

# Green Chemistry

Cutting-edge research for a greener sustainable future

[www.rsc.org/greenchem](http://www.rsc.org/greenchem)

Volume 12 | Number 3 | March 2010 | Pages 353–524



Downloaded on 30 October 2019  
 Published on 10 March 2010 on <http://pubs.rsc.org> | doi:10.1039/C003436N

ISSN 1463-9262

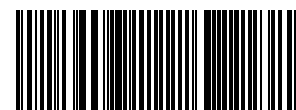
RSC Publishing

Pereira *et al.*  
Dissolution of cork biopolymers in ionic liquids

Zhang and Han *et al.*  
CO<sub>2</sub>-controlled reactors

Gilmore *et al.*  
Antimicrobial and antibiofilm ionic liquids

Lou *et al.*  
Palladium-catalyzed decarboxylation



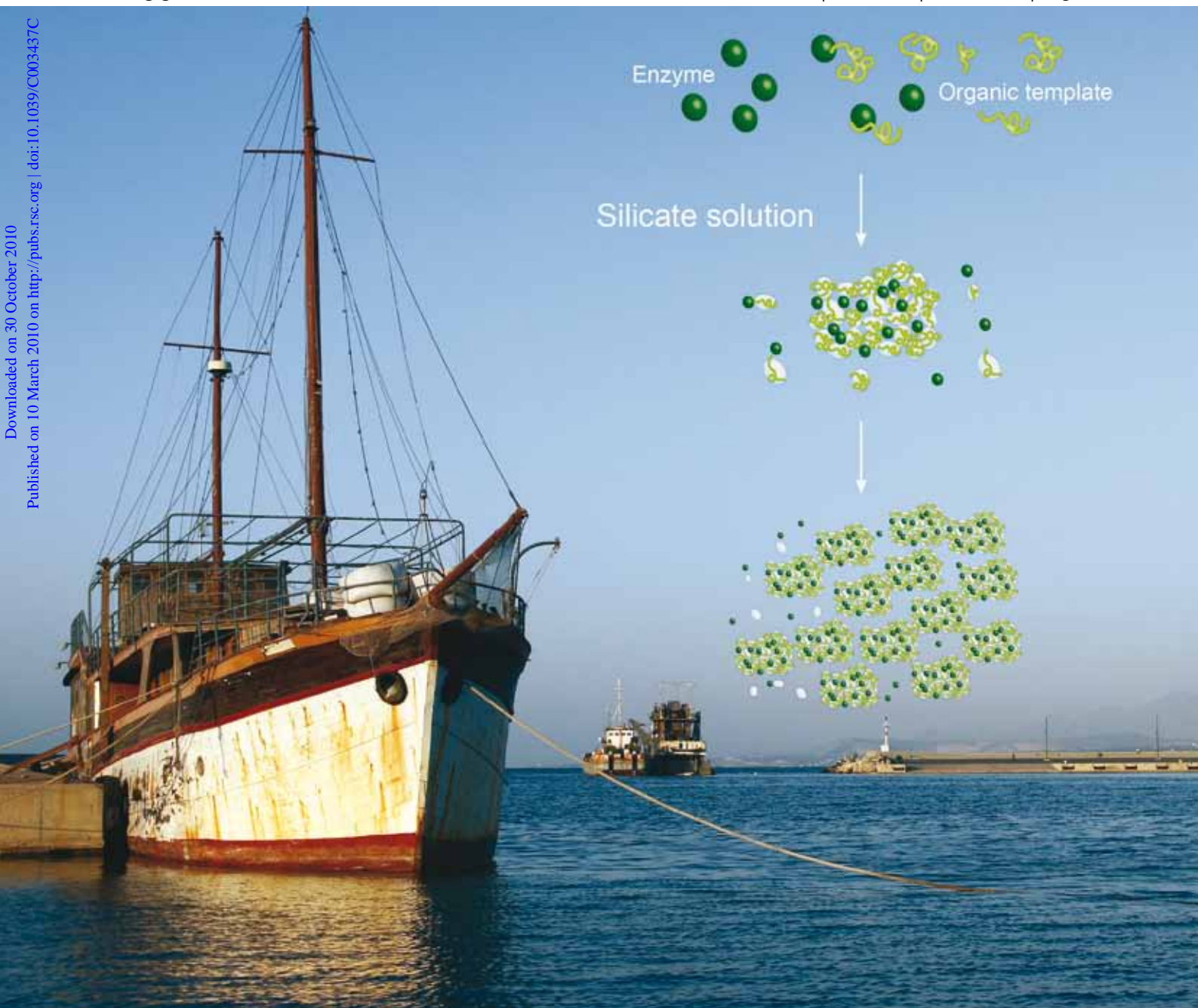
1463-9262(2010)12:3;1-#

# Green Chemistry

Cutting-edge research for a greener sustainable future

[www.rsc.org/greenchem](http://www.rsc.org/greenchem)

Volume 12 | Number 3 | March 2010 | Pages 353–524



Downloaded on 30 October 2010  
Published on 10 March 2010 on <http://pubs.rsc.org> | doi:10.1039/C003437C

ISSN 1463-9262

RSC Publishing

Laursen *et al.*  
Encapsulation of enzymes for  
antifouling coatings

Wang *et al.*  
Knoevenagel condensation

Mascal and Nikitin  
Conversion of plant biomass into  
feedstocks

Schmidt *et al.*  
Utilization of biomass-derived carbon

# Green Chemistry

Cutting-edge research for a greener sustainable future

[www.rsc.org/greenchem](http://www.rsc.org/greenchem)

RSC Publishing is a not-for-profit publisher and a division of the Royal Society of Chemistry. Any surplus made is used to support charitable activities aimed at advancing the chemical sciences. Full details are available from [www.rsc.org](http://www.rsc.org)

## IN THIS ISSUE

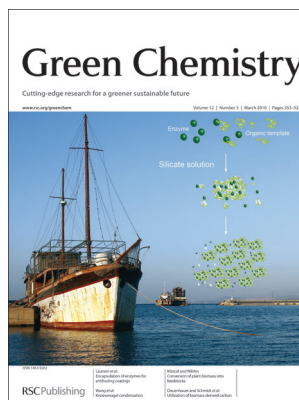
ISSN 1463-9262 CODEN GRCHFJ 12(3) 353–524 (2010)



### Cover

See Pereira *et al.*, pp. 367–369. There is more to cork than sealing wine. Suberin, the highly valuable principal component of cork, is now extractable by a class of biodegradable ionic liquids, the cholinium alkananoates. Photo by Luís Paulo N. Rebelo, design by Luís Morgado.

Image reproduced by permission of Cristina Silva Pereira from *Green Chemistry*, 2010, **12**, 367.



### Inside cover

See Laursen *et al.*, pp. 387–394. A biomimetic process inspired by diatoms, polycation-templated silica co-precipitation, can help enzymes replace persistent biocides in marine coatings. Original photo: Masoud Zargahi.

Image reproduced by permission of Brian Søgaard Laursen from *Green Chemistry*, 2010, **12**, 387.

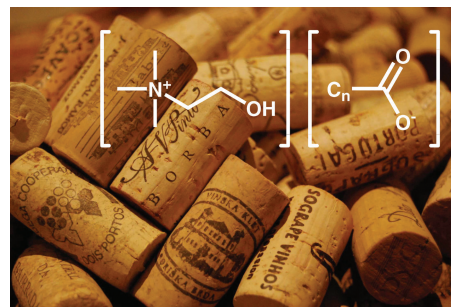
## COMMUNICATIONS

367

### Dissolution of cork biopolymers in biocompatible ionic liquids

Helga Garcia, Rui Ferreira, Marija Petkovic, Jamie L. Ferguson, Maria C. Leitão, H. Q. Nimal Gunaratne, Kenneth R. Seddon, Luis Paulo N. Rebelo and Cristina Silva Pereira\*

We report a class of biocompatible and biodegradable cholinium-based ionic liquids, the cholinium alkananoates, which show a highly efficient and specific dissolution of the suberin domains from cork biopolymers.

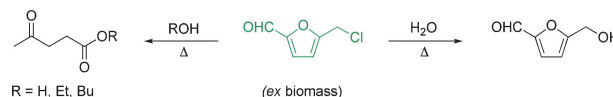


370

### High-yield conversion of plant biomass into the key value-added feedstocks 5-(hydroxymethyl)furfural, levulinic acid, and levulinic esters via 5-(chloromethyl)furfural

Mark Mascall\* and Edward B. Nikitin

5-(Chloromethyl)furfural is proposed as a new cellulose-derived platform chemical for the production of biofuels and value-added products.



## EDITORIAL STAFF

**Editor**

Sarah Ruthven

**Deputy editor**

Kathleen Too

**Senior publishing editor**

Elinor Richards

**Publishing editors**Mary Badcock, David Barden, David Parker,  
Michael Townsend**Publishing assistants**

Anna Anderson, Jackie Cockrill

**Publisher**

Erma Wilson

For queries about submitted articles please contact Elinor Richards, Senior publishing editor, in the first instance. E-mail [green@rsc.org](mailto:green@rsc.org)

For pre-submission queries please contact Sarah Ruthven, Editor. E-mail [green-rsc@rsc.org](mailto:green-rsc@rsc.org)

Green Chemistry (print: ISSN 1463-9262; electronic ISSN 1463-9270) is published 12 times a year by the Royal Society of Chemistry, Thomas Graham House, Science Park, Milton Road, Cambridge, UK CB4 0WF.

All orders, with cheques made payable to the Royal Society of Chemistry, should be sent to RSC Distribution Services, c/o Portland Customer Services, Commerce Way, Colchester, Essex, UK CO2 8HP. Tel +44 (0) 1206 226050; E-mail [sales@rscdistribution.org](mailto:sales@rscdistribution.org)

2010 Annual (print + electronic) subscription price: £1078; US\$2013. 2010 Annual (electronic) subscription price: £970; US\$1811. Customers in Canada will be subject to a surcharge to cover GST. Customers in the EU subscribing to the electronic version only will be charged VAT.

If you take an institutional subscription to any RSC journal you are entitled to free, site-wide web access to that journal. You can arrange access via Internet Protocol (IP) address at [www.rsc.org/ip](http://www.rsc.org/ip). Customers should make payments by cheque in sterling payable on a UK clearing bank or in US dollars payable on a US clearing bank. Periodicals postage paid at Rahway, NJ, USA and at additional mailing offices. Airfreight and mailing in the USA by Mercury Airfreight International Ltd., 365 Blair Road, Avenel, NJ 07001, USA.

US Postmaster: send address changes to Green Chemistry, c/o Mercury Airfreight International Ltd., 365 Blair Road, Avenel, NJ 07001. All despatches outside the UK by Consolidated Airfreight.

Advertisement sales: Tel +44 (0) 1223 432246; Fax +44 (0) 1223 426017; E-mail [advertising@rsc.org](mailto:advertising@rsc.org)

For marketing opportunities relating to this journal, contact [marketing@rsc.org](mailto:marketing@rsc.org)

# Green Chemistry

Cutting-edge research for a greener sustainable future

[www.rsc.org/greenchem](http://www.rsc.org/greenchem)

Green Chemistry focuses on cutting-edge research that attempts to reduce the environmental impact of the chemical enterprise by developing a technology base that is inherently non-toxic to living things and the environment.

## EDITORIAL BOARD

**Chair**

Professor Martyn Poliakoff,  
Nottingham, UK

**Scientific Editor**

Professor Walter Leitner,  
RWTH-Aachen, Germany

**Associate Editor**

Professor C. J. Li,  
McGill University, Canada

**Members**

Professor Paul Anastas,  
Yale University, USA  
Professor Joan Brennecke,  
University of Notre Dame, USA  
Dr Peter Dunn, Pfizer, UK  
Professor Mike Green,  
Newcastle University, UK

Professor Buxing Han,  
Chinese Academy of Sciences,  
China  
Professor Shu Kobayashi,  
University of Tokyo, Japan  
Professor Steven Ley,  
Cambridge, UK  
Professor Tom Welton,  
Imperial College, UK

## ADVISORY BOARD

Tad Adschiri, Tohoku University, Japan

Yonas Chebude, Addis Ababa

University, Ethiopia

Cinzia Chiappe, University of Pisa,  
Italy

James Clark, York University, UK

Avelino Corma, Universidad  
Politecnica de Valencia, Spain

Robert H Crabtree, Yale University,  
USA

Pierre Dixneuf, University of Rennes,  
France

Alexey M. Egorov, Moscow State  
University, Russia

Ronald Hoffmann, Cornell University,  
USA

Istvan Horvath, City University of  
Hong Kong, Hong Kong

Graham Hutchings, Cardiff University,  
UK

Philip Jessop, Queen's University,  
Canada

Kyoko Nozaki, University of Tokyo,  
Japan

Sang-Eon Park, Inha University,  
Korea

Alvise Perosa, Università Ca Foscari,  
Italy

Colin Raston, University of Western  
Australia, Australia

Robin Rogers, University of Alabama,  
USA

Gadi Rothenberg, University of  
Amsterdam, The Netherlands

Janet Scott, JLS Chem Consult Ltd, UK

Ken Seddon, Queen's University,  
Belfast, UK

Roger Sheldon, Delft, The Netherlands

Christian Stevens, Ghent University,  
Belgium

Barry M. Trost, Stanford University,  
USA

Richard Wool, University of Delaware,  
USA

## INFORMATION FOR AUTHORS

Full details on how to submit material for publication in Green Chemistry are given in the Instructions for Authors (available from <http://www.rsc.org/authors>). Submissions should be made via the journal's homepage: <http://www.rsc.org/greenchem>.

Authors may reproduce/republish portions of their published contribution without seeking permission from the RSC, provided that any such republication is accompanied by an acknowledgement in the form: (Original Citation)—Reproduced by permission of The Royal Society of Chemistry.

This journal is © The Royal Society of Chemistry 2010. Apart from fair dealing for the purposes of research or private study for non-commercial purposes, or criticism or review, as permitted under the Copyright, Designs and

Patents Act 1988 and the Copyright and Related Rights Regulation 2003, this publication may only be reproduced, stored or transmitted, in any form or by any means, with the prior permission in writing of the Publishers or in the case of reprographic reproduction in accordance with the terms of licences issued by the Copyright Licensing Agency in the UK. US copyright law is applicable to users in the USA.

The Royal Society of Chemistry takes reasonable care in the preparation of this publication but does not accept liability for the consequences of any errors or omissions.

© The paper used in this publication meets the requirements of ANSI/NISO Z39.48-1992 (Permanence of Paper).

Royal Society of Chemistry: Registered Charity No. 207890.

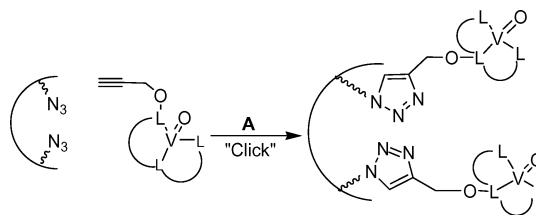
## COMMUNICATIONS

374

**An improved high yielding immobilization of vanadium Schiff base complexes on mesoporous silica *via* azide–alkyne cycloaddition for the oxidation of sulfides**

Suman L. Jain,\* Bharat S. Rana, Bhawan Singh, Anil K. Sinha,\* Asim Bhaumik, Mahasweta Nandi and Bir Sain

“Click chemistry” was found to be an improved and high yielding approach for the covalent immobilization of vanadium Schiff bases onto SBA-15 support as compared to its direct anchoring to the functionalized silica support.

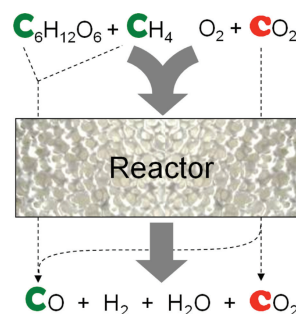


378

**Improved utilization of biomass-derived carbon by co-processing with hydrogen-rich feedstocks in millisecond reactors**

Joshua L. Colby, Paul J. Dauenhauer, Brian C. Michael, Aditya Bhan and Lanny D. Schmidt\*

A reactor capable of improving the utilization of biomass-derived carbon by co-processing hydrogen-deficient biomass ( $H/C \sim 2$ ) with hydrogen-rich feedstocks ( $H/C \geq 4$ ) during thermochemical conversion to synthesis gas is demonstrated experimentally.

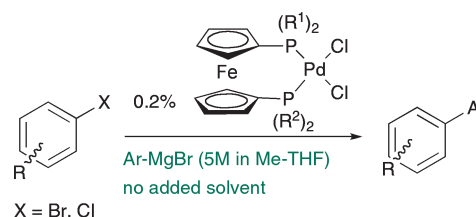


381

**Palladium-catalysed Grignard cross-coupling using highly concentrated Grignards in methyl-tetrahydrofuran**

Edward J. Milton and Matthew L. Clarke\*

Cross-coupling of Grignard reagents at 5 molar concentration is possible in methyl-tetrahydrofuran using just 0.2% of a palladium catalyst with no added reaction solvent, and solvent use was also minimised in the work-up procedure.

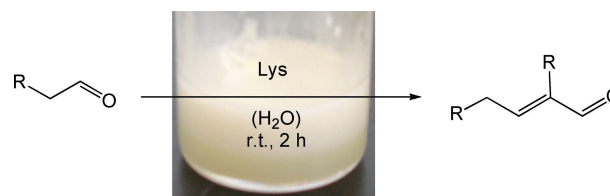


384

**A green method for the self-aldol condensation of aldehydes using lysine**

Yutaka Watanabe,\* Kazue Sawada and Minoru Hayashi

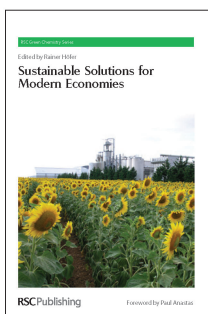
A self-condensation of aldehydes has been conveniently accomplished by the catalytic action of lysine in water or a solvent-free system under specific emulsion. This process is applicable to various aldehydes, especially to long-chain aldehydes.



# Discover Green Chemistry with RSC Publishing

The RSC Green Chemistry book series is a timely and unique venture aimed at providing high level research books at the cutting edge of Green Chemistry

Series Editors James H Clark, University of York, UK | George A Kraus, Iowa State University, USA



## Sustainable Solutions for Modern Economies

This fascinating book outlines the contribution of chemistry and renewable chemical or biological resources to the sustainability concept and potential resolution of the world's energy problems.

**Hardback | ISBN 9781847559050 | 2009 | £90.00**

## Alternative Solvents for Green Chemistry

This book, appropriate for newcomers to the field, gives an overview of the many different



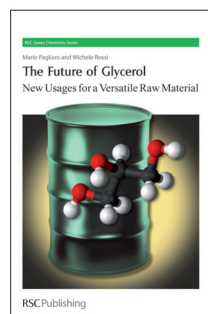
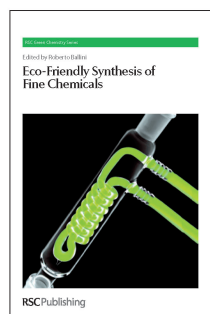
kinds of solvents including alternative greener solvent choices.

**Hardback | ISBN 9780854041633 | 2009 | £89.00**

## Eco-Friendly Synthesis of Fine Chemicals

This book is devoted to the preparation of fine chemicals by new emerging approaches in the field of eco-friendly processes and procedures. A valid resource for researchers and industrialists as well as academia.

**Hardback | ISBN 9781847559081 | 2009 | £99.95**



## The Future of Glycerol

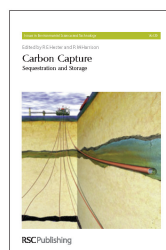
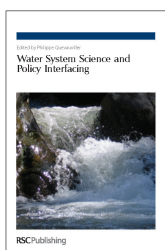
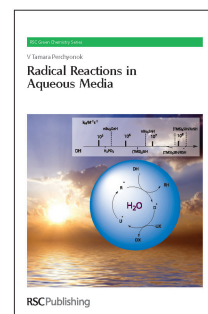
This book depicts how practical limitations posed by glycerol chemistry are solved based on the understanding of the fundamental chemistry of glycerol.

**Hardback | ISBN 9780854041244 | 2008 | £65.00**

## Radical Reactions in Aqueous Media

This exceptional book describes carbon-hydrogen bond formations in aqueous media via radical reactions with a specific focus on Hydrogen Atom Transfer.

**Hardback | ISBN 9781849730006 | 2009 | £70.00**



Also available from RSC Publishing...

## Carbon Capture

**Hardback | ISBN 9781847559173 | 2009 | £54.95**

## Water System Science and Policy Interfacing

**Hardback | ISBN 9781847558619 | 2009 | £120.00**

Visit the website to find out about the new RSC eBook Subject Collections! (Including an Environmental Sciences package)

RSC Publishing

[www.rsc.org/books](http://www.rsc.org/books)

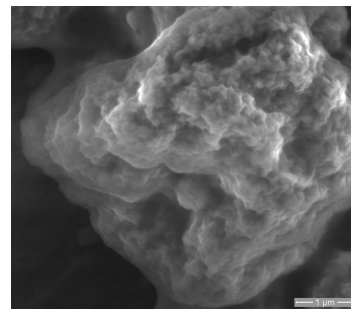
Registered Charity Number 207890

387

### Biomimetic silica encapsulation of enzymes for replacement of biocides in antifouling coatings

Jakob Broberg Kristensen, Rikke Louise Meyer, Charlotte Horsmans Poulsen, Karsten Matthias Kragh, Flemming Besenbacher and Brian Søgaard Laursen\*

A coating system that generates hydrogen peroxide by the action of an encapsulated enzyme is presented. The system has the potential for prolonged action through incorporation in a self-polishing coating.

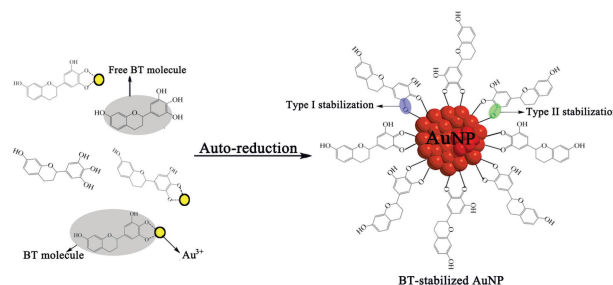


395

### One-step, size-controlled synthesis of gold nanoparticles at room temperature using plant tannin

Xin Huang, Hao Wu, Xuepin Liao\* and Bi Shi

Preparation of BT-stabilized gold nanoparticles (BT-stabilized AuNPs).

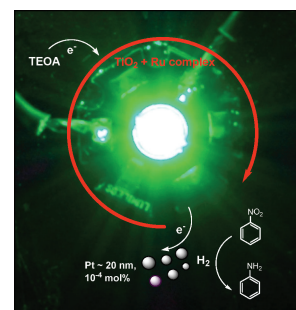


400

### Green-light photocatalytic reduction using dye-sensitized TiO<sub>2</sub> and transition metal nanoparticles

Stefan Fuldner, Ralph Mild, Heiko Ingo Siegmund, Josef A. Schroeder, Michael Gruber and Burkhard König\*

Very clean green light photoreductions of nitrobenzenes are achieved by Ru(bipy)<sub>3</sub>/TiO<sub>2</sub> photocatalysts if small amounts of transition metal salts are added, which form metal particles of a narrow size distribution under experimental conditions.

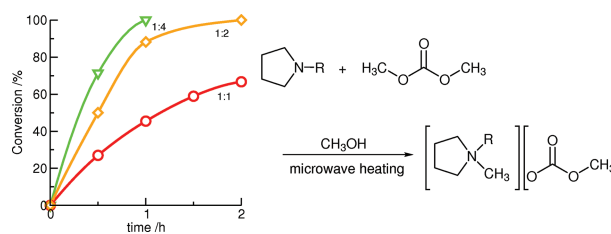


407

### Optimised microwave-assisted synthesis of methylcarbonate salts: a convenient methodology to prepare intermediates for ionic liquid libraries

John D. Holbrey,\* Robin D. Rogers, Saloni S. Shukla and Cecilia D. Wilfred

The synthesis of methylcarbonate salts, which have utility as clean ionic liquid precursors, has been optimised; for example, 1-butyl-1-methylpyrrolidinium methylcarbonate was obtained in 100% yield in 1 h.



The aim of the conference is to highlight innovative concepts for the substitution of volatile organic solvents in solution phase synthesis. Emphasis will be laid on the development and application of alternative reaction media based on advanced fluids such as aqueous phases, ionic liquids, supercritical phases, green organic solvents, or soluble polymers, but includes also phase-separable reagents and related separation strategies in all areas of chemical synthesis.



**October 10 – 13, 2010**  
**Berchtesgaden/Germany**

# Green Solvents Conference

[www.dechema.de/gsfs2010](http://www.dechema.de/gsfs2010)



## INVITED SPEAKERS

**A.T. Bell**, University of California, Berkeley, CA/USA  
**P.J. Dunn**, Pfizer Global Research and Development, Sandwich/UK  
**C. Fischmeister**, University of Rennes/F  
**J.A. Gladysz**, Texas A&M University, College Station, TX/USA  
**L. Greiner**, RWTH Aachen/D  
**J.-D. Grunwaldt**, KIT – Karlsruhe Institute of Technology/D  
**S.M. Howdle**, University of Nottingham/UK  
**T. Ikariya**, Tokyo Institute of Technology/J  
**P.G. Jessop**, Queen's University, Kingston Ontario/CDN  
**U. Kragl**, University of Rostock/D  
**Y.-W. Lee**, Seoul National University/ROK  
**L. Szarvas**, K. Müller, BASF SE, Ludwigshafen/D  
**S. Sarrade**, CEA Marcoule, Bagnols-sur-Cèze/F  
**N. Szesni**, Süd-Chemie AG, Bruckmühl/D  
**D. Vogt**, TU Eindhoven/NL

## ORGANISING COMMITTEE

**W. Leitner**, RWTH Aachen/D, Chairman  
**K.R. Seddon**, The Queen's University of Belfast/UK  
**P. Wasserscheid**, University of Erlangen-Nuremberg/D  
**A. Wells**, AstraZeneca, Loughborough/UK  
**D. Demtröder**, DECHEMA e. V., Frankfurt am Main/D  
**B. Feisst**, DECHEMA e. V., Frankfurt am Main/D

## SUBMISSION OF ABSTRACTS

The submission of abstracts proceeds via file upload at the website effective until **April 30, 2010**.

Full information and submission:  
[www.dechema.de/gsfs2010](http://www.dechema.de/gsfs2010)



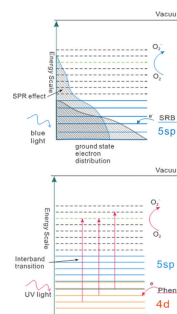


414

### Supported silver nanoparticles as photocatalysts under ultraviolet and visible light irradiation

Xi Chen, Zhanfeng Zheng, Xuebin Ke, Esa Jaatinen, Tengfeng Xie, Dejun Wang, Cheng Guo, Jincai Zhao and Huaiyong Zhu\*

Silver nanoparticles are good photocatalysts under visible light for dye and phenol degradation, and can drive selective alcohol oxidation under UV light. Surface plasmon resonance effect and interband transition of silver nanoparticles can activate organic molecules for oxidation.

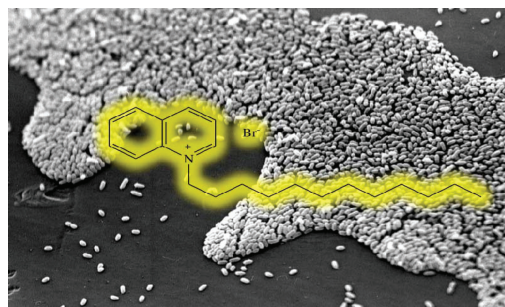


420

### Antimicrobial and antibiofilm activities of 1-alkylquinolinium bromide ionic liquids

Alessandro Buseti, Deborah E. Crawford, Martyn J. Earle, Manuela A. Gilea, Brendan F. Gilmore,\* Sean P. Gorman, Garry Laverty, Andrew F. Lowry, Martin McLaughlin and Kenneth R. Seddon

1-Alkylquinolinium bromide ionic liquids are potent antimicrobial and antibiofilm agents, with a broad spectrum of activity against bacteria and fungi.

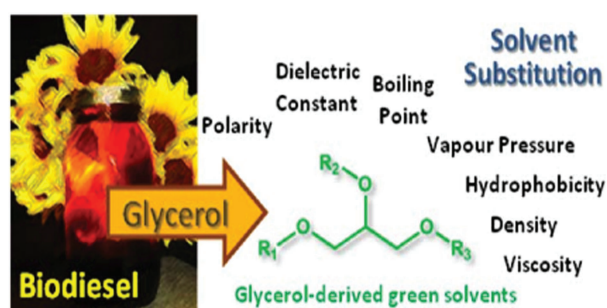


426

### Green solvents from glycerol. Synthesis and physico-chemical properties of alkyl glycerol ethers

José I. García,\* Héctor García-Marín, José A. Mayoral and Pascual Pérez

62 glycerol derivatives, 1,3-dialkoxy-2-propanols and 1,2,3-trialkoxypropanes, have been synthesized and their possible role as substitutive solvents has been evaluated through measurements of their physico-chemical properties.

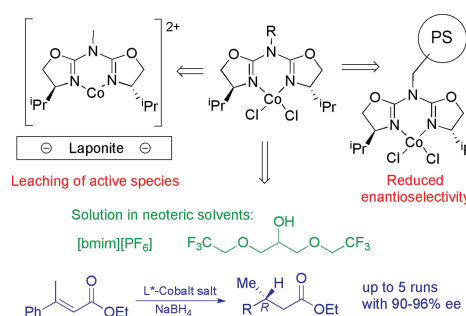


435

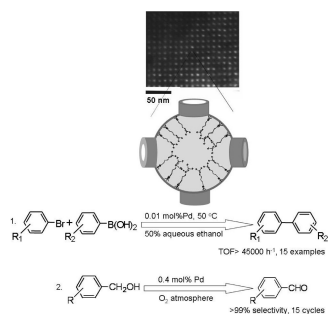
### Study of the recycling possibilities for azabis(oxazoline)-cobalt complexes as catalysts for enantioselective conjugate reduction

Luis Aldea, José M. Fraile,\* Héctor García-Marín, José I. García, Clara I. Herrerías, José A. Mayoral and Ignacio Pérez

Recovery of azabox-Co complexes after enantioselective reduction is not possible by immobilization on solid supports, but the use of a new glycerol-derived solvent and an optimized ligand allows reaching 5 consecutive runs with high enantioselectivity.



441

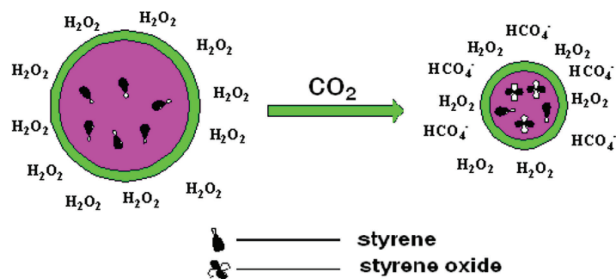


### Palladium-guanidine complex immobilized on SBA-16: a highly active and recyclable catalyst for Suzuki coupling and alcohol oxidation

Hengquan Yang,\* Xiaojing Han, Zhancheng Ma, Runqin Wang, Jing Liu and Xiangfei Ji

By immobilizing a mixture of palladium-guanidine complex and guanidine in the nanocages of SBA-16, an efficient solid catalyst for Suzuki coupling and the aerobic oxidation of alcohols was prepared.

452

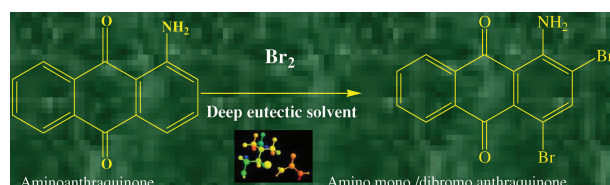


### CO<sub>2</sub>-controlled reactors: epoxidation in emulsions with droplet size from micron to nanometre scale

Yueju Zhao, Jianling Zhang,\* Buxing Han,\* Suqin Hu and Wei Li

The emulsion droplet size can be tuned from microns to nanometres by controlling pressure, and the conversion increased dramatically with the decreasing droplet size of the emulsion.

458

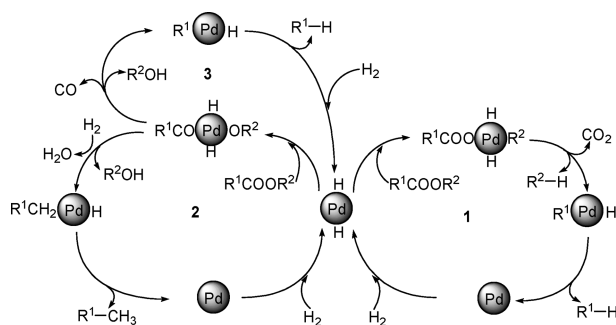


### Halogenation reactions in biodegradable solvent: Efficient bromination of substituted 1-aminoanthra-9,10-quinone in deep eutectic solvent (choline chloride : urea)

Sunanda Balaso Phadtare and Ganapati Subray Shankarling\*

Biodegradable solvents provide an effective green chemistry method for the bromination of 1-aminoanthra-9,10-quinone under mild conditions and are recyclable.

463



### Palladium-catalyzed decarboxylation of higher aliphatic esters: Towards a new protocol to the second generation biodiesel production

Junxing Han, Hui Sun, Yuqi Ding, Hui Lou\* and Xiaoming Zheng

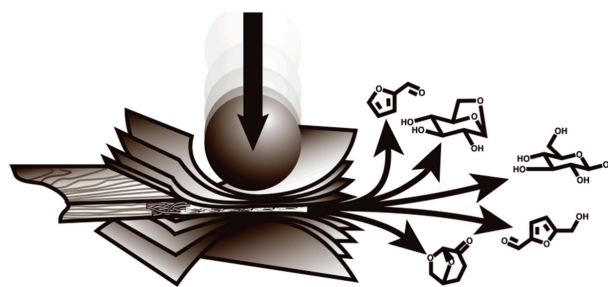
In the present work, we disclosed an effective and highly selective decarboxylation approach to convert higher aliphatic esters into diesel-like paraffins. The methodology described in this paper provides a new protocol to the utilization of biomass-based resources, especially to the second generation biodiesel production.

468

**Mechanocatalysis for biomass-derived chemicals and fuels**

Sandra M. Hick, Carolin Griebel, David T. Restrepo, Joshua H. Truitt, Eric J. Buker, Caroline Bylda and Richard G. Blair\*

The application of mechanical force and layered catalysts can efficiently depolymerize cellulosic materials (up to 84% conversion). The most effective mechanocatalysts are aluminosilicates based on the kaolinite structure.

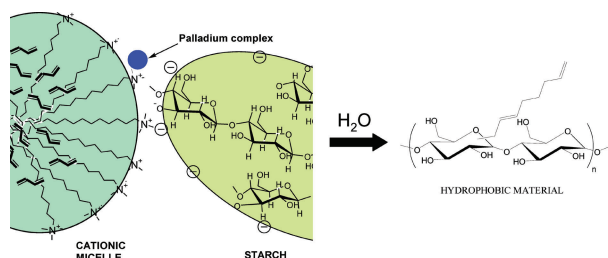


475

**Telomerization of butadiene with starch in water: role of the surfactants**

Julien Mesnager, Claude Quettier, Anne Lambin, Franck Rataboul, Alain Perrard and Catherine Pinel\*

Efficient telomerization of starch was carried out in water in the presence of  $[(\pi\text{-allyl})\text{Pd}(\text{TPPTS})_2]\text{Cl}$  catalyst and surfactant at 50 °C. After optimization, TON up to 4000 was achieved.

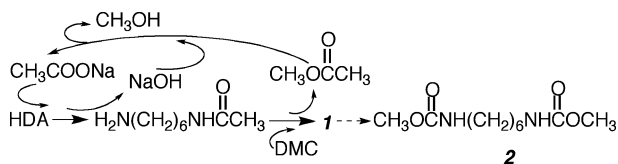


483

**CH<sub>3</sub>COONa as an effective catalyst for methoxycarbonylation of 1,6-hexanediamine by dimethyl carbonate to dimethylhexane-1,6-dicarbamate**

Da-Lei Sun, Shun-Ji Xie, Jian-Ru Deng, Cai-Juan Huang, Eli Ruckenstein\* and Zi-Sheng Chao\*

CH<sub>3</sub>COONa is employed, for the first time, as catalyst for the methoxycarbonylation of HDA by DMC. A 99.0% yield of dimethylhexane-1,6-dicarbamate under mild conditions has been obtained. A possible mechanism is also proposed.

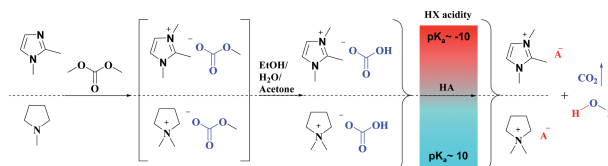


491

**New hydrogen carbonate precursors for efficient and byproduct-free syntheses of ionic liquids based on 1,2,3-trimethylimidazolium and N,N-dimethylpyrrolidinium cores**

Marcin Smiglak, C. Corey Hines and Robin D. Rogers\*

A generalized synthetic protocol for the formation of ionic liquids free of halide and metal ions from  $[\text{HCO}_3]^-$  salt precursors is demonstrated with 1,2-dimethylimidazole and N-methylpyrrolidine.



# Stimulating reviews on natural products and related areas

*Natural Product Reports* publishes highlights (topical areas of interest) and reviews in key areas including: bioorganic chemistry, chemical biology, chemical ecology and carbohydrates



- Impact factor 7.450\*
- High visibility – cited in MEDLINE
- Hot off the Press literature highlights published in each issue for the benefit of the community



\*2008 Thomson Scientific (ISI) Journal Citation Reports®

RSCPublishing

[www.rsc.org/npr](http://www.rsc.org/npr)

Registered Charity Number 207890

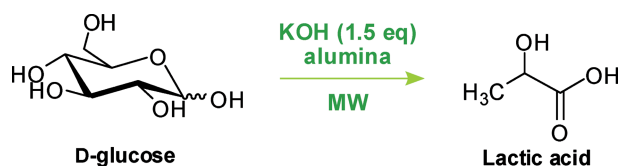
## PAPERS

502

**Microwave-assisted conversion of D-glucose into lactic acid under solvent-free conditions**

Géraldine Epane, Jean Claude Laguerre, Anne Wadouachi\* and Delphine Marek\*

Efficient conversion of D-glucose into lactic acid is described using microwave irradiation in solventless condition with alumina supported potassium hydroxide.

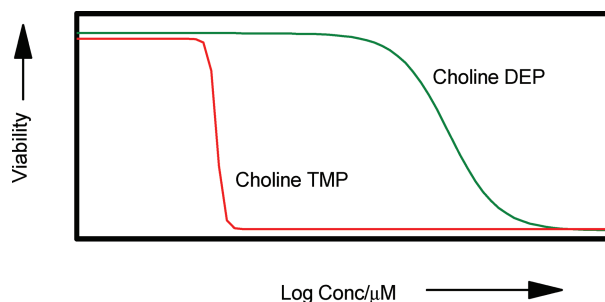


507

**Cyto-toxicity and biocompatibility of a family of choline phosphate ionic liquids designed for pharmaceutical applications**

Katherine D. Weaver, Hye Jin Kim, Jiazeng Sun, Douglas R. MacFarlane and Gloria D. Elliott\*

A set of choline-based ionic liquids are investigated for J774 mouse macrophage cytotoxicity. Manipulating the structure of the phosphate-based anion moiety modulates the cytotoxicity and solution behavior.

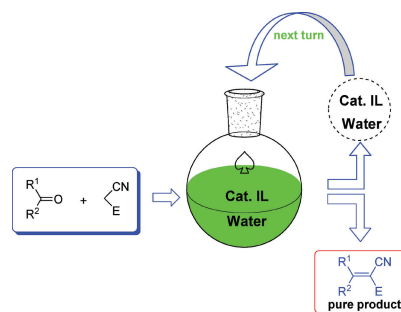


514

**A simple, efficient and green procedure for Knoevenagel condensation catalyzed by [C<sub>4</sub>dabco][BF<sub>4</sub>] ionic liquid in water**


Da-Zhen Xu, Yingjun Liu, Sen Shi and Yongmei Wang\*

The use of DABCO-base ionic liquid catalysts in water as an efficient, green and reusable catalyst system for the Knoevenagel condensation within a short time is presented.



## FREE E-MAIL ALERTS AND RSS FEEDS


Contents lists in advance of publication are available on the web *via* [www.rsc.org/greenchem](http://www.rsc.org/greenchem) – or take advantage of our free e-mail alerting service ([www.rsc.org/ej\\_alert](http://www.rsc.org/ej_alert)) to receive notification each time a new list becomes available.

 Try our RSS feeds for up-to-the-minute news of the latest research. By setting up RSS feeds, preferably using feed reader software, you can be alerted to the latest Advance Articles published on the RSC web site. Visit [www.rsc.org/publishing/technology/rss.asp](http://www.rsc.org/publishing/technology/rss.asp) for details.

## ADVANCE ARTICLES AND ELECTRONIC JOURNAL

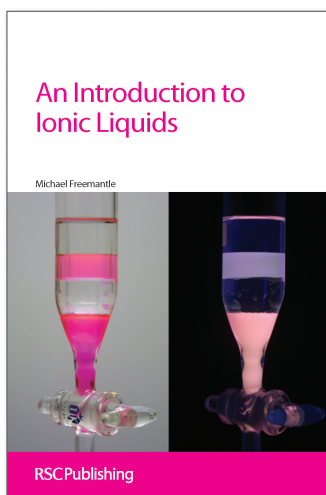
Free site-wide access to Advance Articles and the electronic form of this journal is provided with a full-rate institutional subscription. See [www.rsc.org/ejs](http://www.rsc.org/ejs) for more information.

\* Indicates the author for correspondence: see article for details.

 Electronic supplementary information (ESI) is available *via* the online article (see <http://www.rsc.org/esi> for general information about ESI).

## AUTHOR INDEX

- Aldea, Luis, 435  
 Besenbacher, Flemming, 387  
 Bhan, Aditya, 378  
 Bhaumik, Asim, 374  
 Blair, Richard G., 468  
 Buker, Eric J., 468  
 Buseti, Alessandro, 420  
 Bylda, Caroline, 468  
 Chao, Zi-Sheng, 483  
 Chen, Xi, 414  
 Clarke, Matthew L., 381  
 Colby, Joshua L., 378  
 Crawford, Deborah E., 420  
 Dauenhauer, Paul J., 378  
 Deng, Jian-Ru, 483  
 Ding, Yuqi, 463  
 Earle, Martyn J., 420  
 Elliott, Gloria D., 507  
 Epane, Géraldine, 502  
 Ferguson, Jamie L., 367  
 Ferreira, Rui, 367  
 Fraile, José M., 435  
 Földner, Stefan, 400  
 Garcia, Helga, 367  
 García, José I., 426, 435  
 García-Marín, Héctor, 426, 435  
 Gilea, Manuela A., 420  
 Gilmore, Brendan F., 420  
 Gorman, Sean P., 420  
 Griebel, Carolin, 468  
 Gruber, Michael, 400  
 Gunaratne, H. Q. Nimal, 367
- Guo, Cheng, 414  
 Han, Buxing, 452  
 Han, Junxing, 463  
 Han, Xiaojing, 441  
 Hayashi, Minoru, 384  
 Herrerías, Clara I., 435  
 Hick, Sandra M., 468  
 Hines, C. Corey, 491  
 Holbrey, John D., 407  
 Hu, Suqin, 452  
 Huang, Cai-Juan, 483  
 Huang, Xin, 395  
 Jaatinen, Esa, 414  
 Jain, Suman L., 374  
 Ji, Xiangfei, 441  
 Ke, Xuebin, 414  
 Kim, Hye Jin, 507  
 König, Burkhard, 400  
 Kragh, Karsten Matthias, 387  
 Kristensen, Jakob Broberg, 387  
 Laguerre, Jean Claude, 502  
 Lambin, Anne, 475  
 Laursen, Brian Sogaard, 387  
 Laverty, Garry, 420  
 Leitão, Maria C., 367  
 Li, Wei, 452  
 Liao, Xuepin, 395  
 Liu, Jing, 441  
 Liu, Yingjun, 514  
 Lou, Hui, 463  
 Lowry, Andrew F., 420  
 Ma, Zhancheng, 441
- MacFarlane, Douglas R., 507  
 Marek, Delphine, 502  
 Mascal, Mark, 370  
 Mayoral, José A., 426, 435  
 McLaughlin, Martin, 420  
 Mesnager, Julien, 475  
 Meyer, Rikke Louise, 387  
 Michael, Brian C., 378  
 Mild, Ralph, 400  
 Milton, Edward J., 381  
 Nandi, Mahasweta, 374  
 Nikitin, Edward B., 370  
 Pérez, Ignacio, 435  
 Pérez, Pascual, 426  
 Perrard, Alain, 475  
 Petkovic, Marija, 367  
 Phadtare, Sunanda Balaso, 458  
 Pinel, Catherine, 475  
 Poulsen, Charlotte Horsmans, 387  
 Quettier, Claude, 475  
 Rana, Bharat S., 374  
 Rataboul, Franck, 475  
 Rebelo, Luís Paulo N., 367  
 Restrepo, David T., 468  
 Rogers, Robin D., 407, 491  
 Ruckenstein, Eli, 483  
 Sain, Bir, 374  
 Sawada, Kazuo, 384  
 Schmidt, Lanny D., 378  
 Schroeder, Josef A., 400  
 Seddon, Kenneth R., 367, 420  
 Shankarling, Ganapati Subray, 458
- Shi, Bi, 395  
 Shi, Sen, 514  
 Shukla, Saloni S., 407  
 Siegmund, Heiko Ingo, 400  
 Silva Pereira, Cristina, 367  
 Singh, Bhawan, 374  
 Sinha, Anil K., 374  
 Smiglak, Marcin, 491  
 Sun, Da-Lei, 483  
 Sun, Hui, 463  
 Sun, Jiazeng, 507  
 Truitt, Joshua H., 468  
 Wadouachi, Anne, 502  
 Wang, Dejun, 414  
 Wang, Runqin, 441  
 Wang, Yongmei, 514  
 Watanabe, Yutaka, 384  
 Weaver, Katherine D., 507  
 Wilfred, Cecilia D., 407  
 Wu, Hao, 395  
 Xie, Shun-Ji, 483  
 Xie, Tengfeng, 414  
 Xu, Da-Zhen, 514  
 Yang, Hengquan, 441  
 Zhang, Jianling, 452  
 Zhao, Jincai, 414  
 Zhao, Yueju, 452  
 Zheng, Xiaoming, 463  
 Zheng, Zhanfeng, 414  
 Zhu, Huaiyong, 414



## An Introduction to Ionic Liquids

Michael Freemantle

This is the first single-author book on ionic liquids and the first introductory book on the topic. *An Introduction to Ionic Liquids* is written in a clear, concise and consistent way and provides a useful introduction to ionic liquids for those readers who are not familiar with the topic. It is also wide ranging, embracing every aspect of the chemistry and applications of ionic liquids. The book draws extensively on the primary scientific literature to provide numerous examples of research on ionic liquids. These examples will enable the reader to become familiar with the key developments in ionic liquids chemistry over recent years.

Science students, researchers, teachers in academic institutions and chemists and other scientists in industry and government laboratories will find the book an invaluable introduction to one of the most rapidly advancing and exciting fields of science and technology today.

BB Hardback | 281 pages | ISBN 9781847551610 | 2009 | £39.95

RSC Publishing

www.rsc.org/books  
 Registered Charity Number 207890

# Dissolution of cork biopolymers in biocompatible ionic liquids

Helga Garcia,<sup>†a</sup> Rui Ferreira,<sup>†a</sup> Marija Petkovic,<sup>a</sup> Jamie L. Ferguson,<sup>b</sup> Maria C. Leitão,<sup>a</sup>  
H. Q. Nimal Gunaratne,<sup>b</sup> Kenneth R. Seddon,<sup>a,b</sup> Luís Paulo N. Rebelo<sup>a</sup> and Cristina Silva Pereira<sup>\*a,c</sup>

Received 28th October 2009, Accepted 4th December 2009

First published as an Advance Article on the web 5th January 2010

DOI: 10.1039/b922553f

Classically, the best attempts to separate suberin from cork biopolymers have resulted in low efficiency; here, we report a class of biocompatible and biodegradable cholinium-based ionic liquids, the cholinium alkanooates, which show a highly efficient and specific dissolution of the suberin domains from cork biopolymers.

Worldwide, the annual production of cork, which is the external bark of *Quercus suber* L., is 300 000 tonnes, half of which forms the basis of the Portuguese cork manufacturing industry.<sup>1</sup> Cork is a remarkable biocomposite, showing a very specific combination of properties, such as elasticity, compressibility, low permeability of liquids and significant chemical/microbial resistance;<sup>2</sup> there is thus a significant interest in suberin (its major component) as a valuable source of property-enhancing additives.<sup>3</sup> The conventional pre-treatment of cork<sup>4</sup> removes the soluble components (extractives), but leaves an essentially insoluble matrix (extractive-free, or refined, cork) whose main components are polysaccharides, “lignin-like” poly(phenolics) and suberin (~20, ~30 and ~50 wt%, respectively).<sup>5</sup> Suberin is a complex cross-linked polymer composed of aromatic and aliphatic domains.<sup>6</sup> The former domain is relatively similar to lignin, and possesses a very complex structure comprising units of hydroxycinnamic acid and, to a minor extent, monolignols (*p*-coumaryl, coniferyl and sinapyl alcohols); the latter domain is composed mostly of units of C<sub>16</sub>–C<sub>26</sub> hydroxyacids that are primarily linked *via* ester bonds to glycerol.<sup>2,7</sup> This means that, structurally, cork has a strong relationship with lignocellulosic materials.

Ionic liquids exhibit a set of unique and astonishing properties, such as negligible vapour pressure, bulk non-flammability, and high thermal and chemical stability. Because their thermophysical and chemical properties can be fine-tuned through slight alterations to the cations, anions or both, they can address very specific requirements.<sup>8</sup> A major industrial interest in ionic liquids is the dissolution and processing of cellulose, which has been successfully achieved with some 1,3-dialkylimidazolium ionic liquids.<sup>9,10</sup> The basis of their outstanding solvation behaviour results from their Coulombic environment,<sup>8</sup> and is

thought to be due to an ionic liquid's ability to disrupt intermolecular hydrogen bonding networks and interact with the hydroxyl groups of cellulose.<sup>9,11</sup> However, the scope of possible applications of 1,3-dialkylimidazolium ionic liquids is restricted due to their cost, toxicity<sup>12</sup> and/or environmental persistence due to the non-biodegradability<sup>13</sup> of the imidazolium ring.

Refined cork has been reported to be insoluble in many common solvents,<sup>3</sup> but its apparent similarities with other lignocellulosic materials suggest that it might be soluble in tailor-made ionic liquids. Here, we report the first example of refined cork dissolution by ionic liquids. Moreover, the ionic liquids selected are both biocompatible and biodegradable.

Learning from both previous experience of the dissolution of lignocellulosic materials, and the extant toxicological and biodegradation data of ionic liquid cations and anions, a test group of ionic liquids was selected by combining three different cations (1-ethyl-3-methylimidazolium [C<sub>2</sub>mim]<sup>+</sup>, 1-butyl-3-methylimidazolium [C<sub>4</sub>mim]<sup>+</sup> and cholinium [N<sub>111</sub>C<sub>2</sub>H<sub>4</sub>OH]<sup>+</sup>) and six different anions. The effect of the anion was studied by focusing initially on chloride, ethanoate and lactate anions, and, in the case of the cholinium ionic liquids,<sup>14</sup> on a further three alkanooates.

Cork samples were initially ground to a fine powder, and the soluble cork extracts (extractives) were removed as previously described by Gil *et al.*<sup>4</sup> Prior to the dissolution tests (all performed in triplicate), the ionic liquid and refined cork powder were vacuum dried in order to remove water. The ionic liquid (*ca.* 1.6 g) was added to the refined cork powder (*ca.* 0.025 g) (ionic liquid : cork ≈ 2 : 1 v/v) and the mixture held at 100 °C (which is below the degradation temperature of all the ionic liquids) without any stirring for 4 h. The dissolution was then stopped by adding an excess of de-ionised water (*ca.* 20 cm<sup>3</sup>), and the insoluble residue was recovered by filtration and dried. Under these conditions, in separate experiments, no significant decomposition was detected for either the cork or the ionic liquids.

Attenuated total reflectance Fourier transform infrared (ATR-FTIR) spectroscopy has successfully been used for cork characterisation, and consequently it has been selected here for qualitative assessment of the dissolution process.<sup>2,5,6</sup> These studies determined quite precisely the infrared absorption features of the primary components of refined cork:

Suberin: 2921, 2852, 1737, 1242, 1158 and 724 cm<sup>-1</sup>.

Lignin: 1511, 855 and 819 cm<sup>-1</sup>.

Polysaccharides: 1092 and 1034 cm<sup>-1</sup>.

The samples of refined cork powder prepared for this study, both before and after heating, correspond exactly to these literature data.

<sup>a</sup>Instituto de Tecnologia Química e Biológica, Universidade Nova de Lisboa, Apartado 127, 2781-901, Oeiras, Portugal.

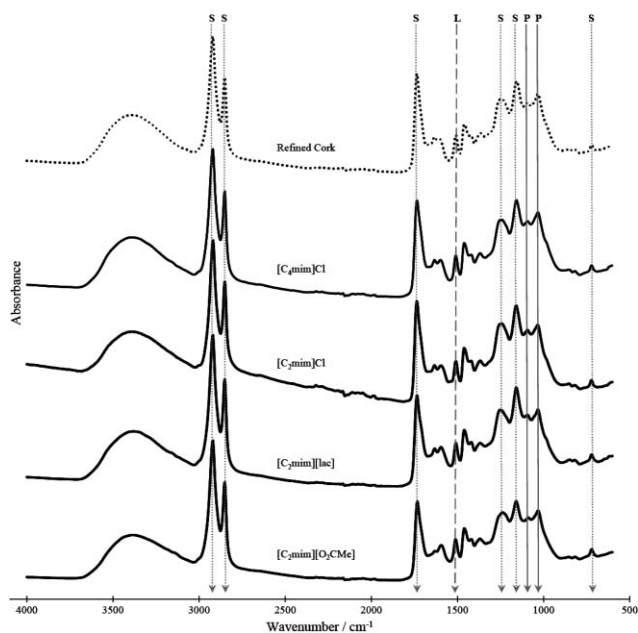
E-mail: spereira@itqb.unl.pt

<sup>b</sup>The Queen's University Ionic Liquid Laboratories (QUILL), The Queen's University of Belfast, Belfast, UK BT9 5AG

<sup>c</sup>Instituto de Biologia Experimental e Tecnológica, Apartado 12, 2781-901, Oeiras, Portugal

† Equally contributing authors.

ATR-FTIR analyses of the cork residue after its extraction by ionic liquids from the 1,3-dialkylimidazolium family are presented in Fig. 1. Neither  $[C_2\text{mim}]\text{Cl}$  nor  $[C_4\text{mim}]\text{Cl}$  were able to dissolve significant amounts of the refined cork, even though they have been previously observed to enable significant dissolution of polysaccharides in lignocellulosic composites.<sup>11,15</sup> However, replacing the chloride with various carboxylate anions, namely lactate ( $[\text{lac}]^-$ ) and ethanoate, caused the dissolution efficiency to increase significantly. The latter was more efficient and led to a greater dissolution of the aromatic suberin (Fig. 1, shown by the decreasing intensity of the peaks at 1737, 1242 and 1158  $\text{cm}^{-1}$ ). Both anions led to a small solubility of the polysaccharides, as illustrated by the changes in the intensity of the peaks at 1092 and 1034  $\text{cm}^{-1}$ .



**Fig. 1** ATR-FTIR spectra of the insoluble cork fraction after treatment with different 1,3-dialkylimidazolium ionic liquids. The vertical lines represent the major cork components: suberin (S), lignin (L) and polysaccharides (P).

The results for the cholinium,  $[\text{Me}_3\text{NCH}_2\text{CH}_2\text{OH}]^+$  or  $[\text{N}_{111}\text{C}_2\text{H}_4\text{OH}]^+$ , salts are presented in Fig. 2 and Table 1. The cholinium ethanoate showed, relative to the 1,3-dialkylimidazolium ionic liquids, a significant increase in dissolution of the refined cork, especially of the aromatic suberin component. The lack of efficiency of the lactate anion relative to the ethanoate (cork weight losses of 20.7 and 39.7%, respectively) is unsurprising as the lactate anion is less basic than the ethanoate anion. Further support for this simple concept is that the cholinium alkanates of increasing alkyl chain length (ethanoate, butanoate, hexanoate) showed augmented dissolution efficiency since the basicity of the anion increases with chain length (Table 1).

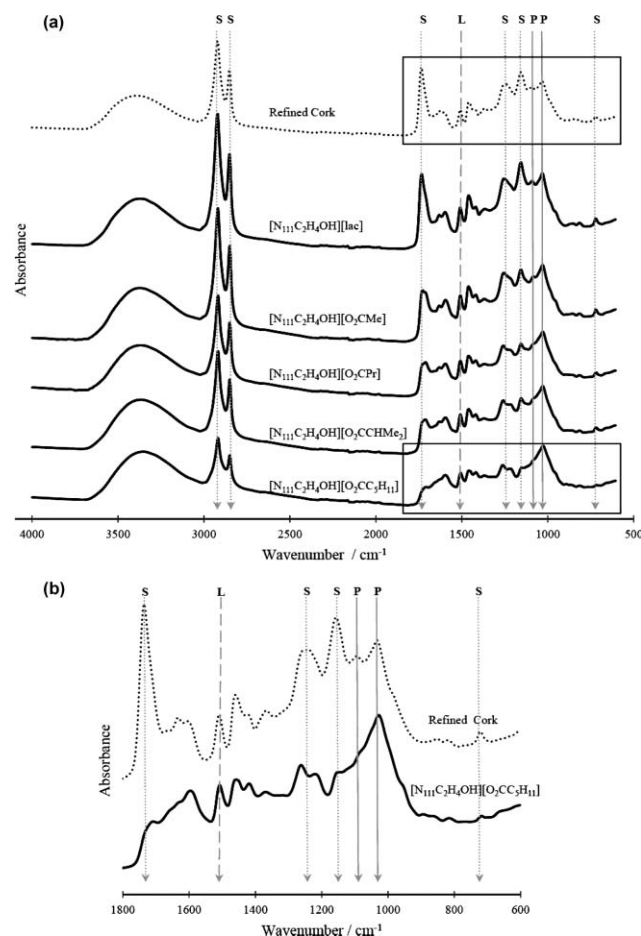
**Table 2** The extraction efficiency of four cholinium ionic liquids

<b>Anion</b>	$[\text{O}_2\text{CMe}]^-$	<	$[\text{O}_2\text{CPr}]^-$	<	$[\text{O}_2\text{CCHMe}_2]^-$	<	$[\text{O}_2\text{CC}_5\text{H}_{11}]^-$
<b>Cork weight loss</b>	40%	<	44%	<	55%	<	65%

**Table 1** Data on the dissolution efficiency of refined cork in a range of cholinium alkanates,  $[\text{N}_{111}\text{C}_2\text{H}_4\text{OH}]\text{Y}$ . The  $\text{pK}_a$  values of the conjugate acid of the anion of each ionic liquid is also presented

$\text{Y}^-$	$E_{\text{solv}}$ (%) <sup>a</sup>	STD <sup>b</sup>	$\text{pK}_a$ (HY)
$[\text{O}_2\text{CMe}]^-$	39.7	2.5	4.76
$[\text{O}_2\text{CPr}]^-$	44.1	10.8	4.84
$[\text{O}_2\text{CCHMe}_2]^-$	55.1	5.8	4.83
$[\text{O}_2\text{CC}_5\text{H}_{11}]^-$	64.9	7.9	4.85
$[\text{lac}]^-$	20.7	4.1	3.86

<sup>a</sup> Extraction efficiency,  $E_{\text{solv}}$  (%) =  $100 \times (m_{\text{cork}, t=0} - m_{\text{cork}, t=4\text{h}}) / m_{\text{cork}, t=0}$ .  
<sup>b</sup> STD = standard deviation.



**Fig. 2** (a) ATR-FTIR spectra of the cork residue after treatment with different cholinium ionic liquids. (b) An expansion of the ATR-FTIR spectra of the cork residue after treatment with cholinium hexanoate. The vertical lines represent the major cork components: suberin (S), lignin (L) and polysaccharides (P).

The efficiency of the anions can be ranked as follows (Table 2).

The dissolution efficiency tracks the  $\text{pK}_a$  values of the conjugate acid of the anion, chloride being the least efficient.



This contrasts with the dissolution of cellulose in ionic liquids, which shows no such correlation and appears to be more associated with the ability of the anion to disrupt the hydrogen-bonded matrix. The lack of any of obvious steric effect here may be a reflection of the porosity of the cork.

The dissolution of cork by  $[N_{111}C_2H_4OH][O_2CMe]$ ,  $[N_{111}C_2H_4OH][O_2CPr]$ ,  $[N_{111}C_2H_4OH][O_2CCHMe_2]$  and  $[N_{111}C_2H_4OH][O_2CC_5H_{11}]$  resulted, progressively, in a remarkable reduction (Fig. 2) of the intensity of the bands due to the aromatic (1242, 1158 and  $1737\text{ cm}^{-1}$ ) and aliphatic (2921, 2852 and  $724\text{ cm}^{-1}$ ) suberin component in the insoluble cork residue. The peak at  $1737\text{ cm}^{-1}$  (associated with the carbonyl stretch of the ester groups) was virtually absent in the case of hexanoate, with concomitant formation of a small shoulder at  $1712\text{ cm}^{-1}$ . This effect has been reported to be possibly associated with the formation of acidic cork decomposition products.<sup>5</sup>

To eliminate the possibility that dissolution was due to hydrolysis of the ionic liquid, control tests were performed using the conjugate acids of the ionic liquids' anions. Butanoic and hexanoic acids (pure and dried with molecular sieves) were tested, resulting in a weight loss of 10.3 and 17.2% respectively, and no evident alterations were observed in the ATR-FTIR spectra.

The cholinium family of ionic liquids present a very low toxicity,<sup>16</sup> especially to some eukaryotic organisms (e.g., ref. 17), due to the benign nature of the cation and its high biodegradation potential.<sup>18</sup> The toxicity (i.e., growth inhibition effect<sup>17</sup>) of  $[N_{111}C_2H_4OH][O_2CPr]$ ,  $[N_{111}C_2H_4OH][O_2CCHMe_2]$  and  $[N_{111}C_2H_4OH][O_2CC_5H_{11}]$  towards *P. corylophilum*, which has been previously demonstrated to show a moderate susceptibility to several ionic liquids,<sup>17</sup> were evaluated here. They exhibited very low inhibitory capacities, with MIC values of 150, 250 and 62.5 mM, respectively. The biodegradation of the most efficient system was then evaluated under aerobic conditions. After four weeks of incubation, the residual concentration of  $[O_2CC_5H_{11}]^-$  in *P. corylophilum* cultures was <12%, as determined by liquid chromatography. The biodegradation of the anion was confirmed by <sup>1</sup>H NMR spectroscopy and shown by the disappearance of the anion peaks in the spectrum relative to the cation.

The biocompatible and biodegradable cholinium hexanoate ionic liquid appears to be the most promising solvent for refined cork dissolution, particularly with respect to the separation of large quantities of suberin. Taking advantage of their synthetic tunability,<sup>8</sup> there is clearly a huge potential for developing and exploring even more efficient systems. Nevertheless, the results reported here are almost an order of magnitude more efficient than any system reported so far, whether it be molecular or ionic.

## Acknowledgements

R. F. is grateful to FC&T for the fellowship SFRH/BD/48286/2008 and H. G. is indebted to FCG for the fellowship 21-95587-B. The work was partially supported by a grant from Iceland, Liechtenstein and Norway through the EEA financial mechanism (Project PT015) and by FC&T (Project REDE/1504/REM/2005). The authors wish to acknowledge Dr M. Vitória San Romão for providing the cork powder used in this study. J. L. F. and K. R. S. wish to thank the QUILL Industrial Advisory Board and the EPSRC (Portfolio Partnership Scheme, grant number EP/D029538/1) for their continued support.

## Notes and references

- J. A. Maga and J. L. Puech, *Food Rev. Int.*, 2005, **21**, 53–68.
- M. H. Lopes, A. S. Barros, C. P. Neto, D. Rutledge, I. Delgadillo and A. M. Gil, *Biopolymers*, 2001, **62**, 268–277.
- N. Cordeiro, N. M. Belgacem, A. Gandini and C. P. Neto, *Bioresour. Technol.*, 1998, **63**, 153–158.
- A. M. Gil, M. Lopes, J. Rocha and C. P. Neto, *Int. J. Biol. Macromol.*, 1997, **20**, 293–305.
- C. P. Neto, J. Rocha, A. Gil, N. Cordeiro, A. P. Esculcas, S. Rocha, I. Delgadillo, J. D. P. Dejesus and A. J. F. Correia, *Solid State Nucl. Magn. Reson.*, 1995, **4**, 143–151.
- M. H. Lopes, C. P. Neto, A. S. Barros, D. Rutledge, I. Delgadillo and A. M. Gil, *Biopolymers*, 2000, **57**, 344–351.
- M. A. Bernards, *Can. J. Bot.*, 2002, **80**(3), 227–240.
- A. Stark and K. R. Seddon, in *Kirk-Othmer Encyclopaedia of Chemical Technology*, ed. A. Seidel, John Wiley & Sons, Inc., Hoboken, New Jersey, USA, 2007, pp. 836–920.
- D. A. Fort, R. C. Remsing, R. P. Swatloski, P. Moyna, G. Moyna and R. D. Rogers, *Green Chem.*, 2007, **9**, 63–69.
- Y. Fukaya, K. Hayashi, M. Wada and H. Ohno, *Green Chem.*, 2008, **10**, 44–46.
- I. Kilpeläinen, H. Xie, A. King, M. Granström, S. Heikkinen and D. S. Argyropoulos, *J. Agric. Food Chem.*, 2007, **55**, 9142–9148.
- P. Stepnowski, A. C. Składanowski, A. Ludwiczak and E. Łaczyńska, *Hum. Exp. Toxicol.*, 2004, **23**, 513–517.
- S. Stolte, S. Abdulkarim, J. Arning, A. K. Blomeyer-Nienstedt, U. Bottin-Weber, M. Matzke, J. Ranke, B. Jastorff and J. Thöming, *Green Chem.*, 2008, **10**, 214–224.
- A. P. Abbott and D. L. Davies, Ionic liquids prepared as low melting salts and compounds of quaternary ammonium halides with metal halides, *World Pat.*, WO 0056700, 2000; A. P. Abbott, D. L. Davies, G. Capper, R. K. Rasheed and V. Tambyrajah, Ionic liquids and their use as solvents, *World Pat.*, WO 2002 026701, 2002.
- R. P. Swatloski, S. K. Spear, J. D. Holbrey and R. D. Rogers, *J. Am. Chem. Soc.*, 2002, **124**, 4974–4975.
- P. Nockemann, B. Thijs, K. Driesen, C. R. Janssen, K. Van Hecke, L. Van Meervelt, S. Kossmann, B. Kirchner and K. Binnemans, *J. Phys. Chem. B*, 2007, **111**, 5254–5263.
- M. Petkovic, J. Ferguson, A. Bohn, J. R. Trindade, I. Martins, M. Carvalho, M. C. Leitão, C. Rodrigues, H. Garcia, R. Ferreira, K. R. Seddon, L. P. N. Rebelo and C. Silva Pereira, *Green Chem.*, 2009, **11**, 889–894.
- R. S. Boethling, E. Sommer and D. DiFiore, *Chem. Rev.*, 2007, **107**, 2207–2227.

# High-yield conversion of plant biomass into the key value-added feedstocks 5-(hydroxymethyl)furfural, levulinic acid, and levulinic esters *via* 5-(chloromethyl)furfural

Mark Mascal\* and Edward B. Nikitin

Received 11th September 2009, Accepted 26th November 2009

First published as an Advance Article on the web 15th December 2009

DOI: 10.1039/b918922j

5-(Hydroxymethyl)furfural, levulinic acid, ethyl levulinate and butyl levulinate are produced by the solvolysis of 5-(chloromethyl)furfural (CMF). Since CMF can be derived in high yield from sugars, cellulose, or lignocellulosic feedstocks, the process described here presents an efficient entry into the value-added manifold of biomass-derived products of relevance to the organic materials and fuel industries.

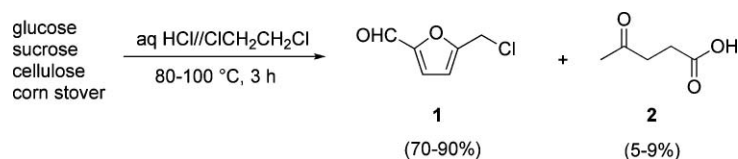
As and when the global petroleum economy draws to a close, the portfolio of derived products from biomass will need to diversify in order to satisfy feedstock requirements across a range of markets. Bioethanol and biobutanol, for example, have primarily uses as fuel oxygenates, and can be used in the production of biodiesel from vegetable oil, but they can also be dehydrated to give the major industrial feedstocks ethylene and 1-butene. Similarly, biogenic methane can be catalytically converted into methanol which, like ethanol and butanol, can be used to prepare biodiesel, but can also be submitted to oxidative coupling processes to give ethylene and higher olefins.<sup>1-3</sup> Yet as versatile as these mainstream biomass derivatives are, they

cannot cover the breadth of chemical feedstock classes available from petroleum.

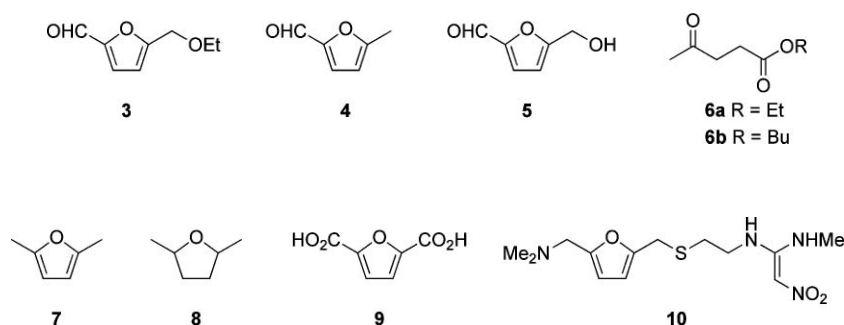
Recently, we described the digestion of sugars, cellulose, or cellulosic biomass with hydrochloric acid in a biphasic reactor which resulted in the isolation of a mixture of 5-(chloromethyl)furfural **1** (CMF) and levulinic acid **2** in up to 95% combined yield (Scheme 1).<sup>4</sup> The major product of the reaction is by far CMF **1**, which accounts for between 70 and 90% of the organic material isolated, depending on the feedstock loading, while levulinic acid comprises less than 10% of the product mixture.

While our earlier work focused on CMF **1** as a precursor to the new generation biofuels 5-(ethoxymethyl)furfural **3** and 5-methylfurfural **4** by reaction of **1** with ethanol and hydrogen, respectively,<sup>5</sup> in this report we describe the efficient conversion of CMF **1** into the value-added products 5-(hydroxymethyl)furfural **5** (HMF), levulinic acid **2** (LA), ethyl levulinate **6a** (EL) and n-butyl levulinate **6b** (BL) by reaction with water or alcohols at elevated temperatures.

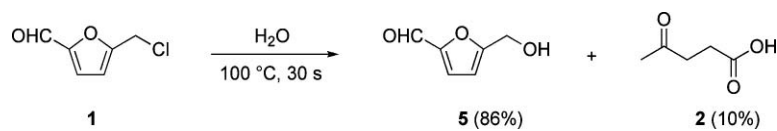
HMF **5** is a versatile platform chemical for the synthesis of a wide range of industrially important materials, including biofuels.<sup>6</sup> For example, **5** is a starting material in Dumesic's approach to the production of biomass-derived hydrocarbons.<sup>7</sup> It can also be reduced to 2,5-dimethylfuran **7** or 2,5-dimethyltetrahydrofuran **8**, both high energy liquids which have been proposed as fuel additives.<sup>8</sup> HMF **5** is also



Scheme 1



Department of Chemistry and Bioenergy Research Group, University of California, Davis, 1 Shields Avenue, Davis, CA, 95616, USA



Scheme 2

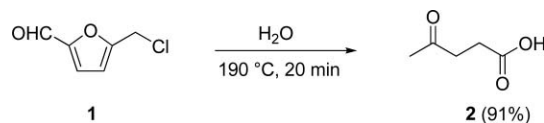
a precursor to the polyester monomer furan-2,5-dicarboxylic acid **9**, a molecule that has the distinction of appearing on the list of Top Value-Added Chemicals From Biomass published by the US Department of Energy's National Renewable Energy Laboratory (NREL). This list of twelve, mainly sugar-derived products was assembled in order to identify major opportunities for "the production of value-added chemicals from biomass that would economically and technically support the production of fuels and power in an integrated biorefinery, and identify the common challenges and barriers of associated production technologies."<sup>9</sup> Finally, the core structure of **5** also appears in the blockbuster antiulcer drug Ranitidine (Zantac<sup>®</sup>) **10**.

Although HMF **5** can be prepared from fructose in good yield,<sup>10</sup> fructose itself is sourced from the food chain, and it would be far too expensive to produce **5** on an industrial scale in this manner. Interestingly, a report as far back as 1912 describes the hydrolysis of **1** to **5** in unspecified yield.<sup>11</sup> This paper was cited by Haworth and Jones in 1944 in their repetition of the procedure,<sup>12</sup> which again lacked experimental detail. We thus undertook a careful study of this conversion with the benefit of modern analytical techniques. The results are quantified as shown in Scheme 2. Thus, under optimized conditions (hydrolysis in boiling water for 30 s), HMF **5** is produced in 86% yield from **1** alongside 10% LA **2**. Formation of the latter product **2**, observed across a range of conditions, appears to be unavoidable in this reaction. In the case, however, where LA **2** is actually the desired product, it can be produced with high efficiency (see below).

LA **2**, like furan-2,5-carboxylic acid **9**, also appears on the NREL Top 12 Value-Added Chemical list.<sup>9</sup> In its candidate summary biography, LA **2** is referred to as "one of the more recognized building blocks available from carbohydrates," the derivatives of which "address a number of large volume chemical markets." These derivatives include levulinate esters and 2-methyltetrahydrofuran (fuel additives),  $\delta$ -aminolevulinic acid (herbicide), and  $\beta$ -acetylacrylic acid, diphenolic acid and 1,4-pentanediol (polymer building blocks).<sup>9</sup> The technical barrier to development of an LA-based chemical intermediate trade is indicated to be the moderate selectivity of the process used to derive LA **2** from biomass.

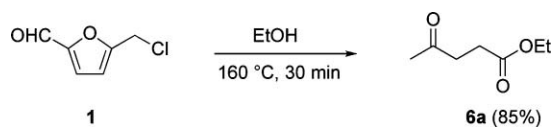
When CMF **1** is heated for longer periods in water, the amount of LA **2** grows at the expense of HMF **5**, but even after 15 h reflux the reaction is not complete, and increasing amounts of decomposition products (dark solids) are seen to accumulate. The addition of acid to the reaction mixture increases the initial

rate of the conversion, such that after only 30 s heating in dilute HCl the ratio of LA to HMF approaches 1 : 1. However, sampling the reaction mixture at subsequent intervals shows little in the way of further progress over the course of the next hour. Heating CMF in water at temperatures  $>100\text{ }^\circ\text{C}$  in a closed vessel was also shown to accelerate the reaction, and it was by a combination of higher temperature and acid catalysis that a high yielding route to **2** was first developed. Thus, heating **1** in dilute HCl at  $150\text{ }^\circ\text{C}$  for 5 h gave a 94% isolated yield of LA. In an attempt to further shorten the reaction time, the temperature was raised to  $190\text{ }^\circ\text{C}$ , which resulted in the complete conversion of **1** into **2** within 20 minutes without the need for additional acid (Scheme 3).



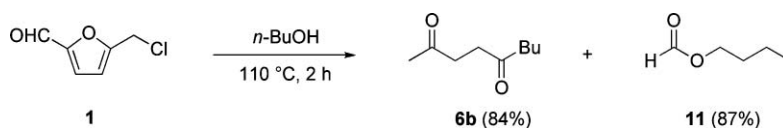
Scheme 3

When CMF **1** is stirred with ethanol at room temperature, 5-(ethoxymethyl)furfural **3** is produced in high yield.<sup>5</sup> As was the case with the CMF **1** to HMF **5** conversion, more severe conditions shift the product distribution from the substituted furan toward the levulinate. Thus, heating CMF **1** in ethanol at  $160\text{ }^\circ\text{C}$  for 30 min gave EL **6a** in 85% isolated yield (Scheme 4).



Scheme 4

The analogous reaction of **1** with *n*-butanol at  $110\text{ }^\circ\text{C}$  for 2 h likewise gave BL **6b** (Scheme 5). In the conversion of  $\text{C}_6$  furfurals to levulinates, there is a loss of a one-carbon fragment at the formate oxidation state, *i.e.* formic acid in the hydrolysis of CMF **1** or the corresponding formate ester in the alcoholysis. In the reactions in Schemes 3 and 4, no attempt was made to recover the formic acid or ethyl formate by-products. In the reaction with *n*-butanol, however, *n*-butyl formate **11** (BF) was isolated in approximately equal amounts to that of butyl levulinate **6b**, although it could not be completely separated from the excess butanol by distillation.<sup>13</sup>



Scheme 5

**Table 1** Yields of value-added products from carbohydrate and biomass feedstocks determined as the following expression: (yield of CMF **1** and LA **2** from either glucose, sucrose, cellulose, or corn stover)<sup>a</sup> × (yield of HMF **5**, LA **2**, EL **6a**, BL **6b**, or BF **11** from CMF **1**)

derivative	feedstock			
	glucose	sucrose	cellulose	corn stover
HMF <b>5</b> (LA <b>2</b> ) <sup>a</sup>	70.0 (12.6)	77.3 (14.2)	72.0 (13.6)	69.1 (15.8)
LA <b>2</b> <sup>a</sup>	78.7	87.1	81.5	81.0
EL <b>6a</b> <sup>b</sup>	72.7	80.5	75.2	74.6
BL <b>6b</b> (BF <b>11</b> )	72.4 (70.4)	80.2 (77.8)	74.9 (72.4)	74.4 (69.5)

<sup>a</sup> The LA **2** yield is a combination of that produced by both reactions.

<sup>b</sup> Assumes conversion of both CMF **1** and LA **2** into EL **6a** in the same percent yield. <sup>c</sup> Assumes conversion of both CMF **1** and LA **2** into BL **6b** in the same percent yield.

If the results in Scheme 2–5 are superimposed upon the high yields of CMF **1** and LA **2** from glucose, sucrose, cellulose, and corn stover recently described by our group,<sup>4</sup> the overall yield of value-added products from these substrates can be reckoned as shown in Table 1. To our knowledge, these levels of conversion from carbohydrate feedstocks are largely unrivalled in the literature.

While a comprehensive review of developments in the area of biomass conversion cannot be given here, the results given in Table 1 can be shown to compare favorably to approaches to LA **2** and HMF **5** at the forefront of the field. Thus, a recent report by Yong and co-workers described the conversion of glucose into HMF **5** in up to 81% yield (by GC and NMR analysis) using a chromium(II) catalyst and N-heterocyclic carbene ligand system.<sup>14</sup> However, the method requires the use of expensive 1-butyl-3-methylimidazolium chloride ([BMIM]Cl) ionic liquid as the solvent. Practical questions remain about this process, not least of which being the activity of the catalytic system after multiple cycles. Along the same lines, Dumesic and co-workers have published a study in which HMF **5** is derived from glucose with 53% selectivity at high conversion in 60% aqueous DMSO in a biphasic reactor.<sup>15</sup> While promising, the separation of DMSO from the HMF product remains an issue. Most recently, Binder and Raines have shown that corn stover can be processed directly into HMF **5** in 48% yield (by HPLC analysis) in a medium loaded with 10 mol% CrCl<sub>3</sub>, 10 mol% HCl, and 60 wt% [EMIM]Cl in *N,N*-dimethylacetamide-LiCl solution.<sup>16</sup>

As concerns LA **2**, although a multitude of routes have been described over the years, the highest yields to date from biomass are claimed for the “Biofine Process,” a two-stage protocol involving high pressures and temperatures, for which yields of between 70–80% of **2** are reported.<sup>17</sup> The technology we have developed, however, operates under substantially milder conditions and is more versatile with respect to product output, *i.e.* includes furfurals such as **3**, **4**, and **5** and their derivatives.

In conclusion, we have described a simple, efficient processes for the conversion of biomass-derived 5-(chloromethyl)furfural **1** into the mainstream value-added products 5-(hydroxymethyl)furfural **5**, levulinic acid **2**, ethyl levulinate **6a** and butyl levulinate **6b**, which may be applied to a variety of purposes in the materials and fuel industries that would otherwise involve the expenditure of petroleum. We foresee a time when CMF **1** may emerge as

a central organic platform chemical, and biphasic acid/solvent carbohydrate digesters as the method of choice for exploiting cellulosic biomass.

## Experimental

### Hydrolysis of CMF **1** to HMF **5**

CMF **1** (0.9490 g, 6.565 mmol) was added in a single portion to boiling water (900 mL) in a 2 L round-bottomed flask with fast stirring. After 30 s the reaction was quickly cooled to room temperature in an ice/water bath. The mixture was extracted with ethyl acetate (5 × 100 mL), the aqueous layer was saturated with sodium chloride, and extraction with ethyl acetate was continued (5 × 100 mL). The combined organic extracts were dried (MgSO<sub>4</sub>) and the solvent was evaporated. Column chromatography (silica, 1 : 1 Et<sub>2</sub>O–CH<sub>2</sub>Cl<sub>2</sub>) gave HMF **5** (0.7137 g, 86.2%) and LA **2** (0.0751 g, 9.9%).

### Hydrolysis of CMF **1** to LA **2**

A 150 mL sealed glass vessel was charged with CMF (0.9889 g, 6.84 mmol) and water (30 mL) and the mixture was heated in an oil bath at 190 °C with stirring for 20 min. The reaction was allowed to cool to room temperature and filtered. The filtrate was extracted with ethyl acetate (5×100 mL), the aqueous layer was saturated with sodium chloride, and extraction with ethyl acetate was continued (5×100 mL). The combined organic extracts were dried (MgSO<sub>4</sub>) and the solvent was evaporated to give LA **2** (0.7248 g, 91.2 %).

### Ethanolysis of CMF **1** to EL **6a**

A 150 mL sealed glass vessel was charged with CMF (3.1662 g, 21.90 mmol) and absolute EtOH (80 mL) and the mixture was heated in an oil bath at 160 °C with stirring for 30 min. The reaction was allowed to cool to room temperature and the excess ethanol was evaporated. Chromatography (silica, 1 : 1 hexane–ethyl acetate) gave EL **6a** (2.6746 g, 84.7%).

### Butanolysis of CMF **1** to BL **6b** and BF **11**

A solution of CMF (9.2211 g, 63.79 mmol) in *n*-BuOH (50 mL) was heated at 110 °C with stirring for 2 h. Distillation gave a mixture of BF **11** (5.65 g, 86.7%) and *n*-BuOH (16.40 g) (by NMR integration) between 104–110 °C and BL **6b** (9.2770 g, 84.4%) between 90–91 °C at 2 Torr.

## Acknowledgements

This work was supported by the US Department of Energy (award number DE-FG36-08GO88161) and the Nevada Institute for Renewable Energy Commercialization (award number 2008/11/002).

## References

- 1 L. Chen, X.-W. Zhang, L. Huang and L.-C. Lei, *Chemical Engineering and Processing*, 2009, **48**, 1333.
- 2 T. Ren, M. K. Patel and K. Blok, *Energy*, 2008, **33**, 817.
- 3 J. H. Lunsford, *Catal. Today*, 2000, **63**, 165.
- 4 M. Mascal and E. B. Nikitin, *ChemSusChem*, 2009, **2**, 859.

- 5 M. Mascal and E. B. Nikitin, *Angew. Chem., Int. Ed.*, 2008, **47**, 7924.
- 6 J. Lewkowski, *ARKIVOC*, 2001, (i), 17.
- 7 G. W. Huber, J. N. Chheda, C. J. Barrett and J. A. Dumesic, *Science*, 2005, **308**, 1446.
- 8 Y. Román-Leshkov, C. J. Barrett, Z. Y. Liu and J. A. Dumesic, *Nature*, 2007, **447**, 982.
- 9 "Top Value Added Chemicals From Biomass. Volume I: Results of Screening for Potential Candidates from Sugars and Synthesis Gas." Technical report identifier PNNL-14804, Pacific Northwest National Laboratory and the National Renewable Energy Laboratory, August 2004 (<http://www1.eere.energy.gov/biomass/pdfs/35523.pdf>).
- 10 B. F. M. Kuster, *Starch/Staerke*, 1990, **42**, 314.
- 11 W. F. Cooper and W. H. Nuttall, *J. Chem. Soc. Trans.*, 1912, **101**, 1074.
- 12 W. N. Haworth and W. G. M. Jones, *J. Chem. Soc.*, 1944, 667.
- 13 It should be pointed out here that the solvolytic reactions described in Schemes 2–5 involve the liberation of a molecule of hydrogen chloride into the reaction medium, *i.e.* water (Schemes 2 and 3), ethanol (Scheme 4), or butanol (Scheme 5). In terms of atom economy, the hydrogen chloride produced can be recovered for recycling back into the acid/solvent digestion reaction wherein the biomass was first processed into CMF **1**. Industrial HCl recovery modules may be based on distillation,<sup>18</sup> pervaporation,<sup>19</sup> acid–base-couple extraction,<sup>20</sup> solvent extraction,<sup>21,22</sup> or electro dialysis.<sup>23</sup> In the reactions where alcohols were both reagent and solvent, small quantities of the corresponding chloroalkane substitution products could be detected in the reaction mixture (by NMR and GC-MS). Chloroethane (bp 12 °C) is much more volatile than the desired product **6a** (204 °C) and the ethanol solvent (78 °C). Likewise, chlorobutane (bp 78 °C) is more volatile than the desired products **6b** (238 °C) and **11** (107 °C), and the butanol solvent (117 °C). Hence, separation of these minor products, which are themselves commercially traded organic intermediates, would be uncomplicated. If desired, the occurrence of haloalkanes could be avoided altogether by practicing the hydrolysis of **1** to levulinic acid **2** (Scheme 3) followed by standard esterification of **2** with ethanol or butanol using a non halogen-containing catalyst.
- 14 G. Yong, Y. Zhang and J. Y. Ying, *Angew. Chem., Int. Ed.*, 2008, **47**, 9345.
- 15 J. N. Chheda, Y. Román-Leshkov and J. A. Dumesic, *Green Chem.*, 2007, **9**, 342.
- 16 J. B. Binder and R. T. Raines, *J. Am. Chem. Soc.*, 2009, **131**, 1979.
- 17 D. J. Hayes, S. W. Fitzpatrick, M. H. B. Hayes and J. R. H. Ross, The Biofine Process—Production of Levulinic Acid, Furfural, and Formic Acid from Lignocellulosic Feedstocks. In: B. Kamm, P. R. Gruber and M. Kamm, (ed.), *Biorefineries—Industrial Processes and Products: Status Quo and Future Directions*, Wiley-VCH, Weinheim, 2006, vol. 1, pp. 144–160.
- 18 A. Regnault, J.-P. Sachetto, H. Tournier, T. Hamm and J. M. Armanet, *US Patent* 4,304,608, 1981 (*Chem. Abstr.* 89: 217099).
- 19 U. Schuchardt, I. Joeke and H. C. Duarte, *J. Chem. Technol. Biotech.*, 1988, **41**, 51.
- 20 A. Baniel and A. Eyal, *PCT Int. Appl.*, 2009(*Chem. Abstr.* 2009: 1263571).
- 21 J. L. Gaddy and E. C. Clausen, *US Patent* 4,645,658 (*Chem. Abstr.* 106: 140514).
- 22 A. V. Forster, L. E. Martz, D. E. Leng and D. Ellis, *Eur. Pat. Appl.*, 1980(*Chem. Abstr.* 94: 176995).
- 23 J. Wiśniewski and G. Wiśniewska, *Desalination*, 1997, **109**, 187.

# An improved high yielding immobilization of vanadium Schiff base complexes on mesoporous silica *via* azide–alkyne cycloaddition for the oxidation of sulfides†‡

Suman L. Jain,\*<sup>a</sup> Bharat S. Rana,<sup>b</sup> Bhawan Singh,<sup>b</sup> Anil K. Sinha,\*<sup>b</sup> Asim Bhaumik,<sup>c</sup> Mahasweta Nandi<sup>c</sup> and Bir Sain<sup>a</sup>

Received 22nd August 2009, Accepted 3rd December 2009

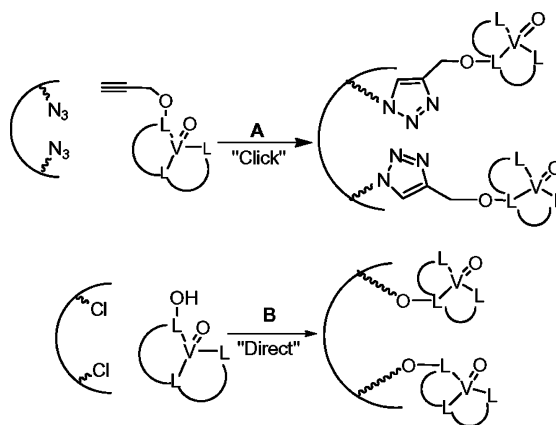
First published as an Advance Article on the web 7th January 2010

DOI: 10.1039/b917382j

Azide–alkyne [3+2] cycloaddition “click reaction” was found to be a simple yet improved approach for the efficient immobilization of oxo–vanadium(IV) tridentate Schiff base complexes to mesoporous silica *via* covalent attachment as it occurred under mild reaction conditions and provided high catalyst loading compared to the direct immobilization of oxo–vanadium(IV) tridentate Schiff base complex to 3-chloropropylsilyl functionalized silica support.

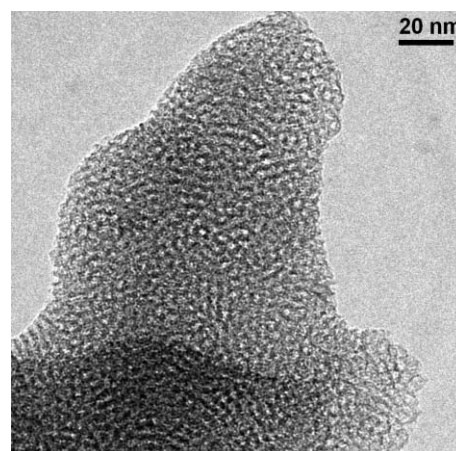
Immobilization of metal complexes onto the surfaces of solid supports is highly desirable in the development of reusable catalysts.<sup>1</sup> Most importantly, the immobilization strategy used for linking metal complexes to supports must be mild, give quantitative conversion, preserve the chemical integrity/functional activity of the metal complex and prevent the leaching of the complex from the support during the reaction. Immobilization methods that are often used for the attachment of metal complexes to a surface either involve non-covalent interactions based on physical adsorption<sup>2</sup> or direct covalent immobilization to chemically functionalized activated supports.<sup>3</sup> However, these methods suffer from certain drawbacks such as lower catalyst loading on the support, use of excess metal complex and harsh reaction conditions. Recently, the Cu(I)-catalyzed azide–alkyne reaction<sup>4</sup> ‘click chemistry’ has, owing to its simplicity, mild reaction conditions, quantitative conversions and high tolerance of functional groups, proved to be one of the most powerful tools for covalent attachment between appropriately functionalized molecules or their ligation to solid supports *via* a 1,2,3-triazole linkage.<sup>5</sup> Although, this approach has extensively been used for the functionalization of surfaces with biomolecules,<sup>6</sup> few reports are known for the immobilization of metal complexes using the click reaction.<sup>7</sup> The present paper describes the synthesis of a silica-immobilized oxo–vanadium(IV) tridentate Schiff base complex *via* covalent attachment using the click

reaction (Fig. 1, A), a mild ligation strategy providing high catalyst loading compared to the direct immobilization of oxo–vanadium(IV) tridentate Schiff base to chloro-functionalized silica support (Fig. 1, B).



**Fig. 1** Covalent immobilization of oxo–vanadium(IV) tridentate Schiff base complex to silica support *via* click method A and direct immobilization B.

For this purpose, we prepared a large (>5 nm) pore-size (3-azidopropyl) functionalized mesoporous SBA-15 support **3** (0.62 mmol N<sub>3</sub> per g) (ESI, Fig. S1†).<sup>6a</sup> The TEM of the (3-azidopropyl) functionalized mesoporous SBA-15 support **3** is shown in Fig. 2. The required oxo–vanadium(IV) tridentate



**Fig. 2** TEM of azidopropyl-functionalized mesoporous SBA-15 support **3**.

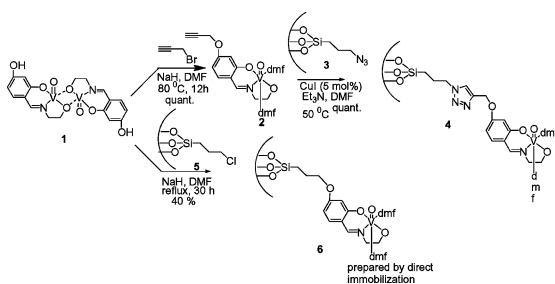
<sup>a</sup>Process Engineering Applied Chemistry and Biotechnology Division, Indian Institute of Petroleum, Dehradun, India 248005. E-mail: suman@iip.res.in

<sup>b</sup>Catalytic Conversion and Process Division, Indian Institute of Petroleum, Dehradun, India 248005. E-mail: asinha@iip.res.in

<sup>c</sup>Department of Materials Science, Indian Association for the Cultivation of Science, Jadavpur, Kolkata, India 700032

† Electronic supplementary information (ESI) available: IR spectra of the materials **3**, **4**, **6**; low angle XRD of **4** and **6**; nitrogen sorption isotherm and pore-size distribution of **4** and **6**. See DOI: 10.1039/b917382j

Schiff base **1** was prepared from 2,4-dihydroxybenzaldehyde, 2-aminoethanol and vanadyl acetylacetonate following the literature procedure.<sup>8</sup> Attachment of the oxo–vanadium complex **1** to azido-functionalized silica **3** could be achieved in an easy two step sequence: propargylation of **1** gave rise to **2**, which, on subsequent copper(I) iodide (5 mol%) catalyzed [3+2] azide–alkyne cycloaddition with azido-functionalized mesoporous silica **3** resulted in covalently attached silica-immobilized oxo–vanadium Schiff base **4** with high catalyst loading (Scheme 1, upper path) as evidenced by the reduced intensity of the typical IR absorbance band of the azide in the functionalized mesoporous silica (2106 cm<sup>-1</sup>) (ESI, Fig. S2†). The obtained dark brown colored solid **4** was separated by filtration, washed thoroughly with acetonitrile, dichloromethane, dried and then Soxhlet extracted in acetonitrile for 8 h. The prepared mesoporous silica immobilized oxo–vanadium Schiff base complex **4** was characterized by IR, elemental analysis, XRD, nitrogen-sorption and thermogravimetric analysis (TGA). Low-angle XRD analysis showed a clear prominent peak at  $2\theta = 0.86^\circ$  with *d* (100) spacing of 10.0 nm, confirming the hexagonal mesoporous structure of the silica support material (ESI, Fig. S3†). The nitrogen-sorption analysis showed a narrow pore-size distribution with mean pore-size of 7.0 nm (ESI, Fig. S4†). The material had 440 m<sup>2</sup> g<sup>-1</sup> surface area and 0.53 cc/g pore volume (cc/g = cubic centimetres per gram), which is considerably lower in comparison to that observed for pristine mesoporous silica support (1.1 cc/g pore volume and 910 m<sup>2</sup> g<sup>-1</sup> surface area), indicating considerable loading of the complex inside the mesopores. The covalent attachment of oxo–vanadium complex **2** to the mesoporous silica supports **3** was judged by IR spectroscopy as it exhibits a sharp band at 961 cm<sup>-1</sup> characteristic to the V=O and a lower shift from 1669 to 1661 cm<sup>-1</sup> of the band corresponds to the C=N of the Schiff base. In addition, the disappearance of a band at 3300 cm<sup>-1</sup> characteristics to the acetylenic C–H further reveals the covalent attachment of complex **2** to the silica support. The observed percentage (2.8%) of nitrogen in elemental analysis suggests the loading of Schiff base per gram of silica to be 0.33 mmol g<sup>-1</sup>.<sup>9</sup>



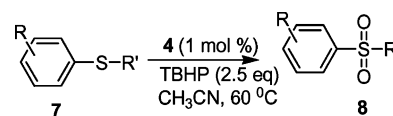
**Scheme 1** Immobilization of oxo–vanadium(IV) tridentate Schiff base **1** complex to the mesoporous silica support.

The percentage of vanadium in the prepared catalyst was estimated by thermogravimetric analysis (TGA) under an oxygen atmosphere. The catalyst **4** started losing weight at *ca.* 75–150 °C, probably due to the loss of coordinated DMF molecules (and other adsorbed species) followed by maximum weight loss between 200–450 °C probably due to the decomposition of ligand moiety. However, the stability of final residue at *ca.* 900–950 °C revealed the formation of V<sub>2</sub>O<sub>5</sub> at the end and by its

weight we estimated the approximate percentage of vanadium ions to be 1.7%.<sup>10</sup>

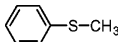
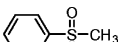
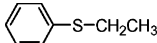
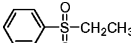
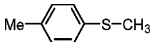
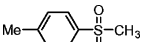
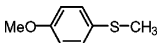
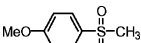
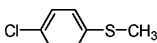
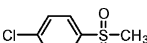
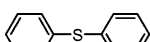

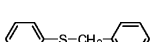
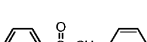
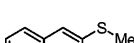


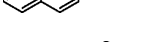
In order to establish the superiority of the click reaction, we prepared silica-immobilized vanadium Schiff base **6** by the direct reaction of 3-chloropropylsilyl functionalized silica **5** (0.52 mmol g<sup>-1</sup>) with oxo–vanadium Schiff base **1** (Scheme 1, lower path). Again, the covalent attachment of complex **1** with silica support **5** was confirmed by the presence of sharp IR bands at 961 characteristic of the V=O; 1657 cm<sup>-1</sup> corresponds to the C=N band and the disappearance of bands at 961 characteristic of the V=O, 1657 cm<sup>-1</sup> corresponds to the C=N band and the disappearance of phenolic band at 3219 cm<sup>-1</sup> (ESI, Fig. S5†). The material did not show a well-defined XRD peak in the low angle region indicating poorly formed mesopores (ESI, Fig. S6†), and nitrogen sorption analysis showed a very broad pore-size distribution and low surface area of 390 m<sup>2</sup> g<sup>-1</sup> (pore volume: 0.79 cc/g) (ESI, Fig. S7†). The TGA analysis revealed the approximate percentage of vanadium to be 0.08%, indicating the lower catalyst loading in comparison to catalyst **4**, prepared *via* a click reaction. Further, direct immobilization of complex **1** to the silica support **5** required a four-fold excess of expensive metal complex and occurred under stringent reaction conditions. However, the click method required a nearly equivalent amount of metal complex, proceeded under mild reaction conditions and afforded better catalyst loading. These facts establish the superiority of the click method over existing methods known for the immobilization of metal complexes to the solid supports.

The catalytic potential of the prepared catalyst **4** was tested for oxidation of sulfides **7** using aq. TBHP as oxidant (Scheme 2). A variety of sulfides were oxidized using aq. TBHP (2.5 mmol) as oxidant in presence of a catalytic amount of silica supported oxo–vanadium Schiff base **4** (1 mol%) in acetonitrile at 60 °C under N<sub>2</sub> atmosphere. At the end of the reaction (monitored by TLC) the catalyst was separated from the reaction mixture by simple filtration, washed thoroughly with acetonitrile and reused for subsequent experiments. The obtained filtrate was subjected to the usual workup to afford the corresponding oxidized product. All the substrates were efficiently and smoothly converted to the corresponding sulfones **8** in near quantitative yields. The results of these experiments are summarized in Table 1. We also compared the catalytic activity of the immobilized catalyst **4** with **6** and its corresponding homogeneous oxo–vanadium Schiff base **1** by carrying out the oxidation of diphenyl sulfide under described reaction conditions (Table 1, entry 1). Although catalytic efficiency of immobilized Schiff bases **4** and **6** were found to be comparable with homogeneous catalyst **1**, the facile recovery as well as recycling ability of immobilized complexes makes them superior catalysts. The oxidation of diphenylsulfide in the presence of unfunctionalized silica (before loading vanadium Schiff base) using aq. TBHP as oxidant under described reaction conditions did not occur even after prolonged reaction time (6 h) and unreacted substrate could only be recovered at the end of the



**Scheme 2** Oxidation of sulfides using catalyst **4**.

**Table 1** Oxidation of sulfides using catalyst **4**<sup>a</sup>

Entry	Sulfide <b>7</b>	Catalyst	Sulfone <b>8</b>	Reaction time/h	Yield (%) <sup>b</sup>
1		<b>4</b> <b>6</b> <b>1</b>		3.0	98
				3.5	96
				2.5	98
2		<b>4</b>		3.5	97
3		<b>4</b>		2.5	98
4		<b>4</b>		2.75	98
5		<b>4</b>		3.5	98
6		<b>4</b>		4.5	98
7		<b>4</b>		4.5	97
8		<b>4</b>		6.5	95
9		<b>4</b>		5.0	62

<sup>a</sup> Reaction conditions: sulfide (1 mmol), aq. TBHP (2.5 mmol), catalyst (1 mol%), acetonitrile (3 ml) at 60 °C under N<sub>2</sub> atm. <sup>b</sup> Isolated yields.

reaction. Similarly, the addition of the catalytic amount of the CuI and azido functionalized silica **3** to the reaction mixture containing diphenylsulfide and aq. TBHP did not give any oxidized product under similar reaction conditions. Reaction of propargyl bromide with 3-azidopropyltrimethoxysilane in the presence of the catalytic amount of CuI (5 mol%) gave free triazole moieties of the similar structure, which are known to bind copper. Addition of diphenylsulfide and aq. TBHP in the above mixture did not give any oxidation product under similar reaction conditions. Similarly, the combination of the catalytic amounts of unfunctionalized silica, CuI, free 1,2,3-triazole and homogeneous oxo-vanadium Schiff base **1**, when added to the reaction mixture containing diphenylsulfide and aq. TBHP and continued the reaction under similar reaction conditions, was found to proceed, albeit affording a lower yield of the corresponding sulfone (80%).

Next, the recyclability and reusability of immobilized catalyst **4** was checked by using the diphenyl sulfide as a model substrate. At the end of the reaction the catalyst was recovered by simple filtration, washed thoroughly with acetonitrile, dried and reused for subsequent experiments (six runs) by adding fresh substrate and oxidant under similar reaction conditions. In all cases reaction times and yield (98%, 98%, 97%, 97%, 97%, 96%) of the desired product remained almost same, establishing the recyclability and reusability of the immobilized oxo-vanadium Schiff base **4**. In a controlled blank experiment, no oxidation of diphenyl sulfide occurred in the absence of catalyst under

otherwise similar experimental conditions. Similarly the reaction was found to be very slow at room temperature, yielded the mixture of sulfoxide and sulfone however at 60 °C sulfones were obtained exclusively in near quantitative yields.

To check the leaching, the immobilized catalyst **4** in acetonitrile was stirred at 60 °C for 3 h. The supported catalyst was then removed by the filtration of the hot solution and the filtrate thus obtained was charged with diphenyl sulfide and aq. TBHP. No oxidation occurred under similar reaction conditions even after prolonged reaction time (5 h). Also the selected filtrate samples during the recycling experiments were analyzed by inductive coupled plasma atomic emission spectroscopy (ICP-AES) and no solvated vanadium could be detected (0.1 ppm detection limit), which established that there was no leaching and the reaction is truly heterogeneous in nature.

In summary, we demonstrated that click chemistry is a simple yet improved approach to immobilization of oxo-vanadium(IV) tridentate Schiff base to azido-functionalized mesoporous silica in high yields. We believe that the key advantages of click chemistry such as simplicity in use and high efficiency in terms of better catalyst loading without using excess of reagents or metal under mild reaction conditions will definitely open a wide scope in developing reusable catalysts for organic transformations.

We are thankful to Director, IIP, for his kind permission to publish these results. DST is acknowledged for funding. BS is thankful to CSIR for his research fellowship. BSR acknowledge IIP for his fellowship.



## Notes and references

‡ The melting points were determined in open-capillaries on a Buchi apparatus and are uncorrected. The  $^1\text{H}$  and  $^{13}\text{C}$  NMR spectra were recorded on a Bruker Avance 300 Spectrometer in  $\text{CDCl}_3$  with  $\text{CHCl}_3$  (7.27 ppm for  $^1\text{H}$ , 77 ppm for  $^{13}\text{C}$ ) as a standard and the chemical shifts are expressed in  $\delta$  parts per million relative to tetramethylsilane (TMS) as the internal standard. The IR spectra were recorded on a Perkin-Elmer FT-IR X 1760 instrument. Elemental analyses were done by using ASTM D-3828 (Kjeldhal method). Analyses of metal content (for leaching experiments) were carried out by using inductively coupled plasma atomic emission spectrometer (ICP-AES, PS-3000UV) by Leeman Labs.

**Preparation of propargylated oxo-vanadium(IV) tridentate Schiff base 2:** Oxo-vanadium(IV) tridentate Schiff base **1** (2.3 g, 5.0 mmol) was added in the stirred mixture of  $\text{Na}_2\text{CO}_3$  (40 mmol, 4.02 g) in DMF (30 mL). Propargyl bromide (80 wt% in toluene, 12 mL, 10 mmol) was added dropwise slowly and the resulting mixture was heated at 80 °C for 8 h. The solvent was removed under reduced pressure and the residue was dissolved in dichloromethane (30 ml). The organic layer was washed with brine solution (20 mL  $\times$  3) and water. The organic layer was dried over anhydrous  $\text{MgSO}_4$  and concentrated under reduced pressure. The dark brown solid thus obtained was dried under vacuum for 5 h. IR ( $\text{cm}^{-1}$ ): 3283, 2953, 1659, 1590, 1544, 1232, 984. ESMS ( $\text{M} + \text{CH}_3\text{COO}^-$ ): 488.

**Preparation of organo-functionalized mesoporous silica supports 3 and 5:** Mesoporous silica materials with a large pore size of 10 nm were synthesized to accommodate the bulky Schiff base complexes using a triblock-copolymer template  $\text{EO}_{20}\text{PO}_{70}\text{EO}_{20}$  ( $\text{MW}_n$  ca. 5800), tetraethylorthosilicate as silica source, and a hydrothermal synthesis method. Mesoporous SBA-15 material functionalized with 3-azidopropylsilyl groups, **3**, was prepared by adding (3-azidopropyl)trimethoxysilane (4 mol%) during the synthesis of mesoporous silica materials (0.62 mmol  $\text{g}^{-1}$ ). Mesoporous silica functionalized with 3-chloropropylsilyl groups, **5**, was prepared by adding (3-chloropropyl)trimethoxysilane (4 mol%) during the synthesis of mesoporous silica materials. The percentage of chloro-functionalization in the prepared material **5** was determined by elemental analysis which was found to be 0.52 mmol  $\text{g}^{-1}$ . During the synthesis of mesoporous SBA-15 materials templates have been removed by Soxhlet extraction in ethanol for 24 h.

**Immobilization of propargylated oxo-vanadium(IV) Schiff base 2 to mesoporous silica 3 via click chemistry:** To the solution of propargylated oxo-vanadium(IV) Schiff base (0.53 g, 1.25 mmol) in dry DMF (25 ml) was added azido-functionalized mesoporous silica (0.62 mmol  $\text{g}^{-1}$ , 2.0 g, 1.24 mmol),  $\text{CuI}$  (5 mol%),  $\text{Et}_3\text{N}$  (1.0 ml). The resulting suspension was vigorously stirred at 50 °C for 24 h under nitrogen. The progress was checked by IR as it showed the reduction of  $\text{N}_3$  band (2106  $\text{cm}^{-1}$ ). After completion, the silica-supported catalyst **4** was filtered off and washed thoroughly with acetonitrile, dried and then removed by Soxhlet extraction in acetonitrile for 8 h and dried under vacuum for 5 h, yield 2.20 g (84%). IR ( $\text{cm}^{-1}$ ): 2994, 1661, 1441, 1391, 1083, 961, 802. TG weight loss to final oxide: found 1.7% (calculated 2.1%). Nitrogen percentage ( $\text{N}_2\%$ ) determined by elemental analysis: found 2.8% (calculated 3.5%).

**Immobilization of oxo-vanadium(IV) Schiff base 1 to mesoporous silica 5 via direct method:** To the stirred suspension of mesoporous silica **5** (0.52 mmol  $\text{g}^{-1}$ , 2.0 g, 1.04 mmol) and  $\text{NaH}$  (0.12 g, 5 mmol) in dry DMF (15 ml) was added dropwise a solution of oxo-vanadium Schiff base **1** (1.21 g, 2.48 mmol) in dry DMF (10 ml) over the period of 15 min. The resulting mixture was refluxed for 30 h under nitrogen atmosphere. The resulting silica supported catalyst was separated via filtration and washed thoroughly with acetonitrile, methanol, dried and then subjected to Soxhlet extraction in acetonitrile for 8 h and dried under vacuum for 5 h, yield 1.5 g (57%). IR ( $\text{cm}^{-1}$ ): 2962, 1657, 1498, 1439, 1419, 1088, 961, 798.

**General experimental procedure for oxidation of sulfides:** To the stirred mixture of sulfide (1 mmol) and aq. 70% TBHP (2.5 mmol) in acetonitrile

(3 ml) was added catalyst (1 mol%) under  $\text{N}_2$  atmosphere. The resulting mixture was kept at 60 °C for the times reported in Table 1. Progress of the reaction was monitored by TLC. After completion, the catalyst was separated by filtration and washed with acetonitrile, dichloromethane and dried under vacuum for further use. The filtrate was concentrated under reduced pressure and the residue dissolved in dichloromethane (10 ml). The organic layer was washed with water (2  $\times$  15 ml), dried over anhydrous  $\text{MgSO}_4$  and concentrated to yield the corresponding sulfone.

- (a) A. D. Pomogaĭlo, *Catalysis by Polymer-immobilized Metal Complexes*, CRC Press, New York, 1998; (b) N. E. Leadbeater and M. Marco, *Chem. Rev.*, 2002, **102**, 3217–3274; (c) K. Burgess, *Solid Phase Organic Synthesis*, John-Wiley, New York, 2000.
- (a) K. Yao, M. Taniguchi, M. Nakata, M. Takahashi and A. Yamagishi, *Langmuir*, 1998, **14**, 2410; (b) A. R. Silva, M. M. A. Freitas, C. Freire, B. de Castro and J. L. Figueiredo, *Langmuir*, 2002, **18**, 8017; (c) P. Van Der Voort, M. Mathieu, E. F. Vansant, S. N. R. Rao and M. G. White, *J. Porous Mater.*, 1998, **5**, 305; (d) M. Bartok, G. Szollosi, A. Mastalir and I. Dekany, *J. Mol. Catal. A: Chem.*, 1999, **139**, 227.
- (a) T. Ray, S. F. Mapolie and J. Darkwa, *J. Mol. Catal. A: Chem.*, 2007, **267**, 143; (b) T. Luts, W. Suprun, D. Hofmann, O. Klepel and H. Papp, *J. Mol. Catal. A: Chem.*, 2007, **261**, 16; (c) M. R. Maurya, U. Kumar and P. Manikandan, *Dalton Trans.*, 2006, 3561–3575; (d) A. Corma, C. González-Arellano, M. Iglesias, M. T. Navarro and F. Sánchez, *Chem. Commun.*, 2008, 6218; (e) C. González-Arellano, A. Corma, M. Iglesias and F. Sánchez, *Chem. Commun.*, 2005, 1990; (f) A. Corma, E. Gutiérrez-Puebla, M. Iglesias, A. Monge, S. Pérez-Ferreras and F. Sánchez, *Adv. Synth. Catal.*, 2006, **348**, 1899; (g) C. González-Arellano, A. Corma, M. Iglesias and F. Sánchez, *Adv. Synth. Catal.*, 2004, **346**, 1758; (h) V. Ayala, A. Corma, M. Iglesias and F. Sánchez, *J. Mol. Catal. A: Chem.*, 2004, **221**, 201.
- (a) C. W. Tornøe and M. Meldal, in *American Peptide Symposium*, ed. M. Lebl and R. A. Houghten, American Peptide Society and Kluwer Academic Publishers, San Diego, CA, 2001, p. 263; (b) V. V. Rostovtsev, L. C. Green, V. V. Fokin and K. B. Sharpless, *Angew. Chem., Int. Ed.*, 2002, **41**, 2596; (c) C. W. Tornøe, C. Christensen and M. Meldal, *J. Org. Chem.*, 2002, **67**, 3057; (d) Q. Wang, T. R. Chan, R. Hilgraf, V. V. Fokin, K. B. Sharpless and M. G. Finn, *J. Am. Chem. Soc.*, 2003, **125**, 3192; (e) H. C. Kalb and K. B. Sharpless, *Drug Discovery Today*, 2003, **8**, 1128.
- R. Huisgen, *Pure Appl. Chem.*, 1989, **61**, 613.
- (a) J. Nakazawa, T. Daniel and P. Stack, *J. Am. Chem. Soc.*, 2008, **130**, 14360; (b) A. Schlossbauer, D. Schaffert, J. Kecht, E. Wagner and T. Bein, *J. Am. Chem. Soc.*, 2008, **130**, 12558.
- (a) A. R. McDonald, H. P. Dijkstra, B. M. J. M. Suijkerbuijk, G. P. M. van Klink and G. van Koten, *Organometallics*, 2009, **28**, 4689; (b) A. Schätz, M. Hager and O. Reiser, *Adv. Funct. Mater.*, 2009, **19**, 2109; (c) A. R. McDonald, N. Franssen, G. P. M. van Klink and G. van Koten, *J. Organomet. Chem.*, 2009, **694**, 2153; (d) J. Y. Ying, J. Lim, S. S. Lee and S. N. B. Riduan, *Int. Appl. No. PCT/SG2008/000088* (WO 2008/115 154); (e) G. Lv, W. Mai, R. Jin and L. Gao, *Synlett*, 2008, 1418; (f) A. Bastero, D. Font and M. A. Pericás, *J. Org. Chem.*, 2007, **72**, 2460; (g) X.-Y. Wang, A. Kimyonok and M. Weck, *Chem. Commun.*, 2006, 3933; (h) S. Jain and O. Reiser, *ChemSusChem*, 2008, **1**, 534; (i) M. Tilliet, S. Lundgren, C. Moberg and V. Levacher, *Adv. Synth. Catal.*, 2007, **349**, 2079; (j) S. Jain, J. K. Joseph, F. E. Kuhn and O. Reiser, *Adv. Synth. Catal.*, 2009, **351**, 230; (k) S. Jain and B. Sain, *Adv. Synth. Catal.*, 2008, **350**, 1479.
- R. Ando, T. Yagyū and M. Maeda, *Inorg. Chim. Acta*, 2004, **357**, 2237.
- Starting from the 0.62 mmol  $\text{N}_3$  per g silica support, theoretical loading of vanadium Schiff base onto support is 0.42 mmol  $\text{g}^{-1}$ .
- Starting from 0.42 mmol  $\text{g}^{-1}$  loading of complex to the support, calculated percentage of vanadium ions is 2.1%.

# Improved utilization of biomass-derived carbon by co-processing with hydrogen-rich feedstocks in millisecond reactors†

Joshua L. Colby,<sup>a</sup> Paul J. Dauenhauer,<sup>b</sup> Brian C. Michael,<sup>a</sup> Aditya Bhan<sup>a</sup> and Lanny D. Schmidt<sup>\*a</sup>

Received 30th September 2009, Accepted 7th December 2009

First published as an Advance Article on the web 8th January 2010

DOI: 10.1039/b920387g

A reactor capable of improving the utilization of biomass-derived carbon during thermochemical conversion to synthesis gas is demonstrated experimentally. By co-processing hydrogen-deficient biomass ( $H/C \sim 2$ ) with hydrogen-rich feedstocks ( $H/C \geq 4$ ) through catalytic partial oxidation, 100% of the fuel carbon atoms fed to the reactor can be converted to CO.

Liquid hydrocarbons are appealing for their high energy density and ease of storage. Collectively, these characteristics are unique to carbon-rich liquid fuels produced almost entirely from petroleum. Biomass, the only source of renewable carbon, represents the only sustainable feedstock for the production of carbon-rich fuels.<sup>1</sup> It will, therefore, become important to develop processes that effectively utilize all of the biomass-derived carbon. No commercial process capable of converting biomass into useful fuels and chemicals, without significant carbon losses to char or CO<sub>2</sub>, exists presently because of process or thermodynamic constraints.<sup>2,3</sup>

Thermochemical conversion of biomass to synthesis gas, a mixture of H<sub>2</sub> and CO, is a route for the production of synthetic, carbon-rich liquid fuels. The gasification of biomass by partial oxidation, used commercially to make synthesis gas, produces some combustion products in an overall exothermic, char-free reaction.



With existing technology, only ~50% of biomass carbon is converted to CO, and the remainder is emitted as CO<sub>2</sub>.<sup>4</sup> Ideally, gasification would convert 100% of the carbon in biomass to CO, eliminating the generation of CO<sub>2</sub>.

CO yields can be improved by co-feeding CO<sub>2</sub> with biomass and O<sub>2</sub>. The addition of CO<sub>2</sub> favors a reverse water-gas shift (RWGS), increasing CO production at the expense of molecular hydrogen.



<sup>a</sup>Department of Chemical Engineering and Materials Science, University of Minnesota–Twin Cities, 421 Washington Avenue SE, Minneapolis, MN, 55455, USA. E-mail: schmi001@umn.edu; Fax: +1 612-626-7246; Tel: +1 612-625-9391

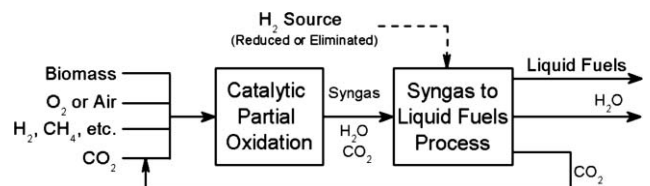
<sup>b</sup>Department of Chemical Engineering, University of Massachusetts Amherst, 686 North Pleasant Street, Amherst, MA, 01003, USA. E-mail: dauenhauer@ecs.umass.edu

† Electronic supplementary information (ESI) available: Experimental details, calculation algorithms and the construction of Table 1. See DOI: 10.1039/b920387g

However, CO<sub>2</sub> addition under typical biomass gasification conditions does not provide the thermodynamic driving force necessary to convert all of the biomass-derived carbon to CO. To overcome this thermodynamic limitation, H<sub>2</sub> must be co-fed into the reaction, supplying the energy needed to drive the RWGS reaction, as discussed in greater detail by Xiaoding *et al.*<sup>5</sup>

The addition of molecular hydrogen to traditional biomass processes has been considered for improving product quality and yield by improving carbon utilization and increasing product H<sub>2</sub>/CO ratios.<sup>6–8</sup> It has also been considered as a method for mitigating CO<sub>2</sub> emissions by chemical reduction, rather than sequestration.<sup>5,9</sup> With advancing technologies, H<sub>2</sub> may ultimately be obtained from alternative sources such as electrochemical or photochemical conversion of water.<sup>1,10</sup> However, until more efficient technologies are developed for producing H<sub>2</sub>, inexpensive hydrocarbons rich in hydrogen, such as natural gas or biogas, may be exploited as a cheap hydrogen source.

We hypothesize that biomass partial oxidation with CO<sub>2</sub> addition can be exploited to recover all fuel carbon atoms as CO by generating molecular hydrogen *in situ* from hydrogen-rich sources (Fig. 1). Previously, we have shown that through a process called reactive flash volatilization, cellulose can be rapidly converted to synthesis gas by catalytic partial oxidation (CPO) over Rh-based catalysts without the formation of char.<sup>11,12</sup> The results presented here suggest that biomass reforming, CH<sub>4</sub> reforming and water-gas shift reactions (WGS) can be integrated into one catalytic reactor stage. Our results show that a mixture of cellulose (a biomass surrogate), CO<sub>2</sub>, and CH<sub>4</sub> can be converted to synthesis gas with no char formation and >100% yield of CO, defined here to be the ratio of the moles of CO produced to the moles of carbon in the fuel feed.



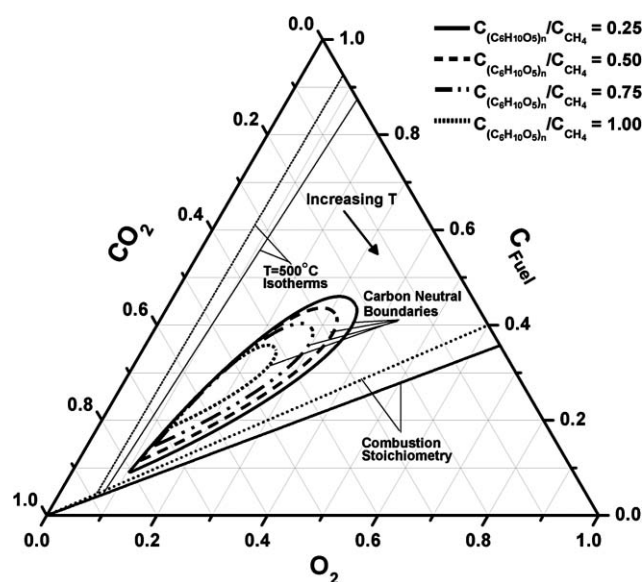
**Fig. 1** A possible schematic of the proposed process. An optimum process design would require, among other things, a coupled economic and process analysis, and detailed product specifications. Furthermore, depending on the CO<sub>2</sub> source, recycling may not be preferred.

The relevant feed ratios for experimental consideration were predicted by calculating the adiabatic equilibrium of all possible feed combinations of carbohydrates (cellulose), CH<sub>4</sub>, air and

CO<sub>2</sub> (the calculation algorithm is presented in Section 2 of the ESI†). Under the considered carbon fuel feed ratios of  $0.25 < C_{(C_6H_{10}O_5)_n}/C_{CH_4} < 1.00$ , there exists a distinct division (Fig. S1 of the ESI†) between the operating conditions that generate CO<sub>2</sub> and a region for which there is no net generation of CO<sub>2</sub> from the fuel.

This complex chemistry can only occur rapidly with heterogeneous catalysts, at high temperatures, near adiabatic reactor conditions, where there is no steady build-up of surface coke. There also exists a distinct set of reactor feed ratios for which no solid graphitic or amorphous carbon is predicted at equilibrium (Fig. S2 of the ESI†).

Under feed conditions where the fuel carbon is not converted to CO<sub>2</sub> or solid carbon, the carbon is converted to CO. Therefore, the overlap of these two regions on the ternary diagram in Fig. 2 depicts a narrow region of feed conditions that will permit CO yields >100% through catalytic biomass and CH<sub>4</sub> co-processing. These inlet concentrations minimize complete fuel combustion and result in temperatures higher than those at which methanation and carbon formation occurs (~500 °C). Details of the calculations that were used to construct Fig. 2 can be found in the ESI.†

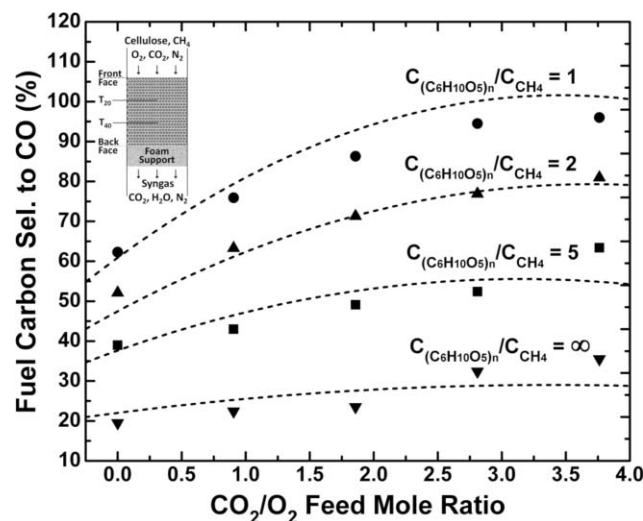


**Fig. 2** An operating diagram derived from adiabatic equilibrium calculations for the CPO of cellulose and CH<sub>4</sub> at four constant feed ratios in air with no pre-heat, and varying air/fuel and air/CO<sub>2</sub> ratios over all possible concentrations. The results (re-normalized without N<sub>2</sub>) describe a regime of operation where solid carbon is not a thermodynamic product and there is zero net generation of CO<sub>2</sub>, corresponding to CO yields of >100%. Details of the calculations and the assembly of this figure can be found in the ESI.†

The results predicted by these equilibrium calculations were tested in experiments conducted with 300 μm cellulose particles with CH<sub>4</sub>, O<sub>2</sub>, CO<sub>2</sub> and N<sub>2</sub> in a 20 mm ID quartz reactor tube over a Rh–Ce/γ–Al<sub>2</sub>O<sub>3</sub> catalyst supported on a 6 cm bed of 1.3 mm diameter α–Al<sub>2</sub>O<sub>3</sub> spheres (inset, Fig. 3; described in detail elsewhere<sup>13†</sup>). The Rh–Ce/γ–Al<sub>2</sub>O<sub>3</sub> catalyst was selected for its high WGS and reforming activity, and stability.<sup>14</sup> Temperatures measured at 20 and 40 mm below the front of

the catalyst surface ranged from 850–1125 °C, depending on the operating conditions and the position in the catalyst bed. Complete conversion to synthesis gas and combustion products with no observable char or tar formation was observed at a <30 ms gas residence time under continuous operation for all of the experiments reported.

The selectivity to CO in the reactor effluent showed that increasing the concentration of CO<sub>2</sub> in the absence of CH<sub>4</sub> co-feed had a weak effect on CO yield, consistent with the thermodynamic calculations represented by the dashed lines in Fig. 3. Alternatively, increasing the concentration of CH<sub>4</sub> in the absence of CO<sub>2</sub> co-feed significantly improved the CO yield, increasing the selectivity to CO from 19 to 62% for C<sub>(C<sub>6</sub>H<sub>10</sub>O<sub>5</sub>)<sub>n</sub>/C<sub>CH<sub>4</sub></sub> feed ratios of ∞ and 1, respectively. Furthermore, increasing the concentration of CO<sub>2</sub> with high concentrations of CH<sub>4</sub> increased the CO yield by as much as 34% at the ratio C<sub>(C<sub>6</sub>H<sub>10</sub>O<sub>5</sub>)<sub>n</sub>/C<sub>CH<sub>4</sub></sub> = 1. At CO<sub>2</sub>/O<sub>2</sub> = 3.76 and CH<sub>4</sub>/O<sub>2</sub> = 0.6, the system approached a CO yield of 100%, indicating a zero net generation of CO<sub>2</sub> in the reactor.</sub></sub>



**Fig. 3** Fuel carbon selectivity to CO rapidly approaches equilibrium-predicted concentrations (dashed lines) in the reforming of cellulose at a constant flow rate of 50 g h<sup>-1</sup> and a fuel carbon to oxygen from O<sub>2</sub> ratio (C/O) of 0.6, while varying the ratio of the two fuels (cellulose and CH<sub>4</sub>), N<sub>2</sub>/O<sub>2</sub> and CO<sub>2</sub>/O<sub>2</sub>. At CO<sub>2</sub>/O<sub>2</sub> = 3.76 and CH<sub>4</sub>/O<sub>2</sub> = 0.6, the system approached CO yields of 100%.

Selected experimental (experiments 1–5) and theoretical (calculations 6–10) results are presented in Table 1. The results from experiment 5 show a condition with >100% CO yield in the laboratory reactor, indicating complete conversion of carbon in cellulose and CH<sub>4</sub>, and partial conversion of CO<sub>2</sub> carbon to CO.

The theoretical data presented in calculation 9 of Table 1 shows a condition with ~100% CO yield and a H<sub>2</sub>/CO ratio of 1.46, compared to a H<sub>2</sub>/CO ratio of 1 for traditional biomass gasification. The theoretical data presented in calculation 10 shows >130% CO yield, compared to ~50% for traditional biomass gasification, which can be achieved at a cost to the product H<sub>2</sub>/CO ratio.

This process works by co-reforming carbohydrate pyrolysis vapors with CH<sub>4</sub> and CO<sub>2</sub> in one heat-integrated catalyst bed.

**Table 1** Selected experimental and theoretical (italics) data for the millisecond CPO of cellulose and CH<sub>4</sub> with CO<sub>2</sub> addition<sup>a</sup>

Experiment/calculation	1	2	3	4	5	6	7	8	9	10
<b>Parameters</b>										
Catalyst bed length/mm	60	60	60	60	60	—	—	—	—	—
C/O ratio	0.6	0.6	0.6	0.6	0.6	0.82	0.79	1.00	0.91	0.70
C <sub>(C<sub>6</sub>H<sub>10</sub>O<sub>5</sub>)<sub>n</sub></sub> /C <sub>CH<sub>4</sub></sub>	∞	5	2	1	0.5	0.50	0.25	0.75	0.25	0.5
CH <sub>4</sub> /O <sub>2</sub> ratio	0	0.2	0.4	0.6	0.8	1.09	1.27	1.14	1.45	0.93
CO <sub>2</sub> /O <sub>2</sub> ratio	0	0.91	1.86	2.81	3.76	1.81	1.59	0.57	0.31	2.6
N <sub>2</sub> /O <sub>2</sub> ratio	3.76	2.86	1.91	0.95	0	3.76	3.76	0	0	0
Cellulose flow/g h <sup>-1</sup>	50	50	50	50	50	—	—	—	—	—
<b>Results</b>										
<i>T</i> /°C										
20 mm	1061	1108	1040	1056	1139	—	—	—	—	—
40 mm	1018	965	897	916	985	—	—	—	—	—
Adiabatic	—	—	—	—	—	652	643	895	892	953
H selectivity (%)										
H <sub>2</sub>	14.9	27.4	26.3	23.7	29.6	63.9	66.4	74.9	83.6	36.6
H <sub>2</sub> O	85.1	72.6	72.9	74.1	68.8	33.7	29.3	25.0	16.2	63.3
C selectivity (%)										
CO yield <sup>b</sup>	19.5	43.0	71.3	94.5	107.6	100.9	101.6	101.6	101.4	131.4
CO <sub>2</sub>	80.5	57.0	28.2	3.9	-8.7	-2.8	-5.4	-1.7	-1.5	-31.4
CH <sub>4</sub>	0	0	0.5	1.6	1.1	1.8	3.7	0.0	0.1	0.0
Residence time/ms										
28.1	23.4	19.1	13.7	9.3	—	—	—	—	—	—
Mass velocity/h <sup>-1</sup>										
43.0	51.6	64.5	86.1	129.1	—	—	—	—	—	—
H <sub>2</sub> /CO ratio										
0.74	0.55	0.46	0.40	0.41	1.02	1.15	1.11	1.46	0.45	—
Synthesis gas yield (%)										
6.5	16.1	27.5	40.0	51.1	41.6	42.8	85.1	89.6	65.1	—

<sup>a</sup> Details of the calculations and assumptions that went into the assembly of this table can be found in the ESI. <sup>b</sup> The results for CO selectivity are identical to CO yield because there is always 100% conversion of the cellulose to C<sub>1</sub> products in the reactor.

The high temperatures generated in the oxidation zone allow rapid heat conduction through the catalyst support, powering endothermic pyrolysis at the front of the catalyst and reforming within the catalyst bed, eliminating char generation.<sup>13,15</sup> The CPO of CH<sub>4</sub> in similar reactors has been shown to readily form CO and H<sub>2</sub>, a crucial step that provides the H<sub>2</sub> necessary to drive the RWGS reaction (eqn 1).<sup>16</sup>

Experiments show a rapid approach to equilibrium with minimal heat loss, validating the use of adiabatic equilibrium calculations to model reactor operation, as noted by the experiments and calculations presented in Fig. 3. The calculations indicate at least 20% lower CO selectivities are achieved for certain feeds with independent carbohydrate and CH<sub>4</sub> reforming, showing the importance of co-reforming CH<sub>4</sub> and biomass in one integrated reaction system (Table S2 of the ESI†). Similar results could be achieved with three reactors individually undergoing CH<sub>4</sub> CPO, carbohydrate reforming and product gas equilibration by water-gas shift. However, this arrangement is considerably more complex and increases the overall process cost.

Our research demonstrates for the first time that equilibrated, adiabatic, char-free biomass processing by co-feeding CH<sub>4</sub> at specific concentrations produces 100% carbon recovery as CO. Future research will focus on the mechanisms of the RWGS reaction in the presence of biomass-derived oxygenate CPO, as well as hydrogen-coupling by CH<sub>4</sub> decomposition, both of which are currently unknown. Utilizing the benefit of this reactor scheme requires considerable process design in conjunction with full biomass life-cycle and economic analysis. Finally, although lignocellulosic biomass has been experimentally shown to yield similar results to a pure cellulose feedstock,<sup>11</sup> in-depth experiments assessing the long-term effect of ash on catalyst site deactivation must be performed.

## Acknowledgements

This research was partially supported by the Initiative for Renewable Energy and the Environment (IREE) at the University of Minnesota, the US Department of Energy (DOE), the National Renewable Energy Laboratory (NREL) and the 3M Corporation.

## Notes and references

- G. W. Huber, S. Iborra and A. Corma, *Chem. Rev.*, 2006, **106**, 4044–4098.
- C. Schubert, *Nat. Biotechnol.*, 2006, **24**, 777–784.
- A. V. Bridgwater, *Chem. Eng. J.*, 2003, **91**, 87–102.
- R. D. Perlack, L. L. Wright, A. F. Turhollow, R. L. Graham, B. J. Stokes, D. C. Erblich, *Biomass as Feedstock for a Bioenergy and Bioproducts Industry: The Technical Feasibility of a Billion-Ton Annual Supply*, Oak Ridge National Laboratory, Oak Ridge, TN, USA, DOE/GO-102005-2135, 2005.
- X. Xu and J. A. Moulijn, *Energy Fuels*, 1996, **10**, 305–325.
- R. Shinnar and F. Citro, *Science*, 2006, **313**, 1243–1244.
- R. Agrawal, N. R. Singh, F. H. Ribeiro and W. N. Delgass, *Proc. Natl. Acad. Sci. U. S. A.*, 2007, **104**, 4828–4833.
- D. Hildebrandt, D. Glasser, B. Hausberger, B. Patel and B. J. Glasser, *Science*, 2009, **323**, 1680–1681.
- B. C. Gates, G. W. Huber, C. L. Marshall, P. N. Ross, J. Siirola and Y. Wang, *MRS Bull.*, 2008, **33**, 429–435.
- R. Agrawal and N. R. Singh, *AIChE J.*, 2009, **55**, 1898–1905.
- P. J. Dauenhauer, B. J. Dreyer, N. J. Degenstein and L. D. Schmidt, *Angew. Chem., Int. Ed.*, 2007, **46**, 5864–5867.
- J. R. Salge, B. J. Dreyer, P. J. Dauenhauer and L. D. Schmidt, *Science*, 2006, **314**, 801–804.
- J. L. Colby, P. J. Dauenhauer and L. D. Schmidt, *Green Chem.*, 2008, **10**, 773–783.
- A. Donazzi, B. C. Michael and L. D. Schmidt, *J. Catal.*, 2008, **260**, 270–275.
- P. J. Dauenhauer, J. L. Colby, C. M. Balonek and L. D. Schmidt, *Green Chem.*, 2009, **11**, 1555–1561.
- D. A. Hickman and L. D. Schmidt, *Science*, 1993, **259**, 343–346.

# Palladium-catalysed Grignard cross-coupling using highly concentrated Grignards in methyl-tetrahydrofuran†

Edward J. Milton and Matthew L. Clarke\*

Received 13th October 2009, Accepted 25th November 2009

First published as an Advance Article on the web 12th January 2010

DOI: 10.1039/b921026a

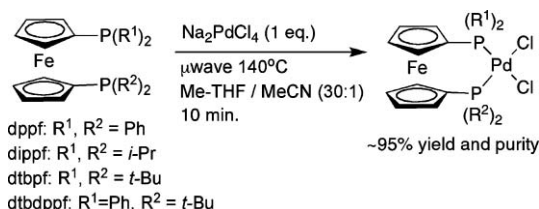
The cross-coupling of Grignard reagents at 5 molar concentration in methyl-tetrahydrofuran with no added reaction solvents can be achieved with the appropriate matching of catalyst to substrate, significantly reducing solvent use when compared to a typical protocol in tetrahydrofuran. Me-THF was also used in an improved microwave accelerated synthesis of the  $[\text{Pd}(\text{L})\text{Cl}_2]$  pre-catalysts from sodium tetrachloropalladate in very high yield.

Palladium-catalysed cross-couplings are now very widely used in both academic and industrial synthesis. There are many studies where important breakthroughs in the cross-coupling of low-reactivity electrophilic partners such as aryl chlorides have become possible after optimisation of ligand structure.<sup>1</sup> On the other hand, our interest has been the investigation of problematic nucleophiles in cross-coupling catalysis,<sup>2</sup> and as part of this effort, we turned our attention to the Grignard cross-coupling (Kumada coupling).<sup>3</sup> There are certainly examples where the use of Grignard reagents, one of the most economical nucleophiles, creates difficulties. An obvious potential problem is reduced functional group tolerance, but there are also reports that suggest problems with low yields and increased homo-coupling for these nucleophiles on a given substrate relative to organo-zinc or organoborane nucleophiles.

Grignard cross-couplings typically use solutions of Grignard reagents in the increasingly environmentally unacceptable solvent, tetrahydrofuran (THF) at concentrations of between 1 and 2.5 molar, often with an added reaction solvent. Most Grignard reagents are not soluble at higher concentrations. At the end of a typical cross-coupling procedure, additional organic solvents (generally diethyl ether) have to be added prior to quenching with water, since THF is miscible with water. The products are then isolated from the Mg salts by washing with organic solvent, and then generally further purified. There has been increasing interest in the THF surrogate, methyl-tetrahydrofuran (Me-THF) as it can be produced from waste biomass, and has some desirable features relative to THF.<sup>4</sup> Me-THF has been reported to be more stable to acids, and to be a better solvent for Grignard reagents allowing more concentrated solutions to be used. In addition, Me-THF is not miscible with water which suggests less solvent can be used in the work-up

stage and energy-intensive clean-up of aqueous waste streams can be reduced. Me-THF is more expensive than THF, in part due to not being produced in such large quantities, but we felt that if solvent usage during cross-coupling could be reduced significantly then the protocols would have very significant environmental and economic advantages relative to traditional procedures. Grignard synthesis or cross-coupling reactions in Me-THF are not a new invention<sup>4</sup> since this solvent has been slowly gaining popularity in industrial research, but to the best of our knowledge, no report has evaluated a range of commonly employed Pd catalysts in Grignard cross-coupling under the rather challenging conditions that enable reduced solvent usage. In this communication, we report that Grignard cross-coupling is possible at 5 molar concentration with no added reaction solvents and using reasonably low catalyst loadings.

We predominantly focussed on ferrocene-type ligands, since dppf has a strong track record in Kumada and Negishi cross-coupling.<sup>5</sup> More recently, 1,1'-ditert-butylphosphinoferrocene (dtbpf) has been found to be a very good ligand in difficult Pd-catalysed Suzuki reactions,<sup>5b</sup> giving superior activity relative to dppf and 1,1'-bis-diisopropylphosphino-ferrocene (dippf). Johnson Matthey have developed this chemistry to a synthetically useful level and sell  $[\text{PdCl}_2(\text{L})]$  complexes of the above ligands. 1-Ditert-butyl-1'-diphenylphosphino-ferrocene (dtbdppf) has barely been studied in cross-coupling or organometallic chemistry, something that we also wished to rectify. An improved synthesis of  $[\text{Pd}(\text{L})\text{Cl}_2]$  complexes was first devised (Scheme 1) that benefits from simplicity and reduced solvent usage, eliminates the need to convert simple Pd salts to  $[\text{PdCl}_2(\text{PhCN})_2]$  using excess PhCN, and the subsequent ligand displacement encountered in the most common method for synthesising  $[\text{PdCl}_2(\text{P}\wedge\text{P})]$  complexes. Equimolar amounts of  $\text{Na}_2[\text{PdCl}_4]$  and diphosphine are simply treated with Me-THF–MeCN solvent (Me-THF–MeCN = 30 : 1) and heated using microwave heating at 140 °C for 10 min. The desired complexes precipitate on cooling and are filtered and then washed with water. Yield and purity are very high.



**Scheme 1** Microwave accelerated synthesis of  $[\text{PdCl}_2(\text{L})]$  pre-catalysts direct from  $\text{Na}_2\text{PdCl}_4$  in Me-THF.

School of Chemistry, University of St Andrews, EaStCHEM, St Andrews, Fife, UK. E-mail: mc28@st-andrews.ac.uk; Fax: (44) 1334 463808; Tel: (44) 1334 463850

† Electronic supplementary information (ESI) available: Experimental procedures. See DOI: 10.1039/b921026a

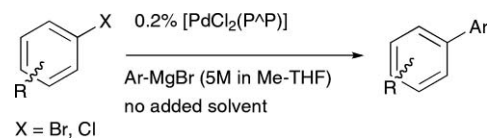
**Table 1** Grignard cross-coupling at high concentration: ligand effects<sup>a</sup>

Entry	Aryl halide	Grignard reagent	L in [PdCl <sub>2</sub> /L <sub>n</sub> ]	T/°C	Time/h	Starting material (%)	Product (%)
1	2-bromo-4-fluoro-anisole	PhMgBr	dppf	50	2	19	76
2	2-bromo-4-fluoro-anisole	PhMgBr	dippf	50	2	60	20
3	2-bromo-4-fluoro-anisole	PhMgBr	dtbpf	50	2	61	30
4	2-bromo-4-fluoro-anisole	PhMgBr	dtbdppf	50	2	28	56
5	2-bromo-4-fluoro-anisole	PhMgBr	dppe	50	2	21	71
6	2-bromo-4-fluoro-anisole	PhMgBr	dppb	50	2	19	75
7	2-bromo-4-fluoro-anisole	PhMgBr	dppp	50	2	1	96
8	4-bromo-anisole	PhMgBr	dppp	50	2	78	22
9	4-bromo-anisole	PhMgBr	dippf	50	2	33	67
10	4-bromo-anisole	PhMgBr	dtbpf	50	2	76	24
11	4-bromo-anisole	PhMgBr	dppf	50	2	54	46
12	4-bromo-anisole	PhMgBr	dtbpf	50	2	40	60
13	4-(Me <sub>2</sub> N)C <sub>6</sub> H <sub>4</sub> Br	PhMgBr	dppp	55	6	39	61
14	4-(Me <sub>2</sub> N)C <sub>6</sub> H <sub>4</sub> Br	PhMgBr	dippf	55	6	51	49
15	4-(Me <sub>2</sub> N)C <sub>6</sub> H <sub>4</sub> Br	PhMgBr	dtbpf	55	6	59	41
16	4-(Me <sub>2</sub> N)C <sub>6</sub> H <sub>4</sub> Br	PhMgBr	dppf	55	6	37	63
17	4-(Me <sub>2</sub> N)C <sub>6</sub> H <sub>4</sub> Br	PhMgBr	dtbpf	55	6	77	23
18	4-(CF <sub>3</sub> )C <sub>6</sub> H <sub>4</sub> Cl	PhMgBr	dippf	75	6	15	82
19	4-(CF <sub>3</sub> )C <sub>6</sub> H <sub>4</sub> Cl	PhMgBr	dtbpf	75	6	74	13
20	4-(CF <sub>3</sub> )C <sub>6</sub> H <sub>4</sub> Cl	PhMgBr	dppf	75	6	25	93
21	4-(CF <sub>3</sub> )C <sub>6</sub> H <sub>4</sub> Cl	PhMgBr	dtbpf	75	6	7	75
22	2-bromo-4-fluoro-anisole	4-(CF <sub>3</sub> )C <sub>6</sub> H <sub>4</sub> MgBr	2 × PPh <sub>3</sub>	50	2	79	21
23	2-bromo-4-fluoro-anisole	4-(CF <sub>3</sub> )C <sub>6</sub> H <sub>4</sub> MgBr	dppe	50	2	75	25
24	2-bromo-4-fluoro-anisole	4-(CF <sub>3</sub> )C <sub>6</sub> H <sub>4</sub> MgBr	dppp	50	2	44	56
25	2-bromo-4-fluoro-anisole	4-(CF <sub>3</sub> )C <sub>6</sub> H <sub>4</sub> MgBr	dppb	50	2	79	21
26	2-bromo-4-fluoro-anisole	4-(CF <sub>3</sub> )C <sub>6</sub> H <sub>4</sub> MgBr	dippf	50	2	96	4
27	2-bromo-4-fluoro-anisole	4-(CF <sub>3</sub> )C <sub>6</sub> H <sub>4</sub> MgBr	dtbpf	50	2	98	2
28	2-bromo-4-fluoro-anisole	4-(CF <sub>3</sub> )C <sub>6</sub> H <sub>4</sub> MgBr	dppf	50	2	34	66
29	2-bromo-4-fluoro-anisole	4-(CF <sub>3</sub> )C <sub>6</sub> H <sub>4</sub> MgBr	dtbpf	50	2	33	67

<sup>a</sup> Reactions conducted at 1 mmol scale using 1.2 mmol of 5M Grignard reagent in 0.24 mL Me-THF for time given. Conversions were determined by <sup>19</sup>F NMR spectroscopy, and checked using H NMR spectroscopy against an internal standard with product identity and side products further examined by GCMS (entries 8–17 by H NMR using methyl naphthalene as internal standard and GCMS only). In the majority of the reactions, GCMS indicates that homo-coupled aryl halide is only present in trace amounts, but exceptions are entry 2 (20% homocoupled), entry 3 (14% homocoupled), entry 4 (16% h) and entries 5 and 6 (6%h).

With these and several other common pre-catalysts in hand, we turned our attention to the synthesis of the Grignards and evaluating the catalysts in cross-coupling. ‡ Most of our studies were carried out with PhMgBr. This can be made as a rather viscous solution at concentrations as high as 5 M. (SAFETY NOTE: We have not experienced any difficulties making small scale solutions (~30 mmol) of highly concentrated Grignard reagents at the temperatures described, but it is essential that great care is taken in synthesising new Grignard reagents at this concentration, in particular monitoring reaction exotherms. While this is the case for any Grignard reagent, it can be envisaged that extra caution is needed at higher concentration. Scale up of these reactions, in common with all Grignard reactions, should first be evaluated using calorimetry.) In order to facilitate transfer of the Grignard reagents, they are heated to 50–75 °C to give less viscous solutions and transferred to the reaction vessel. Alternatively, a very concentrated solution of catalyst and substrate can be added to ArMgBr.

The catalyst screening studies have been carried out using no extra reaction solvents other than the minimal solvent solvating the Grignard reagent (around 800 mg (~4 mmol) of aryl halide per mL solvent), at low catalyst loadings (0.2 mol%) and at moderate temperatures (50–75 °C) since we envisaged these sorts of conditions would be needed in a real application. Table 1 and Scheme 2 show these results. In the case of 2-bromo-4-fluoro-anisole, palladium catalysts derived from dppp stand out

**Scheme 2** Protocol for Grignard cross-coupling reactions in Me-THF.

as being able to operate well under this challenging regime. It is interesting to note that dtbpf, that has been shown to give superb Pd catalysts for the Suzuki coupling of boronic acids with both aryl bromides and deactivated chlorides under conditions where dppf fails, is a poor catalyst in these reactions with significant amounts of starting material and homo-coupling product. Given that the Suzuki results in reference 5b infer high activity in oxidative addition, and that this ligand has been shown to promote reductive elimination over a hundred times faster than dppf complexes,<sup>6</sup> this suggests inefficient transmetalation, a reaction known to be incredibly sensitive to steric effects.<sup>7</sup> We have not optimised these reactions, but the dppp/Pd catalysed reaction gives essentially quantitative yields of a crude material (~95% purity) after work up in which only a further 0.6 ml MeTHF added to assist work-up. While this material that will be contaminated with traces of Pd might be sufficiently pure for further application and downstream purification, it can be further purified by column chromatography (86% isolated yield) in a standard purification procedure. A procedure that is greener

still would use a recyclable catalyst that could be separated prior to the work up; we are optimistic that such a catalyst could be developed given the considerable advances that have been made in catalyst recycling. In any case, this procedure used < 1 ml of Me-THF per mmol of Grignard reagent for the Grignard synthesis, catalytic reaction and aqueous extraction of magnesium salts. Hardly any reports in the literature give amounts of solvent used, but one of best Pd-catalysed procedures reported that does give full details uses over 30 mL of THF and Et<sub>2</sub>O per mmol reaction.<sup>3b</sup> Although this amount could probably be reduced, we would argue that this shows that the saving in solvent could be considerable and make this approach practical. A few other aryl halides were investigated, and one aspect of this study worth highlighting is that the ligand must be matched to the aryl halide, and in this case, this is not easily predicted based on the rather limited range of reactions we have examined thus far; dppf and the previously unstudied ligand dtbdppf appear to be the best catalysts in general. Significant optimisation of Grignard synthesis and cross-coupling would need to be carried out as this type of protocol is transferred to other Grignard reagents or scaled up, but to check that this type of approach would work on another Grignard reagent, *p*-CF<sub>3</sub>C<sub>6</sub>H<sub>5</sub>MgBr was synthesised and coupled with 2-bromo-4-fluoro-anisole at 5M concentration. This Grignard did not store well, needing to be prepared the same day as the coupling reaction in order to obtain reproducible results, but none-the-less good conversions can be obtained in just 2 h.

In summary, we have used a convenient microwave-assisted synthesis of some typical Pd catalysts used for cross-coupling, and investigated the forgotten ferrocene ligand, 1-*di*-*tert*-butyl-1'-diphenylphosphino-ferrocene, and studied how ligand structure alters reactivity in the Grignard cross-coupling under challenging conditions in Me-THF, a new solvent that is beginning to attract attention as a greener replacement to THF if the process economics can overcome its higher cost.<sup>4c</sup> These studies show a significant saving in solvent use in both Grignard synthesis (expected from the literature), but also the Grignard cross-coupling and the work-up; good conversions were obtained in short times at S/C of 500 in the few examples we have examined thus far. The reaction is strongly dependent on ligand structure, but 1-*di*-*tert*-butyl-1'-diphenylphosphino-ferrocene and 1,1'-bis-diphenylphosphino-ferrocene seem to be the preferred ligands at present. A more thorough investigation into the full scope of this reaction will be carried out and reported in full in due course. It is hoped that this study suggests that Grignard cross-coupling in Me-THF might be ecologically and economically attractive and worth developing further in industrial synthesis.

We acknowledge the EPSRC for funding, Johnson-Matthey for the loan of some of the Pd salts, and IMCD for a donation of Me-THF.

## Notes and references

‡ **Example experimental procedure:** Bromobenzene (5 g, 3.36 mL, 32 mmol) in Me-THF (6.4 mL) was added DROPPWISE to magnesium

turnings (0.789 g, 1.02 eq., 32.5 mmol) *via* an addition funnel. NO INITIATOR NEEDED. CAUTION, EXOTHERM! (Heat generated sufficient to maintain gentle reflux.) After addition, the reaction mixture was warmed to 90 °C for 4 h (until the Mg was consumed) to give a bright orange solution. To a solution of the Grignard (PhMgBr) in Me-THF (0.24 mL, 1.2 eq., 1.2 mmol), 2-bromo-4-fluoroanisole (0.205 g, 0.13 mL, 1 mmol) was added followed by the catalyst [Pd(DPPP)Cl<sub>2</sub>] (0.2 mol%, 1.2 mg) and the reaction mixture heated to 50 °C for 2 h. <sup>1</sup>H NMR spectroscopy and GCMS showed the desired product. Excess Grignard reagent was quenched with solid NH<sub>4</sub>Cl, organics filtered through a plug of MgSO<sub>4</sub> (washed with 0.6 mL MeTHF) and concentrated *in vacuo* to give a yellow oil in essentially quantitative yield. GCMS: Retention time, MS (EI) *m/z* (%): 18.706 mins (96%), [M<sup>+</sup>] = 202.1; C<sub>14</sub>H<sub>10</sub>F<sub>2</sub>O requires 202.08. Although this material is of high purity, column chromatography (petroleum ether 40–60) yielded the product as a colourless liquid (0.173 g, 0.86 mmol, 86%). This compound has been reported previously.<sup>5b</sup> <sup>1</sup>H NMR (400 MHz, CDCl<sub>3</sub>) δ = 3.82 (3H, s, OCH<sub>3</sub>), 6.81 (1H, dd, *J* = 4.62, 8.8 Hz, ArCH), 6.87–6.94 (1H, m, ArCH), 6.96 (1H, dd, *J* = 3.2, 9.2 Hz, ArCH), 7.25 (1H, tt, *J* = 7.54, 1.4 Hz, ArCH), 7.34 (2H, t, *J* = 6.96 Hz, ArCH), 7.4–7.45 (2H, m, ArCH); <sup>19</sup>F{<sup>1</sup>H} NMR (376.5 MHz, CDCl<sub>3</sub>) δ = -124.51; <sup>13</sup>C NMR (100 MHz, CDCl<sub>3</sub>) δ = 56.2, 112.3, 112.4, 114.2, 114.4, 117.3, 117.6, 127.4, 128.2, 129.4, 132.0, 132.1, 137.5, 152.7, 156.7 (d, *J* = 236.4 Hz); MS (EI) *m/z* (%): 202.1 (100.0) [M<sup>+</sup>]. Similar protocols were used for the other screening experiments, with product identities, and conversions determined by <sup>1</sup>H NMR spectroscopy against an internal standard and GCMS analysis. The data obtained matched literature values and samples prepared in our laboratory by other methods.

- (a) A. Zapf and M. Beller, *Top. Catal.*, 2002, **19**, 101; (b) C. E. Tucker and J. G. DeVries, *Top. Catal.*, 2002, **19**, 111; (c) C. Barnard, *Platinum Met. Rev.*, 2008, **52**, 38; (d) M. L. Clarke and J. J. R. Frew, *Specialist Periodical Reports: Organometallic Chemistry*, Royal Society of Chemistry, Ed. I. J. S. Fairlamb and J. Lynam, 2009, **35**, 19.
- (a) M. L. Clarke, *Adv. Synth. Catal.*, 2005, **347**, 303; (b) J. A. Fuentes, M. E. France, G. J. Roff, E. J. Milton and M. L. Clarke, *Beilstein J. Org. Chem.*, 2007, **3**, art.18; (c) E. J. Milton, J. A. Fuentes and M. L. Clarke, *Org. Biomol. Chem.*, 2009, **7**, 2645; (d) K. Damian, M. L. Clarke and C. J. Copley, *Appl. Organomet. Chem.*, 2009, **23**, 272.
- (a) K. Tamao, K. Sumitani and M. Kumada, *J. Am. Chem. Soc.*, 1972, **94**, 4374; (b) G. Y. Li, *J. Organomet. Chem.*, 2002, **653**, 63; (c) A. Alimardanov, L. Schmieder-van de Vondervoort, A. H. M. de Vries and J. G. de Vries, *Adv. Synth. Catal.*, 2004, **346**, 1812; (d) J. A. Miller and R. P. Farrell, *Tetrahedron Lett.*, 1998, **39**, 7275; (e) R. Martin and S. L. Buchwald, *J. Am. Chem. Soc.*, 2007, **129**, 3844; (f) C. E. Hartmann, S. P. Nolan and C. J. Cazin, *Organometallics*, 2009, **28**, 2915; (g) Iron catalysed Grignard cross-coupling has developed further recently, but further studies are needed to lower catalysts loadings and determine mechanism (no reports use concentrated Me-THF solutions). For some examples, see: T. Hatekeyama and M. Nakamura, *J. Am. Chem. Soc.*, 2007, **129**, 9844; R. B. Bedford, M. Betham, D. W. Bruce, S. A. Davis, R. M. Frost and M. Hird, *Chem. Commun.*, 2006, 1398; R. B. Bedford, D. W. Bruce, R. M. Frost and M. Hird, *Chem. Commun.*, 2005, 4161.
- (a) D. F. Aycock, *Org. Process Res. Dev.*, 2007, **11**, 156; (b) C. Werner, F. Platz, A. Kanschlik-Conradson, US Patent (to Honeywell International) US 7205,414 (2007); (c) Our interest to follow up our initial finding (that dtbdppf was a better ligand than dtbpf for this reaction) was crystallised by an interesting debate, where the issue of overcoming the extra cost of this green solvent was highlighted. See: <http://gaussling.wordpress.com/2006/10/18/fabulous-2-methyltetrahydrofuran/>.
- (a) T. Hayashi, M. Konishi, Y. Kobori, M. Kumada, T. Higuchi and K. Kirotsu, *J. Am. Chem. Soc.*, 1984, **106**, 158; (b) T. J. Colacot and H. A. Shea, *Org. Lett.*, 2004, **6**, 3731; (c) A. L. Boyles, I. R. Butler and S. C. Quayle, *Tetrahedron Lett.*, 1998, **39**, 7766; I. R. Butler, W. R. Cullen, T. J. Kim, S. J. Rettig and J. Trotter, *Organometallics*, 1985, **4**, 972.
- G. Mann, Q. Shelby, A. H. Roy and J. F. Hartwig, *Organometallics*, 2003, **22**, 2775.
- M. L. Clarke and M. Heydt, *Organometallics*, 2005, **24**, 6475.

# A green method for the self-aldol condensation of aldehydes using lysine†

Yutaka Watanabe,\* Kazue Sawada and Minoru Hayashi

Received 7th September 2009, Accepted 30th November 2009

First published as an Advance Article on the web 13th January 2010

DOI: 10.1039/b918349c

A self-condensation of aldehydes has been conveniently accomplished by the catalytic action of lysine in water or a solvent-free system under specific emulsion conditions to give  $\alpha$ -branched  $\alpha,\beta$ -unsaturated aldehydes in good yields.

## Introduction

The quest for environment friendly or green methods for chemical synthesis is attracting more and more attention.<sup>1</sup> To achieve such a green process, especially for industrial applications it is desirable (1) either to adopt a solvent-free system or to use water as solvent, (2) to use biogenic catalysts but not petroleum products, (3) to avoid heating, and (4) to follow a simple work-up procedure and waste treatment. Aldol condensation is an important synthetic method widely used in organic synthesis.<sup>2</sup> A typical process involves the self-condensation of aldehydes catalyzed by alkalis or acids.<sup>3</sup> Several alternative methods for aldol condensation have been reported.<sup>4</sup> However, in an era when green methods are warranted, many of these methods are not satisfactory with respect to reaction temperature, reaction time, solvent, yield, and simplicity of the catalyst. Aldol condensation is an industrially important process. For example, the condensation product of butanal is the important synthetic intermediate in the preparation of 2-ethylhexanol which is widely used for making plasticizers, surfactants, *etc.* The industrial process for the self-aldol condensation of aldehydes is usually carried out in an aqueous alkaline solution. While condensation of medium carbon-chain aldehydes such as octanal and nonanal can be conducted by heating under alkaline conditions,<sup>5</sup> water-insoluble higher aldehydes are not suitable for the alkaline process. A unified procedure for aldol condensation that can be applied to all kinds of aldehydes is lacking. We herein report a very general and an environmentally benign method for aldol condensation of all range of aldehydes (medium to high carbon aldehydes). The use of biogenic lysine (Lys) as the catalyst and the solvent-free/aqueous conditions make this method very attractive.

## Results and discussion

In addition to the common self-aldol condensation of aldehydes using an alkali, the majority of the reported procedures employ secondary amines and their derivatives as catalysts. As excep-

tional cases, simple aldehydes such as butanal and acetaldehyde were shown to be converted to the condensation products by the catalysis of  $\alpha$ -amino acids in the mechanistic studies.<sup>6</sup> We have now found that Lys and ornithine (Orn) catalyze the self-condensation of aldehydes in water. Thus, the treatment of 10 mol% of Lys in water with 3-phenylpropanal (1 M) for 2 h at room temperature, resulted in the formation of the condensation product in 65% yield (Table 1). Orn also yielded the same product in a comparable yield (59%). However, arginine, despite being a comparably basic amino acid, was not as effective as Lys and Orn (only 24% yield). From this, it is very clear that the presence of an amino group in the side chain is essential for smooth reaction.

In order to investigate the effect of concentration of the aldehyde in the feasibility of reaction, the condensation reaction was carried out at different molar concentrations of the aldehyde. It was found that as the concentration of the aldehyde increases, the yield also increased. For example, 0.25 M, 0.5 M, 1 M and 2 M nonanal in water gave 13%, 21%, 62% and 64% yield of the condensation product, respectively. After various experimental studies, 1–2 M solution of aldehydes with more than seven carbons underwent condensation smoothly in the presence of 10 mol% of Lys at room temperature (Table 1). Even water-insoluble solid octadecanal (entry 9) was found to furnish the coupling product in 61% although a larger amount of Lys and longer reaction time were required.

In order to understand the role of water, we next carried out the reaction without water. Thus, treatment of higher aldehydes (more than C<sub>6</sub>) with 10 mol% of Lys with stirring at room temperature for 2 h gave the condensation products in good yields, which are comparable with those in the reactions in aqueous medium (Table 2). The solvent-free condensation of hexanal (C<sub>6</sub>) gave a yield identical to that obtained in the water solvent system, in which concentration of the aldehyde was exceptionally higher (8 M), as shown in Table 2. It is noteworthy that the short chain aldehydes such as pentanal (C<sub>5</sub>) and butanal (C<sub>4</sub>) provided the condensation product in moderate yields under solvent-free conditions, but when the reaction was done in water (1 M), the yields dropped by half.

The Lys-catalyzed self-condensation of aldehydes in water or without a solvent, as described, would be a synthetically useful alternative; it can be applied to various aldehydes with low to high carbon numbers, in contrast to the common alkaline condensation that requires heating in the case of moderate chain aldehydes (C<sub>7</sub>–C<sub>9</sub>) and is not suitable for higher chain ones. The reaction is especially emphasized to be a green procedure judging from the following: (1) the solvent-free or aqueous condition, (2) the catalyst used, Lys, is of bio-origin, (3) no heating is required, (4) short reaction time and simple work-up

Department of Materials Science and Biotechnology, Graduate School of Science and Engineering, Ehime University, Matsuyama, 790-8577, Japan. E-mail: wyutaka@dpc.ehime-u.ac.jp; Fax: +81-89-927-9921

† Electronic supplementary information (ESI) available: <sup>1</sup>H- and <sup>13</sup>C-NMR spectra and data. See DOI: 10.1039/b918349c



**Table 1** Lys-catalyzed self-condensation of various aldehydes in water

Entry	Aldehyde	Conc./M	Lys (mol%)	Time/h	Yield (%)	E/Z
1	CH <sub>3</sub> (CH <sub>2</sub> ) <sub>7</sub> CH=CH(CH <sub>2</sub> ) <sub>7</sub> CHO	1.0	10	2	70	94/6
2	n-C <sub>9</sub> H <sub>19</sub> CHO	1.0	10	2	75	99/1
3	n-C <sub>8</sub> H <sub>17</sub> CHO	2.0	10	2	64	98/2
4	n-C <sub>7</sub> H <sub>15</sub> CHO	2.0	10	2	68	98/2
5	n-C <sub>6</sub> H <sub>13</sub> CHO	2.0	10	2	69	98/2
6	n-C <sub>5</sub> H <sub>11</sub> CHO	8.0	10	2	63	95/5
7	Ph(CH <sub>2</sub> ) <sub>2</sub> CHO	1.0	10	2	65	98/2
8	n-C <sub>12</sub> H <sub>25</sub> SCH(CH <sub>3</sub> )CH <sub>2</sub> CHO	1.0	10	2	78	25/75
9	n-C <sub>17</sub> H <sub>35</sub> CHO	1.0	30	10	61	99/1

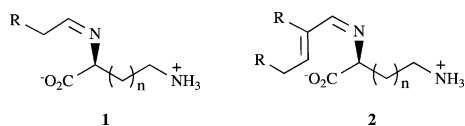
**Table 2** The self-condensation of aldehydes in no solvent<sup>a</sup>

Entry	Aldehyde	Yield (%)	
		No solvent	H <sub>2</sub> O (conc.)
1	n-C <sub>9</sub> H <sub>19</sub> CHO	74	
2	n-C <sub>8</sub> H <sub>17</sub> CHO	66	
3	n-C <sub>7</sub> H <sub>15</sub> CHO	62	
4	n-C <sub>6</sub> H <sub>13</sub> CHO	64	
5	n-C <sub>5</sub> H <sub>11</sub> CHO	62	63 (8 M)
6	n-C <sub>4</sub> H <sub>9</sub> CHO	52	23 (1 M)
7	n-C <sub>3</sub> H <sub>7</sub> CHO	46	23 (1 M)

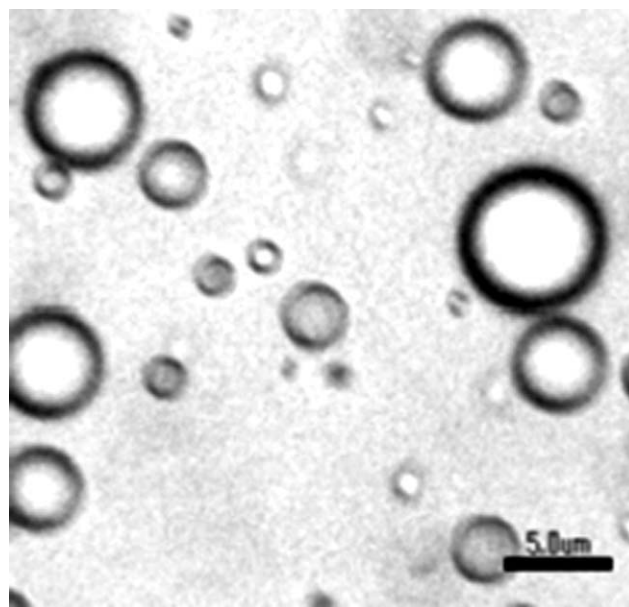
<sup>a</sup> A mixture of an aldehyde and 10 mol% Lys was stirred for 2 h (3 h in the case of entries 6 and 7) at r.t.

procedure, and (5) the waste, containing the basic amino acid, is non-toxic. Furthermore, since by-products were highly polar in all cases carried out this time, chromatographic isolation was accomplished without using a large amount of elution solvents and silica gel. Although the solvent-free process is greener than the reaction in water, when the starting aldehyde is a solid, the water media is essential to promote the condensation.

The reaction mixture in water formed an emulsion. This observation suggests that a micelle or micelle-like colloidal aggregate is formed by assembly of an amphiphilic imine **1** derived from Lys or Orn and aldehyde (Scheme 1). Indeed, the formation of spherical droplets in water was observed by an optical microscope (Fig. 1). The yield of the condensation products depended remarkably upon the concentration of an aldehyde and carbon number of its chain. Thus, 1.0 and 2.0 M of octanal gave the dimer in 53 and 68% yields, respectively, while in the case of the concentration of 0.25 and 0.5 M, 21 and 15% of the product were obtained (Table 3). This tendency was observed in the case of aldehydes with more than seven carbon atoms. These results suggest that the reaction of heptanal and higher aldehydes has a critical concentration between 1.0 and 0.5 M for reaction promotion. On the other hand, in the case of hexanal and lower aldehydes, yields for 1.0 M concentration

**Scheme 1****Table 3** Concentration vs. yield

Entry	Concentration/M	Yield (%)
1	0.25	21
2	0.5	15
3	1.0	53
4	2.0	68

**Fig. 1** Optical micrograph of the mixture of 3-phenylpropanal and Orn in water (scale bar = 5 μm).

decreased dramatically and to gain yields similar to those in higher aldehydes, higher concentration around 4.0–8.0 M was required. Based on these findings, the present aqueous reaction is indicated to occur in assembled particles. Recently, there have been many reports on the reactions in colloidal particles like micelles.<sup>7</sup> Such media were generally constructed by adding a surfactant to a reactant and a catalyst in water.<sup>8</sup> Catalysts themselves are sometimes designed to behave as surfactants.<sup>9</sup> In contrast to these reports, the present emulsion is formed by the

reaction intermediate imine **1** and its condensation product **2**, and the reaction proceeds in assembled sphere. The solvent-free process also proceeds under emulsified conditions. The water to form the emulsion may be generated by imine formation.

## Conclusion

The Lys-promoted reaction of aldehydes in water or under solvent-free conditions has furnished the corresponding condensation products in good yields. The reaction takes place in the emulsion media, which assemble both lipophilic aldehydes and hydrophilic Lys in the same specific micelles, resulting in the promotion of smooth reaction, in spite of an aqueous system. This process is environmentally benign and applicable to various aldehydes, especially to long-chain aldehydes. Therefore, the procedure would provide a practical synthetic method for the self-condensation of aldehydes.

## Experimental

Lys was purchased from Aldrich Chemical Co, and dried by heating (120 °C, for a few hours) *in vacuo*. Normal tap water was used for the reaction. Aldehydes were purchased and distilled under reduced pressure. Some aldehydes were prepared by usual 1,4-addition of thiol to crotonaldehyde (entry 8 in Table 1) and Swern oxidation of stearyl alcohol (entry 9).

### General procedure for the Lys-catalyzed condensation of aldehydes in water

An aldehyde (10 mmol) was added to a solution of Lys (1.0 mmol) in water (10 mL) under vigorous stirring, and the resulting emulsion was stirred for 2 h at room temperature. After addition of water and extraction with ether, the condensation product was isolated by chromatography or distillation. In order to facilitate the extraction, the emulsion was eliminated by adding NaCl to the aqueous layer in some cases.

### General procedure for the solvent-free condensation of aldehydes

To an aldehyde (10 mmol), Lys (1.0 mmol) was added and the mixture was vigorously stirred for 2 h at room temperature. The work-up and isolation procedure were the same as described above.

## Acknowledgements

We thank Venture Business Laboratory (VBL) and Institute for Cooperative Science (INCS), Ehime University for NMR and elemental analysis.

## Notes and references

- 1 P. T. Anastas and J. C. Warner, *Green Chemistry: Theory and Practice*, Oxford University Press, Oxford, 1998; R. Mestres, *Green Chem.*, 2004, **6**, 583; C.-J. Li and B. M. Trost, *Proc. Natl. Acad. Sci. U. S. A.*, 2008, **105**, 13197; R. A. Sheldon, *Chem. Commun.*, 2008, 3352.
- 2 A. T. Nielsen and W. J. Honlikan, *Org. React.*, 1968, **16**, 1.
- 3 M. Häussermann, *Helv. Chim. Acta*, 1951, **34**, 1482.
- 4 M. J. Astle and J. A. Zaslowsky, *Ind. Eng. Chem.*, 1952, **44**, 2867; R. D. Offenhauer and S. F. Nelsen, *J. Org. Chem.*, 1968, **33**, 775; T. Takahashi and H. O. Schmid, *Chem. Phys. Lipids*, 1969, **3**, 185; R. Mahrwald and H. Schick, *Synthesis*, 1990, 592; T. Ishikawa, E. Uedo, S. Okada and S. Saito, *Synlett*, 1999, 450; C. P. Mehnert, N. C. Dispenziere and R. A. Cook, *Chem. Commun.*, 2002, 1610; K. Shimizu, E. Hayashi, T. Inokuchi, T. Kodama, H. Hagiwara and Y. Kitayama, *Tetrahedron Lett.*, 2002, **43**, 9073; S. Kiyooka, H. Fujimoto, M. Mishima, S. Kobayashi, K. Md. Uddin and M. Fujio, *Tetrahedron Lett.*, 2003, **44**, 927; J. Hamaya, T. Suzuki, T. Hoshi, K. Shimizu, Y. Kitayama and H. Hagiwara, *Synlett*, 2003, 873; H. Hagiwara, J. Hamaya, T. Hoshi and C. Yokoyama, *Tetrahedron Lett.*, 2005, **46**, 393; A. Arnold, M. Markert and R. Mahrwald, *Synthesis*, 2006, 1099.
- 5 F. Robert, J. Héritier, J. Quiquerez, H. Simian and I. Blank, *J. Agric. Food Chem.*, 2004, **52**, 3525.
- 6 For a model study on aldolase action, kinetic experiments of the reaction of butanal (Lys/K<sub>2</sub>CO<sub>3</sub>/50 °C at pH around 9.0) have been carried out: A. A. Yasnikov, T. S. Boiko, N. V. Volkova and I. V. Mel'nichenko, *Biokhimiya*, 1966, **31**, 969, (*Biochem. USSR*, 1966, **31**, 841). For a model study on the investigation of the contents in atmospheric aerosols, the aldol condensation of acetaldehyde was demonstrated by the catalysis of amino acids such as Gly, Ala, Ser, Pro and Arg, but not Lys and Orn, in the presence of inorganic salts; B. Nozière, P. Dziedzic and A. Córdova, *Geophys. Res. Lett.*, 2007, **34**, L21812; B. Nozière and A. Córdova, *J. Phys. Chem. A*, 2008, **112**, 2827.
- 7 G. Oehme, E. Paetzold and R. Selke, *J. Mol. Catal.*, 1992, **71**, L1; S. Tascioglu, *Tetrahedron*, 1996, **52**, 11113; J. B. F. N. Engberts and M. J. Blandamer, *Chem. Commun.*, 2001, 1701; U. M. Lindström, *Chem. Rev.*, 2002, **102**, 2751; T. Dwars, E. Paetzold and G. Oehme, *Angew. Chem., Int. Ed.*, 2005, **44**, 7174.
- 8 B. H. Lipshutz and S. Ghorai, *Aldrichim. Acta*, 2008, **41**, 59.
- 9 K. Manabe, Y. Mori, T. Wakabayashi, S. Nagayama and S. Kobayashi, *J. Am. Chem. Soc.*, 2000, **122**, 7202; K. Manabe, X.-M. Sun and S. Kobayashi, *J. Am. Chem. Soc.*, 2001, **123**, 10101.

# Biomimetic silica encapsulation of enzymes for replacement of biocides in antifouling coatings

Jakob Broberg Kristensen,<sup>a,b</sup> Rikke Louise Meyer,<sup>a,c</sup> Charlotte Horsmans Poulsen,<sup>a,b</sup> Karsten Matthias Kragh,<sup>b</sup> Flemming Besenbacher<sup>a,d</sup> and Brian Søgaard Laursen<sup>\*b</sup>

Received 10th July 2009, Accepted 30th October 2009

First published as an Advance Article on the web 27th November 2009

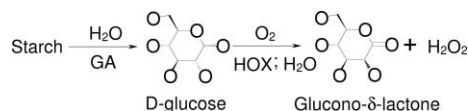
DOI: 10.1039/b913772f

Current antifouling technologies for ship hulls are based on metals such as cuprous oxide and co-biocides like zinc pyrithione. Due to the persistent adverse environmental effects of these biocides, enzyme-based antifouling paints are proposed as a bio-based, non-accumulating alternative. Here, a hydrogen peroxide-producing system composed of hexose oxidase (HOX, EC 1.1.3.5), glucoamylase (GA, EC 3.2.1.3) and starch is tested for the chemical and physical functionalities necessary for successful incorporation into a marine coating. The activity and stability of the enzymes in seawater was evaluated at different temperatures, and paint compatibility was assessed by measuring the distribution and activity of the enzymes incorporated into prototype coating formulations. We used a biomimetic encapsulation procedure for HOX through polyethylenimine-templated silica co-precipitation. The co-precipitation and formulation of a powder for mixing into a marine paint was performed in a one-step economical and gentle formulation process, in which silica co-precipitated HOX was combined with GA and starch to form the antifouling system. Silica co-precipitation significantly improved the stability and performance of the antifouling system in marine-like conditions. For example, encapsulation of HOX resulted in 46% higher activity at pH 8, and its stability in artificial seawater increased from retaining only 3.5% activity after 2 weeks to retaining 55% activity after 12 weeks. A coating comprising the full enzyme system released hydrogen peroxide at rates exceeding a target of 36 nmol cm<sup>-2</sup> d<sup>-1</sup> for 3 months in a laboratory assay, and had potential for prolonged action through incorporation in a self-polishing coating.

## Introduction

Marine biofouling, defined as the adhesion and growth of various microscopic and macroscopic organisms on surfaces immersed in the sea, has been a problem for marine constructions for centuries, including commercial and recreational crafts, oil platforms, bridges, *etc.* Over the years, coating systems have been developed to reduce biofouling, often by the use of metal-based biocides such as tributyltin (now effectively banned), cuprous oxide, and co-biocides (*e.g.* copper pyrithione or irgarol). Many of the current antifouling technologies are under suspicion of long-term harmful environmental effects due to bioaccumulation and ecotoxicity, which was also the reasoning behind the ban on tin-based marine coatings.<sup>1</sup> As an alternative to persistent, toxic compounds in existing antifouling

paints, enzyme-based antifouling technologies are emerging. Many of these aim at hydrolysing adhesives used for the settlement of marine organisms,<sup>2,3</sup> but Poulsen and Kragh<sup>4</sup> also proposed the use of a coupled enzyme system to produce a short-lived antifouling agent, hydrogen peroxide (Fig. 1). In this enzyme system, glucoamylase (GA, EC 3.2.1.3) releases glucose by hydrolysis of starch to provide a substrate for the enzyme hexose oxidase (HOX, EC 1.1.3.5), which catalyses oxidation of glucose, leading to hydrogen peroxide production.<sup>4</sup>



**Fig. 1** Reaction scheme for the coupled enzymatic production of hydrogen peroxide. GA: Glucoamylase hydrolyses starch to release D-glucose. HOX: Hexose oxidase oxidises D-glucose in the presence of water to glucono- $\delta$ -lactone with the concomitant production of hydrogen peroxide.

Hydrogen peroxide is hypothesized to deter fouling organisms due to its toxicity<sup>5,6</sup> and solubility in water. The hypothesis is partly based on the compound's function in nature: excretion of hydrogen peroxide upon wounding (the so-called oxidative burst) has been observed in various terrestrial and aquatic

<sup>a</sup>The Interdisciplinary Nanoscience Center (iNANO), Aarhus University, DK-8000, Aarhus C, Denmark

<sup>b</sup>Genencor–A Danisco Division, Danisco A/S, Edwin Rahrs Vej 38, DK-8220, Brabrand, Denmark.  
E-mail: brian.sogaard.laursen@danisco.com; Fax: +45 86 25 10 77;  
Tel: +45 89 43 53 27

<sup>c</sup>Department of Biological Sciences, Aarhus University, DK-8000, Aarhus C, Denmark

<sup>d</sup>Department of Physics and Astronomy, Aarhus University, DK-8000, Aarhus C, Denmark

plants, most likely to ward off herbivores and pathogens.<sup>7,8</sup> The compound is also widely used as a disinfectant.<sup>5,9,10</sup>

Hydrogen peroxide is naturally present in surface waters, and concentrations ranging from 0.12  $\mu\text{M}$  to 0.28  $\mu\text{M}$  are common,<sup>11</sup> although local coastal concentrations as high as 50  $\mu\text{M}$  have been reported.<sup>12</sup> Certain marine organisms have some adaptation to certain levels of hydrogen peroxide,<sup>13</sup> but the presence of locally elevated levels at a surface is expected to deter the settlement of fouling organisms.<sup>4</sup> Furthermore, hydrogen peroxide degrades rapidly in seawater,<sup>10</sup> and is a common intermediate in various natural metabolic processes, such as photosynthesis.<sup>13</sup> The hydrogen peroxide-producing enzyme system therefore has the potential to fulfil the requirements for an “ideal novel antifoulant” described by Rittschof *et al.*:<sup>14</sup> besides preventing fouling, such agents should have a minimal effect on the environment and human health, they should not be persistent or able to accumulate in living organisms, they should preferably be based on organics rather than metal, and, finally, they should have known environmental fates.

For an enzyme-based antifouling system to work in paints for marine applications, the properties of the enzymes and the coating design must fulfil the following criteria, as described by Olsen *et al.*:<sup>3</sup> the enzymes must be sufficiently robust towards solvents, mechanical stress, and other conditions present during the manufacture of the coating, and the coating technology must provide conditions that will not irreversibly inactivate the enzymes.<sup>3</sup> Conversely, the enzymes must not compromise other coating components or coating functionality. This can be achieved by mutually tailoring the choice of coating components and the physicochemical properties of the enzymes.<sup>3</sup> Meeting these requirements takes a concerted engineering effort for both coating and enzymes.

For application in the marine environment, the moderately alkaline pH (7.5 to 8.5)<sup>15</sup> and high salt concentration (approx. 3.5%), as well as the fluctuating water temperature (from freezing to 35 °C) as ships move from arctic to tropical regions, poses a particular problem to maintaining the activity of many enzymes; most enzymes are optimally active at neutral pH or lower.<sup>16</sup>

The lifespan of enzymes may exceed several months, but they cannot be expected to function adequately in paint for year-long sailing and harbouring periods. A method for gradually activating stored enzyme throughout the lifetime of a coating could provide a solution to this problem. Such gradual activation can be achieved by incorporating the enzyme system in a self-polishing marine paint, which is already the most widespread principle of current antifouling technologies.<sup>1</sup> A self-polishing composition consists of a very slowly dissolving binder matrix and a more soluble, but still quite slowly dissolving, pigment phase (*e.g.* less than 100  $\mu\text{m}$  coating thickness per year). The solubilisation of pigments results in a leached layer of hydrated pores separated by binder forming in the outer region of the coating as it gets thinner during the polishing action.<sup>1</sup> In this work, the enzyme system forms part of the coating pigment. The key is that hydration in the leached layer promotes enzyme activity, and a reserve of dormant enzyme is present in the dry layer. This ensures prolonged catalytic lifetime of the self-polishing coating as compared to a coating in which all enzymes are active from the time of application.

While it is essential that enzymes are active and stable, it is equally important that they can be retained in the coating for extended periods of time. The binder phase of a marine coating will typically behave as a relatively hydrophobic, solid matrix compared to the high-ionic strength seawater.<sup>1</sup> In order for an enzyme to resist immediate solubilisation in the hydrated layer of the coating, it must either possess some form of binding affinity for the coating matrix (*e.g.* high relative hydrophobicity) or be bound to something, which is retained in the matrix.

The present work explores the incorporation of GA and HOX in an antifouling coating for marine application. While studies on the antifouling effects of this enzyme system will be published elsewhere, we focus here on the challenges of incorporating the enzymes into a marine paint, while optimising enzyme activity, stability, and retention in the paint.

GA binds strongly to its insoluble substrate, starch.<sup>17</sup> This is expected to allow mechanical entrapment and retention of GA bound to starch granules inside a coating matrix. HOX, however, has no means of adsorbing to its substrate or other objects in its proximity.<sup>18,19</sup> Since this enzyme lacks the starch binding properties of GA, retention of HOX in the paint is a potential problem. Furthermore, both enzymes have pH optima much below the pH of seawater, and ensuring high enzyme activity in sea water poses another important challenge.

We propose to meet the challenges of securing retention and stability of HOX by physical encapsulation. In this study, we encapsulated HOX in silica by polycation-templated silica co-precipitation, which involves adding polyethylenimine (PEI) to an enzyme suspension. The enzyme and PEI will interact and form a polycation template for particle formation by silicate condensation when the enzyme/PEI is added to a sodium silicate solution.<sup>20</sup> Small primary particles of enzyme/PEI/silica biocomposite aggregate into secondary particles containing several enzyme molecules and further into water insoluble amorphous agglomerates that precipitate out of the aqueous solution, hence the term co-precipitation.<sup>20–22</sup> Other enzymes that have successfully been encapsulated by silica co-precipitation include  $\beta$ -glucosidase, glucose isomerase, lactase, lipase, acyltransferase and glucose oxidase.<sup>20</sup> The present work aims to determine the performance of the enzyme/PEI/silica biocomposite and compare it to the corresponding native enzyme in the conditions relevant to marine application, paint incorporation and in-paint performance.

## Experimental

All chemicals were obtained from Sigma-Aldrich unless otherwise stated. Glucoamylase from *Trichoderma reesei*<sup>23</sup> and HOX originating from *Chondrus crispus* and produced in *Hansenula polymorpha*<sup>24</sup> were products of Genencor–A Danisco Division, Denmark. Glucoamylase is 66 kDa, has a pI of 4.0, a pH optimum of 5.5, a temperature optimum of 70 °C, and an observed  $K_m$  of 0.61 mM for soluble starch (by glucose equivalents).<sup>25</sup> Hexose oxidase is a 126 kDa dimeric enzyme with a pI of approximately 4.7, and a  $K_m$  of 2.7 mM for D-glucose.<sup>19</sup> The GA was used in the form of a concentrate obtained from commercial production before the addition of preserving agents or other formulation additives, while HOX was purified as described by Rand *et al.* (2006).<sup>26</sup>

Artificial seawater (ASW) had the following composition: NaCl 24.0 g L<sup>-1</sup>, MgCl<sub>2</sub> 5.1 g L<sup>-1</sup>, Na<sub>2</sub>SO<sub>4</sub> 4.0 g L<sup>-1</sup>, CaCl<sub>2</sub> 1.1 g L<sup>-1</sup>, KCl 0.67 g L<sup>-1</sup>, KBr 0.098 g L<sup>-1</sup>, H<sub>3</sub>BO<sub>3</sub> 0.027 g L<sup>-1</sup>, SrCl<sub>2</sub> 0.024 g L<sup>-1</sup>, NaF 0.003 g L<sup>-1</sup>, NaHCO<sub>3</sub> 0.196 g L<sup>-1</sup>.<sup>27</sup>

### Enzyme activities and stability

Glucosylase activity (one U equals one μmol glucose equivalents per minute at 25 °C in 200 mM sodium acetate pH 4.5) was measured according to McCleary *et al.* (1991)<sup>28</sup> using an assay kit (Megazyme R-AMGR3), while HOX activity (one U equals 1 μmol hydrogen peroxide per minute at 25 °C in 100 mM potassium phosphate pH 6.3) was measured as described by Savary *et al.*<sup>29</sup>

Standard assay buffers for GA and HOX were replaced by artificial seawater (ASW)<sup>27</sup> when evaluating enzyme activity in marine conditions. To determine the stability of enzyme activity, enzymes were diluted 2000-fold in buffer (pH 6.3 for HOX, diluted activity 0.25 U mL<sup>-1</sup>; pH 4.5 for GA, diluted activity 28 U mL<sup>-1</sup>) or ASW and stored at 10, 20, 25, 30 and 35 °C for up to 12 weeks and aliquots taken out at regular intervals for activity measurements at 25 °C in standard assay buffers.

### Starch binding of glucosylase

GA was analysed for starch binding by dissolving the enzyme to activities of 46 and 92 U per g starch in a 20% cornstarch suspension (Cargill C\*gel 03401) in ASW buffered to pH 8.0 with 50 mM Tris-HCl at 40 °C. The enzyme–starch blend was allowed to incubate for 10 min at 40 °C before centrifuging at 10 000 g for 2 min and measuring the non-bound enzyme activity remaining in the supernatant. Samples were produced in 6 replicates. The degree of starch binding was calculated in relation to the same enzyme treated as described above but suspended in buffered ASW without added cornstarch.

### Spray-drying HOX, GA and starch, and preparation of enzyme-based coating

Cornstarch was spray-dried with GA or HOX or no enzyme using a Büchi Labortechnik Mini Spray Dryer B-191 (inlet 135 °C, outlet 80 °C with 0 °C water cooling at spray nozzle). The products of this process are referred to as “starch formulation” in the following.

Xylene-based rosin self-polishing coatings provided by Hempel A/S, Kongens Lyngby, Denmark were formulated with a volume composition of solids of 50% rosin, 10% polyvinyl-methylether (PVME), 10% coloured pigments and filler, and 30% starch formulation, in which HOX or GA were provided to end concentrations in the dry coating corresponding to nominal enzyme activities of 8.7 μmol min<sup>-1</sup> g<sup>-1</sup> (in pH 6.3 phosphate buffer and pH 4.5 sodium acetate buffer, respectively). The paints were applied to plastic films. Coupons of 1.5 cm<sup>2</sup> were cut out of the painted films. Painted coupons were submerged in ASW, and in-coating enzyme activity was monitored over a 6-week period. At intervals throughout the 6 weeks, H<sub>2</sub>O<sub>2</sub> production from the HOX-containing coating was measured as modified from Savary *et al.*<sup>29</sup> phosphate buffer (pH 6.3) with 55 mM glucose was stirred in 6-well microtiter plates using small magnets. The paint coupons were placed paint-side down,

floating on the buffer, and samples of 275 μL were extracted from the buffer at appropriate times and added to 25 μL of a 1 : 1 mixture of the 5 g L<sup>-1</sup> 2,2'-azino-bis(3-ethylbenzthiazoline-6-sulfonic acid) (ABTS) and 0.1 g L<sup>-1</sup> horseradish peroxidase (Sigma P-6782) in 96-well microtiter plates. The reagents were allowed to react in the wells for 2 min before OD<sub>405nm</sub> was measured and related to a standard curve for hydrogen peroxide concentration. The change in concentration between time points was used to calculate a release rate in μmol min<sup>-1</sup> cm<sup>-2</sup>. GA activity was measured as the glucose release rate, monitoring the glucose concentration with a YSI 2700 Select Biochemical Analyser with glucose analysis enzyme membrane using a glucose reference (YSI 2747). GA activity was also measured independently of in-coating substrate availability according to the method described by McCleary *et al.*,<sup>28</sup> which relies on the external supply of a synthetic substrate.

### Silica co-precipitation of HOX (SiHOX) and formulation of SiHOX coating

HOX was encapsulated in a silica matrix by polyamine-templated silica co-precipitation essentially as described by Chang *et al.*<sup>20</sup> a mixture of 1 mg mL<sup>-1</sup> HOX and 5 mg mL<sup>-1</sup> polyethylenimine (PEI; *M<sub>n</sub>* 60 kDa, *M<sub>w</sub>* 750 kDa, 50% w/v in H<sub>2</sub>O, Fluka P3143) was mixed in a ratio of 1 : 4 into pre-chilled 100 mM sodium silicate solution adjusted to pH 9.0 with phosphoric acid. Mixing was maintained for 30 min at 4 °C, before pH was adjusted to 6.3 to ensure stability of the enzymes through the rest of the process.

The co-precipitate was spray-dried (inlet 180 °C, outlet 85 °C with 0 °C water cooling at spray nozzle on a Büchi Mini Spray Dryer B-191) to form a particle powder (called “SiHOX”). For use in an antifouling coating, cornstarch and GA were added directly to the co-precipitate slurry immediately before spray drying, and inlet temperature of the spray dryer was reduced to 130 °C.

The assay from Savary *et al.*<sup>29</sup> was used with modified pH values for tests of pH optimum and pH tolerance as well as Michaelis–Menten enzyme kinetics based on specific activity of the enzyme. A Lowry method modified as described by Bickerstaff<sup>30</sup> was used for protein measurement in relation to the specific activity of SiHOX and HOX.

The particle size distribution of SiHOX was analysed by Mie light scattering in ethanol suspension using a Malvern Master-sizer magnet cell. Particles were imaged using low vacuum field emission scanning electron microscopy (FEI Nova nanoSEM 600) at an acceleration voltage of 5 kV, and by atomic force microscopy (JPK NanoWizard) in intermittent contact mode using a NSG01 cantilever (NT-MDT) at ambient conditions after dispersing the particles in ethanol and fixing them to a solid support by evaporation.

SiHOX-containing coatings were prepared by mixing a commercial Mille Light paint (Hempel A/S, Kongens Lyngby, Denmark) with 10% w/w (*i.e.* approx. 14% dry mass) starch formulations containing 0.21 mg g<sup>-1</sup> GA (pure protein) and 1.1 mg g<sup>-1</sup> SiHOX (corresponding to 0.13 mg g<sup>-1</sup> HOX (pure protein)).

The paints were coated on the inside of wells in 6-well microtiter plates that were immersed in 2.5 L ASW and stored

in the dark at 25 °C for 136 d, exchanging the ASW weekly. Hydrogen peroxide release was measured weekly as modified from Savary *et al.*:<sup>29</sup> 3 mL of 100 mM sodium phosphate buffer (pH 6.3) containing 4.0 µg mL<sup>-1</sup> horseradish peroxidase and 200 µg mL<sup>-1</sup> ABTS was added to each well resulting in 13 cm<sup>2</sup> coated area in contact with buffer. Aliquots of 200 µL from each well were extracted at 2, 5, 10, 30 and 60 min and placed in a 96-well microtiter plate for OD<sub>405nm</sub> measurement and hydrogen peroxide quantification as described above. Hydrogen peroxide release was measured in the presence and absence of 55 mM glucose. In the absence of glucose, the hydrogen peroxide release rate reflected the rate of starch hydrolysis by GA, as this was the rate-limiting step.

Cross-sections of coatings formulated with rosin, PVME, coloured pigments and filler as described above and with 30% dry weight cornstarch added were painted on plastic film and imaged using scanning electron microscopy (Nova nanoSEM 600). The plastic film was cut by cryo-sectioning through and the coating then broken to allow for topography of the resulting cross-section. Imaging the starch granules in the coating gave an illustration of the distribution of granular products of the size of starch and SiHOX in a rosin-based coating matrix.

## Results and discussion

### Enzyme activity and stability in sea water

GA and HOX activities were assayed in buffers with optimal conditions for the enzymes and in ASW to determine the level of activity in marine conditions compared to standard assay conditions, which are closer to the enzymes' activity optima (Table 1). GA activity was dramatically reduced in ASW, whereas HOX maintained almost full activity when transferred from pH 6.3 buffer to pH 8.2 ASW.

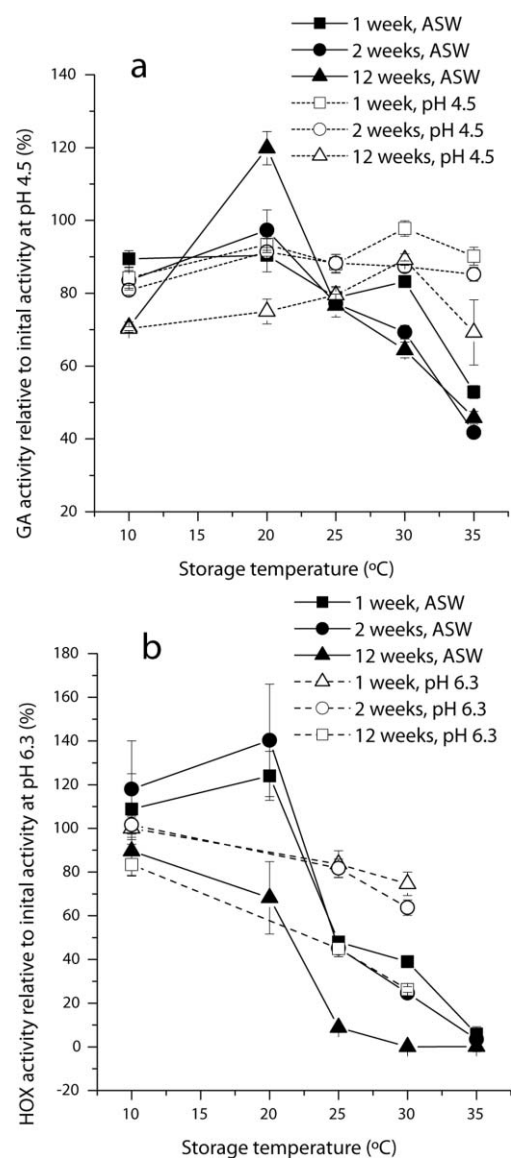
For the enzymes to be applicable to marine coatings, they must be able to maintain an adequate catalytic activity over an extended time-period in seawater. Storage for 12 weeks in pH 4.5 buffer conserved GA activity at a virtually constant level (Fig. 2a), while a moderate decrease in activity was observed after storage in ASW. The highest loss in activity was observed for enzyme stored in ASW at 35 °C. Here, activity dropped to 50% after 1 week, but remained around 40% relative activity throughout the following 11 weeks. GA stored in ASW at 30 °C and below did not lose activity over the 12 week period.

HOX generally lost more activity during storage compared to GA. This was the case both in ASW and in the pH 6.3 buffer

**Table 1** Enzyme activity in buffer at pH optimum and in ASW. The relative activity in ASW is calculated in percent of the activity in the corresponding buffer

Enzyme	Glucosylase	Hexose oxidase
pH 4.5	605.9 ± 8.3 U mL <sup>-1a</sup>	—
pH 6.3	—	343.1 ± 29.4 U g <sup>-1b</sup>
ASW, pH 8.2	3.54 ± 1.09 U mL <sup>-1</sup>	327.2 ± 33.7 U g <sup>-1</sup>
% Relative activity ASW/buffer	0.58 ± 0.18	95.4 ± 9.8

<sup>a</sup>) Buffer: pH 4.5 200mM sodium acetate. <sup>b</sup>) Buffer: pH 6.3 100mM potassium phosphate.



**Fig. 2** The stabilities of GA (a) and HOX (b) were tested by measuring activity at 25 °C/pH 4.5 (a) and 25 °C/pH 6.3 (b) in a series of time-points after storage as indicated. Storage temperatures were 10, 20, 25, 30, and 35 °C.

(Fig. 2b). Activity loss was most notable above 30 °C in buffer and above 25 °C in ASW. While the loss of enzyme activity when transferring from buffer to ASW was higher for GA than for HOX (Table 1), GA had a notably better long-term stability (Fig. 2). This was an indication that HOX would need stabilising to work adequately in marine environment, whereas native GA appeared better suited for marine applications.

### Activity and retention of enzymes in coating

The paint compatibility of HOX and GA was evaluated by testing enzyme activity over 6 weeks after incorporation into model coatings formulated with rosin, PVME, coloured pigments, filler and 30% starch formulation (Table 2). The coating containing HOX and starch had an initial nominal activity in pH 6.3 buffer of 8.7 U per g coating dry weight. The coating containing GA and starch had an initial nominal activity in pH 4.5 buffer of

**Table 2** In-paint activity of HOX and GA. The coatings contained either GA and starch or HOX and starch; n.d. indicates non-detectable activity, while n.a. indicates that measurements were not performed

Day	GA activity in-paint substrate $\mu\text{mol cm}^{-2} \text{d}^{-1}$	GA activity external substrate, $\mu\text{mol cm}^{-2} \text{d}^{-1}$	HOX activity external substrate $\mu\text{mol cm}^{-2} \text{d}^{-1}$
0	15.4	29.0	112
8	0.20	21.1	2.20
15	0.18	28.4	n.d.
22	0.12	28.4	n.d.
43	n.a.	13.7	n.d.

8.7 U per g coating dry weight. A control coating formulated with starch but without enzymes, and this coating showed no activity (data not shown).

GA activity measured in the presence of unlimited externally-supplied substrate was constant for the first three weeks (average  $26.2 \pm 3.8 \mu\text{mol}$  glucose equivalents per  $\text{cm}^2$  per day), but had decreased by approximately 50% after 6 weeks. When GA was dependent on starch in the coating as a substrate, the activity dropped by almost 99% in the first week, and then remained almost constant. The high initial glucose release rate may not have been linked to GA activity, but due to free glucose present in the GA/starch formulation due to starch hydrolysis by GA during the spray drying process. HOX activity measured in the presence of unlimited externally-supplied substrate also dropped by 98% in the first week, and after two weeks no activity was observed. This loss of activity may have been the result of enzyme leaching out of the coating or enzyme inactivation.

Anchoring of enzymes in the coating matrix is highly important to prevent leaching of enzymes, thereby securing the long-term efficacy of an enzyme-based coating. In order to test if the starch binding domain of GA would aid retention, we evaluated the starch binding capacity of GA in a solution system, *i.e.* outside of a coating matrix. Glucoamylase was mixed with excess starch, and unbound GA was subsequently separated from starch-bound GA by centrifugation. Starch binding of an initial GA activity of  $46 \mu\text{mol min}^{-1} \text{g}^{-1}$  in  $0.2 \text{ g mL}^{-1}$  starch was highest at pH 4.5, where  $77.6 \pm 3.7\%$  of the GA activity was bound to starch, based on the synthetic substrate analysis described by McCleary.<sup>28</sup> Conversely, the binding was reduced to  $35.1 \pm 9.0\%$  bound activity in pH 8.0 Tris-buffered ASW. There was no statistically significant difference between starch binding, when increasing the GA concentration (activity) from 46 to  $92 \mu\text{mol min}^{-1}$  per g starch (data not shown). Given the length of the 10-minute incubation to obtain binding between GA and starch, initial activity loss was assessed to be negligible. The strong binding of GA to starch suggests that starch granules may act as anchors promoting the in-paint retention of GA, since their size and low solubility keep them trapped inside the binder matrix while being hydrolysed by the enzyme. A similar binding of HOX to an insoluble, retainable substrate did not occur, and it was concluded that practical application of the enzymes in a coating would call for a modification of HOX.

#### Silica co-precipitation of HOX (SiHOX) for improved stability and activity

The activity and stability of GA was promising for application in a marine coating, but HOX had obvious shortcomings in

**Table 3** Comparison of enzyme kinetics for HOX and SiHOX

Enzyme	$v_{\text{max}}/\mu\text{mol min}^{-1}$ per g protein	$K_{\text{M}}/\text{mM}$
HOX	$53 \pm 6$	$3.2 \pm 0.5$
SiHOX	$3.1 \pm 0.7$	$2.9 \pm 0.9$

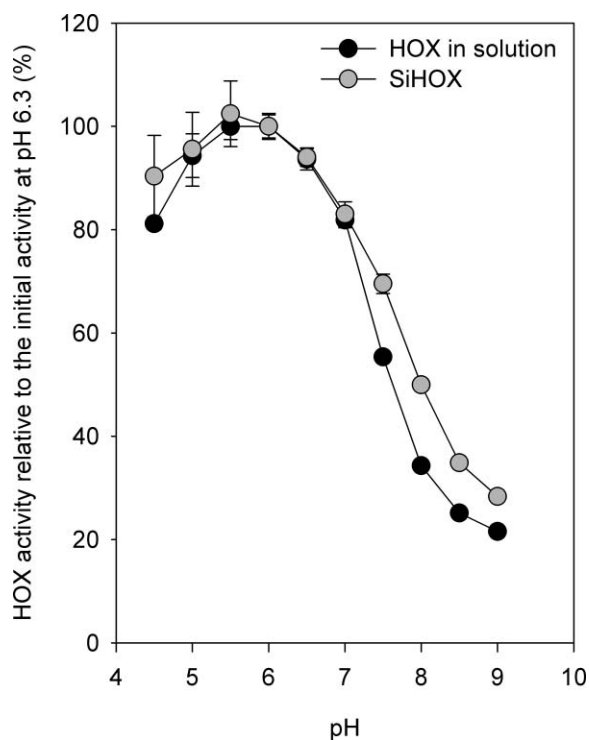
terms of stability and possibly leaching. A silica co-precipitation process, as described in the introduction, was hypothesised to increase enzyme retention in the marine coating by capturing the enzyme in solid aggregates, which would provide mechanical retention due to their large size and lack of solubility. It may furthermore increase enzyme stability, which may be related to higher structural stability, for instance due to reduced unfolding in denaturing media as has been seen for other co-precipitation immobilized enzymes.<sup>20</sup>

Silica co-precipitation is a biomimetic protocol inspired by the polycation-templated silicification of diatom and sponge exoskeletons, which has the advantage of being performed under mild conditions in easily manageable and tuneable steps. The size of the resulting insoluble particles may be controlled by *e.g.* the enzyme/template/silicate ratio, stirring, temperature and reaction time. After optimisation (data not shown) the co-precipitation process applied in this study had a high activity yield with 60% of the initial HOX enzyme activity found in the solid SiHOX fraction after co-precipitation, whereas no activity was detectable in the co-precipitate supernatant. The activity yield was equivalent to the best yields in previous reports relating to the process.<sup>20</sup> After spray-drying, the recovery was 13% of the initial enzyme activity.

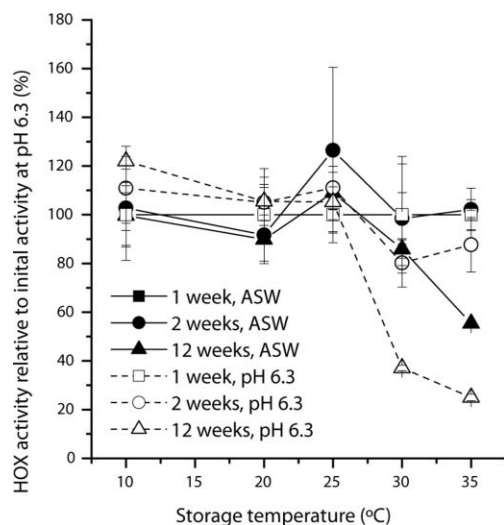
The effect of silica co-precipitation on enzyme kinetics in pH 6.3 buffer was evaluated. SiHOX contained 0.11 mg protein per mg. While  $K_{\text{M}}$  of HOX and SiHOX were similar,  $v_{\text{max}}$  was reduced 17-fold after silica co-precipitation (Table 3). In other words, while the catalytic rate ( $v_{\text{max}}$ ) of SiHOX was significantly lower than HOX in Michaelis–Menten kinetics, SiHOX had the same substrate affinity ( $K_{\text{M}}$ ), which would be consistent with a reduction in enzyme performance due to non-competitive inhibition (lower  $v_{\text{max}}$ , constant  $K_{\text{M}}$ ) of HOX in the SiHOX formulation. This could be due to a reduction of available enzyme, *e.g.* by steric hindrance.

The pH-dependent activity profile for SiHOX was compared to HOX in phosphate buffer adjusted to pH 4.5–9.0 (Fig. 3). Expressed as the activity relative to the activity at pH 6.3, SiHOX performed 25% better than HOX at pH 7.5, 46% better at pH 8.0, 39% better at pH 8.5 and 31% better at pH 9.0. The loss of activity at pH values relevant for marine applications was thus substantially less for SiHOX compared to HOX. Comparing these data with measurements of HOX activity in ASW, it should be noted that HOX did not exhibit a similar loss of activity in ASW (pH 8.2) as in the pH 8.0 phosphate buffer used here (Table 1). This could be due to the high salt concentration in ASW. Comparison of the temperature stability of HOX and SiHOX between 25 and 70 °C showed no effect of Si-precipitation on temperature stability (data not shown).

In order to better describe the applicability of SiHOX for marine coatings where long-term stability is crucial, the activity of SiHOX suspended in ASW and pH 6.3 buffer was monitored for 12 weeks (Fig. 4). The stability of HOX in ASW was markedly



**Fig. 3** Comparison of SiHOX and HOX activity at pH in the range 4.5-9.0, relative to the activity at pH 6.3. Compared to HOX, SiHOX retained its relative activity at a higher level when tested in pH above 7.5.



**Fig. 4** The stability of SiHOX was tested by measuring activity at 25 °C/pH 4.5 in a series of time-points after storage as indicated. Storage temperatures were 10, 20, 25, 30, and 35 °C.

improved by silica co-precipitation. The activity of SiHOX did not change over 12 weeks when stored in ASW at temperatures between 10 and 30 °C, or in pH 6.3 buffer at temperatures from 10 to 25 °C. However, up to 75% activity loss occurred at higher temperatures. In comparison, HOX lost activity at most temperatures when stored in ASW (Fig. 2b). It should also be noted that while transfer from pH 6.3 buffer to ASW negatively affected the stability of native HOX (Fig. 2b), the opposite was the case for SiHOX (Fig. 4). This difference could be related

to a stabilising effect; the salt in ASW enhancing the structural stability of the silica-PEI biocomposite. Investigations into the interactions between the silica-PEI matrix and dissolved salts in the medium could be the subject of further work in this field.

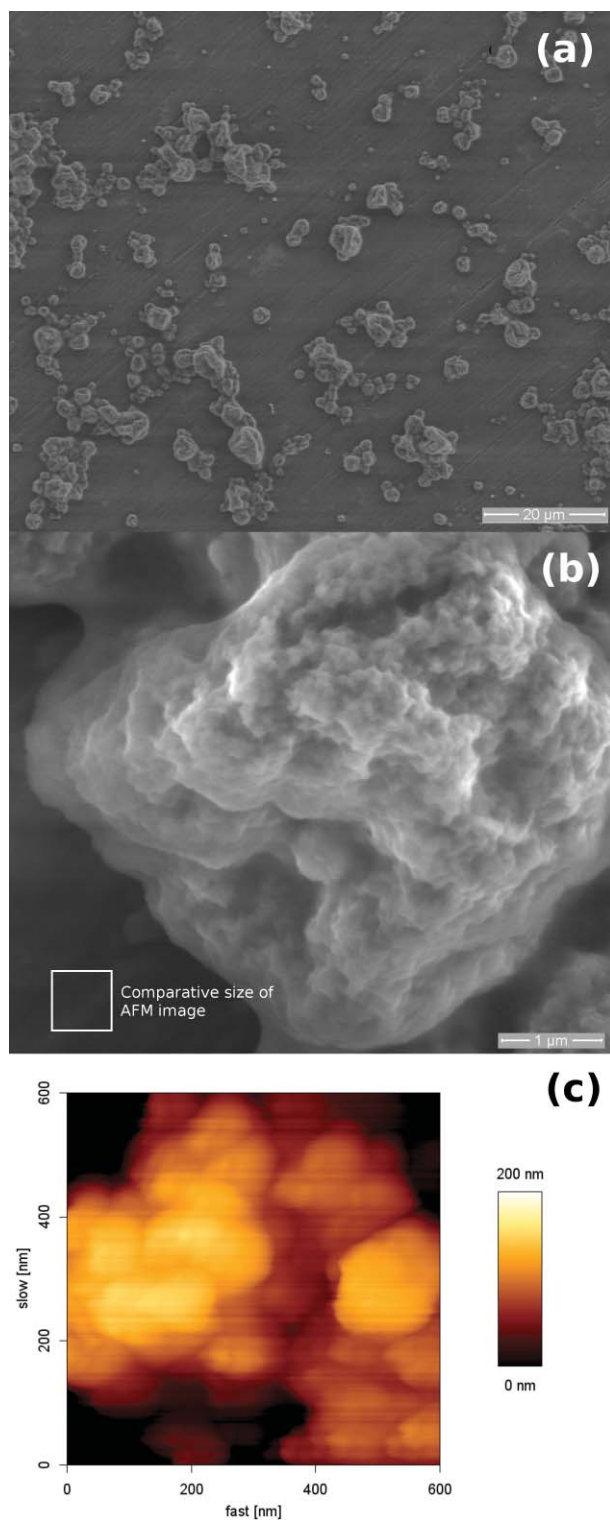
### A SiHOX-based coating

The improvements in stability at high pH and in ASW that silica co-precipitation had brought to HOX were promising for the applicability of SiHOX in marine coatings. With the expectation that co-precipitation would also improve retention, we evaluated the performance and compatibility of SiHOX with GA and starch in experimental coatings.

From a coating technology point-of-view, the particle size of paint constituents is essential, as it affects the polishing and hydrodynamic properties of the coated hull. If particles in the paint are too large, the coating can become rough and self-polishing becomes uncontrolled. The physical dimensions and structure of SiHOX particles were therefore analysed quantitatively by dynamic light scattering and qualitatively by high-resolution microscopy. The particle size distribution showed a peak at 6  $\mu\text{m}$  diameter and 95% of the colloidal volume had particle sizes in the range of 0.7–14  $\mu\text{m}$  (data not shown). The particles were irregular, spheroid structures, which appeared to have a rough surface (Fig. 5a and b). High resolution atomic force microscopy revealed that spheroid structures were aggregates of sub-100 nm particles (Fig. 5c). A SiHOX particle may therefore be an assembly of nanoparticles containing single HOX molecules encapsulated in the PEI-silica co-precipitate. The particle size of SiHOX was in accordance with the theoretical size expected to result from the co-precipitation mechanism.<sup>20,21</sup> It was similar to the 15  $\mu\text{m}$  starch granules and was therefore not expected to alter the surface structure or polishing properties of the paint.

In order to incorporate SiHOX, GA and starch into a coating, the enzyme system had to be formulated as a dry powder. This was done by using the aqueous suspension of SiHOX after co-precipitation as the solvent for starch and GA in a “one-step” spray drying process producing a high-yield powder blend ready for mixing into a coating formulation. This rapid process used mild conditions and standard enzyme formulation equipment, which would allow for simple up-scaling and implementation in modern processing plants. The first model coating was formulated with starch and contained large, spherical starch granules homogeneously distributed throughout the coating (data not shown), which led to the conclusion that the constituents of the enzyme-based antifouling system could be adequately dispersed in the coating matrix. A new coating was formulated by mixing the spray-dried SiHOX–GA–starch formulation into commercial xylene-based paint (Mille Light) as 10% mass fraction of the wet formulation. The enzyme activities in the SiHOX–GA–starch formulation corresponded to 0.21 mg GA protein per g of dry coating and 1.1 mg SiHOX per g (*i.e.* 0.13 mg HOX protein per g) (data not shown). This coating maintained a high level of hydrogen peroxide release when immersed in ASW in static conditions where polishing did not occur, and the release rate decreased gradually over the first 70 d, after which it levelled out (Fig. 6). Measurement of the exact concentration of hydrogen peroxide in the surface boundary layer would be highly relevant to understanding the

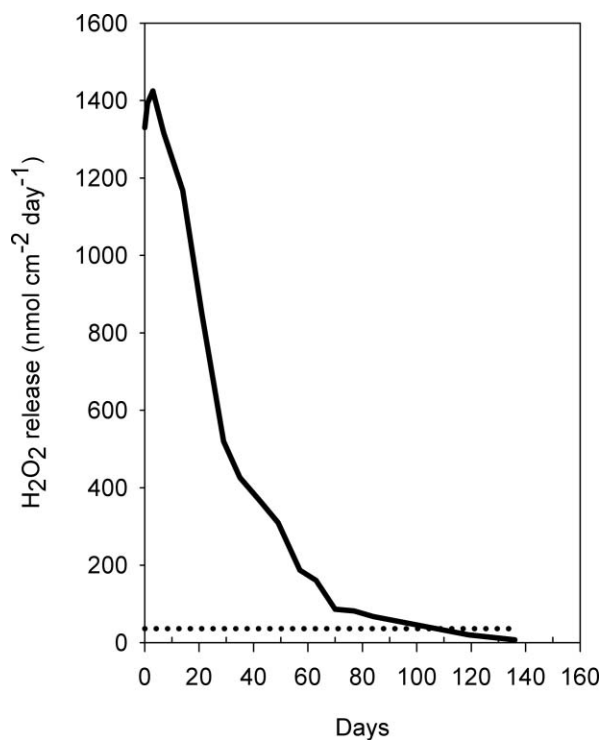




**Fig. 5** Scanning electron microscopy (a + b) and atomic force microscopy (c) of SiHOX particles.

antifouling potential of the coating. However, this was not measured or calculated in the present study, as the boundary layer hydrodynamics were not known.

The key question in evaluating the antifouling potential of the paint is the hydrogen peroxide release rate required to obtain



**Fig. 6** The release rate of hydrogen peroxide from a coating comprising SiHOX, GA and starch. The release was measured over a 136-day period of static immersion in ASW. The dotted line indicates the release rate of 36 nmol cm<sup>-2</sup> day<sup>-1</sup> reported to show antifouling activity<sup>31</sup> (see text for details).

an antifouling effect. A target hydrogen peroxide release rate of 36 nmol cm<sup>-2</sup> d<sup>-1</sup> has been proposed in a patent by Cape Cod Research,<sup>31</sup> who tested the antifouling properties of paint producing hydrogen peroxide by photocatalysis. The release rate of 36 nmol cm<sup>-2</sup> d<sup>-1</sup> was determined by titration with potassium permanganate solution at 0, 48, 72 and 200 h<sup>31</sup> for a coating composition which was observed to prevent biofouling in the Atlantic ocean in a one-year field trial. Furthermore, Nippon Paint Co. has detailed a H<sub>2</sub>O<sub>2</sub> release rate with antifouling activity of 21 nmol cm<sup>-2</sup> d<sup>-1</sup>.<sup>32</sup> The hydrogen peroxide release rate of our coating exceeded 36 nmol cm<sup>-2</sup> d<sup>-1</sup> for approximately 100 d (Fig. 6). Without significant self-polishing, the active enzymes can thus be expected to have a lifespan of 3 months, but a self-polishing coating will continually expose new enzyme and starch in the hydrated layer, and potentially prolong the period of high hydrogen peroxide release.

Detailed knowledge of solubility and the dissolution rate of pigments are necessary to model the full self-polishing behaviour of marine coatings,<sup>33</sup> but the longevity of a coating can be estimated from its dimensions: a paint film as used in the present trials is 300–500 μm thick<sup>34</sup> and the leached/hydrated layer is typically 5–15 μm, resulting in a total film thickness between 20 and 100× that of the leached layer. A 3 month lifespan of hydrated enzyme in the hydrated layer with 20- to 100-fold turnover corresponds to a potential for enzyme activity at the desired level for 5–25 years, but the availability of starch substrate will be limiting. Assuming complete conversion of starch, a 300 μm coating with 30% dry mass of starch will

yield an average of 228 nmol cm<sup>-2</sup> d<sup>-1</sup> for full depletion within 1 year, 76 nmol cm<sup>-2</sup> d<sup>-1</sup> for 3 years or 46 nmol cm<sup>-2</sup> d<sup>-1</sup> for 5 years.

In summary, the activity, stability and retention of enzyme in the coatings formulated in this study was sufficient to provide hydrogen peroxide release from a coating for more than 3 months, at a rate proposed (on the basis of relatively few trials<sup>31,32</sup>) to be sufficient to prevent marine biofouling. However, the effective release of hydrogen peroxide has yet to be demonstrated for the broad diversity in biofouling, and its effect will depend largely on the type of fouling organisms as well as environmental and surface phenomena. Notably, some photosynthetic organisms, including several species of macroalgae, can, in their mature state, protect themselves from the oxidative effect of hydrogen peroxide.<sup>13</sup> This evidence corroborates the need for extensive investigations of the effect of hydrogen peroxide released from immersed surfaces on the settlement and adhesion of variety of biofouling organisms in various environments.

## Conclusions

This study presents an enzyme-based hydrogen peroxide-producing coating with potential antifouling properties. The system comprising HOX, GA and starch needs a certain level of stability and compatibility with common constituents of marine coatings. We identified the stability and retention of HOX in a coating as the main challenge for obtaining prolonged hydrogen peroxide production in seawater. To meet this challenge, HOX was encapsulated by polyethylenimine-templated silica co-precipitation, in a one-step spray drying formulation protocol, allowing rapid, safe and economical production of a powder containing SiHOX, GA and starch. This powder could be readily mixed with solvent and coating components to form an antifouling paint for ships or other structures. The resulting coating showed convincing release of hydrogen peroxide over a three month period without significant aid of polishing to renew the active enzymes, which promises strong performance in continually releasing hydrogen peroxide from a self-polishing coating.

## Acknowledgements

This work was partly funded as an industrial research project under the Danish Industrial PhD programme. Funding was provided the Danish Ministry of Science, Technology and Innovation jointly with the company. Additional funding was obtained through the ProSURF grant from the Danish National Advanced Technology Foundation.

The authors wish to express their gratitude to Charlotte A. Bak of Genencor, Brabrand, Denmark, for her contribution in the lab; to Jacques Chevallier of Aarhus University, Denmark, for his SEM expertise; and to Stefan M. Olsen and Lars T. Pedersen of Hempel A/S, Kongens Lyngby, Denmark, for their collaboration and for providing the paint materials used in this article.

## References

- 1 D. Yebra, S. Kiil and K. Dam-Johansen, *Prog. Org. Coat.*, 2004, **50**, 75–104.
- 2 J. B. Kristensen, R. L. Meyer, B. S. Laursen, S. Shipovskov, F. Besenbacher and C. H. Poulsen, *Biotechnol. Adv.*, 2008, **26**, 471–481.
- 3 S. M. Olsen, L. T. Pedersen, M. H. Laursen, S. Kiil and K. Dam-Johansen, *Biofouling*, 2007, **23**, 369–383.
- 4 C. H. Poulsen and K. M. Kragh, *US Pat. app.* 2002/106361, 2002.
- 5 S. Jacobi, Hydrogen peroxide. In *Ullmann's Encyclopedia of Industrial Chemistry*. Wiley-VCH Verlag, Weinheim, 2002.
- 6 J. Thomassen, In: *Pathogens of wild and farmed fish: sea lice*. G. Boxshall and D. DeFaye, (eds.), pp. 290–295. Ellis Horwood Limited, Chichester, 1993.
- 7 M. Orozco-Cardenas and C. A. Ryan, *Proceedings of the National Academy of Science USA*, 1999, **96**, 6553–6557.
- 8 K. Bouarab, P. Potin, F. Weinberger, J. Correa and B. Kloareg, *J. Appl. Phycol.*, 2001, **13**, 185–193.
- 9 ECETOC. Joint Assessments of Commodity Chemicals No. 22, Hydrogen Peroxide. Brussels, ECETOC - European Center of Ecotoxicology and Toxicology of Chemicals, 1993.
- 10 W. Eul, A. Moeller, U. Stewen, Hydrogen peroxide. In: *Kirk-Othmer Encyclopedia of Chemical Technology*. W. Hess (ed.), vol. 13. John Wiley & Sons, New York, 2002.
- 11 R. G. Petasne and R. G. Zika, *Mar. Chem.*, 1997, **56**, 215–225.
- 12 D. M. McMaster, S. M. Bennett, Y. Tang, J. A. Finlay, G. L. Kowalke, B. Nedved, F. V. Bright, M. E. Callow, J. A. Callow, D. E. Wendt, M. G. Hadfield and M. R. Detty, *Biofouling*, 2009, **25**, 21–23.
- 13 A. L. Dummermuth, U. Karsten, K. M. Fisch, G. M. König and C. Wiencke, *J. Exp. Mar. Biol. Ecol.*, 2003, **289**, 103–121.
- 14 D. Rittschof, C.-H. Lai, L.-M. Kok and S.-M. Teo, *Biofouling*, 2003, **19**, 207–212.
- 15 E. Prenesti, E. Ferrara, S. Berto, P. Fisicaro and P. G. Daniele, *Anal. Bioanal. Chem.*, 2007, **388**, 1877–1883.
- 16 W. Aehle, *Enzymes in industry - Production and applications*, ed. 2. Wiley-VCH, Weinheim, 2003.
- 17 J. R. Daniel, R. L. Whistler, H. Röper, Starch. In *Ullman's Encyclopedia of Industrial Chemistry*. M. Bohnet (ed.). Wiley-VCH Verlag, Weinheim, 2002.
- 18 B. Groen, S. De Vries and J. Duine, *Eur. J. Biochem.*, 1997, **244**, 858–861.
- 19 C. H. Poulsen and P. Høstrup, *Cereal Chem.*, 1998, **75**, 51–57.
- 20 C. Chang, D. E. Ward, B. Kelemen, J. C. McAuliffe, In: *Biomolecular catalysis: Nanoscale science and technology*. J. Kim, S. Kim and P. Wang, (eds.), pp. 183–198. Oxford University Press, New York, 2008.
- 21 J. C. McAuliffe, W. C. Smith, D. E. Ward, C. Chang, K. Sanford and T. H. Lane, Washington, DC, American Chemical Society. Nanoscale science and technology in biomolecular catalysis, 230th ACS National Meeting, 2005.
- 22 T. Coradin and J. Livage, *Colloids Surf., B*, 2001, **21**, 329–336.
- 23 N. Dunn-Coleman, P. Neefe-Kruithof, C. E. Pilgrim, D. E. Ward and P. Van Solingen. *WIPO Pat. app.* 2006/060062, 2006.
- 24 M. Cook and H. Thygesen, *Food Chem. Toxicol.*, 2003, **41**, 523–529.
- 25 R. Fagerström and N. Kalkkinen, *Biotechnol. Appl. Biochem.*, 1995, **21**, 223–231.
- 26 T. Rand, K. B. Qvist, C. P. Walter and C. H. Poulsen, *FEBS J.*, 2006, **273**, 2693–2703.
- 27 K. Grasshof, K. Kremling, M. Ehrhardt, *Methods of seawater analysis*. Ed. 3. Wiley-VCH Verlag, Weinheim, 1999.
- 28 B. V. McCleary, F. Bouhet and H. Driguez, *Biotechnol. Tech.*, 1991, **5**, 255–258.
- 29 B. Savary, K. Hicks and J. O'Connor, *Enzyme Microb. Technol.*, 2001, **29**, 42–51.
- 30 G. F. Bickerstaff, *Methods in Biotechnology, Vol. 1: Immobilization of enzymes and cells*. Humana Press, Totowa, 1997.
- 31 R. S. Morris and M. A. Walsh, *US Pat.* 6 063 849, 2000.
- 32 R. Hamade and N. Yamamori, *US Pat.* 6 150 146, 2000.
- 33 S. Kiil, C. Weinell, M. Stanley Pedersen and K. Dam-Johansen, *Ind. Eng. Chem. Res.*, 2001, **40**, 3906–3920.
- 34 S. M. Olsen, Personal communication. 2007.

# One-step, size-controlled synthesis of gold nanoparticles at room temperature using plant tannin†

Xin Huang,<sup>a</sup> Hao Wu,<sup>b</sup> Xuepin Liao<sup>\*a</sup> and Bi Shi<sup>a,b</sup>

Received 3rd September 2009, Accepted 6th October 2009

First published as an Advance Article on the web 11th November 2009

DOI: 10.1039/b918176h

Bayberry tannin (BT), a natural plant polyphenol, was used for one-step synthesis of gold nanoparticles (AuNPs) in aqueous solution at room temperature. During the synthetic process, BT simultaneously serves as a reducing agent and stabilizing agent, while no additional reagent (surfactant, template, and capping agent) or treatment (heat and photo-irradiation) is needed. The particle diameter and size distribution of BT-stabilized AuNPs (BT-AuNPs) can be facily controlled by varying the concentration of BT, and the particle size of BT-AuNPs is as small as  $1.8 \pm 0.3$  nm when the BT concentration was  $800 \text{ mg L}^{-1}$ . Furthermore, this green approach for the auto-reduction synthesis of AuNPs can be completed in several minutes and exhibits high reproducibility, which shows great potential for practical applications.

## Introduction

Gold nanoparticles (AuNPs) ranging from 2.0 to 50.0 nm in diameter have attracted tremendous attention due to their unique optical, electronic, magnetic and catalytic properties.<sup>1–3</sup> Nowadays AuNP-based nanotechnology is becoming more and more important in modern science, and a wide range of applications of AuNPs have been explored both in chemical and biological research.<sup>4</sup> Depending on their size, shape, and degree of aggregation, AuNPs appear red, blue and other colors, and therefore, AuNPs have been explored as probes for highly sensitive colorimetric detection of heavy metal ions.<sup>5</sup> A particular attraction is the use of functional AuNPs in biological and pharmaceutical fields, such as drug delivery,<sup>6</sup> photothermal ablation therapy,<sup>7</sup> and molecular diagnostics,<sup>8</sup> because AuNPs have excellent biological biocompatibility and low toxicity. There are already many methods for the preparation of AuNPs, but most are either complex, time-consuming, or require strict synthetic conditions.<sup>9–12</sup> From the viewpoint of practical applications, it would be of great value to find a convenient method for the preparation of uniform AuNPs with small particle sizes (2.0–30.0 nm).

The “bottom-up” method of wet chemical nanoparticle preparation is the most commonly used and by far the simplest method for the synthesis of AuNPs.<sup>13,14</sup> Gold precursors (salts or organic complexes) in aqueous or organic media are reduced to zerovalent gold atoms by reducing agent (sodium citrate and sodium borohydride, *etc.*), and the gold atoms collide with each

other to form AuNPs. Simultaneously, the formed AuNPs are stabilized with stabilizing agents to prevent further agglomeration. In this way, AuNPs are separated from each other, and their particle size can be controlled by varying the concentration of stabilizing agent.<sup>13,15,16</sup> In recent studies, it has been shown that by using linear or hyperbranched reducible polymers it is possible to synthesize AuNPs in an environmentally-friendly way without the use of reducing agent and/or surfactant which is much more environmentally benign compared with the conventional “bottom-up” method.<sup>17,18</sup> According to these synthetic procedures, the AuNPs can be easily prepared just by mixing gold precursor and polymer together. But they are often time-consuming, and sometimes photo-irradiation is required.<sup>19–21</sup> Additionally, AuNPs with small particle sizes (2.0–10.0 nm) are difficult to obtain from this auto-reduction process and a slow auto-reduction process inevitably leads to difficult control over the particle size and size distribution.<sup>22</sup> These obstacles have to be overcome before the routine use of such auto-reduction synthesis is possible.

Herein, we report a one-step, and size-controlled fabrication of tannin-stabilized AuNPs in aqueous solution at room temperature. Condensed tannins, which are widely distributed in plants, are soluble polyphenols with multifunctional groups. The general characteristics of condensed tannins are that they are able to chelate with many kinds of metal ions ( $\text{Cu}^{2+}$ ,  $\text{Pt}^{4+}$  and  $\text{Pd}^{2+}$ , *etc.*) through their dense *ortho*-phenolic hydroxyls, and serve as reducing agents to scavenge free radicals.<sup>23,24</sup> The molecular backbone of condensed tannins mainly consists of rigid aromatic rings, which could prevent particle aggregation due to their steric hindrance. All these properties of condensed tannins imply that they could be used as ideal materials for the preparation of stabilized AuNPs. In this study, AuNPs colloids with good morphology and dispersion can facily be obtained by mixing  $\text{HAuCl}_4$  with bayberry tannin (BT, a typical condensed tannin) solution where BT serves as a reducing agent as well as a stabilizing agent, and no additional reagents or treatment are needed. This approach therefore provides a

<sup>a</sup>Department of Biomass Chemistry and Engineering, Sichuan University, Chengdu, P. R. China. E-mail: xpliao@scu.edu.cn; Fax: +86-28-85400356; Tel: +86-28-85400382

<sup>b</sup>National Engineering Laboratory for Clean Technology of Leather Manufacture, Sichuan University, Chengdu, P. R. China. E-mail: sibtannin@vip.163.com

† Electronic supplementary information (ESI) available: XRD pattern of  $\text{BT}_{800}$ -AuNPs and XPS Au 4f spectra of  $\text{BT}_{800}$ -AuNPs. See DOI: 10.1039/b918176h

new strategy for the environmentally benign and size-controlled synthesis of AuNPs.

## Experimental

All chemicals were purchased from commercial suppliers and used without further purification.  $\text{HAuCl}_4 \cdot 3\text{H}_2\text{O}$  was dissolved in deionized water to get a  $10.0 \text{ mmol L}^{-1} \text{ Au}^{3+}$  solution. Then  $2.0 \text{ mL}$  of  $\text{Au}^{3+}$  solution was added drop-wise into  $48.0 \text{ mL}$  of BT solution at different concentrations to prepare a series of BT-stabilized AuNPs ( $\text{BT}_x\text{-AuNPs}$ ) colloids where  $x$  is the concentration of BT varying from  $25.0$  to  $800.0 \text{ mg L}^{-1}$  and the concentration of  $\text{Au}^{3+}$  was fixed at  $0.4 \text{ mmol L}^{-1}$ . UV-vis measurements of the colloids were carried out immediately after  $\text{HAuCl}_4$  and BT were mixed together. The FTIR spectrum of samples was analyzed using a FTIR-7600 instrument. TEM images of  $\text{BT}_x\text{-AuNPs}$  colloids were taken on a FEI-Tecna G2 Transmission Electron Microscope (TEM). Wide-angle X-ray diffraction (XRD) patterns of the samples were recorded by an X'Pert PRO MPD diffractometer (PW3040/60) with  $\text{Cu-K}\alpha$  radiation. X-ray photoelectron spectra (XPS) of the samples were recorded by a Shimadzu ESCA-850.

## Results and discussion

BT, the flavan-3-ols and flavan-3-ols gallate, is a typical kind of condensed tannin and its molecular structure is shown in Fig. 1a. It can be observed that BT mainly consists of polymerized flavan-3-ols, and a large number of multiple phenolic hydroxyls are located at its B-rings. These phenolic hydroxyls are able to chelate with metal ions forming five-membered chelate rings (Fig. 1b), and can also be easily oxidized to the corresponding benzoquinones (Fig. 1c), when exposed in air or if they come into contact with electrophilic ions,<sup>25</sup> which suggests that BT can be used as an effective reducing agent. On the other hand,  $\text{Au}^{3+}$  has high oxidation-reduction potential, which suggests that  $\text{Au}(\text{III})$  ions may play a role as oxidants when they come into contact with BT.<sup>26</sup> Thus we believe that BT could serve as a reducing agent for the reduction of  $\text{Au}^{3+}$  to form AuNPs.

In the present work,  $\text{BT}_x\text{-AuNPs}$  colloids were facilely obtained *via* the addition of  $\text{Au}^{3+}$  into BT solution. After they were mixed together for about  $5.0 \text{ min}$ , the mixture became red (insets in Fig. 2b), signifying the formation of AuNPs. The comparison of the UV-vis spectra of  $\text{HAuCl}_4$  solution before and after mixing with BT is shown in Fig. 2. Initially,  $\text{HAuCl}_4$  shows a strong absorption peak at  $220 \text{ nm}$  and a shoulder at  $290 \text{ nm}$  due to charge transfer between the metal and chloro ligands. After mixing with BT, these two peaks vanished, which corresponds to the complete reduction of  $\text{Au}^{3+}$ . Additionally, two new peaks, located at  $275 \text{ nm}$  and  $206 \text{ nm}$ , appear and increase with the increase of BT concentration. According to the literature,<sup>27</sup> the absorption peak at  $275 \text{ nm}$  would correspond to a gold cluster or AuNPs. In general, the AuNPs often show an intensive surface plasma resonance (SPR) band around  $520 \text{ nm}$  at the UV-vis spectroscopy. But for the BT-AuNPs prepared here, these SPR bands are very weak (magnified regions in Fig. 2b). According to the literature,<sup>28–30</sup> the intensity of SPR absorption depends on the size and shape of the metal nanoparticles as well as the surrounding medium. Possibly, the dense BT molecules on the

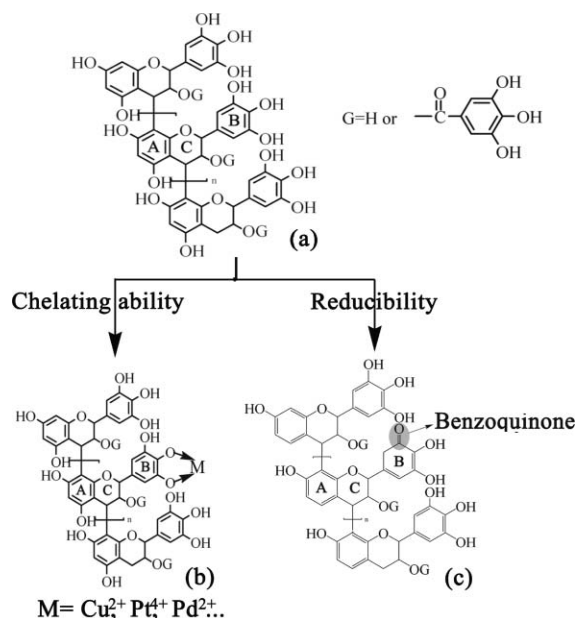


Fig. 1 Molecular structure and chemical properties of BT.

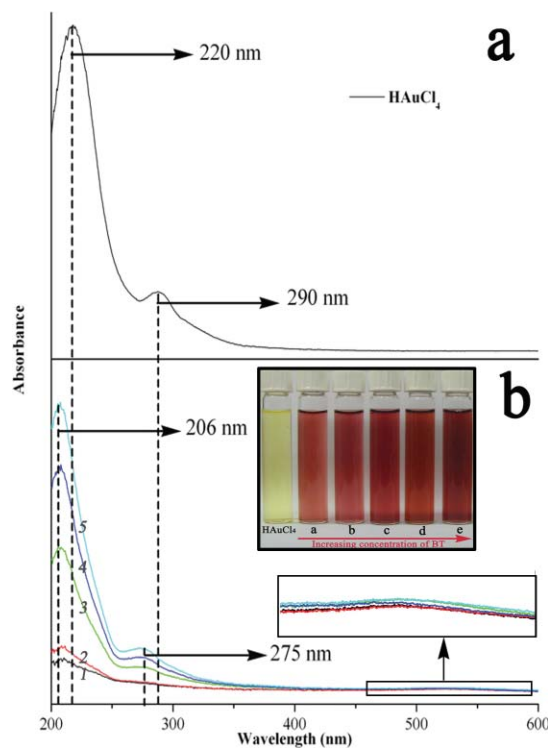
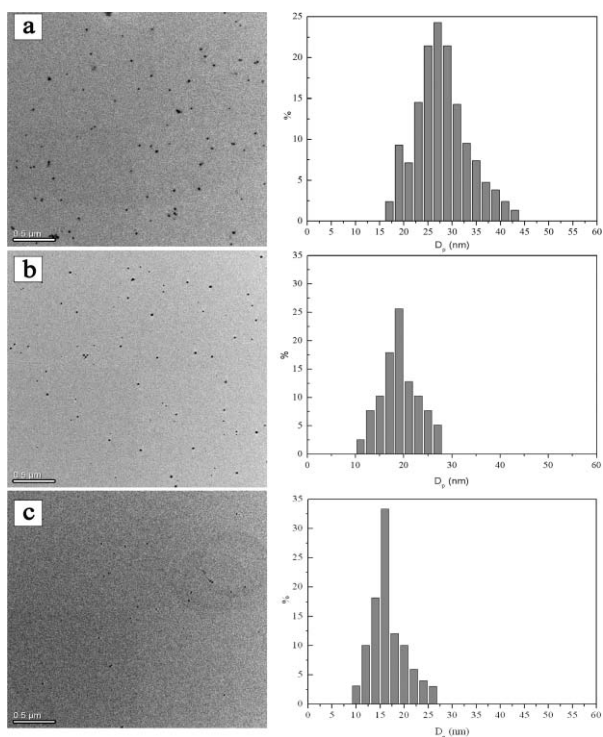


Fig. 2 UV-vis spectra of  $\text{HAuCl}_4$  (a),  $\text{BT}_{100}\text{-AuNPs}$  (b1),  $\text{BT}_{200}\text{-AuNPs}$  (b2),  $\text{BT}_{400}\text{-AuNPs}$  (b3),  $\text{BT}_{600}\text{-AuNPs}$  (b4) and  $\text{BT}_{800}\text{-AuNPs}$  (b5) colloid; the inset in (b) is the photos taken from different BT-AuNPs colloids.

surface of AuNPs significantly change the interface conditions of AuNPs (such as dielectric constant and critical angle of total reflection), which leads to a sharp decrease in the intensity of SPR absorption. The XRD pattern of  $\text{BT}_{800}\text{-AuNPs}$  shows intensive characteristic peaks of metallic gold ( $38.2^\circ$ ,  $44.4^\circ$ ,  $64.6^\circ$  and  $77.6^\circ$ , JCPDS-4784), which confirms the reduction of  $\text{Au}(\text{III})$  to  $\text{Au}(0)$  [see Supporting Information 1 (S1) for details].

Further XPS analysis suggested that about 58.5% of Au(III) ions were reduced to metallic species in the BT<sub>800</sub>-AuNPs (S2) colloid.<sup>31,32</sup>

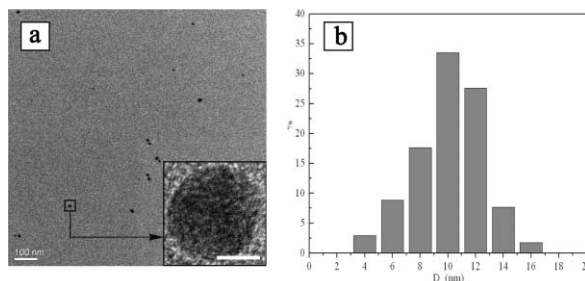
With the use of BT, the synthesis of AuNP colloids is so simple that no surfactant, photo-irradiation, or heat treatment is required. The preparation of BT-AuNP colloids is so efficient that the synthetic process can be completed within 5.0 min, which shows great practical value for the large-scale preparation of AuNP colloids. Additionally, the synthetic procedure for BT<sub>x</sub>-AuNPs preparation showed high reproducibility. In most cases, the color of the mixture quickly changed to red after HAuCl<sub>4</sub> and BT were mixed together. Except the sample with a low concentration of BT (25.0 mg L<sup>-1</sup>), its color gradually turned pink within several minutes and remained unchanged even after 24 h.



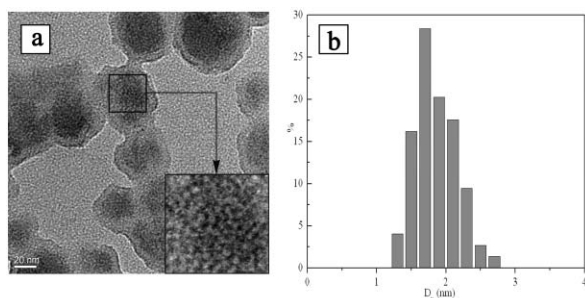
**Fig. 3** TEM images of BT<sub>100</sub>-AuNPs (a), BT<sub>200</sub>-AuNPs (b), and BT<sub>400</sub>-AuNPs (c) (scale bar = 0.5  $\mu$ m).

The morphology and size distribution of BT<sub>x</sub>-AuNP colloids ( $x = 100, 200$  and  $400$ ) are determined by Transmission Electron Microscope (TEM). Fig. 3a shows the TEM image of BT<sub>100</sub>-AuNPs and the corresponding histogram of particle size distribution. The mean particle diameter of BT<sub>100</sub>-AuNPs is  $29.9 \pm 12.3$  nm, and no agglomeration of AuNPs was observed. Hence, BT is able to reduce Au<sup>3+</sup> to form AuNPs and serve as a stabilizing agent to prevent agglomeration of AuNPs. But the particle size distribution of BT<sub>100</sub>-AuNPs is in a wide range, which suggests that BT with relatively low concentration is not efficient enough for the stabilization and/or dispersion of AuNPs. Smaller AuNPs with slightly narrower size distribution ( $19.1 \pm 6.1$  nm) are formed if the concentration of BT increases to 200.0 mg L<sup>-1</sup>, as shown in Fig. 3b. A similar trend can also be observed in Fig. 3c. The particle size distribution of BT<sub>400</sub>-AuNPs is  $17.3 \pm 5.8$  nm. The appearance of fringes in the

corresponding HR-TEM micrograph of BT<sub>600</sub>-AuNPs (Fig. 4a) suggests that BT-AuNPs are crystalline. For the BT<sub>600</sub>-AuNPs colloid, the particle size of AuNPs further decreases to  $10.7 \pm 3.4$  nm, and their size distribution is mainly in the range of 7.2 to 12.8 nm (Fig. 4b). Markedly, the mean particle diameter of AuNPs drastically decreases as the concentration of BT reaches to 800.0 mg L<sup>-1</sup>. The inset in Fig. 5a shows magnified regions of the small AuNPs below 3.0 nm. The AuNPs with mean particle diameters of  $1.8 \pm 0.3$  nm are found to be predominant in the BT<sub>800</sub>-AuNPs colloid (Fig. 5b). These observations may suggest that different stabilization mechanisms are responsible for BT-AuNPs at low and high concentrations of BT.

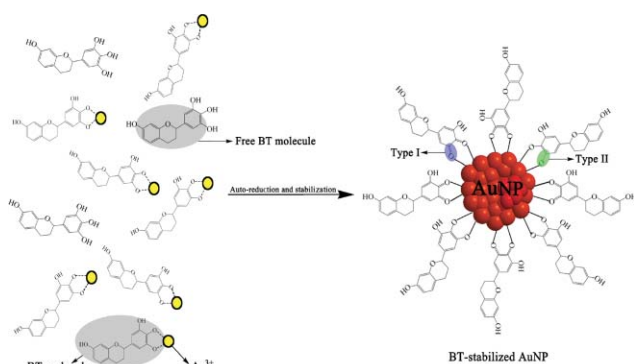


**Fig. 4** TEM images of BT<sub>600</sub>-AuNPs and the inset shows a HR-TEM micrograph of an individual BT<sub>600</sub>-AuNPs (scale bar 5 nm) (a), and the particle size distribution of BT<sub>600</sub>-AuNPs (b).



**Fig. 5** TEM images of BT<sub>800</sub>-AuNPs; the inset is the magnification of the indicated region (a), and the particle size distribution of BT<sub>800</sub>-AuNPs (b).

A possible mechanism for the preparation and stabilization of BT-AuNPs is shown in Fig. 6. The BT molecule first chelates with Au<sup>3+</sup> through its adjacent phenolic hydroxyls to form a five-membered chelate ring. Due to the high oxidation-reduction potential of Au<sup>3+</sup>, the reacted adjacent phenolic hydroxyls of BT are inductively oxidated to the corresponding quinones, and thus the Au<sup>3+</sup> are reduced to Au(0) atoms.<sup>33</sup> These neighbor Au(0) atoms further collide with each other to form AuNPs. Recently, Kim and Nakano found that condensed-tannin gels are able to reduce palladium ions to metallic palladium species, which are simultaneously stabilized by the corresponding formed quinones.<sup>34</sup> Consequently, it is logical to reason that the AuNPs prepared in this study should be stabilized by BT molecules through the quinones (Type I in Fig. 6). The excessive free BT molecules in solution may also interact with the surface atoms of AuNPs *via* its adjacent hydroxyls (Type II in Fig. 6), thereby contributing to the stabilization of AuNPs.<sup>35</sup> Furthermore, the Type II stabilization effect is gradually strengthened with the

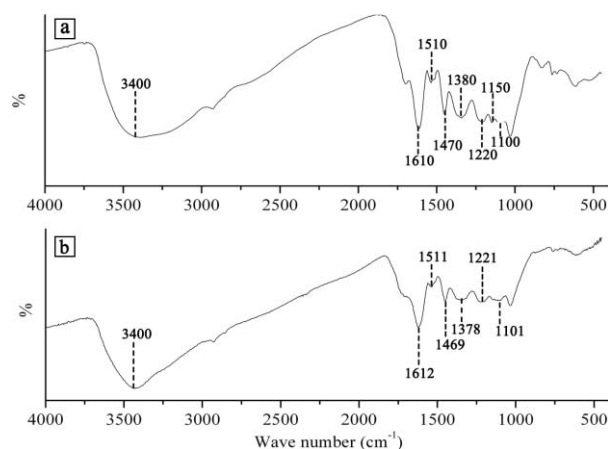


**Fig. 6** Schematic illustration showing a possible mechanism for the stabilization of AuNPs with BT.

increase of BT concentration, which promotes the formation of smaller AuNPs. Possibly, BT molecules may construct a protective shell around AuNPs, which is beneficial for the stabilization of AuNPs.<sup>36</sup>

Additionally, we propose that the formation of BT-AuNPs is a kinetic-controlled process. At low concentrations of BT, the auto-reduction rate of  $\text{Au}^{3+}$  is much faster than the coating speed of AuNPs with BT molecules, which leads to the aggregation of AuNPs to form large ones. For the BT<sub>100</sub>-AuNPs colloid, the aggregation of small AuNPs is obvious, because its size particle is relatively large ( $D_p \approx 30.0$  nm) and the size distribution is in a wide range ( $\pm 12.3$  nm). As the concentration of BT increases, the coating speed is gradually comparable with the auto-reduction of  $\text{Au}^{3+}$ , and the aggregation of AuNPs is effectively suppressed. Thus smaller AuNPs with narrower size distribution can be obtained as the concentration of BT increases from 200.0 to 600.0 mg L<sup>-1</sup>. At even higher concentrations of BT, like BT<sub>800</sub>-AuNPs, the intermolecular interactions among BT molecules are intensively strengthened *via* the formation of hydrogen bonds and/or hydrophobic bonds, and thus some dense supramolecular shells around Au(0) nanoparticles may be formed from the self-aggregation of BT molecules.<sup>37</sup> In the dense shells, the initial growth of AuNPs is limited and the aggregation among AuNPs is also prevented, resulting in the formation of very small Au(0) nanoparticles ( $D_p \approx 2.0$  nm). Hence, for the BT<sub>800</sub>-AuNPs colloid, small AuNPs with very narrow size distribution are preferably enveloped inside the dense shells. Recently, polymer-stabilized AuNPs with small particle size were observed only for a few dendrimers with high-generation ( $G = 4, 5, \dots$ ).<sup>36,38</sup>

Fig. 7a shows the FTIR spectrum of BT. The peak at 3400 cm<sup>-1</sup> can be attributed to the stretching vibration of phenolic hydroxyls (O–H bond) in tannin, and its broad range is due to the formation of hydrogen bonds among BT molecules. The peaks in the vicinity of 1620–1450 cm<sup>-1</sup> (1610, 1510, and 1470 cm<sup>-1</sup>) indicate the presence of aromatic rings of tannin. The absorption peak at 1380 cm<sup>-1</sup> arises from the inplane deformation of phenolic hydroxyls (O–H bond).<sup>39,40</sup> However, in the FTIR spectrum of BT-AuNPs (Fig. 7b), the stretching vibration peak of phenolic hydroxyls (3400 cm<sup>-1</sup>) becomes relatively narrow, which should attribute to the interactions of phenolic hydroxyls with AuNPs, resulting in the partial destruction of hydrogen bonds among BT molecules. Additionally, the inplane deformation of phenolic hydroxyls (1378 cm<sup>-1</sup>) is weaker



**Fig. 7** FTIR spectra of BT (a) and BT-AuNPs (b).

than that of BT, which also indicates that BT interacts with AuNPs through its adjacent phenolic hydroxyls and/or formed quinones.

The present study outlines the use of BT to efficiently auto-reduce  $\text{Au}^{3+}$  to form small AuNPs in an environmentally friendly way, in comparison to those large ones ( $> 20$  nm) obtained from other auto-reduction methods. It appears that BT in solution not only yields excellent reduction power compared with other reductive polymers but also enables the formation and stabilization of small AuNPs ( $\sim 2$  nm). As a result, BT at high concentration can be used to fabricate BT-stabilized AuNPs in the range of 2–3 nm, which have the potential to be utilized in screening applications and therapeutics as well as drug carriers. In this aspect, the BT shell may also provide another benefit to the AuNPs as it enhances the biocompatibility of AuNPs.

## Conclusions

This study described an extremely simple and effective approach for the preparation of AuNPs colloids. In this method, BT serves as a reducing agent as well as a stabilizing agent. It was found that BT was effective in reducing  $\text{Au}^{3+}$  to form AuNPs at room temperature without any additional reagent or treatment. The mean diameter and size distribution of AuNPs can be facilely controlled by varying the concentration of BT. BT is biocompatible, which increases the biocompatibility of AuNPs. Furthermore, this green approach for the synthesis of AuNPs is extremely efficient and highly reproducible, which shows great potential for practical applications.

## Acknowledgements

We acknowledge financial support provided by the Key Program of National Science Foundation of China (20536030), National Natural Science Foundation of China (20776090) and A Foundation for the Author of National Excellent Doctor Dissertation of P. R. China (FANEDD200762). We also give thanks to the Test Center of Sichuan University for the help of TEM and XRD tests.

## Notes and references

- 1 J. J. Storhoff, R. Elghanian, R. C. Mucic, C. A. Mirkin and R. L. Letsinger, *J. Am. Chem. Soc.*, 1998, **120**, 1959.
- 2 T. Li, L. P. Guo and Z. X. Wang, *Biosens. Bioelectron.*, 2008, **23**, 1125.
- 3 C. Marsden, E. Taarning, D. Hansen, L. Johansen, S. K. Klitgaard, K. Egeblad and C. H. Christensen, *Green Chem.*, 2008, **10**, 168.
- 4 N. L. Rosi and C. A. Mirkin, *Chem. Rev.*, 2005, **105**, 1547.
- 5 J. W. Liu and Y. Lu, *J. Am. Chem. Soc.*, 2003, **125**, 6642.
- 6 P. K. Jain, X. Huang, I. H. El-Sayed and M. A. El-Sayed, *Acc. Chem. Res.*, 2008, **41**, 1578.
- 7 M. C. Daniel and D. Astruc, *Chem. Rev.*, 2004, **104**, 293.
- 8 M. P. Melancon, W. Lu, Z. Yang, R. Zhang, Z. Cheng, A. M. Elliot, J. Stafford, T. Olson and J. Z. Zhang, *Mol. Cancer Ther.*, 2008, **7**, 1730.
- 9 K. Yamaguchi and H. Asakawa, *Anal. Biochem.*, 1988, **172**, 104.
- 10 M. Moeremans, G. Daneels and J. D. Mey, *Anal. Biochem.*, 1985, **145**, 315.
- 11 S. Kundu and H. Liang, *Colloids Surf., A*, 2008, **330**, 143.
- 12 X. L. Zhou, E. I. Khoury, L. T. Qu, L. M. Dai and Q. Li, *J. Colloid Interface Sci.*, 2007, **308**, 381.
- 13 N. Toshima and T. Yonezawa, *New J. Chem.*, 1998, **22**, 1179.
- 14 J. F. Zhou, J. Ralston and R. Sedev, *J. Colloid Interface Sci.*, 2009, **331**, 251.
- 15 M. Watzky and R. Finke, *J. Am. Chem. Soc.*, 1997, **119**, 10382.
- 16 J. Rothe, J. Hormes, H. Bonnemann, W. Brijoux and K. Siepen, *J. Am. Chem. Soc.*, 1998, **120**, 6019.
- 17 X. P. Sun, S. J. Dong and E. K. Wang, *Polymer*, 2004, **45**, 2181.
- 18 C. Note, S. Kosmella and J. Koetz, *Colloids Surf., A*, 2006, **290**, 150.
- 19 M. E. Garcia, L. A. Baker and R. M. Crooks, *Anal. Chem.*, 1999, **71**, 256.
- 20 K. Esumi, A. Suzuki, N. Aihara, K. Usui and K. Torigoe, *Langmuir*, 1998, **14**, 3157.
- 21 A. Henglein, *Langmuir*, 1999, **15**, 6738.
- 22 K. Zhu, L. Q. Huang, J. Zhu and Z. Y. Zhuang, *Spectrochim. Acta, Part A*, 2008, **69**, 566.
- 23 S. M. Mohsen and A. S. M. Ammar, *Food Chem.*, 2009, **112**, 595.
- 24 L. Manzocco, D. Mastrocola and M. C. Nicoli, *Food Res. Int.*, 1998, **31**, 673.
- 25 C. W. Oo, M. J. Kassim and A. Pizzi, *Ind. Crop. Prod.*, 2009, **30**, 152.
- 26 M. Ferrer, R. Reina, O. Rossell and M. Seco, *Coordin. Chem. Rev.*, 1999, **193-5**, 619.
- 27 K. Esumi, A. Suzuki, A. Yamahira and K. Torigoe, *Langmuir*, 2000, **16**, 2604.
- 28 S. Szunerits and R. Boukherroub, *Electrochem. Commun.*, 2006, **8**, 439.
- 29 J. G. Gordon II and J. D. Swalen, *Opt. Commun.*, 1977, **22**, 374.
- 30 W. Rechberger, A. Hohenau and A. Leitner, *Opt. Commun.*, 2003, **220**, 137.
- 31 X. Zhang, H. Shi and B. Q. Xu, *Catal. Today*, 2007, **122**, 330.
- 32 G. J. Hutchings, M. S. Hall, A. F. Carley, P. Landon, B. E. Solsona, C. J. Kiely, A. Herzing, M. Makkee, J. A. Moulijn, A. Overweg, J. C. Fierro-Gonzalez, J. Guzman and B. C. Gates, *J. Catal.*, 2006, **242**, 71.
- 33 D. Parajuli, H. Kawakita, K. Inoue, K. Ohto and K. Kajiyama, *Hydrometallurgy*, 2007, **87**, 133.
- 34 Y. H. Kim and Y. Nakano, *Water Res.*, 2005, **39**, 1324.
- 35 J. C. Liu, F. He, E. Durham, E. Durham, D. Zhao and C. B. Roberts, *Langmuir*, 2008, **24**, 328.
- 36 T. Pietsch, D. Appelhans, N. Gindy, B. Voit and A. Fahmi, *Colloid Surface. A*, 2009, **341**, 93.
- 37 S. Kallithraka, C. Garcia-Viguera, P. Bridle and J. Bakker, *Phytochem. Analysis*, 1995, **6**, 265.
- 38 K. Esumi, T. Matsumoto, Y. Seto and T. Yoshimura, *Colloid Interf. Sci.*, 2005, **284**, 199.
- 39 C. W. Oo, M. J. Kassim and A. Pizzi, *Ind. Crop. Prod.*, 2009, **30**, 152.
- 40 Y. Nakano, K. Takeshita and T. Tsutsumi, *Water Res.*, 2001, **35**, 496.

# Green-light photocatalytic reduction using dye-sensitized TiO<sub>2</sub> and transition metal nanoparticles

Stefan Földner,<sup>a</sup> Ralph Mild,<sup>a</sup> Heiko Ingo Siegmund,<sup>b</sup> Josef A. Schroeder,<sup>b</sup> Michael Gruber<sup>c</sup> and Burkhard König<sup>\*a</sup>

Received 3rd September 2009, Accepted 6th October 2009

First published as an Advance Article on the web 19th November 2009

DOI: 10.1039/b918140g

Nitrobenzenes are cleanly reduced to anilines using Ru-sensitized TiO<sub>2</sub> photocatalysts and green light irradiation, if very small amounts of transition metal salts are added, which form metal nanoparticles of narrow size distribution under the experimental conditions. The catalyst system is prepared by simple mixing of the components and is therefore easy to apply in organic synthesis. As light sources, commercial high power LEDs or sunlight are used. We report the optimization of the reaction conditions, the effect of trace amounts of added metal salts and demonstrate the use of green light photoreduction in the conversion of several nitrobenzene derivatives.

## Introduction

Sunlight is our largest energy resource by far. Photovoltaic systems for the conversion of solar energy into electrical power have already evolved into a wide range of applications.<sup>1</sup> Photocatalysts, which utilize light to drive chemical reactions,<sup>2</sup> are less developed and typical applications are the photodegradation of organic pollutants with TiO<sub>2</sub> and UV irradiation in waste water treatment<sup>3</sup> or self-cleaning surfaces.<sup>4</sup> Large scale photocatalytic fuel generation,<sup>5</sup> e.g. by water splitting,<sup>6</sup> still lacks endurance and efficiency, but photocatalytic fine chemical synthesis has been achieved. Recent examples of homogeneous photocatalysis<sup>7</sup> include alkyne hydrogenation,<sup>8</sup> the direct asymmetric alkylation of aldehydes,<sup>9</sup> enantioselective cyclisation reactions<sup>10</sup> and methanol addition to glycals.<sup>11</sup> Heterogeneous photocatalysts are typically based on doped TiO<sub>2</sub><sup>12</sup> or TiO<sub>2</sub> sensitized by dyes<sup>13</sup> to extend its absorption beyond the UV range. Cadmium sulfide-based photocatalysts have been developed for the synthesis of unsaturated  $\alpha$ -cyano-homoallyl amines from imines and olefins.<sup>14</sup> In addition, metal complexes<sup>15</sup> and metals<sup>16</sup> are deposited on TiO<sub>2</sub> to increase its photocatalytic efficiency.<sup>17</sup> A recent example of the application of sensitized TiO<sub>2</sub> photocatalysis to organic synthesis is the TEMPO-mediated aerobic oxidation of alcohols using blue light irradiation and oxygen,<sup>18</sup> whereas non-modified TiO<sub>2</sub> was used to mediate the oxidative addition of THF to quinolines.<sup>11</sup>

Here, we describe photocatalytic reductions of nitrobenzene derivatives using green LED light irradiation or sun light. Our

simple but effective heterogeneous photocatalysts are derived from commercial Degussa P25 TiO<sub>2</sub>, ruthenium complex **N3** and trace amounts of added metal salts. The catalyst preparation is achieved by simple mixing and does not require any special procedures. The photoconversions of organic substrates are very clean, as verified by gas chromatography monitoring, and, in many cases, quantitative.

## Results and discussion

The photoreduction of nitrobenzenes to anilines<sup>19</sup> has been reported using TiO<sub>2</sub> and UV irradiation<sup>20</sup> or transition metal-doped TiO<sub>2</sub> and visible blue light,<sup>21</sup> but these conditions still show some disadvantages: a sunlight-mediated reduction is typically not effective, the reported TONs with respect to the added metal catalysts are below 1000, partial conversions and side-product formation are observed, and metal-doped titanium dioxide must be specially prepared.<sup>22</sup>

As in a Grätzel cell (dye sensitized solar cell),<sup>23</sup> we have used commercial TiO<sub>2</sub>, which was surface-functionalized by a Ru-complex, to absorb green light; this region of the solar spectrum has the highest intensity. Scheme 1 shows the proposed mechanism of the photoreduction process: The excited dye injects electrons into the conduction band (CB) of TiO<sub>2</sub>. Added transition metal ions are reduced by the TiO<sub>2</sub>, form clusters and mediate the reduction of nitroarene substrates, which are reduced to anilines. The catalytic cycle is closed by TEOA oxidation to reduce the dye.

High power LEDs with a narrow emission wavelength bandwidth (530  $\pm$  10 nm) and a high light intensity of more than 60 lm, generated from approximately 3 W electrical power according to their specifications, are used as energy-efficient light sources to drive the catalysis. Fig. 1 shows the experimental set up.

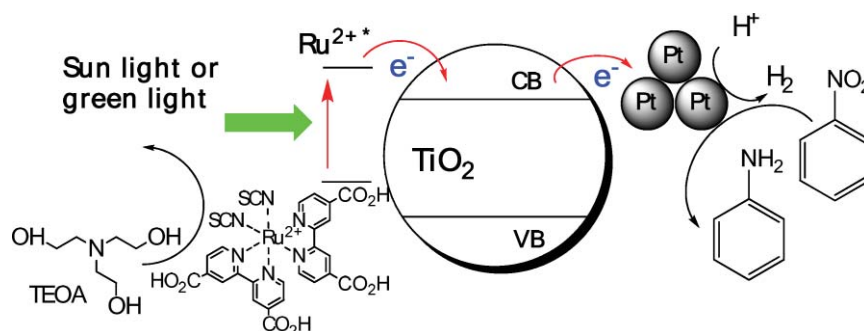
The photocatalysts were prepared by deposition of the ruthenium complex **N3** on P-25 TiO<sub>2</sub> ( $8 \times 10^{-8}$  mmol mg<sup>-1</sup>) followed by addition of different amounts of transition metals (see Experimental section for details). A solution of nitrobenzene

<sup>a</sup>Institute of Organic Chemistry, University of Regensburg, Universitätsstr., 31, 93040, Regensburg, Germany. E-mail: Burkhard.koenig@chemie.uni-regensburg.de; Fax: +49 941 9434566; Tel: +49 941 9434575

<sup>b</sup>Department of Pathology, Central EM Labor, University Hospital Regensburg, Regensburg, 93051, Germany. E-mail: josef.schroeder@klinik.uni-regensburg.de; Fax: +49 941 944 6602

<sup>c</sup>Department of Anaesthesia, University Hospital Regensburg, Regensburg, 93051, Germany. E-mail: michael.gruber@klinik.uni-regensburg.de; Fax: +49 941 944 7801





**Scheme 1** Proposed mechanism of green-light-mediated reduction of nitrobenzenes by dye-sensitized TiO<sub>2</sub> and transition metal clusters. TEOA: triethanolamine.



**Fig. 1** Reaction vials irradiated by an array of high power green light LEDs.

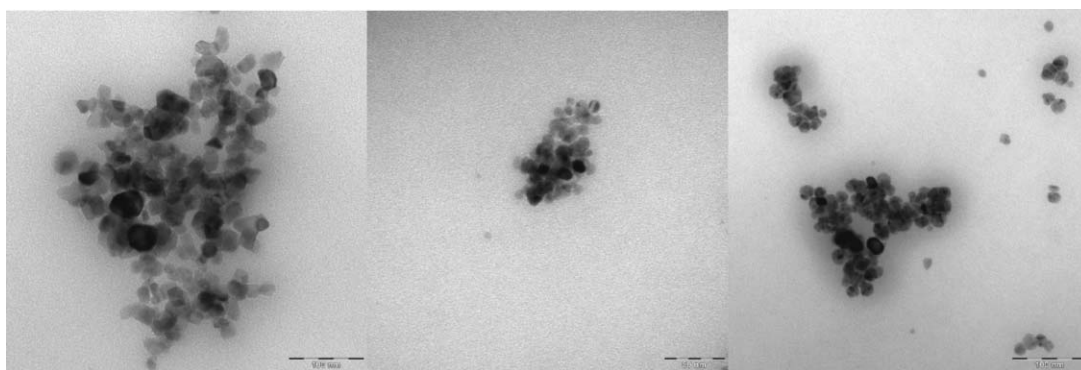
[ $c = 8 \times 10^{-2} \text{ mol L}^{-1}$ ] in acetonitrile (2.5 mL) and 50 mg of the TiO<sub>2</sub> photocatalyst was irradiated with a 3 W green LED at room temperature for 24 h. The reaction conversion was monitored by gas chromatography (GC) and GC/MS analysis.

Irradiation of unmodified TiO<sub>2</sub> at 530 nm leads to low nitrobenzene conversions of about 2% (Table 1, entry 2). TiO<sub>2</sub> modified with N3 but with no deposited transition metal ions gave conversions of nitrobenzene to aniline of 39% (Table 1, entry 3). No conversion was detected without green light irradiation or by irradiating N3 without TiO<sub>2</sub> (Table 1, entry 1). The addition of small amounts of transition metal ions to the reaction mixture led to a significant enhancement of the photocatalytic activity: 67% conversion for 0.1 mol% and 51% for 0.001 mol% K<sub>2</sub>PtCl<sub>6</sub> (Table 1, entries 7, 8 and 9). Quantitative conversions of nitrobenzene to aniline were observed with 0.1 mol% of Pt(II) or even smaller amounts of Pd(II) salts. A similar effect in non-sensitized reactions has been previously reported for silver clusters deposited on TiO<sub>2</sub>.<sup>21</sup> Systematic variation of the transition metals, their amounts and the method of their reduction revealed a relationship between the nature of the metal and the optimal catalytic amount (Table 1): quantitative conversions >99% are observed for 0.5–0.01 mol%

**Table 1** Green light photoreduction of nitrobenzene to aniline in the presence of different transition metal salts

		<chem>c1ccc(cc1)[N+](=O)[O-]</chem> $\xrightarrow[\text{MeCN, 530 nm}^{[b]}, 24 \text{ h}]{\text{N3/ TiO}_2^{[a]} \text{ cat.}, \text{TEOA (10 equiv.)}}$ <chem>c1ccc(cc1)N</chem>							
		$2 \times 10^{-4} \text{ mol}$							
		Nitrobenzene conversion [%] <sup>c</sup>							
Entry	Added metal salt [mol%]	No metal salt	Pt <sup>4+</sup>	Pt <sup>2+</sup>	Pt <sup>0g</sup>	Pt <sup>0h</sup>	Au <sup>3+</sup>	Pd <sup>2+</sup>	Ag <sup>+</sup>
1 <sup>d</sup>	0	0							
2 <sup>e</sup>	0	2							
3 <sup>f</sup>	0	39							
4	0.000001		37	46	46	> 99	44	50	46
5	0.00001		27	39	32	> 99	32	39	29
6	0.0001		51	90	49	99	> 99	49	49
7	0.001		51	41	49	> 99	83	40	39
8	0.01		43	> 99	28	> 99	85	> 99	59
9	0.1		67	> 99	39	72	> 99	> 99	65
10	0.5		38	36	32	40	49	> 99	30
11	1.75		25	27	26	23	12	56	7
12 <sup>i</sup>	0.1		—	99 (91) <sup>j</sup>	—	—	—	99 (93) <sup>j</sup>	—
13 <sup>k</sup>	0.001		—	—	—	—	99 (92) <sup>j</sup>	—	—

<sup>a</sup> 50 mg TiO<sub>2</sub> with immobilized N3 (2 mol%). <sup>b</sup> 3 W electrical power. <sup>c</sup> Integration of signals in GC chromatograms. <sup>d</sup> 50 mg TiO<sub>2</sub> with 0.01 mol% K<sub>2</sub>PtCl<sub>6</sub> in the dark. <sup>e</sup> 50 mg TiO<sub>2</sub> without immobilized dye and without transition metal salt. <sup>f</sup> 50 mg TiO<sub>2</sub> with immobilized dye, without transition metal salt. <sup>g</sup> Particles synthesized by reduction with NaBH<sub>4</sub> and mercaptosuccinic acid.<sup>32</sup> <sup>h</sup> Particles synthesized by reduction with UV light < 300 nm. <sup>i</sup>  $2 \times 10^{-3}$  mmol nitrobenzene are converted; 36 h irradiation time. <sup>j</sup> Isolated aniline yields after distillations are given in parentheses.

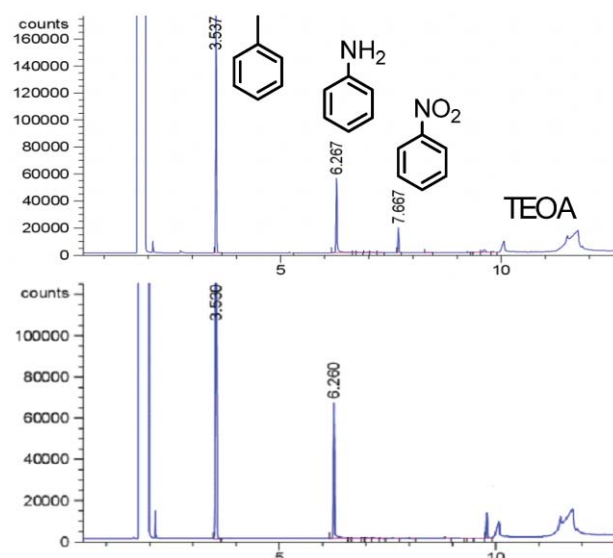


**Fig. 2** TEM-pictures of nanoparticles found in solution after the photocatalytic reduction (a) 0.01 mol% Pt(II), (b) 0.01 mol% Pd(II) and (c) 0.0001 mol% Au(III).

using Pt(II) and Pd(II), while reduced Pt(IV) and Ag(I) salts did not lead to complete conversions under the experimental conditions, with the best results of 67% for 0.1 mol% Pt(IV) and 65% for 0.1 mol% Ag(I).

The photocatalytic activity of the Pt(0) species depended on their preparation: the reduction of Pt(IV) and stabilization of the colloid by mercaptosuccinic acid yielded less active catalysts. On the other hand, photochemically-prepared Pt colloids showed quantitative conversion of nitrobenzene to aniline in the range  $10^{-1}$ – $10^{-6}$  mol% (Table 1, entries 4–8). The photocatalytic activity depends on the oxidation state of the platinum source, which is either Pt(IV), Pt(II) or Pt(0). This has been observed earlier by Remita *et al.* in photodegradations by platinum-doped TiO<sub>2</sub>: under visible light irradiation, the photodegradation activities followed the order Pt cluster > Pt(II)  $\gg$  Pt(IV) and was explained by the ability of the Pt clusters to act as weak temporary electron scavengers.<sup>24</sup> Using Au(III) salts led to quantitative conversions at  $10^{-1}$  and  $10^{-4}$  mol%. For every metal salt, an optimum quantity range was found. All were below 1 mol%, some as low as  $10^{-4}$  mol%. Amounts higher than 1 mol% decreased the catalytic activity. Ozin *et al.* recently reported that the size distribution of deposited platinum clusters on TiO<sub>2</sub> depends on the platinum loading, and that the photocatalytic activity of the material in photodecomposition increased beyond a critical cluster size of 2 nm.<sup>25</sup> TEM pictures from our reaction solutions with the optimum catalytic amounts for Pt(II) and Pd(II) in  $10^{-2}$  mol% and Au(III) in  $10^{-4}$  mol% showed a similar morphology for each of the resulting particles (Fig. 2). No transition metal particles were found on the surface of TiO<sub>2</sub>. This indicates that (a) for every transition metal, a specific amount is needed to get the optimum particle size for the photocatalytic reduction under these conditions and (b) the active catalyst is prepared heterogeneously, but the reduction reaction is homogeneously mediated by nanometer size metal clusters.

The reactions in Table 1 correspond to minimum turnover numbers of 1000 for Pt(II) (0.1 mol%), 9996 for Pd(II) (0.01 mol%) and 995900 for Au(III) ( $10^{-4}$  mol%). The selective green light irradiation requires longer irradiation times for complete conversion compared to UV experiments; however, no side products of the reduction were detected when analyzing the samples by GC and GC-MS (see Fig. 3). A quantum efficiency of 8% was determined for the reduction reaction under the optimized conditions.



**Fig. 3** Gas-chromatographic analyses of nitrobenzene reductions. Toluene was used as internal standard. Upper trace: entry 9, Table 1, Pt(0) from UV reduction, 72% conversion; lower trace: entry 8, Table 1, Pt(II) from Vis reduction, 99%.

To demonstrate the use of the green light photoreduction on a laboratory preparative scale,  $2 \times 10^{-3}$  mmol of nitrobenzene were reduced and the product was isolated by distillation (Table 1, entries 12 and 13). Quantitative conversions and high yields were obtained for 0.1 mol% Pd<sup>2+</sup> and Pt<sup>2+</sup> and for 0.0001 mol% of Au<sup>3+</sup> when irradiating the samples for 36 h.

As the composition of our catalyst system is similar to reported hydrogen-generating photocatalysts, consisting in the simplest case of a ruthenium complex, an electron mediator and colloidal palladium, we suspected hydrogen as an intermediate and the chemical reduction reagent. Gas chromatographic analyses of the head space of a reaction sample using the conditions of entry 9, Table 1 for 0.1 mol% Pd<sup>2+</sup>, clearly showed the presence of 6% hydrogen gas after 10 h of irradiation. We therefore conclude that the role of the metal clusters in our catalytic system is twofold: they accept electrons from the conduction band of the TiO<sub>2</sub> and generate dihydrogen by reduction of protons provided by the TEOA,<sup>26</sup> but they also catalyze the hydrogenation of the organic substrate. Monitoring the photoreduction (see Experimental section for data) shows

an induction period for the reaction of about 8–12 h. A likely explanation for this observation is the necessary formation of the reduced metal clusters and the build up of a hydrogen gas pressure before an effective substrate conversion starts.

After the optimization of the reaction conditions, the substrate scope was investigated. Table 2 summarizes the results for standard reaction conditions of 24 h irradiation at room temperature. Ethyl 4-nitrobenzoate, 4-nitrobenzonitril, 4-nitrobenzaldehyde and 4-bromonitrobenzene are reduced to the corresponding anilines, with smaller amounts of added  $K_2PtCl_6$  giving better conversions under the experimental conditions. No reduction of the aldehyde functional group is observed. In the case of 4-bromonitrobenzene, dehalogenation occurs as a competing process at high platinum concentrations. No other side products were detected by GC analysis for the photoreductions. 4-Nitrophenol is not reduced under the experimental conditions and 1,4-dinitrobenzene gives nitroaniline, but only in small yields.<sup>27</sup> In contrast, 1,2-dinitrobenzene is reduced to 2-nitroaniline in good yields with small amounts of the corresponding nitrohydroxylamine as a side product. 2-Nitrobenzaldehyde and 2-nitroacetophenone are reduced to the corresponding anilines. However, depending on the amount of platinum salt added the corresponding 1,2-benzisoxazole becomes the major product. The preparation of 1,2-benzisoxazoles has been previously described using 2–5 equivalents of indium as the reduction reagent.<sup>28</sup>

As expected, the conversion of benzaldehyde to benzyl alcohol is low under the experimental conditions. However, pyridine-4-carbaldehyde is reduced to the corresponding benzyl alcohol in up to 80%. The reduction of stilbene to 1,2-diphenylethane is possible under the reaction conditions, but the conversions remain incomplete within 24 h.

The photocatalyst system absorbs in the most intense region of the solar spectrum and is therefore suitable to work in sun light. Photocatalytic reduction reactions using the standard apparatus and a  $TiO_2/N3/K_2PtCl_6$  photocatalyst were performed at different weather conditions with daylight and sun irradiation (late summer, south of Germany). Table 3 summarizes the results. On a rainy and overcast day, the conversion in nitrobenzene reduction is, as expected, only small. However, with increasing sunshine the nitrobenzene conversion reached 80% and maximal TON, with respect to the added platinum catalyst, of more than 67 000 after 11 h.

## Conclusions

The combination of ruthenium dye-sensitized  $TiO_2$ , as used in the photovoltaic Grätzel cell, with *in situ*-generated transition metal nanoparticles of a size in the order of 10 to 20 nm leads to photoreduction catalysts that work with green light irradiation. The catalysts are simple to prepare and apply, and allow the complete, selective and clean conversion of nitrobenzene derivatives to the corresponding anilines. The use of green light irradiation of low energy avoids the formation of unwanted side products and rapid catalyst decomposition. Optimization studies revealed the amount of transition metal salts initially added to be critical for effective catalysis, as it determines the size of the *in situ*-formed nanoparticles. Their activity as hydrogen

evolution and hydrogenation catalysts is size dependent, as known from other studies.

The described photocatalyst may find applications in synthesis, as the metal salts exhibit some selectivities in the reduction reaction and conversions can be performed using energy-efficient high power green light LEDs or direct sunlight.

## Experimental

### Synthesis of the ruthenium complex-modified titanium dioxide

**4,4'-Dicarboxylic acid-2,2'-bipyridine (1)**<sup>29</sup>. 4,4'-Dimethyl-2,2'-bipyridyl (2 g, 10.9 mmol) in 50 mL conc.  $H_2SO_4$  was heated to 70 °C. At this temperature,  $K_2Cr_2O_4$  (9.6 g, 33 mmol) was added slowly and the solution stirred for another hour at this temperature. The hot solution was poured into 300 mL crushed ice and stirred for 1 h. The green-yellow solid was filtered and washed with  $2 \times 50$  mL water. The yellow residue was refluxed in 50%  $HNO_3$  for 4 h, cooled to room temperature and poured into 300 mL crushed ice. Crystals were obtained from this water phase over night.

The solid was filtered and dried at high vacuum ( $8 \times 10^{-2}$  mbar) for 4 h at room temperature. A colourless solid (2.3 g) was obtained (yield: 87%; lit<sup>29</sup>: 90%). Mass analysis and melting point were identical to the reported data:  $m/z = 244.1$ ; m.p. = 97 °C.

**cis-Diaquadithiocyanatobis(2,2'-bipyridyl-4,4'-dicarboxylate)-ruthenium(II) (N3)**<sup>30,31</sup>. 4,4'-Dicarboxylic acid-2,2'-bipyridine **1** (2.3 g, 9.4 mmol) and  $RuCl_3 \cdot H_2O$  (1.01 g, 4.5 mmol) were suspended in 25 mL DMF and refluxed overnight. DMF was evaporated, the dark solid dried at high vacuum ( $5 \times 10^{-2}$  mbar, room temperature) for 2 h. The solid (1.28 g) was used without further purification, dissolved in 160 mL DMF, and a solution of NaOH (430 mg, 10.6 mmol) in 100 mL  $H_2O$  was added. NaSCN (1.93 g, 23.8 mmol) in 11 mL  $H_2O$  was added dropwise under argon and the solution was allowed to reflux for 6 h. The solvents were evaporated, the crude residue dissolved in 100 mL  $H_2O$  and acidified to pH = 2 by  $HClO_4$ . The dark red solid was filtered, dried at high vacuum and stored in the dark. 1.1 g of a dark solid (**2**) was obtained (yield: 80%, lit<sup>31</sup>: 80%). UV and ESI-MS data of complex **2** were identical to reported values:  $m/z = 724.1$  ( $M + NH_4^+$ ): UV-VIS (MeCN):  $\lambda_{max}$  (nm)/ $\epsilon$  ( $M^{-1} cm^{-1}$ ) = 546/14.000; 401/13.800; 316/31.000.

**Dye immobilization on  $TiO_2$** .  $TiO_2$  (4 g, 50 mmol) and dye **N3** (229 mg,  $3.2 \times 10^{-4}$  mol) were suspended in 25 mL MeCN and stirred for 12 h in the dark under an argon atmosphere. The solvent was evaporated and the remaining violet solid dried at high vacuum ( $2 \times 10^{-2}$  mbar).

### General procedure for the reduction of nitrobenzene derivatives and alkenes

A mixture of the nitro compound or alkene ( $2 \times 10^{-4}$  mmol),  $TiO_2$  with **N3** (50 mg, containing  $4 \times 10^{-6}$  mol **N3**), stock solution of the transition metal salt, TEOA ( $2 \times 10^{-3}$  mol) and 2.5 mL MeCN were transferred into a glass vial. The reaction mixture was frozen in liquid nitrogen, evacuated and allowed to warm up to room temperature at 50 mbar. The procedure was repeated and finally the reaction vial was flushed with nitrogen.

**Table 2** Photoreduction of nitrobenzenes and alkenes using 50 mg TiO<sub>2</sub> with immobilized N3 (2 mol%) in acetonitrile solution (2 × 10<sup>-4</sup> mol L<sup>-1</sup>); 10 equiv. TEOA; irradiation with green light (530 nm) LED (3 W) for 24 h

Starting material	K <sub>2</sub> PtCl <sub>6</sub> [mol%]	Products [%] <sup>a</sup>			
	0.0001		89		
	0.001		79		
	0.01		69		
	0.5		87		
	0.0001		58		
	0.001		85		
	0.01		60		
	0.5		59		
	0.0001		76		
	0.001		89		
	0.01		85		
	0.5		63		
	0.0001 <sup>b</sup>		84		
	0.001 <sup>b</sup>		49		6
	0.01 <sup>b</sup>		48		—
	0.5 <sup>b</sup>		23		64
	0.0001		21		
	0.001		20		
	0.01		24		
	0.5		21		
	0.0001		75		
	0.001		91		22
	0.01		85		9
	0.5		88		15
	0.0001		15		
	0.001		26		29
	0.01		18		62
	0.5		22		62
	0.0001		66		
	0.001		66		33
	0.01		79		21
	0.5		79		20
	0.0001		6		
	0.001		12		
	0.01		7		
	0.5		7		
	0.0001		80		
	0.001		73		
	0.01		78		
	0.5		76		
	0.0001		36		
	0.001		44		
	0.01		33		
	0.5		40		

<sup>a</sup> Determined by gas chromatography. <sup>b</sup> Pd(OAc)<sub>2</sub> was used as added metal salt.

**Table 3** Reduction of nitrobenzene to aniline using sunlight and an N3/TiO<sub>2</sub>/K<sub>2</sub>PtCl<sub>6</sub> photocatalyst

2 x 10<sup>-4</sup> mol

Weather	Temp./°C	Platinum catalyst [mol%]	Irradiation time/h	Nitrobenzene conversion <sup>c</sup> [%]	TON with respect to Pt
	15	0.1	11	4	40
	15	0.001	11	5	5000
	20	0.1	11	15	150
	20	0.001	11	11	11000
	35	0.1	11	80	800
		0.001	11	67	67000

<sup>a</sup> 50 mg TiO<sub>2</sub> with immobilized N3 (2 mol%). <sup>b</sup> Direct sunlight. <sup>c</sup> Integration of signals in GC chromatograms.

The sample was irradiated with a high power LED (Luxeon, 3 W, 530 nm) for 24 h. 500 µL of the reaction mixture were diluted with 500 µL of 6.7 × 10<sup>-2</sup> M stock solution of toluene in MeCN as standard. Analytical data of all isolated compounds corresponded to literature values.

#### General procedure for the large-scale reduction of nitrobenzene

A mixture of the nitrobenzene (2 × 10<sup>-3</sup> mmol), TiO<sub>2</sub> with N3 (500 mg, containing 4 × 10<sup>-5</sup> mol N3), stock solution of the transition metal salt, TEOA (2 × 10<sup>-2</sup> mol) and 10 mL MeCN was transferred into a glass vial. The reaction mixture was frozen in liquid nitrogen, evacuated and allowed to warm up to room temperature at 150 mbar. The procedure was repeated and finally the reaction vial was flushed with nitrogen. The sample was irradiated with a high power LED (Luxeon, 3 W, 530 nm) for 36 h. The N3/TiO<sub>2</sub> was filtered off over Celite, the filtrate was evaporated and distilled under high vacuum. Analytical data of all isolated compounds corresponded to literature values.

#### Gas chromatographic analyses

Monitoring of the reaction and product analysis was performed by gas chromatographic analysis (GC 5890 Series II from Hewlett-Packard, capillary column J+W Scientific—DB-5MS/30 m × 0.25 mm/0.25 µm film). The structures of the products were confirmed by comparison with standard samples and by GC-MS analyses (GC-MS 5973 MSD from Agilent Technologies, capillary column from Agilent 19091S-433 HP-5MS/30 m × 0.25 mm/0.25 µm film).

#### Reaction kinetics

A mixture of the nitro compound (2 × 10<sup>-4</sup> mmol), TiO<sub>2</sub> with N3 (50 mg, containing 4 × 10<sup>-6</sup> mol N3), stock solution of the transition metal salt, TEOA (2 × 10<sup>-3</sup> mol) and 2.5 mL MeCN were transferred into a glass vial. The reaction mixture was frozen in liquid nitrogen, evacuated and allowed to warm up to room temperature at 50 mbar. The procedure was repeated and finally the reaction vial was flushed with nitrogen. The mixture

was irradiated with a high power LED (Luxeon, 3 W, 530 nm) for 1 h. To monitor the reaction progress, 20 µL samples of the reaction mixture were taken and diluted with 20 µL of 6.7 × 10<sup>-2</sup> M stock solution of toluene in MeCN as standard and analyzed by GC.

#### TEM material and method

The sample solution drops were placed on Formvar- and carbon-coated positive glow-discharge treated copper grid (400 mesh) and subsequently blotted dry with filter paper. The samples were examined in a LEO912AB electron microscope (Zeiss, Oberkochen, Germany) operating at 100 kV, equipped with a bottom-mounted CCD-camera capable to record images with 1k × 1k pixels. The documentation was done with the iTEM software, ver. 5.0 (Olympus Soft Imaging Solutions GmbH, Muenster, Germany).

#### Acknowledgements

This work was supported by DFG (GRK 640, Sensory Photoreceptors), the University of Regensburg and a scholarship of the Bayerische Eliteförderung for S.F.

#### Notes and references

- 1 S. Westenhoff, I. A. Howard, J. M. Hodgkiss, K. R. Kirov, H. A. Bronstein, C. K. Williams, N. C. Greenhorn and R. H. Friend, *J. Am. Chem. Soc.*, 2008, **130**, 13653–13658.
- 2 P. Esser, B. Pohlmann and H.-D. Scharf, *Angew. Chem.*, 1994, **106**, 2093–2108.
- 3 (a) A. L. Linsebigler, G. Lu and J. T. Yates, *Chem. Rev.*, 1995, **95**(3), 735–758; (b) M. Barbeni, M. Morello, E. Pramauro, M. Vincenti, E. Borgarello and N. Serpone, *Chemosphere*, 1987, **16**(6), 1165–1179.
- 4 T. Yuranova, R. Mosteo, J. Bandava, D. Laub and J. Kiwi, *J. Mol. Catal. A: Chem.*, 2006, **244**, 160–167.
- 5 (a) B. Kayes and M. Filler, *Nature*, 2008, **452**, 400–402; (b) M. Hamburger, P. A. Liddell, D. Gust, A. L. Moore and T. A. Moore, *Photochem. Photobiol. Sci.*, 2007, **6**, 431–437.
- 6 (a) M. W. Kanan and D. G. Nocera, *Science*, 2008, **321**, 1072–1075; (b) J. Tang, J. R. Durrant and D. R. Klug, *J. Am. Chem. Soc.*, 2008, **130**(42), 13885–13891; (c) R. Brimblecombe, G. Swiegers, G. C. Dismukes and L. Spiccia, *Angew. Chem.*, 2008, **120**, 7445–7448.

- 7 (a) S. Rau, D. Walthera and J. G. Vosb, *Dalton Trans.*, 2007, 915–919; (b) M. A. Ischay, M. E. Anzovino, J. Du and T. P. Yoon, *J. Am. Chem. Soc.*, 2008, **130**(39), 12886–12887; (c) H. Schmaderer, P. Hilgers, R. Lechner and B. König, *Adv. Synth. Catal.*, 2009, **351**, 163–174; (d) G. Imperato and B. König, *ChemSusChem*, 2008, **1**, 993–996; (e) J. Svoboda, H. Schmaderer and B. König, *Chem.–Eur. J.*, 2008, **14**, 1854–1865; (f) R. Cibulka, R. Vasold and B. König, *Chem.–Eur. J.*, 2004, **10**, 6223–6231; (g) J. Du and T. P. Yoon, *J. Am. Chem. Soc.*, 2009, **131**, 14604.
- 8 S. Rau, B. Schäfer, D. Gleich, E. Anders, M. Rudolph, M. Friedrich, H. Görls, W. Henry and J. G. Vos, *Angew. Chem.*, 2006, **118**, 6361–6364.
- 9 D. A. Nicewicz and D. W. C. MacMillan, *Science*, 2008, **322**, 77–80.
- 10 (a) A. Bauer, F. Westkämpfer, S. Grimme and T. Bach, *Nature*, 2005, **436**, 1139–1140; (b) J. Svoboda and B. König, *Chem. Rev.*, 2006, **106**, 5413–5430.
- 11 M. Fagnoni, D. Dond, D. Ravelli and A. Albini, *Chem. Rev.*, 2007, **107**, 2725–2756.
- 12 (a) S. In, A. Orlov, R. Berg, F. García, S. Pedrosa-Jimenez, M. S. Tikhov, D. S. Wright and R. M. Lambert, *J. Am. Chem. Soc.*, 2007, **129**, 13790–13791; (b) R. Nakamura, A. Okamoto, H. Osawa, H. Irie and K. Hashimoto, *J. Am. Chem. Soc.*, 2007, **129**, 9596–9597; (c) S. S. Srinivasan, J. Wade and E. K. Stefanakos, *J. Nanomat.*, 2006, 1–4.
- 13 (a) W. R. Duncan, C. F. Craig and O. V. Prezhdo, *J. Am. Chem. Soc.*, 2007, **129**, 8528–8543; (b) H. Qin, S. Wenger, M. Xu, F. Gao, X. Jing, P. Wang, S. M. Zakeeruddin and M. Grätzel, *J. Am. Chem. Soc.*, 2008, **130**, 9202–9203; (c) F. Gao, Y. Wang, D. Shi, J. Zhang, M. Wang, X. Jing, R. Humphry-Baker, P. Wang, S. M. Zakeeruddin and M. Grätzel, *J. Am. Chem. Soc.*, 2008, **130**, 10720–10728.
- 14 H. C. Pehlivanugullari, E. Sumer and H. Kisch, *Res. Chem. Intermed.*, 2007, **33**, 297–309.
- 15 (a) H. Takeda, K. Koike, H. Inoue and O. Ishitani, *J. Am. Chem. Soc.*, 2008, **130**, 2023–2031; (b) W. R. McNamara, R. C. Snoberger, G. Li, J. M. Schleicher, C. W. Cady, M. Poyatos, C. A. Schmuttenmaer, R. H. Crabtree, G. W. Brudvig and V. S. Batista, *J. Am. Chem. Soc.*, 2008, **130**, 14329–14338; (c) P. Du, J. Schneider, F. Li, W. Zhao, U. Patel, F. N. Castellano and R. Eisenberg, *J. Am. Chem. Soc.*, 2008, **130**, 5056–5058.
- 16 O. Ozcan, F. Yukruk, E. U. Akkaya and D. Uner, *Top. Catal.*, 2007, **44**(4), 523–528.
- 17 G. Li, N. M. Dimitrijevic, L. Chen, J. M. Nichols, T. Rajh and K. A. Gray, *J. Am. Chem. Soc.*, 2008, **130**, 5402–5403.
- 18 M. Zhang, C. Chen, W. Ma and J. Zhao, *Angew. Chem.*, 2008, **120**, 9876–9879.
- 19 For typical chemical methods of reduction, see: (a) Y. Zheng, K. Ma, H. Wang, X. Sun, J. Jiang, C. Wang, R. Li and J. Ma, *Catal. Lett.*, 2008, **124**, 268–276; (b) M. O. Sydnes and M. Isobe, *Tetrahedron Lett.*, 2008, **49**, 1199–1202; (c) H. H. Hodgson and E. R. Ward, *J. Chem., Soc.*, 1949, 1316; (d) D. S. Wulfinson and C. F. Cooper, *Synthesis*, 1978, 924–925.
- 20 (a) H. Tada, A. Takao, T. Akita and K. Tanaka, *ChemPhysChem*, 2006, **7**, 1687–1691; (b) Y. Matsushita, S. Kumada, K. Wakabayashi, K. Sakeda and T. Ichimura, *Chem. Lett.*, 2006, **35**(4), 410–411; (c) H. Tada, T. Ishida, A. Takao, S. Ito, S. Mukhopadhyay, T. Akita, K. Tanaka and H. Kobayashi, *ChemPhysChem*, 2005, **6**, 1537–1543; (d) J. L. Ferry and W. H. Glaze, *J. Phys. Chem. B*, 1998, **102**, 2239–2244; (e) V. Brezová, A. Blažková, I. Šurina and B. Havlinová, *J. Photochem. Photobiol., A*, 1997, **107**, 233–237.
- 21 H. Tada, T. Ishida, A. Takao and S. Ito, *Langmuir*, 2004, **20**, 7898–7900.
- 22 S. O. Flores, O. Rios-Bernij, M. A. Valenzuela, I. Cordova, R. Gomez and R. Gutiérrez, *Top. Catal.*, 2007, **44**(4), 507–511.
- 23 Recent review: J.-H. Yum, P. Chen, M. Graetzel and M. K. Nazeeruddin, *ChemSusChem*, 2008, **1**, 699–707.
- 24 S. Chen and K. Kimura, *J. Phys. Chem. B*, 2001, **105**, 5397–5403.
- 25 E. Kolwaska, H. Remita, C. Colbeau-Justin, J. Hupka and J. Belloni, *J. Phys. Chem. C*, 2008, **112**(4), 1124–1131.
- 26 J. I. L. Chen, E. Loso, N. Ebrahim and G. A. Ozin, *J. Am. Chem. Soc.*, 2008, **130**, 5420–5421.
- 27 The use of TEOA for the photoreduction is essential. A replacement by  $\text{NEt}_3$  as the terminal reductant leads to a drastically decreased activity, which indicates the importance of the presence of protons for the overall photoreduction.
- 28 The chemoselective hydrogenation of substituted nitrobenzenes depending on the nature of the catalytically active metal and the catalyst support was described recently: A. Corma, P. Serna, P. Concepción and J. J. Calvino, *J. Am. Chem. Soc.*, 2008, **130**, 8748–8753.
- 29 B. H. Kim, Y. Jin, Y. M. Jun, R. Han, W. Baik and B. M. Lee, *Tetrahedron Lett.*, 2000, **41**, 2137–2140.
- 30 P. G. Hoertz, A. Staniszewski, A. Marton, G. T. Higgins, C. D. Incarvito, A. L. Rheingold and G. J. Meyer, *J. Am. Chem. Soc.*, 2006, **128**, 8234–8245.
- 31 M. K. Nazeeruddin, A. Kay, I. Rodicio, R. Humphry-Baker, E. Müller, P. Lisa, N. Vlachopoulos and M. Grätzel *et al.*, *J. Am. Chem. Soc.*, 1993, **115**, 6382–6390.
- 32 P. Svoboda, R. Saf and K. Hummel, *Macromolecules*, 1995, **28**, 4255–4259.

# Optimised microwave-assisted synthesis of methylcarbonate salts: a convenient methodology to prepare intermediates for ionic liquid libraries

John D. Holbrey,<sup>\*a</sup> Robin D. Rogers,<sup>a</sup> Saloni S. Shukla<sup>a</sup> and Cecilia D. Wilfred<sup>a,b</sup>

Received 10th September 2009, Accepted 26th October 2009

First published as an Advance Article on the web 18th November 2009

DOI: 10.1039/b918713h

The reaction of 1-butylpyrrolidine with dimethyl carbonate to yield the ionic liquid precursor, 1-butyl-1-methylpyrrolidinium methylcarbonate, has been investigated under microwave heating conditions and the reaction parameters optimised to achieve 100% yield of the pyrrolidinium salt with no by-products in under 1 h. The reactions of tributylamine, trioctylphosphine, and 1-butylimidazole with dimethyl carbonate under comparable conditions have also been evaluated, yielding the corresponding methylcarbonate salts which can be used as intermediates for the preparation of halide-free ionic liquids without generating any undesirable salt wastes.

## Introduction

The most versatile and commonly studied types of ionic liquids, referred to as *aprotic ionic liquids*, contain a fully alkylated organic cation.<sup>1</sup> These ionic liquids are generally prepared by initial alkylation of an organic base to yield the cation of choice followed, optionally, by a metathesis step to substitute the anion formed from the leaving group of the alkylating agent with a more desirable species following the general scheme below:

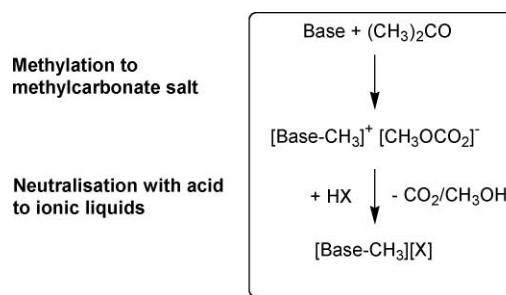


Alkylation with haloalkanes, such as chloroethane or bromobutane, has been the method of choice since the earliest studies on ionic liquids.<sup>2</sup> The haloalkanes are relatively cheap, simple to use, and reaction optimisation methods including the use of microwave<sup>3</sup> or ultrasonic induction,<sup>4</sup> high-shear mixing<sup>5</sup> and microchannel reactor arrays<sup>6</sup> have been reported. However, unless halide or halometallate ionic liquids are the desired products (for example as solvents for cellulose,<sup>7</sup> as Lewis-acidic catalysts,<sup>8</sup> or electrochemical solvents<sup>9</sup>), then a subsequent metathesis step to exchange the anion is required. Anion metathesis is usually achieved through the precipitation of insoluble silver,<sup>10</sup> or other halide salts,<sup>11</sup> although the use of anion exchange columns<sup>12</sup> and electro dialysis cells to form hydroxide solutions<sup>13</sup> have also been described. In all cases, salt wastes are produced as by-products and can leave a legacy of halide contamination in the final products which can lead to catalyst poisoning and unforeseen plant corrosion problems.

A better approach is to design the ionic liquid syntheses so that the anion required in the final product is introduced as the leaving group of the alkylating agent. A variety of alkylating agents have been used in this way including alkyl triflates, trifluoroacetates and sulfonates,<sup>14</sup> and alkylsulfates,<sup>15</sup>

*etc.* – all of which are hazardous, highly reactive and toxic reagents – to prepare ionic liquids. For those times when this approach is not practical, for example when the desired alkylating agent is too reactive (*e.g.* alkyl nitrates) or unreactive (*e.g.* simple alkylcarboxylate esters such as ethyl ethanoate), then a reasonable compromise is the formation of intermediate salts in which the anion of choice can be subsequently introduced simply, safely, at low cost, and with the least possible generation of waste.

Using these criteria, one of the most appealing reagents is dimethyl carbonate (DMC).<sup>16,17</sup> DMC is a non-toxic compound with a versatile and tuneable chemical reactivity, and can function as either a methoxycarbonylating or as a methylating agent<sup>18</sup> depending on the experimental conditions.<sup>19</sup> For methylation reactions the reaction temperature must typically be >120 °C, *i.e.* under pressure. DMC has been used as a replacement for highly toxic and hazardous conventional methylating agents such as methyl halides, methyl triflate and dimethyl sulfate<sup>20</sup> in the synthesis of surfactants, detergents, and phase transfer reagents from amines and phosphines.<sup>21</sup> More recently, ionic liquids have also been synthesised by methylation with DMC followed by reaction of the methylcarbonate salts formed with Brønsted acids, as shown schematically in Fig. 1.<sup>22-24</sup>



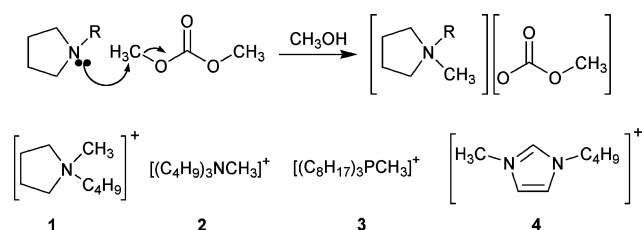
**Fig. 1** Schematic of the two-stage ionic liquid synthesis using DMC as a clean methylating agent to form intermediate methylcarbonate salts followed by neutralisation with Brønsted acids producing only molar equivalents of carbon dioxide and methanol as by-products.

<sup>a</sup>The QUILL Research Centre, School of Chemistry and Chemical Engineering, The Queen's University of Belfast, Belfast, BT9 5AG, Northern Ireland, UK. E-mail: j.holbrey@qub.ac.uk

<sup>b</sup>Foundation and Applied Science Department, Universiti Teknologi PETRONAS, Bandar Seri Iskandar, 31750, Tronoh, Perak, Malaysia

In contrast to the salt waste generated from the more traditional metathesis approaches, forming methylcarbonate salts and then neutralising with a Brønsted acid produces only carbon dioxide and methanol as by-products which are facile to remove and yields ionic liquids that are intrinsically halide-free. As such, the methodology is widely applicable, although with 1-alkylimidazoles, additional reaction pathways can yield C(2)- and C(4)-carboxylation, as well as *N*-methylation, so that 1,3-dialkylimidazolium-2-carboxylate<sup>25</sup> and 1,3-dialkyl-4-carboxylate zwitterions<sup>26</sup> are formed in addition to 1,3-dialkylimidazolium methylcarbonate salts.<sup>27</sup> Importantly, though, the zwitterions still react with acids, liberating CO<sub>2</sub>, and so can be used as precursors to ionic liquids.<sup>28</sup>

Despite the clear interest in the opportunities to use DMC as a methylating agent to yield ionic liquid precursors, almost all the available data from the literature relates to unoptimised batch reactions with time-scales on the order of tens of hours to days. Here we describe the results of studies into the optimisation of the reaction of DMC with a range of organic bases: 1-butylpyrrolidine, tributylamine, trioctylphosphine, and 1-butylimidazole (Fig. 2), in a microwave reactor under autogeneous pressure to yield quaternised methylcarbonate salts in high yield in a conveniently short time-frame.



**Fig. 2** Reaction scheme for the synthesis of 1-butyl-1-methylpyrrolidinium methylcarbonate from the reaction of 1-butylpyrrolidine with dimethyl carbonate in methanol, and the structures of the cations synthesised here: 1-butyl-1-methylpyrrolidinium (1), tributylmethylammonium (2), trioctylmethylphosphonium (3), and 1-butyl-3-methylimidazolium (4).

Our objective was to identify conditions where methylcarbonate salts could be rapidly synthesised in high purity, in order to obtain useful intermediates for the synthesis of ionic liquid libraries with common cations and a wide variety of anions, with minimal toxic or hazardous by-product formation.

## Experimental

Dimethyl carbonate, methanol, 1-butylpyrrolidinium, tributylamine, 1-butylimidazole, and trioctylphosphine of AR grade were purchased from Aldrich and used as received. Reactions were carried in quartz pressure vessels using a Milestone Microsynth microwave reactor. Reaction products were characterised by <sup>1</sup>H and <sup>13</sup>C NMR spectroscopy in DMSO-*d*<sub>6</sub> using a JEOL 300 MHz NMR spectrometer. Melting points and glass transition temperatures were determined using a TA Instruments Q2000 DSC. Thermal decomposition temperatures were determined from the onset to 5 wt% mass loss heating at 5 °C min<sup>-1</sup> in nitrogen, using a TA Instruments Q5000 TGA. Water content was measured using a Cou-Lo Aquamax KF Moisture meter (GRS Scientific). CHN elemental analyses and

electrospray MS were conducted by ASEP, Queen's University Belfast.

### Reaction of 1-butylpyrrolidinium with DMC

The reaction of 1-butylpyrrolidine with dimethyl carbonate in methanol was screened as a function of temperature (from 130–170 °C), 1-butylpyrrolidine:DMC ratio (from 1 : 1–1 : 4), and reaction time (*t* = 0–5 h). In a typical procedure, 1-butylpyrrolidine (5.66 g, 0.0445 mol), dimethyl carbonate (4.10 g, 0.0445 mol) and methanol (10 cm<sup>3</sup>) were placed in a microwave quartz reaction tube, sealed and heated with magnetic stirring to 130 °C.

Under the efficient microwave heating, the internal temperature of the reaction vessel reached the reaction set-points in 3–5 min. and was maintained at temperature ±5 °C using the power compensation feedback control. After defined times, the microwave heating was stopped and the reaction vessel cooled to room temperature quenching the reaction. The reaction mixture was sampled and analysed by <sup>1</sup>H NMR spectroscopy, and the product distribution and conversion of 1-butylpyrrolidine to 1-butyl-1-methylpyrrolidinium methylcarbonate were determined as a function of time, initial reagent composition and temperature from the relative integrals of the *N*-CH<sub>2</sub> signals of the reagent and product at ~3 ppm.

For optimised reactions (1 : 4 base:DMC, 130 °C, 1 h), the solvent and the excess alkylating agent were removed under reduced pressure at 50 °C and the resulting pale brown ionic liquid was recrystallised from methanol–ethyl ethanoate at 4 °C as colourless hygroscopic plates, mp 63 °C. (Found: C, 54.72; H, 10.79; N, 5.48. [C<sub>13</sub>H<sub>30</sub>N][C<sub>2</sub>H<sub>3</sub>O<sub>3</sub>] requires C, 60.80; H, 10.67; N, 6.45(6)†; δ<sub>H</sub> (300 MHz, DMSO-*d*<sub>6</sub>) 3.60 (4H, m, NCH<sub>2</sub>), 3.43 (5H, m, NCH<sub>2</sub>, NCH<sub>3</sub>), 3.10 (3H, s, [CH<sub>3</sub>OCO<sub>2</sub>]), 2.18 (4H, m, NCH<sub>2</sub>CH<sub>2</sub>), 1.76 (2H, m, NCH<sub>2</sub>CH<sub>2</sub>), 1.38 (2H, m, CH<sub>2</sub>CH<sub>3</sub>), 0.98 (3H, t, CH<sub>2</sub>CH<sub>3</sub>); δ<sub>C</sub> (125 MHz, DMSO-*d*<sub>6</sub>) 156.2, 63.5, 53.9, 51.5, 47.3, 25.2, 21.2, 19.4, 12.5. Decomp. 163 °C, water content 0.2157 wt%.

### Reaction of tributylamine with DMC

The reaction of tributylamine with dimethyl carbonate in methanol was screened as a function of temperature (from 110–160 °C), tributylamine:DMC ratio (from 1 : 2–1 : 4), and reaction time (*t* = 0–10 h). In a typical procedure, tributylamine (9.27 g, 0.05 mol), dimethyl carbonate (4.50 g, 0.05 mol) and methanol (10 cm<sup>3</sup>) were placed in a microwave quartz reaction tube, sealed and heated to 130 °C. The internal pressure and temperature of the reaction vessel were monitored. The reaction mixture was sampled and analysed by <sup>1</sup>H NMR spectroscopy, the product distribution and conversion being determined from the relative integrals of the *N*-CH<sub>2</sub> signals of the reagent and product at ~3 ppm.

Tributylmethylammonium methylcarbonate was isolated from the reaction under optimised conditions (1 : 2 base:DMC, 160 °C, 10 h) after removing the volatile solvent and excess DMC under reduced pressure as a brown oil, *T*<sub>g</sub> –59.5 °C. (Found: C, 62.01; H, 12.26; N, 5.03. [C<sub>13</sub>H<sub>30</sub>N][C<sub>2</sub>H<sub>3</sub>O<sub>3</sub>] requires C, 65.42;

† Typical results; it was not possible to obtain stable, reproducible elemental analyses of these extremely hygroscopic materials.



H, 12.07; N, 5.09%)<sup>†</sup>;  $\delta_{\text{H}}$  (300 MHz, DMSO- $d_6$ ) 3.17–3.21 (9H, s and m,  $[\text{CH}_3\text{OCO}_2^-]$  and  $\text{NCH}_2$ ), 2.97 (3H, s,  $\text{NCH}_3$ ), 1.62 (6H, m,  $\text{NCH}_2\text{CH}_2$ ), 1.32 (6H, m,  $-\text{CH}_2\text{CH}_3$ ), 0.954 (9H, t,  $J = 7.9$  Hz,  $\text{CH}_3$ );  $\delta_{\text{C}}$  (125 MHz, DMSO- $d_6$ ) 149.8, 60.9, 49.1, 48.0, 23.9, 19.9, 14.0. ESI-MS; +ve mode: 200.24 (100%,  $[\text{C}_{13}\text{H}_{30}\text{N}]^+$ ); –ve mode: 75.01 (100%,  $[\text{C}_2\text{H}_3\text{O}_3]^-$ ). Decomp. 150 °C, water content 2.14 wt%.

### Reaction of trioctylphosphine with DMC

The reaction of trioctylphosphine with dimethyl carbonate in methanol was performed at 140 °C with a 1:3 base:DMC ratio over 5 h. Trioctylphosphine (18.53 g, 0.05 mol), dimethyl carbonate (12.30 g, 0.15 mol) and methanol (10 cm<sup>3</sup>) were loaded under a dry dinitrogen atmosphere into a microwave quartz reaction tube, sealed and heated to 140 °C for 5 h, then cooled rapidly to room temperature. The internal pressure and temperature of the reaction vessel were monitored. The reaction mixture was sampled and analysed by <sup>1</sup>H NMR spectroscopy, showing complete conversion to the product.

1,1,1-Trioctyl-1-methylphosphonium methylcarbonate was isolated from the reaction mixture as a pale yellow oil, after removing the volatile solvent and excess DMC under reduced pressure.  $\delta_{\text{H}}$  (300 MHz, DMSO- $d_6$ ) 3.36 (3H, s,  $[\text{CH}_3\text{OCO}_2^-]$ ), 1.89 (6H, m,  $\text{NCH}_2$ ), 1.49 (3H, d,  $\text{NCH}_3$ ), 1.10–1.21 (12H, m), 0.92 (24H, m), 0.52 (9H, t,  $\text{CH}_3$ ).

### Reaction of 1-butylimidazole with DMC

A quartz microwave vessel was charged with 1-butylimidazole (6.378 g, 0.05 mol), dimethyl carbonate (6.756 g, 0.075 mol) and methanol (10 cm<sup>3</sup>). After sealing and placing in the microwave reactor, the vessel was heated to 150 °C. The internal pressure in the reactor increased on heating to 8–12 bar. Reactions were quenched after 3, 6, 9, and 12 h and sampled for analysis by <sup>1</sup>H NMR, using the downfield ring-hydrogen signals of the heterocycle.

The crude reaction mixture showed the presence of two products, 1-butyl-3-methylimidazolium methylcarbonate and 1-butyl-3-methylimidazolium-2-carboxylate, identified by <sup>1</sup>H NMR.  $\delta_{\text{H}}$  (300 MHz, DMSO- $d_6$ ) 6.86 (s, 1H, C(4)-H 1-butylimidazole), 7.15 (s, 1H, C(5)-H 1-butylimidazole), 7.575 (d, 1H,  $J = 2$  Hz, C(4)-H 1-butyl-3-methylimidazolium-2-carboxylate), 7.61 (s, 1H, C(2)-H 1-butylimidazole), 7.64 (d, 1H,  $J = 2$  Hz, C(5)-H 1-butyl-3-methylimidazolium-2-carboxylate), 7.73 (dd, 1H, C(4)-H,  $J_1 = J_2 = 1.5$  Hz 1-butyl-3-methylimidazolium), 7.8 (dd, 1H, C(5)-H,  $J_1 = J_2 = 1.5$  Hz, 1-butyl-3-methylimidazolium), 9.392 (s, 1H, C(2)-H 1-butyl-3-methylimidazolium). The major product, 1-butyl-3-methylimidazolium methylcarbonate, was confirmed by ESI-MS; +ve mode: 139.1218 (100%,  $[\text{C}_8\text{H}_{15}\text{N}_2]^+$ ); –ve mode: 75.0082 (100%,  $[\text{C}_2\text{H}_3\text{O}_3]^-$ ).

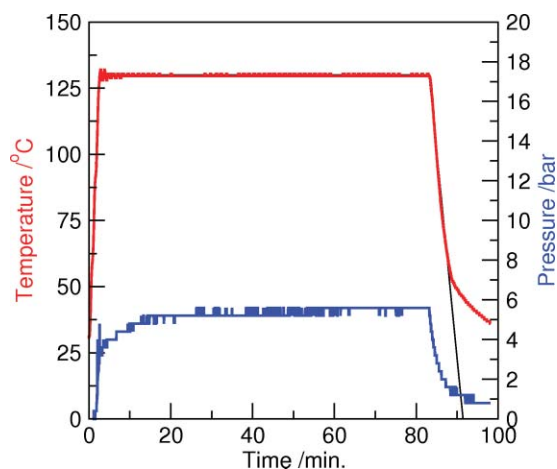
## Results and discussion

### 1-Butylpyrrolidine + DMC

DMC and 1-butylpyrrolidine were reacted in methanol in a Milestone MicroSynth microwave reactor under autogeneous pressure in a sealed 100 cm<sup>3</sup> quartz reaction vessels with

magnetic stirring, varying the reagent ratios between 1:1 and 1:4 1-butylpyrrolidine:DMC and reaction temperature between 130–170 °C using a controlled, programmed heating profile where the sample was heated to reaction temperature, held at temperature, and then rapidly cooled to room temperature for analysis.

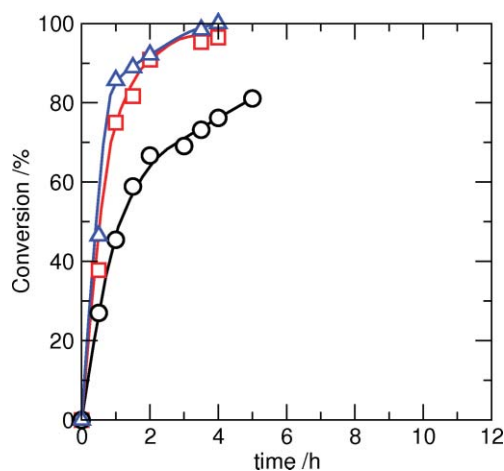
The internal reaction temperature was monitored using an *in situ* fibre-optic probe placed in the reaction solution and the temperature maintained using a feedback control to moderate the power output of the microwave magnetron. In a typical heating profile, the sample is heated with stirring, over 3–5 min, from ambient to the defined reaction temperature and then held for the duration of the reaction. This short initial ramping of the temperature resulted in an excellent correspondence between the programmed and actual monitored temperatures during the initial heating (Fig. 3) with little observed thermal lag. If an instantaneous temperature jump to (high) reaction temperatures was programmed, the finite time required for the power compensation feedback control to kick-in could result in initial overheating and temperature oscillation. From this point of view, the presence of methanol as a moderately polar cosolvent is advantageous in acting as a microwave adsorbant during the early stages of the reaction, allowing even heat distribution through the reaction media.



**Fig. 3** The short initial heating ramp (heating from ambient to final reaction temperature over the first 0–5 min) in a typical reaction profile gives excellent thermal control with the internal reaction temperature (red line) corresponding excellently with the set-point programmed temperature (black line). During the initial heating step, the internal reactor pressure (blue line) increases, but then remains constant for the remainder of the reaction time.

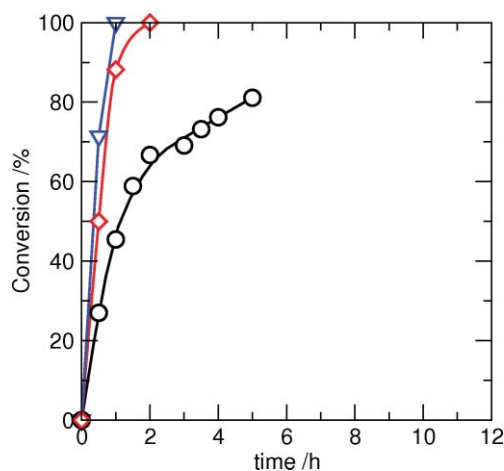
Set-point and internal temperature and pressure were monitored as the reaction progressed. On heating, the internal pressure in the vessels increased to a maximum of 8–12 bar. Reactions were quenched and sampled at times between 0–5 h for analysis.

Reactions were followed by <sup>1</sup>H NMR spectroscopy. The conversion of 1-butylpyrrolidine was monitored by comparing the relative values of the integrated signals from the amine and product. The percentage conversion of 1-butylpyrrolidine with reaction time is shown in Fig. 4 at constant 1:1 base:DMC



**Fig. 4** Conversion of 1-butylpyrrolidine to 1-butyl-1-methylpyrrolidinium methylcarbonate with time at 130 °C (○), 140 °C (□), and 170 °C (△) using a 1:1 base:DMC ratio.

ratio as a function of temperature and in Fig. 5 as a function of base:DMC ratio at 130 °C.



**Fig. 5** Conversion of 1-butylpyrrolidine to 1-butyl-1-methylpyrrolidinium methylcarbonate with time using 1:1 (○), 1:2 (◇), and 1:4 (▽) base:DMC ratios at 130 °C.

Only one product, 1-butyl-1-methylpyrrolidinium methylcarbonate, was identified in the reaction mixtures on the basis of  $^1\text{H}$  and  $^{13}\text{C}$  NMR spectroscopy, and was isolated from the optimised syntheses (see Experimental section) as an extremely hygroscopic low-melting crystalline solid after evaporation of the excess DMC and methanol followed by recrystallisation from methanol–ethyl ethanoate, and was fully characterised.

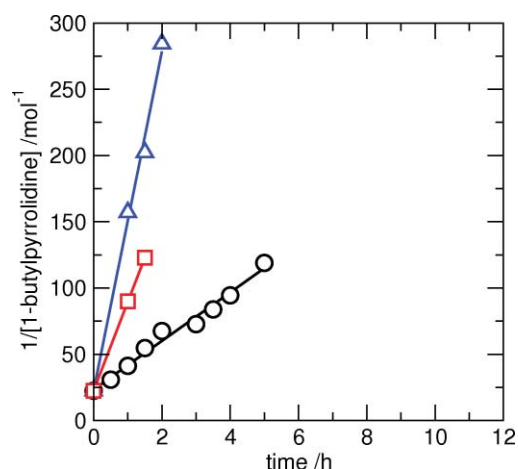
Using a 1:1 reagent ratio, 80% conversion of 1-butylpyrrolidine to 1-butyl-1-methylpyrrolidinium methylcarbonate was achieved after 5 h at 130 °C (Fig. 4). Increasing the reaction temperature to 140 °C resulted in both a significant increase in the initial rate of reaction and in the overall conversion (~98%), although further increments in the reaction temperature to 170 °C gave rise to much smaller changes to either the rate or final conversion; discolouration of the reaction mixtures was observed, indicating the start of undesirable decomposition pathways.

**Table 1** Second-order rate coefficients ( $k_2$ ) for the methylation of 1-butylpyrrolidinium with dimethyl carbonate at 1:1 reagent ratios obtained from the gradients of the linear fit to the data plotted in Fig. 6.

$T/^\circ\text{C}$	$k_2/\text{mol}^{-1}\text{ s}^{-1}$
130	$5.08 \times 10^{-3}$
140	$18.6 \times 10^{-3}$
170	$35.5 \times 10^{-3}$

The influence of base:DMC ratio was examined at 130 °C (Fig. 5). The addition of excess methylating agent resulted in a marked increase on the rate of reaction and also enabled the reaction to proceed to completion, with no 1-butylpyrrolidine detectable in the reaction mixtures after 2 h at 1:2 base:DMC and after 1 h at 1:4 base:DMC.

The initial rates of reaction at 1:1 base:DMC ratio were investigated by plotting the reciprocal of 1-butylpyrrolidine content ( $\text{mol}^{-1}$ ) against time for reactions at 130, 140, and 170 °C. The data (Fig. 6) show linear dependence of  $1/[\text{1-butylpyrrolidine}]$  with time indicating, as anticipated, overall second-order rate kinetics for the  $[\text{A}] + [\text{B}] \rightarrow [\text{C}]$  reaction. The second-order rate coefficients ( $k_2$ ) were determined at the three temperatures from the slopes of the plots of  $1/[\text{conc}]$  vs. time and are listed in Table 1. It is worth noting that  $k_2$  determined for the 1:1 composition at 130 °C ( $5 \times 10^{-3} \text{ mol}^{-1} \text{ s}^{-1}$ ) is comparable in magnitude with that reported for the alkylation of 1-methylimidazole with bromohexane ( $k_2 = 1.1 \times 10^{-3} \text{ mol}^{-1} \text{ s}^{-1}$ ) at 60 °C.<sup>29</sup>



**Fig. 6** Variation of the reciprocal concentration of 1-butylpyrrolidine ( $1/[\text{1-butylpyrrolidine}]$ ) present in the reaction mixtures as a function of time at 1:1 base:DMC at 130 °C (○), 140 °C (□), and 170 °C (△), showing the linear dependence of  $1/[\text{conc}]$  with  $t$  indicating initial second-order rate kinetics.

Taking the data points for conversion after 1 h, the temperature dependence of the rate coefficient was fitted using the Arrhenius equation ( $k_2 = A \exp(-E_a/RT)$ ) and gave a pre-exponential factor ( $A$ ) of  $1.3 \times 10^{-6} \text{ mol}^{-1} \text{ s}^{-1}$  and activation energy  $E_a = 64 \text{ kJ mol}^{-1}$  (though we do note that there is a significant uncertainty implicit in extrapolating from just three points, and from such a narrow temperature range).

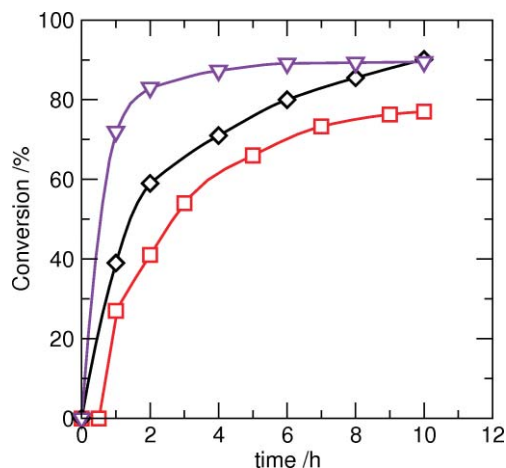
With efficient heat transfer, the reaction of 1-butylpyrrolidine with dimethyl carbonate was optimised to give complete

conversion of the amine to quaternary methylcarbonate salt in <1 h using an excess 1:4 ratio of DMC as methylating agent at 130 °C with overall second-order kinetics. Methylation of 1-butylpyrrolidine was observed with all reagent ratios from 1:1 to 1:4 base:DMC at temperatures above 130 °C with only one product, 1-butyl-1-methylpyrrolidinium methylcarbonate, observed by  $^1\text{H}$  NMR spectroscopy. Notably, the addition of a 2–4-fold excess of DMC resulted in the rapid, complete conversion of 1-butylpyrrolidine to product, from which the unreacted DMC and methanol solvent could be easily removed under reduced pressure. The product, 1-butyl-1-methylpyrrolidinium methylcarbonate, was isolated as a pale brown low-melting hygroscopic solid. Recrystallisation from methanol–ethyl ethanoate gave the salt as extremely hygroscopic colourless plates.

It is worth noting that during similar studies on the synthesis of quaternary ammonium methylcarbonate surfactants, Earl *et al.*<sup>18</sup> comment that products containing a brown colouration were obtained when the methylation reactions were performed in the presence of atmospheric oxygen – presumably due to formation of an oxidation product – and that colourless or very pale yellow salts were formed when reactions were performed in the absence of oxygen. In the reactions performed in this work, no special precautions were taken to exclude air from the reaction mixtures.

### Reaction of DMC with other organic bases

The reactivity of other organic bases with DMC was explored under analogous conditions to that used above with 1-butylpyrrolidine. Methylation of tributylamine with DMC was much slower than for 1-butylpyrrolidine under comparable conditions. Using a 1:2 base:DMC ratio, less than 20% methylation of tributylamine was observed at 110 °C after 7 h. Increasing the temperature led to increased reactivity and to an increase in the apparent initial rate and the overall yield, from 77% at 140 °C to 90% at 160 °C after 10 h (Fig. 7), in contrast to 98% conversion of 1-butylpyrrolidine at 140 °C after 4 h.

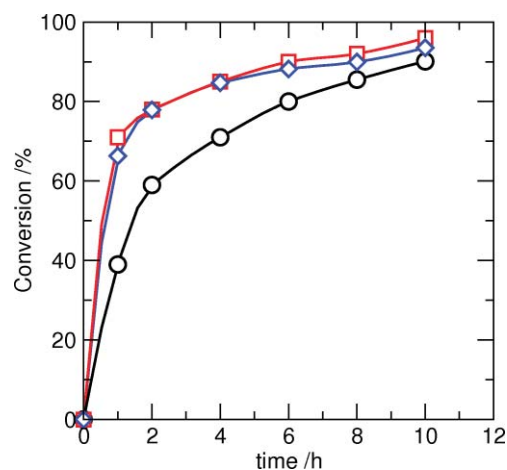


**Fig. 7** Conversion of tributylamine to tributylmethylammonium methylcarbonate with time at 140 °C (□), 150 °C (◇), and 160 °C (▽) using 1:2 base:DMC ratios.

On increasing the temperature further, to 160 °C, the rate of reaction increased, but no further enhancement in the

overall conversion of tributylamine to tributylmethylammonium methylcarbonate was observed, and the maximum yield (~90%) was achieved in 4–6 h. Examination of the thermal stability of isolated tributylmethylammonium methylcarbonate by TGA under dinitrogen showed that the onset of thermal decomposition at ambient pressure started at around 150 °C (most likely *via* Hoffmann E2 elimination pathways to generate volatile organic fragments<sup>30</sup>), and it is likely that the limiting conversion in the higher temperature reaction is a result of competing thermal decomposition. When the methylation reaction was attempted at higher temperatures, an increase in the reactor pressure was observed that approached the defined safe limits of operation of the microwave, and reactions were abandoned. These results, for the reaction of tributylamine with DMC, are consistent with data previously reported under conventional heating at moderate pressures, where yields of 91–96% were recorded using comparable reagent ratios and temperatures.<sup>18</sup>

As anticipated from classical kinetics, and from the comparative reaction of 1-butylpyrrolidine, increasing the concentration of DMC in the reaction mixture gave an increase in the reaction rate, although this was accompanied by only a small increment in the overall conversion, from 90 to around 95%. Data for reactions at 1:2, 1:3 and 1:4 base:DMC ratio at 150 °C are shown in Fig. 8. The results at 1:3 and 1:4 base:DMC ratio are effectively identical within experimental error.



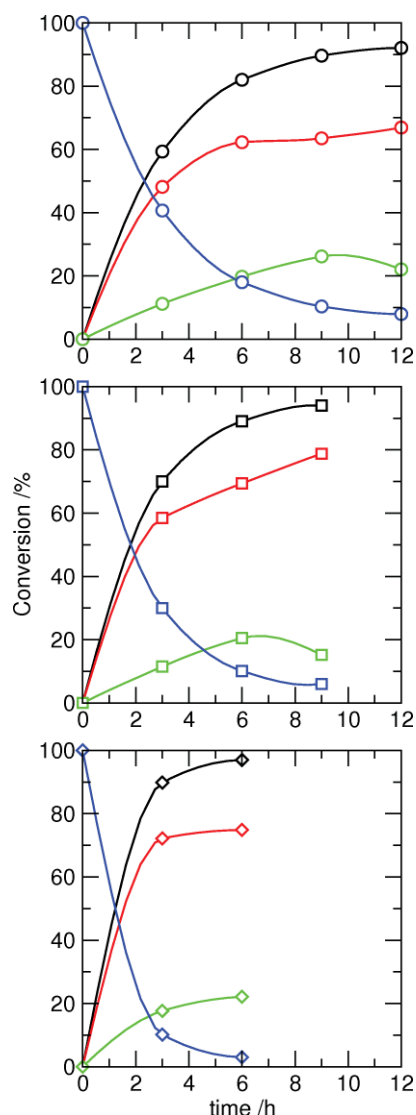
**Fig. 8** Conversion of tributylamine to tributylmethylammonium methylcarbonate with time using 1:2 (○), 1:3 (□), and 1:4 (◇) base:DMC ratios at 150 °C.

To examine whether thermal decomposition of the quaternary ammonium methylcarbonate salt was the limiting factor in the reactions at elevated temperatures, the reaction of trioctylphosphine with DMC at 140 °C with a 1:3 phosphine:DMC ratio for 5 h reaction time was performed. It was anticipated that the greater thermal stability of tetraalkylphosphonium salts compared to tetraalkylammonium salts should allow quantitative formation of the phosphonium methylcarbonate with no thermal degradation. The reaction of a 1:3 ratio of trioctylphosphine:DMC at 140 °C for 5 h gave complete methylation and formation of the trioctylmethylphosphonium methylcarbonate salt.

The reaction of 1-butylimidazole with DMC was conducted using 1:1–1:4 ratios of 1-butylimidazole:DMC at 140 °C

and 150 °C. The reaction rate was slower than that with 1-butylpyrrolidine though similar to that with tributylamine. In contrast to the reactions with the saturated amines, where only one reaction product was observed, with 1-butylimidazole two products, 1-butyl-3-methylimidazolium methylcarbonate and 1-butyl-3-methylimidazolium-2-carboxylate, were formed during the reaction.

At 140 °C and 1:1 1-butylimidazole:DMC ratio, only 35% conversion of 1-butylimidazole to products was observed after 7 h compared to 98% conversion of 1-butylpyrrolidine after 4 h. When an excess of DMC was used and the temperature was raised to 150 °C, both reactivity and total conversion to products were increased. Fig. 9 shows the total conversion, and distribution of the two products with time for reactions at 1:1.5, 1:2 and 1:4 1-butylimidazole:DMC ratio conducted at 150 °C.



**Fig. 9** Change in percentage composition with time for the reaction of 1-butylimidazole with DMC in 1:1.5 (*top*) 1:2 (*middle*) and 1:4 (*bottom*) base:DMC ratios (total conversion, *black*; 1-butylimidazole starting material, *blue*; 1-butyl-3-methylimidazolium methylcarbonate, *red*; 1-butyl-3-methylimidazolium-2-carboxylate, *green*) at 150 °C.

At 1:1.5 ratio, the conversion of 1-butylimidazole to products peaked at 92% after 12 h, whereas with increasing the 1-butylimidazole:DMC ratio further, a slight increase in total conversion was achieved, to 94% with 1:2 ratio and to 97% at 1:4. The rate of conversion increased in each case, so that the reaction was complete after 12 h at 1:1.5, 9 h at 1:2, and 6 h at 1:4 1-butylimidazole:DMC. In all the reactions, the ratio of imidazolium salt to imidazolium-2-carboxylate zwitterion formation remained consistent at approximately 4:1 irrespective of temperature and composition.

Unusually, the product distribution for the reactions here of 1-butylimidazole with DMC differs from that previously reported for reaction of 1-methylimidazole,<sup>24,27</sup> in which the 1,3-dimethylimidazolium-2-carboxylate zwitterion was isolated in up to 85% yield. The reasons for this inversion is not apparent, but may be the result of greater steric hindrance in 1-butylimidazole compared to 1-methylimidazole, or the formation of solid 1,3-dimethylimidazolium-2-carboxylate displacing the product equilibrium.

Compared to 1-butylpyrrolidine, which gave complete conversion at the same reagent ratios in less than 1 h at 130 °C, both tributylamine and 1-butylimidazole were significantly less reactive, although reactions could be run to completion in 6 h. The probable cause for the differences in reactivity of the amines is most likely steric crowding at the reaction centre, rather than differences in the  $pK_a$  of the different bases.

## Conclusions

Methylcarbonate salts are versatile halide-free intermediates for ionic liquid synthesis. Clean, quantitative formation of the methylcarbonate salts with no waste provides a platform to access large libraries of ionic liquids around common cations that are entirely halide-free, with only carbon dioxide and methanol produced as by-products through simple acid/base chemistry. This presents a highly desirable alternative to the conventional salt–salt metatheses usually used for ionic liquid synthesis.

While enhanced reaction kinetics arising from ‘microwave effects’ have been largely dispelled following careful experimentation,<sup>31</sup> there is still a clear utility in using microwave reactors, not least of which is the ability to heat samples rapidly with good thermal control. This provides a very useful methodology for screening and development, and, more importantly, with rapid heating to reaction temperature, potential side-reactions arising with dimethyl carbonate at intermediate temperatures (for example from the carboxylation pathway) can be reduced or eliminated.

The microwave batch synthesis of 1-butyl-1-methylpyrrolidinium methylcarbonate has been optimised in a Milestone Microsynth microwave reactor with 100% yield of the desired product obtained in 1 h using a 1:4 base:DMC ratio at 130 °C. For the reaction with tributylamine, 98% conversion to the desired product could be achieved after 6 h, however increasing the temperature to >140 °C to enhance the reaction rate initiated thermal decomposition of the ammonium methylcarbonate salts, resulting in poorer yields. Under comparable conditions, the more thermally stable trioctylmethylphosphonium methylcarbonate could be obtained quantitatively.

The reaction of 1-butyylimidazole with DMC yielded two products, the desired imidazolium methylcarbonate and zwitterionic imidazolium-2-carboxylate salts, in approximately 4 : 1 ratio irrespective of the conditions used. Interestingly, both the methylcarbonate salt and zwitterionic carboxylate can be converted to ionic liquids by reaction with acid.<sup>28</sup> Further work will examine a wider reaction space for the imidazolium salts, to try to identify conditions where carboxylate formation is suppressed and the imidazolium methylcarbonate is formed as the sole product.

Work is ongoing to extend optimisation to other useful ionic liquid-forming cations and to transfer the reaction to a continuous flow microwave reactor.

## Acknowledgements

The authors wish to thank Petrolia Nasional Berhad (PETRONAS) for financial support for this project (and particularly the Management of Petronas Research Sdn Bhd and Universiti Teknologi Petronas for initiating and establishing the collaborative program with QUB), Milestone Microwave Laboratory Systems for the loan of microwave reactors, and Prof. C. R. Strauss for invaluable discussions.

## References

- Ionic Liquids in Synthesis*, eds. P. Wasserscheid and T. Welton, Wiley-VCH, Weinheim, 2nd edn, 2008.
- J. S. Wilkes, J. A. Levisky, R. A. Wilson and C. L. Hussey, *Inorg. Chem.*, 1982, **21**, 1263.
- E. Boros, K. R. Seddon and C. R. Strauss, *Chim. Oggi*, 2008, **26**(6), 28.
- J. M. Leveque, S. Desset, J. Suptil, C. Fachinger, M. Draye, W. Bonrath and G. Cravotto, *Ultrasonics*, 2006, **13**, 189.
- M. A. Gonzalez and J. T. Ciszewski, *Org. Process Res. Dev.*, 2009, **13**, 64.
- D. A. Waterkamp, M. Heiland, M. Schlueter, J. C. Sauvageau, T. Beyersdorff and J. Thoeming, *Green Chem.*, 2007, **9**, 1084; D. Wilms, J. Klos, A. F. M. Kilbinger, H. Löwe and H. Frey, *Org. Process Res. Dev.*, 2009, **13**, 961.
- R. P. Swatloski, S. K. Spear, J. D. Holbrey and R. D. Rogers, *J. Am. Chem. Soc.*, 2002, **124**, 4974.
- R. Sheldon, *Chem. Commun.*, 2001, 2399–2407; C. M. Gordon, *Appl. Catal., A*, 2001, **222**, 101.
- Y. Ito and T. Nohira, *Electrochim. Acta*, 2000, **45**, 2611–2622; M. Galinski, A. Lewandowski and I. Stepniak, *Electrochim. Acta*, 2006, **51**, 5567.
- J. S. Wilkes and M. J. Zaworotko, *J. Chem. Soc., Chem. Commun.*, 1992, 965.
- L. Cammarata, S. Kazarian, P. Salter and T. Welton, *Phys. Chem. Chem. Phys.*, 2001, **3**, 5192.
- H. Ohno and K. Fukumoto, *Acc. Chem. Res.*, 2007, **40**, 1122.
- S. Himmler, A. Koenig and P. Wasserscheid, *Green Chem.*, 2007, **9**, 935.
- P. Bonhôte, A.-P. Dias, M. Armand, N. Papageorgiou, K. Kalyanasundaram and M. Grätzel, *Inorg. Chem.*, 1996, **35**, 1168.
- J. D. Holbrey, W. M. Reichert, R. P. Swatloski, G. A. Broker, W. R. Pitner, K. R. Seddon and R. D. Rogers, *Green Chem.*, 2002, **4**, 407.
- P. Tundo, F. Aricò, A. E. Rosamilia, S. Grego and L. Rossi, in *Green Chemical Reactions*, NATO Science for Peace and Security Series C: Environmental Security, 2008, pp. 213–232.
- M. Selva and A. Perosa, *Green Chem.*, 2008, **10**, 457.
- W.-C. Shieh, S. Dell and O. Repič, *J. Org. Chem.*, 2002, **67**, 2188; P. Tundo, *Continuous Flow Methods in Organic Synthesis*, Horwood, Chichester, UK, 1991.
- P. Tundo and M. Selva, *Acc. Chem. Res.*, 2002, **35**, 706.
- U. Romano, F. Rivetti and N. Di Muzio, *US Pat.* 4318862, 1981, CA 80141, 1979; F. Rivetti, U. Romano and D. Delledonne, in *Green Chemistry: Designing Chemistry for the Environment*, eds. P. Anastas and T. Williamson, ACS Symposium Series, American Chemical Society, Washington, DC, 1996, vol. 626, pp. 70–80.
- J. H. Wernitz, *US Pat.* 2635100, 1953; S. Mori, K. Ida and M. Ue, *Eur. Pat. Appl.* 88107735.8, 1988; B. Albert and M. Jansen, *Z. Anorg. Allg. Chem.*, 1995, **621**, 173; G. W. Earl, D. E. Weisshaar, D. Paulson, M. Hanson, J. Uilk, D. Wineinger and S. Moeckly, *J. Surfactants Deterg.*, 2005, **8**, 325.
- R. Kalb, *PCT* EP2004/009296; R. Kalb, W. Staber, M. Schelch, M. Kotschan, R. Hermann and W. Wesner, *US Pat. Appl.*, 2008251759(A1); C. Adelwohrer, Y. Yoneda, T. Takano, F. Nakatsubo and T. Rosenau, *Cellulose*, 2009, **16**, 139.
- R. Kalb and M. J. Kotschan, CBILS<sup>®</sup> A Revolutionary Tool for Ionic Liquid Synthesis, *ChemFiles*, 2006, **6**(9), 8.
- M. Aresta, I. Tkatchenko and I. Tommasi, in *Ionic Liquids as Green Solvents*, eds. R. D. Rogers and K. R. Seddon, ACS Symposium Series 856, Washington DC, 2002, p. 93.
- J. D. Holbrey, W. M. Reichert, I. Tkatchenko, E. Bouajila, O. Walter, I. Tommasi and R. D. Rogers, *Chem. Commun.*, 2003, 28.
- J. Fisher, W. Seigel, V. Bomm, M. Fisher and K. Mundinger, *US Pat.* 6175019, 1999.
- Z.-B. Zhou, M. Takeda and M. Ue, *J. Fluorine Chem.*, 2004, **125**, 471; Q. Zhu, Y. Song, X. Zhu and X. Wang, *J. Electroanal. Chem.*, 2007, **601**, 229.
- M. Smiglak, J. D. Holbrey, S. T. Griffin, W. M. Reichert, R. P. Swatloski, A. R. Katritzky, H. Yang, D. Zhang, K. Kirichenko and R. D. Rogers, *Green Chem.*, 2007, **9**, 90; N. J. Bridges, C. C. Hines, M. Smiglak and R. D. Rogers, *Chem. Eur. J.*, 2007, **13**, 5207.
- J. C. Schleicher and A. M. Scurto, *Green Chem.*, 2009, **11**, 694.
- B. K. M. Chan, N. H. Chang and M. R. Grimmitt, *Aust. J. Chem.*, 1977, **30**, 2005.
- S. Garbacia, B. Desai, O. Lavastre and C. O. Kappe, *J. Org. Chem.*, 2003, **68**, 9136; C. R. Strauss and R. S. Varma, *Microwave Methods in Organic Synthesis*, *Topics in Organic Chemistry*, 2006, **266**, 199; C. R. Strauss, *Aust. J. Chem.*, 2009, **62**, 3.

# Supported silver nanoparticles as photocatalysts under ultraviolet and visible light irradiation

Xi Chen,<sup>a</sup> Zhanfeng Zheng,<sup>a</sup> Xuebin Ke,<sup>a</sup> Esa Jaatinen,<sup>a</sup> Tengfeng Xie,<sup>b</sup> Dejun Wang,<sup>b</sup> Cheng Guo,<sup>c</sup> Jincai Zhao<sup>d</sup> and Huaiyong Zhu<sup>\*a</sup>

Received 16th October 2009, Accepted 2nd December 2009

First published as an Advance Article on the web 26th January 2010

DOI: 10.1039/b921696k

The significant activity for dye degradation by silver nanoparticles (NPs) on oxide supports was better than popular semiconductor photocatalysts. Moreover, silver photocatalysts can degrade phenol and drive oxidation of benzyl alcohol to benzaldehyde under ultraviolet light. We suggest that surface plasmon resonance (SPR) effect and interband transition of silver NPs can activate organic molecules for oxidation under ultraviolet and visible light irradiation.

## Introduction

Photocatalysts show great potential as drivers of chemical reactions when illuminated by sunlight at ambient temperatures.<sup>1–3</sup> One of the great challenges in this field is devising new catalysts that consist of nanoparticles (NPs) usually below 10 nm size regime and possess high activity when illuminated with either visible light or ultraviolet (UV) light.<sup>1</sup> The new photocatalysts will enable us to use sunlight, the abundant and green energy source, to drive useful chemical reactions. Once sunlight is utilized as a substitute of fossil fuel to drive reactions for production of important chemicals and environmental remediation, this will alleviate our reliance on fossil fuel energy and reduce energy consumption and CO<sub>2</sub> emissions. Conventional semiconductor photocatalysts, in particular TiO<sub>2</sub> based materials have been extensively investigated.<sup>2</sup> As these photocatalysts have a large band gap, photocatalysis can only occur when UV light is absorbed. Since more than 43% of the solar energy is in the visible part of the spectrum,<sup>3</sup> many approaches have been proposed to develop photocatalysts that can perform under visible light.<sup>1,3–4</sup> It is well known that gold, silver and copper NPs strongly absorb visible-light due to the so-called surface plasmon resonance (SPR) effect.<sup>5</sup> The SPR effect is the collective oscillation of conduction electrons in the NPs, which resonate with the electromagnetic field of the incident light. Also these excited electrons will return to their thermal equilibrium states and release heat to the lattice and surrounding medium.<sup>6</sup> This heating effect may also induce reactions of the molecules adsorbed on the particles. Indeed, we found that when illuminated with visible light, gold NPs dispersed on oxide supports exhibited significant activity for oxidation of formaldehyde and methanol in air at room temperature due to

the SPR effect.<sup>7</sup> Since visible light absorption heats the electrons and excites them from ground state to higher energy levels, the probability that a conduction electron participates in chemical reactions involving electron transfer is greater.

Silver NPs also exhibit considerable UV light absorption due to the interband transition (the transition of 4*d* electrons to the 5*sp* band).<sup>8</sup> Therefore, silver NPs are potentially photocatalysts that utilize the full solar spectrum. Silver NPs on the surface of semiconductors and electron-donor substances cause charge separation of photogenerated electron-hole pairs, thus enhancing the overall photocatalytic activity.<sup>9</sup> However, the photocatalytic activity of the silver NPs themselves has not been recognized. While silver ions were reported to be photoactive for certain reactions, such as nitric oxide decomposition and carbon-hydrogen bond activation,<sup>10</sup> to date even the precise nature of the reaction mechanism for the catalysis involving plasmonic silver materials has not been clarified. Here we verify that silver NPs at room temperature can be used to drive chemical reactions when illuminated with light throughout the solar spectrum, and in the process gain some understanding into the mechanism behind the photocatalytic process (which is different from that for the conventional semiconductor photocatalysts).

## Experimental

### Silver NPs preparation

Solution-phase reduction methods<sup>11</sup> were used to prepare the silver NPs supported on different oxides. ZrO<sub>2</sub>, Zeolite Y and amorphous SiO<sub>2</sub> powders were chosen as supports because of their band gaps (above ~5.0 eV), which are much larger than the energies of the photons of visible light (below 3.0 eV). Hence, the light cannot excite electrons from the valence band to the conduction band of the support. It is also impossible for the silver NPs on the support to reduce its band gap enough for visible light photons to be absorbed. Thus, the observed visible light absorption and catalytic activity by the photocatalysts is due to the supported silver NPs. The AgNO<sub>3</sub> solution (3 × 10<sup>-3</sup> M) containing suspended 0.5 g ZrO<sub>2</sub>, SiO<sub>2</sub> or zeolite Y

<sup>a</sup>School of Physical and Chemical Sciences, Queensland University of Technology, Queensland, 4001, Australia. E-mail: hy.zhu@qut.edu.au; Fax: +61 731381804; Tel: +61 731381581

<sup>b</sup>College of Chemistry, Jilin University, Changchun, 130012, China

<sup>c</sup>College of Science, Nanjing University of Technology, Nanjing, 210009, China

<sup>d</sup>Institute of Chemistry, Chinese Academy of Science, Beijing, 100080, China

(surface areas are 34, 47, 653 m<sup>2</sup> g<sup>-1</sup>, respectively) was irradiated with six UV lamps (20 W/tube, from Philips). The irradiated mixture was then centrifuged for 2 h, and the obtained Ag/oxide precipitate was washed with deionized water, dried at 80 °C and heated at 450 °C for 6 h.

### Sample characterization

Transmission electron microscopy (TEM) studies of supported silver NPs were carried out on Philips CM200 TEM with an accelerating voltage of 200 kV. The silver content was determined by energy dispersive X-ray spectroscopy (EDS) using FEI Quanta 200 Environmental SEM. X-ray photoelectron spectroscopy (XPS) analysis was performed on a Kratos Analytical Axis Ultra X-ray photoelectron spectrometer. X-ray diffraction (XRD) was carried out using a PANalytical with Cu-K $\alpha$  radiation. The surface photocurrent (SPC) measurements were performed on the system constituted of a source of monochromatic light, a lock-in amplifier (SR830-DSP) with a light chopper (SR540), and a photovoltaic cell. A 500 W xenon lamp (CHFXQ500W, Global xenon lamp power) and a double-prism monochromator (Hilger and Watts, D300) provide monochromatic light. A comb-like ITO electrode with an external bias (10.0 V) on its two sides was used. The sample chamber for transient photovoltage (TPV) measurements consists of an ITO electrode, a 10  $\mu$ m thick mica spacer as electron isolator, and a platinum wire gauze electrode (with a transparency of about 50%). The construction is a sandwich-like structure of ITO electrode-sample-mica-gauze platinum electrode. During the measurement, the gauze platinum electrode was connected to the core of a BNC cable which input signals to the oscilloscope. The samples were excited from platinum wire gauze electrode with a laser radiation pulse (wavelength of 532 nm and pulse width of 5 ns) from a third-harmonic Nd:YAG laser (Polaris II, New Wave Research, Inc.). The intensity of the pulse was regulated with a neutral gray filter and determined with an EM500 single-channel joulemeter (Molelectron, Inc.). The TPV signals were registered with a 500 MHz digital phosphor oscilloscope (TDS 5054, Tektronix).

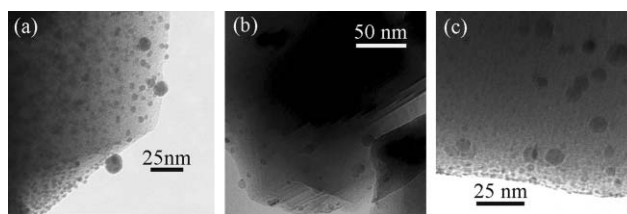
### Photocatalytic tests

In the photocatalytic dye sulforhodamine-B (SRB) degradation experiment under air atmosphere, aqueous suspensions of SRB (50 mL, 2  $\times$  10<sup>-5</sup> M) and 50 mg of photocatalyst were placed in a glass vessel, which was in a chamber with 6 light tubes (18 W/tube, Philips, light intensity 0.011 W cm<sup>-2</sup>, wavelength around 450 nm) as the light source. The pH of the solutions was adjusted to 2.5 with 0.1 M HNO<sub>3</sub>. An air conditioner was installed in the chamber to maintain the temperature at 25 °C as the light illumination could cause an increase in temperature of the vessel. Before irradiation the suspensions were magnetically stirred in the dark for 30 min to establish adsorption/desorption equilibrium between the dye and the catalyst. At given irradiation time intervals, 4 mL aliquots were collected, centrifuged, and then filtered through a Millipore filter (pore size 0.45  $\mu$ m) to remove the catalyst particulates. The filtrates were analyzed at the wavelength of maximal absorption (565 nm) in the UV-vis spectra of SRB using a Varian 5000. For comparison we also product nitrogen-doped TiO<sub>2</sub> by annealing

TiO<sub>2</sub> at 550 °C in N<sub>2</sub> gas for 4 h to test SRB photodegradation. In the photocatalytic phenol degradation experiment, aqueous suspensions of organic compounds (100 mL, 1 mM) and 100 mg of silver photocatalyst powders were placed in the vessel. Then the vessel was in a chamber with 6 UV light tubes as the light source (20 W/tube, NEC, light intensity was 0.014 W cm<sup>-2</sup>, wavelength around 365 nm). The filtrates were analysed at 270 nm in the UV-vis spectra using the Varian 50. In the benzyl alcohol degradation experiment, 50 ml toluene suspensions of benzyl alcohol (10%) and 50 mg of silver photocatalyst powders were placed in the glass vessel. Then the vessel was in a chamber with 6 UV light tubes as the light source. In order to increase photocatalytic activity, 30 mg NaOH was added into the benzyl alcohol solution and the vessel was filled with pure oxygen as the reaction atmosphere. The filtrates were analysed in GC HP6890 Prometheus to measure the concentration change of benzyl alcohol.

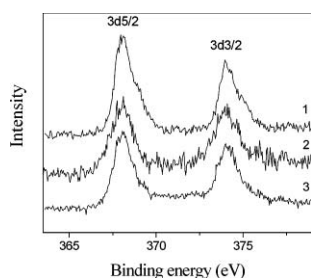
### Results and discussion

In this study, we loaded silver NPs onto various typical oxide supports<sup>12</sup> and used these photocatalysts for degrading a range of organic compounds in aqueous solution under either visible light or UV irradiation at room temperature. TEM images of silver NPs supported on ZrO<sub>2</sub> (Ag/ZrO<sub>2</sub>), amorphous SiO<sub>2</sub> (Ag/SiO<sub>2</sub>) and Zeolite Y (Ag/Zeolite Y) are shown in Fig. 1. These images indicate that silver exists in these samples as NPs. Most of the silver particles (the dark-colour substance) on these supports were found to have dimensions below 10 nm, which can lead to changes in surface and electronic structure providing an opportunity to control catalytic activity and selectivity.<sup>13</sup> The silver contents in Ag/Zeolite Y, Ag/ZrO<sub>2</sub> and Ag/SiO<sub>2</sub> samples were found by EDS to be 7.39, 7.48 and 7.56 wt% of the overall photocatalyst mass, respectively. XPS analysis shown in Fig. 2 indicated that the silver exists in metal state. However, no silver peaks can be identified through XRD pattern of our photocatalysts (shown in Fig. 3), probably due that the loaded silver did not form large particles, but was dispersed in the support structure.

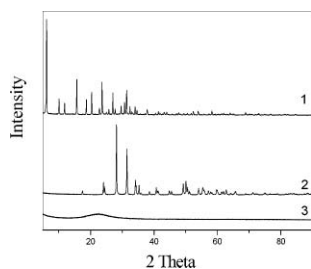


**Fig. 1** Transmission electron microscopy images of the photocatalysts of silver NPs on supports. (a) Silver on zeolite Y, Ag-zeolite Y. (b) Silver on zirconia, Ag-ZrO<sub>2</sub>. (c) Silver on silica, Ag-SiO<sub>2</sub>.

Dyes are of special interest as their use in the textile and industrial industries is becoming a significant source of environmental contamination.<sup>14</sup> Under visible light irradiation silver NPs dispersed on oxide supports exhibited significant activity for SRB degradation at 25 °C (An air conditioner was installed to maintain the temperature as the light illumination could cause an increase in the vessel temperature), which is even better than can be achieved with the widely reported nitrogen

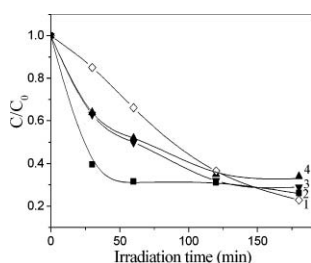


**Fig. 2** Binding energy of Ag 3d<sub>5/2</sub> and Ag 3d<sub>3/2</sub> for silver photocatalysts. (1) Ag/ZrO<sub>2</sub>; (2) Ag/SiO<sub>2</sub>; (3) Ag/Zeolite Y.



**Fig. 3** XRD analysis of silver photocatalysts. (1) Ag/ZrO<sub>2</sub>; (2) Ag/SiO<sub>2</sub>; (3) Ag/Zeolite Y.

doped TiO<sub>2</sub> photocatalysts. The comparison of degradation curves of SRB in aqueous solutions using silver photocatalysts after 180 min of blue light irradiation are shown in Fig. 4. Silver supported on zeolite exhibited the highest degradation ability among these materials. SRB content decreased by 74% in 3 h under blue light irradiation with intensity of 0.011 W cm<sup>-2</sup>. The photocatalysts of silver supported on zirconia and silica (Ag/ZrO<sub>2</sub> and Ag/SiO<sub>2</sub>) are also very active for SRB degradation (shown in Fig. 4). After 3 h of blue light irradiation, 71% and 66% of the dye were degraded with Ag/SiO<sub>2</sub> and Ag/ZrO<sub>2</sub>, respectively, slightly lower than the degradation rate with Ag/Zeolite Y. We also found a trend that the ability of the photocatalysts to degrade SRB increased with the increasing silver content. The Ag/Zeolite Y samples containing 4.5 wt% and 1.5 wt% of silver were also prepared. The SRB content decreased to 56% and 40% under blue light irradiation in 3 h, respectively. In the dark, SRB was not decomposed with any one of the three silver photocatalysts. A blank experiment under the otherwise identical conditions but without silver NPs (solutions with these oxide supports - Zeolite Y, ZrO<sub>2</sub> or SiO<sub>2</sub> powder only) was also conducted, and no SRB conversion above 3% was observed. Moreover, silver photocatalysts were stable under repeated application. About 82% SRB conversion catalyzed by



**Fig. 4** Degradation curves of SRB under blue light using different photocatalysts. (1) N-doped TiO<sub>2</sub>. (2) Ag/Zeolite Y. (3) Ag/SiO<sub>2</sub>. (4) Ag/ZrO<sub>2</sub>.

Ag/Zeolite Y can be maintained within 5 photodegradation recycles.

We also studied the effect that the intensity of the light irradiation had on the SRB degradation reaction. No concentration changes were detected if the experiment was conducted without light irradiation. When the light intensity was reduced to 0.008 and 0.006 W cm<sup>-2</sup> (by turning off 2 or 4 blue light tubes, respectively), the SRB conversion by Ag/SiO<sub>2</sub> decreased from 71% to 50% and 27%, respectively. The wavelength of the irradiation also affects the photocatalytic activity. Under red light irradiation (of 6 light tubes from Philips, with overall light intensity 0.010 W cm<sup>-2</sup> and wavelength around 650 nm) about 56% and 39% of SRB was converted by using Ag/SiO<sub>2</sub> and Ag/ZrO<sub>2</sub> as catalysts in 3 h, which is substantially lower than that under blue light (71% and 66%). These observations show that the SRB degradation is undoubtedly driven by visible light. Next, as the calcination temperature of silver samples was 300 °C, only 49% SRB was degraded over Ag/Zeolite Y under blue light for 3 h due to weak interaction between silver and support. While high calcination temperature (600 °C) can lead to big silver particles. 53% SRB was converted under the same experimental condition except the calcination temperature.

Moreover, these silver photocatalysts also can degrade organic compounds under UV light irradiation at room temperature. The UV light absorption by silver NPs can excite interband transition and be utilized to drive photoreactions. TiO<sub>2</sub> is the most widely studied photocatalyst under UV light irradiation, and nitrogen-doped TiO<sub>2</sub> can exhibit high activity when illuminated by visible light.<sup>4</sup> We compare the SRB photodegradation activity of the supported silver particles with that of TiO<sub>2</sub> material in Table 1. SRB conversions from replicate runs agree to each other within ±3%. The results confirm that silver NPs supported on oxides are superior to TiO<sub>2</sub> based photocatalysts for SRB degradation under both blue and UV light irradiation, given that the silver particles are the active photocatalysis component and that silver accounts for about 7.5 wt% of the catalyst mass.

The silver photocatalysts exhibited better catalytic activity under UV irradiation than under blue light. They not only decompose dye molecules under UV light faster than under visible light, but also are able to oxidize phenol in aqueous solution, which they cannot catalyze under visible light. After 120 h of UV light irradiation 41% of phenol was degraded by Ag/ZrO<sub>2</sub>. The photocatalytic conversion of phenol by Ag/Zeolite and Au/SiO<sub>2</sub> was 37% and 38%, respectively. The conversion of blank experiment (without catalyst under UV irradiation) was below 1%. These experimental results indicate that silver particles supported on oxides can catalyze the degradation of organic compounds without involving photosensitization process like dyes in aqueous solution at ambient temperature.<sup>15</sup>

The photocatalytic decomposition of organic compounds discussed above involves transfer of multiple electrons from the organic molecules to oxygen—the oxidant. In principle, selective (or partial) oxidation of an organic compound can be achieved with these photocatalysts if we regulate the electron transfer process by tuning the experimental conditions. Indeed, supported silver NPs were found to be effective catalysts for oxidation of benzyl alcohol in toluene to benzaldehyde. 11% benzyl alcohol conversion was achieved in 48 h under UV light irradiation with 62% of the product being benzaldehyde, when



**Table 1** Absorption of irradiation energy and catalytic activity of the photocatalysts to degrade SRB

Photocatalyst	Under blue light				Under UV light			
	Conversion <sup>a</sup>	Absorb energy	TOF <sup>b</sup>	Normalized TOF <sup>b</sup>	Conversion <sup>a</sup>	Absorb energy	TOF <sup>b</sup>	Normalized TOF <sup>b</sup>
	%	W cm <sup>-2</sup>	atom <sup>-1</sup> s <sup>-1</sup>	cm <sup>2</sup> J <sup>-1</sup> (Ag or TiO <sub>2</sub> )-atom <sup>-1</sup> s <sup>-1</sup>	%	W cm <sup>-2</sup>	atom <sup>-1</sup> s <sup>-1</sup>	cm <sup>2</sup> J <sup>-1</sup> (Ag or TiO <sub>2</sub> )-atom <sup>-1</sup> s <sup>-1</sup>
Ag-zeolite Y	68	0.007	1.6 × 10 <sup>-5</sup>	2.3 × 10 <sup>-3</sup>	75	0.007	1.8 × 10 <sup>-5</sup>	2.6 × 10 <sup>-3</sup>
Ag-ZrO <sub>2</sub>	48	0.007	1.1 × 10 <sup>-5</sup>	1.6 × 10 <sup>-3</sup>	55	0.006	1.3 × 10 <sup>-5</sup>	2.2 × 10 <sup>-3</sup>
Ag-SiO <sub>2</sub>	50	0.004	1.2 × 10 <sup>-5</sup>	3.0 × 10 <sup>-3</sup>	64	0.004	1.5 × 10 <sup>-5</sup>	3.8 × 10 <sup>-3</sup>
N-doped TiO <sub>2</sub>	34	0.001	1.5 × 10 <sup>-7</sup>	1.5 × 10 <sup>-4</sup>	49	0.005	2.2 × 10 <sup>-7</sup>	4.4 × 10 <sup>-5</sup>
TiO <sub>2</sub> (P25)	14	0.001	8.8 × 10 <sup>-9</sup>	8.8 × 10 <sup>-6</sup>	75	0.006	3.3 × 10 <sup>-7</sup>	5.5 × 10 <sup>-5</sup>

<sup>a</sup> SRB conversions from replicate runs agree to within ±3%. <sup>b</sup> Turnover frequency data in the table were calculated from the conversion after 1 h of irradiation.

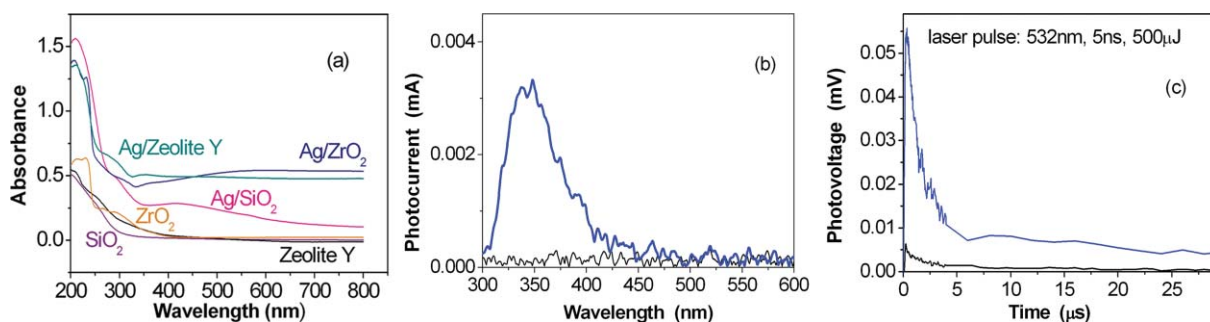
Ag/zeolite Y was used as the photocatalyst. Partial oxidation for producing aldehydes from corresponding alcohols is a very important process for the fine chemical industry.<sup>16</sup> We also increased the selectivity for producing benzaldehyde to 100% by adjusting the pH with NaOH solution<sup>17</sup> and using pure oxygen instead of air, though the overall conversion fell to 4% in 48 h.

Based on these facts, we conclude that the photocatalytic process with supported silver NPs does not occur *via* the same mechanism as found for semiconductor photocatalysts, such as TiO<sub>2</sub>.<sup>2</sup> In our study the silver NPs were supported on zeolite, ZrO<sub>2</sub> and SiO<sub>2</sub>. ZrO<sub>2</sub> has a band gap of about 5 eV.<sup>7</sup> The band gaps of zeolite Y and SiO<sub>2</sub> are slightly larger than that for ZrO<sub>2</sub>, according to the UV-vis absorption measurements shown in Fig. 5a by Cary5000 UV-Vis spectrometer. These supports alone (in the absence of the NPs) exhibit little light absorption. When light wavelengths are above 330 nm, the illumination cannot excite electrons of the supports from the valence band to the conduction band. Thus, all the photogenerated charges that lead to catalytic activity originate from the silver NPs. The silver in the photocatalysts remains in a metal state as indicated by the XPS analysis (Fig. 2), which is dissimilar to AgCl which can donate electrons and exhibit photocatalytic activity by the oxidation of Cl<sup>-</sup> ions to Cl<sup>0</sup> atoms under light irradiation.<sup>9</sup>

The photocatalytic reactions (degradation and selective oxidation) involve electron transfer from the molecules of the oxidized reactant to those of the reduced reactant. We believe that the silver NPs initialize and mediate the electron transfer for the photooxidation reactions. It has been reported that the

silver doped on TiO<sub>2</sub> surface can interact strongly with the oxygen atoms and give rise to an electron transfer to the Ti 3d states.<sup>18</sup> In order to determine whether light irradiation can induce electron transfer from the silver particle to the oxygen molecules (or oxygen adsorbed on the support), SPC and TPV spectra of the samples were also analysed and shown in Fig. 5. A surface current and a transient photovoltage will arise whenever excess light-induced charge carriers are separated in space, with the signal intensity being proportional to the number of the photogenerated charges.<sup>19</sup>

These spectra also explicitly exhibit the dependence of the electron transfer on the illumination wavelength allowing the spectral regions under which electron transfer occurs to be identified. For typical isolated spherical silver NPs the SPR absorption is generally around 380 nm, but the absorption band of the supported NPs is significantly red-shifted to above 410 nm.<sup>20</sup> Aggregation of the silver NPs and non-spherical shaped particles, which we observed in the samples in the present study, broaden the absorption resonance at low light intensity.<sup>21</sup> The silver NPs exhibit UV absorption, due to the interband excitation of electrons from 4d to 5sp. From the SPC spectra (Fig. 5b) it is apparent that UV absorption produces a much larger surface photocurrent than that induced by the SPR absorption under visible light irradiation. Also, a large initial photovoltage is observed in the TPV spectrum (Fig. 5c) which was measured with a 532 nm laser that has a much higher intensity than the light used for the SPC measurement. This indicates that visible light irradiation does generate electrical



**Fig. 5** (a) Light absorption of silver photocatalysts, zeolite Y and oxides in UV and visible light range. (b) Surface photocurrent spectra of silver NPs supported on zeolite Y (trace in blue) and zeolite Y (trace in black). (c) Transient photovoltage spectra of silver NPs supported on zeolite Y (trace in blue) and zeolite Y (trace in black).

surface charges when sufficiently intense. The SPC spectrum also indicates that the interband absorption (UV) results in a much larger proportion of electron transfer from silver NPs to the oxygen molecules than the SPR absorption (visible). Consequently, more positive charges (holes) are left in the silver NPs under UV illumination.

To explain these photocatalytic observations, we propose a tentative transfer mechanism as illustrated in Scheme 1. Before light illumination the silver electron occupancy obeys the Fermi–Dirac distribution. Blue light irradiation will excite the SPR and is strongly absorbed. Silver electrons are excited from within the outermost *sp* band to higher energy states.<sup>5</sup> Soon after light absorption the plasmon loses energy causing rapid heating of electron gas to an elevated temperature (about 400–2000 K) within a time scale of the order of 100 fs or less through electron–electron collision.<sup>22</sup> Then the electrons share the heat energy from the ‘hot’ electron gas with the NP lattice through electron–phonon collisions. The time scale varies from 500 fs to 10 ps.<sup>23</sup> Therefore, it is possible that the electrons with enough energy may be captured by a body once the capture process takes within 1 ps, according to Furube’s finding that the electron transfer from gold NPs to titanium oxide takes less than 240 fs.<sup>24</sup> We suggested that under visible light irradiation at moderate intensity, a very small number of silver electrons with high temperature gain sufficient energy (above the green line in Scheme 1) to be captured by oxygen molecules. However, most of the electrons are excited to lower energy levels (below

the green line in Scheme 1), which cannot be captured. Thus, a weak SPC signal and slow dye degradation are observed under moderate visible light illumination. The holes left in the *5sp* band can capture electrons from excited SRB molecules (SRB\*), due that the photosensitization process under light irradiation which involves initial excitation of the dye molecules can be helpful for injecting dye electrons.<sup>15</sup>

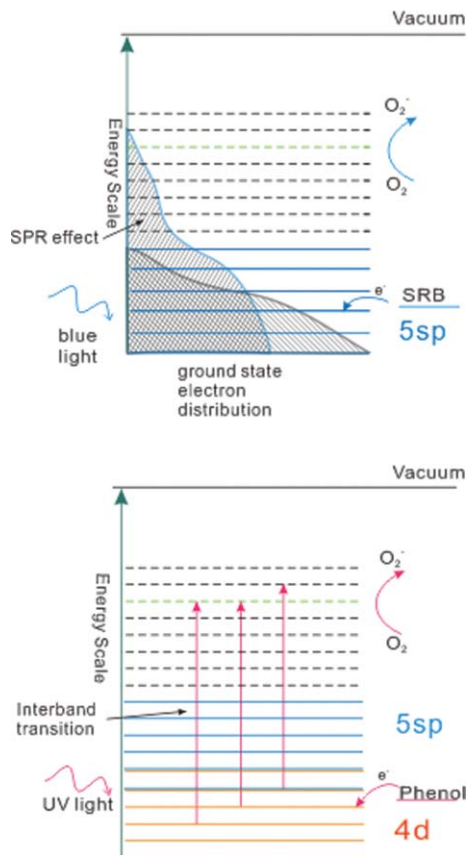
When silver particles absorb UV irradiation, electrons of the *4d* band can be excited to the *5sp* states band,<sup>8</sup> and many photogenerated electrons are in high energy (the green line or above in Scheme 1) where oxygen molecules can seize them, yielding large surface photovoltage signals under UV light. The holes left in the inner *d* band have a greater affinity for capturing electrons from the adsorbed organic molecules than those in the outermost *sp* band. Thus the presence of holes in the *d* band allows any attached phenol to be degraded by accepting its electrons. Since different mechanisms are responsible for degrading organic compounds under visible and UV light, the photocatalysts ability to oxidize specific compounds will depend on the illumination wavelength. This property can be utilized for two reaction regimes. First, under UV illumination, the photocatalysts can oxidize the compounds that they cannot oxidize under visible light, such as phenol. However, further research can be done with other reduction substances whose reduction potential is lower than that of  $O_2/O_2^-$ . Probably this will provide visible light driven catalytic activity of phenol degradation to silver photocatalysts. Second, the illumination wavelength can be used as a control parameter to determine whether a specific reaction will take place or not. The ability for the photocatalysts to capture electrons under UV light is a useful feature that can be used for producing desired chemicals under the experimental conditions which can prevent further oxidation, such as selective oxidation of benzyl alcohol to benzaldehyde by silver photocatalysts.

## Conclusions

In summary, silver NPs are good photocatalysts under ambient temperature for degrading organic compounds. Silver NPs supported on oxides can exhibit significant oxidation activity for a synthetic dye under visible light illumination. These photocatalysts can also catalyze phenol degradation as well as selective oxidation of benzyl alcohol under UV light. The findings indicate conceptually that it is possible to drive various chemical reactions with visible light. Therefore, as in the case of photochemistry driven by surface plasmon, it is a distinct possibility that environmental remediation and fine chemical production can be performed using the most efficient light source available—visible light. This will alleviate our reliance on fossil fuel energy and concerns in regards to global warming. Our findings also show the potential to switch on or off specific reactions by tuning the light wavelength. This development will lead to a new direction in photocatalysis research.

## Acknowledgements

Financial Supports from the Australian Research Council (ARC), and 973 program (2007CB613306) and NSFC (20537010) of China are gratefully acknowledged.



**Scheme 1** The diagram of the band structures of the supported silver NPs and the proposed photocatalysis mechanism.

## Notes and references

- 1 N. S. Lewis, *Nature*, 2001, **414**, 589–590; T. L. Thompson and J. T. Yates, *Chem. Rev.*, 2006, **106**, 4428–4453; S. U. M. Khan and M. Al-Shahry, *Science*, 2002, **297**, 2243–2245; M. Zhang, C. C. Chen, W. H. Ma and J. C. Zhao, *Angew. Chem., Int. Ed.*, 2008, **47**, 9730–9733.
- 2 M. I. Litter, *Appl. Catal., B*, 1999, **23**, 89–114; A. L. Linsebigler, G. Q. Lu and J. T. Yates, *Chem. Rev.*, 1995, **95**, 735–758; X. B. Chen and S. S. Mao, *Chem. Rev.*, 2007, **107**, 2891–2959.
- 3 Z. G. Zou, J. H. Ye, K. Sayama and H. Arakawa, *Nature*, 2001, **414**, 625–627.
- 4 R. Asahi, T. Morikawa, T. Ohwaki, K. Aoki and Y. Taga, *Science*, 2001, **293**, 269–271.
- 5 H. Yuan, *Chem. Mater.*, 2007, **19**, 1592–1600; G. C. Schatz, *Acc. Chem. Res.*, 1984, **17**, 370–376; X. H. Huang, I. H. El-Sayed, W. Qian and M. A. El-Sayed, *J. Am. Chem. Soc.*, 2006, **128**, 2115–2120; X. L. Zheng, W. Q. Xu, C. Corredor, S. P. Xu, J. An, B. Zhao and J. R. Lombardi, *J. Phys. Chem. C*, 2007, **111**, 14962–14967; S. Eustis and M. A. El-Sayed, *Chem. Soc. Rev.*, 2006, **35**, 209–217; K. L. Kelly, E. Coronado, L. L. Zhao and G. C. Schatz, *J. Phys. Chem. B*, 2003, **107**, 668–677; P. Mulvaney, *Langmuir*, 1996, **12**, 788–800; L. M. Liz-Marzán, *Langmuir*, 2006, **22**, 32.
- 6 S. Link, C. Burda, Z. L. Wang and M. A. El-Sayed, *J. Chem. Phys.*, 1999, **111**, 1255–1264; K. Yamada, K. Miyajima and F. Mafune, *J. Phys. Chem. C*, 2007, **111**, 11246–11251.
- 7 X. Chen, H. Y. Zhu, J. C. Zhao, Z. F. Zheng and X. P. Gao, *Angew. Chem., Int. Ed.*, 2008, **47**, 5353–5357.
- 8 P. V. Kamat, *J. Phys. Chem. B*, 2002, **106**, 7729–7744; P. P. Kiran, B. N. Bhaktha, D. N. Rao and G. De, *J. Appl. Phys.*, 2004, **96**, 6717–6723; C. Voisin, N. Del Fatti, D. Christofilos and F. Vallee, *J. Phys. Chem. B*, 2001, **105**, 2264–2280.
- 9 Y. H. Zheng, C. Q. Chen, Y. Y. Zhan and X. Y. Lin, *J. Phys. Chem. C*, 2008, **112**, 10773–10777; P. Wang, B. B. Huang, X. Y. Qin, X. Y. Zhang, Y. Dai, J. Wei and M. Whangbo, *Angew. Chem., Int. Ed.*, 2008, **47**, 7931–7933.
- 10 M. Matsuoka and M. Anpo, *Curr. Opin. Solid State Mater. Sci.*, 2003, **7**, 451–459; G. A. Ozin and F. Hugues, *J. Phys. Chem.*, 1982, **86**, 5174–5179.
- 11 R. Hu, L. Y. Xie, S. Ding, J. Hou, Y. Cheng and D. Z. Wang, *Catal. Today*, 2008, **131**, 513–519; Y. Shi, H. Pan, Y. T. Zhang and W. Li, *Catal. Commun.*, 2008, **9**, 796–800; F. C. Meunier, J. P. Breen, V. Zuzaniuk, M. Olsson and J. R. H. Ross, *J. Catal.*, 1999, **187**, 493–505.
- 12 M. M. Schubert, S. Hackenberg, C. Andre, M. Muhler and V. Plzak, *J. Catal.*, 2001, **197**, 113–122; L. Tosheva and V. P. Valtchev, *Chem. Mater.*, 2005, **17**, 2494–2513.
- 13 A. T. Bell, *Science*, 2003, **299**, 1688–1691.
- 14 E. J. Weber and R. L. Adams, *Environ. Sci. Technol.*, 1995, **29**, 1163–1170.
- 15 J. C. Zhao, C. C. Chen and W. H. Ma, *Top. Catal.*, 2005, **35**, 269–278.
- 16 V. R. Choudhary, P. A. Chaudhari and V. S. Narkhede, *Catal. Commun.*, 2003, **4**, 171–175.
- 17 J. J. Zhu, J. L. Figueiredo and J. L. Faria, *Catal. Commun.*, 2008, **9**, 2395–2397; S. K. Klitgaard, A. T. DeLa Riva, S. Helveg, R. M. Werchmeister and C. H. Christensen, *Catal. Lett.*, 2008, **126**, 213–217.
- 18 L. Giordano, G. Pacchioni, T. Bredow and J. F. Sanz, *Surf. Sci.*, 2001, **471**, 21–31.
- 19 P. Wang, B. B. Huang, X. Y. Zhang, X. Y. Qin, H. Jin, Y. Dai, Z. Y. Wang, J. Wei, J. Zhan, S. Y. Wang, J. P. Wang and M. Whangbo, *Chem.–Eur. J.*, 2009, **15**, 1821–1824.
- 20 T. Hirakawa and P. V. Kamat, *J. Am. Chem. Soc.*, 2005, **127**, 3928–3934.
- 21 J. A. Creighton and D. G. Eadon, *J. Chem. Soc., Faraday Trans.*, 1991, **87**, 3881–3891.
- 22 A. Takami, H. Kurita and S. Koda, *J. Phys. Chem. B*, 1999, **103**, 1226–1232; D. K. Roper, W. Ahn and M. Hoepfner, *J. Phys. Chem. C*, 2007, **111**, 3636–3641.
- 23 S. Link and M. A. El-Sayed, *Int. Rev. Phys. Chem.*, 2000, **19**, 409–453.
- 24 A. Furube, L. C. Du, K. Hara, R. Katoh and M. Tachiya, *J. Am. Chem. Soc.*, 2007, **129**, 14852–14853.

# Antimicrobial and antibiofilm activities of 1-alkylquinolinium bromide ionic liquids

Alessandro Buseti,<sup>a</sup> Deborah E. Crawford,<sup>a</sup> Martyn J. Earle,<sup>b</sup> Manuela A. Gilea,<sup>b</sup> Brendan F. Gilmore,<sup>\*a</sup> Sean P. Gorman,<sup>a</sup> Garry Laverty,<sup>a</sup> Andrew F. Lowry,<sup>a</sup> Martin McLaughlin<sup>a</sup> and Kenneth R. Seddon<sup>b</sup>

Received 24th September 2009, Accepted 7th December 2009

First published as an Advance Article on the web 26th January 2010

DOI: 10.1039/b919872e

Quinoline derivatives are known to possess a range of bioactive and medicinal activities, which have been exploited in the design of antibacterial, antifungal and antimalarial compounds. In this study, we report on the microbiological toxicity of a series of 1-alkylquinolinium bromides against a range of clinically relevant microorganisms, in both planktonic and sessile (biofilm) cultures. A comparison of antimicrobial activity against planktonic bacteria and established biofilms is presented. In general, 1-alkylquinolinium ionic liquids possess excellent, broad spectrum antimicrobial activity against microorganisms grown in both the planktonic and sessile, or biofilm, mode of growth. Importantly, these compounds are potent against Gram positive and Gram negative bacteria, as well as fungi, with a clear dependency on length of the alkyl substituent for activity, with compounds containing twelve and fourteen carbons in the alkyl group exhibiting highest antimicrobial and antibiofilm activity.

## Introduction

The ‘tunable’ nature of ionic liquids, whereby physical, chemical and biological property sets may be altered by independent modification of the constituent anions and cations, has been the major driving force behind the huge interest in this rapidly expanding field of chemistry. ‘Tuneability’ of ionic liquids introduces an unparalleled flexibility in the design of reagents for a particular functional niche, such designer solvents<sup>1,2</sup> have the potential to deliver a range of new reaction media potentially having greater diversity of character and application than that of the traditional solvents they are designed to replace,<sup>3,4</sup> whilst generally having negligible vapour pressure thus reducing the likely risk of atmospheric pollution.<sup>5</sup> As such, the major thrust of ionic liquids research in the past two decades has been towards ‘greening’ chemical processes *via* replacement of volatile organic compounds as solvents in the chemical industry.<sup>6,7,8</sup> Apart from direct replacement of organic solvents, ionic liquids have been shown to deliver improved reaction rate and yields in a number of chemical reactions<sup>9</sup> and may be suitable replacements for toxic catalysts, facilitate product recovery and have the potential for recyclability.<sup>10</sup>

Commonly employed classes of ionic liquids have recently been shown to exhibit toxicity towards both prokaryotic and eukaryotic organisms.<sup>10</sup> Since many classes of ionic liquids described in the literature exhibit varying degrees of aqueous

solubility, the potential for contamination and elaboration of toxicity in aquatic ecosystems will be important considerations in the design of processes utilising such compounds in place of traditional solvents. Ecotoxicological studies on several classes of ionic liquid demonstrated that some 1,3-dialkylimidazolium and 1-alkylpyridinium compounds exhibit toxicity towards the freshwater algae *Pseudokirchneriella subcapitata*,<sup>11</sup> while 1,3-dialkylimidazolium ionic liquids are toxic to the freshwater crustacean *Daphnia magna*,<sup>12</sup> the phytoplankton *Selenastrum capricornutum*,<sup>13</sup> and the nematode *Caenorhabditis elegans*.<sup>14</sup> To date, numerous studies have demonstrated the antimicrobial activity of various classes of ionic liquids against both environmental and clinically important microorganisms.<sup>15,16,17,18,19,20,21</sup> Biological issues relating to the widespread use of ionic liquids, such as stability, toxicity, biodegradability and recyclability (which are themselves ‘tunable’) have become increasingly important considerations. However, appropriate design and judicious use of ionic liquids having antimicrobial activity may equally deliver significant benefits in infection control through, for example, improved disinfectants, biocides and antiseptics. Microbial biofilms (matrix encased surface adherent microbial populations) are, according to a recent NIH announcement,<sup>22</sup> implicated in *ca.* 80% of chronic infections and constitute a significant public health risk for patients requiring indwelling medical devices,<sup>23</sup> with medical device usage implicated in approximately half of all incidences of nosocomial infections.<sup>24</sup> Furthermore, the biofilm represents an important survival strategy for microorganisms and, as such, is the predominant mode of growth for microorganisms in natural ecosystems,<sup>25,26</sup> where their presence may be desirable for ecological balance. Therefore, no assessment of either the microbiological/environmental toxicity or potential utility of ionic liquids as antimicrobial agents

<sup>a</sup>School of Pharmacy, The Queens University of Belfast, Medical Biology Centre, 97 Lisburn Road, Belfast, UK BT9 7BL.  
E-mail: b.gilmore@qub.ac.uk; Fax: +44 (0) 28 90 247 794; Tel: +44 (0) 28 90 972 047

<sup>b</sup>The QUILL Research Centre, School of Chemistry, The Queen's University of Belfast, Belfast, UK BT9 5AG

would be complete without attention to the antibiofilm efficacy of ionic liquids, since the biofilm affords significant tolerance to antimicrobial agents, when compared to the planktonic mode of microbial growth.<sup>23,27</sup>

Recently, we reported for the first time the *in vitro* antibiofilm activity of a series of 1-alkyl-3-methylimidazolium chloride ionic liquids against clinically relevant pathogenic bacteria (including MRSA) and fungi<sup>21</sup> using the Calgary Biofilm Device (CBD).<sup>27</sup> We now wish to report on the antimicrobial and antibiofilm activities of a series on 1-alkylquinolinium bromide ionic liquids, against a panel of clinically relevant pathogens, for example, methicillin resistant *Staphylococcus epidermidis* (MRSE) and *Pseudomonas aeruginosa*. To our knowledge, this is the first assessment of the antimicrobial and antibiofilm efficacy of 1-alkylquinolinium ionic liquids in the literature. However, the *in vitro* cytotoxicity of 1-alkylquinolinium ionic liquids (assessed against rat IPC-81 promyelocytic cells) has been discussed previously.<sup>28</sup>

## Experimental

### Synthesis of 1-alkylquinolinium bromide ionic liquids

A mixture of quinoline (0.100 mol) and a slight excess (0.105 mol) of either 1-bromooctane, 1-bromodecane, 1-bromododecane, 1-bromotetradecane, 1-bromohexadecane or 1-bromooctadecane was heated for 3 d at 80 °C under dinitrogen. When the reaction was completed (verified by <sup>1</sup>H NMR spectroscopy), the solid was obtained and purified *via* recrystallisation from boiling toluene/ethyl ethanoate mixtures. This mixture was then cooled at –15 °C, filtered under vacuum, washed with cold toluene (*ca.* 50 cm<sup>3</sup>) and dried under vacuum. This re-crystallisation process was repeated twice. The compound was then dried in a vacuum oven overnight at 70 °C. For each compound in the series, purity was found to be 98–99% by <sup>1</sup>H NMR spectroscopy. The <sup>1</sup>H and <sup>13</sup>C NMR data was as expected for 1-alkylquinolinium bromide ionic liquids<sup>29,30</sup> and revealed no organic impurities; the detailed characterisation will be reported in detail in a future manuscript. All salts were solid at room temperature, the melting points were determined using differential scanning calorimetry (DSC); [C<sub>6</sub>quin]Br m.p. = 66.0 °C; [C<sub>8</sub>quin]Br m.p. = 66.5 °C; [C<sub>10</sub>quin]Br m.p. = 86.6 °C; [C<sub>12</sub>quin]Br m.p. = 92.0 °C; [C<sub>14</sub>quin]Br m.p. = 102.5 °C; [C<sub>16</sub>quin]Br m.p. = 113 °C; [C<sub>18</sub>quin]Br m.p. = 116 °C. The general structure of 1-alkylquinolinium bromide is shown in Fig. 1.

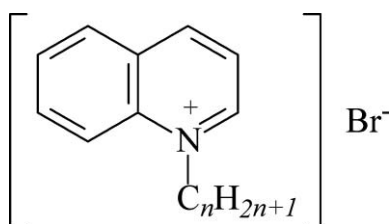


Fig. 1 General structure of [C<sub>n</sub>quin]Br.

### Strains and growth media

The following strains were used in this study: *Staphylococcus epidermidis* ATCC 12228 (non-biofilm forming), methicillin resistant *Staphylococcus epidermidis* (MRSE) ATCC 35984 (biofilm forming), *Staphylococcus aureus* ATCC 29213, methicillin resistant *Staphylococcus aureus* (MRSA) ATCC 43300, *Escherichia coli* NCTC 8196, *Klebsiella aerogenes* NCTC7427, *Bacillus cereus* NCTC 2599, *Proteus mirabilis* NCTC 12442, *Pseudomonas aeruginosa* PA01 and *Candida tropicalis* NCTC 7393. All microbial strains were stored at –70 °C in Microbank vials (Pro-Lab Diagnostics, Cheshire, UK), and subcultured in Müller Hinton Broth (MHB) before testing.

### MIC/MBC determination

Broth microdilution tests were carried out according to NCCLS guidelines, and as previously described.<sup>21</sup> An original working solution of each ionic liquid was prepared in MHB, and 0.22 μm sterile filtered. From this stock solution, serial two-fold dilutions in MHB were carried out in 96-well microtitre plates over the concentration range 0.00000763–1% w/v. Microorganisms under investigation were grown over 18–24 h at 37 °C in MHB, from which an inoculum was taken and adjusted to optical density 0.3 at 550 nm, which is the equivalent to 1 × 10<sup>8</sup> CFU cm<sup>-3</sup>. This suspension was further diluted to give a final inoculum density of 2 × 10<sup>5</sup> CFU cm<sup>-3</sup>, as verified by total viable count. The microtitre plate for determination of MIC (minimum inhibitory concentration) and MBC (minimum bactericidal concentration) was set up as described elsewhere,<sup>21</sup> and positive and negative controls included in each plate. All controls and test concentrations were prepared as six replicates. The microtitre plates were then incubated for 24 h at 37 °C in a stationary incubator. Following determination of the MIC for each compound, the minimum bactericidal concentrations (MBC) were derived by transferring 20 μL of the suspension from the wells, which displayed no signs of growth to MHA plates. The MHA plates were then incubated in a stationary incubator at 37 °C for 24 h and examined for 99.9% killing.

### Biofilm susceptibility assay

Biofilm susceptibility assays were performed using the Calgary Biofilm Device (MBEC Assay for Physiology & Genetics (P&G), Innovotech Inc., Edmonton, Alberta, Canada), a rapid, high throughput assay for the determination of microbial biofilm susceptibility to antimicrobial challenge. The biofilm assay was conducted essentially according to the manufacturer's instructions with some slight modifications as previously described.<sup>21</sup> Positive and negative controls (6 replicates) were included in each challenge plate alongside serial two-fold dilutions of the compound under test (6 replicates). After exposure of 24 h biofilms to challenge concentrations of 1-alkylquinolinium bromide ionic liquids, the recovery plate was incubated for a further 24 h at 37 °C and visually checked for turbidity, clear wells indicating biofilm eradication. The lowest concentration at which no observable growth was apparent after 24 h was designated the minimum biofilm eradication concentration (MBEC). For verification purposes, optical density in each well was recorded at 550 nm and compared with a negative (no-growth) control.

**Table 1** MIC and MBC values ( $\mu\text{M}$ ) of 1-alkyl-quinolinium ( $[\text{C}_n\text{quin}]\text{Br}$ )

Organism	$n$	$n$						
		8	10	12	14	16	18	
<i>S. aureus</i> (MRSA)	MIC		121.2	55.7	12.9	5.8	35.1	104.9
ATCC 43300	MBC		242	111.5	25.8	5.8	35.1	209.8
<i>S. epidermidis</i>	MIC		121.2	55.7	12.9	3	35.1	104.9
ATCC 12228	MBC		242	111.4	25.8	5.8	35.1	104.9
<i>S. epidermidis</i> (MRSE)	MIC		242	55.7	25.8	5.8	35.1	209.8
ATCC 35984	MBC		484	111.5	25.8	5.8	70.2	209.8
<i>S. aureus</i>	MIC		242	111.5	25.8	5.8	70.2	209.8
ATCC 29213	MBC		484	111.5	51.6	5.8	70.2	419.5
<i>B. cereus</i>	MIC		484.8	223	51.6	23.9	140.5	419.5
NCTC 2599	MBC		726	278.7	77.4	29.8	561.9	839
<i>E. coli</i>	MIC		121.2	55.7	25.81	11.6	35.12	104.9
NCTC 8196	MBC		242	167.2	38.7	11.6	70.24	209.8
<i>K. aerogenes</i>	MIC		60	55.7	12.9	5.8	35.12	104.9
NCTC 7427	MBC		242	167.2	38.7	11.6	35.12	104.9
<i>P. mirabilis</i>	MIC		242	111.5	25.8	5.8	70.2	104.9
NCTC 12442	MBC		363	167.2	51.6	5.8	140.5	209.7
<i>P. aeruginosa</i>	MIC		484.8	223	51.6	23.9	70.2	419.5
PA01	MBC		605	446	90.3	23.9	280.9	419.5
<i>C. tropicalis</i>	MIC		242	55.7	12.9	3	35.1	104.9
NCTC 7393	MBC		363	111.5	25.8	3	70.2	419.5

Recovery plates were incubated for a further 24 h at 37 °C to confirm minimum biofilm eradication concentrations.

### Haemolysis assay

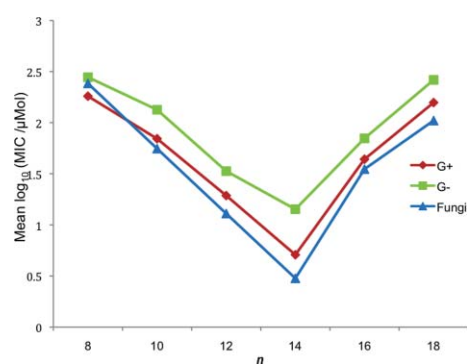
In order to assess the potential for 1-alkylquinolinium bromide ionic liquids to elicit haemolysis, 1-alkylquinolinium bromides  $[\text{C}_n\text{quin}]\text{Br}$  ( $n = 8, 10, 12, \text{ or } 14$ ) were spectrophotometrically assayed for their ability to induce haemoglobin release from fresh equine erythrocytes according to the method of Shin *et al.*<sup>31</sup> Essentially, fresh defibrinated equine erythrocytes (Laboratory Supplies & Instruments Ltd., Antrim, UK), were rinsed three times with equal volumes of phosphate buffered saline (PBS), following centrifugation for 15 min at 900 g, the erythrocytes were re-suspended 4% (v/v) in PBS. Equal volumes (100  $\mu\text{L}$ ) of the erythrocyte suspension were added to each well of a 96-well microtitre plate. Erythrocytes were subsequently exposed to selected ionic liquid concentrations, incubated at 37 °C for 1 h and centrifuged at 1000 g. Aliquots of the supernatant were transferred to a fresh 96-well microtitre plate, and haemoglobin release measured spectrophotometrically at 405 nm. As a positive control (100% haemolysis), erythrocytes were treated with 0.1% Triton X-100, whilst PBS (0% haemolysis) acted as a negative control. All samples (and controls) were assayed in quadruplicate. Percentage haemolysis was calculated as follows:

$$\% \text{Haemolysis} = \frac{(\text{Abs}_{405} \text{ ionic liquid solution}) - (\text{Abs}_{405} \text{ PBS})}{(\text{Abs}_{405} \text{ 0.1\% Triton X-100}) - (\text{Abs}_{405} \text{ PBS})}$$

## Results and discussion

Quinoline derivatives are known to possess a range of bioactive and medicinal activities, which have been exploited in the design of antibacterial,<sup>32</sup> antifungal<sup>33</sup> and antimalarial<sup>34</sup> compounds. In this study, we have examined a series of 1-alkylquinolinium bromides for their microbiological toxicity against a range

of clinically relevant microorganisms, in both planktonic and sessile (biofilm) cultures. Minimum inhibitory concentrations (MIC) and minimum bactericidal/fungicidal concentration (MBC) values determined for a range of 1-alkylquinolinium bromide ionic liquids  $[\text{C}_n\text{quin}]\text{Br}$  (where  $n = 8, 10, 12, 14, 16 \text{ or } 18$ ) against a range of pathogenic organisms are shown in Table 1. The mean MIC values for Gram positive bacteria (*S. epidermidis* ATCC 12228 and ATCC 35984 (MRSE), *S. aureus*, *B. cereus*), Gram negative bacteria (*E. coli*, *P. aeruginosa*, *P. mirabilis*, *K. aerogenes*) and fungi (*C. tropicalis*) are shown in Fig. 2. The determined MIC values for the 1-alkylquinolinium bromide ionic liquids were consistent with those previously published by Pernak and co-workers.<sup>35</sup>



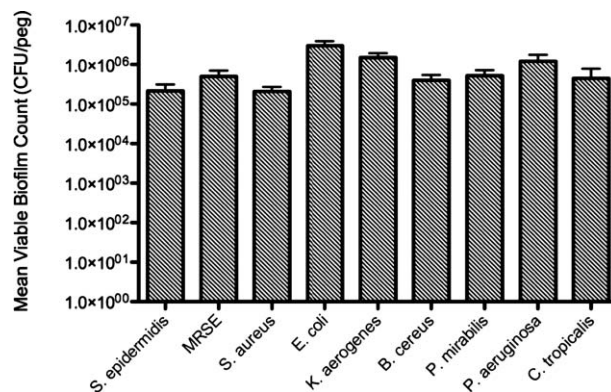
**Fig. 2** Mean [1-alkylquinolinium]Br ionic liquid minimum inhibitory concentrations (MIC) values for Gram positive cocci, Gram negative rods and fungi.

All compounds tested exhibited broad spectrum antimicrobial activity; the data presented here are in general agreement with previous studies of antimicrobial ionic liquids<sup>21</sup> whereby antimicrobial activity increases with increasing alkyl chain length, up to a maximum of 14–16, whence it decreased. Taken together, these data indicate that antimicrobial activity is likely to be governed by maximal interaction with the microbial cell

**Table 2** MIC and MBEC values ( $\mu\text{M}$ ) of 1-alkylquinolinium bromides [ $C_n$ quin]Br

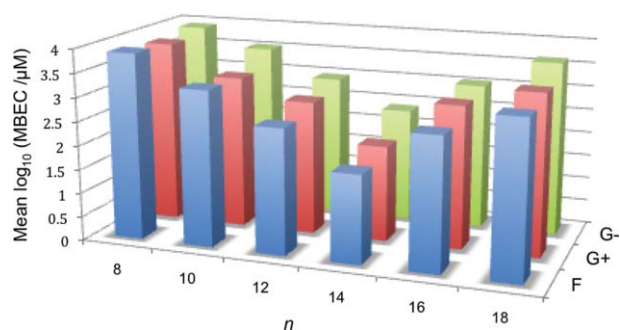
	<i>n</i>						
		8	10	12	14	16	18
<i>S. aureus</i> (MRSA)	<b>MIC</b>	121.2	55.7	12.9	5.8	35.1	104.9
ATCC 43300	<b>MBEC</b>	3913	896	413.9	68.3	561.9	1678.1
<i>S. epidermidis</i> (MRSE)	<b>MIC</b>	242	55.7	25.8	5.8	35.1	209.8
ATCC 35984	<b>MBEC</b>	7826	1792	827.9	136.7	1123.8	1678.1
<i>S. aureus</i>	<b>MIC</b>	242	111.5	25.8	5.8	70.2	209.8
ATCC 29213	<b>MBEC</b>	7826	1956	619.5	91.1	1123.8	3356.2
<i>B. cereus</i>	<b>MIC</b>	484.78	223	51.6	23.95	140.5	419.5
NCTC 2599	<b>MBEC</b>	7826	3584	774.2	273.3	1123.8	3356.2
<i>E. coli</i>	<b>MIC</b>	121.2	55.7	25.8	11.6	35.1	104.9
NCTC 8196	<b>MBEC</b>	8315	3584	827.9	136.7	561.9	1678.1
<i>K. aerogenes</i>	<b>MIC</b>	60	55.7	12.9	5.8	35.1	104.9
NCTC 7427	<b>MBEC</b>	9782	4568	981.2	136.7	561.9	6712.3
<i>P. mirabilis</i>	<b>MIC</b>	242	111.5	25.8	5.8	70.2	104.9
NCTC 12442	<b>MBEC</b>	7826	3584	1655.9	546.6	2247.7	3356.2
<i>P. aeruginosa</i>	<b>MIC</b>	484.8	223	51.6	23.9	70.2	419.5
PA01	<b>MBEC</b>	8315	1792	413.9	136.7	1123.8	6712.3
<i>C. tropicalis</i>	<b>MIC</b>	242	55.7	12.9	3	35.1	104.9
NCTC 7393	<b>MBEC</b>	7826	1792	413.9	68.3	561.9	1678.1

membrane and hydrophobicity. A recent study of the antimicrobial effects of fatty acids and amines against MRSA found optimal antimicrobial activity (though relatively low compared with compounds quoted here) with lauric acid (dodecanoic acid;  $C_{11}H_{23}CO_2H$ ) and myristylamine ( $C_{14}H_{29}NH_2$ ),<sup>36</sup> confirming the observations regarding influence of chain length on antimicrobial activity. Again, in keeping with previous studies, Gram positive organisms (with the exception of *B. cereus*) and fungi are more sensitive to these compounds than Gram negative organisms, although the relative differences in susceptibilities are not as pronounced as those previously reported for 1-alkyl-3-methylimidazolium ionic liquids,<sup>21</sup> indicating that 1-alkylquinolinium bromides exhibit excellent broad spectrum activity against all organisms tested. The Gram negative outer membrane may serve as a barrier to the entry of antimicrobial molecules, particularly those which interact with the membrane (such as fatty acids and acylated/alkylated compounds) whereas the bacterial cell wall of gram positive organism may absorb such compounds and transport them to the inner cell membrane,<sup>37,38</sup> thus potentially explaining the observed differences in susceptibility to 1-alkylquinolinium bromides between Gram positive and Gram negative bacteria. Minimum inhibitory concentrations and minimum bactericidal/fungicidal concentrations for these compounds are superior when compared to previously reported ionic liquids (1-alkyl-3-methylimidazolium chlorides,<sup>21</sup> 1-alkoxymethyl-3-methylimidazolium chlorides and tetrafluoroborates,<sup>16</sup> and 1-alkylimidazolium DL-lactates),<sup>19</sup> and comparable to reported phosphonium ionic liquids.<sup>39</sup> Furthermore, these compounds generally have superior antimicrobial activity compared to 3-alkylpyridinium salts isolated from the marine sponge *Reniera sarai* and their synthetic analogues.<sup>40</sup> Biofilm cultures of each target microbial species were grown for 24 h before exposure them to varying concentrations of 1-alkylquinolinium bromide ionic liquids. As a positive control, viable counts of 24 h biofilms (6 replicates) were performed to ascertain mean viable biofilm counts, given in Fig. 3. These data demonstrate the extent of biofilm formation after 24 h incubation, with an adherent population on each peg of greater



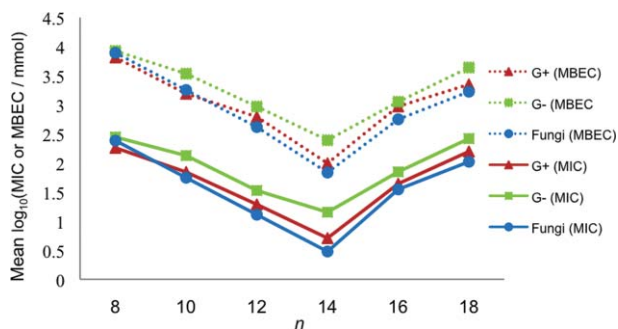
**Fig. 3** Mean biofilm viable cell counts for each organism grown on the Calgary Biofilm Device. Each value is expressed as the mean of six replicates.

than  $1 \times 10^5$  viable bacteria per peg (CFU per peg). Minimum biofilm eradication concentrations for each biofilm forming species, are given in Table 2, where corresponding MIC values are also included for comparison. The data from Table 2 are represented as the mean  $\log_{10}(\text{MBEC})$  values ( $\mu\text{M}$ ) in Fig. 4,



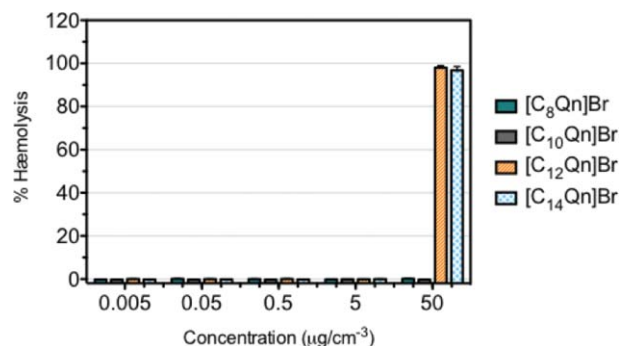
**Fig. 4** Mean minimum biofilm eradication concentration (MBEC) values for [1-alkylquinolinium]Br ionic liquids where ( $n = 8, 10, 12, 14, 16$  or  $18$ ) for the representative fungi, *C. tropicalis* (F), Gram positive (G+) cocci and Gram negative (G-) rods.

and comparison of the MIC/MBEC values {as mean  $\log_{10}(\mu\text{M})$  values} in Fig. 5. In keeping with our previously reported study of 1-alkyl-3-methylimidazolium chlorides ionic liquids<sup>21</sup> (and planktonic data from the current study), these data demonstrate that MBEC values for the 1-alkylquinolinium bromides are dependent on the length of alkyl chain. 1-Alkylquinolinium bromide ionic liquids with an alkyl chain of  $n > 8$  possess antimicrobial activity against both biofilm and planktonic microorganisms, with maximum antimicrobial and antibiofilm activity where the number of carbons in the alkyl chain is 14. The minimum biofilm eradication concentrations of the most potent compound in the range (1-tetradecylquinolinium bromide) against Gram positive organisms are comparable to those for the most potent antibiofilm compound in the previous study, 1-tetradecyl-3-methylimidazolium chloride.<sup>21</sup> However, average 1-tetradecylquinolinium bromide MBEC values are significantly lower for Gram negative bacteria and the representative fungi, *C. tropicalis*, than the corresponding 1-tetradecyl-3-methylimidazolium chloride. The data indicate that, in general, the 1-alkylquinolinium bromide ionic liquids are more potent broad spectrum antimicrobials (against both planktonic and sessile microorganisms) than the corresponding 1-alkyl-3-methylimidazolium chloride ionic liquids and that modifications to the head group can yield differences in both potency and spectrum of antimicrobial activity, further validating the ability to 'tune' the antimicrobial toxicity of ionic liquids. In addition, we have observed that modification of the quinoline head group has the ability to alter microbiological toxicity (data not shown), in keep with observations that not only head group, but substitution and functionalisation of head group, has the ability to alter biological toxicity.<sup>41</sup>



**Fig. 5** Comparison of mean MIC and MBEC values for [1-alkylquinolinium]Br ionic liquids where ( $n = 8, 10, 12, 14, 16, 18$ ) for Gram positive and Gram negative bacteria, and the representative fungi, *C. tropicalis*.

Finally, the haemolytic activity of the 1-alkylquinolinium bromide ionic liquids ( $n = 8, 10, 12, \text{ or } 14$ ) was evaluated against fresh equine erythrocytes (Fig. 6). The results of the haemolytic assay indicate that the compounds tested exhibit no haemolytic activity up to  $50 \mu\text{g cm}^{-3}$ , at this concentration 1-dodecylquinolinium bromide ( $[\text{C}_{12}\text{quin}]\text{Br}$ ,  $142.85 \mu\text{M}$ ) and 1-tetradecylquinolinium bromide ( $[\text{C}_{14}\text{quin}]\text{Br}$ ,  $132.6 \mu\text{M}$ ) caused  $97.7 \pm 2.6\%$  and  $97.3 \pm 5.1\%$  haemolysis, respectively. This is unsurprising given the high antimicrobial potency of these compounds, which is most likely due to their ability to disrupt cellular membranes. Even at  $50 \mu\text{g cm}^{-3}$ , 1-octylquinolinium



**Fig. 6** Haemolytic activity [1-alkylquinolinium]Br ( $[\text{C}_8\text{--C}_{14}\text{quin}]\text{Br}$ ) ionic liquids against equine erythrocytes. Each value is expressed as the mean of six replicates.

bromide ( $[\text{C}_8\text{quin}]\text{Br}$ ,  $155.1 \mu\text{M}$ ) and 1-decylquinolinium bromide ( $[\text{C}_{10}\text{quin}]\text{Br}$ ,  $142.7 \mu\text{M}$ ) exhibit no haemolytic activity. Concentrations of ionic liquid at minimum inhibitory concentrations would not be expected to produce haemolysis, since these concentrations are inhibitory to growth rather than producing a killing, or cidal, effect which is observed at and above the minimum bactericidal concentrations. In the case of both  $[\text{C}_{12}\text{quin}]\text{Br}$  and  $[\text{C}_{14}\text{quin}]\text{Br}$ , almost total haemolysis is observed at  $50 \mu\text{g cm}^{-3}$ , which is unsurprising given the average MBCs for the range of organisms tested is  $45.15 \mu\text{M}$  and  $9.89 \mu\text{M}$ , respectively. From these data, it is clear that 1-alkylquinolinium bromide ionic liquids are highly membrane active and bring about cidal activity *via* disruption of the cell membrane.

## Conclusions

The economic impact of healthcare-associated infections (HAIs) or nosocomial infections imposes significant financial burdens on healthcare systems worldwide, primarily due to increased hospital stay and associated costs. In a recently published report on the financial burden of HAIs in the USA, the direct (Consumer Price Index adjusted) costs associated with such infections may be as high as \$45 billion for inpatient hospital services, with the attributable costs per patient of all HAIs estimated to be between \$20549 and \$25903.<sup>42</sup> In the UK, approximately 9% of hospitalised patients acquire an infection post-admission to hospital,<sup>43</sup> representing a significant imposition on an already over-stretched NHS budget. Patients acquiring nosocomial infections incurred hospitalisation costs three times that of uninfected patients and had, on average, prolonged hospital stays in the region of 2.5 times that of uninfected patients.<sup>42</sup> Significant scope therefore exists to not only reduce the costs associated with such infections, but more importantly to improve patient quality of life by reduction in morbidity and mortality associated with hospital acquired infections.<sup>42,43</sup> Ionic liquids could prove attractive reagents for the control and prevention of infection and may be employed in a diverse range of antimicrobial applications.

In summary, 1-alkylquinolinium ionic liquids possess excellent, broad spectrum antimicrobial activity against microorganisms grown in both the planktonic and sessile, or biofilm, mode of growth. Importantly, these compounds are potent against Gram positive and Gram negative bacteria, as well as fungi, with a clear dependency on length of the alkyl substituent for activity,



with compounds containing twelve and fourteen carbons in the alkyl group exhibiting highest antimicrobial and antibiofilm activity. The data presented here indicate that antimicrobial potency and spectrum of activity of ionic liquids can be tuned by alteration of not only alkyl chain length but also by head group modification. This will permit flexibility in the design of antimicrobial agents, such as antiseptics and biocides targeted to particular applications where known microorganisms are predominant, (for example, pulmonary infections, such as pneumonia, urinary tract infections and catheter-associated infections), where gram negative bacteria are major causative species.

## Acknowledgements

We are grateful to the Industrial Advisory Board of QUILL and the EPSRC (Portfolio Partnership Scheme, grant number EP/D029538/1) for their continuing support and to the Society for Applied Microbiology for funding AFL through a 'Students into Work' grant.

## References

- 1 *Ionic Liquids in Synthesis*, ed. P. Wasserscheid and T. Welton, Wiley-VCH, Weinheim, 2003.
- 2 A. Stark and K. R. Seddon, in *Kirk-Othmer Encyclopaedia of Chemical Technology*, ed. A. Seidel, John Wiley & Sons, Inc., Hoboken, New Jersey, 2007, vol. 26, pp. 836–920.
- 3 M. J. Earle and K. R. Seddon, *Pure Appl. Chem.*, 2000, **72**, 1391–1398.
- 4 N. V. Plechkova and K. R. Seddon, *Chem. Soc. Rev.*, 2008, **37**, 123–150.
- 5 M. J. Earle, J. M. S. S. Esperança, M. A. Gilea, J. N. C. Lopes, L. P. N. Rebelo, J. W. Magee, K. R. Seddon and J. A. Widegren, *Nature*, 2006, **439**, 831–834.
- 6 N. V. Plechkova and K. R. Seddon, in *Methods and Reagents for Green Chemistry: An Introduction*, ed. P. Tundo, A. Perosa and F. Zecchini, John Wiley & Sons, Inc., New York, 2007, pp. 105–130.
- 7 *Ionic Liquids: Industrial Applications for Green Chemistry*, ed. R. D. Rogers and K. R. Seddon, ACS Symposium Series, vol. 818, American Chemical Society, Washington, 2002, pp. 90–105.
- 8 R. D. Rogers and K. R. Seddon, *Science*, 2003, **302**, 792–793.
- 9 A. J. Carmichael, M. J. Earle, J. D. Holbrey, P. B. McCormac and K. R. Seddon, *Org. Lett.*, 1999, **1**, 997–1000.
- 10 P. J. Scammells, J. L. Scott and R. D. Singer, *Aust. J. Chem.*, 2005, **58**, 155–169.
- 11 T. P. T. Pham, C. W. Cho, J. Min and Y. S. Yun, *J. Biosci. Bioeng.*, 2008, **105**, 425–428.
- 12 A. Wells and V. T. Coombe, *Org. Process Res. Dev.*, 2006, **10**, 794–798.
- 13 C.-W. Cho, T. P. T. Pham, Y.-C. Jeon and Y.-S. Yun, *Green Chem.*, 2008, **10**, 67–72.
- 14 R. P. Swatloski, J. D. Holbrey, S. B. Memon, G. A. Caldwell, K. A. Caldwell and R. D. Rogers, *Chem. Commun.*, 2004, 668–669.
- 15 K. M. Docherty and C. F. Kulpa Jr., *Green Chem.*, 2005, **7**, 185–189.
- 16 J. Pernak, K. Sobaszekiewicz and I. Mirska, *Green Chem.*, 2003, **5**, 52–56.
- 17 J. Pernak, K. Sobaszekiewicz and J. Foksowicz-Flaczyk, *Chem.–Eur. J.*, 2004, **10**, 3479–3485.
- 18 D. Demberelymba, K. S. Lim, S. Choi, S. Y. Park, H. Lee, C. J. Kim and I. D. Yoo, *Bioorg. Med. Chem.*, 2004, **12**, 853–857.
- 19 J. Pernak, I. Goc and I. Mirska, *Green Chem.*, 2004, **6**, 323–329.
- 20 J. Pernak and J. Feder-Kubis, *Chem.–Eur. J.*, 2005, **11**, 4441–4449.
- 21 L. Carson, P. K. W. Chau, M. J. Earle, M. A. Gilea, B. F. Gilmore, S. P. Gorman, M. T. McCann and K. R. Seddon, *Green Chem.*, 2009, **11**, 492–497.
- 22 A. Dongari-Bagtzoglou, *Expert Rev. Anti-Infect. Ther.*, 2008, **6**, 141–144.
- 23 R. M. Donlan and J. W. Costerton, *Clin. Microbiol. Rev.*, 2002, **15**, 167–193.
- 24 M. J. Richards, J. R. Edwards, D. H. Culver and R. P. Gaynes, *Crit. Care Med.*, 1999, **27**, 887–892.
- 25 J. W. Costerton and M. Wilson, *Biofilms*, 2004, **1**, 1–4.
- 26 P. Gilbert, J. Das and I. Foley, *Adv. Dent. Res.*, 1997, **11**, 160–167.
- 27 H. Ceri, M. E. Olson, C. Stremick, R. R. Read, D. Morck and A. Buret, *J. Clin. Microbiol.*, 1999, **37**, 1771–1776.
- 28 J. Ranke, A. Müller, U. Bottin-Weber, F. Stock, S. Stolte, J. Arning, R. Störmann and B. Jastorff, *Ecotoxicol. Environ. Saf.*, 2004, **58**, 396–404.
- 29 T. Fuji, K. Fujio, S. Ozeki, in *Studies in Surface Science and Catalysis*, ed. Y. Iwasawa, N. Oyama and H. Kunieda, Elsevier Science B. V., 2001, vol. 132, pp. 129–132.
- 30 C. M. Lee, *J. Korean Chem. Soc.*, 1972, **16**, 205–207.
- 31 S. Y. Shin, S. H. Lee, S. T. Yang, E. J. Park, D. G. Lee, M. K. Lee, S. H. Eom, W. K. Song, Y. Kim, K. S. Hahm and J. I. Kim, *J. Pept. Res.*, 2001, **58**, 504–514.
- 32 D. Dube, M. Bloun, C. Brideau, C. Chan, S. Desmarais, D. Eithier, J. P. Falgoutier, R. W. Friesen, M. Girard, Y. Girard, J. Guay, P. Tagri and R. N. Yong, *Bioorg. Med. Chem. Lett.*, 1998, **8**, 1255–1260.
- 33 M. Azad, M. Ali Munawar and H. L. Siddiqui, *J. Appl. Sci.*, 2007, **7**, 2485–2489.
- 34 D. Larsen, E. G. Corley, A. O. King, J. D. Carrol, P. Davis, T. R. Verhoeven, P. J. Reider, M. Labelle, J. Y. Gauthier, Y. B. Xiang and R. Zamboni, *J. Org. Chem.*, 1996, **61**, 3398–3405.
- 35 J. Pernak, J. Krysinski, L. Michalak and W. Karminski, *Arch. Pharm.*, 1985, **318**, 410–415.
- 36 T. Kitahara, N. Koyama, J. Matsuda, Y. Aoyama, Y. Hirakata, S. Kamihira, S. Kohno, M. Nakashima and H. Sasaki, *Biol. Pharm. Bull.*, 2004, **27**, 1321–1326.
- 37 C. W. Sheu and E. Freese, *J. Bacteriol.*, 1973, **115**, 869–875.
- 38 H. Galbraith and T. B. Miller, *J. Appl. Bacteriol.*, 1973, **36**, 647–658.
- 39 A. Cieniecka-Roslonkiewicz, J. Pernak, J. Kubis-Feder, A. Ramani, A. J. Robertson and K. R. Seddon, *Green Chem.*, 2005, **7**, 855–862.
- 40 E. Chelossi, I. Mancini, K. Sepcic, T. Turk and M. Faimali, *Biomol. Eng.*, 2006, **23**, 317–323.
- 41 S. Stolte, M. Matzke, J. Arning, A. Boschen, W.-R. Pitner, U. Welz-Biermann, B. Jarstoff and J. Ranke, *Green Chem.*, 2007, **9**, 1170–1179.
- 42 R. D. Scott II, *The direct medical costs of Healthcare-Associated Infections in U.S. Hospitals, and benefits of prevention*, Centers for Disease Control and Prevention USA, 2009.
- 43 R. Plowman, N. Graves, M. A. S. Griffin, J. A. Roberts, A. V. Swan, B. Cookson and L. Taylor, *J. Hosp. Infect.*, 2001, **47**, 198–209.

# Green solvents from glycerol. Synthesis and physico-chemical properties of alkyl glycerol ethers†‡

José I. García,\*<sup>a</sup> Héctor García-Marín,<sup>a</sup> José A. Mayoral<sup>a,b</sup> and Pascual Pérez<sup>c</sup>

Received 10th November 2009, Accepted 14th December 2009

First published as an Advance Article on the web 26th January 2010

DOI: 10.1039/b923631g

A family of glycerol derivatives, consisting of over sixty 1,3-dialkoxy-2-propanols and 1,2,3-trialkoxypropanes, both symmetrically and unsymmetrically substituted at terminal positions, have been synthesized and the possible role of these glycerol derivatives as substitutive solvents has been evaluated through measurements of their physico-chemical properties. The molecular diversity of the derivatives prepared results in significant variations of polarity properties, facilitating the identification of possible candidates for solvent substitution.

## Introduction

Glycerol (1,2,3-propanetriol) is a well-known substance, that can be naturally found under the form of fatty acid esters, also known as triglycerides. Traditionally, glycerol is obtained as a by-product in four different processes: soap manufacture, fatty acid production, fatty ester production,<sup>1</sup> and microbial fermentation.<sup>2</sup> It can also be synthesized from propylene oxide.<sup>1</sup>

In recent years, the increase in the production of fatty acid methyl esters from vegetal oils to be used as biofuels (known popularly as “biodiesel”), has lead to a surplus in the production of glycerol, normally generated at the rate of 1 mol of glycerol for every 3 mol of methyl esters synthesized; which is approximately 10 wt% of the total product. Today, close to two-thirds of world glycerol production comes from biodiesel. Combined U.S. and European output last year was 1.2 million metric tons.<sup>3</sup>

Recently, a European Union Directive stated that by the end of 2010, traffic fuels should contain at least 5.75% of renewable bio-components.<sup>4</sup> However, if the target of this directive is to be achieved, European biodiesel demand could increase to 10 million metric tons per year by 2010, producing already about one million metric tons of glycerol as by-product only in Europe.<sup>5</sup> A similar situation arises in the United States and other countries. Obviously the question arises how this additional

glycerol can be used wisely. New uses for glycerol should require high amounts of substance, to absorb the surpluses, and simple and minimal chemical transformation, to minimize transformation costs and produce low price derivatives, and of course these transformations should be compatible with the Green Chemistry principles. This topic has attracted much attention from researchers and industries, and some reviews have appeared very recently dealing with the use of glycerol as a source of commodity chemicals.<sup>6</sup>

Solvents are chemical substances used in huge amounts for many different applications. In many cases, organic solvents are chemical substances derived from petrol, and have a negative impact on the health and the environment. The great majority of air contaminants in indoor atmospheres are organic solvents. If valuable solvents are synthesized from glycerol, not only a new application, able to consume high quantities of glycerol surpluses will be found, but also some of the most dangerous organic solvent could be replaced by less harmful, biodegradable glycerol-derived solvents.

Some solvents derived from glycerol are already known and used in different applications. More than 2000 applications are spread out in different fields such as the cosmetic, pharmaceutical or food industry. Glycerol itself has been recently proposed as a green solvent.<sup>7</sup> However, as different application fields require different physico-chemical properties, it would be convenient to have a high degree of versatility in the preparation of the glycerol derivatives, keeping the simplicity of the derivatization process, and it would be also necessary to have a methodology to find quickly the possible fields of application of the new substances prepared.

In this paper we present our first results in the characterization and classification, based on a series of physico-chemical properties, of new solvents derived from glycerol, consisting of 1,3-dialkoxy-2-propanols and 1,2,3-trialkoxypropanes (glycerol diethers and triethers), with the same or different alkyl groups on both terminal positions, with the aim to identify similarities with traditional organic solvents that can provide clues for solvent substitution applications.

Graphical classification of these new solvents will help us to choose quickly which solvent has the best properties to be a

<sup>a</sup>Dept. Organic Chemistry, Instituto de Ciencia de Materiales de Aragón, Facultad de Ciencias, Univ. de Zaragoza-CSIC, Pedro Cerbuna, 12, E-50009, Zaragoza, Spain. E-mail: jig@unizar.es; Fax: +34 976762077; Tel: +34 976762271

<sup>b</sup>Instituto Universitario de Catálisis Homogénea, Facultad de Ciencias, Univ. de Zaragoza, Pedro Cerbuna, 12, E-50009, Zaragoza, Spain. E-mail: mayoral@unizar.es; Fax: +34 976762077; Tel: +34 976762077

<sup>c</sup>Dept. Physical Chemistry and Organic Chemistry, Facultad de Ciencias, Univ. de Zaragoza, Pedro Cerbuna, 12, E-50009, Zaragoza, Spain. E-mail: pascual@unizar.es; Fax: +34 976761205; Tel: +34 976761202

† Dedicated to Prof. Pelayo Camps on the occasion of his 65th birthday.

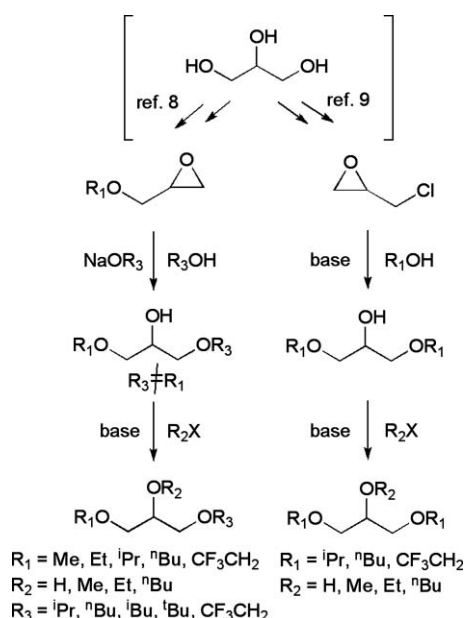
‡ Electronic supplementary information (ESI) available: Full data of physico-chemical properties measured for the glycerol-derived solvents described. Experimental procedures used for the properties measurements. Characterization of the compounds prepared. See DOI: 10.1039/b923631g

good candidate in order to substitute a classical solvent in an existing application.

## Results and discussion

### Glycerol derivative synthesis

As our priority target in this work was to dispose of a large variety of alkyl glycerol ethers to investigate their physico-chemical properties and to correlate them with their structural features, we used simple yet versatile synthetic schemes, starting from commercial glycidol ethers and epichlorohydrin (Scheme 1). It is worth noting that efficient transformation of glycerol into both glycidol<sup>8</sup> and epichlorohydrin<sup>9</sup> is possible in large scale, so the synthetic scheme proposed should be feasible for industrial solvents production with relatively small modifications.



**Scheme 1** Synthetic pathways to symmetrical and unsymmetrical 1,3-dialkyl glycerol derivatives.

As can be seen, the possibility of unsymmetrical substitution allows obtaining an interesting structural diversity, which should result in adjustable physico-chemical properties. In some cases, fluorinated substituents were used, to introduce a new feature that might strongly modify both polarity and solvophobicity of the corresponding solvents.

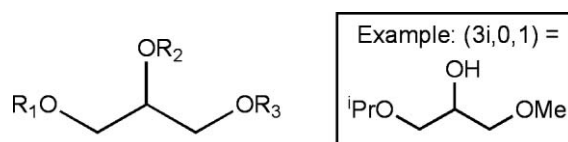
Using these synthetic strategies, a family of 62 1,3-dialkoxy-2-propanols and 1,2,3-trialkoxypropanes (glycerol diethers and triethers), both symmetrically and unsymmetrically substituted, was prepared. It is important to note that more than half of the structures prepared were not previously known.

To clarify the identification of the glycerol-derived solvents in figures, schemes and tables we have used coded names to represent the substitution patterns on each glycerol hydroxyl group. These code names use three combinations of digits and letters representing the corresponding ether alkyl chain. The codes used are summarized in Table 1.

An example of a glycerol-derived solvent structure and its codification is shown in Scheme 2.

**Table 1** Substituting groups in the structures of glycerol-derived solvents

Digits and letters	Group	Structure
0	H	free hydroxyl group
1	CH <sub>3</sub>	methyl
2	CH <sub>3</sub> CH <sub>2</sub>	ethyl
3i	(CH <sub>3</sub> ) <sub>2</sub> CH	<i>iso</i> -propyl
4	CH <sub>3</sub> (CH <sub>2</sub> ) <sub>2</sub> CH <sub>2</sub>	<i>n</i> -butyl
4i	(CH <sub>3</sub> ) <sub>2</sub> CHCH <sub>2</sub>	<i>iso</i> -butyl
4t	(CH <sub>3</sub> ) <sub>3</sub> C	<i>tert</i> -butyl
3F	CF <sub>3</sub> CH <sub>2</sub>	2,2,2-trifluoroethyl
5F	CF <sub>3</sub> CF <sub>2</sub> CH <sub>2</sub>	2,2,3,3,3-pentafluoro- <i>n</i> -propyl
7F	CF <sub>3</sub> (CF <sub>2</sub> ) <sub>2</sub> CH <sub>2</sub>	2,2,3,3,4,4,4-heptafluoro- <i>n</i> -butyl



**Scheme 2** Structures and simplified nomenclature for glycerol based solvents.

Of course, because of symmetry reasons,  $R_1$  and  $R_3$  substituents are fully exchangeable, so (3i,0,1) and (1,0,3i) represent the same compound. The order of these substituents has been arbitrarily chosen.

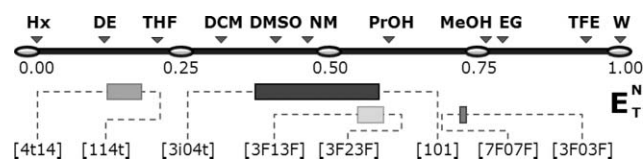
### Solvent polarity

Solvent polarity parameters have demonstrated their usefulness not only to classify organic solvents but also to explain solvent effects on very different physical and chemical processes. An excellent overview of solvent polarity parameters and their applications can be found in the outstanding Reichardt's book.<sup>10</sup> Although there are several procedures to quantify solvent polarity, solvatochromism measurements of probe dyes is undoubtedly the most successful methodology for an accurate determination of this solvent feature due to their easy determination and the high sensitivity to small polarity changes. In this regard, the Dimroth and Reichardt  $E_T(30)$  parameter<sup>11</sup> is the most used and known, and not only has it been determined for most of the common (and not so common) organic solvents,<sup>10,12</sup> but also for neoteric solvents, such as supercritical fluids<sup>13</sup> and ionic liquids.<sup>14</sup>

$E_T(30)$  values represent a blend of dipolarity/polarizability and hydrogen bond donor solvation abilities of the solvent, the latter feature contributing to a greater extent. Very often, normalized  $E_T(30)$  values, known as  $E_T^N$  are used, where tetramethyl silane (TMS) and water are arbitrarily chosen as 0.0 and 1.0 values of the normalized scale.<sup>10</sup> In line with the previous comments, it can be observed that  $E_T$  values behaves consistently along the solvent series (Table 1S in the Electronic Supporting Information, ESI<sup>†</sup>). Thus, 1,3-dialkoxy-2-propanols have  $E_T^N$  values in the range 0.37–0.50, which are normal for alcohols. 1,2,3-trialkoxypropanes have much lower values, in the range 0.15–0.20, also normal for less polar, non-protic solvents, like ethers. The presence of fluorinated substituents results in an increase of the corresponding  $E_T^N$  values, which is a well-known effect for alcohols. However, this effect is particularly noticeable in the case of glycerol triethers, which present  $E_T^N$

values over 0.50 (*i.e.*, similar to those of many alcohols) in spite of being formally non-protic solvents. The absence of traces of alcohol in the samples was carefully checked, and finally discarded, by gas chromatography analyses. The presence of acid traces could also be discarded, because protic acids protonate the Dimroth–Reichardt dye, resulting in the disappearance of the characteristic absorption band in the UV-visible spectra.<sup>10</sup>

To put these values in the context of common solvents, Figure 1 represent the range of values of  $E_T^N$  determined for glycerol-derived solvents compared with those of a series of common organic solvents covering a wide spectrum of polarities (from *n*-hexane to water).



**Fig. 1** Different common solvents and glycerol-based solvents on the  $E_T^N$  polarity line.

Glycerol-based solvents cover a wide range of polarities grouped in four families: 1,3-dialkoxy-2-propanols, 1,2,3-trialkoxypropanes, fluorinated 1,3-dialkoxy-2-propanols, and fluorinated 1,3-dialkoxy-2-alkoxypropanes. As previously mentioned, the latter are in the same zone that the most polar 1,3-dialkoxy-2-propanols, so they could be considered as strong C–H hydrogen bond donors. In order to get some insights on this hypothesis, a computational molecular modelling study has been carried out, comparing the behaviour of (2,1,2) and (3F,1,3F).

First of all we localized the minimum energy conformer for both compounds, and we calculated the electronic distribution of both molecules at the B3LYP/6-31G\* theory level. Figure 2 shows the Molecular Electrostatic Potential corresponding to these electronic distributions mapped onto the van der Waals molecular surface. As can be seen, the hydrogen atoms of (3F,1,3F) (and especially those of the trifluoroethyl groups) are more positively charged (dark blue colour), whereas oxygen atoms are less negatively charged (light red colour), when compared with (2,1,2).

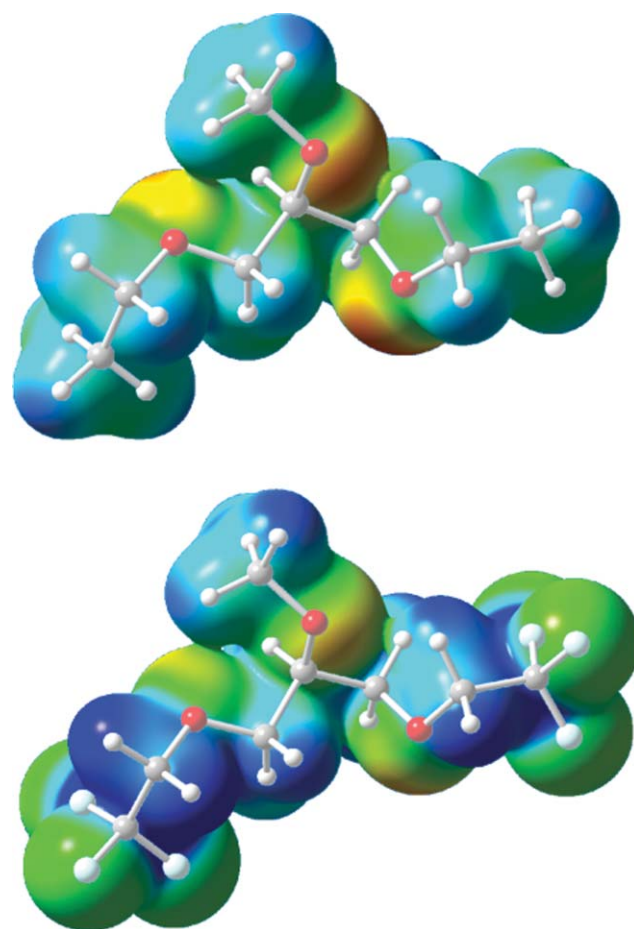
To model the possible hydrogen bonding interaction between the solvent and the Dimroth–Reichardt betaine, we also calculated the complexes fenolate–solvent. The calculated solvation energies are gathered in Table 2. In gas phase, the interaction energies are both stabilizing, but solvation energy with (3F,1,3F) is *ca.* 9 kcal mol<sup>−1</sup> higher than with (2,1,2).

Of course, the ion-molecule interaction values in the gas phase must be higher than in solution. We carried out single point energy calculations on the gas phase optimized geometries

**Table 2** Calculated (B3LYP/6-31G\*) Fenolate–Solvent interaction energies (in kcal mol<sup>−1</sup>) in gas phase and in solution

Solvent	Gas phase	PCM <sup>a</sup>	PCM+opt <sup>b</sup>
(2,1,2)	−10.0	0.4 <sup>c</sup>	—
(3F,1,3F)	−18.9	−1.4 <sup>d</sup>	−7.4

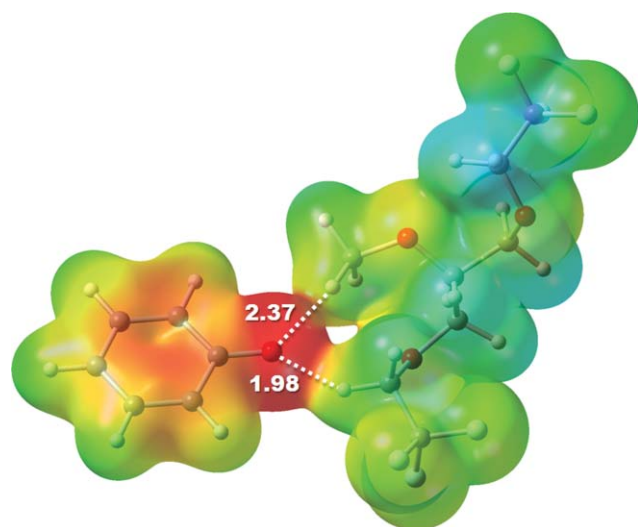
<sup>a</sup> Single point energies on gas-phase optimized geometries. <sup>b</sup> Geometry optimization in solution, using 3F,1,3F parameters. <sup>c</sup> Using diethyl ether parameters. <sup>d</sup> Using 1,2-dichloroethane parameters.



**Fig. 2** Calculated (B3LYP/6-31G\*) Molecular Electrostatic Potential (MEP) of (2,1,2) (upper) and (3F,1,3F) (lower) glycerol-derived solvents. Blue colour corresponds to more positive zones, and red colour to more negative zones.

by considering electrostatic solvation effects through the PCM continuum model.<sup>15</sup> In these conditions, the interaction energy fenolate–(2,1,2) turns to be positive (destabilizing), whereas that of (3F,1,3F) remains negative, indicating a weak association (1.4 kcal mol<sup>−1</sup>). To have a more reliable value, we reoptimized the fenolate–(3F,1,3F) complex in solution, using the physical properties determined for this solvent (density, dielectric constant and refraction index) in the PCM calculations. The calculated solvation energy increases up to 7.4 kcal mol<sup>−1</sup>, indicating a rather strong association. Figure 3 shows the optimized fenolate–(3F,1,3F) geometry, in which the interactions between the negative fenolate oxygen and the positively charged solvent hydrogen atoms are clearly seen.

It can be then concluded that these fluorinated solvents can act as moderate hydrogen bond donors, as suggested by their relatively high  $E_T^N$  values. This may confer to these molecules interesting features, since they participate simultaneously in solvent properties associated to high and low polarities (*vide infra*), for instance moderately high HBD ability linked to immiscibility with water, which can constitute an interesting combination of properties, difficult to attain for common organic solvents.



**Fig. 3** Calculated (PCM-B3LYP/6-31G\*) geometry and Molecular Electrostatic Potential (MEP) of the fenolate-(3F,1,3F) complex in solution.

Multiparametric Abboud–Abraham–Kamlet–Taft equation is also very popular for solvent effect studies, and the corresponding  $\pi^*$  (dipolarity-polarizability)<sup>16</sup> and  $\alpha$  (hydrogen-bond donor, HBD, ability)<sup>17</sup> are among the most known solvent parameters. This approach presents the advantage that each contribution to the total solvation can be determined independently, but on the other hand, neither  $\pi^*$  nor  $\alpha$  are as sensitive as  $E_T(30)$  to small polarity changes.  $E_T(30)$ ,  $\pi^*$  and  $\alpha$  parameters are linearly related so that usually  $\alpha$  values can be determined from  $E_T(30)$  and  $\pi^*$  measurements.<sup>18</sup> In our case, we use the following expression to calculate the  $\alpha$  values of our solvents (eq. 1):

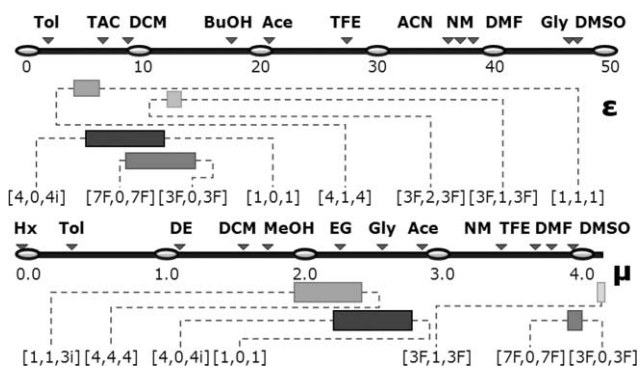
$$E_T(30)(\text{kcal mol}^{-1}) = 11.5 \cdot \pi^* + 15.2 \cdot \alpha + 31.2 \quad (1)$$

The corresponding  $\pi^*$  and  $\alpha$  values are gathered in Table 1S<sup>†</sup> and will not be further discussed here.

### Physico-chemical properties

**Dielectric and related properties.** Measurements of different physico-chemical properties of the compounds prepared have been made, some of them also related with solvent polarity features such as dielectric permittivity and dipolar moment, in order to characterize completely the polarity of these new solvents.

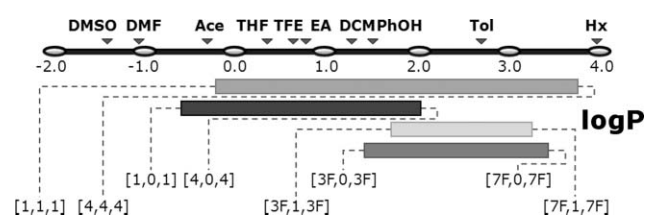
Dielectric permittivities are lower when free hydroxyl groups are not present in the structure, as is reflected in Figure 4 and in the values gathered in Table 1S,<sup>†</sup> when comparing trialkyl and dialkyl derivatives. Moreover, when fluorinated atoms are introduced in the structure, polarity increases. Dipole moments of these new solvents can be estimated from permittivity values through the Onsager's equation.<sup>19</sup> Dipole moment values in each of the glycerol-derived families are relatively high and in some cases very high, as in the case of glycerol–diether derivatives containing fluorinated atoms. It is worth noting the relatively high  $\epsilon$  and  $\mu$  values obtained for ( $R_1^F, R_2, R_3^F$ ) albeit not having free hydroxyl groups, in line with that observed in the case of the  $E_T^N$  parameter.



**Fig. 4** Different common solvents and glycerol-based solvents on the permittivity ( $\epsilon$ ) and dipole moment ( $\mu$ ) lines.

Other related property is the refraction index, which can be connected with the polarizability of the molecules. The determined values for this property are gathered in Table 1S.<sup>‡</sup>

**Water compatibility.** The hydrophobic or lipophilic character of organic compounds plays an important role in many fields. Water miscibility and hydrophobicity issues are so important that systematic efforts have been made to obtain numerically defined constants to assess the hydrophobic character of organic compounds. One of the best is Hansch–Leo 1-octanol/water partition coefficient ( $P_{O/W}$ )<sup>20</sup> which is usually expressed under logarithmic form as the  $\log P$  parameter. The huge amount of experimental data for  $\log P$  has allowed the development of many calculation schemes, based on molecular topology, group contribution and atom contribution models that allow estimating good  $\log P$  values from virtually any chemical structure.<sup>21</sup> In our case, we used the Ghose and Crippen atom contribution method through the  $\Delta\text{LogP98}$  refinement.<sup>22</sup> Due to the high variability in their structures (see Scheme 1), the hydrophobicity range covered by these glycerol-derived solvents is very wide, covering almost five magnitude orders (Figure 5).



**Fig. 5** Different common solvents and glycerol-based solvents on the hydrophobicity line.

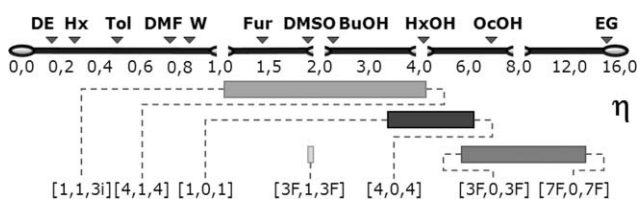
This parameter is narrowly related to miscibility with water, an important feature if applications in biphasic catalysis or extractions are envisaged. Two different determinations of water content were carried out with a selected set of glycerol-derived solvents (Table 3). The first one corresponds to the water content under storage conditions, *i.e.*, the amount of water gained when the solvent is stored for six months with no particular precaution measures (without inert atmosphere or molecular sieves, for instance). These values give an idea of the hygroscopicity of the solvents, which is quite low in all cases (0.1% wt. or less). The second one, water solubility under saturation conditions, is generally low for glycerol triethers and is roughly related to their hydrophobicity. Not surprisingly, the solubility of water in

**Table 3** Solubility of water in some glycerol-based solvents under different conditions

Solvent	mg H <sub>2</sub> O g <sup>-1</sup> solvent under storage conditions	mg H <sub>2</sub> O g <sup>-1</sup> solvent under saturation conditions
1,0,4t	1.123	Miscible
3i,0,3i	0.926	120.774
4,0,4	1.140	44.691
4,0,4t	0.755	38.515
3F,0,3F	0.650	28.483
1,1,4t	1.586	21.158
1,1,4i	1.402	12.211
3i,1,4	1.145	8.050
4,1,4t	0.605	5.252
3i,1,3F	1.493	4.525
4,1,4	1.420	4.438
4t,1,3F	0.450	4.361
4,1,3F	0.919	4.061
3F,1,3F	0.438	3.238
4,4,4	0.530	2.262

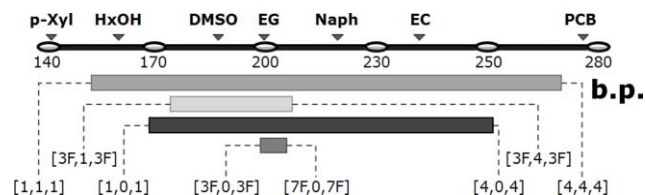
the 1,3-dialkoxy-2-propanols (diethers) is much higher in most cases, and even in one case (1,0,4t) the solvent results completely miscible with water. Anyway, as indicated above, it is possible to have completely anhydrous solvents without particular effort if the corresponding application would require it.

**Viscosity.** The determination of this property is particularly interesting from the viewpoint of possible large scale industrial applications, where big solvent volumes have to be stirred and pumped from one tank to another. Although glycerol-based solvents with free hydroxyl groups have viscosities higher than those of typical polyethers, they do not have extremely high viscosities, and most values fall within reasonable values for organic solvents (Table 1S<sup>†</sup> and Figure 6), being well below from usual values for other families of green solvents, as are ionic liquids. It is worth mentioning that these values will further decrease with temperature, and that glycerol-derived solvents allow working at relatively high temperatures, so, in general, viscosity should not constitute an issue with these solvents.

**Fig. 6** Kinematic viscosities of different common and glycerol-based solvents.

**VOC character.** One major problem concerning the use of organic solvents is the presence of traces of these compounds in the air. The most common volatile organic compounds (VOC's) are solvents indeed. Nowadays a big effort is being done to solve the problem trying to substitute these volatile solvents with others that are less or non-volatile.

All the glycerol-based solvents included in this work have a high boiling point (Table 1S<sup>†</sup>) and low volatility, for this reason they can be considered as good candidates for substitution of volatile organic compounds. In Figure 7 it can be seen that most boiling points determined for glycerol-derived solvents are higher than those of organic solvents traditionally considered as

**Fig. 7** Different common solvents and glycerol-based solvents on the boiling point line.

having high b.p., such as DMSO and ethylene glycol (EG). In many cases, they are even higher than that of ethylene carbonate (EC).

Even better than boiling points, vapour pressures at different temperatures allow to determine if the glycerol-derived solvents prepared are more or less volatile than other common organic solvents. Given the difficulty of having accurate measurements of this property, it has been only determined for a selected set of solvents including representatives of non-fluorinated and fluorinated diethers and triethers of glycerol. Table 2S in the ESI<sup>†</sup> gathers the vapour pressures of the selected solvents at ten temperatures ranging between 293.25 and 373.15 K. The vapour pressures are in general low but somewhat higher than those of 1-alkanols with a similar number of C atoms (for example, the vapour pressure of 1-decanol is around 0.1 mmHg at 323.15 K). On the other hand, they are much lower than those of conventional organic solvents (Figure 8). The behaviour of this property seems to be mostly controlled by intermolecular hydrogen bonding, it can be observed by comparing the vapour pressure of (1,0,4t) against (1,1,4t) and (3F,0,3F) against (3F,1,3F), in both cases the pressure increases with the change from the -OH group to the -OCH<sub>3</sub> group. On the other hand, by comparing the vapour pressure of (4,0,4) against (4,0,4t) we can see as the vapour pressure decreases in the linear isomer, which is probably related to the lower shielding of the -OH group, which favours the intermolecular hydrogen bonding, but also with the London dispersion forces between alkyl chains.

The experimental vapour pressure data were fitted to the Antoine equation (eq. 2), which allows calculating vapour pressures within the temperature range used (Figure 8). It can be concluded from these measurements that glycerol-derived solvents have considerably less VOC character than most common organic solvents.

$$\log P(\text{mmHg}) = A - \frac{B}{T(^{\circ}\text{K}) - C} \quad (2)$$

### Insights on solvent substitution and possible uses

In order to find possible applications of the prepared glycerol-derived solvents, it is necessary to put the determined physico-chemical properties in context with those of common organic solvents. This has also been partially accomplished in the unidimensional Figures of the precedent sections, but more insights can be obtained with two- and three-dimensional plots, gathering several different (and preferably independent) properties.

Thus, Figure 9 gathers the plot of logP vs. E<sup>N</sup><sub>T</sub> solvent parameters for a series of common organic solvents, comprising

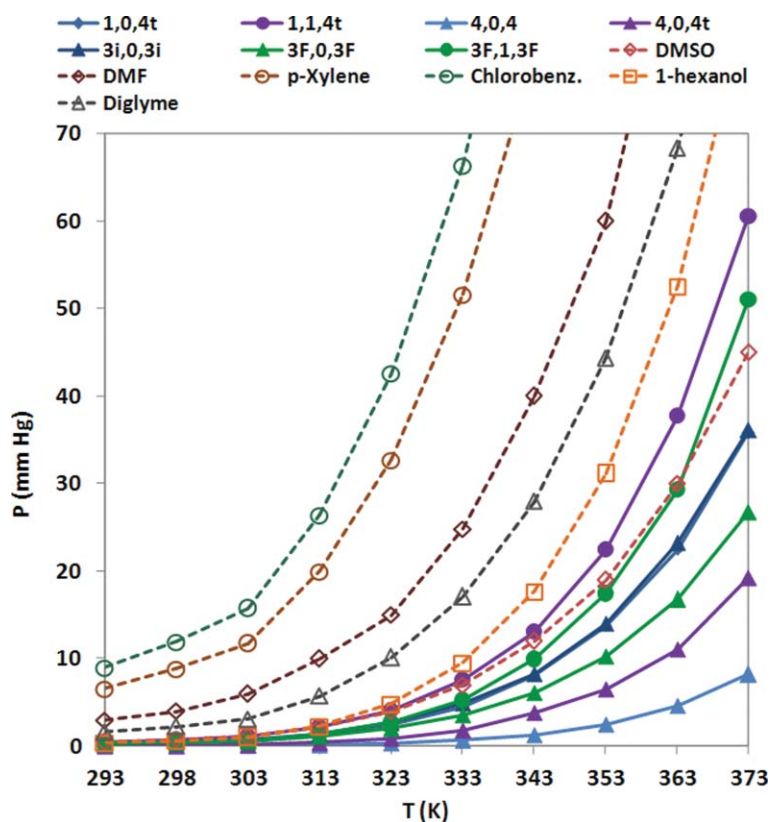


Fig. 8 Antoine plots of some common (--- lines) and glycerol-based (— lines) solvents (values for common solvents taken from ref. 23).

different chemical families and solvation abilities (see Table 3S in the ESI for a comprehensive list of solvents considered<sup>†</sup>), as well as a selection of glycerol-derived solvents, for which both parameters have been determined.

As already mentioned,  $\log P$  is a measure of solvent hydrophobicity, and it is therefore more related to non-polar solvation, whereas  $E^N_T$  is a blend of dipolarity and hydrogen bond solvation mechanisms, *i.e.*, with polar solvation. Not surprisingly, there is a rough correlation between both parameters in the case of common organic solvents ( $r = -0.769$ ), since the most polar solvents are usually the least hydrophobic and vice-versa. As a consequence, in the  $\log P$  vs.  $E^N_T$  plot, all common solvents are placed in the lower left triangular zone, as indicated by the dashed line. We can see that many glycerol-derived solvents also fall within this zone, and therefore they are candidates for solvent substitution in the case of ethers and aromatic hydrocarbons (R,R,R or glycerol triether solvents), also of polar aprotic and protic solvents (R,O,R or glycerol diether solvents), and even in some cases of chlorinated solvents. But more interestingly, there is a set of glycerol-derived solvents falling beyond the dashed line, indicating that they possess unusual combinations of solvation abilities, being at the same time moderately hydrophobic, but also highly polar. In most cases, these glycerol-derived solvents bear fluorinated alkyl chains in their structures. This result suggests that these solvents could be good candidates for new applications. Since they have relatively high boiling points, low vapour pressures and low viscosities, they can be seen as alternatives to ionic liquids, with which they share many common properties.

Of course, if glycerol-derived solvents are considered together with common solvents, the correlation between  $\log P$  and  $E^N_T$  decreases ( $r = -0.562$ ), and both indicators become more independent.

Similar plots can be drawn with other pairs of properties. In the ESI we show the result of plotting the Kirkwood and Dielectric functions (Figure 1S<sup>†</sup>), depending respectively on solvent dielectric permittivities and refraction indices. These functions have been traditionally used in the Koppel and Palm multiparametric solvation model,<sup>24</sup> under the name of Y and P, respectively, as representatives for the dipolar and dispersive forces involved in the solvation mechanism.

Finally, a more illustrative plot can be obtained by combining the four parameters used in the above-mentioned plots. To this end, a Factor analysis was carried out and a plot of the three first factors, representing 96% of the total variance, is shown in Figure 10. As can be seen in this plot, glycerol triethers fall in a zone shared with aliphatic and aromatic hydrocarbons, polar aprotic and chlorinated solvents. Glycerol diethers clearly fall in the zone occupied also by polar protic solvents, and, to some extent, also by polar aprotic solvents. Finally, glycerol-derived solvents with two fluorinated alkyl chains are relatively isolated from common organic solvents, indicating again that they can probably be used for new applications in which conventional solvents are less adequate. A preliminary work where one of such special applications is proposed has been published very recently,<sup>25</sup> and another appears in this very issue.<sup>26</sup> Other new possible applications are currently under investigation in our group.

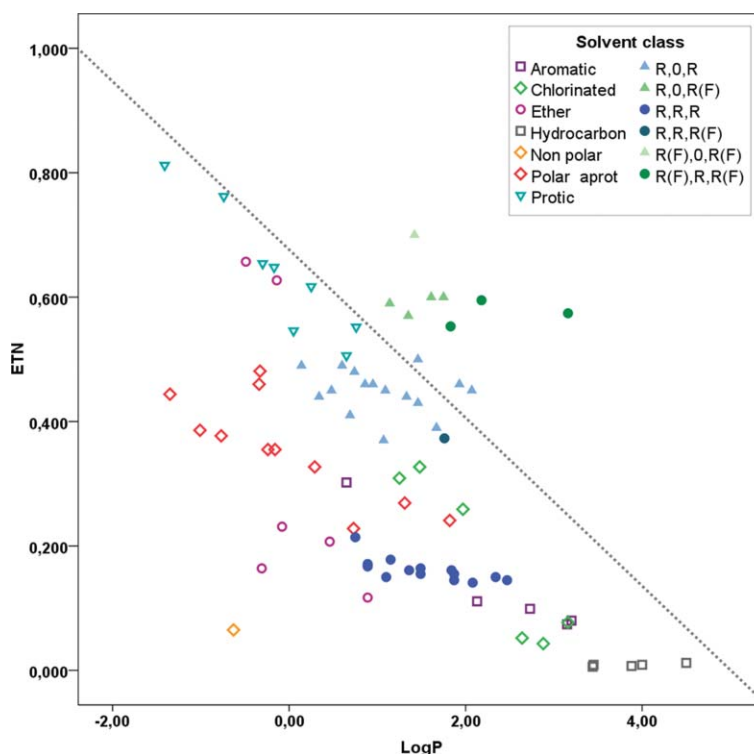


Fig. 9 Log P vs.  $E^N_T$  plot for a series of common organic solvents and glycerol-derived solvents.

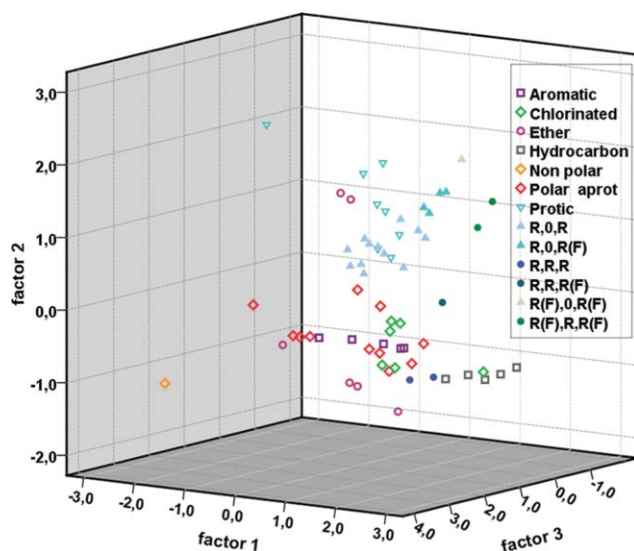


Fig. 10 Factor analysis plot for a series of common organic solvents and glycerol-derived solvents.

## Experimental

Glycerol-based solvents were obtained by ring opening of either the appropriate glycidol ether (non-symmetric glycerol-based solvents) or epichlorohydrin (symmetric glycerol-based solvents) with corresponding alkoxide in alcoholic media. After that, opening glycerol-based solvents were purified by vacuum distillation.

### General procedure for the synthesis of non-fluorinated non-symmetric 1,3-dialkoxyglycerols from glycidol ethers

In a round bottom flask cooled in an ice bath, 300 mL of  $R_3OH$  ( $R_3 = \text{Me, Et, } ^i\text{Pr, } ^n\text{Bu}$ ) then 1 mol (24 g) of sodium were added to generate the corresponding alkoxide. When the sodium reacted completely, the flask was heated up at 70 °C, and 1 mol of  $R_1$ -glycidol (glycidyl isopropyl ether ( $R_1 = ^i\text{Pr}$ ) 118 g; butyl glycidyl ether ( $R_1 = ^n\text{Bu}$ ) 137 g; glycidyl isobutyl ether ( $R_1 = ^i\text{Bu}$ ) 135 g; tert-butyl glycidyl ether ( $R_1 = ^t\text{Bu}$ ), 134 g) was dropped into the flask. After 30 min the reaction has been completed. After cooling down the flask in an ice bath, 25 mL of water were added. Water and the rest of the alcohol were removed after heating under vacuum. The product was dried out with magnesium sulphate. Non-fluorinated 1,3-dialkoxyglycerols were purified by vacuum distillation (yield > 85%, GC purity > 99.5%).

### General procedure for the synthesis of fluorinated non-symmetric 1,3-dialkoxyglycerols from glycidol ethers

75 mL of  $R_3OH$  ( $R_3 = \text{CF}_3\text{CH}_2$ ) then 1 mol (140 g) of potassium carbonate was added to a round bottom flask. The flask was heated up at 70 °C, and 1 mol of  $R_1$ -glycidol (glycidyl isopropyl ether ( $R_1 = ^i\text{Pr}$ ) 118 g; butyl glycidyl ether ( $R_1 = ^n\text{Bu}$ ) 137 g; glycidyl isobutyl ether ( $R_1 = ^i\text{Bu}$ ) 135 g; tert-butyl glycidyl ether ( $R_1 = ^t\text{Bu}$ ), 134 g) was dropped into the flask. After 1 hour the reaction was complete. Cooling down the flask, the mixture was filtered to remove the carbonate. The rest of the fluorinated alcohol were removed by heating under vacuum. Fluorinated 1,3-dialkoxyglycerols were purified by vacuum distillation (yield > 85%, GC purity > 99.5%).



### General procedure for the synthesis of non-fluorinated symmetric 1,3-dialkoxyglycerols from epichlorohydrin

In a round bottom flask cooled in an ice bath, 300 mL of  $R_3OH$  ( $R_3 = Me, Et, ^iPr, ^nBu$ ) then 1 mol (24 g) of sodium was added to generate the corresponding alkoxide. When the sodium reacted completely, the flask was heated up to 70 °C, and 1 mol of epichlorohydrin (94 g) was dropped into the flask. After 1 hour the reaction was completed. Cooling down the flask in an ice bath, 25 mL of water were added. Water and the rest of the alcohol were removed by heating under vacuum. The product was dried out with magnesium sulphate. Non-fluorinated 1,3-dialkoxyglycerols were purified by vacuum distillation (yield > 85%, GC purity > 99.5%).

### General procedure for the synthesis of fluorinated symmetric 1,3-dialkoxyglycerols from epichlorohydrin

In a round bottom flask were placed 75 mL of  $R_3OH$  ( $R_3 = CF_3CH_2, CF_3CF_2CH_2, CF_3CF_2CF_2CH_2$ ) then 1 mol (140 g) of potassium carbonate was added. The flask was heated up at 70 °C, and 1 mol of epichlorohydrin (94 g) was dropped into the flask. After 2 hours the reaction was complete. Cooling down the flask, the mixture was filtered to remove the carbonate. The rest of the fluorinated alcohol was removed by heating under vacuum. Fluorinated 1,3-dialkoxyglycerols were purified by vacuum distillation (yield > 85%, GC purity > 99.5%).

### Characterization of glycerol-based solvents

All data are compiled in the electronic supporting information (ESI).<sup>‡</sup>

Nuclear magnetic resonance was done in  $CDCl_3$  in a Bruker ARX 300 MHz.

Infrared spectra were obtained from the pure liquid using an infrared spectrometer Ati Mattson Genesis series FTIR.

Mass spectrometry was carried out in a Bruker MicroTof-Q, by electrospray ionization.

Gas chromatography was carried out in a Hewlett Packard 5890 series II Gas Chromatograph using a column of phenyl silicone 5.5% (supelco spb-s 30 m × 0.25 mm × 0.25 μm) and Helium as carrier gas.

### Polarity and physico-chemical properties

Details of the experimental measurements of the different solvent polarity parameters and physico-chemical properties of the solvents prepared are available in the Electronic Supporting Information.<sup>‡</sup>

### Toxicity issues

In some cases there are some experimental data, for instance toxicities of glycerol based solvents like 101, 202 or 404 are very low ( $LD_{50} > 3000$  mg/kg, oral in mice),<sup>27</sup> which are even lower than butanol ( $LD_{50} = 2680$  mg/kg). Unfortunately there is not data for all of them. Fluorinated solvents will be more toxic than aliphatic ones but not having experimental data for them it would be reasonable to think in the toxicities of compounds produced in their probable decomposition, like trifluoroethanol ( $LD_{50} = 366$  mg/kg, oral in mice),<sup>28</sup> trifluoroacetic acid ( $LD_{50} =$

150 mg/kg, intraperitoneal in mice)<sup>28</sup> or 2,2,2-trifluoroethyl ethyl ether ( $LD_{50} = 5100$  mg/kg, intraperitoneal in rats).<sup>29</sup>

Moreover using these glycerol derivatives allows to reduce some hazardous aspects. For instance, they have low volatility, so the concentration in the air using them is lower than using other conventional solvents. Albeit toxicities of these solvents are not well known at this moment it is clear they are not extremely toxic, meeting one of the key requirements for green applications.

### Theoretical calculations.

Theoretical calculations were carried out using the Gaussian 03 program.<sup>30</sup> Geometrical optimizations and single point energy calculations were performed within the Density Functional Theory formalism using the B3LYP/6-31G(d) theoretical level. Solvent effects were taken into consideration through the PCM formalism,<sup>15</sup> as implemented in the Gaussian program. The built-in parameterization for diethyl ether and 1,2-dichloroethane was used to model solvent effects in the case of 2,1,2 and 3F,1,3F, respectively, because of the similar dielectric constant values.

### Conclusions

A family of glycerol derivatives, consisting of 62 1,3-dialkoxy-2-propanols and 1,2,3-trialkoxypropanes, both symmetrically and unsymmetrically substituted at terminal positions, and 34 of them not previously described, have been synthesized, characterized, and the possible role of these glycerol derivatives as substitutive solvents has been evaluated through measurements of their physico-chemical properties. Nearly 400 experimental data have been collected for these solvents, and compared with analogous properties of common organic solvents. The molecular diversity of the derivatives prepared results in significant variations of polarity properties, facilitating the identification of possible candidates for solvent substitution, which will undoubtedly help to find applications for the glycerol-derived solvents as substitutes of more harmful, petrol-derived, conventional organic solvents and, even more interestingly, to find new applications based on the particular combination of solvent properties displayed by some of the substances described.

### Acknowledgements

Financial support from the European Union (project Solvsafe, NMP2-CT-2005-011774 and European Regional Development Funds) and the Spanish MCIMM (project CTQ2008-05138 and Consolider Ingenio 2010 CSD 2006-0003) is gratefully acknowledged. H. Garcia-Marin thanks the Gobierno de Aragón and Caja de Ahorros de la Inmaculada for grants. The authors also thank Dr. José M. Peiró for his assistance in the water content measurements.

### Notes and references

- 1 Kirk-Othmer *Encyclopedia of Chemical Technology*, John Wiley & Son, Inc., New York, 2001.
- 2 (a) Z. Z. J. Wang, J. Zhuge, H. Fang and B. A. Prior, *Biotechnol. Adv.*, 2001, **19**, 201; (b) M. J. Taherzadeh, L. Adler and G. Liden, *Enzyme Microb. Technol.*, 2002, **31**, 53.
- 3 M. McCoy, *Chem. Eng. News*, 2009, **87**, 16.

- 4 (a) EU-Directive, 2003/30/EC, 2003, 8th May; (b) EU-Directive, 2009/28/EC, 2009, 23th April.
- 5 L. Ott, M. Bicker and H. Vogel, *Green Chem.*, 2006, **8**, 214.
- 6 (a) M. Pagliaro, R. Ciriminna, H. Kimura, M. Rossi and C. Della Pina, *Angew. Chem., Int. Ed.*, 2007, **46**, 4434; (b) A. Behr, J. Eilting, K. Irawadi, J. Leschinski and F. Lindner, *Green Chem.*, 2008, **10**, 13; (c) Y. Zheng, X. Chen and Y. Shen, *Chem. Rev.*, 2008, **108**, 5253; (d) C. H. Zhou, J. N. Beltrami, Y. X. Fan and G. Q. Lu, *Chem. Soc. Rev.*, 2008, **37**, 527.
- 7 A. Wolfson, C. Dlugy and Y. Shotland, *Environ. Chem. Lett.*, 2007, **5**, 67.
- 8 J. W. Yoo, Z. Mouloungui and A. Gaset, *World Pat.*, 1998, WO 9840371.
- 9 (a) T. Aoki, T. Ohe and H. Ishikami, *Eur. Pat.*, 2000, 1059278; (b) P. Gilbeau, *World Pat.*, 2006, WO 2006106154; (c) P. Gilbeau, *World Pat.*, 2006, WO 2006100311; (d) D. Siano, E. Santacesaria, V. Fiandra, R. Tesser, G. Di Nuzzi, M. Di Serio and M. Nastasi, *World Pat.*, 2006, WO 2006111810.
- 10 C. Reichardt, *Solvents and Solvent Effects in Organic Chemistry*, 3<sup>rd</sup> ed., Ed. Wiley-VCH, Weinheim, 2003.
- 11 K. Dimroth, C. Reichardt, T. Siepmann and F. Bohlmann, *Liebigs Ann. Chem.*, 1963, **1**, 661.
- 12 C. Reichardt, *Chem. Rev.*, 1994, **94**, 2319.
- 13 Y. Marcus, *J. Phys. Org. Chem.*, 2005, **18**, 373.
- 14 C. Reichardt, *Green Chem.*, 2005, **7**, 339.
- 15 (a) M. Cossi, V. Barone, B. Mennucci and J. Tomasi, *Chem. Phys. Lett.*, 1998, **286**, 253; (b) J. Tomasi, B. Mennucci and E. Cancès, *THEOCHEM*, 1999, **464**, 211; (c) M. Cossi, G. Scalmani, N. Rega and V. Barone, *J. Chem. Phys.*, 2002, **117**, 43. (and references cited therein).
- 16 M. J. Kamlet, J. L. Abboud and R. W. Taft, *J. Am. Chem. Soc.*, 1977, **99**, 6027.
- 17 M. J. Kamlet, J. L. Abboud, M. H. Abraham and R. W. Taft, *J. Org. Chem.*, 1983, **48**, 2877.
- 18 Y. Marcus, *Chem. Soc. Rev.*, 1993, **22**, 409.
- 19 L. Onsager, *J. Am. Chem. Soc.*, 1936, **58**, 1486.
- 20 A. Leo, C. Hansch and D. Elkins, *Chem. Rev.*, 1971, **71**, 525.
- 21 R. Mannhold and H. van Waterbeemd, *J. Comput.-Aided Mol. Des.*, 2001, **15**, 337.
- 22 (a) A. K. Ghose, V. N. Viswanadhan and J. J. Wendoloski, *J. Phys. Chem.*, 1998, **102**, 3762–3772; (b) S. A. Wildman and G. M. Crippen, *J. Chem. Inf. Comput. Sci.*, 1999, **39**, 868.
- 23 H. Y. Afeefy, J. F. Liebman and S. E. Stein, Neutral Thermochemical Data, in, *NIST Chemistry WebBook*, NIST Standard Reference Database Number 69, P. J. Linstrom and W. G. Mallard (Ed.), National Institute of Standards and Technology, Gaithersburg MD, 20899, <http://webbook.nist.gov>.
- 24 I. A. Koppel and V. A. Palm, The Influence of the Solvent on Organic Reactivity, in, *Advances in Linear Free Energy Relationships*, Ed. Plenum Press, London, 1972.
- 25 H. García-Marín, J. C. Van Der Toorn, J. A. Mayoral, J. I. García and I. W. C. E. Arends, *Green Chem.*, 2009, **11**, 1605.
- 26 L. Aldea, J. M. Fraile, H. García-Marín, J. I. García, C. I. Herrerías, J. A. Mayoral and I. Pérez, *Green Chem.*, 2010, **12**, DOI: 10.1039/b923137d, next paper in this issue.
- 27 J. Wagner and H. Grill, *US. Pat.*, 1975, 3888994.
- 28 D. A. Blake, H. F. Cascorbi, R. S. Rozman and F. J. Meyer, *Toxicol. Appl. Pharmacol.*, 1969, **15**, 83.
- 29 M. J. Murphy, D. A. Dunbar and L. S. Kaminsky, *Toxicol. Appl. Pharmacol.*, 1983, **71**, 84.
- 30 *Gaussian03, Revision C.02*, M. J. Frisch, G. W. Trucks, H. B. Schlegel, G. E. Scuseria, M. A. Robb, J. R. Cheeseman, J. A. Montgomery, Jr., T. Vreven, K. N. Kudin, J. C. Burant, J. M. Millam, S. S. Iyengar, J. Tomasi, V. Barone, B. Mennucci, M. Cossi, G. Scalmani, N. Rega, G. A. Petersson, H. Nakatsuji, M. Hada, M. Ehara, K. Toyota, R. Fukuda, J. Hasegawa, M. Ishida, T. Nakajima, Y. Honda, O. Kitao, H. Nakai, M. Klene, X. Li, J. E. Knox, H. P. Hratchian, J. B. Cross, V. Bakken, C. Adamo, J. Jaramillo, R. Gomperts, R. E. Stratmann, O. Yazyev, A. J. Austin, R. Cammi, C. Pomelli, J. W. Ochterski, P. Y. Ayala, K. Morokuma, G. A. Voth, P. Salvador, J. J. Dannenberg, V. G. Zakrzewski, S. Dapprich, A. D. Daniels, M. C. Strain, O. Farkas, D. K. Malick, A. D. Rabuck, K. Raghavachari, J. B. Foresman, J. V. Ortiz, Q. Cui, A. G. Baboul, S. Clifford, J. Cioslowski, B. B. Stefanov, G. Liu, A. Liashenko, P. Piskorz, I. Komaromi, R. L. Martin, D. J. Fox, T. Keith, M. A. Al-Laham, C. Y. Peng, A. Nanayakkara, M. Challacombe, P. M. W. Gill, B. Johnson, W. Chen, M. W. Wong, C. Gonzalez and J. A. Pople, Gaussian, Inc., Wallingford CT, 2004.

# Study of the recycling possibilities for azabis(oxazoline)–cobalt complexes as catalysts for enantioselective conjugate reduction†

Luis Aldea, José M. Fraile,\* Héctor García-Marín, José I. García, Clara I. Herrerías, José A. Mayoral and Ignacio Pérez

Received 5th November 2009, Accepted 14th December 2009

First published as an Advance Article on the web 26th January 2010

DOI: 10.1039/b923137d

Azabis(oxazoline)–cobalt(II) complexes have been tested in multiphase catalytic systems for enantioselective conjugate reduction of (*E*)-3-phenylbut-2-enoate with NaBH<sub>4</sub>. Immobilization by electrostatic interactions with laponite clay leads to excellent results in the first run, as a consequence of the role of the clay as an anion. However most of the reaction takes place in solution due to leaching of active complex, and the solids are not reusable. Covalent immobilization to Merrifield's resin does not allow the high enantioselectivity obtained in solution to be reached, and heterogeneous catalysts are again not reusable. Only the use of biphasic liquid systems allows an efficient recovery of the catalyst. The combination of a new ditopic ligand and 1,3-bis(2,2,2-trifluoroethoxy)propan-2-ol as a solvent for the catalyst phase is optimal to recycle the catalytic system with 90–96% ee for 5 runs.

## Introduction

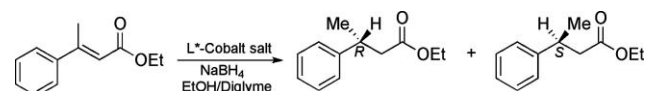
The selective reduction of double bonds in  $\alpha,\beta$ -unsaturated carbonyl compounds has become an important tool for the synthesis of organic compounds. Hence, many systems have been described to improve this selective process.<sup>1</sup> The use of metal hydrides as well as the combination of hydrides, such as sodium borohydride or aluminium hydrides, and transition metal salts have allowed the selective reduction of double bonds conjugated with electron-withdrawing groups.<sup>2</sup> However, there are very few examples in the literature about the asymmetric version of this type of reduction.<sup>3</sup> One of these examples was reported by Pfaltz and co-workers who described the use of semicorrin–cobalt complexes in the enantioselective reduction of  $\alpha,\beta$ -unsaturated esters and amides with sodium borohydride, obtaining high enantioselectivities.<sup>4</sup> Afterwards, other chiral cobalt complexes were used in the reduction of acrylamides with very good results.<sup>5</sup> Recently, Reiser and co-workers have described the use of azabis(oxazoline)–Co complexes, which proved to be highly efficient and selective in the reduction of esters, lactams and amides with NaBH<sub>4</sub>.<sup>6</sup>

During the last few years, the immobilization of chiral catalysts<sup>7</sup> has emerged as a powerful tool in order to improve the applicability of enantioselective processes, due to the easier catalyst separation in comparison with the analogous homogeneous counterparts. However, this is not the only advantage that would

justify the use, in some cases, of supported systems prepared by easy non-covalent immobilization methods.<sup>8</sup>

It has been shown that immobilized catalysts can afford additional advantages related to site-isolation or to the possibility of using them as true multitask catalysts.<sup>9</sup> More recently, it has been shown that the support can be used as an active part of the enantioselection process,<sup>10</sup> leading to catalytic reactions with improved stereoselectivity<sup>11</sup> or even with a reversal in the stereochemical result in comparison with the behavior of the same catalysts in solution.<sup>12</sup> The easy separation and purification of the catalyst, as well as the improved activity and selectivity are clearly desirable objectives of Green Chemistry.

In this paper, we describe the efforts carried out in the recycling of azabis(oxazoline)–cobalt complexes, used as catalysts for the reduction of ethyl (*E*)-3-phenylbut-2-enoate with NaBH<sub>4</sub> (Scheme 1), through immobilization on solid supports and the use of liquid–liquid biphasic systems.



**Scheme 1** Conjugated reduction of ethyl (*E*)-3-phenylbut-2-enoate with NaBH<sub>4</sub>.

## Results and discussion

### Assessment of the ligand effect

In a first set of experiments, three azabis(oxazoline) (azabox, **2**, Fig. 1) and two bis(oxazoline) ligands (box, **1**, Fig. 1) were tested in the homogeneous enantioselective reduction of ethyl (*E*)-3-phenylbut-2-enoate (Table 1), in order to compare them with the results reported in the literature with other substrates.

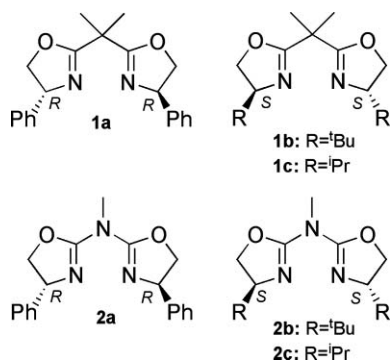
Departamento de Química Orgánica, Instituto de Ciencia de Materiales de Aragón and Instituto Universitario de Catálisis Homogénea, Facultad de Ciencias, Universidad de Zaragoza-C.S.I.C., 50009, Zaragoza, Spain. E-mail: jmfraile@unizar.es; Fax: +34 976762077

† Electronic supplementary information (ESI) available: Experimental details for preparation and characterization of heterogeneous catalysts, and catalytic tests with homogeneous and heterogeneous catalysts. See DOI: 10.1039/b923137d

**Table 1** Results obtained in the conjugated reduction of ethyl (*E*)-3-phenylbut-2-enoate with NaBH<sub>4</sub> catalyzed by CoCl<sub>2</sub> complexes<sup>a</sup>

Entry	Ligand	Yield (%) <sup>b</sup>	e.e. (%) <sup>c</sup>
1	—	<5	n.d.
2	<b>1a</b>	14	8 ( <i>S</i> )
3	<b>1c</b>	21	27 ( <i>R</i> )
4	<b>2a</b>	82	91 ( <i>S</i> )
5	<b>2b</b>	22	14 ( <i>R</i> )
6	<b>2c</b>	83	72 ( <i>R</i> )

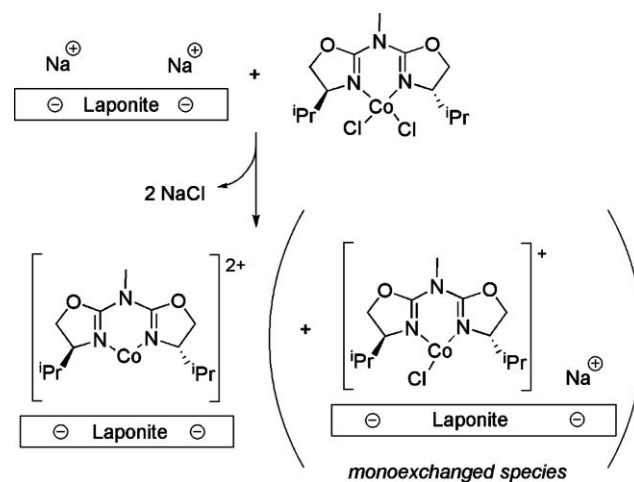
<sup>a</sup> Reaction conditions: 1 mmol of ethyl (*E*)-3-phenylbut-2-enoate, 0.025 mmol (2.5 mol %) of CoCl<sub>2</sub>, 0.028 mmol (2.8 mol %) of ligand, 4 ml EtOH–diglyme (1 : 1), 2.5 mmol NaBH<sub>4</sub>, 24 h, rt. <sup>b</sup> Determined by gas chromatography. <sup>c</sup> Determined by gas chromatography (β-cyclodextran column).

**Fig. 1** Chiral bis(oxazoline) (box, **1**) and azabis(oxazoline) (azabox, **2**) ligands.

As can be seen, when the reaction was carried out without a chiral ligand, the yield was less than 5%, confirming the result obtained by Reiser *et al.*<sup>6</sup> The use of the bis(oxazoline) complexes (**1a**–CoCl<sub>2</sub> and **1c**–CoCl<sub>2</sub>) did not lead to good results either, although box(*i*-Pr) (**1c**) performed slightly better than box(Ph) (**1a**), mainly in enantioselectivity (27% ee vs. 8% ee). In good agreement with previous results,<sup>6</sup> the use of azabis(oxazoline) ligands leads to a great increase in activity and enantioselectivity (91% ee with **2a** and 72% ee with **2c**) with respect to the results obtained using bis(oxazoline) ligands bearing the same substituents. However, the results with azabox bearing *tert*-butyl groups (**2b**) were not so satisfactory (22% yield, 14% ee).

### Immobilization by cation exchange

Given the results obtained in solution, only complexes **2a**–CoCl<sub>2</sub> and **2c**–CoCl<sub>2</sub> were supported by electrostatic interactions onto laponite. This clay was chosen due to its good behavior in other enantioselective reactions catalyzed by bis(oxazoline)–Cu complexes.<sup>13</sup> Immobilization was carried out by cationic exchange (Scheme 2) using the sodium form of the laponite<sup>14</sup> and ethanol as solvent instead of the frequently used methanol

**Scheme 2** Cation exchange process of **2c**–CoCl<sub>2</sub>.

to prevent possible stability problems of NaBH<sub>4</sub>.<sup>15</sup> Solids were characterized by cobalt analysis, elemental analysis and FT-IR spectroscopy.

FT-IR spectra of immobilized species (see the ESI†) show the C=N band at around 1670 cm<sup>-1</sup>, shifted from the position at 1638 cm<sup>-1</sup> of the free ligand, together with the typical bands of the complex in the skeletal region of 1400–1600 cm<sup>-1</sup>. Metal and elemental analyses are gathered in Table 2. The cobalt loading (around 0.15 mmol g<sup>-1</sup>) is in good agreement with previous results of exchange obtained with related copper complexes and the same support.<sup>16</sup> As can be seen, the ligand:Co ratio (calculated from N analysis) was higher than 1 in all cases. Decomplexation/ligand adsorption phenomena, and/or deproportionation of oligomeric species may account for this ratio.

The results of the conjugated reduction of ethyl (*E*)-3-phenylbut-2-enoate with NaBH<sub>4</sub> (Scheme 1), promoted by laponite-based catalysts are gathered in Table 3. The immobilized **2a**–Co(II) complex showed an activity (entry 1) similar to that obtained in homogeneous phase with slightly lower enantioselectivity. However, **2c**–Co(II) immobilized onto laponite led to much better results (entry 3) than those obtained in solution, with quantitative yield and improved enantioselectivity (95% vs. 72% e.e.). Laponite has proven to be a less coordinating anion than chloride,<sup>13</sup> and this might be the origin of this effect. In fact, experiments in solution with ligand **2c** and Co(BF<sub>4</sub>)<sub>2</sub> showed 97% e.e., enantioselectivity noticeably improved from 72% e.e. obtained with CoCl<sub>2</sub>. It is worth mentioning that these are the best results obtained in this reaction with azabox(*i*-Pr) ligand (**2c**), proving the importance of the cobalt counter-ion on the catalytic performance.

The recoverability of laponite catalysts was very poor (entries 2 and 4), with a considerable drop in activity and

**Table 2** Characterization of the different complexes immobilized onto laponite by cationic exchange

Ligand	Starting Co salt	N/mmol g <sup>-1</sup>	Co/mmol g <sup>-1</sup>	ligand:Co	B/mmol g <sup>-1</sup>	Cl/mmol g <sup>-1</sup>
<b>2a</b>	CoCl <sub>2</sub>	1.95	0.16	4.1	—	0.11
<b>2c</b>	CoCl <sub>2</sub>	1.00	0.15	2.2	—	0.06
<b>2c</b>	Co(BF <sub>4</sub> ) <sub>2</sub>	0.96	0.20	1.6	0.054	—

**Table 3** Results obtained in the conjugated reduction of ethyl (*E*)-3-phenylbut-2-enoate with NaBH<sub>4</sub> promoted by chiral cobalt complexes immobilized onto laponite<sup>a</sup>

Entry	Ligand	Co precursor	Run	Time/h	Yield (%) <sup>b</sup>	e.e. (%) <sup>c</sup>
1	<b>2a</b>	CoCl <sub>2</sub>	1	24	83	81 ( <i>S</i> )
2			24	12	43 ( <i>S</i> )	
3	<b>2c</b>	CoCl <sub>2</sub>	1	24	100	95 ( <i>R</i> )
4			2	24	16	n.d.
5			1	3	95	92 ( <i>R</i> )
6			2	3	19	35 ( <i>R</i> )
7	<b>2c</b>	Co(BF <sub>4</sub> ) <sub>2</sub>	1	72	100	92 ( <i>R</i> )
8			2	72	46	68 ( <i>R</i> )
9 <sup>d</sup>			1	24	53	88 ( <i>R</i> )
10			2	168	19	55 ( <i>R</i> )

<sup>a</sup> Reaction conditions: 1 mmol of ethyl (*E*)-3-phenylbut-2-enoate, 2.5 mmol NaBH<sub>4</sub>, 0.025 mmol (2.5 mol %) of catalyst, 4 ml EtOH:diglyme (1:1), rt. <sup>b</sup> Determined by gas chromatography. <sup>c</sup> Determined by gas chromatography (β-cyclodextran column). <sup>d</sup> Catalyst filtered after 30 min of reaction.

enantioselectivity. Shorter reaction times (entry 5) allowed the same results to be obtained in the first run but it did not prevent any deleterious effects of the prolonged contact with the borohydride solution. The analysis of the recovered solids (up to 0.04 mmol g<sup>-1</sup>) showed a great decrease in Co content.

Filtration experiments after 30 min of reaction showed an important contribution of homogeneous reaction (80% yield, 90% e.e.) and the complete deactivation of the solid. The analysis of the freshly prepared catalysts (Table 2) showed that a considerable amount of chloride remained on them, probably due to the incomplete exchange of the highly coordinating chloride anion (Scheme 2).

The same type of solid was prepared by exchange of **2c**-Co(BF<sub>4</sub>)<sub>2</sub>. The analysis (Table 2, entry 3) showed a similar cobalt loading (0.20 mmol g<sup>-1</sup>), a ligand:Co ratio closer to the theoretical value, and a significantly lower amount of remaining anion from the boron analysis. As expected, the use of Co(BF<sub>4</sub>)<sub>2</sub> reproduced the good results obtained in homogeneous phase (Table 3, entry 7) and allowed a better recovery of the catalyst achieving a moderate activity and selectivity (Table 3, entry 8). Although the analysis of the recovered catalyst showed an elevated lixiviation (60% of the Co content in the fresh catalyst), the leaching was somewhat lower than that obtained when chloride was used as starting counterion.

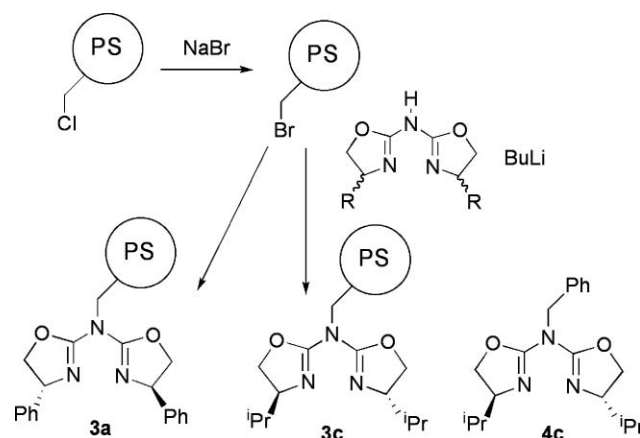
The same filtration experiment at short reaction time (30 min) showed again the presence of active chiral complex in the solution (quantitative yield, 91% e.e.). However, the lixiviation level was lower than in the case of using CoCl<sub>2</sub>, since the recovered solid showed significant activity (53% yield) and enantioselectivity (88% e.e.) (Table 3, entry 9).

The cobalt leaching might be due to two different mechanisms: back-exchange with Na from NaBH<sub>4</sub> and formation of a neutral Co species.

Although the reaction mechanism is unknown, some reactions of Co(II) complexes with NaBH<sub>4</sub> under stoichiometric conditions have been described and can be considered as models. In most cases, a reduction takes place, leading to the formation of Co<sup>0</sup>X,<sup>17</sup> Co<sup>0</sup>(BH<sub>4</sub>),<sup>18</sup> or Co<sup>0</sup>H<sup>19</sup> complexes. The formation of a mixed Co<sup>II</sup>H(BH<sub>4</sub>) complex has been also described.<sup>20</sup> The formation of any of those types of complexes with azabox ligands would account for the observed cobalt leaching.

### Covalent immobilization

Taking into account the results obtained with complexes immobilized by electrostatic interactions, the grafting of the complex through covalent bonds seemed to be a good alternative, as the cationic or neutral character of the intermediates would not be an issue in such case. A chloromethylated polystyrene (Merrifield's resin) was activated by treatment with NaBr under biphasic conditions to obtain the corresponding bromomethylated polymer, which was used to alkylate the imino central bridge of azabox leading to the immobilized ligands **3a** and **3c** (Scheme 3).<sup>9,21</sup> The cobalt complexes were prepared from different precursors and in different solvents (Table 4). Ligand and cobalt contents were analyzed (Table 4) and the immobilized complexes were characterized by IR spectroscopy.

**Scheme 3** Covalent immobilization of azabox.

In the spectra of immobilized complexes (ESI), the band at 1665 cm<sup>-1</sup> is present together with that of the free ligand at 1645 cm<sup>-1</sup>, in agreement with the rather low complexation level obtained in all cases (22–66% of the immobilized ligand, Table 4).

**Table 4** Characterization of the different complexes immobilized onto Merrifield's resin by covalent bond

Catalyst	Co salt	Solvent	N/mmol g <sup>-1</sup>	Azabox/mmol g <sup>-1</sup>	Co/mmol g <sup>-1</sup>	N:Co
<b>3a</b> -C <sub>Me</sub>	CoCl <sub>2</sub>	MeOH	2.34	0.78	0.17	13.8
<b>3c</b> -C <sub>Me</sub>	CoCl <sub>2</sub>	MeOH	2.49	0.83	0.46	5.4
<b>3c</b> -B <sub>Et</sub>	Co(BF <sub>4</sub> ) <sub>2</sub>	EtOH	2.46	0.82	0.27	9.1
<b>3c</b> -B <sub>THF</sub>	Co(BF <sub>4</sub> ) <sub>2</sub>	THF	2.41	0.80	0.53	4.5

**Table 5** Results obtained in the conjugated reduction of ethyl (*E*)-3-phenylbut-2-enoate with NaBH<sub>4</sub> promoted by chiral cobalt complexes immobilized onto Merrifield's resin

Entry	Catalyst	Solvent <sup>a</sup>	NaBH <sub>4</sub> <sup>b</sup>	Time/h	Yield (%) <sup>c</sup>	e.e. (%) <sup>d</sup>
1	<b>3a</b> -C <sub>Me</sub>	EtOH-dig	2.5	24	17	15 ( <i>S</i> )
2	<b>3c</b> -C <sub>Me</sub>	EtOH-dig	2.5	24	13	4 ( <i>R</i> )
3	<b>4c</b> -Co(BF <sub>4</sub> ) <sub>2</sub>	EtOH-dig	2.5	24	98	91 ( <i>R</i> )
4	<b>4c</b> -Co(BF <sub>4</sub> ) <sub>2</sub>	EtOH-dig-THF	2.5	24	99	89 ( <i>R</i> )
5	<b>3c</b> -B <sub>Et</sub>	EtOH-dig	1.0	72	30	32 ( <i>R</i> )
6	<b>3c</b> -B <sub>Et</sub>	EtOH-dig-THF	1.0	72	25	46 ( <i>R</i> )
7	<b>3c</b> -B <sub>THF</sub>	EtOH-dig-THF reuse	1.3	72	69	67 ( <i>R</i> )
				168	14	34 ( <i>R</i> )

<sup>a</sup> Reaction solvent: dig. = diglyme. All the mixtures contain the same amount of each solvent (v/v). <sup>b</sup> mmol of NaBH<sub>4</sub> per mmol of substrate. <sup>c</sup> Determined by gas chromatography. <sup>d</sup> Determined by gas chromatography (β-cyclodex column).

These complexes were tested in the conjugated reduction of ethyl (*E*)-3-phenylbut-2-enoate with NaBH<sub>4</sub> (Scheme 1), and the results are gathered in Table 5.

The supported complexes prepared with CoCl<sub>2</sub> in methanol gave rise to very poor results, both in yield and enantioselectivity (entries 1 and 2). The role of substitution in the central imine bridge was discarded by testing the analogous homogeneous ligand **4c** (Scheme 3), able to achieve excellent results (entry 3). A new solid prepared with Co(BF<sub>4</sub>)<sub>2</sub> in ethanol (32% e.e., entry 5) excludes an important role of methanol traces. Trying to improve polymer swelling, THF was added to the reaction mixture, leading to slightly better enantioselectivity (46% e.e., entry 6). The problem of swelling in complexation of the supported ligands was solved by carrying out the complexation with Co(BF<sub>4</sub>)<sub>2</sub> also in THF. In agreement with this hypothesis, the cobalt loading was much higher than that obtained in ethanol (Table 4) and the catalytic performance was also improved, with higher yield and enantioselectivity (67% e.e., entry 7).

It can be seen that the immobilized catalyst, even under optimized conditions, does not reach the high performance of the homogeneous catalyst (entry 4), and moreover it is not recyclable, in spite of the lack of cobalt leaching from the polymer (0.51 mmol g<sup>-1</sup>).

### Biphasic liquid systems

Given the limitations of supported catalysts regarding enantioselectivity, leaching, and/or recovery, the use of biphasic liquid systems<sup>22</sup> was considered as an interesting alternative. As water is detrimental for this reaction, ionic liquids<sup>23</sup> were first considered to carry out the reduction in solution, allowing the final extraction of the products with an immiscible solvent. The chosen solvent was 1-butyl-3-methylimidazolium hexafluorophosphate [bmim][PF<sub>6</sub>].

The first tests with complex **2c**-Co(BF<sub>4</sub>)<sub>2</sub> in [bmim][PF<sub>6</sub>] showed the need for a proton source to complete the catalytic cycle. Hence, ethanol was used as proton donor together with the ionic liquid. Ethanol had to be evaporated before extraction of the reaction product with hexane. In such case a remarkable

**Table 6** Results obtained in the conjugated reduction of ethyl (*E*)-3-phenylbut-2-enoate with NaBH<sub>4</sub> promoted by chiral cobalt complexes in alternative solvents

Entry	Catalyst	Solvent <sup>a</sup>	Run	Yield (%) <sup>b</sup>	e.e. (%) <sup>c</sup>
1	<b>2c</b> -Co(BF <sub>4</sub> ) <sub>2</sub>	[bmim][PF <sub>6</sub> ]	1	51	81 ( <i>R</i> )
2	<b>2c</b> -Co(BF <sub>4</sub> ) <sub>2</sub>	BTfEP	1	89	88 ( <i>R</i> )
3	<b>5c</b> -Co(BF <sub>4</sub> ) <sub>2</sub>	[bmim][PF <sub>6</sub> ]	1	75	85 ( <i>R</i> )
4			2	67	82 ( <i>R</i> )
5			3	60	77 ( <i>R</i> )
6			4	44	61 ( <i>R</i> )
7			5	48	40 ( <i>R</i> )
8	<b>5c</b> -Co(BF <sub>4</sub> ) <sub>2</sub>	BTfEP	1	99	96 ( <i>R</i> )
9			2	91	95 ( <i>R</i> )
10			3	41	96 ( <i>R</i> )
11			4	41	96 ( <i>R</i> )
12			5	48	90 ( <i>R</i> )

<sup>a</sup> Reaction solvent. In all cases the same volume of EtOH is added to act as proton donor. <sup>b</sup> Determined by gas chromatography. <sup>c</sup> Determined by gas chromatography (β-cyclodex column).

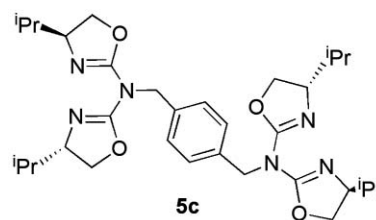
51% yield with 81% ee was obtained (Table 6, entry 1), but the catalyst phase was not recoverable.

In view of those results in ionic liquid solution and the incompatibility of the reaction with water, a new type of solvent was considered. *O*-Alkylated glycerol derivatives<sup>24</sup> are interesting solvents that are currently being studied as potential alternatives to "classical" harmful organic solvents.

Among the large amount of solvents (around 75) prepared, characterized and tested in our group,<sup>24</sup> BTfEP (1,3-bis(2,2,2-trifluoroethoxy)propan-2-ol) was chosen because of its good behavior in catalyzed oxidation reactions.<sup>25</sup>

In this case results with **2c**-Co(BF<sub>4</sub>)<sub>2</sub> were improved up to 89% yield and 88% ee (Table 6, entry 2), but again the catalyst phase was not recoverable. In both media the formation of a large amount of a black solid was observed. This seems to indicate that the cobalt complex is broken and an inactive cobalt derivative, probably cobalt boride, is formed. A possible solution will be the use of a more stable complex.

In view of those results, a ditopic azabis(oxazoline) **5c** (Fig. 2) was prepared by alkylation of 2,2'-iminobis[(4*S*)-4-isopropyl-4,5-dihydro-1,3-oxazole] with 1,4-di(bromomethyl)benzene<sup>26</sup> and it was tested as a ligand.

**Fig. 2** Chiral ditopic azabis(oxazoline) **5c** ligand.

As can be seen in Table 6, results with this ligand are clearly better than those obtained with azabox in the same solvent. In [bmim][PF<sub>6</sub>] 85% e.e. was obtained in the first reaction along with 75% yield, and recoverability was excellent in the second run, but a decay in catalytic activity and enantioselectivity

was observed from the third run (entries 3–7). The higher stability of the complex was demonstrated by the slower formation of the black residue, only observable after the second reaction.

On the contrary the complex **5c**–Co(BF<sub>4</sub>)<sub>2</sub> shows an excellent performance in BTFEP, 99% yield and 96% ee. Interestingly, the catalyst solution is recoverable with no significant drop in enantioselectivity up to the fifth run. However activity is reduced to 40–50% yield from the third run but it remains stable. This is probably due to the unavoidable slow formation of CoB particles, detected in the form of black powder, which significantly reduces the true amount of catalyst after the second recovery. In any case these results represent the first recyclable system for this reaction, showing that the biphasic liquid system using a glycerol derivative is the most suitable method of recovery in this case.

## Experimental

### Representative procedure for the biphasic conjugated reduction of ethyl (*E*)-3-phenylbut-2-enoate

A suspension of the corresponding ligand (0.025 mmol) and the cobalt salt (0.028 mmol) in anhydrous solvent (ionic liquid or BTFEP) (1 ml) was stirred for 15 min under an inert atmosphere. After this time, a solution of ethyl (*E*)-3-phenylbut-2-enoate (1 mmol) in ethanol (1 ml) was added, and the mixture was cooled to 0 °C. NaBH<sub>4</sub> (2.5 mmol) was slowly added in portions and, after the addition was completed, the reaction mixture was stirred 24 h at room temperature under inert atmosphere. The resulting crude was evaporated to eliminate the ethanol, and extracted with hexane (3 × 2 ml). The combined organic layers were washed with H<sub>2</sub>O (3 × 10 ml), dried with anhydrous MgSO<sub>4</sub> and concentrated under vacuum. The results were analyzed by HPLC. After extraction the catalyst solution in ionic liquid or BTFEP was evaporated to eliminate the remaining hexane and it was reused under the same conditions.

## Conclusions

Azabox–Co complexes can be immobilized on solids by either electrostatic interactions or covalent bonding. In the first case the solid anion plays a role, as it happens in solution, leading to an improvement in the catalytic performance. However, a large amount of active complex is leached to the solution, and hence the reaction mostly takes place in homogeneous phase. As a consequence the catalysts are not reusable. Complexes formed on Merrifield's resin are much less active and enantioselective than the homogeneous counterparts.

The best method for recycling is the use of a liquid–liquid biphasic system. Both ionic liquids and fluorinated glycerol derivatives are good media to perform the reaction, but again the catalytic medium is not recoverable, unless a new ditopic ligand containing two azabis(oxazoline) moieties is used. In such case the glycerol derivative BTFEP is more efficient, mainly regarding the enantioselectivity, which is maintained at 90–96% ee for five consecutive runs.

## Acknowledgements

Financial support from the European Union (project Solvsafe, NMP2-CT-2005-011774), the Spanish Ministerio de Ciencia e Innovación (projects CTQ2008-05138 and Consolider Ingenio 2010 CSD2006-0003), and the Diputación General de Aragón (E11 Group co-financed by the European Regional Development Funds) is gratefully acknowledged.

## Notes and references

- 1 E. Keinan and N. Greenspoon, in *Comprehensive Organic Synthesis*, ed. B. M. Trost and I. Fleming, vol. 8, Pergamon Press, Oxford, 1991, p. 523.
- 2 J. H. Schauble, G. J. Walter and J. G. Morin, *J. Org. Chem.*, 1974, **39**, 755; S. Antus, A. Gottsegen and M. Nogradi, *Synthesis*, 1981, 574; N. Satyanarayana and M. Periasamy, *Tetrahedron Lett.*, 1984, **25**, 2501; W. S. Mahoney, D. M. Brestensky and J. M. Stryker, *J. Am. Chem. Soc.*, 1988, **110**, 291; T. Kawakami, M. Miyatake, I. Shibata and A. Baba, *J. Org. Chem.*, 1996, **61**, 376; J. M. Khurana and P. Sharma, *Bull. Chem. Soc. Jpn.*, 2004, **77**, 549.
- 3 For examples of reductions with CuH systems see: C. Deutsch, N. Krause and B. H. Lipshutz, *Chem. Rev.*, 2008, **108**, 2916.
- 4 U. Leutenegger, A. Madin and A. Pfaltz, *Angew. Chem., Int. Ed. Engl.*, 1989, **28**, 60; P. Von Matt and A. Pfaltz, *Tetrahedron: Asymmetry*, 1991, **2**, 691; M. Misun and A. Pfaltz, *Helv. Chim. Acta*, 1996, **79**, 961.
- 5 T. Yamada, Y. Ohtsuka and T. Ikeno, *Chem. Lett.*, 1998, 1129; Y. Ohtsuka, T. Ikeno and T. Yamada, *Tetrahedron: Asymmetry*, 2003, **14**, 967.
- 6 C. Geiger, P. Kreitmeier and O. Reiser, *Adv. Synth. Catal.*, 2005, **347**, 249.
- 7 *Chiral Catalysts Immobilization and Recycling*, ed. D. E. De Vos, I. F. J. Vankelecom and P. A. Jacobs, Wiley-VCH, Weinheim, 2000.
- 8 J. M. Fraile, J. I. García and J. A. Mayoral, *Chem. Rev.*, 2009, **109**, 360.
- 9 J. M. Fraile, I. Pérez, J. A. Mayoral and O. Reiser, *Adv. Synth. Catal.*, 2006, **348**, 1680.
- 10 J. M. Fraile, J. I. García, C. I. Herrerías, J. A. Mayoral and E. Pires, *Chem. Soc. Rev.*, 2009, **38**, 695.
- 11 J. M. Fraile, J. I. García, J. A. Mayoral and M. Roldán, *Org. Lett.*, 2007, **9**, 731; M. J. Fabra, J. M. Fraile, C. I. Herrerías, F. J. Lahoz, J. A. Mayoral and I. Pérez, *Chem. Commun.*, 2008, 5402.
- 12 A. I. Fernández, J. M. Fraile, J. I. García, C. I. Herrerías, J. A. Mayoral and L. Salvatella, *Catal. Commun.*, 2001, **2**, 165; H. Wang, X. Liu, H. Xia, P. Liu, J. Gao, P. Ying, J. Xiao and C. Li, *Tetrahedron*, 2006, **62**, 1025; M. R. Castillo, L. Fousse, J. M. Fraile, J. I. García and J. A. Mayoral, *Chem.–Eur. J.*, 2007, **13**, 287; J. I. García, B. López-Sánchez, J. A. Mayoral, E. Pires and I. Villalba, *J. Catal.*, 2008, **258**, 378.
- 13 J. M. Fraile, J. I. García, J. A. Mayoral and T. Tarnai, *Tetrahedron: Asymmetry*, 1998, **9**, 3997.
- 14 J. M. Fraile, J. I. García, C. I. Herrerías, J. A. Mayoral and M. A. Harmer, *J. Catal.*, 2004, **221**, 532; J. M. Fraile, J. I. García, M. A. Harmer, C. I. Herrerías, J. A. Mayoral, O. Reiser and H. Werner, *J. Mater. Chem.*, 2002, **12**, 3290.
- 15 R. C. Wade, *J. Mol. Catal.*, 1983, **18**, 273.
- 16 J. M. Fraile, J. I. García, C. I. Herrerías, J. A. Mayoral, O. Reiser, A. Socuélamos and H. Werner, *Chem.–Eur. J.*, 2004, **10**, 2997.
- 17 M. Aresta, M. Rossi and A. Sacco, *Inorg. Chim. Acta*, 1969, **3**, 227.
- 18 D. G. Holah, A. N. Hughes, B. C. Hui and K. Wright, *Can. J. Chem.*, 1974, **52**, 2990; E. J. Corey, N. J. Cooper, W. M. Canning, W. N. Lipscomb and T. F. Koetzle, *Inorg. Chem.*, 1982, **21**, 192; D. J. Wink and N. J. Cooper, *J. Chem. Soc., Dalton Trans.*, 1984, 1257.
- 19 C. A. Ghilardi, S. Midollini and L. Sacconi, *Inorg. Chem.*, 1975, **14**, 1790; D. G. Holah, A. N. Hughes, S. Maciaszek, V. R. Magnuson and K. O. Parker, *Inorg. Chem.*, 1985, **24**, 3956.
- 20 M. Nakajima, T. Saito, A. Kobayashi and Y. Sasaki, *J. Chem. Soc., Dalton Trans.*, 1977, 385.

- 
- 21 H. Werner, C. I. Herrerías, M. Glos, A. Gissibl, J. M. Fraile, I. Pérez, J. A. Mayoral and O. Reiser, *Adv. Synth. Catal.*, 2006, **348**, 125.
- 22 See for example: B. E. Hanson, in ref. 7, p. 81.
- 23 C. E. Song, *Chem. Commun.*, 2004, 1033; *Ionic Liquids in Synthesis*, ed. P. Wasserscheid and T. Welton, Wiley-VCH, Weinheim, 2003; J. Dupont, R. F. de Souza and P. A. Z. Suarez, *Chem. Rev.*, 2002, **102**, 3667.
- 24 J. I. García, H. García-Marín, J. A. Mayoral and P. Pérez, *Green Chem.*, 2010, **12**, DOI: 10.1039/b923631g, previous paper in this issue.
- 25 H. García-Marín, J. C. van der Toorn, J. A. Mayoral, J. I. García and I. W. C. E. Arends, *Green Chem.*, 2009, **11**, 1605.
- 26 J. I. García, B. López-Sánchez and J. A. Mayoral, *Org. Lett.*, 2008, **10**, 4995.



# Palladium-guanidine complex immobilized on SBA-16: a highly active and recyclable catalyst for Suzuki coupling and alcohol oxidation†

Hengquan Yang,<sup>\*a,b</sup> Xiaojing Han,<sup>a</sup> Zhancheng Ma,<sup>a</sup> Runqin Wang,<sup>a</sup> Jing Liu<sup>a</sup> and Xiangfei Ji<sup>a,b</sup>

Received 16th September 2009, Accepted 6th November 2009

First published as an Advance Article on the web 13th January 2010

DOI: 10.1039/b919175e

By immobilizing a mixture of a palladium-guanidine complex and guanidine on the mesoporous cage-like material SBA-16 via a one-pot silylation, we have successfully prepared a new solid catalyst for Suzuki coupling and the aerobic oxidation of alcohols. The structure and composition of the solid catalyst were characterized with N<sub>2</sub> sorption, XRD, TEM, FT-IR and solid state NMR. The coordination state of the palladium-guanidine complex supported on the solid catalyst was preliminarily investigated with XPS and UV-vis spectroscopy. This catalyst afforded fast conversions for the Suzuki coupling of various aryl bromides and arylboronic acids in a 50% aqueous ethanol solution at 50 °C even at loadings of 0.01–0.001 mol%, and the TOF (turn-over frequency) for the Suzuki coupling of bromobenzene and arylboronic acids could be up to 45 700 h<sup>-1</sup> under mild conditions. A satisfactory yield was obtained even after the catalyst was reused several times. The developed solid catalyst combined with the mild conditions investigated represents one of the most efficient heterogeneous systems for the Suzuki coupling of bromides. Furthermore, it was found that the solid catalyst could also work well for the aerobic oxidation of benzylic alcohols and cinnamyl alcohol, affording over 99% selectivity. The catalyst could be reused 15 times without a significant decrease in activity and selectivity.

## Introduction

Pd-catalyzed reactions, such as Suzuki coupling and alcohol oxidation, are of significant importance in modern chemical transformations.<sup>1</sup> Various palladium complex catalysts for these reactions have been successfully established.<sup>2</sup> These metal complexes, however, suffer from practical problems such as catalyst separation, catalyst recycling and product contamination. To address these problems, palladium complexes as well as Pd nanoparticles have been immobilized on various supports such as silica, alumina, zeolites, organic polymers and dendrimers to create heterogeneous catalysts because these heterogeneous systems are easy to handle, recover and are “green” processes.<sup>3</sup> Although significant efforts and advances have been made along this line, the development of highly recyclable and active heterogeneous catalytic systems that could work well under mild conditions still remains a major challenge in view of the practical applications.

Our previous investigations and other groups' reports revealed that it was possible to improve the recyclability and activity of the immobilized catalyst by choosing a suitable support and ligand to be grafted on the support.<sup>4</sup> For both the Suzuki

coupling and alcohol oxidation, it was found that the supported molecular catalysts were converted to palladium nanoparticles as the reaction proceeded.<sup>3g,4a,5</sup> Driven by the high surface energy, the palladium nanoparticles on the support are prone to aggregate and agglomerate into less active larger particles, and the recyclability of the immobilized catalyst was thus discounted. Accordingly, limiting the growth of Pd nanoparticles into the less active larger particles (even Pd black) is one of the key factors for improving the recyclability. Among various supports for efficiently preventing the growth of metal nanoparticles, mesoporous materials are very promising because of their regularly arranged pore structure on a mesoscopic scale. More interestingly, different to the widely used channel-like mesoporous materials MCM-41 and SBA-15, the recently synthesized SBA-16 (cubic, *Im3m*) is one of the new ordered mesoporous materials with cage-like structures.<sup>6</sup> This mesoporous cage-like material has tunable cage sizes (4–10 nm) and pore entrance sizes (generally less than 4 nm). The isolated nanocages are three-dimensionally interconnected by the pore entrances. Such isolated nanocages of SBA-16 could not only accommodate metal complexes and particles formed *in situ* during the catalytic reaction, but also limit the growth of metal nanoparticles by the spatial restrictions. Meanwhile, the smaller pore entrances may inhibit the motion of metal nanoparticles, thereby preventing undesired agglomeration. In our very recent study, it has been demonstrated that the cage-like SBA-16 exhibited a much better capability to prevent the growth of metal nanoparticles than the channel-like SBA-15 as well as amorphous silica, and the recyclability of the complex catalyst immobilized on SBA-16 was significantly improved.<sup>4a</sup>

<sup>a</sup>School of Chemistry and Chemical Engineering, Shanxi University, Taiyuan, 030006, China. E-mail: hqyang@sxu.edu.cn; Fax: +86-351-7011688; Tel: +86-351-7018371

<sup>b</sup>Fine Chemical Engineering Centre of Education Ministry, Shanxi University, Taiyuan, 030006, China

† Electronic supplementary information (ESI) available: Textural parameters, base screening and XRD patterns. See DOI: 10.1039/b919175e

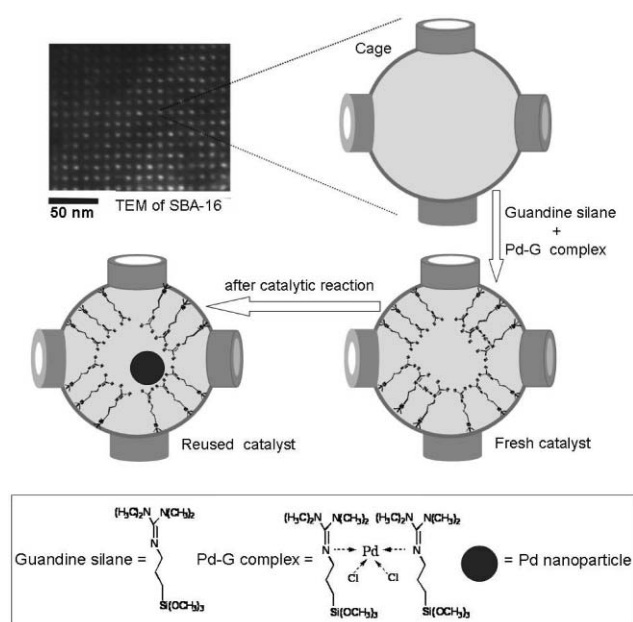
Recently, a palladium-tetramethylguanidine complex was found to be active in the Suzuki reaction.<sup>7</sup> Compared with the well-established phosphine, *N*-heterocyclic carbene and palladacyclic complex system, the palladium-guanidine complex is air-stable, inexpensive, has low toxicity and is easily accessible *via* chemical synthesis. Such advantages could make guanidine a potential ligand for practical applications. However, to the best of our knowledge, there has been no report about the heterogeneous palladium-guanidine complex catalyst.

This work aims to develop a more active and recyclable heterogeneous catalyst for Suzuki coupling and the aerobic oxidation of alcohols. By grafting a mixture of the palladium-guanidine complex and guanidine on SBA-16 *via* a one-pot silylation, we have successfully prepared a new solid catalyst. This catalyst afforded fast conversions for the Suzuki couplings of various aryl bromides and arylboronic acids in an aqueous ethanol solution at 50 °C even at catalyst loadings of 0.01–0.001 mol%. The turnover frequency (TOF) for the Suzuki coupling of bromobenzene and phenylboronic acid could be up to 45 700 h<sup>-1</sup> under mild conditions. Furthermore, it was found that the solid catalyst could also work well for the aerobic oxidation of alcohols with over 99% selectivity.

## Results and discussion

### Catalyst preparation and characterization

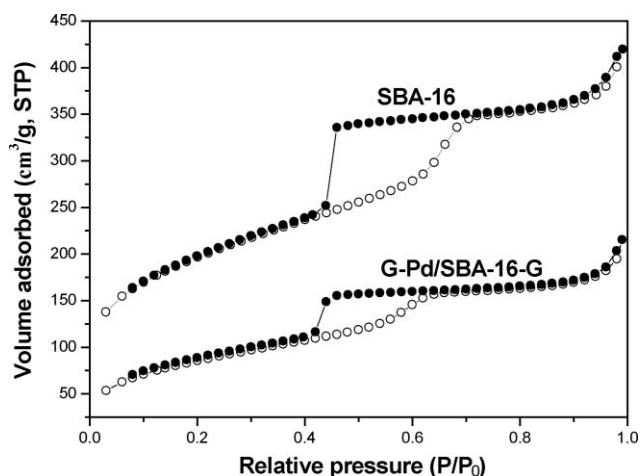
The process for the preparation of the catalyst Pd-G/SBA-16-G is schematically depicted in Scheme 1. To form a covalent linkage with the mesoporous cage-like material SBA-16, tetramethylguanidine was first subjected to a derivation with chloropropyltrimethoxysilane, leading to 1,1,3,3-tetramethyl-2-(3-trimethoxysilylpropyl)-guanidine (G), as described in the Experimental. Then, an excess of G was coordinated with PdCl<sub>2</sub>, resulting in a G solution containing the Pd-G complex. The Pd-G complex and residual G in this solution were grafted onto



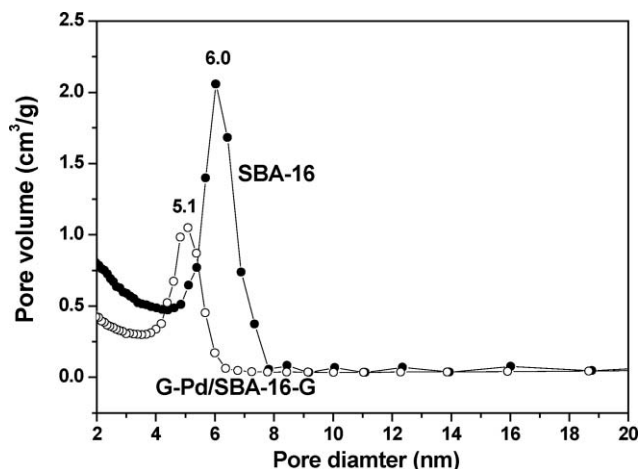
**Scheme 1** Schematic descriptions for preparing the solid catalyst Pd-G/SBA-16-G and the model for the reused catalyst.

SBA-16 through a one-pot silylation. After being thoroughly washed with organic solvents, a solid catalyst denoted as Pd-G/SBA-16-G was obtained. The Pd content of the catalyst Pd-G/SBA-16-G, determined by ICP-AES, is 0.86 wt%. The N and C contents of the catalyst Pd-G/SBA-16-G determined by combustion chemical analysis are 3.58 wt% and 9.28 wt%, respectively. The determined atom ratios of Pd, C and N on the solid catalyst were, broadly, in agreement with the ratios expected.

In order to obtain the structural information about the solid catalyst on a mesoscopic scale, N<sub>2</sub> sorption and powder X-ray diffraction (XRD) were used to characterize Pd-G/SBA-16-G. The N<sub>2</sub> sorption isotherms and pore size distribution plots for SBA-16 and Pd-G/SBA-16-G, are displayed in Fig. 1 and Fig. 2, respectively. The textural parameters determined by the N<sub>2</sub> sorption are listed in the ESI, Table S1.† SBA-16 exhibits a type-IV isotherm pattern with an H2 hysteresis loop, which is characteristic of the mesoporous cage-like structure. Similar to the parent material SBA-16, Pd-G/SBA-16-G also shows a type-IV isotherm with an H2 hysteresis loop, indicating that the catalyst Pd-G/SBA-16-G still maintains a good mesoporous cage-like structure. It is worthwhile to note that the specific surface area, pore volume and pore size of the parent SBA-16



**Fig. 1** N<sub>2</sub> sorption isotherms of SBA-16 and Pd-G/SBA-16-G.



**Fig. 2** Pore size distributions of SBA-16 and Pd-G/SBA-16-G.

undergo a significant decrease after grafting the mixture of the Pd-G complex and G (ESI, Table S1).<sup>†</sup> The significant decrease in these textural parameters may point out a fact that the Pd-G complex and G were introduced into the interior of SBA-16, as expected. The XRD patterns of SBA-16 and Pd-G/SBA-16-G are displayed in the ESI, Fig. S1.<sup>†</sup> Like the parent material SBA-16, Pd-G/SBA-16-G also shows a strong diffraction peak at small angles, further confirming that the periodic mesoporous structure of SBA-16 remained roughly intact during the course of preparing the catalyst.

The composition of the catalyst Pd-G/SBA-16-G was determined by FT-IR and solid state NMR. The FT-IR spectra of SBA-16 and Pd-G/SBA-16-G are shown in Fig. 3. Compared with the FT-IR spectrum of the parent material SBA-16, the FT-IR spectrum of Pd-G/SBA-16-G clearly exhibited three new peaks at 2943, 1590 and 1410  $\text{cm}^{-1}$ , which correspond to the stretching vibrations of the C–H and C=N, and the bending vibration of C–H, respectively. Meanwhile, the intensity of the peak at 960  $\text{cm}^{-1}$  (related to the bending vibration of Si–OH on SBA-16) significantly decreases after grafting with Pd-G complex and G. This can be explained by a fact that the Si–OH groups on the SBA-16 surface were consumed due to the silylation. These results indicate that the Pd-G complex and G were successfully immobilized on SBA-16. Fig. 4 and Fig. 5 show the  $^{29}\text{Si}$  MAS NMR and  $^{13}\text{C}$  CP-MAS NMR spectra of Pd-G/SBA-16-G, respectively. In Fig. 4, the solid state NMR spectrum of Pd-G/SBA-16-G shows a “T<sup>3</sup>” band at *ca.* –63 ppm, indicating that the Pd-G complex and G were immobilized on SBA-16 through a condensation reaction of the surface silanols with silane derivatives. In Fig. 5, the carbon chemical shifts for the catalyst Pd-G/SBA-16-G are broadly in agreement with those values for G in solution (liquid state NMR, see Experimental).

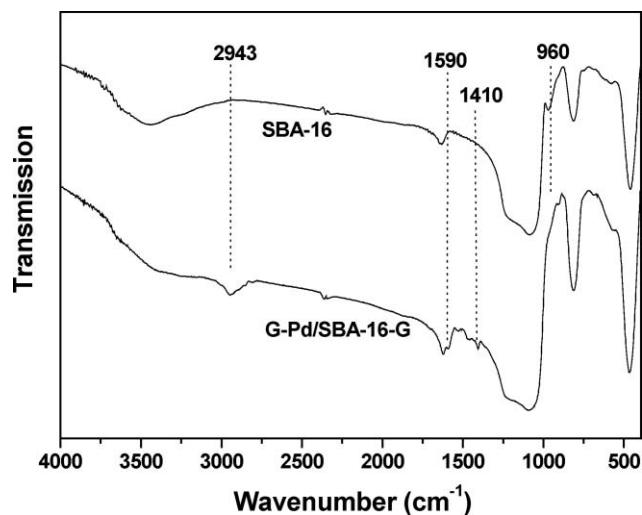


Fig. 3 FT-IR spectra of SBA-16 and G-Pd/SBA-16-G.

In order to get an insight into the coordination state of the Pd complex on the solid catalyst, UV-vis and X-ray photoelectron spectroscopy (XPS) experiments were performed. The UV-vis spectra for the Pd-G complex in solution and Pd-G/SBA-16-G are displayed in Fig. 6. In order to elucidate the coordination state of the complex in solution and on the solid surface, G in

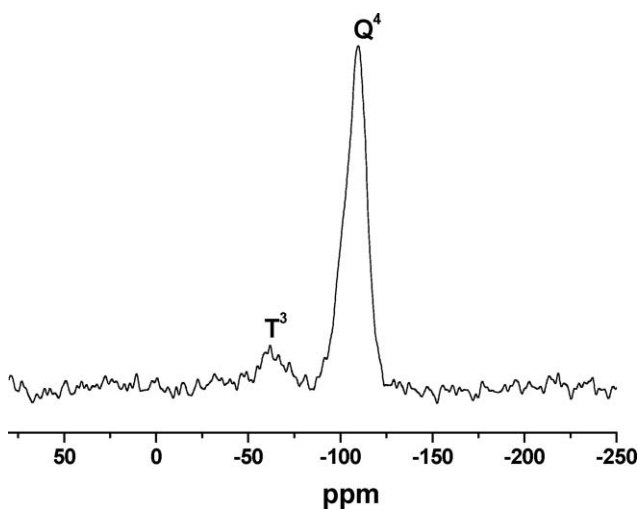


Fig. 4  $^{29}\text{Si}$  MAS NMR spectrum of G-Pd/SBA-16-G.

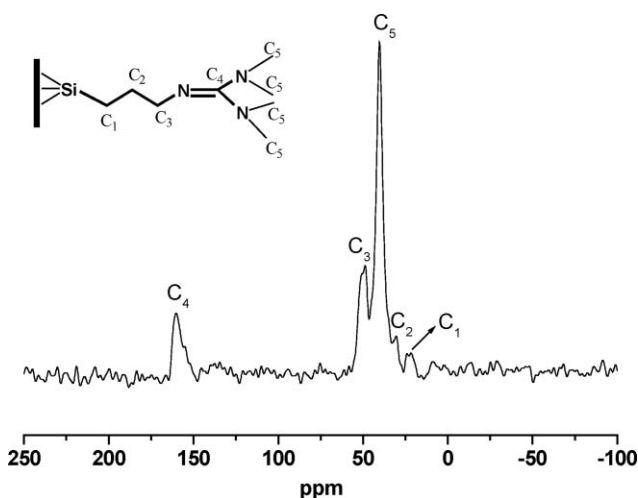


Fig. 5  $^{13}\text{C}$  CP-MAS NMR spectrum of G-Pd/SBA-16-G.

solution and SBA-16-G (G grafted on SAB-16) as references are also included in Fig. 6A and Fig. 6B, respectively. As shown in Fig. 6A, the Pd-G complex in dichloromethane exhibits two new absorption bands around 370 and 445 nm compared with G in dichloromethane. These two bands, attributable to the ligand to metal charge transfer transitions (LMCT), may be characteristics of the Pd-G complex. In Fig. 6B, Pd-G/SBA-16-G also shows two new absorption bands in comparison with the only G grafted on SBA-16 (SBA-16-G), indicating that there is a coordination interaction between PdCl<sub>2</sub> and G on the solid catalyst surface. A further comparison of the UV-vis spectra of Pd-G/SBA-16-G (Fig. 6B) and that of Pd-G complex in solution (Fig. 6A) shows that they have similar absorption bands in the range of 350–700 nm. The similar absorption bands may suggest that Pd exist on the solid catalyst surface in a coordinated fashion, which is similar to the Pd-G complex in solution.

Fig. 7 presents the XPS elemental survey scans of surface of the solid catalyst. The peaks corresponding to silicon, oxygen, carbon, nitrogen, palladium and chlorine are clearly observed. Fig. 8 displays the Pd binding energy of PdCl<sub>2</sub> and Pd-G/SBA-16-G. PdCl<sub>2</sub> exhibits two peaks centered at 342.6 and 337.3

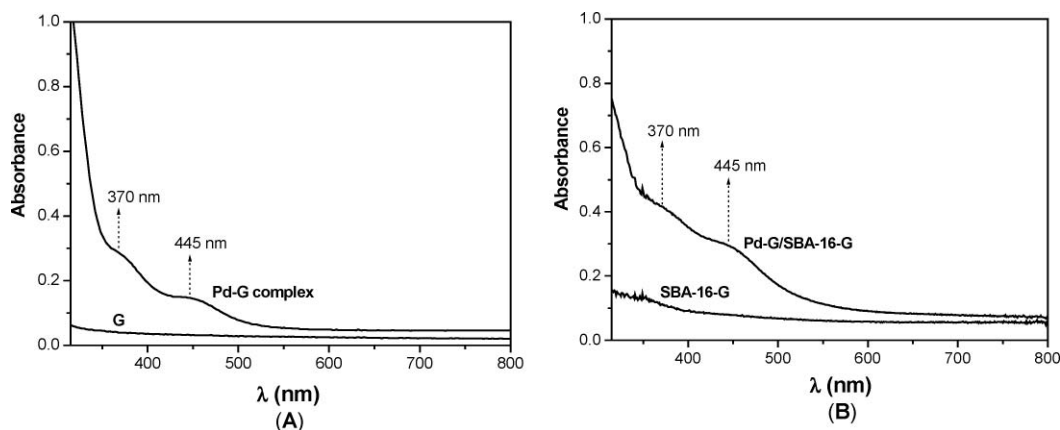


Fig. 6 UV-vis spectra. (A): Pd-G complex and G in dichloromethane; (B) Pd-G/SBA-16-G and SBA-16-G (diffuse reflectance).

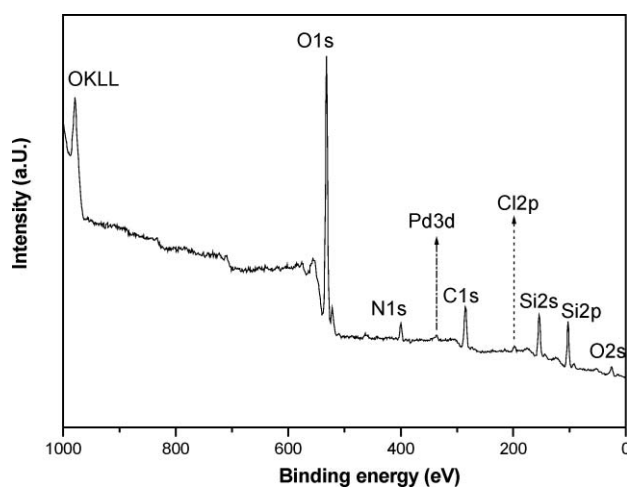


Fig. 7 XPS spectrum of the elemental survey scan of G-Pd/SBA-16-G.

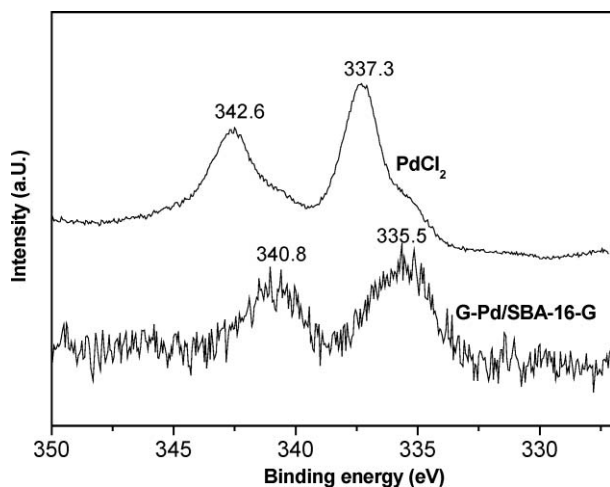


Fig. 8 XPS spectra of G-Pd/SBA-16-G and PdCl<sub>2</sub>.

eV, which are assigned to Pd 3d<sub>3/2</sub> and Pd 3d<sub>5/2</sub>, respectively. Compared with PdCl<sub>2</sub>, the Pd 3d<sub>3/2</sub> and Pd 3d<sub>5/2</sub> peaks for Pd-G/SBA-16-G significantly shift to 340.8 and 335.5 eV, respectively. The remarkable decrease in Pd binding energy implies that there is a strong coordination interaction between

Pd and G. These results are in agreement with the UV-vis observations.

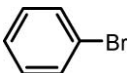
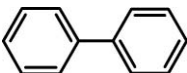
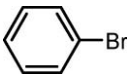
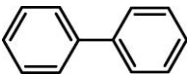
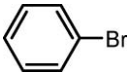
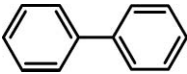
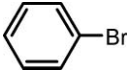
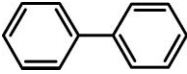
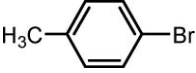
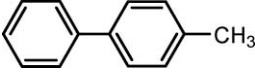
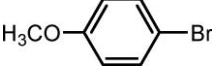
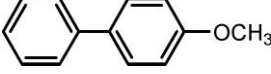
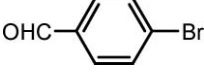
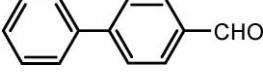
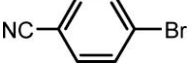
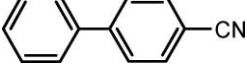
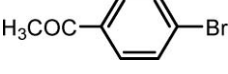

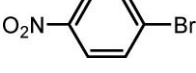
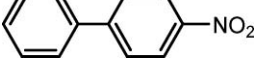
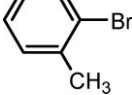
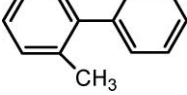
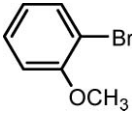
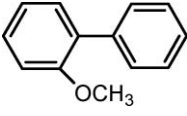
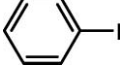
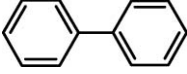
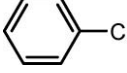
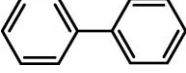
The above characterization experiments confirm that the Pd-G complex and G were successfully immobilized onto SBA-16 through a covalent linkage, the catalyst Pd-G/SBA-16-G still maintains its unique pore structure of the parent material SBA-16, and the Pd-G complex immobilized on the solid catalyst surface has a coordination state similar to the Pd-G complex in solution.

### The Suzuki reaction

The catalytic activity of Pd-G/SBA-16-G was first tested using Suzuki coupling. Previous studies have showed that solvents and base had remarkable influences on the reactivity of the Suzuki reaction.<sup>7,8</sup> We are interested in using water as a medium for the Suzuki coupling because using water as solvent represents a green, safe and cost-effective process. Our preliminary screening of solvent reveals that the presence of ethanol could efficiently promote the Suzuki reaction in water and 50% aqueous ethanol was the best choice for the reaction medium.<sup>4a,7,9</sup> After the reaction medium was chosen, we screened a range of representative bases. As shown in Table S2† lists the results of the Suzuki coupling of bromobenzene and phenylboronic acid in the presence of various bases. Among the bases investigated, K<sub>3</sub>PO<sub>4</sub> was found to be the best choice in view of the highest conversion.

With the optimized solvent and base in hand, we investigated the activity of Pd-G/SBA-16-G for various substrates. All the reactions were carried out at 50 °C in air using a 50% aqueous ethanol solution as a reaction medium. The corresponding results are summarized in Table 1. Using bromobenzene and phenylboronic acid as reactants, Pd-G/SBA-16-G at a loading of 0.1 mol% Pd (with respect to bromobenzene) afforded biphenyl in 95% yield within 20 min and a TOF *ca.* 2850 h<sup>-1</sup> (Table 1, entry 1). Encouraged by so high an activity of the developed catalyst, we decided to explore the potential of the catalyst Pd-G/SBA-16-G at a lower loading. When the catalyst loading was decreased to 0.01 mol%, within 35 min

**Table 1** Suzuki coupling of various bromides with phenylboronic acid in the presence of the catalyst Pd-G/SBA-16-G<sup>a</sup>

Entry	Substrate	Product	Pd/mol%	<i>t</i> /min	Yield <sup>b</sup> (%)	TOF <sup>c</sup> /h <sup>-1</sup>
1			0.1	20	95	2850
2			0.01	35	99	17 000
3			0.002	100	99	29 700
4			0.001	130	99	45 700
5			0.01	50	99	11 880
6			0.01	40	79	11 850
7			0.01	35	99	16 970
8			0.01	40	97	14 550
9			0.01	50	98	11 760
10			0.01	60	93	9300
11			0.01	90	94	6270
12			0.01	100	93	5580
13			0.01	35	88	15 085
14			0.1	180	8	—

<sup>a</sup> The reaction was carried out at 50 °C in air. <sup>b</sup> Isolated yield. <sup>c</sup> TOF is calculated according to the following equation:  $\text{TOF} = N_{\text{product}} / (N_{\text{palladium}} \times t)$ , where *N* denotes molar numbers, and *t* denotes reaction time (h).

Pd-G/SBA-16-G still gave biphenyl in 99% yield and TOF reached 17 000 h<sup>-1</sup> (Table 1, entry 2). The activity of the developed solid catalyst is nearly comparable to its homogeneous counterpart (Pd-tetramethylguanidine complex,

97% yield within 20 min). Further reducing the catalyst loading down to 0.002 mol%, 99% yield was achieved within 100 min and TOF was up to 29 700 h<sup>-1</sup> (Table 1, entry 3). When the catalyst loading was further decreased to 0.001 mol%, 99%

**Table 2** Suzuki coupling of arylboronic acids with bromobenzene in the presence of the catalyst Pd-G/SBA-16-G<sup>a</sup>

Entry	Substrate	Product	<i>t</i> /min	Yield <sup>b</sup> (%)	TOF <sup>c</sup> /h <sup>-1</sup>
1			35	95	16 280
2			35	84	14 400
3			120	79	3950
4			300	98	1960
5			75	99	7920
6			100	99	5940

<sup>a</sup> The reaction was carried out with 4 mmol of halide, 4.4 mmol of phenylboronic acid, 4.4 mmol of  $K_3PO_4 \cdot 3H_2O$ , 0.01 mol% Pd with respect to bromobenzene (5 mg), 4 mL of water and 4 mL of ethanol at 50 °C in air. <sup>b</sup> Isolated yield. <sup>c</sup> TOF is calculated according to the method used in Table 1.

yield could be still obtained within 130 min and TOF was 45 700 h<sup>-1</sup> (Table 1, entry 4). The activity of the developed catalyst is much higher than that of the *N*-heterocyclic carbene palladium complex grafted on SBA-16 (reported in our very recent study) under the same conditions.<sup>4a</sup> To the best of our knowledge, this finding represents one of the best cases for Suzuki coupling of bromobenzene using an immobilized catalyst under mild conditions.<sup>10</sup>

In order to verify the high activity of Pd-G/SBA-16-G, we examined its activity towards other substrates with variation of different substituents. These results are included in Table 1. At a catalyst loading of 0.01 mol%, Pd-G/SBA-16-G also afforded a satisfactory yield for bromides containing –CH<sub>3</sub> and –OCH<sub>3</sub> groups within 40–50 min (Table 1, entries 5 and 6). For other bromides with substituents such as –CHO, –CN, –COCH<sub>3</sub> and –NO<sub>2</sub> complete conversions were observed and 93–99% yields for the corresponding biaryl products were also achieved within one hour under mild reaction conditions (Table 1, entries 7–10). With regard to 2-substituted bromides, it took a slightly longer time to complete the reaction, probably due to steric hindrance, but TOFs still exceeded 5500 h<sup>-1</sup> (Table 1, entries 11 and 12). Additionally, Pd-G/SBA-16-G showed high activity towards iodobenzene but low activity towards chlorobenzene (Table 1, entries 13 and 14).

Pd-G/SBA-16-G also showed a high activity for the Suzuki couplings of other arylboronic acids with different substituents. The results are listed in Table 2. For *p*-methylphenylboronic acid and *p*-methoxyphenylboronic acid, satisfactory yields could be obtained within 35 min (Table 2, entries 1 and 2). For

arylphenylboronic acid with electron-withdrawing groups such as –Cl and –CF<sub>3</sub>, good yields were still afforded although a longer time was required to complete the reaction (Table 2, entries 3 and 4). When these substituents changed to the *o*-position, a longer time was needed to achieve excellent yields compared with *p*-substituted phenylboronic acids (Table 2, entries 5 and 6). The prolonged reaction time may reflect the steric hindrance effects.

The recyclability of Pd-G/SBA-16-G was investigated with consecutive Suzuki coupling reactions. Due to the unavoidable loss of solid catalyst during the course of recovery and washing, the reaction scale was amplified 5 times to ensure catalyst quality to perform the several consecutive recycling reactions, as described in the Experimental. The recycling results of the catalyst Pd-G/SBA-16-G are summarized in Table 3. The catalyst Pd-G/SBA-16-G gave complete conversion of bromobenzene, and 99% yield was still achieved within 35 min under the scale-up conditions. The determined palladium content in the product from the first reaction cycle was below 0.1 ppm. After the first reaction cycle, the catalyst could be recovered by simple centrifugation and filtration. After being washed and dried, the recovered catalyst was directly used for the next reaction cycle. For the second reaction cycle, biphenyl in 99% yield was still obtained within 40 min. From the second to sixth reaction cycle, 84–91% yield were achieved although a longer reaction time was needed to complete the reaction. For the seventh reaction cycle, 77% yield could be attained within 15 h. Although the activity of Pd-G/SBA-16-G was decreased during the consecutive recycling reactions, it still represents one of

**Table 3** Recyclability test of the catalyst Pd-G/SBA-16-G in the Suzuki reaction<sup>a</sup>

Cycle	1	2	3	4	5	6	7
<i>t</i>	35 min	40 min	100 min	3 h	5.5 h	12 h	15 h
Yield (%)	99	99	97	87	84	91	77

<sup>a</sup> The first reaction cycle was carried out with 40 mmol of halide, 44 mmol of phenylboronic acid, 44 mmol of  $K_3PO_4 \cdot 3H_2O$ , 0.05 mol% Pd with respect to bromobenzene (246 mg), 40 mL of water and 40 mL of ethanol at 50 °C in air. For the following reaction cycles, the recovered catalyst was weighed again and the fresh solvent and substrates was added, but the molar ratios of substrates and solvent to Pd remained the same to the first run.

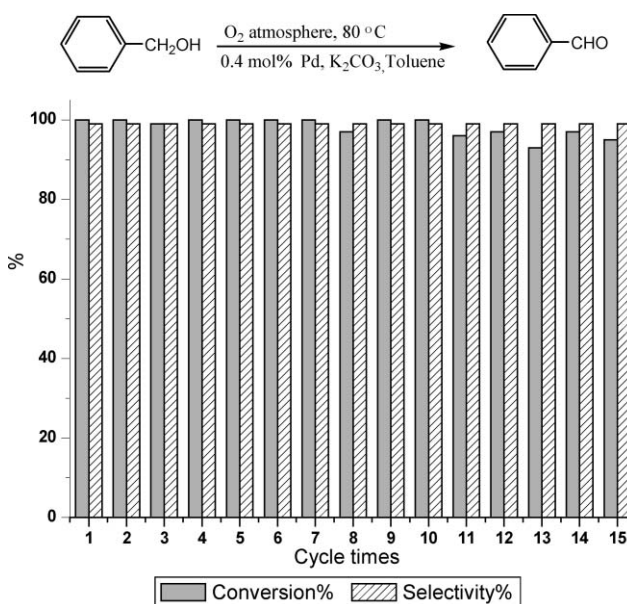
the most durable catalysts in view of the low catalyst loading (0.05 mol%) employed in the recycling test. The loss in activity is mainly due to the collapse of pore structure, which leads to the inability to limiting the growth of Pd nanoparticles into less active larger particles.

### The aerobic oxidation of alcohols

Selective oxidation of alcohols to carbonyl compounds is one of the most important transformations in the synthesis of fine chemicals. Currently, of particular interest in this field is the use of molecular oxygen as oxidant because it represents a green and facile chemical process in contrast to the use of toxic and expensive stoichiometric metal oxidants.<sup>11</sup> Encouraged by the obtained results in the Suzuki reaction, we attempted to examine the catalytic performances of Pd-G/SBA-16-G in the aerobic oxidation of alcohols.

Selected examples are listed in Table 4. The oxidation reactions were conducted in toluene under air or O<sub>2</sub> atmosphere using K<sub>2</sub>CO<sub>3</sub> as a base. The catalyst Pd-G/SBA-16-G shows moderate activity in the oxidation of benzyl alcohol in air. Within 8 h, 48.5% conversion for benzyl alcohol was obtained at 80 °C and the selectivity for benzaldehyde was more than 99% (Table 4, entry 1). When the reaction was carried out in an O<sub>2</sub> atmosphere, which was introduced by using an O<sub>2</sub> balloon under an atmospheric pressure, complete conversion of benzyl alcohol was achieved within 8 h (Table 4, entry 2). No by-products (*e.g.* carboxylic acid) were observed. When the reaction temperature was increased to 100 °C, the reaction proceeded faster, and nearly complete conversion of benzyl alcohol was observed within a shorter time (Table 4, entry 3). The catalyst Pd-G/SBA-16-G also showed good activity towards the oxidation of other benzyl alcohol containing substituents such as methyl, methoxy and nitro groups (Table 4, entries 4–6). Carboxylic acids were not detected for all these substrates investigated. Interestingly, the catalyst Pd-G/SBA-16-G is also active for the oxidation of less reactive  $\alpha$ ,  $\beta$ -unsaturated alcohols like cinnamyl alcohol. 93.9% conversion and more than 99% selectivity could be obtained at the catalyst loading of 1 mol% (Table 4, entry 7). For secondary and heterocyclic alcohols, the catalyst Pd-G/SBA-16-G also shows satisfactory activity (Table 4, entries 8 and 9).

Further experiments were performed to verify the catalyst recyclability. The results of the recycling tests of the oxidation of benzyl alcohol are displayed in Fig. 9. After the first reaction cycle, the catalyst Pd-G/SBA-16-G was recovered by a simple filtration, washed with toluene and acetone, and eventually dried

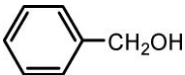
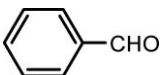
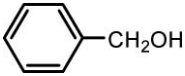
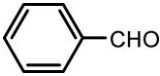
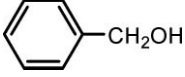
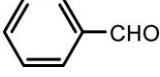
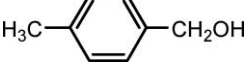

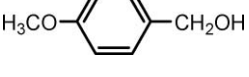
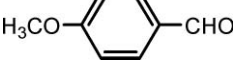
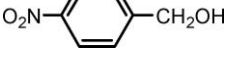
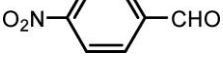
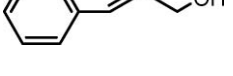
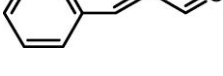
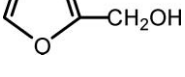
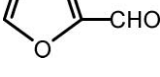
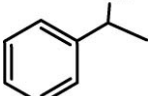
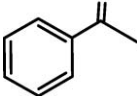


**Fig. 9** Recycling test of G-Pd/SBA-16-G. The reaction time for the first to eighth cycle was 8 h, and the reaction time for the ninth to fifteenth cycle was 11 to 14.5 h.

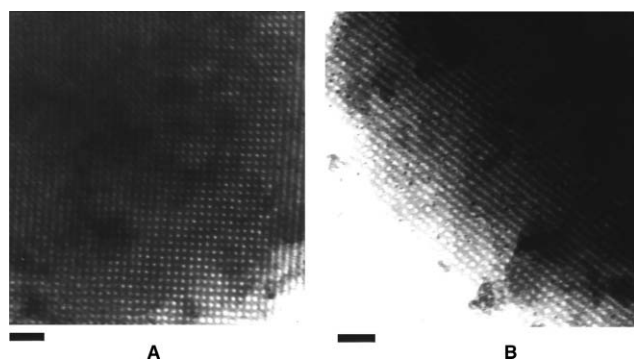
for the next cycle. For the second reaction cycle, Pd-G/SBA-16-G still furnished a complete conversion and over 99% selectivity within the same reaction time as the first reaction cycle (8 h). From the third to seventh reaction cycle, over 99% conversion was achieved without any prolonged time and 99% selectivity was maintained. For the eighth cycle reaction, although the activity of the reused catalyst began to decrease, 97% conversion was still obtained within 8 h. From the ninth to fourteenth reaction cycle, above 93% conversions were still afforded within a slightly prolonged time (11–13.5 h). For the fifteenth reaction cycle, 95% conversion was obtained within 14.5 h. The total TON (turnover numbers) for fifteen cycles was up to 3700. Interestingly, the selectivity for benzaldehyde was maintained over 99% throughout all the reaction cycles. These results are very encouraging in view of the previously reported results.<sup>4g,12</sup>

The impressive recyclability of the catalyst may be partially attributable to the unique pore structure of SBA-16. To confirm the role of the pore structure, TEM was employed to characterize the fresh catalyst Pd-G/SBA-16-G and the catalyst Pd-G/SBA-16-G that had been used twice. Their TEM images are shown in Fig. 10. For the fresh catalyst, Pd-G/SBA-16-G, the (100)

**Table 4** The aerobic oxidation of alcohols in the presence of the catalyst Pd-G/SBA-16-G<sup>a</sup>

Entry	Substrates	Product	Pd mol%	T/°C	t/h	Conv. (%)	Selectivity (%)
1 <sup>b</sup>			0.4	80	8	49	> 99
2 <sup>c</sup>			0.4	80	8	> 99	> 99
3 <sup>c</sup>			0.4	100	7	99	> 99
4 <sup>c</sup>			0.4	100	6	98	> 99
5 <sup>c</sup>			0.4	100	7	> 99	> 99
6 <sup>c</sup>			0.4	110	20	91	> 99
7 <sup>c</sup>			1	100	24	94	> 99
8			1	110	24	79	78
9			1	110	24	99	> 99

<sup>a</sup> The reactions were carried out with alcohol (2 mmol), K<sub>2</sub>CO<sub>3</sub> (2 mmol), the catalyst Pd-G/SBA-16-G and toluene (2 mL) under atmospheric pressure of O<sub>2</sub> or air. <sup>b</sup> In air. <sup>c</sup> In an O<sub>2</sub> atmosphere that was introduced by an O<sub>2</sub> balloon under atmospheric pressure.



**Fig. 10** TEM images for the fresh catalyst G-Pd/SBA-16-G (A) and the catalyst G-Pd/SBA-16-G used two times (B). The bar is 50 nm.

projection corresponding to a cubic *Im3m* structure was clearly observed (Fig. 10A). After the catalyst had been used twice, the cage-like structure of the catalyst was still observed and fine Pd particles appeared (Fig. 10B). Interestingly, the Pd particles with sizes of only a few nanometres were dispersed in the cages

of SBA-16. This observation is in agreement with the previous reports that Pd nanoparticle was formed once the catalytic reaction started.<sup>3g</sup> Due to the high surface area and surface energy, the unstable nanoparticles are prone to aggregation and agglomeration into larger particles. Owing to the spatial restriction of the isolated nanocages and smaller pore entrances of SBA-16, the growth of Pd nanoparticles is efficiently prevented, as shown in Scheme 1. The Pd nanoparticles stabilized by the nanocages of SBA-16 may account for the high recyclability.

## Conclusions

By grafting a mixture of a palladium-guanidine complex and guanidine on SBA-16 *via* a one-pot silylation, a new solid catalyst for the Suzuki coupling reaction and the aerobic oxidation of benzyl alcohols was successfully prepared. This catalyst can afford complete conversions of various aryl bromides and arylboronic acids in an aqueous ethanol solution at 50 °C even at catalyst loadings of 0.01–0.001 mol%, and the TOF for the Suzuki coupling of bromobenzene and phenylboronic acid is up



to 45 700 h<sup>-1</sup> under mild conditions in air. The developed solid catalyst combined with the mild conditions represents one of the most efficient heterogeneous systems for the Suzuki reaction of aryl bromides. Furthermore, it was found that the catalyst could work well for the aerobic oxidation of benzylic alcohols and cinnamyl alcohol under an atmospheric pressure of O<sub>2</sub>, affording over 99% of selectivity. This catalyst could be reused 15 times without a significant decrease in activity and selectivity.

## Experimental

### Reagents and materials

Pluronic P123 copolymer (EO<sub>20</sub>PO<sub>70</sub>EO<sub>20</sub>), Pluronic copolymer F127 (EO<sub>106</sub>PO<sub>70</sub>EO<sub>106</sub>) and PdCl<sub>2</sub> were purchased from Sigma Company. Various arylboronic acids were obtained from Beijing Pure Chemical Co. Ltd. (3-Chloropropyl)trimethoxysilane was purchased from Jiangnan Fine Chemical Company (China, distilled). 1,1,3,3-Tetramethylguanidine, aryl bromides and most of other reagents were obtained from Shanghai Chemical Reagent Company of Chinese Medicine Group.

Mesoporous cage-like material SBA-16 was synthesized according to a modified method.<sup>6</sup> A mixture of Pluronic F127 (EO<sub>106</sub>PO<sub>70</sub>EO<sub>106</sub>, 7.42 g) and Pluronic P123 (EO<sub>20</sub>PO<sub>70</sub>EO<sub>20</sub>, 1.19 g) were used as the templates. After the mixed templates were completely dissolved in a solution of 300 mL of distilled water and 52.5 g of concentrated hydrochloric acid (36%), the solution was further stirred at 308 K for 4 h. 28 mL of tetraethyl orthosilicate was added dropwise to the solution. After being stirred for 40 min, the resulting suspension was transferred into autoclaves. The autoclaves were placed under static conditions at 308 K for 24 h. Afterwards the temperature of the autoclaves was raised up to 373 K and kept at that temperature for 32 h. After the hydrothermal treatment, the precipitated solid was isolated by filtration and dried at 373 K for 24 h, yielding white solid powders. This powdered sample was then subjected to calcination at 825 K for 10 h and the mesoporous cage-like material SBA-16 was eventually obtained.

### Preparation of 1,1,3,3-tetramethyl-2-(3-trimethoxysilylpropyl)-guanidine (G)<sup>13</sup>

In a dry flask, 1,1,3,3-tetramethylguanidine (17.39 g, 0.151 mol) and xylene (1.8 mL) were mixed together. After being evacuated and purged with N<sub>2</sub> five times, the system was heated up to 120 °C and maintained at this temperature for 2 h, and then (3-chloropropyl)trimethoxysilane (14.93 g, 0.076 mol) was added dropwise over 2 h. After being stirred at 120 °C for 7 h under an N<sub>2</sub> atmosphere, the resulting mixture was allowed to cool down to room temperature. The formed salt precipitates 1,1,3,3-tetramethylguanidine·HCl was filtrated out. The filtrate liquid was distilled under reduced pressure and 1,1,3,3-tetramethyl-2-(3-trimethoxysilylpropyl)-guanidine was thus obtained (yield: ca.18%). 1,1,3,3-tetramethyl-2-(3-trimethoxysilylpropyl)-guanidine was denoted as G hereafter. <sup>1</sup>H NMR (CDCl<sub>3</sub>, 300 MHz, ppm): δ 0.63 (m, 2 H, SiCH<sub>3</sub>); 1.57 (m, 2 H, SiCH<sub>2</sub>CH<sub>2</sub>); 2.58–2.73 (m, 12 H, NCH<sub>3</sub>); 3.05 (m, 2 H, CH<sub>2</sub>N=C); 3.55 (s, 9 H, CH<sub>3</sub>O). <sup>13</sup>C NMR (CDCl<sub>3</sub>, 300 MHz, ppm): δ 6.55 (SiCH<sub>3</sub>); 24.78 (SiCH<sub>2</sub>CH<sub>2</sub>); 39.75 (NCH<sub>3</sub>); 50.5 (CH<sub>3</sub>O, CH<sub>2</sub>N=C); 160.65 (N=C(N(CH<sub>3</sub>))<sub>2</sub>).

### Preparation of a G solution containing Pd-G complex (Pd-G)

In a dried flask, PdCl<sub>2</sub> (0.032 g) was added to 1,1,3,3-tetramethyl-2-(3-trimethoxysilylpropyl)-guanidine (G, 0.5 g). The system was evacuated and purged four times with N<sub>2</sub>. The mixture was stirred at 55 °C for 12 h and was then cooled to room temperature, affording a red liquid, which was named as G solution containing the Pd-G complex.

### One-pot immobilization of Pd-G complex and G on SBA-16

The above G solution containing the Pd-G complex was diluted with 10 mL of dry toluene. Into this solution, 1.6 g of SBA-16 was added under a N<sub>2</sub> atmosphere and the mixture was stirred at 80 °C for 8 h. On cooling, the solid material was isolated by filtration, and repeatedly washed with toluene, dichloromethane and acetone in sequence, and then dried under vacuum overnight to give the yellowish solid catalyst Pd-G/SBA-16-G. The Pd content of Pd-G/SBA-16-G determined by ICP-AES is 0.86 wt%. The N and C contents of Pd-G/SBA-16-G determined by combustion chemical analysis are 3.58 wt% and 9.28 wt%, respectively.

### Typical procedures for the Suzuki reaction

A mixture of bromobenzene (8 mmol), phenylboronic acid (8.8 mmol), K<sub>3</sub>PO<sub>4</sub>·3H<sub>2</sub>O (8.8 mmol), ethanol (8 mL), H<sub>2</sub>O (8 mL), and Pd-G/SBA-16-G (9.86 mg) were stirred at 50 °C in air. The reaction process was monitored by TLC. After the reaction, the mixture was cooled down to room temperature and repeatedly extracted with diethyl ether (8 × 8 mL). The combined organic layers were concentrated and the resulting product was purified by column chromatography on silica gel. The product was confirmed by <sup>1</sup>H NMR.

Recyclability tests for the Suzuki reaction were as follows: for the first run, the mixture of 40 mmol of bromobenzene, 44 mmol of phenylboronic acid, 44 mmol of K<sub>3</sub>PO<sub>4</sub>·3H<sub>2</sub>O, 0.05 mol% Pd with respect to bromobenzene (246 mg), 40 mL of water and 40 mL ethanol were stirred at 50 °C. The reaction was monitored by TLC. At the end of the reaction the system was cooled down to room temperature and repeatedly extracted with diethyl ether. The obtained catalyst was washed with diethyl ether, water, methanol and acetone in sequence and dried under vacuum. The recovered catalyst was weighed again. Fresh solvent and substrates were added, but the molar ratios of substrates and solvent to Pd remained the same to the first run.

### Typical procedures for the oxidation of benzyl alcohol by O<sub>2</sub>

Benzyl alcohol (2 mmol), K<sub>2</sub>CO<sub>3</sub> (2 mmol), the catalyst Pd-G/SBA-16-G (0.4 mol% equiv. to benzyl alcohol, 98.6 mg) and toluene (2 mL) were combined in a dry flask, and the mixture was stirred at a given temperature in air or O<sub>2</sub> for a given time. Oxygen gas was introduced into the flask from an O<sub>2</sub> balloon under atmospheric pressure. After the reaction, the liquid obtained by filtration was diluted with toluene and then analyzed with GC to determine the conversion and selectivity.

Recyclability tests for the oxidation of benzyl alcohol were as follows: for the first cycle, the procedure was the same to the above description. After the first cycle reaction, the solid catalyst was recovered by centrifugation, and washed repeatedly with dry toluene and acetone. The recovered catalyst was dried

under vacuum and was directly used for the next cycle reaction. For each cycle reaction, 0.2 mmol of  $K_2CO_3$  (10% equiv. to the first reaction cycle) was supplied into the reaction system.

### Characterization and analysis

Small-angle powder X-ray powder diffraction was performed on a Rigaku diffractometer (Cu  $K\alpha$ , 40 kV, 30 mA).  $N_2$  physical adsorption was carried out on Micromeritics ASAP2020 volumetric adsorption analyzer (before the measurements, samples were out gassed at 393 K for 6 h). The Brunauer–Emmett–Teller (BET) surface area was evaluated from the data in the relative pressure range of 0.05 to 0.25. The total pore volume of each sample was estimated from the amount adsorbed at the highest  $P/P_0$  (above 0.99). Pore diameters were determined from the adsorption branch using the Barrett–Joyner–Halenda (BJH) method. FT-IR spectra were collected on Thermo-Nicolet-Nexus 470 infrared spectrometer. UV-vis spectra were recorded on the JASCOV-550 UV-vis spectrophotometer. Diffuse-reflectance UV-vis spectra were also recorded on the CARY300 spectrophotometer (Varian Co.). Pd content was analyzed by inductively coupled plasma-atomic emission spectrometry (ICP-AES, AtomScan16, TJA Co.). C and N content analysis was conducted on a vario EL (Elementar). X-Ray photoelectron spectroscopy (XPS) was recorded on Perkin-Elmer 5400 ESCA, and  $C_{1s}$  line at 284.9 eV was used as a reference. TEM micrographs were taken with a JEM-2000EX transmission electron microscope at 120 kV. Solid-state NMR spectra were recorded on an Infinityplus 300 MHz spectrometer: for  $^{13}C$  CP-MAS NMR experiments, 75.4 MHz resonant frequency, 4 kHz spin rate, 4 s pulse delay, 1.0 ms contact time, hexamethyl benzene as a reference compound; for  $^{29}Si$  MAS NMR experiments, 79.6 MHz resonant frequency, 4 kHz spin rate, 4.0 s pulse delay, TMS as a reference compound. GC analysis was conducted on SP-6800A equipped with SE-54 capillary column.

### The $^1H$ NMR data for the coupling products

Biphenyl ( $CDCl_3$ , 300 MHz, ppm):  $\delta$  7.57 (d, 4 H,  $J = 9$  Hz); 7.41–7.46 (m, 4 H); 7.34 (t, 2 H,  $J = 7.5$  Hz). 4-Biphenylcarbaldehyde ( $CDCl_3$ , 300 MHz, ppm):  $\delta$  10.07 (s, 1 H); 7.95 (d, 2 H,  $J = 7.8$  Hz); 7.75 (d, 2 H,  $J = 7.8$  Hz), 7.43–7.66 (m, 5 H). 4-Acetylbiphenyl ( $CDCl_3$ , 300 MHz, ppm):  $\delta$  8.06 (d, 2 H,  $J = 6$  Hz); 7.39–7.68 (m, 7 H); 2.67 (s, 3 H). 4-Cyanobiphenyl ( $CDCl_3$ , 300 MHz, ppm):  $\delta$  7.53–7.64 (m, 4 H); 7.50 (d, 2 H,  $J = 7.8$  Hz); 7.35–7.42 (m, 3 H). 4-Nitrobiphenyl ( $CDCl_3$ , 300 MHz, ppm):  $\delta$  8.29 (d, 2 H,  $J = 8.7$  Hz); 7.73 (d, 2 H,  $J = 8.7$  Hz); 7.45–7.62 (m, 5 H). 4-Methylbiphenyl ( $CDCl_3$ , 300 MHz, ppm):  $\delta$  7.52 (d, 2 H, 6 Hz); 7.43 (d, 2 H, 6 Hz); 7.37 (t, 2 H, 6 Hz); 7.27 (d, 1 H, 6 Hz); 7.21 (d, 2 H, 9 Hz); 2.34 (s, 3 H). 4-Methoxybiphenyl ( $CDCl_3$ , 300 MHz, ppm):  $\delta$  7.55–7.60 (m, 4 H); 7.45 (t, 2 H,  $J = 7.5$  Hz); 7.33 (m, 1 H); 7.00 (d, 2 H,  $J = 9$  Hz); 3.88 (s, 3 H). 2-Methoxybiphenyl ( $CDCl_3$ , 300 MHz, ppm):  $\delta$  7.48–7.51 (m, 2 H); 7.19–7.36 (m, 5 H); 6.86–6.98 (m, 2 H); 3.66 (s, 3 H). 2-Methoxybiphenyl ( $CDCl_3$ , 300 MHz, ppm):  $\delta$  7.09–7.24 (m, 9 H); 2.14 (s, 3 H). 4-Trifluoromethylbiphenyl ( $CDCl_3$ , 300 MHz, ppm):  $\delta$  7.67 (s, 4 H), 7.57–7.59 (d,  $J = 6.9$  Hz, 2 H), 7.38–7.48 (m, 3 H). 4-Chlorobiphenyl ( $CDCl_3$ , 300 MHz, ppm):  $\delta$  7.53–7.56 (m, 4 H), 7.35–7.50 (m, 5 H).

### Acknowledgements

We acknowledge the New Teacher Foundation from Education Ministry of China (200801081035) and Shanxi Natural Science Foundation for Youths (2009021009). We also thank Dr Lei Zhang (BASF, Nederland, BV, De Meern) for his good suggestions to this manuscript.

### References

- (a) N. Miyaura, T. Yanagi and A. Suzuki, *Synth. Commun.*, 1981, **11**, 513; (b) A. Biffis, M. Zecca and M. Basato, *J. Mol. Catal. A: Chem.*, 2001, **173**, 249; (c) L. Yin and J. Liebscher, *Chem. Rev.*, 2007, **107**, 133; (d) Gerd-Jan ten Brink, I. W. C. E. Arends and R. A. Sheldon, *Science*, 2000, **287**, 1636.
- (a) H. Doucet, *Eur. J. Org. Chem.*, 2008, 2013; (b) T. Fujihara, S. Yoshida, J. Terao and Y. Tsuji, *Org. Lett.*, 2009, **11**, 2121; (c) E. A. B. Kantchev, C. J. O'Brien and M. G. Organ, *Angew. Chem., Int. Ed.*, 2007, **46**, 2768; (d) S. S. Stahl, *Angew. Chem., Int. Ed.*, 2004, **43**, 3400; (e) S. Mannam, S. K. Alamsetti and G. Sekara, *Adv. Synth. Catal.*, 2007, **349**, 2253–2258; (f) K. P. Peterson and R. C. Larock, *J. Org. Chem.*, 1998, **63**, 3185; (g) M. Janssen, C. Muller and D. Vogt, *Adv. Synth. Catal.*, 2009, **351**, 313.
- (a) A. Corma, H. Garcia and A. Primo, *J. Catal.*, 2007, **251**, 39; (b) B. M. Choudary, S. Madhi and N. S. Chowdari, *J. Am. Chem. Soc.*, 2002, **124**, 14127; (c) G. Wei, W. Q. Zhang, F. Wen, Y. Wang and M. C. Zhang, *J. Phys. Chem. C*, 2008, **112**, 10827; (d) N. Jamwal, M. Gupta and S. Paul, *Green Chem.*, 2008, **10**, 999; (e) H. Q. Yang, L. Zhang, P. Wang, Q. H. Yang and C. Li, *Green Chem.*, 2009, **11**, 257; (f) N. Erathodiyil, S. Ooi, A. M. Seayad, Y. Han, S. S. Lee and J. Y. Ying, *Chem.–Eur. J.*, 2008, **14**, 3118; (g) B. Karimi, S. Abedi, J. H. Clark and V. Budarin, *Angew. Chem., Int. Ed.*, 2006, **45**, 4776; (h) T. Mallat and A. Baiker, *Chem. Rev.*, 2004, **104**, 3037; (i) H. L. Wu, Q. H. Zhang and Y. Wang, *Adv. Synth. Catal.*, 2005, **347**, 1356; (j) T. Matsumoto, M. Ueno, N. Wang and S. Kobayashi, *Chem.–Asian J.*, 2008, **3**, 196; (k) J. Shin, J. Bertoia, K. R. Czerwinski and C. Bae, *Green Chem.*, 2009, **11**, 1576, DOI: 10.1039/b913060h.
- (a) H. Q. Yang, X. J. Han, G. Li and Y. W. Wang, *Green Chem.*, 2009, **11**, 1184; (b) H. Q. Yang, G. Y. Zhang, X. L. Hong and Y. Y. Zhu, *J. Mol. Catal. A: Chem.*, 2004, **210**, 143; (c) C. M. Crudden, M. Sateesh and R. Lewis, *J. Am. Chem. Soc.*, 2005, **127**, 10045; (d) X. M. Ma, Y. X. Zhou, J. C. Zhang, A. L. Zhu, T. Jiang and B. X. Han, *Green Chem.*, 2008, **10**, 59.
- N. T. S. Phan, M. V. D. Sluys and C. W. Jones, *Adv. Synth. Catal.*, 2006, **348**, 609.
- (a) H. Skaff and T. Emrick, *Chem. Commun.*, 2003, 52; (b) T. W. Kim, R. Ryoo, M. Kruk, K. P. Gierszal, M. Jaroniec, S. Kamiya and O. Terasaki, *J. Phys. Chem. B*, 2004, **108**, 11480; (c) H. Q. Yang, J. Li, J. Yang, Z. M. Liu, Q. H. Yang and C. Li, *Chem. Commun.*, 2007, 1086.
- S. H. Li, Y. J. Lin, J. G. Cao and S. B. Hang, *J. Org. Chem.*, 2007, **72**, 4067.
- (a) L. F. Liu, Y. H. Zhang and B. W. Xin, *J. Org. Chem.*, 2006, **71**, 3994; (b) M. Trilla, Roser Pleixats, M. W. C. Man, C. Bied and J. J. E. Moreau, *Adv. Synth. Catal.*, 2008, **350**, 577; (c) J. Z. Zhang, W. Q. Zhang, Y. Wang and M. C. Zhang, *Adv. Synth. Catal.*, 2008, **350**, 2065.
- (a) H. Hagiwara, K. H. Ko, T. Hoshi and T. Suzuki, *Chem. Commun.*, 2007, 2838.
- (a) J. H. Kim, J. W. Kim, M. Shokouhimehr and Y. S. Lee, *J. Org. Chem.*, 2005, **70**, 6714; (b) B. W. Glasspoole, J. D. Webb and C. M. Crudden, *J. Catal.*, 2009, **265**, 148; (c) P. D. Stevens, J. Fan, H. M. R. Gardimalla, M. Yen and Y. Gao, *Org. Lett.*, 2005, **7**, 2085; (d) M. J. Gronnow, R. Luque, D. J. Macquarrie and J. H. Clark, *Green Chem.*, 2005, **7**, 552; (e) C. Ornelas, J. Ruiz, L. Salmon and D. Astruc, *Adv. Synth. Catal.*, 2008, **350**, 837; (f) H. Hattori, K. I. Fujita, T. Muraki and A. Sakaba, *Tetrahedron Lett.*, 2007, **48**, 6817.
- (a) Y. H. Ng, S. Ikeda, T. Harada, Y. Morita and M. Matsumura, *Chem. Commun.*, 2008, 3181; (b) Y. M. A. Yamada, T. Arakawa, H. Hocke and Y. Uozumi, *Angew. Chem., Int. Ed.*, 2007, **46**, 704; (c) D. D. Caspi, D. C. Ebner, J. T. Bagdanoff and B. M. Stoltz, *Adv. Synth. Catal.*, 2004, **346**, 185; (d) A. Abad, A. Corma and H. Garcia,

- Chem.–Eur. J.*, 2008, **14**, 212; (e) I. A. Ansari and R. Gree, *Org. Lett.*, 2002, **4**, 1507; (f) J. Chen, Q. H. Zhang, Y. Wang and H. L. Wan, *Adv. Synth. Catal.*, 2008, **350**, 453; (g) J. Yang, Y. J. Guan, T. Verhoeven, R. V. Santen, C. Li and E. J. M. Hensen, *Green Chem.*, 2009, **11**, 322; (h) A. Biffis and L. Minati, *J. Catal.*, 2005, **236**, 405; (i) B. A. Steinhoff, A. E. King and S. S. Stahl, *J. Org. Chem.*, 2006, **71**, 1861; (j) B. Karimi, A. Biglari, J. H. Clark and V. Budarin, *Angew. Chem., Int. Ed.*, 2007, **46**, 7210.
- 12 (a) B. Karimi, A. sghar Zamani, S. edigheh Abedi and J. H. Clark, *Green Chem.*, 2009, **11**, 109; (b) B. Karimi, A. Zamani and J. H. Clark, *Organometallics*, 2005, **24**, 4695; (c) Y. Uozumi and R. Nakao, *Angew. Chem., Int. Ed.*, 2003, **42**, 194; (d) A. Bleloch, B. F. G. Johnson, S. V. Ley, A. J. Price, D. S. Shephard and A. W. Thomas, *Chem. Commun.*, 1999, 1907.
- 13 A. C. Blanc, D. J. Macquarrie, S. Valle, G. Renard, C. R. Quinn and D. Brunel, *Green Chem.*, 2000, **2**, 283.

# CO<sub>2</sub>-controlled reactors: epoxidation in emulsions with droplet size from micron to nanometre scale†

Yueju Zhao, Jianling Zhang,\* Buxing Han,\* Suqin Hu and Wei Li

Received 14th October 2009, Accepted 21st November 2009

First published as an Advance Article on the web 13th January 2010

DOI: 10.1039/b921538g

The epoxidation of styrene in the cetyltrimethylammonium bromide (CTAB)/H<sub>2</sub>O/heptane/styrene/H<sub>2</sub>O<sub>2</sub> emulsion system was investigated in the presence of compressed CO<sub>2</sub>. It was found that by controlling the CO<sub>2</sub> pressure, the emulsion droplets can be changed in a wide range from micron to nanometre size; accordingly, the conversion was enhanced significantly with the reduced droplet size. At 5.27 MPa, the conversion in the emulsion (with droplet size of 39.5 nm) could be about 10 times higher than that in a surfactant-free system at the same pressure. The effects of other experimental conditions of CTAB concentration, reaction time, styrene concentration, amounts of H<sub>2</sub>O<sub>2</sub>, and alkalinity on the efficiency of the epoxidation were also studied, and a possible mechanism for the enhanced reaction efficiency with reduced droplet size was presented. This process has some unique advantages. For example, the reactant conversion can be easily tuned by controlling the pressure of CO<sub>2</sub>; CO<sub>2</sub> can be used as bicarbonate source and no additional catalyst was used; CO<sub>2</sub> can be easily removed by depressurization; the separation for the product is simple. It is believed that the CO<sub>2</sub>-tuned emulsions can be easily applied to many other chemical reactions.

## Introduction

Emulsions have ability to dissolve both polar and non-polar components in large quantities with the aid of surfactants. Generally, macroemulsions have large droplet sizes up to tens of microns. For chemical reactions at water/oil interfaces,<sup>1</sup> enlargement of the interfacial area or reduction of droplet size of emulsion is crucial for accelerating the reaction rate.<sup>2</sup> Nanoemulsions are a class of emulsions with droplet sizes on the nano-scale.<sup>3</sup> They have been widely applied in polymerizations.<sup>4</sup> However, the application of nanoemulsion in other chemical reactions is very limited. As far as we know, the only report was about the lipase-catalyzed reaction of racemic  $\alpha$ - and  $\beta$ -amino acid esters to the respective homochiral free acids in nanoemulsion.<sup>5</sup> Studying the effect of the emulsion droplet size on chemical reaction by controlling the size from the micron to nanometre scale continuously is very interesting, but it is challenging due to the lack of an efficient method for tuning the emulsion droplet size in such a wide range.

Epoxides and their derivatives are widely used as intermediates.<sup>6</sup> For the epoxidation reaction, H<sub>2</sub>O<sub>2</sub> is a commonly used oxidant with innocuous decomposition byproducts of water and oxygen. Generally, the reaction is promoted by catalysts. Homogeneous catalysts such as porphyrin,<sup>7</sup> salen,<sup>8</sup> BI-

NOL ((*R*)-(+)-1,1'-bi-2-naphthol) systems<sup>9</sup> and heterogeneous catalysts such as supported porphyrin<sup>10</sup> and salen systems<sup>11</sup> and silica-supported tantalum complexes<sup>12</sup> have been used to catalyze the reaction. The high cost of the catalysts and the difficulty of catalyst separation and recovery cause economic and environmental problems. Recently, an inexpensive and convenient method to activate H<sub>2</sub>O<sub>2</sub> using bicarbonate ion was reported.<sup>13,14</sup> In this bicarbonate-activated peroxide system, the active species peroxymonocarbonate ion, HCO<sub>4</sub><sup>-</sup>, is formed in the CO<sub>2</sub>-H<sub>2</sub>O<sub>2</sub>-H<sub>2</sub>O biphasic system in the presence of base (NaOH or Na<sub>2</sub>CO<sub>3</sub>).<sup>14</sup> This method is greener and simple because both H<sub>2</sub>O<sub>2</sub> and CO<sub>2</sub> are green agents. However, the conversion was very low (less than 10%) in the CO<sub>2</sub>-H<sub>2</sub>O<sub>2</sub>-H<sub>2</sub>O biphasic system, mainly due to the interphase mass-transfer limitation.<sup>14</sup> Exploring new routes for enhancing the conversion of epoxidation in CO<sub>2</sub>-H<sub>2</sub>O<sub>2</sub>-H<sub>2</sub>O system is highly desirable.

Recently, we found that CO<sub>2</sub> could tune the droplet size of AOT/isooctane/water emulsion from the micron to nanometre scale<sup>15</sup> because the gas can change the properties of the solvent<sup>16</sup> and insert into the tail region of the surfactant film. This unique method to tune the droplet size of emulsions continuously provides the possibility to study the effect of droplet size of emulsions on chemical reactions in a wide droplet size range. In this work, we conducted styrene epoxidation in a cetyltrimethylammonium bromide (CTAB)/H<sub>2</sub>O/*n*-heptane/styrene/H<sub>2</sub>O<sub>2</sub> emulsion system in the presence of CO<sub>2</sub>. CO<sub>2</sub> acts not only as a modulator for the emulsion droplet size, but also as bicarbonate source to catalyze the reaction. To the best of our knowledge, this is the first work to study the effect of droplet size of an emulsion on a reaction in a wide size range from microns to tens of nanometres.

Beijing National Laboratory for Molecular Sciences, CAS Key Laboratory of Colloid and Interface and Thermodynamics, Institute of Chemistry, Chinese Academy of Sciences, Beijing, China.

E-mail: zhangjl@iccas.ac.cn, hanbx@iccas.ac.cn;

Fax: (+) 86-10-62559373

† Electronic supplementary information (ESI) available: <sup>1</sup>H NMR spectra, SAXS data analysis and nanoemulsion formation with different styrene concentrations. See DOI: 10.1039/b921538g

## Experimental

### Materials

The surfactant cetyltrimethylammonium bromide (CTAB), styrene, hydrogen peroxide aqueous solution (30 wt.%), and KOH were provided by Beijing Chemical Reagent Company (A. R. grade). *n*-Heptane, benzaldehyde and phenylacetaldehyde were supplied by Beijing Chemical Plant were A. R. grade. Styrene oxide (98%) was produced by ACROS. CO<sub>2</sub> was provided by Beijing Analytical Instrument Factory with a purity of >99.99%. Deuteriochloroform (CDCl<sub>3</sub>) (D, 99.8%, contains 0.03% v/v TMS) was purchased from Beijing Tengdayuan Science and Technology Co., Ltd.

### Apparatus and procedures

The high pressure view cell for observing phase behavior of the H<sub>2</sub>O/CTAB/heptane/H<sub>2</sub>O<sub>2</sub>/styrene and nanoemulsion formation was similar to that used previously,<sup>17</sup> which had a volume of 40 mL. It was also used as the reactor for the styrene epoxidation reaction. A YKKY A2 digital temperature controller was used to control the temperature of the water bath. The pressure gauge used was composed of a pressure transducer (FOXBORO/ICT, Model 93) and an indicator, which was accurate to ± 0.025 MPa in the pressure range of 0–20 MPa. In the experiment, a suitable amount of water, *n*-heptane, styrene, H<sub>2</sub>O<sub>2</sub> aqueous solution, KOH, and CTAB (heptane : water (v/v) = 4 : 5, total volume of emulsion system is 6 mL) were added into the view cell after the air in the cell was replaced by CO<sub>2</sub>. The temperature of the system was controlled at 40.0 °C. After thermal equilibrium had been reached, CO<sub>2</sub> was charged into the view cell to the desired pressure and the stirrer was started. The CO<sub>2</sub> in the view cell was released after a suitable reaction time and the stirrer was stopped. The reaction mixture separated into two phases. The upper oil phase was collected. Then the mixture in the view cell was extracted with heptane (4 × 5 mL) and mixed with the oil phase. The sample was analyzed by GC (Agilent 4890D) with a flame ionization detector (FID). An external standard of known concentrations was used to calibrate the GC for quantification. The products were confirmed by gas chromatography/mass spectrometry (GC-MS) (QP 2010). The <sup>1</sup>H NMR spectra were also used to confirm the components of the oil phase, which were recorded on a Bruker Model Advance DMX 300 spectrometer in CDCl<sub>3</sub> as the solvent. Chemical shift values were reported in parts per million (ppm) relative to those for tetramethylsilane (TMS) used as an internal reference standard.

### SAXS experiments

SAXS experiments were carried out at Beamline 4B9A at the Beijing Synchrotron Radiation Facility (BSRF). The data were collected using a CCD detector (MAR) having a maximum resolution of 3450 × 3450 pixels. The wavelength used was 1.38 Å, and the distance of sample to detector was 1.873 m. The detailed description of the spectrometer was given elsewhere.<sup>18</sup> The 2-D SAXS images were azimuthally averaged to produce one-dimensional profiles of intensity, *I*, vs. wavevector, *q*, using the two-dimensional data reduction program FIT2D. The background from the empty high-pressure SAXS cell was also

collected and the scattering data were normalized and then subtracted from the corresponding data of empty cell. The high-pressure SAXS cell was the same as that used previously.<sup>19</sup> It was composed mainly of a stainless steel body and two diamond windows of 8 mm in diameter and 0.4 mm in thickness. The cell body was coiled with an electric heater and heat-insulate ribbon outside, which was electrically heated to ±0.1 K of the desired temperature by using a temperature controller with a platinum resistance temperature probe (Model XMT, produced by Beijing Chaoyang Automatic Instrument Factory). The X-ray path length of the cell was 1.5 mm and the internal volume of the cell was 2.7 cm<sup>3</sup>. The high-pressure pump that was used to charge CO<sub>2</sub> into the system was model DB-80. The accuracy of the pressure gauge, which composed of a transducer (FOXBORO/ICT) and an indicator, was ±0.025 MPa in the pressure range of 0–20 MPa. In a typical experiment, the air in the sample cell was replaced by CO<sub>2</sub>. The desired amount of emulsion system was added into the sample cell, and after the system had reached thermal equilibrium, CO<sub>2</sub> was pumped into the cell until the desired pressure was reached. The X-ray scattering data was recorded after enough equilibration time.

### SAXS data analysis

Irena is a tool suite for analysis of small-angle X-ray scattering (SAXS) data within the commercial Igor Pro application.<sup>20</sup> The pair-distance distribution function is an important tool in the suite. The resulting intensity *I*(*q*) at different scattering vectors *q* is expressed by eqn (1).

$$q = \frac{4\pi}{\lambda} \sin \theta \quad (1)$$

The Indirect Fourier Transformation method can be used to determine size, shape, and internal structure of colloidal particles with high accuracy in the size range of 1 to 100 nanometres.<sup>21</sup> This distance distribution function is expressed by eqn (2).

$$p(r) = \frac{r^2}{2\pi^2} \int_0^\infty q^2 I(q) \frac{\sin qr}{qr} dr \quad (2)$$

The radius of gyration *R<sub>g</sub>* is the normalized second moment of the distance distribution of the particle around the centre of its scattering length density distribution. Where *p*(*r*) is the pair-distance distribution function (PDDF). Globular particles display bell-shaped *p*(*r*) functions with a maximum at about *D<sub>max</sub>*/2.<sup>22</sup> The relation between *R<sub>g</sub>* and *p*(*r*) can be expressed by eqn (3).

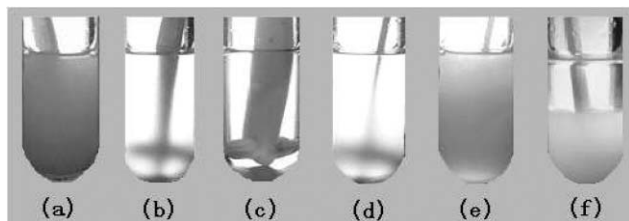
$$R_g = \int_0^{D_{\max}} r^2 p(r) dr \left[ 2 \int_0^{D_{\max}} p(r) dr \right]^{-1} \quad (3)$$

The forward scattering and the radius of gyration can be readily derived from the *p*(*r*) functions following eqn (2) and (3).

## Results and discussion

### Effect of CO<sub>2</sub> on the phase behavior of emulsion system

The effect of CO<sub>2</sub> on the phase behavior of H<sub>2</sub>O/CTAB/heptane/H<sub>2</sub>O<sub>2</sub>/styrene emulsion ( $V_{\text{heptane}}/V_{\text{water}} = 4:5$ ,  $V_{\text{total}} = 6$  mL, 0.055 M CTAB, 4.5 M H<sub>2</sub>O<sub>2</sub>, 1.5 M styrene, 0.3 M KOH) was first investigated using the high pressure view cell.<sup>15</sup> Fig. 1a–1e show the photographs of the emulsion at different CO<sub>2</sub> pressures. In the absence of CO<sub>2</sub>, the emulsion was turbid (Fig. 1a) with droplet size in the micron scale.<sup>23</sup> With the addition of CO<sub>2</sub>, the emulsion became more and more clear (e.g. Fig. 1b). When the pressure reached 5.27 MPa, the emulsion became transparent (Fig. 1c), indicating that the droplet size was in the nanoscale.<sup>15</sup> Given enough time, the transparent system separated into two phases. This indicates that the transparent system was a nanoemulsion instead of a microemulsion because microemulsions are thermodynamically stable. We define the pressure where the transparent nanoemulsion is formed as transparent pressure ( $P_T$ ). The solution was turbid again as pressure exceeded  $P_T$  (Fig. 1d and 1e), indicating that the droplet size of the emulsion became larger again at higher pressure. The above results show that the droplet size of the emulsion can be tuned effectively by CO<sub>2</sub> pressure.

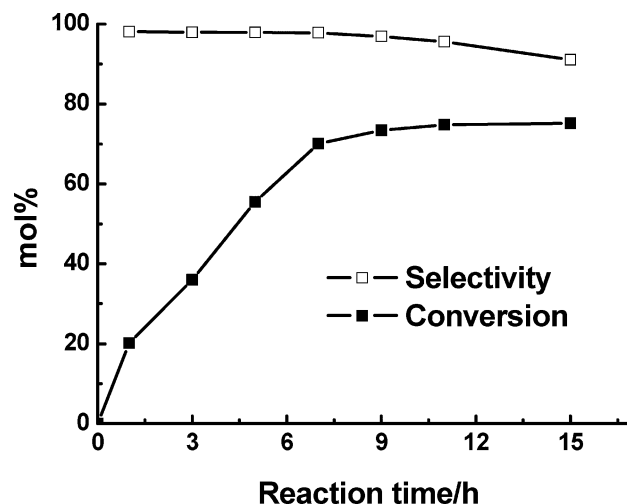


**Fig. 1** Photographs of H<sub>2</sub>O/CTAB/*n*-heptane/styrene/H<sub>2</sub>O<sub>2</sub> system at 40.0 °C ( $V_{\text{heptane}}/V_{\text{water}} = 4:5$ ,  $V_{\text{total}} = 6$  mL, 0.055 M CTAB, 4.5 M H<sub>2</sub>O<sub>2</sub>, 1.5 M styrene, 0.3 M KOH) with CO<sub>2</sub> pressure of 0 MPa (a), 2.50 MPa (b), 5.27 MPa (c), 5.51 MPa (d), 6.71 MPa (e); (f) represents photograph of emulsion c after releasing of CO<sub>2</sub> for 0.5 h.

After reaction and releasing CO<sub>2</sub>, the reaction system separated into two phases, an oil phase containing the product and aqueous phase containing the surfactant, as shown in Fig. 1f. GC-MS analysis indicated that the styrene oxide was the main product in the reaction, with small amounts of byproducts benzaldehyde and phenylacetaldehyde. A direct observation method was used to determine the solubility of CTAB in heptane. The results showed that the solubility was negligibly small (<0.01 wt%), which was further proven by <sup>1</sup>H NMR method (Fig. S1).<sup>†</sup> Therefore, the product could be collected by extraction using heptane as the solvent, and the surfactant and NaOH remained in the aqueous phase.

### Effect of reaction time on the reaction

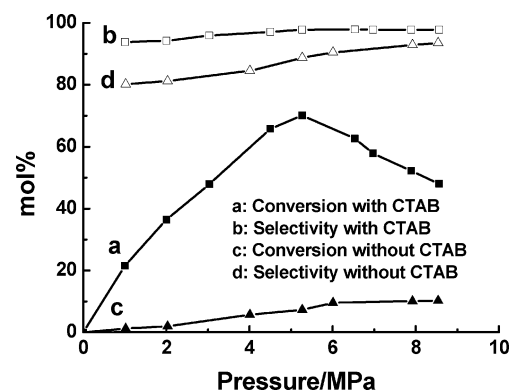
The styrene conversion and the product selectivity at 5.27 MPa with different reaction times are presented in Fig. 2. The styrene conversion increased with reaction time in the range of 0–7 h, and then was not changed considerably with reaction time. The selectivity of styrene oxide decreased slightly with the reaction time. The selectivity could be larger than 97% at conversion of 70.1%.



**Fig. 2** The styrene conversion and the product selectivity with the reaction time at 40.0 °C and 5.27 MPa. The other experimental conditions:  $V_{\text{heptane}}/V_{\text{water}} = 4:5$ ,  $V_{\text{total}} = 6$  mL, 0.055 M CTAB, 4.5 M H<sub>2</sub>O<sub>2</sub>, 1.5 M styrene, 0.3 M KOH.

### Effect of CO<sub>2</sub> pressure on the reaction

Fig. 3 shows the effect of CO<sub>2</sub> pressure on the reaction in the emulsion. Styrene oxide was not detectable without CO<sub>2</sub>. This is understandable because HCO<sub>4</sub><sup>-</sup>, which is necessary for the epoxidation of styrene, can not be formed in the absence of CO<sub>2</sub>.<sup>13,14</sup> It is interesting that with adding CO<sub>2</sub>, the conversion of styrene was gradually increased and reached a maximum of 70.1% at 5.27 MPa, which is the  $P_T$  where the droplet size of the emulsion was the smallest. Then the conversion decreased with further increasing pressure. In order to explain this phenomenon, we conducted the reaction in surfactant-free conditions at different CO<sub>2</sub> pressures, while the other experimental conditions were the same as those for the emulsion system. As shown in Fig. 3, the conversion of styrene increased monotonously with increasing CO<sub>2</sub> pressure. This is attributed to the fact that more CO<sub>2</sub> was dissolved in the system at higher pressure, resulting in more HCO<sub>4</sub><sup>-</sup>, which is favorable to the epoxidation reaction. At the same pressure, the conversion in the emulsion system was much higher than that at the surfactant-free condition, as can be known from Fig. 3. At 5.27 MPa, the



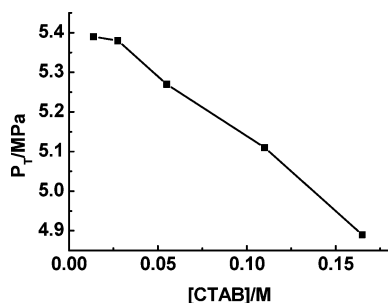
**Fig. 3** The styrene conversion and the product selectivity at different CO<sub>2</sub> pressures with CTAB (0.055 M) (a, b) and without CTAB (c, d) at 40.0 °C for 7 h. The experimental conditions:  $V_{\text{heptane}}/V_{\text{water}} = 4:5$ ,  $V_{\text{total}} = 6$  mL, 4.5 M H<sub>2</sub>O<sub>2</sub>, 1.5 M styrene, 0.3 M KOH.

conversion in the nanoemulsion could be about 10 times higher than that in surfactant-free system at the same pressure. This is mainly due to the enhanced mass transfer in the emulsion. On the basis of the results above, the occurrence of the maximum conversion is explained qualitatively as follows.

Changing of  $\text{CO}_2$  pressure affects the reaction mainly in two ways. First, more  $\text{HCO}_4^-$  is produced at higher pressure, which is favourable to the reaction. Second, the droplet size in the emulsion changes with  $\text{CO}_2$  pressure. The size decreases with increasing pressure below 5.27 MPa, and increases with pressure in the high pressure range, as discussed above. Smaller droplet sizes should be favorable to the reaction because of the enhanced mass transfer across the hydrophile/hydrophobe interface. At pressures below the  $P_T$ , the conversion increased dramatically with raising the pressure because both factors should enhance the conversion. However, when the pressure is higher than the  $P_T$ , the droplet size of the emulsion increased with pressure, which was not favorable to the reaction. Therefore, pressure of  $\text{CO}_2$  influenced the conversion in two opposite ways. The effect of the size change was dominant and the conversion decreased rapidly with pressure. This indicates that the droplet size of the emulsion plays a key role for the reaction. At low pressure the conversion was very low because the droplet size of the emulsion was large and the concentration of  $\text{HCO}_4^-$  was small.

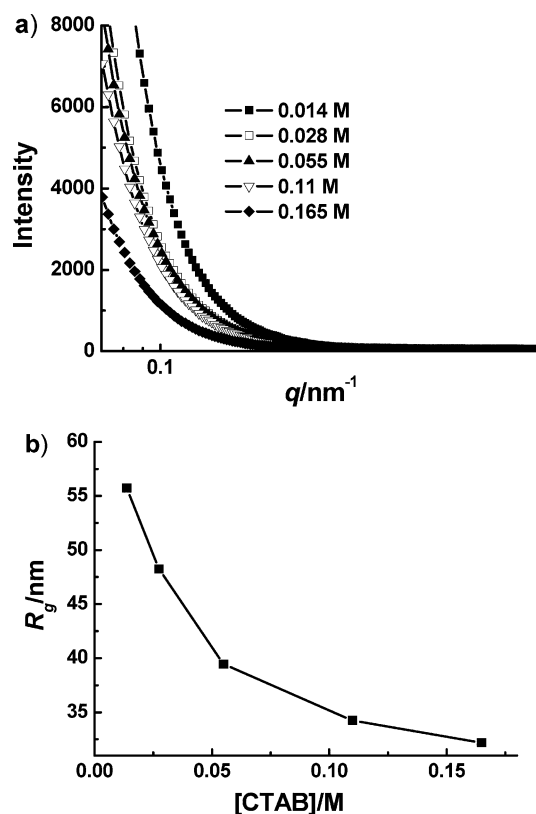
#### Effect of CTAB concentration on the reaction

Our experiments in this work showed that the nanoemulsion could also be formed at other surfactant concentrations (0.014 M, 0.028 M, 0.11 M, and 0.17 M). The  $P_T$ , at which nanoemulsions were formed, increased slightly with decreasing surfactant concentration, as shown in Fig. 4.



**Fig. 4** Dependence of  $P_T$  on CTAB concentration in the  $\text{H}_2\text{O}/\text{CTAB}/\text{heptane}/\text{H}_2\text{O}_2/\text{styrene}/\text{CO}_2$  system at 40.0 °C. The experimental conditions:  $V_{\text{heptane}}/V_{\text{water}} = 4:5$ ,  $V_{\text{total}} = 6$  mL, 4.5 M  $\text{H}_2\text{O}_2$ , 1.5 M styrene, 0.3 M KOH.

The droplet sizes of the nanoemulsions with different CTAB concentrations were studied by using small angle X-ray scattering (SAXS). Fig. 5a shows the typical SAXS curves of the  $\text{H}_2\text{O}/\text{CTAB}/\text{heptane}/\text{H}_2\text{O}_2/\text{styrene}/\text{CO}_2$  nanoemulsions ( $V_{\text{heptane}}/V_{\text{water}} = 4:5$ ,  $V_{\text{total}} = 6$  mL, 4.5 M  $\text{H}_2\text{O}_2$ , 1.5 M styrene, 0.3 M KOH) with different CTAB concentrations at corresponding  $P_T$  (Fig. 4). The decrease of the forward scattering intensity in the small-angle region upon increasing CTAB concentrations can be taken as evidence of the reduced droplet size. The gyration radius  $R_g$  of the droplets in nanoemulsions with different CTAB concentrations was obtained from SAXS curves. As shown in Fig. 5b, the  $R_g$  decreased from 55.7 nm



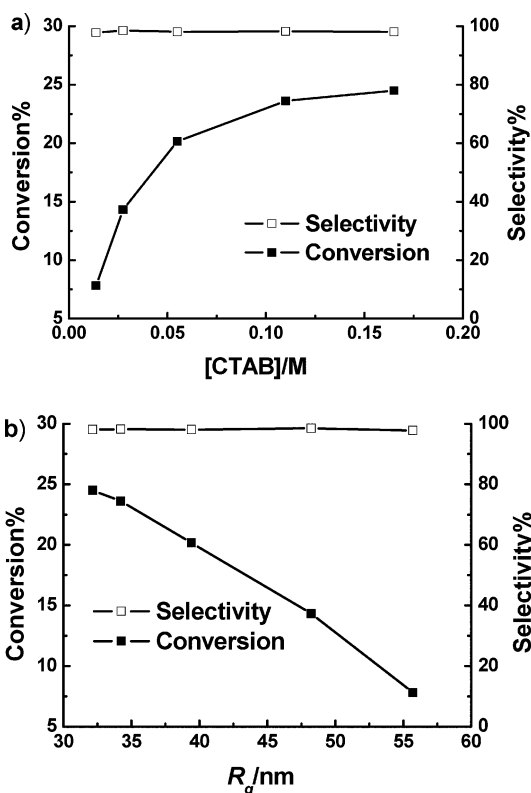
**Fig. 5** Dependence of experimental SAXS profiles (a) and the radius of gyration ( $R_g$ ) (b) on the CTAB concentration in the  $\text{H}_2\text{O}/\text{CTAB}/\text{heptane}/\text{H}_2\text{O}_2/\text{styrene}$  nanoemulsions ( $V_{\text{heptane}}/V_{\text{water}} = 4:5$ ,  $V_{\text{total}} = 6$  mL, 4.5 M  $\text{H}_2\text{O}_2$ , 1.5 M styrene, 0.3 M KOH) at 40.0 °C and corresponding  $P_T$  (Fig. 4).

to 32.2 nm with increasing surfactant concentration from 0.014 M to 0.17 M. The distance distribution function of the nanoemulsion with different CTAB concentrations was also calculated, which showed that globular droplets were formed (Fig. S2 and S3).†

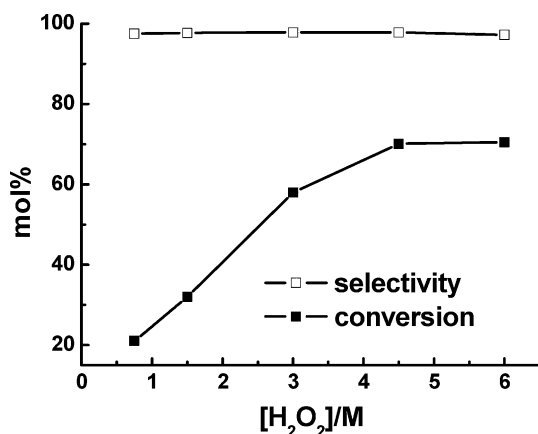
In order to study the effect of the droplet size of the nanoemulsions on the reaction efficiency, the reaction was also carried out in the nanoemulsions of different surfactant concentrations at the corresponding  $P_T$ . The reaction was conducted in a short reaction time (1 h), so that the effect of droplet size on the reaction rate could be clearly shown. As can be seen from Fig. 6a, the conversion increased with increasing CTAB concentration. From Fig. 5b and 6a, the dependence of styrene conversion on the droplet size of the nanoemulsion can be obtained, which is presented in Fig. 6b. Evidently, styrene conversion increased significantly as the droplet size was reduced. This indicates that the droplet size is crucial to the reaction efficiency even the droplet size is in the nano-size region.

#### Effects of other experimental conditions on the reaction

The conversion of styrene depended strongly upon amount of hydrogen peroxide, as can be seen from the data in Fig. 7. The conversion increased with increasing amount of  $\text{H}_2\text{O}_2$ , and when 4.5 M of  $\text{H}_2\text{O}_2$  was used, 70.1% styrene conversion was achieved. The selectivity of styrene oxide was nearly unaffected by the amount of  $\text{H}_2\text{O}_2$ .



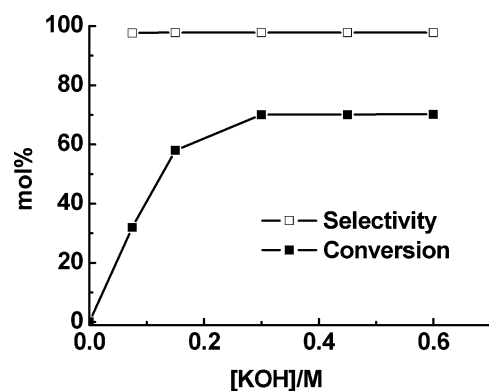
**Fig. 6** Dependence of conversion and selectivity on CTAB concentration (a) and on droplet size ( $R_g$ ) of the H<sub>2</sub>O/CTAB/heptane/H<sub>2</sub>O<sub>2</sub>/styrene nanoemulsions (b) at 40.0 °C for 1 h. The experimental conditions:  $V_{\text{heptane}}/V_{\text{water}} = 4:5$ ,  $V_{\text{total}} = 6$  mL, 4.5 M H<sub>2</sub>O<sub>2</sub>, 1.5 M styrene, 0.3 M KOH.



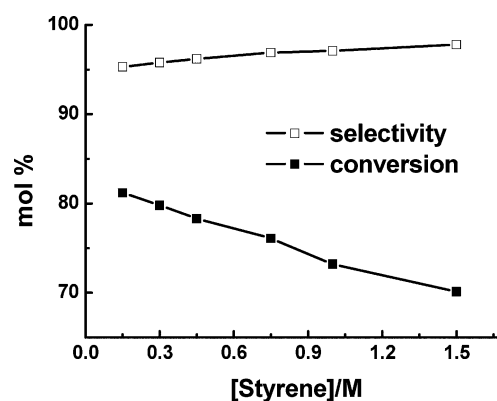
**Fig. 7** The styrene conversion and the product selectivity with amount of H<sub>2</sub>O<sub>2</sub> for 7 h at 40.0 °C and 5.27 MPa. Conditions:  $V_{\text{heptane}}/V_{\text{water}} = 4:5$ ,  $V_{\text{total}} = 6$  mL, 0.055 M CTAB, 1.5 M styrene, 0.3 M KOH.

The dependence of styrene conversion and selectivity of styrene oxide on the amount of KOH at 40.0 °C and 5.27 MPa was shown in Fig. 8. The conversion increased sharply with increasing amount of KOH, and a conversion of 70.1% could be reached at 0.3 M of KOH. Then the conversion remained nearly constant with further increasing amount of KOH.

In this work, it was also found that the nanoemulsion could be formed with different styrene concentrations (Fig. S4).<sup>†</sup> Fig. 9 shows the effect of styrene concentration on the reaction in



**Fig. 8** The styrene conversion and the product selectivity with amount of KOH at 40.0 °C and 5.27 MPa. Conditions:  $V_{\text{heptane}}/V_{\text{water}} = 4:5$ ,  $V_{\text{total}} = 6$  mL, 0.055 M CTAB, 4.5 M H<sub>2</sub>O<sub>2</sub>, 1.5 M styrene, reaction time 7 h.

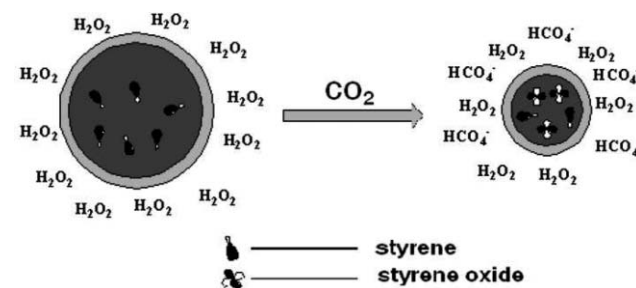


**Fig. 9** The styrene conversion and the product selectivity with different styrene concentrations at 40.0 °C for 7 h at the respective  $P_T$  values. The experimental conditions:  $V_{\text{heptane}}/V_{\text{water}} = 4:5$ ,  $V_{\text{total}} = 6$  mL, 4.5 M H<sub>2</sub>O<sub>2</sub>, 0.3 M KOH.

the H<sub>2</sub>O/CTAB/heptane/H<sub>2</sub>O<sub>2</sub>/styrene/CO<sub>2</sub> nanoemulsions. Evidently, the conversion of styrene increased with decreasing styrene concentrations.

#### Possible mechanism

On the basis of the above results, the main reasons for the very highly efficient epoxidation in the nanoemulsion can be discussed by combination of Scheme 1. In the absence of CO<sub>2</sub>, an oil-in-water (O/W) emulsion with large droplet size is formed (Scheme 1a). H<sub>2</sub>O<sub>2</sub> exists in the aqueous continuous phase, while the styrene resides in the hydrophobic inner core.



**Scheme 1** Schematic illustration for the epoxidation reaction of styrene without CO<sub>2</sub> (a) and in CO<sub>2</sub> induced nanoemulsion (b).



The epoxidation cannot be performed without CO<sub>2</sub> due to the absence of HCO<sub>4</sub><sup>-</sup>. With the addition of CO<sub>2</sub>, HCO<sub>4</sub><sup>-</sup> is produced and the catalytic reaction occurs through transporting the substrates and HCO<sub>4</sub><sup>-</sup> across the oil/water interface, as shown by Scheme 1b. Meanwhile, the droplet size is decreased with increasing pressure and interfacial area becomes larger, which are favorable to the reaction by enhancing the mass transfer. When the nanoemulsion is formed at P<sub>T</sub>, the catalytic reaction is significantly accelerated due to the smallest droplet size of the emulsion and the largest interfacial surface area. Therefore, the maximum conversion of styrene is achieved at this condition. With further increasing CO<sub>2</sub> pressure, the droplet size is increased again and hence the conversion of styrene is decreased.

## Conclusions

In conclusion, the epoxidation of styrene was conducted in a CO<sub>2</sub>-controlled emulsion system. By adding CO<sub>2</sub>, the droplet size of H<sub>2</sub>O/CTAB/heptane/H<sub>2</sub>O<sub>2</sub>/styrene emulsion was reduced from micron to nanometre scale and the styrene conversion was significantly enhanced with the decrease of the droplet size. At the pressure where the nanoemulsion with the smallest droplet size was formed, the conversion of styrene reached a maximum. Study of the effect of CTAB concentration on the reaction further confirmed that the conversion can be enhanced by the reduced droplet size of emulsions. From the practical point of view, this process is advantageous in that the reaction efficiency can be easily tuned by pressure of CO<sub>2</sub>, and CO<sub>2</sub> can be used as bicarbonate source and no additional catalyst is used, and the process is greener. We believe that the concept of tuning the efficiency of reactions in emulsions using CO<sub>2</sub> can also be used for some other reactions.

## Acknowledgements

The authors thank the National Natural Science Foundation of China (20633080, 20873164), Chinese Academy of Sciences (KJCX2.YWH16). The authors are also grateful to Prof. Z. H. Wu and Dr Z. H. Li from Beijing Synchrotron Radiation Facility (BSRF) for their help on the small angle X-ray scattering experiments.

## References

- 1 S. Jew, J. H. Lee, B. S. Jeong, M. S. Yoo, M. J. Kim, Y. J. Lee, J. Lee, S. H. Choi, K. Lee, M. S. Lah and H. Park, *Angew. Chem., Int. Ed.*, 2005, **44**, 1383–1385; K. Manabe, S. Iimura, X. M. Sun and S. Kobayashi, *J. Am. Chem. Soc.*, 2002, **124**, 11971–11978; C. J. Li and L. Chen, *Chem. Soc. Rev.*, 2006, **35**, 68–82; T. Dwars, E. Paetzold and G. Oehme, *Angew. Chem., Int. Ed.*, 2005, **44**, 7174–7199; M. Kunishima, H. Imada, K. Kikuchi, K. Hioki, J. Nishida and S. Tani, *Angew. Chem., Int. Ed.*, 2005, **44**, 7254–7257; H. Ohde, C. M. Wai, H. Kim, J. Kim and M. Ohde, *J. Am. Chem. Soc.*, 2002, **124**, 4540–4541;
- 2 G. B. Jacobson, C. T. Lee, K. P. Johnston and W. Tumas, *J. Am. Chem. Soc.*, 1999, **121**, 11902–11903.
- 3 J. Li, Y. M. Zhang, D. F. Han, G. Q. Jia, J. B. Gao, L. Zhong and C. Li, *Green Chem.*, 2008, **10**, 608–611; S. Z. Luo, X. L. Mi, S. Liu, H. Xu and J. P. Cheng, *Chem. Commun.*, 2006, 3687–3689.
- 4 J. M. Janjic, M. Srinivas, D. K. K. Kadayakkara and E. T. Ahrens, *J. Am. Chem. Soc.*, 2008, **130**, 2832–2841.
- 5 K. Landfester, *Angew. Chem., Int. Ed.*, 2009, **48**, 4488–4507; X. P. Ge, M. Z. Wang, Q. Yuan, H. Wang and X. W. Ge, *Chem. Commun.*, 2009, 2765–2767; G. D. Liang, J. T. Xu and X. S. Wang, *J. Am. Chem. Soc.*, 2009, **131**, 5378–5379.
- 6 H. Groger, O. May, H. Husken, S. Georgeon, K. Drauz and K. Landfester, *Angew. Chem., Int. Ed.*, 2006, **45**, 1645–1648.
- 7 *Kirk-Othmer Encyclopedia of Chemical Technology*, 4th edn, ed. J. Kroschwitz and M. Howe-Grant, John Wiley and Sons, New York, 1991, vol. 6, pp 730–753.
- 8 A. R. Han, Y. J. Jeong, Y. Kang, J. Y. Lee, M. S. Seo and W. Nam, *Chem. Commun.*, 2008, 1076–1078; N. Jin, M. Ibrahim, T. G. Spiro and J. T. Groves, *J. Am. Chem. Soc.*, 2007, **129**, 12416–12417.
- 9 S. J. Wezenberg and A. W. Kleij, *Angew. Chem., Int. Ed.*, 2008, **47**, 2354–2364; S. Jonsson, F. G. J. Odille, P. O. Norrby and K. Warnmark, *Chem. Commun.*, 2005, 549–551; R. I. Kureshy, N. U. H. Khan, S. H. R. Abdi, S. Singh, I. Ahmad, R. V. Jasra and A. P. Vyas, *J. Catal.*, 2004, **224**, 229–235.
- 10 S. Sahoo, P. Kumar, F. Lefebvre and S. B. Halligudi, *J. Catal.*, 2009, **262**, 111–118; M. Schlosser and F. Bailly, *J. Am. Chem. Soc.*, 2006, **128**, 16042–16043.
- 11 S. L. Jain, J. K. Joseph, F. E. Kuhn and O. Reiser, *Adv. Synth. Catal.*, 2009, **351**, 230–234.
- 12 (a) R. F. Bai, X. K. Fu, H. B. Bao and W. S. Ren, *Catal. Commun.*, 2008, **9**, 1588–1594; (b) S. Bhattacharjee and J. A. Anderson, *Adv. Synth. Catal.*, 2006, **348**, 151–158.
- 13 Q. Yang, S. Wang, J. Lu, G. Xiong, Z. Feng, Q. Xin and C. Li, *Appl. Catal., A*, 2000, **194–195**, 507–514.
- 14 D. E. Richardson, H. R. Yao, K. M. Frank and D. A. Bennett, *J. Am. Chem. Soc.*, 2000, **122**, 1729–1739; H. R. Yao and D. E. Richardson, *J. Am. Chem. Soc.*, 2000, **122**, 3220–3221; J. L. Song, Z. F. Zhang, T. Jiang, S. Q. Hu, W. J. Li, Y. Xie and B. X. Han, *J. Mol. Catal. A: Chem.*, 2008, **279**, 235–238.
- 15 S. A. Nolen, J. Lu, J. S. Brown, P. Pollet, B. C. Eason, K. N. Griffith, R. Glaser, D. Bush, D. R. Lamb, C. L. Liotta, C. A. Eckert, G. F. Thiele and K. A. Bartels, *Ind. Eng. Chem. Res.*, 2002, **41**, 316–323; D. Hancu, J. Green and E. J. Beckman, *Acc. Chem. Res.*, 2002, **35**, 757–764; D. Hancu, J. Green and E. J. Beckman, *Ind. Eng. Chem. Res.*, 2002, **41**, 4466–4474.
- 16 J. L. Zhang, B. X. Han, C. X. Zhang, W. Li and X. Y. Feng, *Angew. Chem., Int. Ed.*, 2008, **47**, 3012–3015.
- 17 P. G. Jessop and B. Subramaniam, *Chem. Rev.*, 2007, **107**, 2666–2694; M. Wei, G. T. Musie, D. H. Busch and B. Subramaniam, *J. Am. Chem. Soc.*, 2002, **124**, 2513–2517.
- 18 J. L. Zhang, B. X. Han, J. C. Liu, X. G. Zhang, Z. M. Liu and J. He, *Chem. Commun.*, 2001, 2724–2725; D. Shen, R. Zhang, B. X. Han, Y. Dong, W. Z. Wu and J. L. Zhang, *Chem.–Eur. J.*, 2004, **10**, 5123–5128.
- 19 B. Z. Dong, W. J. Sheng, H. L. Yang and Z. J. Zhang, *J. Appl. Crystallogr.*, 1997, **30**, 877–879.
- 20 D. Li, B. X. Han, Z. M. Liu and J. Liu, *Macromolecules*, 2001, **34**, 2195–2201.
- 21 J. Brunner-Popela, R. Mittelbach, R. Strey, K.-V. Schubert, E. W. Kaler and O. Glatter, *J. Chem. Phys.*, 1999, **110**, 10623–10632.
- 22 L. K. Shrestha, O. Glatter and K. Aramaki, *J. Phys. Chem. B*, 2009, **113**, 6290–6298; L. K. Shrestha, R. G. Shrestha, D. Varade and K. Aramaki, *Langmuir*, 2009, **25**, 4435–4442.
- 23 J. Ilavsky and P. R. Jemian, *J. Appl. Crystallogr.*, 2009, **42**, 347–353.
- 24 S. M. Zhang and J. D. Chen, *Polymer*, 2007, **48**, 3021–3025.

# Halogenation reactions in biodegradable solvent: Efficient bromination of substituted 1-aminoanthra-9,10-quinone in deep eutectic solvent (choline chloride : urea)<sup>†</sup>

Sunanda Balaso Phadtare and Ganapati Subray Shankarling\*

Received 10th November 2009, Accepted 7th December 2009

First published as an Advance Article on the web 26th January 2010

DOI: 10.1039/b923589b

A simple ammonium deep eutectic solvent was used as a dual catalyst and environmentally benign reaction medium for the bromination of 1-aminoanthra-9,10-quinone, eliminating the need for volatile organic solvents and concentrated acids like H<sub>2</sub>SO<sub>4</sub> as solvents or catalysts. This simple ammonium deep eutectic solvent, easily synthesized from choline chloride and urea, is relatively inexpensive and biodegradable, making it applicable for industrial applications. The deep eutectic solvent was easily separated and reused without loss of activity, and thus provides a good alternative for industrial bromination of 1-aminoanthra-9,10-quinone.

## Introduction

Halogenated 1-aminoanthra-9,10-quinones are important intermediates in the dyestuff industry.<sup>1</sup> The halogenation of 1-aminoanthra-9,10-quinone is difficult as anthra-9,10-quinone contains two carbonyl groups that deactivate the ring towards any electrophilic substitution. Several methods can be used to brominate 1-aminoanthra-9,10-quinone, such as bromination of 1-aminoanthra-9,10-quinone in 20% sulfuric acid at 70–80 °C<sup>2</sup> and bromination in 70–95% sulfuric acid at a high temperature to obtain 1-amino-2,4-dibromoanthra-9,10-quinone with or without a catalyst.<sup>3</sup> 1-Amino-2,4-dibromoanthra-9,10-quinone may also be obtained by brominating 1-aminoanthra-9,10-quinone in chloroform.<sup>4</sup> Bromination of 1-methylaminoanthraquinone may be carried out in pyridine solution by treatment with two moles of bromine.<sup>5</sup> These methods, however, all require drastic conditions involving strong acids, high temperature, and chlorinated solvents, all of which are environmentally toxic.

Ionic liquids are attracting increasing interest in the context of green chemistry. Ionic liquids are non-volatile, thermally stable, and their solvation properties can be varied by changing the cation and anion. There are limitations to the use of ionic liquids, however, such as high cost, environmental toxicity, and high purity requirement. Ionic liquids like (BMIM)PF<sub>6</sub> made from 95% pure 1-butyl-3-methylimidazolium chloride are even more expensive than pure acetone or toluene. Ionic liquids were initially introduced as alternative green reaction media because of their unique chemical and physical properties of non-volatility, non-flammability, thermal stability, and controlled miscibility.<sup>6–8</sup> Many ionic liquids, however, are dangerous envi-

ronmental contaminants, with toxicity similar to or even higher than that of organic solvents.<sup>7</sup> Further, high purity is required for ionic liquids, as even trace impurities affect the physical properties of ionic solvents.<sup>9</sup>

The development of alternative solvents from components that are inexpensive, non-toxic towards the environment, and are biodegradable or obtainable from biodegradable resources is therefore highly desirable to overcome these drawbacks.

Stavber *et al.*<sup>10</sup> reviewed halogenations of organic compounds in ionic liquids. Regioselective aromatic ring bromination of aromatics and heteroaromatics has been performed using *N*-bromosuccinimide as the brominating agent and tetrabutylammonium bromide as a phase transfer catalyst in ionic liquid such as (BMIM)PF<sub>6</sub>.<sup>11</sup>  $\alpha$ -Halogenation of  $\beta$ -dicarbonyl compounds and cyclic ketones is also possible using *N*-halosuccinimides in [BMIM]PF<sub>6</sub>.<sup>12</sup> An ionic liquid such as [BMIM][Br<sub>3</sub>] with a tribromide anion functions as both a reagent and solvent. This tribromide-based ionic liquid has been used for the nuclear bromination of activated aromatics.<sup>13</sup> These methods are also limited, however, by their toxicity, and the presence of impurities decreases the activity of the ionic liquids.

We synthesized a deep eutectic solvent composed wholly of biomaterials referred to as “Bio-ILs” or “Deep Eutectic Mixture”. Abbott *et al.*<sup>14</sup> published a series of studies on the low melting point of deep eutectic liquid systems based on choline chloride ([Ch] [Cl]). These studies suggest that choline cations can substitute for synthetic cations. Choline is a naturally occurring biocompatible compound that is not hazardous if it is released back to nature as choline or its deep eutectic mixture.<sup>15</sup> Urea is a compound present in all animals. Because choline chloride and urea are both inexpensive, processes that use this deep eutectic solvent are economically viable.

These deep eutectic mixtures have been used as solvents in biologic transformation such as hydrolase catalyzed biotransformation<sup>16</sup> and extraction of glycerol from biodiesel into a eutectic-based solvent.<sup>17</sup> Deep eutectic solvents are used as electrolytes for dye-sensitized solar cells.<sup>18</sup> The ability of deep

Department of Dyestuff Technology, Institute of Chemical Technology, N. P. Marg, Matunga, Mumbai, 400 019, India.  
E-mail: gss@udct.org, gsshankarling@gmail.com; Fax: +91-22-2414 5614; Tel: +91-22-2414 5616

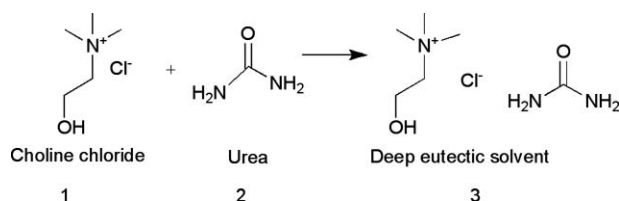
<sup>†</sup> Electronic supplementary information (ESI) available: Characterisation of products. See DOI: 10.1039/b923589b

eutectic mixtures to serve as solvents, however, has not been adequately explored in the field of synthetic organic chemistry field. Deep eutectic mixtures of urea and a range of quaternary ammonium salts are liquid at ambient temperatures and have interesting solvent properties. These mixtures were initially used for biologic conversion because of their biodegradable properties.<sup>17</sup> Deep eutectic solvents composed solely of biomaterials, in particular choline cations combined with propionate, hydrogen succinate, and hydrogen maleate, are ionic liquids with strong hydrogen bonding characteristics at room temperature.<sup>19</sup>

Here, we evaluated the effectiveness of a mixture of choline chloride and urea (1 : 2) as an environmentally benign solvent for use in the electrophilic substitution of 1-aminoanthra-9,10-quinone. The ability to recover and recycle the solvent used in a reaction is an important aspect to green chemistry.<sup>20</sup> Therefore, in the present study, we also evaluated the recyclability and reusability of this deep eutectic solvent.

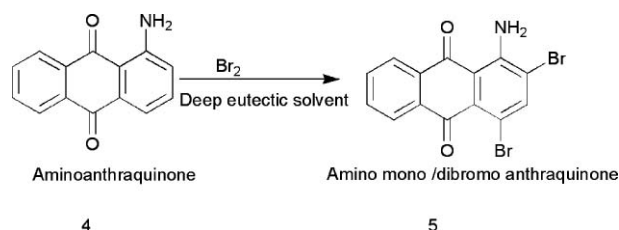
## Results and discussion

A deep eutectic solvent was prepared by a previously reported simple method<sup>14a</sup> with 100% atom economy (Scheme 1). Choline chloride (1 mole) was reacted with urea (2 moles) at 80 °C. The resulting molten salt was used directly in reactions without purification. This method produced no byproducts; therefore there was no loss during isolation of the solvent.



**Scheme 1** Preparation of deep eutectic solvent.

Bromination of an 1-aminoanthra-9,10-quinone derivative was performed at 50–60 °C using molecular bromine (Scheme 2 and Table 1). Monobrominated products **5e**, **5f**, and **5g** were obtained using 1.5 molar equivalents of bromine. Dibrominated products **5a**, **5b**, and **5d** were obtained by using 2.5 molar equivalents of bromine. Tetrabrominated product **5c** was obtained by using 4.5 molar equivalents. During the reaction, unreacted bromine was neutralized with 2 N aqueous Na<sub>2</sub>CO<sub>3</sub> solution. Deep eutectic solvents are miscible with many other solvents such as water, methanol, chloroform, and tetrahydrofuran. The solvent was separated from the product by adding water to the reaction mixture and filtering the product. The deep eutectic solvent was separated from the reaction mixture by phase



**Scheme 2** Bromination of 1-aminoanthra-9,10-quinone using Choline chloride : urea (ChCl : urea).

separation between the product and the aqueous phase. The solvent was recovered easily from the filtrate by evaporating the water under vacuum. This method used no hazardous chemicals, *e.g.*, acetic acid, sulfuric acid, or chloroform.

To compare the results obtained using the deep eutectic solvent and an organic solvent, bromination of 1-aminoanthra-9,10-quinone was performed using two different solvents (Table 2). Compared to the reaction using the organic solvent, the reaction using the deep eutectic solvent was much faster, requiring only 2 to 3 h for completion. Both yield and purity of the brominated product were greater in the reaction using the deep eutectic solvent than the organic solvents such as methanol and chloroform. Results are summarized in Table 2.

All products were confirmed by melting point assay, FTIR spectroscopy, <sup>1</sup>H NMR spectroscopy, and mass spectrometry. The purity of the product was checked by HPLC.

The reaction was effectively scaled-up to 5 g based on a representative reaction of bromination of 1-aminoanthra-9,10-quinone. Therefore, it is easy to scale-up the reaction on an industrial scale.

The deep eutectic solvent was recycled based on the representative reaction of bromination of 1-aminoanthra-9,10-quinone. We recycled the deep eutectic solvent five times without purification. The reactions using recycled deep eutectic solvent continued to produce excellent results without and a decrease in the yield or purity as shown in the Table 3.

## Experimental

### Materials and equipment

All melting points are uncorrected and are presented in degrees Celsius. FT-IR spectra were recorded on a Bomem Hartmann and Braun MB-Series FT-IR spectrometer. <sup>1</sup>H NMR spectra were recorded on Varian 400 MHz mercury plus spectrometer, and chemical shifts are expressed in δ ppm using TMS as an internal standard. Mass spectral data were obtained with a micromass - Q - TOF (YA105) spectrometer. Common reagent grade chemicals were procured from SD Fine Chemical Ltd. (Mumbai, India) and were used without further purification.

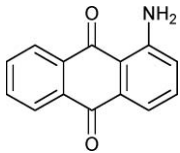
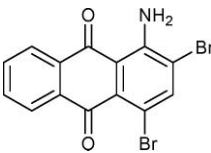
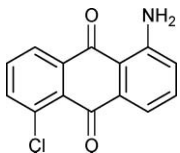
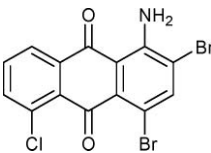
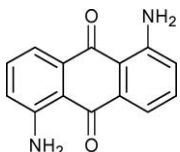
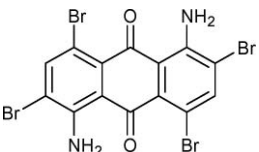
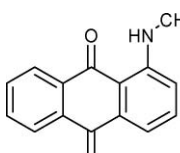
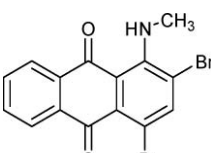
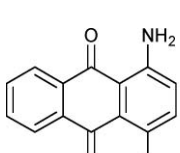
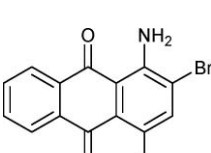
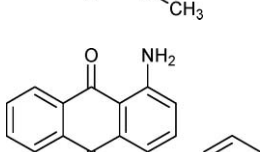
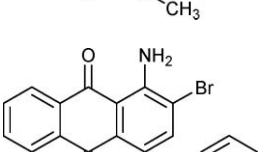
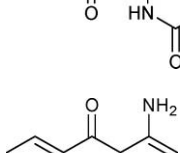
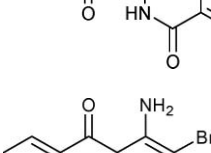
### Preparation of deep eutectic solvent (choline chloride : urea) 3.<sup>10a</sup>

Choline chloride (100 g, 71 mmol) and urea (86 g, 140 mmol) were placed in a round bottom flask and heated to 70 to 80 °C, until liquid began to form. After 15 to 20 min, a homogenous colorless liquid (186 g, 100%) formed, which was used directly for the reactions without purification.

### Bromination of 1-aminoanthra-9,10-quinone using an organic solvent.

1-Aminoanthra-9,10-quinone (1 g, 4.48 mmol) was added to the solvent (dichloromethane or methanol; 7 ml). Bromine (0.6 ml; 11.2 mmol) was slowly added to the reaction mixture. The reaction mixture was stirred at 50–60 °C for 12 h. The reaction was monitored by TLC. After completion of the reaction, water was added, and the mixture filtered and dried in an oven to isolate the product.

**Table 1** Bromination of 1-aminoanthra-9,10-quinone derivative using deep eutectic solvent (ChCl : Urea)

Entry	Amino-anthra-9,10-quinone derivative	Brominated Product	Yield (%) <sup>a</sup>	HPLC Purity (%)	Melting Point
5a			95	97.01	222 °C <sup>21</sup>
5b			87	99.8	249 °C
5c			94	97.8	Decomposes >250 °C
5d			88	99.3	154 °C
5e			84	99.6	176 °C
5f			91	98.8	247 °C
5g			92	98.9	198 °C

<sup>a</sup> Isolated by filtration. †In Reaction **5a**, **5b** and **5d**, 2.5 equivalent bromine was used. In reaction **5e**, **5f**, **5g** and **7**, 1.2 equivalent bromine while in reaction **5c**, 4.5 equivalent of bromine was used. ‡Reaction time is same for all the reactions *i.e.* 2-3 h. <sup>b</sup> In Reaction **5a**, **5b** and **5d**, 2.5 equivalent bromine was used. In reaction **5e**, **5f**, **5g** and **7**, 1.2 equivalent bromine while in reaction **5c**, 4.5 equivalent of bromine was used. <sup>c</sup> Reaction time is same for all the reactions *i.e.* 2-3 h.

**Table 2** Bromination of 1-aminoanthra-9,10-quinone derivative using organic solvents using 2.5 equivalent of bromine at 20-30 °C

Entry	Solvent	Reaction time (hr.)	Yield (%) <sup>a</sup>	HPLC Purity (%)
1	Methanol	10-12	75	95
2	Chloroform	10-12	70	92
3	Deep eutectic solvent	2-3	95	97

<sup>a</sup> Isolated by filtration.

**Table 3** Recycling of deep eutectic solvent in bromination of 1-aminoanthra-9,10-quinone at room temperature

Recycle of IL	Yield (%) <sup>a</sup>
Fresh, Non- Recycled	84.3%
First	97.5%
Second	92.7%
Third	93.4%
Forth	94.1%
Fifth	82.0%

<sup>a</sup> Isolated by filtration.

#### Typical procedure for the bromination of 1-aminoanthra-9,10-quinone (5a, 5b, 5c, 5d, 5e, 5f, 5g).

1-Aminoanthra-9,10-quinone (1 g, 4.48 mmol) was added to the deep eutectic solvent (5 ml) with stirring for 15 min, and bromine (0.6 ml, 11.2 mmol) was slowly added to the reaction mixture. In the case of **5c**, a 4.5-molar equivalent of Br<sub>2</sub> was used and in the cases of **5e**, **5f**, **5g**, 1.1 molar equivalents of Br<sub>2</sub> were used. The reaction mixture was stirred at 50–60 °C for 2 to 3 h. During the reaction, unreacted bromine that was expelled was neutralized in a trap containing aqueous Na<sub>2</sub>CO<sub>3</sub> solution. The reaction was monitored by TLC. After completion of the reaction, water was added, the mixture filtered, and residual product dried in an oven under vacuum.

**1-Amino-2,4-dibromoanthracene-9,10-dione 5a.** (1.6 g, 93.2%) An orange colored solid. Melting point (measured) 222 °C (from water) (lit, 221 °C<sup>17</sup>); λ<sub>max</sub> (methanol)/nm 381; ν<sub>max</sub>/cm<sup>-1</sup> 3396(NH), 1670 and 1577 (CO), and 715 (CBr); δ<sub>H</sub> (400 MHz; DMSO; Me<sub>4</sub> Si) 3.4 (2H, s, NH), 7.6-8.4(5H, m, aromatic); *m/z* (EI) 380 (M-1) for <sup>80</sup>Br. C<sub>14</sub>H<sub>7</sub>Br<sub>2</sub>NO<sub>2</sub> calculated *m/z*: 380.9

**1-Amino-2,4-dibromo-5-chloroanthracene-9,10-dione 5b.** Orange colored solid. Melting point (measured) 249 °C from water; λ<sub>max</sub> (methanol)/nm 415; ν<sub>max</sub>/cm<sup>-1</sup> 3452 and 3307 (NH), 167 and 1635 (CO) and 759 (CBr); δ<sub>H</sub> (400 MHz; DMSO; Me<sub>4</sub> Si) 3.4 (1H, s, NH), 7.6-8.4(5H, m, aromatic); *m/z* (EI) 414 (M-1) for <sup>80</sup>Br. C<sub>14</sub>H<sub>6</sub>Br<sub>2</sub>ClNO<sub>2</sub> calculated *m/z*: 414.9.

**1,5-Diamino-4,8-dibromoanthracene-9,10-dione 5c.** Brown colored solid. Decomposes >250 °C (from water); λ<sub>max</sub> (methanol)/nm 554; ν<sub>max</sub>/cm<sup>-1</sup> 3446 and 3319(NH), 1577 and 1560 (CO) and 759 (CBr); δ<sub>H</sub> (400 MHz; CDCl<sub>3</sub>; Me<sub>4</sub> Si) 2.1 (4H, s, NH) 7.5-7.8 (2H, m, C-H); *m/z* (EI) 553 (M-1) for <sup>80</sup>Br; C<sub>14</sub>H<sub>6</sub>Br<sub>4</sub>N<sub>2</sub>O<sub>2</sub> calculated *m/z*: 553.7.

**2,4-Dibromo-1-(methylamino) anthracene-9,10-dione 5d.** Brown colored solid. Melting point (measured) 154 °C (from water); λ<sub>max</sub> (Methanol)/nm 395; ν<sub>max</sub>/cm<sup>-1</sup> 3458 and 3099(NH), 1672 and 1625 (CO) and 737 (CBr); δ<sub>H</sub>(400 MHz; CDCl<sub>3</sub>; Me<sub>4</sub> Si) 3.5 (3H, s, NHCH<sub>3</sub>), 7.4-8.0(5H, m, C-H aromatic) and 9.9 (1H, s weak, NH); *m/z* (EI) 396 (M+1) for <sup>80</sup>Br; C<sub>15</sub>H<sub>9</sub>Br<sub>2</sub>NO<sub>2</sub> calculated *m/z*: 394.9.

**1-Amino-2-bromo-4-methoxyanthracene-9,10-dione 5e.** Brown colored solid. Melting point (measured) 176 °C (from water); λ<sub>max</sub> (methanol)/nm 411; ν<sub>max</sub>/cm<sup>-1</sup> 3434 and 3284 Br (NH), 1659 and 1625 (CO) and 798 (CBr); δ<sub>H</sub>(400 MHz; CDCl<sub>3</sub>; Me<sub>4</sub> Si) 3.9 (3H, s, OCH<sub>3</sub>), 5.3 (2H, weak s, NH), 7.4-8.4(5H, m C-H

aromatic); *m/z* (EI) 332 (M+1) for <sup>80</sup>Br; C<sub>15</sub>H<sub>10</sub>BrNO<sub>3</sub> calculated *m/z*: 330.9.

**N-(1-Amino-2-bromo-9,10-dihydro-9,10-dioxoanthracen-4-yl) benzamide 5f.** Brown colored solid. Melting point (measured) 247 °C (from water); λ<sub>max</sub> (MeOH)/nm 486; ν<sub>max</sub>/cm<sup>-1</sup> 3460 and 3252 br (NH), 1670,1627 and 1575 (CO) and 736 (CBr); δ<sub>H</sub>(400 MHz; CDCl<sub>3</sub>; Me<sub>4</sub> Si) 1.5(2H, weak s, NH<sub>2</sub>),7.4-8.4 (9H, m, C-H aromatic), 9.6 (1H, s, C-H) and 13.5 (1H, s, NH); *m/z* (EI) 421 (M+1) for <sup>80</sup>Br; C<sub>21</sub>H<sub>13</sub>BrN<sub>2</sub>O<sub>3</sub> calculated *m/z*: 420.0.

**1-Amino-2-bromo-4-hydroxyanthracene-9,10-dione 5g.** Brown colored solid. Melting point (measured) 198 °C (from water); λ<sub>max</sub> (methanol)/nm 397; ν<sub>max</sub>/cm<sup>-1</sup> 3453 and 3306 br (NH), 1670 and 1635 (CO) and 759 (CBr); δ<sub>H</sub> (400 MHz; CDCl<sub>3</sub>; Me<sub>4</sub> Si) 3.4 (2H, s, NH), 7.5-8.4 (5H, m, C-H aromatic); *m/z* (EI) 318 (M+1) for <sup>80</sup>Br; C<sub>14</sub>H<sub>8</sub>BrNO<sub>3</sub> calculated *m/z*: 316.9.

#### Scale-up of bromination of 1-amino-anthra-9,10-quinone and recycling of choline chloride: urea (deep eutectic solvent).

1-Aminoanthra-9,10-quinone 5 g (22.4 mmol) was added to deep eutectic solvent (50 ml). The reaction mixture was stirred for 15 min, bromine (2.9 ml, 56.0 mmol) was added slowly, and the reaction mixture stirred at 50–60 °C for 2 to 3 h. During the reaction, liberated HBr gas was neutralized using 2 N aqueous Na<sub>2</sub>CO<sub>3</sub> solution. The reaction was monitored by TLC. After completion of the reaction, 50 ml of water was slowly added, the mixture was filtered to obtain the product using a Büchner funnel under vacuum and dried in an oven to afford an orange-colored solid of 1-amino-2,4-dibromoanthra-9,10-quinone (8.1 g, 94%). The deep eutectic solvent was recovered from the filtrate by evaporating the water phase at 80 °C under vacuum. The recycled deep eutectic solvent was used for the next batch and recycled again.

#### Conclusion

The present reaction using a readily available and biodegradable ammonium deep eutectic solvent (choline chloride: urea) provides an efficient and convenient method for the bromination of 1-aminoanthra-9,10-quinones using molecular bromine without the use of any other catalyst or organic solvent. This method offers marked improvements in terms of simplicity, decreased reaction time, simple reaction conditions, general applicability, high isolated product yields, and the use of environmentally benign procedures and solvents. This method also eliminates the use of hazardous organic solvents and toxic catalysts, and thus provided a better and practical alternative to the existing procedures. Most significantly, however, this procedure demonstrates that selectivity and balance among yields are achievable. It is easy to separate the catalyst and substrate after completion of the reaction. The halogenated 1-aminoanthraquinones were easily isolated with high purity. These deep eutectic solvents provide a good alternative for industrial synthesis of mono or di-bromo derivatives of 1-aminoanthra-9,10-quinone, as the reaction is readily scalable.

## Acknowledgements

Authors are thankful to SAIF IIT- Bombay for recording  $^1\text{H}$  NMR spectra.

## References

- H. Fierz-David and L. Blangey in *Fundamental Process of Dye Chemistry*, Paul W. Vittum, Eastman Kodak Company, Rochester, Interscience, New York, 1949, pp. 224.
- Ciba Ltd., *GB Pat.*, 957 146, 1962.
- J. Stout, S. Hanahan, *US Pat.*, 4 235 789, 1980.
- M. Priester, P. Loew, *US Pat.*, 4 393 007, 1983.
- C. V. Wilson, *Organic Syntheses, Coll. Vol.*, 1955, **3**, 575.
- T. Welton, *Chem. Rev.*, 1999, **99**, 2071.
- (a) J. Ranke, S. Stolte, R. Stormann, J. Arning and B. Jastorff, *Chem. Rev.*, 2007, **107**, 2183–2206; (b) B. Jastorff, R. Störmann, J. Ranke, K. Molter, F. Stock, B. Oberheitmann, W. Hoffmann, J. Hoffmann, M. Nuhter, B. Ondruschka and J. Filser, *Green Chem.*, 2003, **5**, 136; (c) J. Ranke, K. Moulter, F. Stock, U. Bottin-Weber, J. oczobutt, J. Hoffmann, B. Ondruschka, J. Filser and B. Jastorff, *Ecotoxicol. Environ. Saf.*, 2004, **58**, 396; (d) S. Stolte, J. Arning, Bottin-Weber, M. Matzke, F. Stock, K. Thiele, M. Uerdingen, U. Welz-Biermann, B. Jastorff and J. Ranke, *Green Chem.*, 2006, **8**, 621.
- P. Wasserscheid and W. Keim, *Angew. Chem., Int. Ed.*, 2000, **39**, 3772.
- (a) K. Seddon, A. Stark and M. Torres, *Pure Appl. Chem.*, 2000, **72**, 2275; (b) A. Burrell, R. Del Sesto, S. Baker, T. M. McCleskey and G. A. Baker, *Green Chem.*, 2007, **9**, 449.
- J. Pavlinac, M. Zupan, K. Laali and S. Stavber, *Tetrahedron*, 2009, **65**, 5625.
- N. Ganguly, P. De and S. Dutta, *Synthesis*, 2005, 1103.
- H. Meshram, P. Reddy, P. Vinshnu, K. Sadashiv and J. Yadav, *Tetrahedron Lett.*, 2006, **47**, 991.
- (a) Z. Le, Z. Chen, Y. Hu and Q. Zheng, *Synthesis*, 2004, 2809; (b) Z. Le, Z. Chen, Y. Hu and Q. Zheng, *Chin. Chem. Lett.*, 2005, 1007; (c) Z. Le, Z. Chen and Y. Hu, *Chin. J. Chem.*, 2005, **23**, 1537.
- (a) A. Abbott, G. Capper, D. Davies, H. Munro, R. Rasheed and V. Tambyrajah, *Chem. Commun.*, 2001, 2010; (b) A. Abbott, G. Capper, D. Davies, R. Rasheed and V. Tambyrajah, *Chem. Commun.*, 2003, 70; (c) A. Abbott, D. Boothby, G. Capper, D. Davies and R. Rasheed, *J. Am. Chem. Soc.*, 2004, **126**, 9142.
- J. Gorke, J. Romas and Kazlauskas, *Chem. Commun.*, 2008, 1235.
- A. Abbott, P. Cullis, M. Gibson, R. Harris and E. Raven, *Green Chem.*, 2007, **9**, 868.
- N. Jain, A. Kumar and S. Chauhan, *Tetrahedron*, 2005, **61**, 1015.
- H. Jhong, D. Wonga, C. Wana, Y. Wang and T. Wei, *Electrochem. Commun.*, 2009, **11**, 209.
- R. Boethling, E. Sommer and D. Fiore, *Chem. Rev.*, 2007, **107**, 2207.
- P. Nockemann, K. Binnemans and K. Driesen, *Chem. Phys. Lett.*, 2005, **415**, 131.
- H. Ghaieni, M. Sharifi and M. Fattollahy, *Dyes Pigm.*, 2006, **71**, 73.

# Palladium-catalyzed decarboxylation of higher aliphatic esters: Towards a new protocol to the second generation biodiesel production†

Junxing Han, Hui Sun, Yuqi Ding, Hui Lou\* and Xiaoming Zheng

Received 28th August 2009, Accepted 10th December 2009

First published as an Advance Article on the web 26th January 2010

DOI: 10.1039/b917690j

An effective and highly selective decarboxylation approach to convert higher aliphatic esters into diesel-like paraffins has been developed. The results showed that palladium supported on barium sulfate was a potent catalyst to transform aliphatic esters into high-energy alkanes in supercritical hexane at a much lower temperature. Based on the comprehensive analysis to gas and liquid products, a decarboxylation mechanism was proposed. The methodology described in this paper provides a new protocol to the utilization of biomass-based resources, especially to the second generation biodiesel production.

## Introduction

Diminishing petroleum reserves and growing concerns about global warming make biomass-based energy resources an appealing alternative.<sup>1,2</sup> But it requires removal of most, or all, of the oxygen atoms in the reactant to form energy-rich molecules having desirable properties for combustion.<sup>2</sup> Higher aliphatic esters, a kind of renewable resource, have widespread existence in nature, such as in vegetable oils mainly composed of triglyceride compounds. Although transesterification reactions of triglycerides from natural oils or fats with methanol or ethanol to prepare biodiesel have been extensively studied,<sup>3</sup> high oxygen content, as well as poor heating value, high viscosity, and high cloud point and pour point, of biodiesel limits its direct application in power plants. In current industrial process to produce biodiesel, mineral acid or base catalysts, such as H<sub>2</sub>SO<sub>4</sub>, H<sub>3</sub>PO<sub>4</sub>, NaOH, KOH or CH<sub>3</sub>ONa, are needed to homogeneously catalyze the reversible transesterification reaction, which cause corrosion problems and must be neutralized at the end of the reaction. Heterogeneous catalysts used for biodiesel preparation have been developed in recent years, but they are confronted with problems as well, for instance, they are not as active as homogeneous catalysts and thus higher reaction temperature (200–250 °C) and pressure are required.<sup>4</sup> Additionally, post-treatment of glycerol by-product increases the production cost. Based on similarity in structure between higher aliphatic esters and natural diesel, *i.e.* the long alkyl chain, diesel-like hydrocarbons known as the second generation biodiesel can be produced from higher aliphatic esters *via* decarboxylation route, though harsh reaction conditions (high temperature and/or pressure) may be exerted to realize the conversion.

On the other hand, decarboxylation is a standard organic reaction and has considerable synthetic significance. However, from the viewpoint of advances in organic synthesis, decarboxylation or decarbonylation reactions of higher aliphatic esters have lagged far behind those of carboxylic acids, acyl halides and aldehydes.<sup>5</sup>

Homogeneously palladium-catalyzed decarboxylation reactions of active allyl esters have been reported in the literature. For example, Pd-catalyzed decarboxylation of allyl β-ketoesters was accomplished with Pd(OAc)<sub>2</sub> in acetonitrile,<sup>6</sup> and Pd(PPh<sub>3</sub>)<sub>4</sub> was effective to catalyze decarboxylation of allylic aryl carbonates, allyl α-acetoxyethyl-β-keto carboxylates and allylic alkynoates.<sup>7</sup> But homogeneously palladium-catalyzed decarboxylation of higher aliphatic esters has not been reported due to the low reactivity of these esters.

Recently, several groups have made progress in transforming higher aliphatic esters into hydrocarbons with heterogeneous catalysts. Murzin *et al.*<sup>8</sup> realized the decarboxylation of stearic acid, ethyl stearate and tristearine to diesel-like hydrocarbons over a commercial Pd/C catalyst in a semi-batch reactor under 15–27 bar and 300–360 °C. Among the noble metals they tested, Pd showed a superior decarboxylation activity to Pt, Ni, Rh, Ir, Ru and Os, especially supported on activated carbons. They investigated the effect of metal, support, solvent, temperature, initial concentration and reaction atmosphere on the decarboxylation reaction of fatty acids and their derivatives. Resasco and co-workers indicated that decarbonylation of methylesters to alkenes could occur on stream over CsNaX catalyst containing conjugated Lewis acid–base pairs with methanol co-fed.<sup>9</sup> According to the literature, decarbonylation of methyl octanoate was performed with low hydrogen consumption, but at much higher temperature, 425 °C. In this group, decarboxylation and decarbonylation of methylesters were achieved over Pt/Al<sub>2</sub>O<sub>3</sub> catalyst as well, while yields towards diesel-like hydrocarbons were unsatisfactory.<sup>10</sup> Work from the Krause group was concentrated on hydrodeoxygenation of aliphatic esters over sulfided NiMo/Al<sub>2</sub>O<sub>3</sub> and CoMo/Al<sub>2</sub>O<sub>3</sub> catalysts, and they argued that the high nucleophilic strength

Institute of catalysis, Zhejiang University, Tianmushan Road 138, Hangzhou, 310028, China. E-mail: hx215@zju.edu.cn; Fax: +86 571-88273593; Tel: +86 571-88273593

† Electronic supplementary information (ESI) available: Characterization of catalysts and analysis of products. See DOI: 10.1039/b917690j

of SH<sup>-</sup> groups was important in the hydrodeoxygenation reactions of aliphatic esters.<sup>11</sup> Koivusalmi and Jakkula disclosed a method of manufacturing branched saturated hydrocarbons from unsaturated fatty acids or fatty acid esters with C<sub>1</sub>–C<sub>5</sub> alcohols in an US patent.<sup>12</sup> The process comprised skeletal isomerization, prehydrogenation and deoxygenation carried out by decarboxylation or hydrodeoxygenation with conventional catalysts, *i.e.* Pd/C and NiMo/Al<sub>2</sub>O<sub>3</sub>. However, researchers knew only a little about the exact decarboxylation mechanism of higher aliphatic esters, and a catalytic decarboxylation cycle has not been stated explicitly up to now.

In the present work, we report that decarboxylation of aliphatic esters can be successfully performed over a Pd/BaSO<sub>4</sub> catalyst (Rosenmund catalyst) in supercritical hexane with high selectivity at a much lower temperature. Catalytic performance of Pd/BaSO<sub>4</sub> as well as several palladium-based catalysts including Pd/SrSO<sub>4</sub>, Pd/BaCO<sub>3</sub>, Pd/CaCO<sub>3</sub>, Pd/C and Pd/MWCNTs (Pd metal on multi-walled carbon nanotubes) was examined using aliphatic acid methyl esters and ethyl esters as model compounds. A decarboxylation mechanism was proposed on the foundation of comprehensive analysis to gas and liquid products.

## Results and discussion

### Catalyst performance testing

Initially, our studies were carried out by optimizing catalysts and reaction conditions using methyl stearate as a model substrate, and the results were summarized in Table 1. Among the catalysts examined (Table 1, entries 1–6), only Pd/BaSO<sub>4</sub> showed excellent activity and selectivity and offered the highest yield of heptadecane with one carbon atom less than the fatty acid part of methyl stearate (Table 1, entry 6). Pd/SrSO<sub>4</sub> and Pd/BaCO<sub>3</sub> were not effective for the present transfor-

mation (Table 1, entries 1 and 2). Pd/CaCO<sub>3</sub>, Pd/C and Pd/MWCNTs exhibited high activity but afforded relatively low yields of heptadecane (Table 1, entries 3–5). In the cases of Pd/CaCO<sub>3</sub> and Pd/BaCO<sub>3</sub>, some unidentified floccular species were observed. As could be seen from the results of metal loading experiments (Table 1, entries 6–9), 5% Pd loading was suitable. Decreasing the Pd loading sacrificed the activity and more loading was unnecessary. Temperature was an important parameter of decarboxylation reactions. As expected, the yield significantly increased from 62.6% to 96.6% as the temperature increased from 250 °C to 270 °C (Table 1, entries 6 and 12). Further raising temperatures had an adverse effect on the yields (Table 1, entries 10–11) and hence 270 °C was selected for the following study. As shown in Table 1, decarboxylation of methyl stearate was almost independent on the hydrogen pressure in the scope of our test (Table 1, entries 6 and 13–14). Conversion of substrates and the yield and selectivity of target molecules hardly varied with the hydrogen pressure raised from 0.8 MPa to 2.2 MPa. However, appropriately higher pressure of hydrogen was essential to keep the surface of palladium clean and retard the catalyst deactivation.<sup>13</sup> Therefore, 1.6 MPa of hydrogen pressure was used for the following investigation. Experiments showed that 20 mL of hexane as solvent provided the best yield for the product (Table 1, entries 6 and 15–18). Without the solvent, almost no alkanes could be detected in the product, though the conversion of methyl stearate was 100%. We speculated that macromolecules might have been formed by coupling reactions among intermediates on the surface of the catalyst. It was assumed that compared with the effect of organic solvent on chemical reactions the high diffusivity of supercritical hexane can reduce mass-transfer resistance on reactions,<sup>14</sup> which facilitates contact of hydrogen and esters with catalysts, and the strong solvent power can yield high solubility for alkanes, which enhances the desorption of alkanes generated on the catalyst surface and thus effectively inhibits the coupling

**Table 1** Optimization of catalysts and reaction conditions<sup>a</sup>

Entry	Catalyst	P(H <sub>2</sub> )/MPa	Time/h	T/°C	Solvent amount/mL	Conversion (%)	Yield (%) <sup>d</sup>
1	5%Pd/SrSO <sub>4</sub>	1.6	3.5	270	20	63.6	16.7
2	5%Pd/BaCO <sub>3</sub>	1.6	3.5	270	20	88.3	31.6
3	5%Pd/CaCO <sub>3</sub>	1.6	3.5	270	20	98.9	66.6
4	5%Pd/C	1.6	3.5	270	20	99.3	60.2
5	5%Pd/MWCNTs	1.6	3.5	270	20	98.5	72.0
6	5%Pd/BaSO <sub>4</sub>	1.6	3.5	270	20	99.5	96.6
7	8%Pd/BaSO <sub>4</sub>	1.6	3.5	270	20	98.7	95.8
8	2%Pd/BaSO <sub>4</sub>	1.6	3.5	270	20	94.6	92.8
9	1%Pd/BaSO <sub>4</sub>	1.6	3.5	270	20	57.4	46.2
10	5%Pd/BaSO <sub>4</sub>	1.6	3.5	300	20	99.8	89.1
11	5%Pd/BaSO <sub>4</sub>	1.6	3.5	285	20	99.7	95.6
12	5%Pd/BaSO <sub>4</sub>	1.6	3.5	250	20	75.9	62.6
13	5%Pd/BaSO <sub>4</sub>	2.2	3.5	270	20	99.3	94.9
14	5%Pd/BaSO <sub>4</sub>	0.8	3.5	270	20	99.5	95.7
15	5%Pd/BaSO <sub>4</sub>	1.6	3.5	270	40	51.3	25.8
16	5%Pd/BaSO <sub>4</sub>	1.6	3.5	270	30	51.6	37.9
17	5%Pd/BaSO <sub>4</sub>	1.6	3.5	270	10	99.3	92.6
18	5%Pd/BaSO <sub>4</sub>	1.6	2.5	270	0	100	0
19 <sup>b</sup>	5%Pd/BaSO <sub>4</sub>	1.6	8.0	270	20	93.4	87.2
20 <sup>b</sup>	5%Pd/BaSO <sub>4</sub>	1.6	9.0	270	20	99.3	93.8
21 <sup>c</sup>	5%Pd/BaSO <sub>4</sub>	1.0	3.5	270	20	58.3	9.60

<sup>a</sup> Typical reaction conditions, with 0.1 mmol methyl stearate. The safety range: temperature below 300 °C and hydrogen pressure below 2.2 MPa.

<sup>b</sup> The amount of substrate was tripled. <sup>c</sup> Argon atmosphere. <sup>d</sup> Yield of heptadecane.





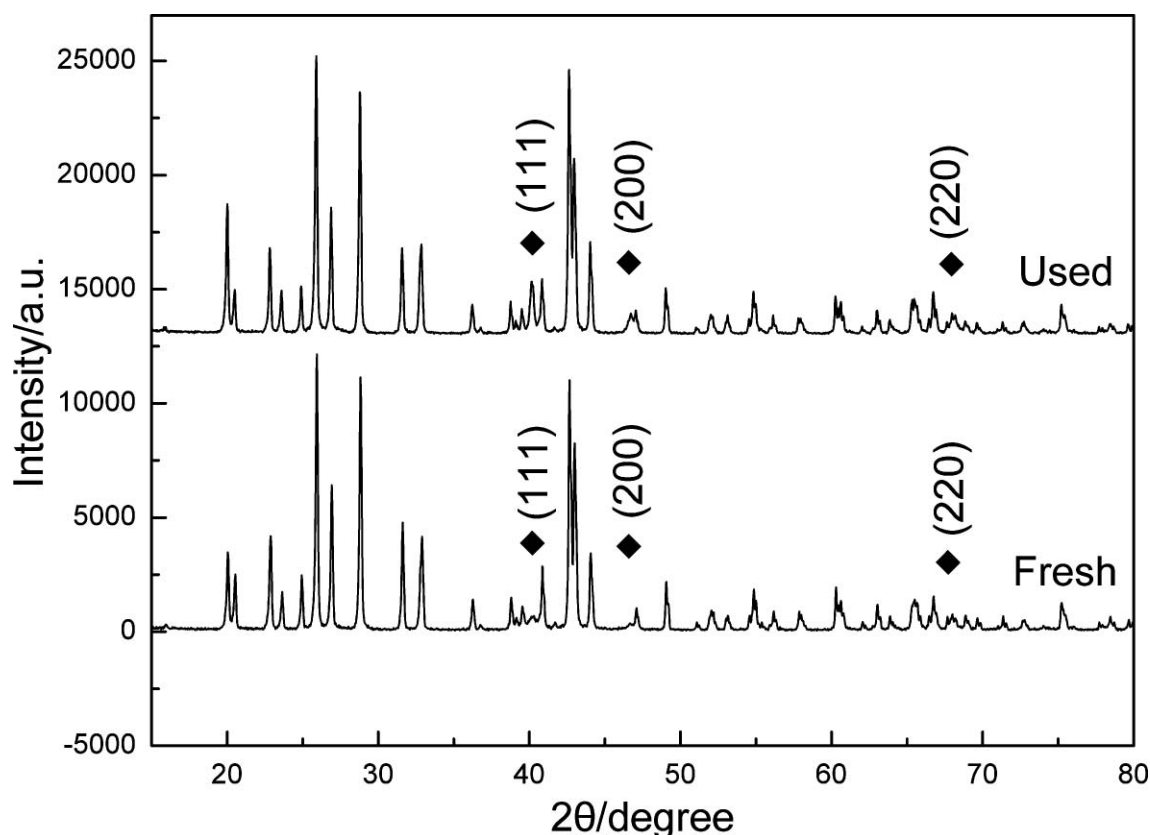
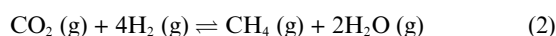


Fig. 1 XRD patterns of freshly prepared and used 5%Pd/BaSO<sub>4</sub>.

the gaseous products in our reaction system and carbon dioxide might be consumed in the presence of hydrogen to form methane.



Trace amounts of ethanol were detected in the liquid products of ethyl esters, whereas no methanol was found in the corresponding products of methyl esters. To our knowledge, the decomposition of methanol might occur on (111) facets of palladium.<sup>17</sup>

Importantly, high selectivity for decarboxylation products can be explained by the mechanism proposed above. There exist three possible routes during the reaction course, two of which (**Cycle 1** and **Cycle 3**) are dominant and offer the same decarboxylated products (R<sup>1</sup>-H).

## Experimental

All of the chemicals used in the following experiments were of analytical grade, provided by local suppliers and used without further purification. Pristine MWCNTs were purchased from Chengdu Organic Chemicals Co. Ltd., China.

### Instrumentation

X-ray powder diffraction (XRD) patterns were recorded on a D8 ADVANCE X-Ray diffractometer using Cu K<sub>α1</sub> radiation ( $\lambda = 0.154056$  nm) at 40 kV and 30 mA, over a  $2\theta$  range of 10–80° at a scanning speed of 6° per minute. The phases

were identified using the Power Diffraction File (PDF) database (JCPDS, International Centre for Diffraction Date). Energy dispersive spectrometry (EDS) was measured on an S-4700 field-emission scanning electron microscope with an accelerating voltage of 15 keV. TEM images were obtained on a JEOL JEM-2010 at 200 kV. Product identifications were using a HP 5973 series GC-MS. Chemical standards were also used to confirm product identification. Reaction mixtures were analyzed using a GC system equipped with a HP-5 capillary column and a flame ionization detector.

### Preparation and characterization of catalysts

1%Pd/BaSO<sub>4</sub>, 2%Pd/BaSO<sub>4</sub>, 5%Pd/BaSO<sub>4</sub>, 8%Pd/BaSO<sub>4</sub>, 5%Pd/SrSO<sub>4</sub>, 5%Pd/BaCO<sub>3</sub>, 5%Pd/CaCO<sub>3</sub> and 5%Pd/C catalysts were prepared according to the literature procedures,<sup>18</sup> and characterized by X-ray diffraction, TEM and EDS. The theoretical Pd loading in each catalyst was calculated based on the amount of metal precursor (H<sub>2</sub>PdCl<sub>4</sub>).

5%Pd/MWCNTs was prepared according to the literature<sup>19</sup> with some modifications: Oxidation of multi-walled carbon nanotubes was carried out by refluxing pristine MWCNTs in 68% HNO<sub>3</sub> at 140 °C for 12 h. After filtered, the sample was washed and dried at 120 °C for 12 h. The oxidized carbon nanotubes (0.25 g) contacted with H<sub>2</sub>PdCl<sub>4</sub> solution by incipient wetness impregnation technique overnight and dried at 120 °C for 0.5 h. Then the sample was heated in argon at 350 °C for 3 h

and subsequently reduced in hydrogen at 350 °C for 3 h. The final obtained sample was cooled to room temperature in argon atmosphere. The catalyst prepared was confirmed using X-ray diffraction, TEM and EDS.

### Decarboxylation procedure

In a typical procedure for decarboxylation, methyl stearate (0.25 mmol), freshly prepared 5%Pd/BaSO<sub>4</sub> catalyst (7.5 mol%, based on Pd) and hexane (20 mL) were added to a 100 mL stainless steel autoclave. The reaction system was pressured with hydrogen to 1.6 MPa and heated to react at 270 °C for 9.0 h. After the reaction, gas and liquid products were collected and then detected by gas chromatography (GC) and GC-MS, respectively. Quantitative calculations of liquid products were performed using the internal standard method. The reaction conditions for other cases were performed accordingly.

### Catalyst recycling

When the reaction was complete, 5%Pd/BaSO<sub>4</sub> catalyst was deposited at the bottom of the autoclave. The precipitate was separated by filtration and washed sufficiently with hexane, then dried in an oven at 70 °C for 0.5 h. The catalyst was recovered and reused in the next run without further activation treatment.

### Conclusion

In summary, we disclosed an efficient decarboxylation method to transform higher aliphatic esters into diesel-like paraffins. Palladium supported on barium sulfate was testified to be a potent catalyst to convert aliphatic esters into high-energy alkanes in supercritical hexane under optimized reaction conditions. High selectivity for the desired decarboxylates could be explained with the decarboxylation mechanism proposed which included both decarboxylation and decarbonylation process. The methodology described in this paper provides a new protocol to decrease the oxygen content of biomass-based resources for their utilization in the future.

### Acknowledgements

This work was supported by the Chinese National Natural Science Foundation (Project No. 20673097), the National Basic Research Program of China (Project No. 2007CB210204) and the Top Key Discipline of Zhejiang Province.

### References

- 1 A. Corma, S. Iborra and A. Velty, *Chem. Rev.*, 2007, **107**, 2411–2502.
- 2 E. L. Kunkes, D. A. Simonetti, R. M. West, J. C. Serrano-Ruiz, C. A. Gärtner and J. A. Dumesic, *Science*, 2008, **322**, 417–421.
- 3 (a) D. E. Lopez, K. Suwannakarn, D. A. Bruce and J. G. Goodwin, *J. Catal.*, 2007, **247**, 43–50; (b) I. N. Martyanov and A. Sayari, *Appl. Catal., A*, 2008, **339**, 45–52; (c) M. D. Serio, R. Tesser, L. Pengmei and E. Santacesaria, *Energy Fuels*, 2008, **22**, 207–217; (d) H. Sun, K. Hu, H. Lou and X. M. Zheng, *Energy Fuels*, 2008, **22**, 2756–2760.
- 4 G. W. Huber, S. Iborra and A. Corma, *Chem. Rev.*, 2006, **106**, 4044–4098.
- 5 (a) Y. Yoshimi, T. Itou and M. Hatanaka, *Chem. Commun.*, 2007, 5244–5246; (b) J. Tsuji and K. Ohno, *J. Am. Chem. Soc.*, 1968, **90**, 94–98; (c) J. M. Anderson and J. K. Kochi, *J. Am. Chem. Soc.*, 1970, **92**, 1652–1659; (d) D. D. Tanner and S. A. A. Osman, *J. Am. Chem. Soc.*, 1968, **90**, 6572–6574.
- 6 C. Mercier, G. Mignani, M. Aufrand and G. Allmang, *Tetrahedron Lett.*, 1991, **32**, 1433–1436.
- 7 (a) R. C. Larock and N. H. Lee, *Tetrahedron Lett.*, 1991, **32**, 6315–6318; (b) J. Tsuji, M. Nisar and I. Minami, *Tetrahedron Lett.*, 1986, **27**, 2483–2486; (c) S. H. Sim, H. J. Park, S. I. Lee and Y. K. Chung, *Org. Lett.*, 2008, **10**, 433–436; (d) K. H. Kim, E. S. Kim and J. N. Kim, *Tetrahedron Lett.*, 2009, **50**, 5322–5325.
- 8 (a) M. Snåre, I. Kubičková, P. Mäki-Arvela, K. Eränen, J. Wärnä and D. Yu. Murzin, *Chem. Eng. J.*, 2007, **134**, 29–34; (b) M. Snåre, I. Kubičková, P. Mäki-Arvela, D. Chichova, K. Eränen and D. Yu. Murzin, *Fuel*, 2008, **87**, 933–945; (c) I. Kubičková, M. Snåre, K. Eränen, P. Mäki-Arvela and D. Yu. Murzin, *Catal. Today*, 2005, **106**, 197–200; (d) M. Snåre, I. Kubičková, P. Mäki-Arvela, K. Eränen and D. Yu. Murzin, *Ind. Eng. Chem. Res.*, 2006, **45**, 5708–5715.
- 9 T. Sooknoi, T. Danuthai, L. L. Lobban, R. G. Mallinson and D. E. Resasco, *J. Catal.*, 2008, **258**, 199–209.
- 10 P. T. Do, M. Chiappero, L. L. Lobban and D. E. Resasco, *Catal. Lett.*, 2009, **130**, 9–18.
- 11 E. M. Ryymin, M. L. Honkela, T. R. Viljava and A. O. I. Krause, *Appl. Catal., A*, 2009, **358**, 42–48.
- 12 E. Koivusalmi and J. Jakkula, *US Pat.*, 7 459 597, 2007.
- 13 P. Mäki-Arvela, I. Kubičková, M. Snåre, K. Eränen and D. Yu. Murzin, *Energy Fuels*, 2007, **21**, 30–41.
- 14 Y. X. Jia, X. Y. Guo and B. Zhong, *J. Supercrit. Fluids*, 2004, **32**, 177–182.
- 15 (a) A. K. Datye, Q. Xu, K. C. Kharas and J. M. McCarty, *Catal. Today*, 2006, **111**, 59–67; (b) R. T. K. Baker, P. S. Harris and R. B. Thomas, *Surf. Sci.*, 1974, **46**, 311–316; (c) P. Stone, S. Poulston, R. A. Bennett and M. Bowker, *Chem. Commun.*, 1998, 1369–1370.
- 16 R. D. Cortright, R. R. Davda and J. A. Dumesic, *Nature*, 2002, **418**, 964–967.
- 17 (a) S. Schauermaier, J. Hoffmann, V. Johánek, J. Hartmann, J. Libuda and H. J. Freund, *Angew. Chem., Int. Ed.*, 2002, **41**, 2532–2535; (b) I. V. Yudanov, A. V. Matveev, K. M. Neyman and N. Rosch, *J. Am. Chem. Soc.*, 2008, **130**, 9342–9352.
- 18 (a) A. Parvulescu, D. D. Vos and P. Jacobs, *Chem. Commun.*, 2005, 5307–5309; (b) R. Mazingo, *Org. Synth., collect. vol. 3*, 685.
- 19 A. M. Zhang, J. L. Dong, Q. H. Xu, H. K. Rhee and X. L. Li, *Catal. Today*, 2004, **93–95**, 347–352.

# Mechanocatalysis for biomass-derived chemicals and fuels

Sandra M. Hick, Carolin Griebel, David T. Restrepo, Joshua H. Truitt, Eric J. Buker, Caroline Bylda and Richard G. Blair\*

Received 4th November 2009, Accepted 8th December 2009

First published as an Advance Article on the web 25th January 2010

DOI: 10.1039/b923079c

Heterogeneous catalysis cannot be easily applied to solids such as cellulose. However, by mechanically grinding the correct catalyst and reactant, it is possible to induce solid–solid catalysis or mechanocatalysis. This process allows a wide range of solids to be effectively utilized as feedstock for commercially relevant compounds. Here we show a set of structural and physical parameters important for the implementation of catalysts in mechanocatalytic processes and their application in the catalytic depolymerization of cellulose. Using the best catalysts, which possess high surface acidities and layered structures, up to 84% of the available cellulose can be converted to water-soluble compounds in a single pass. This approach offers significant advantages over current methods - less waste, insensitivity to feedstock, multiple product pathways, and scalability. It can be easily integrated into existing biorefineries - converting them into multi-feedstock and multi-product facilities. This will expand the use of non-food polysaccharide sources such as switch grass.

## 1. Introduction

Lignocellulosic biomass represents a rich source of feedstock for fuels<sup>1</sup> and chemicals; major work in developing this resource is underway. Biological sources such as switch grass, corn stover, bagasse, and other agricultural waste are largely underutilized. Most lignocellulosic biomass is processed in one of three ways: acid hydrolysis, enzymatic hydrolysis, and pyrolysis.<sup>2,3</sup> New biological<sup>4,5</sup> and chemical<sup>6</sup> approaches seek to circumvent the drawbacks associated with these processes.

Catalytic processing of these materials is an important topic. Although efficient catalysts have been developed for a wide range of heterogeneous systems, they are not suitable for solid–solid catalysis. A major difficulty with these solids is mass transport. High surface area structures suited to liquid and gas systems do not work as efficiently in solid systems. Two typical structures, porous solids and supported particles have limitations when applied to solid systems. Porous solids have pore sizes too small to accommodate molecules much larger than 30 Å; and supported particle systems still require some method to overcome the solid–solid diffusion barrier.

Biochemical pathways are also important in processing these polymers. However, enzymes have limited pressure/temperature regimes in which they can function and are not as robust as inorganic solids.

There are two issues that need to be addressed in order to realize effective catalysis in solid–solid reactions. The solid–solid diffusion barrier (mass transport) must be overcome and the catalyst must be structured to allow access to catalytic sites. Currently, most catalytic depolymerization involves solvent systems to overcome this diffusion barrier.<sup>7–10</sup>

We have found that it is possible to overcome diffusion in a solid–solid reaction by using mechanical force without the addition of solvents. This phenomenon is often referred to as mechanocatalysis or tribocatalysis. Little work has been done on this phenomenon.<sup>11–14</sup> In fact, recent work has focused on using traditional heterogeneous catalysts (such as zeolites) in mechanochemical processes.<sup>15–21</sup> This approach ignores the aggressive nature of mechanical processing. Effective mechanocatalysts must be mechanically robust, and possess sites that are physically accessible and chemically active.

Mechanocatalytic processes require no external heat. All of the energy for the reaction comes from the pressures and frictional heating provided by the kinetic energy of milling media moving in a container. Although there is a large body of work examining mechanochemical syntheses,<sup>22–39</sup> to date no one has examined the properties required for an effective mechanocatalyst.

In a mechanocatalytic system, it is important that intimate contact between the catalyst and reactant be maintained. Although most biomass processing facilities utilize some form of attrition technology, it is usually in the form of hammer mills, disk mills, or roller mills. These technologies are being actively researched,<sup>40–42</sup> but they do not allow good interaction between a solid catalyst and the material being treated. Pebble (or rolling) mills, shaker mills, attrition mills, and planetary mills are a few examples of mills that effectively “push” the catalyst into contact with the material being treated (biomass).<sup>43</sup>

## Experimental

### Reagents

Pure microcrystalline cellulose (Avicel, Brinkmann) was utilized to investigate the performance of different solid catalysts. The natural cellulose sources *Z. mays indurata* (flint corn),

University of Central Florida, Department of Chemistry, P.O. BOX 162366, Orlando, FL, 32816, USA, rblair@mail.ucf.edu; Fax: +1 407-823-2252; Tel: +1 407-823-0639

*Prunus* stone, paper, aspen wood, and mixed biomass were collected from local sources. The grasses: *A. gerardii* (Big Bluestem), *S. scoparium* (Little Bluestem) and *P. virgatum* (Switchgrass) were supplied by Agricol Corporation (Madison, WI). All natural cellulose sources were dried at room temperature to a moisture content of <10% and cut to 2 cm or smaller pieces.

The materials kaolinite (Edgar Plastic Kaolin, Axner Pottery), delaminated kaolinite (Kaopaque 10, IMERYS), aluminium phosphate (Fisher Scientific), aluminium oxide (J.T. Baker), talc (Nytol 100HR, Axner Pottery), Y-type zeolite (HS-320, Hydrogen Y, Wako Chemicals), bentonite (Asbury Carbons), vermiculite, quartz, muscovite mica, silicon carbide (-325 mesh, Electronic Space Products International), graphite (grade TC306, Asbury Carbons), and aluminium sulfate (Fisher Scientific) were used as received. Layered silicates were H<sup>+</sup> exchanged by soaking in 1 M hydrochloric acid for 12 h, filtering and dried at 80 °C overnight. Chemically delaminated kaolinite was prepared by intercalating with urea and deintercalating by washing with water.<sup>44</sup> The super acid was prepared by stirring aluminium oxide (J.T. Baker) in 2.5 M H<sub>2</sub>SO<sub>4</sub> followed by calcination at 600 °C.<sup>45</sup>

### Mechanical processing

Various amounts of cellulose and catalyst were ground using a rolling mill (custom), mixer mill (SPEX Certiprep, Metuchen, NJ), or attrition mill (Union Process Inc., Akron OH). Initial catalyst assessment was performed using a mixer mill. Typically, 2 grams of a 1 : 1 mixture of catalyst and cellulose were ground in a 65 mL vial (1.5" ID × 2.25" deep) made of 440C steel, utilizing three 0.5" balls made of the same material as the milling vial. Attrition milling experiments were performed by Union Process, Inc. in a 1-SD attrition mill run at 350 rpm with a 1.5 gallon tank, 40 lbs of 0.25" chrome steel (SAE 52100) balls as the milling media, and 1200 g of a 1 : 1 mixture of cellulose and catalyst. Rolling mill experiments were performed in a custom rolling mill constructed of 316 stainless steel with a diameter of 1.37" and a length of 4.93". The mill was charged with 25 0.5" balls made of 440C steel and 2 g of a 1 : 1 mixture of cellulose and catalyst.

### Gravimetric analysis

The extent of hydrolysis was monitored gravimetrically. Conversion of cellulose to water-soluble oligosaccharides was determined by stirring 0.1 g of the reaction mixture in 30 mL of water. Any oligosaccharide with a degree of polymerization <5 will be solvated.<sup>46</sup> The production of water-soluble products was measured by filtration through a 47 mm diameter Whatman Nuclepore® track etched polycarbonate membrane filter with a pore size of 0.220 μm. The residue was dried in a 60 °C oven for 12 h and then weighed.

### Gas chromatography with mass sensitive detection

GC-MS analysis was performed on an Agilent 6850 GC with an Agilent 19091-433E HP-5MS column (5% phenyl methyl siloxane, 30 m × 250 μm × 0.25 μm nom.) coupled with a 5975C VL mass selective detector. Saccharide composition was

analyzed by silanizing<sup>47</sup> the product. Dehydration products were extracted with 60 °C chloroform and analyzed by GC-MS.

### Thin layer chromatography

Thin layer chromatography was used to assess the composition of the hydrolysis product. Solutions were spotted onto cellulose plates and developed with a 20 : 7 : 10 mixture of n-butanol, acetic acid, and water. The plates were stained with a 3% urea and 1 M phosphoric acid in n-butanol saturated water solution.

### Discrete element modeling

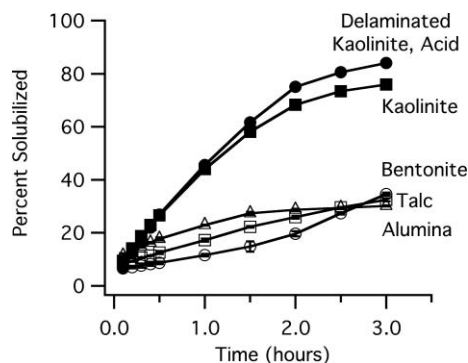
Discrete element models of the milling process were generated using EDEM (DEM Solutions Ltd.).

### Degree of polymerization

The degree of polymerization of the insoluble cellulose residue was determined using viscometry according to the method outlined in ASTM D 4243.

## Results

Three milling modes were investigated for the mechanocatalytic depolymerization of cellulose—shaking, rolling, and stirring. Fig. 1 illustrates solubilization achievable in a SPEX shaker mill. No appreciable solubilization was realized on samples of microcrystalline cellulose milled without a catalyst.

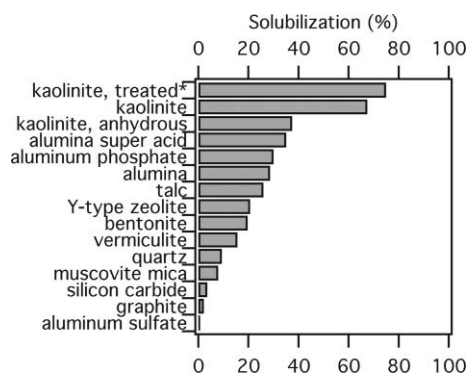


**Fig. 1** Solubilization of cellulose as a function of milling time in a SPEX 8000D mixer mill. Catalysts were milled with microcrystalline cellulose in a 1 : 1 ratio. The most rapid solubilization was measured using 1 : 1 aluminosilicates such as kaolinite.

The catalysts' chemical and physical properties effect on conversion efficiency was studied by choosing materials with specific structural and chemical properties. Fig. 2 summarizes the solubilization results for cellulose mechanocatalytically treated for two hours in a shaker mill.

A shaker mill was chosen to assess catalyst efficacy since cellulose hydrolysis is observed after as little as 6 min of milling. This mode is a high-energy process with the possible realization of localized high pressures. After 3 h of milling, up to 84% of the cellulose can be converted to water-soluble fractions allowing rapid assessment of catalysts parameters.

The layered silicate mineral kaolinite was determined to be a good mechanocatalyst and the composition of the solubilized fraction produced was analyzed utilizing thin layer



**Fig. 2** Mechanocatalytic activity for a sample of compounds investigated. Catalysts were milled with microcrystalline cellulose in a 1 : 1 ratio for 2 h. Layered compounds with a surface acidity,  $H_0$ ,  $< -3.0$ , as determined by dicinnamalacetone gave the best yields. The catalytic efficiency of kaolinite was improved through physical delamination and proton exchange (\*).

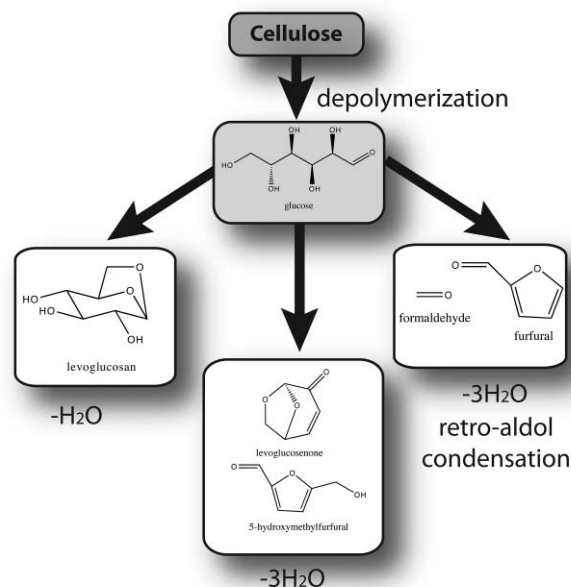
chromatography and gas chromatography with mass sensitive detection. Both methods confirmed that depolymerization occurs rapidly with no oligosaccharides larger than  $n = 2$  detected even after 30 min of treatment. The three major water-soluble components detected were levoglucosan, fructose, and glucose. The degree of polymerization of the insoluble residue was measured and found to decrease linearly with time.

The variation in product composition was studied as a function of milling mode and time. A study of the energy input through milling, and its effect on products, was investigated using a variable speed rolling-mill. Models were developed using discrete element methods (EDEM<sup>TM</sup>, DEM Solutions Ltd.) to estimate the compressive forces achieved during milling. These models indicate that, in a 10 s period, a shaker mill can produce 9 impacts with forces between 400 and 3000 N; an attrition mill can produce 9 impacts between 400 and 2000 N; a rolling mill at 30 rpm generates 4 impacts between 60 and 110 N; and at 100 rpm, 10 impacts between 60 and 130 N.

High-energy processing in a shaker mill resulted in the production of levoglucosan, fructose and glucose with a ratio of 9 : 1 : 4.3 after 30 min of treatment and a ratio of 4.6 : 1 : 4.1 after two hours of treatment. The product distribution was similar for samples prepared in an attrition mill. Low-speed processing in a rolling mill (30 rpm) resulted in no measurable catalytic activity; increasing the rotation velocity to 100 rpm resulted in  $13.2 \pm 0.8\%$  solubilization after 96 h of treatment. The product consisted of levoglucosan, fructose, and glucose in a 1 : 1 : 5.8 ratio. With continued high energy milling the levoglucosan fraction decreased and other dehydration products were observed - levoglucosenone and 5-hydroxymethyl furfural (HMF), as well as the retro-aldol condensation product furfural (Fig. 3). This result is encouraging since HMF is of interest for use as a fuel or chemical feedstock.<sup>1,48,49</sup>

## Discussion

Milling alone (without a catalyst present) is not sufficient to hydrolyze the glycosidic bond in cellulose. Acidic solids such as kaolinite ( $Al_2Si_2O_7 \cdot 2H_2O$ ), alumina super acid, aluminium phosphate ( $AlPO_4$ ), alumina ( $Al_2O_3$ ), Y-type zeolite,

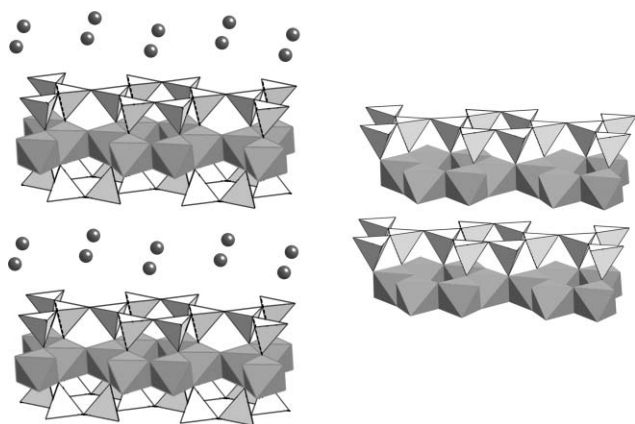


**Fig. 3** Cellulose can be mechanocatalytically converted to glucose and, with prolonged treatment, into a variety of products. The formaldehyde produced was not observed with the analytical techniques utilized.

and bentonite ( $Al_2Si_4O_{11} \cdot H_2O$ ) showed good catalytic ability. Low-acidity solids such as talc ( $H_2Mg_3(SiO_3)_4$ ), vermiculite ( $(MgFe,Al)_3(Al,Si)_4O_{10}(OH)_2 \cdot 4H_2O$ ), quartz ( $SiO_2$ ), mica ( $(KF)_2(Al_2O_3)_3(SiO_2)_6(H_2O)$ ), silicon carbide ( $SiC$ ), graphite ( $C$ ), and aluminium sulfate ( $Al_2(SO_4)_3$ ) were less effective. The hardness of the catalyst did not play a role in the efficiency of the depolymerization. Both kaolinite and talc are soft, but kaolinite is a much more efficient catalyst. Silicon carbide and aluminium oxide are both very hard, but silicon carbide showed little or no catalytic ability. The use of harder catalysts resulted in undesirable wear on the container and milling media. The most effective catalyst is the layered mineral kaolinite. Kaolinite is an aluminosilicate consisting of aluminium-containing (as  $AlO_6$  units) layers covalently bound to silicon-containing (as  $SiO_4$  units) layers as in a 1 : 1 ratio. These layers are held together by hydrogen bonds from protons on open  $Al-O-Al$  sites to open  $Si-O-Si$  sites. The structurally similar bentonite has each aluminium-containing layer covalently bound above and below by a silicon-containing layer in a 2 : 1 configuration; this prevents the active sites from interacting with the cellulose (Fig. 4). The role of aluminium in the active sites was confirmed by comparing the catalytic ability of quartz and aluminium phosphate. These compounds are isostructural; substituting the  $SiO_4$  units in quartz with  $AlO_4$  and  $PO_4$  units, as in aluminium phosphate, results in an increase in active sites and the observed increase in catalytic ability.

Layered compounds are effective mechanocatalysts because the layers are typically held together by weak forces such as hydrogen bonding and van der Waals forces. These bonds can be easily broken *via* mechanical processing (grinding or rubbing).<sup>50</sup> The result is a material with a high specific surface area (SSA) that is only dependent upon the number of layers in each particle.

$$SSA_{\text{hard sphere}} = \frac{3}{rd_{\text{solid}}} \quad (1)$$



**Fig. 4** The structures for the 2:1 smectite bentonite (left) and 1:1 smectite kaolinite (right). The octahedra are  $\text{AlO}_6$  units and the tetrahedra are  $\text{SiO}_4$  units. The sheets in bentonite are charged due to an Al:Si imbalance. The sheets are held together by ionic forces between the sheets and a cation (dark sphere). The sheets in kaolinite are held together by hydrogen bonds from protons on the Al layer to the oxygens on the Si layer.

$$SSA_{\text{layered}} = \frac{2}{(n + nf - 1)td_{\text{solid}}} \quad (2)$$

Eqn (1) and 2 give the specific surface areas (SSA) in area/unit mass for hard spheres and layered materials where  $n$  = the number of layers,  $d_{\text{solid}}$  = the density of the solid,  $r$  = the radius of the particle,  $t$  = the interlayer spacing, and  $f$  = the ratio of the layer thickness to the interlayer spacing. Eqn (1) is derived from the surface area of a solid sphere ( $4\pi r^2$ ) and the mass of the sphere as determined by its density (mass =  $4/3 \pi r^3 d_{\text{solid}}$ ). Eqn (2) is derived from the surface area of a fragment using its length and width ( $2lw$ ) and the mass of  $n$  layers using the material's density and interlayer spacing (mass =  $lw(n+nf-1)td_{\text{solid}}$ ). This derivation assumes both sides of the sheet are catalytically active. For kaolinite, only one side of the sheet (the  $\text{AlO}_6$  side) is catalytically active. This results in a SSA half of that predicted by eqn (2). Using the  $d_{\text{solid}} = 2.599 \text{ g cm}^{-3}$ ,  $t = 2.892 \text{ \AA}$ , and  $f = 1.561$  for kaolinite, we find that reducing it to a collection of single aluminosilicate sheets (through delamination) would result in an active specific surface area of  $852 \text{ m}^2 \text{ g}^{-1}$ . This would be equivalent to  $1.35 \text{ nm}$  spherical particles. Structures consisting of 5 layers would have a specific surface area equivalent to  $10.2 \text{ nm}$  particles ( $113 \text{ m}^2 \text{ g}^{-1}$ ). It has been suggested that mechanochemical processes are dependent on the area of surface sites available.<sup>15</sup> This is in line with our observation that layered materials are the ideal structure for mechanocatalysts. Delamination of kaolinite to single sheets has been observed during grinding.<sup>51</sup> In fact, it is not unreasonable to expect delamination to single layers; this has been observed in talc.<sup>15</sup>

It is important to note that anhydrous kaolinite showed a decrease in catalytic ability. This is due to the fact that water is required to break the cellulose glycosidic bond.

### Kinetics and depolymerization mechanism

Concentrations in chemical reaction are typically expressed in terms of moles/l. In a solventless, solid-solid reaction this

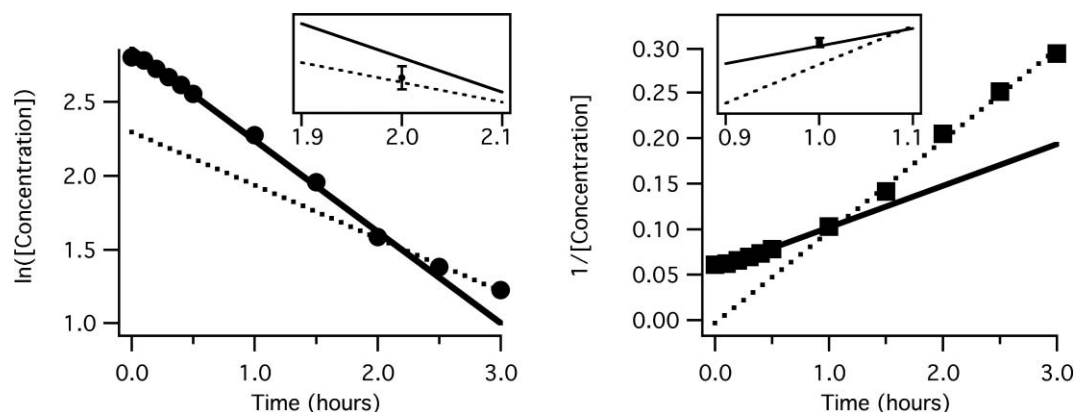
expression is meaningless. If percent composition is used, the resulting expression does not accurately reflect the consequences of increasing the milling load without increasing the vessel size (which results in a decrease in reaction rate). We have found that reaction rates can be examined by expressing the concentration of reactants and products in terms of mass/free volume.<sup>52</sup> Here the free volume is the volume of the milling container not occupied by balls, reactants, or products. This value is calculated by converting the masses of the reactants, products, and milling media to volumes based on the materials' densities. This volume is subtracted from the container volume to give a free volume. This approach indirectly incorporates the motions available to the milling media. The milling media, for the same mode of milling, in systems with large free volumes will have a greater mean free path than in systems with small free volumes.

We determined the reaction order by generating kinetic plots. Although attrition is quite rapid in a SPEX mill, finely ground cellulose (Avicel) and catalysts were used to minimize the effect of initial particle size. The reaction cannot be zeroth order since reaction rate would be independent of concentration. The concentration of the reactants directly affects the free volume and, subsequently, the motion of the milling media. Higher concentrations result in less motion. In the most severe case the concentration would be so high that no media motion is allowed. A zeroth order model would predict yield in this case - an unphysical prediction. Fig. 5 compares a first and second order plot in this system. The differentiation between first and second order behavior is a little more subtle. Both kinetic plots can be fit to lines representing initial and final kinetics. Although the first order plot gives slightly better linear correlation coefficients, a second order model more accurately describes the data. For example, using  $\text{H}^+$  exchanged, physically delaminated kaolin the linear correlation coefficient for the initial kinetics is  $-0.9986$  for first order kinetics and  $0.9974$  for second order kinetics. In the final kinetic region this coefficient is  $-0.9969$  for first order kinetics and  $0.9952$  for second order kinetics. The important feature is the data point near the intersection of the two regression lines (inset Fig. 5). It does not fall on the first order curve that would be generated by the sum of the two linear fits. It does fall on the curve generated by the two linear second order fits. This behavior was observed for all catalysts listed in Table 1 which summarizes the rates observed in several systems. The uncertainties reported are the standard deviations in the slope of the second-order plot calculated using linear regression. The uncertainty in the time change was determined by propagating these uncertainties through the equation describing the intersection of these lines. Second order behavior has also been observed in the hydrolysis of the glucose dimer cellobiose in super critical water.<sup>53</sup>

It was confirmed that the process was catalytic by performing turnover studies using kaolinite and cellulose in a shaker mill. Two hours of milling time resulted in loss of catalytic efficiency over 5 turnovers. One hour of milling resulted in no loss in catalytic efficacy over 8 turnovers. Although extended milling can induce significant defects in the crystal structure of the catalysts, the active sites on these catalysts are surface protons and should be unaffected by the defect structure of the solid. Prolonged milling may, instead, result in the formation of insoluble polymerization products. In particular,

**Table 1** Second-order rates observed in the catalytic depolymerization of cellulose in a SPEX shaker mill. The column labeled “time change” indicates when the rate changes

	Initial Rate (second order) L g <sup>-1</sup> h <sup>-1</sup>	Second Rate (second order) L g <sup>-1</sup> h <sup>-1</sup>	Time Change (hours)
Kaolinite, physically delaminated, H <sup>+</sup> exchanged	0.0522 ± 0.0022	0.1460 ± 0.0058	1.21 ± 0.14
Kaolinite, H <sup>+</sup> exchanged	0.0464 ± 0.0017	0.0836 ± 0.0054	1.08 ± 0.29
Kaolinite, chemically delaminated	0.0433 ± 0.0013	0.0902 ± 0.0035	1.13 ± 0.15
Kaolinite, physically delaminated	0.0330 ± 0.0013	0.0832 ± 0.0027	1.16 ± 0.11
Kaolinite	0.03240 ± 0.00085	0.0825 ± 0.0056	0.75 ± 0.17
Bentonite	0.0268 ± 0.0015	0.00639 ± 0.00018	1.86 ± 0.18
Aluminium oxide	0.01147 ± 0.00050	0.00230 ± 0.00016	1.383 ± 0.049
Talc	0.00943 ± 0.00014	0.00415 ± 0.00026	3.567 ± 0.029

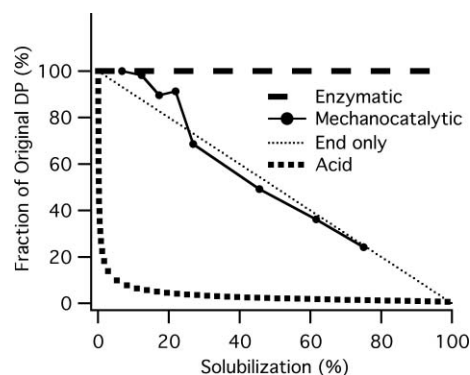


**Fig. 5** A first (left) and second (right) order plot of the hydrolysis of cellulose in a SPEX shaker mill. Both plots show strong linear relations, but the data point near the intersection of the two fit lines (insets) indicates that a second-order process is the more accurate description. The catalyst used was H<sup>+</sup> exchanged, physically delaminated kaolinite.

furfural polymerizes when heated in the presence of an acid. These insoluble by-products would interfere with the interaction between the catalyst and the reactant. Limiting the milling time limits the production of these by-products.

In order to understand the mechanism of cellulose depolymerization, the degree of polymerization (DP) of the insoluble residue was measured. This can be compared to the change in DP observed in acid and enzyme hydrolysis. The three approaches to depolymerization - acid, enzymatic, and mechanocatalytic proceed by quite different kinetics and mechanisms. By examining the change in degree of polymerization of the residue with respect to the fraction of oligomers with a DP < 5 (or degree of solubilization) the role of these factors can be reduced and the approaches can be compared.

Fig. 6 shows the change in DP as a function of degree of solubilization. Values for acid hydrolysis were simulated using a model that all bonds have an equal probability of cleavage.<sup>54</sup> Change in DP from enzyme hydrolysis was taken from the literature.<sup>55</sup> It can be seen that mechanocatalytic depolymerization does not follow a mechanism like acid or enzyme hydrolysis. Mechanocatalytic hydrolysis does not randomly cleave cellulose chains like acid hydrolysis. Initially, depolymerization more closely matches the enzymatic process. The accessibility of surface sites gives rise to the evolution of the degree of polymerization in enzyme hydrolysis.<sup>56</sup> Similarly, mechanocatalysis is dominated by two processes - attrition and hydrolysis. During the initial milling time, cellulose particles are being broken down physically and chemically. There are three main chemical reactions occurring. The reactions are: hydrolysis



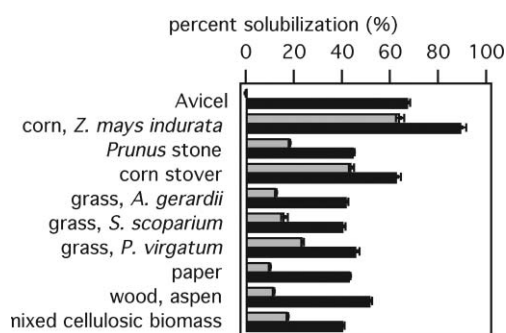
**Fig. 6** Change in the degree of polymerization for the insoluble residue of cellulose hydrolysis as a function of degree of solubilization. The dotted line represents a model where hydrolysis only occurs at the ends of the polymer chain.

catalyzed by the catalyst's surface protons, dehydration by the catalyst, and retro-aldol condensation due to the localized high pressures. The surfaces of these particles are accessible to the catalyst. At a certain point, attrition slows and only the end units of the cellulose chain are accessible. This results in a change in DP that coincides with a model where only the ends of a polymer chain are allowed to react (dashed line in Fig. 6). For the layered catalysts, bentonite, talc, and kaolinites the rate changes (Table 1) when solubilization is between 30 and 40%. This corresponds to the region in Fig. 6 where the DP of the residue matches an end-only hydrolysis model and further corroborates the second-order model.



## Industrial applicability and economics

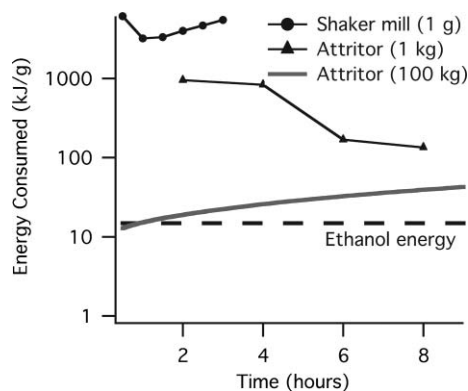
In order for mechanocatalysis to be an effective industrial tool, it must be effective for real world materials. We tested the conversion efficiency for a wide range of relevant cellulose sources. Fig. 7 illustrates the efficiency observed in the depolymerization of cellulose after two hours of milling in a mixer mill. Initial particle size was kept to less than 2 cm. In all cases, the cellulose source and catalyst were reduced to fine powders in 5 to 10 min due to the vigorous nature of the attrition process. Agricultural wastes from corn (corn stover), wood (aspen), and fruit (*Prunus* stone) production were examined; all showed improved water solubility after mechanocatalytic treatment. Commercial and residential waste such as paper and mixed waste from clearing land can also be efficiently treated. The grasses *A. gerardii* (Big Bluestem), *S. scoparium* (Little Bluestem) and *P. virgatum* (Switchgrass) are crops that are of interest for use as a biomass source. It should be noted that 90% of a corn kernel's mass can be converted to soluble matter in a single pass.



**Fig. 7** Unlike current approaches to cellulose hydrolysis, mechanocatalytic hydrolysis is relatively insensitive to feedstock.

Our survey experiments have utilized a SPEX mixer mill, which allows us to rapidly assess the viability of catalytic materials and develop kinetic models for cellulose conversion. We have found that the reaction goes as a second-order process in cellulose. However, this technology is not scalable without significant redesign.<sup>57</sup> Rolling-mode and stirring-mode are among the scalable approaches. Utilizing our DEM model, it was determined that rolling mills do not develop the high pressures encountered in a shaking mill. Processing in a rolling mill produced a product composed primarily of glucose. This suggests that the forces that occur during the milling process are directly related to the composition of the soluble fraction produced. Low forces result in no observable solubilization; increasing the rotational velocity of the roller mill results in compressive forces and a measurable yield of sugars. The most energetic process, shaking-mode, results in an increase in the levoglucosan fraction. This implies that there is a critical energetic region favorable for the production of fructose and glucose.

Attritors are scalable, can be run in a batch or continuous mode, and can produce compressive forces similar to those achieved in a shaker mill (0.4 to 3 GPa, as predicted by our DEM models). We performed a limited number of kilogram-scale tests using a small Union Process attritor. Fig. 8 illustrates the energy costs associated with the two milling technologies. The dashed line is the energy obtainable from the ethanol produced from



**Fig. 8** The energy consumed to produce 1 gram of glucose from 1 gram of cellulose treated in a shaker mill, 1 kg of cellulose treated in an attritor, and modeled consumptions for 100 kg in a large attritor. The dashed line is the energy released by burning the ethanol produced from 1 gram of glucose.

one gram of glucose. It can be seen that the SPEX mill is an energy intensive process. Switching to an attritor allowed the process to be scaled-up by 1000 fold; the result was nearly a 46-fold decrease in the energy consumption as expressed in kJ/gram glucose produced. It was found that conversion in a small attritor required a 4-hour initiation time before the rate became appreciable. The kinetic data from this batch was used, in conjunction with the behavior observed in the shaker mill, to develop a predictive model for a 100 kg batch. The gray trace in Fig. 8 shows the projected energy consumption for an attritor with a 150 hp motor and fast reaction kinetics. It is important to note that the four-hour induction period must be eliminated for this approach to produce glucose at an energy cost lower than the energy released by burning the ethanol prepared from the glucose. This process is energy positive for 0.9 h of milling with a predicted conversion efficiency of 20.2%.

## Conclusions

The natural layered structure of clays is ideally suited for use as a catalyst in milling processes. We have shown that layered structures are particularly suited to mechanocatalytic processes. This opens up a new area for catalyst synthesis. A new set of catalysts based on this paradigm could be synthesized to take advantage of the unique conditions in a ball mill. Using this idea, it may be possible to depolymerize other biopolymers such as chitin or protein as well as synthetic polymers such as nylon, polyethylene terephthalate, polycarbonate, and polylactic acid.

The observation of the glucose dehydration products levoglucosan, levoglucosenone, and 5-hydroxymethylfurfural as well as the retro-aldol condensation product furfural suggest that it will be possible to design mechanocatalysts for the direct conversion of cellulose into these compounds. In fact, many of the synthetic pathways utilized to produce derivatives from these compounds should be directly accessible through solventless milling.

Mechanocatalytic processing of materials has significant advantages over current methods. The best catalyst so far, kaolinite, costs around \$80/ton and can be reused. Any catalyst waste produced is innocuous and there are no toxic solvents needed. Additionally, no heating or high-pressure equipment is

required, simplifying plant design. Mechanocatalytic conversion of cellulose is insensitive to lignin and hemicellulose content allowing any cellulosic biomass source to be utilized. This is an improvement over methods that utilize edible biomass (such as corn) for ethanol production.

## Dedication

This manuscript is dedicated to the memory of Glenn T. Blair (1945–2009).

## Acknowledgements

We thank Agricol Corporation (Madison, WI) for supplying samples of Big Bluestem, Little Bluestem, and Switch grass; IMERYS (Roswell, GA) for supplying samples of physically delaminated kaolinite; and Asbury Carbons (Asbury, NJ) for supplying samples of bentonite and graphite.

## References

- G. W. Huber, S. Iborra and A. Corma, *Chem. Rev.*, 2006, **106**, 4044–4098.
- S. J. B. Duff and W. D. Murray, *Bioresour. Technol.*, 1996, **55**, 1–33.
- A. Demirbas and G. Arin, *Energy Sources*, 2002, **24**, 471–482.
- M. B. Sticklen, *Nat. Rev. Genet.*, 2008, **9**, 433–443.
- T. S. Bayer, D. M. Widmaier, K. Temme, E. A. Mirsky, D. V. Santi and C. A. Voigt, *J. Am. Chem. Soc.*, 2009, **131**, 6508–6515.
- Y. Zhao, W.-J. Lu, H.-T. Wang and D. Li, *Environ. Sci. Technol.*, 2009, **43**, 1565–1570.
- R. Rinaldi, R. Palkovits and F. Schuth, *Angew. Chem., Int. Ed.*, 2008, **47**, 8047–8050.
- T. Iwaya, S. Tokuno, M. Sasaki, M. Goto and K. Shibata, *J. Mater. Sci.*, 2008, **43**, 2452–2456.
- J. Shabtai, X. Xiao and W. Zmierzczak, *Energy Fuels*, 1997, **11**, 76–87.
- R. W. Thring and J. Breau, *Fuel*, 1996, **75**, 795–800.
- T. Ohta, *Appl. Energy*, 2000, **67**, 181–193.
- A. Karpinska, C. Kajdas and K. i. Hiratsuka, *Tribologia*, 2006, **37**, 21–37.
- C. Kajdas and A. Karpinska, *Tribologia*, 2005, **36**, 125–141.
- Y. Momose, *Toraiborojisu*, 2001, **46**, 391–397.
- M. Hasegawa, M. Kimata and I. Takahashi, *Adv. Powder Technol.*, 2007, **18**, 541–554.
- S. Ikeda, T. Takata, M. Komoda, M. Hara, J. N. Kondo, K. Domen, A. Tanaka, H. Hosono and H. Kawazoe, *Phys. Chem. Chem. Phys.*, 1999, **1**, 4485–4491.
- S. Ikeda, T. Takata, T. Kondo, G. Hitoki, M. Hara, J. N. Kondo, K. Domen, H. Hosono, H. Kawazoe and A. Tanaka, *Chem. Commun.*, 1998, 2185–2186.
- S. Murakami, M. Tabata and J. Sohma, *J. Appl. Polym. Sci.*, 1984, **29**, 291–298.
- C. Kajdas, K. Hiratsuka and A. Borkowska, *Tribologia*, 2004, **35**, 11–25.
- T. Shirasaki, *Shikizai Kyokaishi*, 1972, **45**, 737–743.
- S. Murakami, M. Tabata, J. Sohma and M. Hatano, *J. Appl. Polym. Sci.*, 1984, **29**, 3445–3455.
- E. Barraud, S. Begin-Colin, G. Le Caer, O. Barres and F. Villieras, *J. Alloys Compd.*, 2008, **456**, 224–233.
- M. K. Beyer and H. Clausen-Schaumann, *Chem. Rev. (Washington, DC, U. S.)*, 2005, **105**, 2921–2948.
- V. V. Boldyrev and K. Tkacova, *J. Mater. Synth. Process.*, 2000, **8**, 121–132.
- P. G. Fox, *J. Mater. Sci.*, 1975, **10**, 340–369.
- S. Granick and S. C. Bae, *Nature*, 2006, **440**, 160–161.
- S. Kipp, V. Sepelak and K. Dieter Becker, *Chem. Unserer Zeit*, 2005, **39**, 384–392.
- B. Kubias, M. J. G. Fait and R. Schloegl, *Handb. Heterog. Catal. (2nd Ed.)*, 2008, **1**, 571–583.
- V. I. Levitas, *Phys. Rev. B: Condens. Matter Mater. Phys.*, 2004, **70**, 184118.
- B. Rodríguez, A. Bruckmann, T. Rantanen and C. Bolm, *Adv. Synth. Catal.*, 2007, **349**, 2213–2233.
- B. M. Rosen and V. Percec, *Nature*, 2007, **446**, 381–382.
- L. Takacs, *Hyperfine Interact.*, 1997, **111**, 245–250.
- Z. V. Todres, in *Organic Mechanochemistry and Its Practical Applications*, CRC Taylor and Francis, Boca Raton, FL, 2006, pp. 61–102.
- F. K. Urakaev and V. V. Boldyrev, *Powder Technol.*, 2000, **107**, 93–107.
- F. K. Urakaev and V. V. Boldyrev, *Powder Technol.*, 2000, **107**, 197–206.
- K. Wieczorek-Ciurowa and K. Gamrat, *Mater. Sci.*, 2007, **25**, 219–232.
- H. Yang and P. G. McCormick, *Trans. Mater. Res. Soc. Jpn.*, 1994, **14A**, 617–620.
- I. J. Lin and S. Nativ, *Mater. Sci. Eng.*, 1979, **39**, 193–209.
- G. Kaupp, *CrystEngComm*, 2009, **11**, 388–403.
- L. S. Esteban and J. E. Carrasco, *Powder Technol.*, 2006, **166**, 139–151.
- D. Schell and C. Harwood, *Appl. Biochem. Biotechnol.*, 1994, **45–46**, 159–168.
- V. S. P. Bitra, A. R. Womac, N. Chevanan, P. I. Miu, C. Igathinathane, S. Sokhansanj and D. R. Smith, *Powder Technol.*, 2009, **193**, 32–45.
- C. Suryanarayana, *Prog. Mater. Sci.*, 2001, **46**, 1–184.
- K. Tsunematsu and H. Tateyama, *J. Am. Ceram. Soc.*, 1999, **82**, 1589–1591.
- K. Arata, *Appl. Catal., A*, 1996, **146**, 3–32.
- J. B. Taylor, *Trans. Faraday Soc.*, 1957, **53**, 1198–1203.
- M. L. Sanz, J. Sanz and I. Martínez-Castro, *J. Chromatogr., A*, 2004, **1059**, 143–148.
- J. N. Chheda, Y. Roman-Leshkov and J. A. Dumesic, *Green Chem.*, 2007, **9**, 342–350.
- Y. Roman-Leshkov, J. N. Chheda and J. A. Dumesic, *Science*, 2006, **312**, 1933–1937.
- J. Kano and F. Saito, *Powder Technol.*, 1998, **98**, 166–170.
- S. Yariv and I. Lapides, *J. Mater. Synth. Process.*, 2000, **8**, 223–233.
- S. M. Hick, C. Griebel and R. G. Blair, *Inorg. Chem.*, 2009, **48**, 2333–2338.
- M. Sasaki, M. Furukawa, K. Minami, T. Adschiri and K. Arai, *Ind. Eng. Chem. Res.*, 2002, **41**, 6642–6649.
- R. Simha, *J. Appl. Phys.*, 1941, **12**, 569–578.
- Y. H. P. Zhang and L. R. Lynd, *Biomacromolecules*, 2005, **6**, 1510–1515.
- Y. H. P. Zhang and L. R. Lynd, *Biotechnol. Bioeng.*, 2004, **88**, 797–824.
- G. Janke, A. Frenzel and G. Schmidt-Naake, *Chem. Eng. Technol.*, 1999, **22**, 997–1000.

# Telomerization of butadiene with starch in water: role of the surfactants

Julien Mesnager,<sup>a,b,c</sup> Claude Quettier,<sup>c</sup> Anne Lambin,<sup>c</sup> Franck Rataboul,<sup>a,b</sup> Alain Perrard<sup>a,b</sup> and Catherine Pinel<sup>\*a,b</sup>

Received 2nd November 2009, Accepted 14th December 2009

First published as an Advance Article on the web 27th January 2010

DOI: 10.1039/b922781d

Nowadays, the preparation of bio-based polymers remains a challenging issue. The modification of starch by hydrophobic chemical substitutions results in an innovative material. We introduced the hydrophobic part of the derivative *via* catalytic butadiene telomerization using exclusively water as solvent in the presence of surfactants. In this paper, we describe the influence of the nature of the surfactant on the reaction, CTAB (cetyltrimethylammonium bromide) giving the best reactivity. Moreover, some physicochemical properties of modified starches are evaluated showing their hydrophobic behaviours.

## Introduction

Starch is an abundant and inexpensive natural polymer that is widely used as a raw material in the paper, textile and pharmaceutical industries. For such applications, the hydrophobic or hydrophilic character of starch must be tuned, for example for its introduction into polymer matrices. Hydrophobic starches are prepared by formation of an ether or ester from anhydride acetic, fatty acid derivatives or Michael type addition with routes using un-friendly stoichiometric reagents and base reactants.<sup>1–3</sup>

The telomerization of butadiene with alcohols is a green route for the production of ethers catalyzed by palladium complexes. This reaction is 100% atom efficient. Recent studies report the development of new catalytic systems highly efficient for the telomerization of butadiene or isoprene with polyols such as ethylene glycol, glycerol, mono or disaccharides.<sup>4–19</sup> Recently, our group has introduced a catalytic route based on this telomerization reaction to increase the hydrophobic character of starch (Scheme 1).<sup>20–23</sup> We recently reported an efficient method operating under mild conditions (low temperature and butadiene pressure) under heterogeneous conditions: the hydrosoluble complex was efficient enough to modify the solid starch.<sup>23</sup> In this last study, the reaction was performed at 50 °C in water with dimethyl-isosorbide (DMI) as a green co-solvent and in the presence of the water-soluble Pd-catalyst  $[(\pi\text{-allyl})\text{Pd}(\text{TPPTS})_2]\text{Cl}$  [TPPTS = tris(*m*-sulfonato)phenyl phosphine trisodium salt, Fig. 1]. Particularly, we showed that the introduction of Na<sub>2</sub>SO<sub>4</sub> allowed the reaction to be performed at 50 °C without provoking swelling of starch granules. Hydrophobic starch can thus be easily separated from the reaction medium by simple filtration which is classically applied in starch processes. DMI was also introduced to prevent the use of alcohol co-solvent.

The progress of this kind of reaction is evaluated by the degree of substitution (DS) that is defined as the average number of octadienyl chain per anhydroglycosidic unit (AGU) and is determined by liquid NMR analysis. In our recent study, a DS of 0.05 was obtained corresponding to a turn over number (TON) of 550 and 60% conversion of butadiene.<sup>23</sup> This DS is high enough to confer to the materials strong hydrophobic properties and low enough to process the materials in granular state.

In order to enhance the green character of this transformation, we wish to avoid the use of an organic solvent. Ideally, the reaction should be carried out with a neat substrate as recently reported by the group of Weckhuysen using glycerol as the solvent and the nucleophile.<sup>8</sup> However, this approach is not possible with solid starch as substrate. Mortreux *et al.* reported the telomerization of butadiene with sucrose in aqueous solution but an excess of telogen is essential to get the reaction at 80 °C.<sup>24</sup> Moreover, modest activity was reported for the telomerization of butadiene with starch in pure water as the reaction media and we envisaged the addition of surfactants to circumvent this drawback.<sup>23</sup> Very few reports are dealing with the use of surfactants in telomerization.

Here we wish to report the use of surfactants with adjusted catalytic systems to avoid the use of organic co-solvents with aqueous mixture without decreasing the efficiency of the reaction. Some physical properties of the modified starch will also be presented.

## Results and discussion

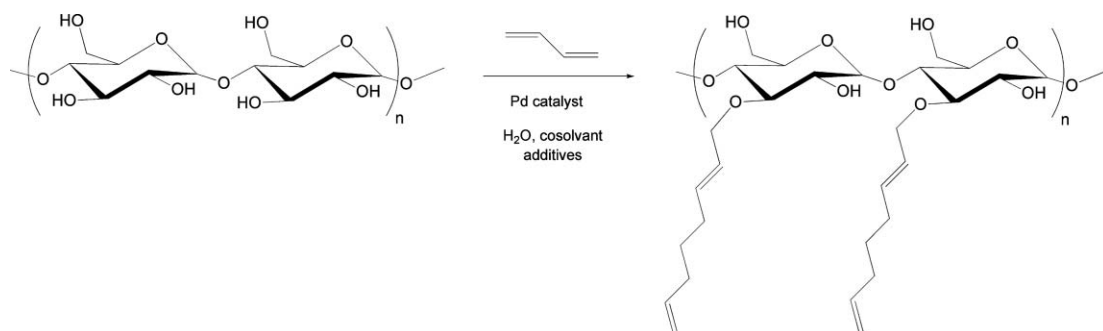
### Butadiene telomerization with starch in the presence of surfactants

**Choice of surfactant.** Monfler *et al.* reported the efficient use of surfactants for butadiene telomerization with water to improve mass transfers in a pure aqueous media.<sup>25–27</sup> Indeed, it was shown that the formation of micelles or colloids increased the solubilisation of butadiene in the water solution thus playing the role of the organic co-solvent. In their reports, several neutral, cationic and anionic surfactants were used in combination with water-soluble phosphines. The best results were obtained with

<sup>a</sup>Université de Lyon, F-69622, Lyon, France

<sup>b</sup>Université Lyon 1; CNRS; UMR 5256, Institut de Recherches sur la Catalyse et l'Environnement de Lyon, 2 avenue Albert Einstein, F-69626, Villeurbanne, France. E-mail: catherine.pinel@ircelyon.univ-lyon1.fr; Tel: 33(4) 7244 5478

<sup>c</sup>Roquette Frères, 62080, LESTREM Cedex, France



Scheme 1 Telomerization of starch with butadiene.

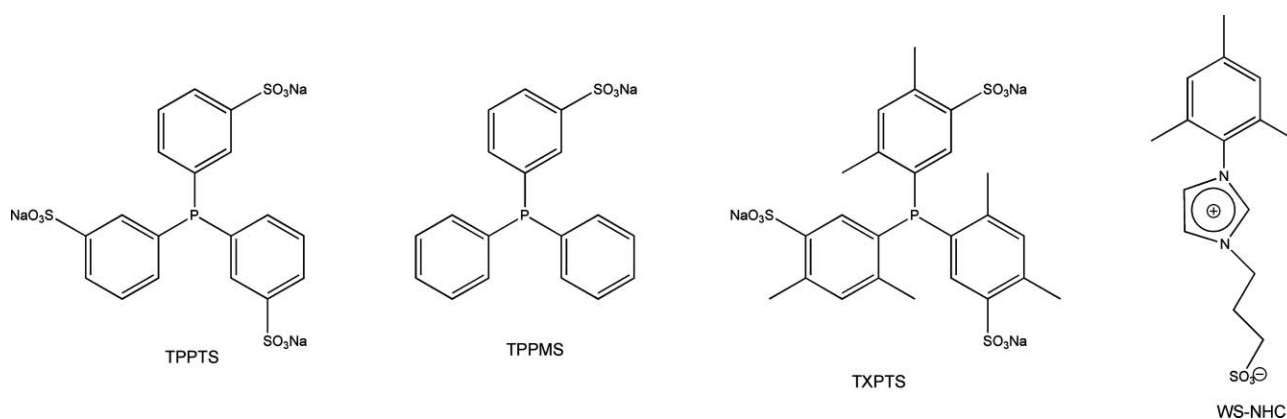


Fig. 1 Hydrosoluble phosphine and NHC ligands used for the telomerization of butadiene with starch.

cationic surfactants or neutral ones like  $C_{12}H_{25}(OCH_2CH_2)_{23}OH$  (DPEG) while anionic surfactants inhibited the reaction.<sup>25</sup>

As introduced above, we showed in our previous study that DMI allowed the reaction to proceed with the same efficiency ( $DS = 0.05$ , butadiene conversion = 60–67%) as with *i*PrOH, which is the classical co-solvent used for this reaction. Interestingly, we also showed that, even in pure water, the reaction was possible but much lower DS and conversion were obtained due to the negligible solubility of butadiene in pure water (Table 1, entries 1–3).<sup>23</sup>

It was estimated that only 2% of introduced butadiene was solubilized in the solution.<sup>28</sup>

**Table 1** Telomerization of butadiene with starch under various conditions<sup>a</sup>

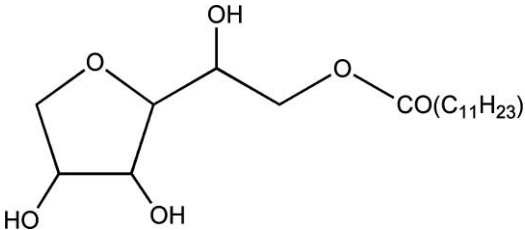
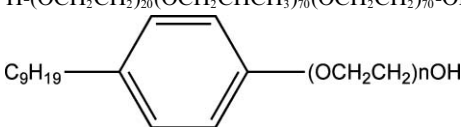
Entry	Co-solvent/ V mL <sup>-1</sup>	Surfactant	DS	Butadiene Conv. (%)
1	<i>i</i> PrOH/5	—	0.05	67
2	DMI/5	—	0.05	60
3	—	—	0.02	30
4 <sup>b</sup>	—	$CH_3CH_2(CH_2CH_2)_x-$ ( $OCH_2CH_2$ ), OH, DPEG	0.065	87

<sup>a</sup> 64 g of dry starch, 3.2 g of butadiene (0.15 equiv./AGU), 100 mL of water, 0.5[( $\pi$ -allyl)PdCl]<sub>2</sub> + 2TPPTS ([Pd] = 0.4%mol), 8 g of Na<sub>2</sub>SO<sub>4</sub>, 1.38%wt of NaOH, 50 °C, 24 h. <sup>b</sup> [DPEG] =  $5 \times 10^{-3}$  mol L<sup>-1</sup>, AGU = anhydroglucosidic unit.

Based on the work of Monflier *et al.*, we wish to perform the telomerization reaction in pure water but in the presence of a small amount ( $5 \times 10^{-3}$  mol L<sup>-1</sup>) of a neutral surfactant such as polyethylene-block-poly(ethylene glycol) DPEG ( $M_n \sim 1400$ ). Under these new reaction conditions, we observe that the introduction of a neutral surfactant leads to a greater DS and a significantly higher butadiene conversion after 24 h (Table 1, entry 4), showing the possibility of running even more efficiently this reaction in the absence of any organic co-solvent. The use of a surfactant presents the advantage of getting an organic solvent-free reaction mixture at the end of the reaction and therefore avoiding a separation step. Under the reaction conditions reported here (50 °C), we did not observe any product issued from hydrodimerization. We previously checked carefully for the formation of octadienol during the telomerization of butadiene with methanol but this product was not detected (NMR or GC analysis).<sup>29</sup> It has to be acknowledged that in their work, Monflier *et al.* performed the hydrodimerization at 85 °C and in the presence of carbonate (formed *in situ* from amine and CO<sub>2</sub>) that is essential to produce octadienol.<sup>25</sup>

Then, a comparative study with a series of various neutral and cationic commercial surfactants was performed. The surfactants having a range of hydrophilic lipophilic balance (HLB), and chemical functions have been evaluated. Moreover, anionic surfactants have been omitted due to their inefficiency established by Monflier *et al.*<sup>27</sup> The reactions were run at 50 °C, over 6 h using 0.15 equiv./AGU of butadiene yielding to a  $DS_{max} = 0.075$ . The palladium content based on butadiene was 0.4%mol

**Table 2** Telomerization of butadiene with starch: influence of the nature of surfactant<sup>a</sup>

Entry	Surfactant	$M_n$	HLB <sup>b</sup>	DS	Butadiene Conv (%)
1	CH <sub>3</sub> CH <sub>2</sub> (CH <sub>2</sub> CH <sub>2</sub> ) <sub>x</sub> (OCH <sub>2</sub> CH <sub>2</sub> ) <sub>n</sub> OH DPEG	1400	10	0.05	60
2	C <sub>18</sub> H <sub>35</sub> (OCH <sub>2</sub> CH <sub>2</sub> ) <sub>n</sub> OH (n ~ 20) BRIJ <sup>®</sup> 98	1150	15	0.075	100
3		346	8	0.01	13
4	SPAN <sup>®</sup> 20	5800	7-9	0.04	47
5	H-(OCH <sub>2</sub> CH <sub>2</sub> ) <sub>20</sub> (OCH <sub>2</sub> CHCH <sub>3</sub> ) <sub>70</sub> (OCH <sub>2</sub> CH <sub>2</sub> ) <sub>70</sub> -OH Pluronic <sup>®</sup> P-123	1982	17	0.075	100
6	 IGEPAL <sup>®</sup> CO-890 C <sub>16</sub> H <sub>33</sub> NMe <sub>3</sub> Br CTAB	364	21.4	0.07	93

<sup>a</sup> 64 g of dry starch, 3.2 g of butadiene (0.15 equiv./AGU), 100 mL of water, [( $\pi$ -allyl)Pd(TPPTS)<sub>2</sub>] ([Pd] = 0.4%mol), 8 g of Na<sub>2</sub>SO<sub>4</sub>, 1.38%wt of NaOH, 5 × 10<sup>-3</sup> mol L<sup>-1</sup> of surfactant, 50 °C, 6 h. <sup>b</sup> Data obtained from Sigma-Aldrich.

corresponding to 0.04%wt based on dry starch. The degree of substitution of starch and the butadiene conversion are reported in Table 2.

In these conditions, the neutral DPEG, SPAN<sup>®</sup> 20 and Pluronic<sup>®</sup> P-123 surfactants gave low to acceptable results with DS from 0.01 to 0.05 and butadiene conversion from 13 to 60% (entries 1, 3, and 4). However, the neutral surfactants BRIJ<sup>®</sup> 98 and IGEPAL<sup>®</sup> CO-890 as well as the cationic cetyltrimethylammonium bromide (CTAB) surfactant gave very good results with DS up to 0.08 corresponding to full butadiene conversion (entries 2, 5 and 6). It is clear that, in the case of neutral surfactants, the butadiene conversion tended to increase with the HLB (hydrophilic lipophilic balance) from 13% (HLB = 8) up to 100% (HLB > 15). It is known that surfactants with a HLB value greater than 8 are water soluble and are able to solubilize a hydrophobic compound above the critical micellar concentration of the surfactant (oil-in-water emulsion).<sup>30</sup> Here, the formation of butadiene/water emulsion during the reaction has not been checked; however, since the best results were obtained with HLB > 15, the efficiency of these additives seemed to correlate with their ability to solubilize butadiene in water.

The nature of the hydrophilic part of the surfactant has an influence on the performances. Indeed, Pluronic<sup>®</sup> P-123 and SPAN<sup>®</sup> 20 have a similar HLB value (7–10) but a very different efficiency corresponding to 47 and 13% butadiene conversion respectively. The hydrophilic part influences the size and the geometry of the micelle<sup>27</sup> and thus the efficiency of the transfer. In this way, the block-copolymer Pluronic<sup>®</sup> P-123 appeared to be more efficient compared to SPAN<sup>®</sup> 20 that can be saponified under the reaction conditions,<sup>31</sup> and can also react with butadiene to give the corresponding octadienyl ether

although this by-product could not be identified in the reaction mixture.<sup>27</sup> Concerning the block-copolymer Pluronic<sup>®</sup> P-123, the maximum solubility in water (1%wt) is lower than the molar concentration we used experimentally (2.4%wt).

The cationic surfactant, CTAB, is almost as efficient as neutral BRIJ<sup>®</sup> and IGEPAL<sup>®</sup> surfactants, giving a DS of 0.07 and 93% of butadiene conversion. This surfactant has a low critical micelle formation temperature (20–25 °C) that is fully compatible with starch modification.

**Adjusted catalytic systems.** To attempt to run this reaction with a lower palladium concentration, we then studied the influence of the catalytic complex considering several ligands and palladium precursors. For that, we used a series of water soluble phosphines such as TPPMS [mono(*m*-sulfonato)phenyl phosphine sodium salt],<sup>32</sup> TXTPS [4,6-dimethyltris(*m*-sulfonato)phenyl phosphine trisodium salt]<sup>33</sup> and P(CH<sub>2</sub>OH)<sub>3</sub>, as well as the water soluble N-heterocyclic carbene 1-(3-sulfonatopropyl)-3-mesityl imidazo-2-ylidene<sup>29,34</sup> (WS-NHC) (Fig. 1). Indeed we showed in one of our recent studies on telomerization of butadiene with MeOH, the high efficiency of the water soluble complexes [( $\pi$ -allyl)Pd(TPPTS)<sub>2</sub>]Cl and [( $\pi$ -allyl)Pd(TPPMS)<sub>2</sub>]Cl as well as the combination [( $\pi$ -allyl)PdCl]<sub>2</sub>/TXTPS.<sup>32</sup>

In the present study, these ligands were associated with [( $\pi$ -allyl)PdCl]<sub>2</sub> or [Pd(OAc)<sub>2</sub>] as palladium precursors, in combination with the two surfactants that gave the best results with TPPTS: the neutral IGEPAL<sup>®</sup> CO-890 and the cationic CTAB. The results are summarized in Table 3.

In the presence of CTAB surfactant, neither the hydrosoluble phosphine P(CH<sub>2</sub>OH)<sub>3</sub> nor the N-heterocyclic carbene led to a

**Table 3** Telomerization of butadiene with starch using surfactants: influence of various catalytic systems<sup>a</sup>

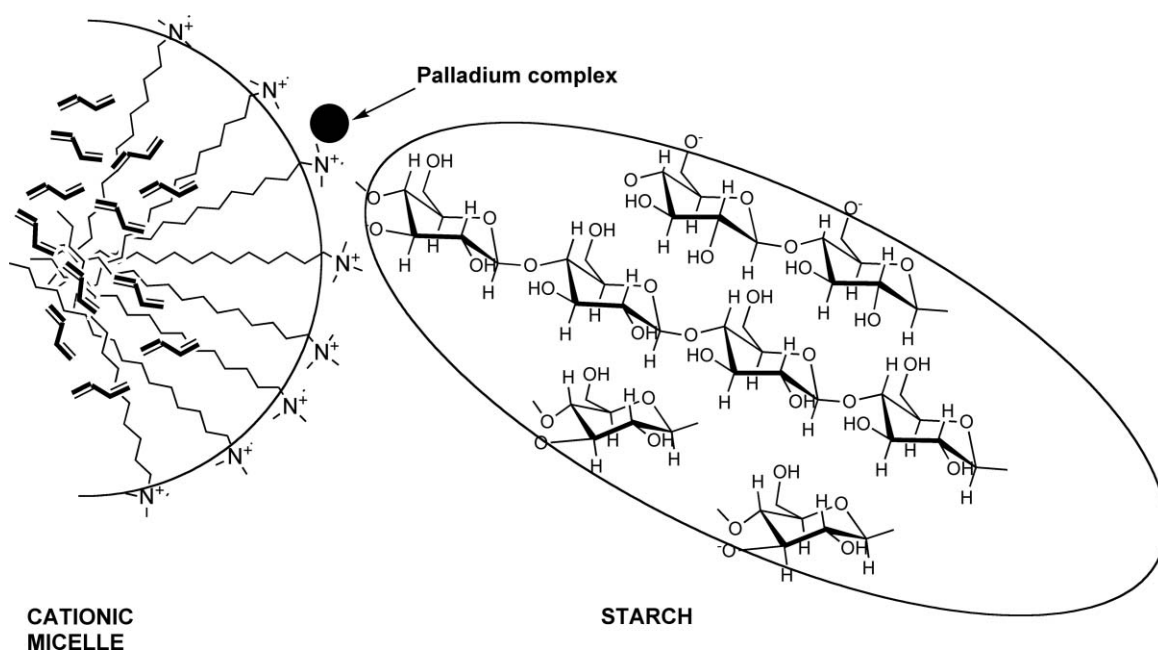
Entry	Catalytic system	Surfactant	DS	Butadiene conv (%)	TON	TOF/h <sup>-1</sup>
1	$[(\pi\text{-allyl})\text{Pd}(\text{TPPTS})_2]\text{Cl}$	IGEPAL <sup>®</sup> CO-890	0.03	38 <sup>b</sup>	180	63
			0.05	38	330	55
2	$[(\pi\text{-allyl})\text{Pd}(\text{TPPMS})_2]\text{Cl}$	IGEPAL <sup>®</sup> CO-890	0.015	20 <sup>b</sup>	200	33
3	0.5 $[(\pi\text{-allyl})\text{PdCl}_2]/\text{TXTPS}$	IGEPAL <sup>®</sup> CO-890	0.02	27 <sup>b</sup>	270	45
4	$[\text{Pd}(\text{OAc})_2]/3 \text{ TPPTS}$	CTAB	0.055	42 <sup>b</sup>	420	53
5	$[(\pi\text{-allyl})\text{Pd}(\text{TPPTS})_2]\text{Cl}$	CTAB	0.05	38 <sup>b</sup>	370	62
6	$[(\pi\text{-allyl})\text{Pd}(\text{TPPMS})_2]\text{Cl}$	CTAB	0.08	59	590	74
7	0.5 $[(\pi\text{-allyl})\text{PdCl}_2]/\text{TXTPS}$	CTAB	0.05	38	380	63
8	$[\text{Pd}(\text{OAc})_2]/3 \text{ PPh}_3$	CTAB	0.02	18	180	7
9	0.5 $[(\pi\text{-allyl})\text{PdCl}_2]/\text{P}(\text{CH}_2\text{OH})_3$	CTAB	0	0	0	0
10	$[\text{Pd}(\text{OAc})_2]/\text{WS-NHC}$	CTAB	0	0	0	0

<sup>a</sup> 64 g of dry starch, 0.27 equiv./AGU of butadiene ( $\text{DS}_{\text{max}} = 0.13$ ), 100 mL of water,  $[\text{Pd}] = 0.1\%$ mol, 8 g of  $\text{Na}_2\text{SO}_4$ , 1.38%wt of NaOH, 0.05 mol L<sup>-1</sup> of surfactant, 50 °C, 6 h. <sup>b</sup> 0.15 equiv./AGU of butadiene ( $\text{DS}_{\text{max}} = 0.075$ ).

reaction (entries 9 and 10). We previously observed that for the butadiene telomerization of methanol, the activity of complex prepared from hydrosoluble N-heterocyclic carbene decreased strongly in the presence of water.<sup>29</sup> This is probably due to the low stability of this complex in water medium and the presence of surfactant should not affect this behaviour. In the case of the phosphine  $\text{P}(\text{CH}_2\text{OH})_3$ , the inefficiency was previously reported for the telomerization of isoprene with ammoniac.<sup>35</sup> The conversion achieved with  $\text{PPh}_3$ -based complex is very low due to its insolubility in water (entry 8). On the other hand, as far as sulfonated hydrosoluble phosphines were considered, the monosulfonated TPPMS was more efficient than the two trisulfonated phosphines TPPTS and TXTPS with DS and TOF up to 0.08 and 74 h<sup>-1</sup>, respectively (entries 5–7). The nature of the palladium precursor did not affect the activity of the catalytic system and similar results were achieved with  $[\text{Pd}(\text{OAc})_2]$  or  $[(\pi\text{-allyl})\text{PdCl}_2]$  as palladium source (entries 4 and 5). The relative reactivity was affected by the nature of the surfactant. Indeed, with neutral IGEPAL<sup>®</sup>, the complex

chelated to TPPTS ligand more efficiently than TXTPS and TPPMS-based complexes (entries 1–3), with DS and TOF up to 0.03 and 63 h<sup>-1</sup>, respectively. Moreover, the butadiene conversions achieved in the presence of IGEPAL<sup>®</sup> were slightly lower than those obtained with CTAB (20–38% and 38–59% respectively).

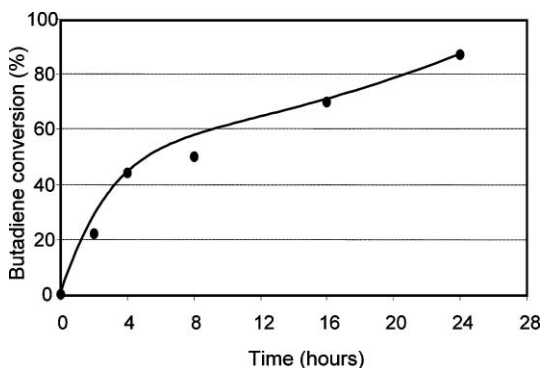
Considering these results, it seems that an optimized combination between the surfactant and the ligand exists depending on the nature of the surfactant (neutral or cationic). Similar phenomena were previously reported by Monflier *et al.* for the hydrodimerization of butadiene.<sup>25</sup> Whatever the surfactant, an oil-in-water emulsion should be formed with high concentration of butadiene within the hydrophobic inner core of the micelle and the water soluble palladium complexes should be located at the micelle-water interface or in the so-called palisade layer. Due to the size of the starch granules, the reaction has to take place outside of the micelle by butadiene or complexed-butadiene diffusion from the inner core, and can be limited by diffusion phenomenon of the different species (Fig. 2). However, as the

**Fig. 2** Schematic representation of interactions between starch and micelles.

reaction is performed in basic conditions, the starch is partly negatively charged and should interact closely with micelles formed from cationic surfactant.

With the system  $[(\pi\text{-allyl})\text{Pd}(\text{TPPMS})_2]\text{Cl}/\text{CTAB}$ , we minimized the concentration of catalyst. When 0.04%mol of palladium was introduced, a DS of 0.11 was obtained with a high conversion of 83% after 24 h of reaction ( $\text{TOF} = 86 \text{ h}^{-1}$ ).

The influence of reaction time in these conditions showed that the reaction rate decreased after 4 h (44% of conversion) (Fig. 3). This could be explained by diffusion limitation of butadiene in the solution when a significant amount has reacted. A concentration of 0.01%mol led to a material with a DS of 0.055 and a lower conversion of butadiene (40%) after 24 h. However, TOF was significantly increased to  $167 \text{ h}^{-1}$  ( $\text{TON} = 4000$ ). Under such optimized conditions, the catalytic activity is even better than that previously achieved in  $\text{H}_2\text{O}/i\text{PrOH}$  medium. At this stage, we evaluated the possibility to reuse the catalytic system in a second run. Indeed, after isolation of starch by filtration, the filtrate containing salts, surfactant and the soluble catalytic system, can be engaged in a second cycle. Unfortunately, under similar conditions, only 5% conversion of butadiene was achieved. It is noteworthy that efficient recycling of catalysts in telomerization reactions was previously reported with ethylene glycol or  $\text{NH}_3$  as the nucleophile in biphasic conditions.<sup>6,7,35,36</sup> In every case, excess of phosphine ( $\text{P}/\text{Pd} > 2$ ) was reported while in the present work, we performed the reaction in the presence of only 2 equivalents of monophosphine per palladium. Degradation of the catalyst during the separation steps could occur and further studies have to be carried out to study the potential reuse of the catalytic system.

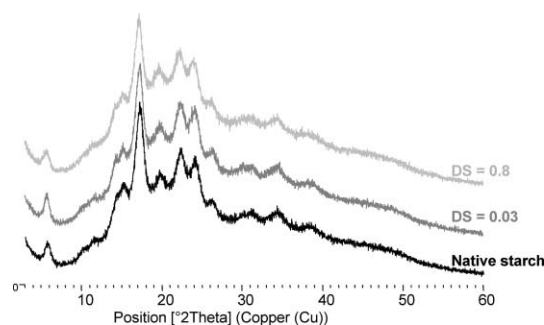


**Fig. 3** Influence of reaction time on the conversion of butadiene. 64 g of dry starch, 0.27 equiv./AGU of butadiene, 100 mL of water,  $[(\pi\text{-allyl})\text{Pd}(\text{TPPMS})_2]\text{Cl}$   $[\text{Pd}] = 0.04\%$ mol, 8 g of  $\text{Na}_2\text{SO}_4$ , 1.38%wt of  $\text{NaOH}$ ,  $0.05 \text{ mol L}^{-1}$  of CTAB,  $50^\circ\text{C}$ .

Even low DS's impart hydrophobic properties to starch as determined by physicochemical analysis.

#### Physicochemical properties of starch modified with octadienyl chains

**X-Ray diffraction analysis.** We have previously shown that under mild conditions the texture of native potato starch was maintained after the reaction.<sup>23</sup> In order to check that the crystallinity was not affected by the transformation, X-ray diffraction spectra of native and telomerized starch with different DS were performed. It is clear from Fig. 4 that there is



**Fig. 4** X-Ray diffraction patterns of native and modified starches.

no difference between the spectra of the native starch and those of the substituted starch even with significant DS ( $\text{DS} = 0.8$ ) indicating that the crystalline structure was not affected by the reaction conditions.<sup>37</sup>

**Rheological properties.** Among the most important functional properties of starches are their thermal and pasting properties. The pasting behaviour is usually studied by observing changes in the viscosity of a starch system based on rheological principles. The viscosity of the modified starches was evaluated by heating a suspension of the material in water (7% dry basis, total mass 28 g) for 15 min. Before the analysis, the material was carefully washed with deionized water to remove the remaining salts (conductivity  $< 50 \mu\text{S}$ ) and surfactants.

Indeed, salt and surfactant can have an influence on the viscosity measurements. In the case of starch modified with octadienyl chains, the viscosity profiles present high swelling temperatures, no viscosity peak and no retrogradation phenomenon. Viscosity increases with time of analysis and are much lower than that for native starch as was already observed.<sup>38</sup> The higher the DS, the lower the viscosity values. High swelling temperatures can be possibly explained by the presence of hydrophobic chains at the surface of the material that prevents water molecules to enter the granules and to diffuse and degrade them. Moreover, the presence of these groups could also prevent the interaction of water molecules with the macromolecules after the splitting, thus avoiding the formation of a gel (no retrogradation).

**Surface properties.** Hydrophobicity of the materials was evaluated by measuring the contact angle formed between water drops and the surface of the modified starch using contact angle measuring system. The surface free energy of the solid was measured from the contact angles of a droplet of various probe liquids (water, ethylene glycol and glycerol) with the surface. The calculations were done using the Owens–Wendt model which allows the separation of the polar (specific component  $\gamma^p$ ) and non-polar contributions (dispersive component  $\gamma^d$ ) of the surface.<sup>39</sup> Higher contact angle values indicate a hydrophobic surface, while lower contact angles will be measured when the sample surface is more hydrophilic, and in the case of a hydrophobic material, the polar component should be low. The contact angle measurements and the surface free energies of modified starch are shown in Table 4.

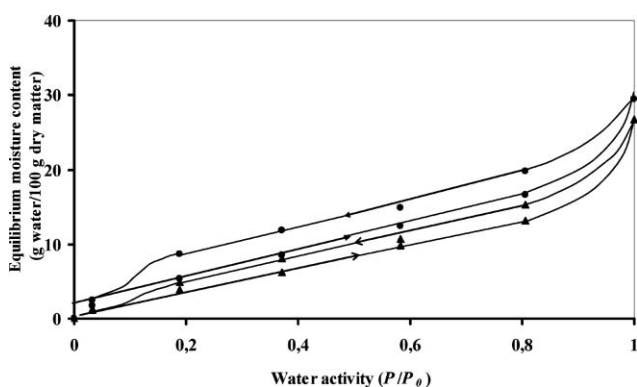
As it can be seen, the DS has a remarkable influence on the hydrophobic character of the modified starches and as it can be expected, increasing the DS decreases the polarity of the surface. For  $\text{DS} > 0.1$  contact angles are greater than  $90^\circ$  with

**Table 4** Surface free energies of starches modified by octadienyl groups estimated from Owens–Wendt method

Entry	DS	$\gamma/\text{mN m}^{-1}$	$\gamma^p/\text{mN m}^{-1}$	$\gamma^d/\text{mN m}^{-1}$	Polarity (%)	Water contact angle/ $^\circ$
1	0.05	512.5	299.6	212.9	71	45
2	0.1	100.0	74.3	25.7	35	99
3	0.3	59.1	3.3	55.8	6	93

quite a low total surface free energy (entries 2 and 3), indicating a hydrophobic character of the material and a low wet ability as previously reported for esterified starches.<sup>40,41</sup>

In parallel, the water adsorption–desorption isotherms were determined at 20 °C for native and modified starches having different DS (DS = 0.05, 0.1 and 0.3). For clarity reasons, Fig. 5 shows the complete measurements for native starch (DS = 0) and one modified starch (DS = 0.3). The water content in samples is given in g of H<sub>2</sub>O per 100 g of dried sample as a function of the relative humidity  $P/P_0$  in the vapour phase.

**Fig. 5** Water adsorption–desorption isotherms at 20 °C of: (●) native starch; (▲) DS = 0.3 modified starch.

All the isotherms develop the same trend. At very low relative pressures close to 0, the adsorption curves must rise steeply and then flatten out for a very linear section in a large range of pressures ( $0.03 < P/P_0 < 0.8$ ) before a significant increase until saturation. The comparison of the four starches reveals that the adsorbed water content decreases as the C<sub>8</sub>H<sub>13</sub> group content in the starch unit increases at any relative humidity. In the course of desorption, the adsorbed water amount decreases with the relative humidity as a straight line parallel to the adsorption branch in the range  $0.2 < P/P_0 < 0.8$ . Finally, branching occurs at a very low relative humidity ( $< 0.2$ ).

These results are quite comparable to those of Luck *et al.*, who studied the water desorption isotherms of cellulose–acetate membranes with different acetyl contents at 10–40 °C.<sup>42,43</sup> More recently, Do *et al.* developed a new model to describe the adsorption and desorption branches of water adsorption in activated carbons, original or acid-treated to make it hydrophilic by increasing the surface functional groups such as carboxylic groups.<sup>44,45</sup> During adsorption, the model is based on the growth of water clusters at the functional groups. The desorption branch resulted from the relaxation of water clusters to form superclusters because of the presence of neighbouring clusters, involving a delay of desorption and thus a larger hysteresis.

We evaluated the hydroxylic group contents present in the four samples and the amount of adsorbed water at particular values of relative humidity:  $P/P_0 = 0^+$ , 0.805 and 1 (Table 5). The intercept obtained from the extrapolation of each adsorption linear region to  $P/P_0 = 0$  allows us to assess the content of water initially adsorbed. As expected, the ratio mol H<sub>2</sub>O/mol OH at  $P/P_0 \neq 0$  decreases from 5.5 to 3.1 when the DS increases from 0 to 0.3, which confirms that the hydrophobic character of starch increases with DS. Moreover, if we link the linear zones of adsorption branches up to  $P/P_0 = 0.805$  to the growth of water clusters, which is reasonable given the same values of the ratios mol H<sub>2</sub>O/mol OH  $\neq 50$  at  $P/P_0 = 0.805$ , the ratios (mol H<sub>2</sub>O) <sub>$P/P_0 = 0.805$</sub> /(mol H<sub>2</sub>O) <sub>$P/P_0 \neq 0$</sub>  leads to a water cluster size of about 10 molecules, value a little greater than the heptamer size given by Do. Moreover, it is worth noting that the amount of water adsorbed at  $P/P_0 = 1$  for the four samples corresponds to that of hydroxylic groups in the fresh samples. This involves the lack of any porosity in the starches, which is not surprising, given the very low specific area of such materials determined from nitrogen adsorption data, *i.e.* less than 1 m<sup>2</sup> g<sup>-1</sup>.<sup>46</sup>

As Luck *et al.* did on the desorption branches, we attempted to estimate the two constants derived from the BET equation from the adsorption branches in the range  $P/P_0 = 0$ –0.4 (Table 5).<sup>42</sup> Whatever the DS, the values for one monolayer of water (g H<sub>2</sub>O/100 g sample)  $W_m$ , are very comparable but they have

**Table 5** Mass balance on hydroxylic groups and adsorbed water. Constants derived from the BET equation

Sample	DS = 0	DS = 0.054	DS = 0.105	DS = 0.3
Mol OH/100 g dry sample	1.85	1.75	1.66	1.38
Mol H <sub>2</sub> O/mol OH at $P/P_0 \neq 0$ ( $\times 100$ )	5.5	4.9	5.7	3.1
Mol H <sub>2</sub> O/mol OH at $P/P_0 = 0.805$ ( $\times 100$ )	50	47	53	53
(Mol H <sub>2</sub> O) <sub><math>P/P_0 = 0.805</math></sub> /(mol H <sub>2</sub> O) <sub><math>P/P_0 \neq 0</math></sub>	9.1	9.5	9.3	17
Mol H <sub>2</sub> O/mol OH at $P/P_0 = 1$ ( $\times 100$ )	89	98	108	107
Water amount of one monolayer (g <sub>H<sub>2</sub>O</sub> /100 g sample) after BET	5.8	5.2	5.5	4.6
BET constant $c^a$	17	16	17	10
$E_1 - E_L$ (kcal mol <sup>-1</sup> )	1.7	1.6	1.7	1.3

<sup>a</sup>  $c = e[(E_1 - E_L)/RT]$ ; water liquefaction heat  $E_L = 10.5$  kcal mol<sup>-1</sup>.



no physical meaning because of the lack of microporosity. Nevertheless, the BET constants  $c$  lead to the evaluation of the adsorption heat  $E_1$  of the water layer in contact with the solid, which slightly decreases from 13 to 12 kcal mol<sup>-1</sup> when the DS increases from 0 to 0.3, indicating the most hydrophobic character of the modified starch.

All these analyses confirmed the hydrophobic character of the modified starches.

## Conclusion

In this study, we have shown that telomerization of butadiene with starch can be performed in pure water with good yields if surfactants are present. In all steps (reaction and work-up) only water was used as the solvent and after optimization almost complete conversion of butadiene was achieved. The best activity was achieved using a cationic surfactant such as CTAB but neutral surfactants having HLB > 15 also displayed high activities. After optimization, TON up to 4000 was achieved with a low active starch substrate. Even at low degree of substitution, the properties of the modified starch were strongly affected and hydrophobic materials which can be useful for specific applications were prepared.

## Experimental

### Generalities

Starches used in this work were food grade quality with relative humidity content of 20%wt for potato starch and 13%wt for maize starch (Roquette Frères). Experiment amounts corresponded to wet starch amounts.  $[(\pi\text{-allyl})\text{PdCl}]_2$  and  $\text{Pd}(\text{OAc})_2$  were purchased from Strem and Aldrich, respectively.  $\text{P}(\text{CH}_2\text{OH})_3$ , TXTPS and the surfactants were purchased from Aldrich. Other sulfonated phosphines were obtained from Strem, Interchim or as a gift from Emile Kuntz. WS-NHC,<sup>29</sup>  $[(\pi\text{-allyl})\text{Pd}(\text{TPPTS})_2]\text{Cl}^{32}$  and  $[(\pi\text{-allyl})\text{Pd}(\text{TPPMS})_2]\text{Cl}^{32}$  were prepared according to the literature. Amounts of NaOH and  $\text{Na}_2\text{SO}_4$  are relative to the weight of dry starch.

Degree of substitution (DS) was defined as the average number of octadienyl chain per anhydroglycosidic unit (AGU). It was obtained from <sup>1</sup>H NMR ( $d_6$  DMSO +  $\text{CF}_3\text{CO}_2\text{H}$ ) as the ratio of protons in the octadienyl chain to the number of C–H protons in one AGU.<sup>20</sup> Maximum DS ( $\text{DS}_{\text{max}}$ ) is 3 for full substitution. Repeated reactions indicated that the accuracy of DS is 0.01.

Butadiene conversion was calculated as the ratio of experimental DS over the  $\text{DS}_{\text{max}}$  which would be obtained at full conversion. For a specific experiment,  $\text{DS}_{\text{max}}$  is equivalent to half the number of equivalents of butadiene per AGU.

NMR was performed on a Bruker 250 spectrometer with deuterated DMSO as solvent with 2 drops of trifluoroacetic acid to displace the signals of hydroxyl groups to the low field region. Chemical shifts are referred to  $\text{SiMe}_4$ . XRD spectra were registered on a Bruker D5005 diffractometer.

### Typical procedure of starch telomerization using a surfactant

Starch (80 g, equivalent to 64 g of dry matter, 0.5 mol of AGU) was suspended in a 70 mL water solution of CTAB (182 mg, 0.5 mmol) with  $\text{Na}_2\text{SO}_4$  (8 g). 30 mL of a NaOH solution

(1.38%wt) were slowly added over 10 min to the suspension under vigorous stirring. The resulting mixture was introduced in a 300 mL autoclave equipped with a heating mantle and mechanical stirring.  $[(\pi\text{-allyl})\text{Pd}(\text{TPPTS})_2]\text{Cl}$  ( $[\text{Pd}] = 0.04\%$ wt) was added. The system was flushed with argon and cooled to  $-30^\circ\text{C}$  using liquid nitrogen. Liquid butadiene (0.3 equiv./AGU) was condensed and the exact mass introduced was determined by weighting. After warming to room temperature, the mixture was heated to  $40^\circ\text{C}$  over 10 min and from  $40^\circ\text{C}$  to  $50^\circ\text{C}$  over 1 h. The reaction was performed at  $50^\circ\text{C}$  under stirring (1800 rpm) for a specified time. After reaction, the system was degassed, purged with argon and the solid was recovered by filtration, washed with distilled water ( $3 \times 100$  mL) and wrung. The resulting wet material was suspended in water and stirred for 30 min. The pH was adjusted to 5–6 by addition of HCl 10%. The solid was then filtered, washed with distilled water ( $2 \times 100$  mL) and dried to give a white powder (97%wt/starting starch).

<sup>1</sup>H NMR (200 Mz,  $d_6$ -DMSO, 25 °C, TMS):  $\delta = 5.74\text{--}5.49$  (3 H), 5.08 (1 H), 5.02–4.91 (2 H), 4.09 (1 H), 3.62 (3 H), 3.34 (2 H), 1.98 (4 H), 1.40 (2 H) ppm. <sup>13</sup>C NMR (200 Mz,  $d_6$ -DMSO, 25 °C, TMS):  $\delta = 138.5, 133.7, 132.9, 126.9, 114.9, 100.2, 78.9, 73.1, 71.7, 71.7, 60.4, 32.6, 31.1, 27.8$  ppm.

**Viscosity profiles.** The RVA parameters were determined using the RVA-4 (Newport Scientific Pvt. Ltd., Australia) with 7%wt (dry basis) starch suspensions in deionized water (total mass 28 g). The temperature profile was set as shown above. The agitation speed was set up as follows: 100 rpm to 500 rpm for the first 10 s, 500 rpm to 960 rpm for the next 10 s, 960 rpm to 160 rpm for the next 10 s then 160 rpm until the end of analysis. In the case of modified starch, the suspension was agitated for 2 h *in situ* and let to deposit for 8 h before the measurements.

**Contact angles.** Before analysis, the starch samples were compressed (1 ton) to form a tablet and dried at  $130^\circ\text{C}$  for 4 h in an oven. The contact angles were measured using a contact angle meter GBX DIGIDROP apparatus with the WINDROP software. Droplets (1  $\mu\text{L}$ ) were deposited on the surface and the evolution of the contact angles was monitored using a CCD camera until equilibrium was reached.

**Water adsorption–desorption isotherms.** The four samples of native and modified starches were previously dried at  $130^\circ\text{C}$  under air for 4 h in an oven. About 1 g of each sample was then placed in a petri cup, weighed and equilibrated successively over aqueous solutions of sulfuric acid with different densities in a desiccator at  $20^\circ\text{C}$  until equilibrium. The relative humidity or pressure of aqueous vapour of air in equilibrium conditions above such acidic aqueous solutions are tabulated.<sup>47</sup> The adsorption branch of isotherm was built by contacting each sample with solutions providing increasing relative humidity values from 0.032 up to 1 (vapor pressure of water at  $20^\circ\text{C}$ :  $P_0 = 17.4$  Torr). The desorption branch was drawn by decreasing the relative humidity  $P/P_0$  from 1 down to 0. Once equilibrium was reached, the equilibrium moisture content of the starch samples was measured gravimetrically by re-weighing the container and the content. Equilibrium was verified to be reached for each relative humidity after three days.

## Acknowledgements

P. Fuertes is warmly acknowledged for helpful discussions. We thank Dr E. Puzenat for help in contact angle measurements, F. Bosselet for X-ray analysis and G. Aubert for technical assistance.

## References

- O. B. Wurzburg, *Food Sci. Technol.*, 1995, **67**, 67.
- W. Jarowenko, *Modif. Starches: Prop. Uses*, 1987, 55.
- D. Bikiaris, J. Aburto, I. Alric, E. Borredon, M. Botev, C. Betchev and C. Panayiotou, *J. Appl. Polym. Sci.*, 1999, **71**, 1089.
- A. Behr, M. Becker, T. Beckmann, L. Johnen, J. Leschinski and S. Reyer, *Angew. Chem., Int. Ed.*, 2009, **48**, 3598.
- A. Behr, J. Leschinski, C. Awungacha, S. Simic and T. Knoth, *ChemSusChem*, 2009, **2**, 71.
- A. Behr and M. Urschey, *J. Mol. Catal. A: Chem.*, 2003, **197**, 101.
- A. Behr and M. Urschey, *Adv. Synth. Catal.*, 2003, **345**, 1242.
- R. Palkovits, I. Nieddu, R. J. M. Klein Gebbink and B. M. Weckhuysen, *ChemSusChem*, 2008, **1**, 193.
- P. J. C. Hausoul, P. C. A. Brujininx, R. J. M. Klein Gebbink and B. M. Weckhuysen, *ChemSusChem*, 2009, **2**, 855.
- R. Palkovits, A. N. Parvulescu, P. J. C. Hausoul, C. A. Kruithof, R. J. M. Klein Gebbink and B. M. Weckhuysen, *Green Chem.*, 2009, **11**, 1155.
- R. Palkovits, I. Nieddu, C. A. Kruithof, R. J. M. Klein Gebbink and B. M. Weckhuysen, *Chem.–Eur. J.*, 2008, **14**, 8995.
- R. Jackstell, A. Grotevendt, D. Michalik, L. El Firdoussi and M. Beller, *J. Organomet. Chem.*, 2007, **692**, 4737.
- R. Jackstell, A. Grotevendt, M. G. Andreu and M. Beller, *Org. Process Res. Dev.*, 2009, **13**, 349.
- A. Grotevendt, R. Jackstell, D. Michalik, M. Gomez and M. Beller, *ChemSusChem*, 2009, **2**, 63.
- S. Bouquillon, F. Henin, J. Muzart and B. Estrine, *Appl. Organomet. Chem.*, 2007, **21**, 945.
- C. Hadad, C. Damez, S. Bouquillon, B. Estrine, F. Henin, J. Muzart, I. Pezron and L. Komunjer, *Carbohydr. Res.*, 2006, **341**, 1938.
- C. Damez, B. Estrine, A. Bessmertnykh, S. Bouquillon, F. Henin and J. Muzart, *J. Mol. Catal. A: Chem.*, 2006, **244**, 93.
- B. Estrine, S. Bouquillon, F. Henin and J. Muzart, *Green Chem.*, 2005, **7**, 219.
- A. Bessmertnykh, F. Henin and J. Muzart, *J. Mol. Catal. A: Chem.*, 2005, **238**, 199.
- C. Donzé, C. Pinel, P. Gallezot and P. L. Taylor, *Adv. Synth. Catal.*, 2002, **344**, 906.
- A. B. Sorokin, S. L. Kachkarova-Sorokina, C. Donzé, C. Pinel and P. Gallezot, *Top. Catal.*, 2004, **27**, 67.
- P. Gallezot, M. Besson, L. Djakovitch, A. Perrard, C. Pinel, A. Sorokin, in *Feedstocks for the Future, Renewables for the Production of Chemicals and Materials* (ed.: J. J. Bozell, M. K. Patel), American Chemical Society, Washington, 2005, pp. 52.
- J. Mesnager, C. Quettier, A. Lambin, F. Rataboul and C. Pinel, *ChemSusChem*, 2010, **2**, 1125.
- I. Pennequin, J. Meyer, I. Suisse and A. Mortreux, *J. Mol. Catal. A: Chem.*, 1997, **120**, 139.
- E. Monflier, P. Bourdauducq, J. L. Couturier, J. Kervennal and A. Mortreux, *Appl. Catal., A*, 1995, **131**, 167.
- E. Monflier, P. Bourdauducq, J. L. Couturier, J. Kervennal and A. Mortreux, *J. Mol. Catal. A: Chem.*, 1995, **97**, 29.
- E. Monflier, P. Bourdauducq, J. L. Couturier, J. Kervennal, I. Suisse and A. Mortreux, *Catal. Lett.*, 1995, **34**, 201.
- At 20 °C, the solubility of butadiene in water is <math>1\text{ g l}^{-1}</math> and at 50 °C the equilibrium vapour pressure is 5 bar.
- J. Mesnager, P. Lammel, E. Jeanneau and C. Pinel, *Appl. Catal., A*, 2009, **368**, 22.
- M. J. Rosen, *Surfactant and Interfacial phenomena*, Wiley-interscience, New-York, 1978.
- C. Larpent, *Techniques de l'ingénieur*, 1995, K342, <http://www.techniques-ingenieur.fr/book/k342/tensioactifs.html>.
- J. Mesnager, E. Kuntz and C. Pinel, *J. Organomet. Chem.*, 2009, **694**, 2513.
- L. R. Moore, E. C. Western, R. Craciun, J. M. Spruell, D. A. Dixon, K. P. Halloran and K. H. Shaughnessy, *Organometallics*, 2008, **27**, 576.
- L. R. Moore, S. M. Cooks, M. S. Anderson, H. J. Schanz, S. T. Griffin, R. D. Rogers, M. C. Kirk and K. H. Shaughnessy, *Organometallics*, 2006, **25**, 5151.
- T. Prinz and B. Driessen-Hölscher, *Chem.–Eur. J.*, 1999, **5**, 2069.
- A. Behr, M. Urschey and V. A. Brehme, *Green Chem.*, 2003, **5**, 198.
- C. Hyun-Wook, L. Jae-Hwang, A. Soon-Chul, K. Byung-Yong and B. Moo-Yeol, *Starch/Staerke*, 2009, **61**, 334.
- M. H. Azizi and G. V. Rao, *Food Hydrocolloids*, 2005, **19**, 739.
- D. K. Owens and R. C. Wendt, *J. Appl. Polym. Sci.*, 1969, **13**, 1741.
- J. Zhou, L. Ren, J. Tong and Y. Ma, *J. Appl. Polym. Sci.*, 2009, **114**, 940.
- H. Chi, K. Xu, X. Wu, Q. Chen, D. Xue, C. Song, W. Zhang and P. Wang, *Food Chem.*, 2008, **106**, 923.
- W. A. P. Luck and K. Rangsrwatananon, *Colloid Polym. Sci.*, 1997, **275**, 964.
- W. A. P. Luck and K. Rangsrwatananon, *Colloid Polym. Sci.*, 1997, **275**, 1018.
- D. D. Do and H. D. Do, *Carbon*, 2000, **38**, 767.
- D. D. Do, S. Junpirom and H. D. Do, *Carbon*, 2009, **47**, 1466.
- M. Włodarczyk and J. Jamroz, *J. Food Eng.*, 2009, **93**, 379.
- Handbook of Chemistry and Physics*, ed. R. C. Weast, CRC press, 55th edn, 1974, p. E-46.

# CH<sub>3</sub>COONa as an effective catalyst for methoxycarbonylation of 1,6-hexanediamine by dimethyl carbonate to dimethylhexane-1,6-dicarbamate†

Da-Lei Sun,<sup>a,c</sup> Shun-Ji Xie,<sup>a</sup> Jian-Ru Deng,<sup>a</sup> Cai-Juan Huang,<sup>a</sup> Eli Ruckenstein<sup>\*b</sup> and Zi-Sheng Chao<sup>\*a</sup>

Received 17th April 2009, Accepted 6th January 2010

First published as an Advance Article on the web 28th January 2010

DOI: 10.1039/b915023b

Methoxycarbonylation of 1,6-hexanediamine (HDA) by dimethyl carbonate (DMC) was carried out, using, for the first time, CH<sub>3</sub>COONa as catalyst. The effects of the solvent, reaction temperature, reaction time, and catalyst amount, were investigated. A yield as high as 99.0% of dimethylhexane-1,6-dicarbamate **2** has been obtained at a temperature of 348 K and a reaction time of 6 h. Mechanistic studies revealed that N-substituted acetamide, as the active intermediate product, and NaOH were first formed *via* the reaction between HDA and CH<sub>3</sub>COONa. A further reaction between the N-substituted acetamide and DMC generated carbamates and methyl acetate, *via* a hexatomic ring intermediate. The CH<sub>3</sub>COONa catalyst was finally recovered through the reaction between NaOH and methyl acetate, which thus completed the catalytic cycle.

## 1. Introduction

Organic carbamates, which are very important starting materials and/or intermediates, have found versatile applications in the production of fine and commodity chemicals<sup>1,2</sup> and in organic synthesis.<sup>1</sup> Currently, the commercial production of carbamates is based mainly on the reaction between alcohols and isocyanates.<sup>3</sup> However, this route is not environmentally friendly, because the industrial production of isocyanates is associated with a high energy input, toxic phosgene as a raw material, and the corrosive hydrochloric acid as a side product.<sup>2</sup> Several phosgene-free processes for the production of organic carbamates have been explored,<sup>4–8</sup> among which the alkoxycarbonylation of amines by alkyl carbonates,<sup>4</sup> particularly dimethyl carbonate (DMC),<sup>5</sup> have received considerable attention. This route appears to be promising, because on the one hand methanol is obtained as the main by-product and on the other hand DMC is non-toxic and can be prepared on a large scale by the oxidative carbonylation of methanol.<sup>9,10</sup> In addition, DMC can be easily handled and is cheap, non-toxic and clean. Thus, if the methoxycarbonylation reaction between an amine and DMC is combined with the oxidative carbonylation of methanol, a green process for the production of organic carbamates, with “zero emission”, can be achieved.

In the synthesis of carbamates from amines and DMC, Lewis acidic catalysts, such as the acetates of Mn, Zr, Sn, Zn and Pb,<sup>4,11–13</sup> the nitrates of Bi and Pb,<sup>14,15</sup> the triflates of IIIB metals (M(OTf)<sub>3</sub> with M = Sc, La),<sup>16,17</sup> and even CO<sub>2</sub>,<sup>18</sup> were often employed, providing appreciable yields of carbamates. Because they can be thermally or catalytically converted into diisocyanates, which are widely used as precursors in polymer preparation,<sup>19</sup> the dicarbamates are of particular industrial interest. Few papers have dealt with the synthesis of dicarbamate from DMC and diamines, especially the aliphatic ones, over catalysts such as Bi(NO<sub>3</sub>)<sub>3</sub>,<sup>14</sup> M(OTf)<sub>3</sub> (with M = Sc, La),<sup>16,17</sup> NaOCH<sub>3</sub>,<sup>20</sup> and ionic liquids MIm(CH<sub>2</sub>)<sub>4</sub>SO<sub>3</sub>HTfO.<sup>21</sup> We have previously reported the synthesis of dimethylhexane-1,6-dicarbamate *via* the methoxycarbonylation of 1,6-hexanediamine (HDA) by DMC over a ZnAlPO<sub>4</sub> berlinite catalyst.<sup>22</sup> In the present paper, sodium acetate was employed, for the first time, as catalyst for this reaction and a yield as large as 99.0% of **2** (dimethylhexane-1,6-dicarbamate) under mild conditions has been obtained. The sodium acetate catalyst is superior to the other catalysts already reported in the literature, because it is cheaper, non-toxic, and much more efficient. In addition, the mechanism of methoxycarbonylation of HDA by DMC using sodium acetate as catalyst was examined.

## 2. Experimental

### 2.1 Reagents

The reagents involved are as follows: HDA (C.P., Shanghai Lingfeng Chemicals Company); CH<sub>3</sub>OH (A.R., Shanghai Ludou Chemicals Company); CH<sub>3</sub>CN (A.R., Tianjin Kemiou Chemicals Reagents Company); CH<sub>3</sub>COONa, DMC, DMF, CH<sub>3</sub>COOH, (CH<sub>3</sub>CO)<sub>2</sub>O, and acetamide (A.R., China National Medicines Chemicals Reagents Corporation Ltd.). Before use, all the agents were pretreated to remove the water they contained: CH<sub>3</sub>COONa was dried at 373 K in a vacuum

<sup>a</sup>College of Chemistry and Chemical Engineering; Key Laboratory of Chemometrics & Chemical Biological Sensing Technologies, Ministry of Education, Hunan University, Changsha, 410082, China. E-mail: zschao@yahoo.com; Tel: +86-731-8713257

<sup>b</sup>Department of Chemical and Biological Engineering, State University of New York at Buffalo, Buffalo, NY, 14260, USA. E-mail: feaeliru@buffalo.edu; Tel: +1-716-6451179

<sup>c</sup>Department of Chemical Engineering and Light Industry, Guangdong University of Technology, Guangzhou, 510006, China

† Electronic supplementary information (ESI) available. See DOI: 10.1039/b915023b

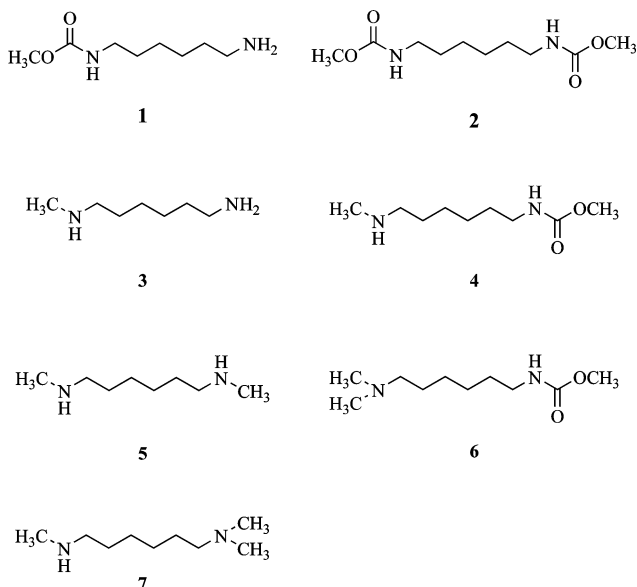
oven and the liquid agents were dehydrated using molecular sieves 4A.

## 2.2. Methoxycarbonylation of HDA by DMC

The methoxycarbonylation of HDA by DMC was performed under a N<sub>2</sub> atmosphere in a 250 ml three-neck flask equipped with a condenser and a magnetic stirrer. A solution was first prepared by mixing selected amounts of HDA, DMC, CH<sub>3</sub>COONa and solvent (CH<sub>3</sub>OH, CH<sub>3</sub>CN, or DMC) with stirring at room temperature, until a small amount of white floccules appeared. Then, a flow of nitrogen was introduced to drive out the air contained in the three-neck flask, and the solution was heated to the desired temperature and kept at that temperature for the reaction to take place. The white floccules disappeared within the first 10 min of reaction, and by prolonging the reaction time, the clear solution turned gradually into a white emulsion. After a certain reaction time, a white viscous gel was generated. This gel was cooled to room temperature and then subjected to GC and GC-MS analysis.

## 2.3. Analysis of intermediates and products

The product mixtures of methoxycarbonylation of HDA by DMC were sampled, dissolved into methanol and analyzed using a Varian Saturn2200-CP3800 GC-MS spectrometer equipped with two 15 m × 0.32 mm CP-Wax 52CB fused silica capillary columns, which were linked to a mass detector for qualitative analysis and to a flame ionization detector (FID) for quantitative analysis. It was reported<sup>14,17</sup> that in the methoxycarbonylation of HDA by DMC, besides the desired product **2** (dimethylhexane-1,6-dicarbamate), a few by-products, such as **1** (methyl-6-amino-hexyl-1-carbamate) and **3–6**, might be generated. In our work, the desired product **2**, the main by-product **1** and the minor by-product **7** have been identified (ESI: Fig. S1 and Tables S1 and S2) in all the runs. Occasionally, depending on reaction conditions, trace amounts of the by-products **3–6** could also be detected. Since the amounts of by-products **3–7** identified in our experiments were small, their selectivities are reported together in this paper. Unless otherwise



mentioned, the conversion of HDA was calculated on the basis of the initial amount of HDA, the selectivities to products were calculated on the basis of the amount of HDA converted, and the yield of **2** was calculated by multiplying the conversion of HDA with the selectivity to **2** (ESI: Section 2). The thus-obtained yield of **2** is denoted as GC yield.

To identify the reaction intermediates and products, FT-IR and <sup>1</sup>H NMR spectroscopies were employed. The FT-IR spectrum was recorded on a Thermo Nicolet Nexus 670 FT-IR spectrometer equipped with a MCTA detector and a ZnSe single-bounce attenuated total reflectance (ATR) accessory, using a 32 scans at 4 cm<sup>-1</sup> resolution. The specimen was prepared *via* a dip-coating procedure using a KBr disk as support. The <sup>1</sup>H NMR spectrum was recorded on a 400 MHz Varian INOVA-400 spectrometer, with tetramethylsilane (TMS) in deuteriochloroform (CDCl<sub>3</sub>) as internal standard.

## 2.4. Purification and identification of dimethylhexane-1,6-dicarbamate

After the methoxycarbonylation of HDA by DMC in the presence of CH<sub>3</sub>COONa as catalyst, the product mixture was cooled to room temperature and an excess amount of dilute aqueous HCl solution was added with stirring. The resulting mixture was allowed to stand until two layers were formed. A hydrophilic layer contained mainly the catalyst (CH<sub>3</sub>COONa), and a hydrophobic layer consisted mainly of the unconverted reactants and products. After the separation of the hydrophilic layer, the hydrophobic layer was vacuum-distilled to remove the DMC, the methanol, and, if any, solvent, yielding a white solid, *i.e.*, the crude **2**. Then, the crude **2** was subjected to re-crystallization, involving the steps of dissolution in water at *ca.* 353 K, aging at room temperature for 2 h, filtration and washing with cold water. The re-crystallization procedure was repeated five times, and after drying in vacuo, the purified **2** was finally obtained. The percentage of the weight of purified **2** relative to that of **2** predicted theoretically by the stoichiometry of the reaction was then obtained and denoted as isolated yield of **2**.

<sup>1</sup>H NMR and GC-MS were employed to identify the purified **2** and the results are as follows: <sup>1</sup>H NMR (ESI: Fig. S2), δ = 1.33 (*m*, 4H; -CH<sub>2</sub>CH<sub>2</sub>CH<sub>2</sub>CH<sub>2</sub>CH<sub>2</sub>CH<sub>2</sub>-), 1.48 (*m*, 4H; -CH<sub>2</sub>CH<sub>2</sub>CH<sub>2</sub>CH<sub>2</sub>CH<sub>2</sub>CH<sub>2</sub>-), 3.14 (*q*, 4H; -NHCH<sub>2</sub>-), 3.66 (*s*, 6H; -OCH<sub>3</sub>) and 4.79 (broad, 2H; -NHCO-); GC-MS (ESI: Fig. S3 and Table S3), *m/z* = 232, 201, 173, 158, 144, 130, 116, 114, 102, 99, 88, 74, 59, 56 and 44.

## 3. Results and discussion

### 3.1. Methoxycarbonylation of HDA by DMC

Table 1 presents the results of methoxycarbonylation of HDA by DMC in the absence and presence of various solvents (methanol, DMC, or CH<sub>3</sub>CN), using CH<sub>3</sub>COONa as catalyst, a reaction time of 10 h and a reaction temperature of 348 K. All the batches consisted of 100 mmol HDA, 200 mmol (16.8 ml) DMC, 24.4 mmol (2 g) CH<sub>3</sub>COONa and 50 ml solvent. Except the batch that employed DMC as solvent, all other batches had a stoichiometric molar ratio of DMC/HDA (= 2) required for the methoxycarbonylation of HDA by DMC. It was found that in the absence of solvent, the conversion of HDA, the selectivity to

**Table 1** Effect of solvent on methoxycarbonylation of HDA by DMC using  $\text{CH}_3\text{COONa}$  as catalyst<sup>a</sup>

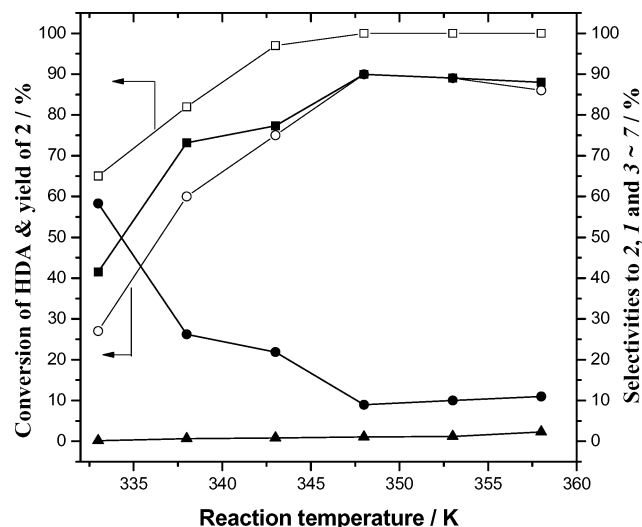
Solvent	$\chi_{\text{HDA}}^c$	$S_i^d$ (%)			$Y_{2,\text{GC}}^e$	$Y_{2,\text{isolated}}^f$
	(%)	1	2	3–7	(%)	(%)
$\text{CH}_3\text{OH}$	100	2.6	96.1	1.3	96.1	87.2
DMC	98	3.9	93.6	2.6	91.7	81.5
$\text{CH}_3\text{CN}$	97	20.4	80.7	2.0	78.3	62.8
None <sup>b</sup>	74	29.2	65.8	5.0	48.7	21.9

<sup>a</sup> HDA: 100 mmol; DMC: 200 mmol (16.8 ml);  $\text{CH}_3\text{COONa}$ : 2.0 g (24.4 mmol); solvent: 50 ml; reaction time: 10 h; reaction temperature: 348 K. <sup>b</sup> No solvent was employed. <sup>c</sup>  $\chi_{\text{HDA}}$ : conversion of HDA. <sup>d</sup>  $S_i$ : selectivity to component  $i$  in the products mixture. <sup>e</sup>  $Y_{2,\text{GC}}$ : GC yield of **2**. <sup>f</sup>  $Y_{2,\text{isolated}}$ : isolated yield of **2**.

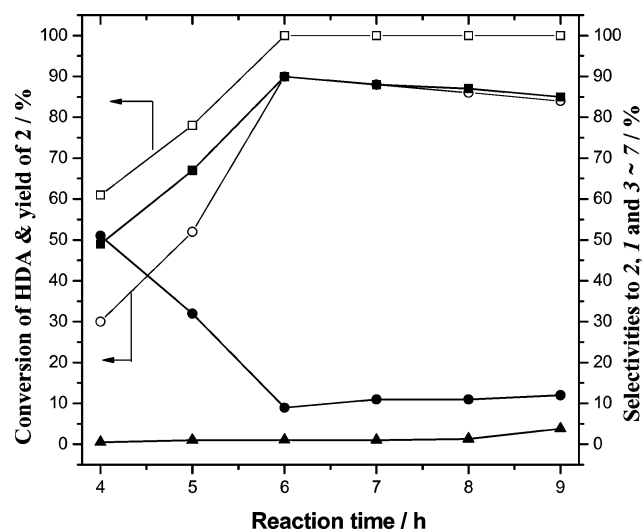
**2** and the yield of **2** were only 74.0, 65.8 and 48.7%, respectively. When a solvent was employed, the conversion of HDA, the selectivity to **2** and the yield of **2** increased to above 97.0, 80.7 and 78.3%, respectively. This indicates that the solvent stimulated the methoxycarbonylation of HDA by DMC. The stimulation by the solvent was in the order  $\text{CH}_3\text{OH} > \text{DMC} > \text{CH}_3\text{CN} >$  no solvent. Though the isolated yields of **2** were lower than the GC ones, due to the loss of **2** during re-crystallization, they still remained in the order  $\text{CH}_3\text{OH} > \text{DMC} > \text{CH}_3\text{CN} >$  no solvent. The above observation is useful, because DMC is, on the one hand, one of the main raw materials employed in the synthesis of **2**, and on the other hand, is currently manufactured *via* the reaction between methanol and  $\text{CO}_2$ .<sup>9,10</sup> Consequently, the product mixture (DMC +  $\text{CH}_3\text{OH}$ ) obtained during the DMC synthesis can be directly employed in the synthesis of **2**. The use of DMC or methanol as solvent is consistent with the “green chemistry rule”, to pursue a synthesis process using as little solvent and operational steps as possible.<sup>23</sup>

The above result reveals that both methanol and DMC are good solvents for the methoxycarbonylation of HDA by DMC. Since methanol is also a by-product and DMC is one of the reactants of the methoxycarbonylation of HDA by DMC, it is kinetically favorable for the amount of methanol to be reduced and that of DMC increased. Therefore, in the following experiments, as illustrated by Fig. 1–3, batches consisting of 50 mmol HDA, 200 mmol (16.8 ml) DMC and 20 ml  $\text{CH}_3\text{OH}$ , which have a higher molar ratio of DMC/HDA and a lower amount of methanol than those used in Table 1, were employed. One can consider that in these experiments the methoxycarbonylation of HDA by DMC takes place in the presence of DMC and methanol as co-solvents. These reactions were conducted at 348 K for 6 h, using 0.6 g (7.3 mmol) of  $\text{CH}_3\text{COONa}$  as catalyst. By changing the reaction temperature, reaction time and amount of  $\text{CH}_3\text{COONa}$ , the effects of these factors were investigated.

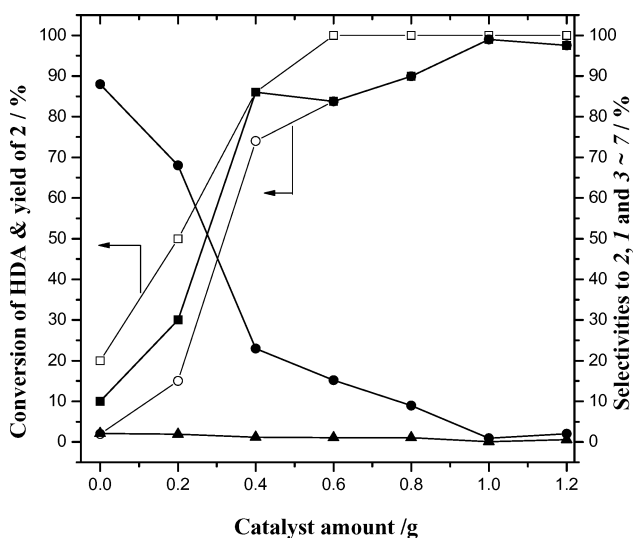
Fig. 1 presents the effect of reaction temperature. One can see that the selectivity to **3–7** is much lower than those to **1** and **2** at all temperatures tested. With increasing reaction temperature, the selectivity to **3–7** increases only slightly. This occurs because the activation energy for N-methylation is much larger than that for methoxycarbonylation.<sup>17</sup> The selectivity to **2** first increases, attains a maximum at 348 K, followed by a slight decrease, with increasing reaction temperature. The change of the selectivity to **1** with temperature exhibits the opposite trend, compared to that to **2**. This indicates that the activation energy for the formation of **2** is higher than that for **1**. The decrease in the selectivity to **2** and



**Fig. 1** Effect of reaction temperature on HDA conversion, yield of **2** and selectivities to reaction products. Reaction conditions: HDA, 50 mmol;  $\text{CH}_3\text{COONa}$ , 0.6 g; DMC, 200 mmol; time, 6 h;  $\text{CH}_3\text{OH}$ , 20 ml. (Legend: (□) HDA conversion; (○) yield of **2**; (■), (●) and (▲), selectivities to **2**, **1** and **3–7**, respectively.)



**Fig. 2** Effect of reaction time on HDA conversion, yield of **2** and selectivities to reaction products. Reaction conditions: HDA, 50 mmol;  $\text{CH}_3\text{COONa}$ , 0.6 g; DMC, 200 mmol; temperature, 348 K;  $\text{CH}_3\text{OH}$ , 20 ml. (Legend: (□) HDA conversion; (○) yield of **2**; (■), (●) and (▲), selectivities to **2**, **1** and **3–7**, respectively.)



**Fig. 3** Effect of amount of catalyst on HDA conversion, yield of **2** and selectivities to reaction products. Reaction conditions: HDA, 50 mmol; DMC, 200 mmol; time, 6 h; temperature, 348 K; CH<sub>3</sub>OH, 20 ml. (Legend: (□) HDA conversion; (○) yield of **2**; (■), (●) and (▲), selectivities to **2**, **1** and **3–7**, respectively.)

the increase of that to **1** at temperatures higher than 348 K may be due to the decomposition of **2** to **1**, because **1** is the primary and **2** the secondary product in the methoxycarbonylation of HDA by DMC.<sup>14</sup> With increasing temperature, both the conversion of HDA and the yield of **2** increase. At temperatures  $\geq 348$  K, the conversion increases to and is maintained at 100%, however, the yield of **2** decreases, as a result of the decrease of the selectivity to **2**. Consequently, the optimum temperature for the production of **2** *via* the methoxycarbonylation of HDA by DMC is around 348 K.

Fig. 2 outlines the effect of reaction time. One can see that for all reaction times tested, the selectivity to **3–7**, which increases very slightly with increasing reaction time, was much lower than those to **1** and **2**. By prolonging the reaction time, the selectivity to **2** increases, attaining a maximum at 6 h, followed by a decrease. The selectivity to **1** exhibits, however, the inverse trend, compared to that to **2**, with increasing reaction time. This occurs because **2** is a secondary product formed *via* the further reaction of **1**. Both the conversion of HDA and the yield of **2**

increase rapidly when the reaction time increases up to 6 h. The further increase of reaction time results in an approach towards a HDA conversion of 100%, but by a decrease of the yield of **2**, caused by the decomposition of **2** to **1**. Consequently, the optimum reaction time is 6 h.

Fig. 3 presents the effect of the amount of CH<sub>3</sub>COONa. One can see that in the presence of this catalyst, the conversion of HDA, the yield of **2** and the selectivity to **2** increase but the selectivity to **1** decreases, compared to those in the absence of this catalyst. The selectivity to **3–7** is much lower than those to **1** and **2** and almost unchanged in the absence or in the presence of various amounts of catalyst. When 0.6 g (7.3 mmol) of catalyst is employed, a 100% conversion of HDA is achieved. With a further increase of the amount of catalyst in the range of 0.6 to 1.0 g (12.2 mmol), the conversion of HDA remains 100%, the selectivity to **2** increases and that to **1** decreases. These results indicate that the catalyst stimulates the formation of both **1** and **2**, with **1** as the primary product and **2** as the secondary one *via* the further reaction of **1**. After HDA was completely converted, the increase of the amount of catalyst stimulated the conversion of **1** to **2**, because HDA is no longer available for the formation of **1**. When the amount of catalyst is higher than 1.0 g, the selectivity to **2** decreases slightly and that to **1** increases. This occurs most likely because the decomposition of **2** to **1** becomes predominant, when **1** is no longer available for the formation of **2**. Consequently, the optimum amount of catalyst is 1.0 g (12.2 mmol).

Table 2 presents the results of methoxycarbonylation of HDA by DMC in the absence and in the presence of CH<sub>3</sub>COONa as catalyst; for comparison, the results obtained with other catalysts reported in the literature are also included. One can see that both the conversion of HDA, the selectivity to **2** and the yield of **2** are small in the absence of the catalyst but large in its presence. CH<sub>3</sub>COONa appears to be the most efficient catalyst for the methoxycarbonylation of HDA by DMC under comparable reaction conditions, exhibiting a 100.0% conversion of HDA and a 99% yield of **2** at 348 K in 6 h.

### 3.2. On the reaction mechanism

It is known that the methoxycarbonylation of amines by DMC is the result of a S<sub>N</sub>2 nucleophilic attack by amines on the carbonyl

**Table 2** Methoxycarbonylation of 1,6-hexanediamine by DMC with various catalysts

Catalyst and its quantity	Batch composition			Reaction conditions			S <sub>i</sub> <sup>b</sup> (%)			Y <sub>2</sub> <sup>c</sup> (%)
	HDA/mmol	DMC/mmol	CH <sub>3</sub> OH/ml	T/K	Time/h	χ <sub>HDA</sub> <sup>a</sup> (%)	1	2	3-7	
None	50.0	200.0	20.0	348	6	16.0	51.9	25.6	22.5	4.1
CH <sub>3</sub> COONa (1.0 g/12.2 mmol)	50.0	200.0	20.0	348	6	100.0	0.9	99.0	0.1	99.0
Bi(NO <sub>3</sub> ) <sub>3</sub> (0.12 mmol) <sup>14</sup>	3.5	21.0	3.0	353	18	100.0	11.0	84.0	5.0	84.0
NaOCH <sub>3</sub> (28.2 mmol) <sup>20</sup>	392.0	2875.0	123.8	343	1	99.5	<i>NA</i> <sup>d</sup>	98.9	<i>NA</i>	98.4
MIm(CH <sub>2</sub> ) <sub>4</sub> SO <sub>3</sub> HTfO (3.26 mmol 1 wt% ionic liquids) <sup>21</sup>	400.0	820.0	0	353	4	100.0	<i>NA</i>	95.0	<i>NA</i>	95.0
Sc(OTf) <sub>3</sub> (0.295 mmol) <sup>17</sup>	11.3	59.4	0	293	144	100.0	<i>NA</i>	88.0	<i>NA</i>	88.0
ZnAlPO <sub>4</sub> (1.0 g) <sup>22</sup>	200.0	1600.0	0	353	8	99.0	3.9	88.6	7.5	87.7

<sup>a</sup> χ<sub>HDA</sub>: conversion of HDA. <sup>b</sup> S<sub>i</sub>: selectivity to component *i* in products mixture. <sup>c</sup> Y<sub>2</sub>: yield of **2**; all the rows in this column are GC yields, except the second row from bottom, which is isolated yield. <sup>d</sup> N. A.: not available.

carbon of DMC. Whereas a significantly higher basicity of the amine than that of the leaving group (methoxyl) is required,<sup>4,24-26</sup> methoxycarbonylation depends mostly upon the reactivity of DMC. The factors that increase the electrophilicity of carbonyl carbon promote this reaction. An electron-withdrawing effect exerted on the carbonyl group facilitates its reaction with a nucleophilic amine.<sup>4,24,27</sup> Lewis acidic catalysts were often employed to promote the methoxycarbonylation of amines by DMC. For example, over the Lewis acidic catalyst ZnAlPO<sub>4</sub>,<sup>22</sup> dimethylhexane-1,6-dicarbamate is formed *via* a catalytic cycle, which involves the activation of DMC due to the coordination of the carbonyl oxygen with Zn(II) and the nucleophilic attack by the amino group of HDA on the carbonyl carbon of the activated DMC. The absence of acidity in the CH<sub>3</sub>COONa catalyst suggests that a different mechanism may be involved in the methoxycarbonylation of HDA by DMC over this catalyst. Mason and Charles<sup>19</sup> found that the organic diisocyanate is formed *via* the reaction between diphenyl carbonate and an organic diformamide at temperatures higher than 473 K. The organic diformamide can be employed as such or can be generated *in situ* by reacting the corresponding diamine with formic acid. Besides the diisocyanate, byproducts such as dicarbamate, mixed isocyanate/carbamate and phenyl formate are also obtained. While the mechanism was not provided by the authors, the carbamate was most likely the key intermediate in the formation of isocyanate from formamide and carbonate, because the thermolysis of the carbamate yields isocyanate. For the methoxycarbonylation of HDA by DMC, catalyzed by CH<sub>3</sub>COONa, it is suggested that the N-substituted acetamide, RNHCOCH<sub>3</sub>, is formed *in situ* *via* the reaction between HDA and CH<sub>3</sub>COONa and further contributes to the formation of carbamate by reacting with DMC. The following experiments provide evidence in this direction.

**Experiment A: Identification of reaction intermediates and products *via* a two-step reaction for the methoxycarbonylation of HAD by DMC using CH<sub>3</sub>COONa as catalyst.** A mixture of HDA (50 mmol), CH<sub>3</sub>COONa (1.0 g/12.2 mmol) and CH<sub>3</sub>OH (20 ml) was first subjected to reaction at 337 K for 1 h. Chemical analysis and FT-IR identified that N-substituted acetamide (ESI: Fig. S4 and Table S4) and NaOH (ESI: Section 5) were formed *via* this reaction. Then, 200 mmol (16.8 ml) of DMC were added to the above products mixture for further reaction. After heating to 348 K and being kept at this temperature for reaction for 5 h, the product mixture was analyzed by GC and GC-MS and the results revealed that the conversion of HDA was 100% and that the selectivities to **1**, **2** and **3–7** were 0.9%, 99% and 0.1%, respectively. The product mixture was also vacuum-distilled until a white powder was generated. The FT-IR characterization of the white powder indicated the presence of mainly **2**, much less **1** and very little **3–7** (ESI: Fig. S5 and Table S5). The above results indicate that both the N-substituted acetamide and NaOH were formed as intermediates, which were consumed during the formation of carbamates, by the reaction between HDA and CH<sub>3</sub>COONa.

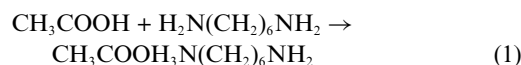
**Experiment B: Role of the reaction intermediates N-substituted acetamide and NaOH.** A mixture of HDA (10 mmol), CH<sub>3</sub>COONa (0.8 g/9.8 mmol) and CH<sub>3</sub>OH (20 ml) was first subjected to reaction at 337 K for 4 h. Then, the formed

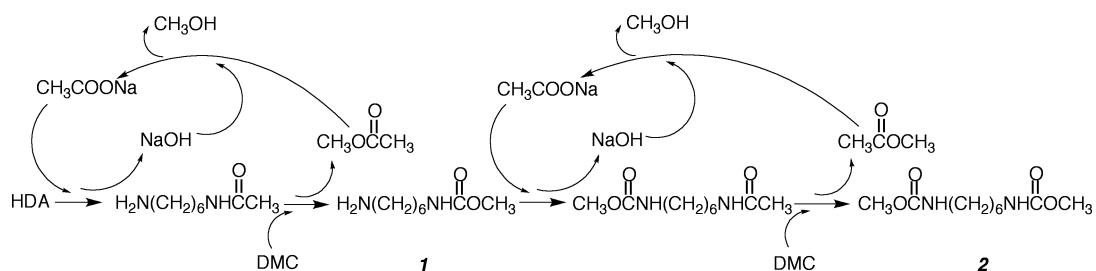
NaOH in the form of white floccules was removed by centrifugal separation. The supernatant liquid was characterized by FT-IR and the results indicated the presence of the N-substituted acetamide, HDA and acetate (the spectrum was similar to that of Fig. S4 in ESI and for this reason is not provided). To the above supernatant liquid, an excess amount of DMC was added. The resulted mixture was heated to 348 K for further reaction, and after 6 h, the product mixture was vacuum-distilled. A white powder was finally obtained and characterized by FT-IR, which indicated the presence of di-carbamate and mono-carbamate (the spectrum was similar to that of Fig. S5 in ESI and therefore is not given). The above results indicate that the N-substituted acetamide plays the role of an active intermediate and that NaOH is not a catalyst for the formation of carbamates during the methoxycarbonylation of HDA by DMC, since the separation of NaOH from the reaction system did not stop the formation of carbamate.

One may argue that a part of NaOH was dissolved into the above supernatant liquid, and after the addition of DMC to the supernatant liquid, this residual NaOH catalyzed the methoxycarbonylation reaction. To clarify this issue, we conducted an experiment, which can be described as follows. HDA (10 mmol), DMC (40 mmol) and NaOH (0.4 g/10 mmol) were dispersed into CH<sub>3</sub>OH (20 ml) with stirring at room temperature. Then, the mixture was heated to 348 K and kept at that temperature for 6 h. After cooling to room temperature, a few white floccules appeared. The floccules were recovered by centrifugal separation and identified to be NaOH. The GC-MS analysis of the supernatant liquid indicated the presence of HDA, DMC and methanol; no other component could be identified. This result confirms the conclusion that NaOH is not a catalyst for the formation of carbamates *via* the methoxycarbonylation of HDA by DMC.

**Experiment C: Methoxycarbonylation of acetamide by DMC in the absence of any catalyst.** Acetamide (50 mmol) was mixed with DMC (200 mmol/16.8 ml) and methanol (20 ml) with stirring at room temperature, and then the temperature was raised to 348 K and kept at that temperature for reacting for 6 h. After that, the reaction mixture was vacuum-distilled, resulting in a white powder, which was characterized by FT-IR (ESI: Fig. S6 and Table S6). The results revealed the presence of methyl carbamate (CH<sub>3</sub>OCONH<sub>2</sub>), besides the unconverted acetamide. It indicates that an amide such as the acetamide can interact directly with DMC to generate carbamate.

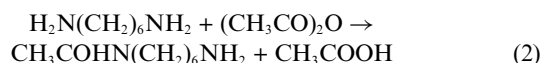
**Experiment D: Methoxycarbonylation of HDA by DMC using either CH<sub>3</sub>COOH or (CH<sub>3</sub>CO)<sub>2</sub>O as catalyst.** DMC (200 mmol/16.8 ml) and methanol (20 ml) were first mixed and then HDA (50 mmol) was added with stirring at room temperature, resulting in a clear solution. After that, CH<sub>3</sub>COOH (0.8 g/13.3 mmol) was added, and it was found that a white fume burst out and a few small white crystals appeared in the solution, releasing a large amount of heat. The crystals were sampled and identified to be N-substituted ammonium acetate, which is formed *via* the neutralization reaction of CH<sub>3</sub>COOH with HDA, as shown by eqn (1):





**Scheme 1** Possible mechanism for the methoxycarbonylation of HDA by DMC using  $\text{CH}_3\text{COONa}$  as catalyst.

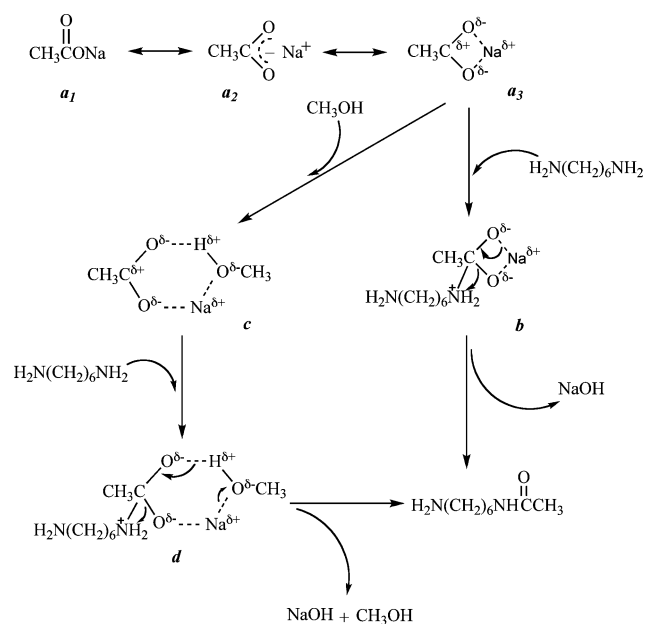
After the batch (HDA + DMC +  $\text{CH}_3\text{COOH}$  +  $\text{CH}_3\text{OH}$ ) was heated to 348 K and kept at that temperature for 6 h, neither **1** nor **2** could be identified. When the  $\text{CH}_3\text{COOH}$  in the (HDA + DMC +  $\text{CH}_3\text{COOH}$  +  $\text{CH}_3\text{OH}$ ) batch was replaced by  $(\text{CH}_3\text{CO})_2\text{O}$  and heated at 348 K for 6 h, again, neither **1** nor **2** could be identified. This occurred because though the N-substituted acetamide may be formed *via* the ammonolysis of  $(\text{CH}_3\text{CO})_2\text{O}$  by HDA (eqn (2)), this reaction is competing with both the alcoholysis of  $(\text{CH}_3\text{CO})_2\text{O}$  by methanol (eqn (3)) and the neutralization of HDA by  $\text{CH}_3\text{COOH}$  (eqn (1)):



Reactions (1) and (3) proceed at much higher rates than reaction (2), thus transforming HDA mainly into the N-substituted ammonium acetate. Thus, not enough N-substituted acetamide remained available for the formation of carbamates (**1** and **2**). The above results indicate that, neither  $\text{CH}_3\text{COOH}$  nor  $(\text{CH}_3\text{CO})_2\text{O}$  play the role of catalyst in the methoxycarbonylation of HDA by DMC, since the acidic environment they provided rapidly transformed HDA into the N-substituted ammonium acetate instead of N-substituted acetamide.

Summing up the results of experiments A to D, one can conclude that during the methoxycarbonylation of amines by DMC,  $\text{CH}_3\text{COONa}$  plays the role of a catalyst. The N-substituted acetamide,  $\text{RNHCOCH}_3$ , and NaOH are first formed *via* the reaction between HDA and  $\text{CH}_3\text{COONa}$ . NaOH does not play the role of a catalyst but provides an alkaline environment that ensures the conversion of HDA to N-substituted acetamide instead of N-substituted ammonium acetate. The observation that an alkaline environment is favorable to the methoxycarbonylation of amines by DMC has already been reported in the literature.<sup>4,9</sup> The N-substituted acetamide constitutes the key intermediate product and its further reaction with DMC results in the formation of the carbamates **1** and **2**. A possible mechanism, shown in Scheme 1, for the methoxycarbonylation of HDA by DMC, with  $\text{CH}_3\text{COONa}$  as catalyst, is proposed, and more details are provided in Schemes 2–4.

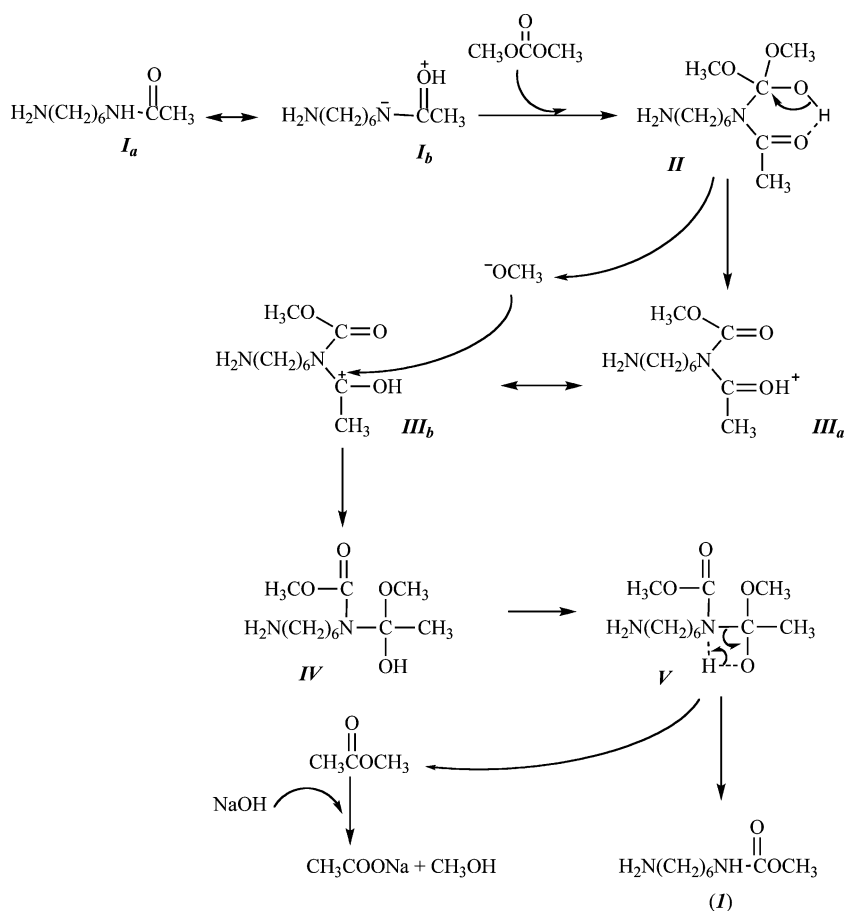
In the methoxycarbonylation of amines by DMC, an acidic catalyst was usually employed to activate the DMC. However, the nucleophilicity of the amine is potentially reduced by the interaction between the basic amine and the acidic catalyst. In the methoxycarbonylation of amines by DMC, in the presence of the basic  $\text{CH}_3\text{COONa}$  catalyst, N-substituted acetamide is first formed *via* the reaction between HDA and  $\text{CH}_3\text{COONa}$ .



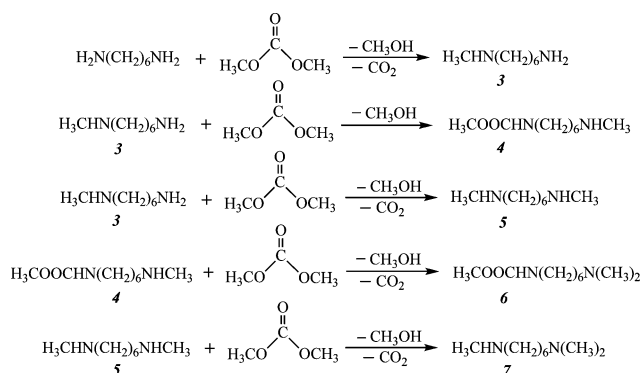
**Scheme 2** Possible mechanism for the formation of N-substituted acetamide *via* the reaction between HDA and  $\text{CH}_3\text{COONa}$ .

As shown in Scheme 2, in the absence of a solvent,  $\text{CH}_3\text{COONa}$  may exist as an equilibrium among a few resonant structures, *e.g.*, **a**<sub>1</sub>, **a**<sub>2</sub> and **a**<sub>3</sub>. The positively charged carbon of **a**<sub>3</sub> is attacked by the nucleophilic HDA, generating the intermediate **b**. The ring-opening and rearrangement of **b** results in N-substituted acetamide and NaOH. Due to the large strain of the tetraatomic ring, the equilibrium among **a**<sub>1</sub>, **a**<sub>2</sub> and **a**<sub>3</sub> may be displaced to **a**<sub>1</sub> and **a**<sub>2</sub>, generating less **a**<sub>3</sub> and in turn less **b** and N-substituted acetamide. While N-substituted acetamide has been identified as the active intermediate product for the formation of carbamates, a relatively low yield of carbamates is expected in the absence of a solvent. When a polar non-protic solvent, *e.g.*,  $\text{CH}_3\text{CN}$ , is employed, **a**<sub>3</sub> can be stabilized by the dipole–dipole interactions between solvent and **a**<sub>3</sub>. As a result, the yield of carbamates is increased. When a non-polar non-protic solvent, *e.g.*, DMC, is employed, a higher yield of carbamates than for the polar non-protic solvent  $\text{CH}_3\text{CN}$  is obtained. This occurs because, whereas no stabilization of **a**<sub>3</sub> is provided by the solvent, the increase in the amount of DMC, as one of the reactants of the methoxycarbonylation, promotes the reaction in the right direction. When a polar protic solvent is employed, *e.g.*,  $\text{CH}_3\text{OH}$ , a hexatom-ringed intermediate **c** may be formed between **a**<sub>3</sub> and  $\text{CH}_3\text{OH}$ . The higher stability of **c** than **a**<sub>3</sub> results in a higher yield





**Scheme 3** Possible mechanism for the formation of carbamate *via* the reaction between N-substituted acetamide and DMC.



**Scheme 4** Possible mechanism for the formation of 3–7 during the methoxycarbonylation of HDA by DMC using  $\text{CH}_3\text{COONa}$  as catalyst.

of carbamates when  $\text{CH}_3\text{OH}$  is employed as solvent rather than  $\text{CH}_3\text{CN}$ .

The formation of carbamates is a result of the reaction between the N-substituted acetamide and DMC. As shown in Scheme 3, the N-substituted acetamide is expected to exist as an equilibrium between the resonant structures **I<sub>a</sub>** and **I<sub>b</sub>**. With the proton of **I<sub>b</sub>** transferred to the carbonyl oxygen of DMC, the DMC becomes activated and the negatively charged N in the **I<sub>b</sub>** becomes more active in the nucleophilic attack on the carbonyl carbon of the DMC. This results in the formation of a hexatomic ring intermediate **II**. The ring-opening and rearrangement of **II**

generates the intermediate **III<sub>a</sub>** and the methoxyl group ( $\text{CH}_3\text{O}^-$ ), both driven by the resonance between **III<sub>a</sub>** and **III<sub>b</sub>**. The positive charge of the carbon in **III<sub>b</sub>** enables its attack by  $\text{CH}_3\text{O}^-$ , resulting in the intermediate **IV**. Due to the hydrogen bonding between N, O and H in **IV**, a tetratomic ring intermediate **V** is formed, and the ring-opening and rearrangement of **V** generates the carbamate **1** and the methyl acetate. The reaction between methyl acetate and NaOH, which occurs concomitantly with the formation of the N-substituted acetamide through the reaction between HDA and  $\text{CH}_3\text{COONa}$ , recovers the  $\text{CH}_3\text{COONa}$  catalyst and produces the byproduct  $\text{CH}_3\text{OH}$ . Similar steps and intermediates are expected to occur for the reaction between **1** and DMC, in the presence of  $\text{CH}_3\text{COONa}$  as catalyst, to produce the desired product **2**. We tried to react N,N'-dimethyl formamide (DMF) with DMC, but no carbamates (**1** and **2**) could be identified. This probably occurred because no hydrogen atom can be provided by DMF for the formation of a hexatomic ring intermediate, and for this reason, it cannot generate carbamates. This indicates that the formation of the intermediate **II** in the above steps is essential.

The formation of the N-alkylated byproducts 3–7, identified in the present work, may be a result of a nucleophilic attack of the amino groups of the amines on the methoxyl carbon of DMC, as shown in Scheme 4. Because of the ambident electrophilicity, DMC may react with nucleophiles not only at the carbonyl group but also at the methyl moiety.<sup>17</sup> When a Lewis acidic

catalyst was employed in the methoxycarbonylation of amines by DMC, the carbonyl in DMC was activated by the catalyst, inducing a positive charge on the carbonyl carbon and further on the methoxyl carbon.<sup>15</sup> The nucleophilic attack of the amines on the positively charged carbons results in the formation of both carbamates and N-alkylated amines. High selectivities to N-alkylated amines were also achieved at relatively high reaction temperatures.<sup>17</sup> In the present work, the basic CH<sub>3</sub>COONa catalyst promotes the methoxycarbonylation of amines by DMC via a mechanism very different from that of the Lewis acidic catalysts. Carbamates are formed as a result of the reaction between DMC and the N-substituted acetamides, which are generated by reacting amines with CH<sub>3</sub>COONa. It is expected that the positive charge of the methoxyl carbon of DMC in the presence of a basic catalyst will be smaller than that for a Lewis acidic catalyst. This might be another reason for the extremely low selectivity to **3–7** observed in our work, besides the relatively low reaction temperature (lower than 360 K) employed compared with that used in the literature for N-alkylation of amines.

#### 4. Conclusion

It is demonstrated, for the first time, that CH<sub>3</sub>COONa is a very effective catalyst for the production of dimethylhexane-1,6-dicarbamate (**2**) via the methoxycarbonylation of HDA by DMC, when CH<sub>3</sub>OH or even DMC itself is used as solvent. At a temperature of 348 K and reaction time of 6 h, a 100% conversion of HDA with a 99% selectivity to **2** could be achieved. It is shown that the catalytic cycle of the methoxycarbonylation of HDA by DMC with CH<sub>3</sub>COONa as catalyst consists mainly of three steps: the formation of the N-substituted acetamide and NaOH via the reaction between HDA and CH<sub>3</sub>COONa, the generation of carbamates and methyl acetate via the reaction between the N-substituted acetamide and DMC, and the regeneration of the CH<sub>3</sub>COONa catalyst, releasing methanol as a byproduct, via the reaction between the NaOH and methyl acetate. The yield of carbamates is affected largely by the solvent, most likely due to the different stabilities of the reaction intermediates, which depend on the nature of the solvent.

#### Acknowledgements

We are grateful for financial support from the Program for New Century Excellent Talents in University, the Ministry of Education of P. R. China; and the Program for Lotus Scholar in Hunan Province, P. R. China.

#### References

- 1 T. W. Greene and P. G. M. Wuts, in *Protective Groups in Organic Synthesis*, Wiley & Sons, New York, 3rd edn, 1999, p. 503.
- 2 P. Adams and F. A. Baron, *Chem. Rev.*, 1965, **65**, 567.
- 3 S. L. Shapiro, V. Bandurco and L. Freedman, *J. Org. Chem.*, 1961, **26**, 3710.
- 4 T. Baba, A. Kobayashi, Y. Kawanami, K. Inazu, A. Ishikawa, T. Echizen, K. Murai, S. Aso and M. Inomata, *Green Chem.*, 2005, **7**, 159.
- 5 P. Tundo and M. Selva, *Acc. Chem. Res.*, 2002, **35**, 706.
- 6 R. A. Jacobson, *J. Am. Chem. Soc.*, 1938, **60**, 1742.
- 7 N. V. Kaminshkia and N. M. Kostic, *Inorg. Chem.*, 1998, **37**, 4302.
- 8 F. Paul, J. Fischer, P. Ochsenbein and J. A. Osborn, *Organometallics*, 1998, **17**, 2199.
- 9 K. T. Jung and A. T. Bell, *J. Catal.*, 2001, **204**, 339.
- 10 D. Delledome, F. Rivetti and U. Romano, *J. Organomet. Chem.*, 1995, **488**, C15.
- 11 W. Briu, *US Pat.*, 3 763 217, 1973.
- 12 E. A. Gurgiolo, *US Pat.*, 4 268 683, 1981.
- 13 C. Calderoni, F. Mizia, F. Rivetti, U. Romano and Vimercate, *US Pat.*, 5 091 556, 1992.
- 14 R. G. Deleon, A. Kobayashi, T. Yamauchi, J. Oishi, T. Baba, M. Sasaki and F. Hiarata, *Appl. Catal. A: Gen.*, 2002, **225**, 43.
- 15 T. Baba, M. Fujiwara, A. Oosaku, A. Kobayashi and R. G. Deleon, *Appl. Catal. A: Gen.*, 2002, **227**, 1.
- 16 D. Monica and Q. Eugenio, *J. Catal.*, 2004, **228**, 36.
- 17 M. Distaso and E. Quaranta, *Appl. Catal. B: Env.*, 2006, **66**, 72.
- 18 A. Inesi, V. Mucciante and L. Rossi, *J. Org. Chem.*, 2001, **66**, 1035.
- 19 R. Mason and L. Charles, *US Pat.*, 6 781 010, 2004.
- 20 T. Yagii, T. Itokazu, and K. Murata, *US Pat.*, 5 773 643, 1994.
- 21 H. C. Zhou, F. Shi, X. Tian, Q. H. Zhang and Y. Q. Deng, *J. Mol. Catal. A: Chem.*, 2007, **271**, 89.
- 22 D. L. Sun, J. R. Deng and Z. S. Chao, *Chem. Cent. J.*, 2007, **1**, 27, DOI: 10.1186/1752-153X-1-27.
- 23 P. T. Anastas and M. M. Kirchhoff, *Acc. Chem. Res.*, 2002, **686**, 35.
- 24 A. B. Shivarkar, S. P. Gupte and R. V. Chaudhari, *J. Mol. Catal. A: Chem.*, 2004, **223**, 85.
- 25 E. A. Castro, *Chem. Rev.*, 1999, **99**, 3505.
- 26 M. J. Gresser and W. P. Jencks, *J. Am. Chem. Soc.*, 1977, **99**, 6963.
- 27 S. Carloni, D. E. Devos, P. A. Jacobs, R. Maggi, G. Sartori and S. Raffaella, *J. Catal.*, 2002, **205**, 199.

# New hydrogen carbonate precursors for efficient and byproduct-free syntheses of ionic liquids based on 1,2,3-trimethylimidazolium and *N,N*-dimethylpyrrolidinium cores†

Marcin Smiglak, C. Corey Hines‡ and Robin D. Rogers\*

Received 29th September 2009, Accepted 14th December 2009

First published as an Advance Article on the web 29th January 2010

DOI: 10.1039/b920003g

Two new hydrogen carbonate IL precursors, 1,2,3-trimethylimidazolium and *N,N*-dimethylpyrrolidinium hydrogen carbonate salts, were synthesized and their structures confirmed by NMR and single-crystal X-ray diffraction. These salts were also evaluated for application in the syntheses of ILs by reacting them with a variety of acids and  $[\text{NH}_4][\text{ClO}_4]$ , which resulted in the clean and quantitative formation of a family of 1,2,3-trimethylimidazolium- and *N,N*-dimethylpyrrolidinium-based salts. Synthetic protocols for the formation of the hydrogen carbonate salts involved simple alkylation reactions of the chosen neutral amines with dimethyl carbonate, and later conversion of the formed methyl carbonate anion-based salts to hydrogen carbonate salts. The reactions proceed in one step at temperatures close to room temperature using only water. The new organic salts with the chosen anions are formed with only gaseous byproducts ( $\text{CO}_2$ ,  $\text{H}_2\text{O}$ , and in the case of  $[\text{NH}_4][\text{ClO}_4]$ ,  $\text{NH}_3$ ), thus eliminating further purification steps. This generalized synthetic protocol for the formation of hydrogen carbonate IL precursors may be used as a cleaner, contaminant-free (halides and metal ions) route to many classes of ILs.

## Introduction

One of the most challenging problems faced by researchers working with ionic liquids (ILs, defined as salts which melt below  $100\text{ }^\circ\text{C}$ ), is difficulty in the reliable and reproducible preparation of pure compounds. Unfortunately, current methods for preparation of various ILs often involve multi-step synthesis, complex purification, and very often result in formation of undesirable and difficult to remove halide- or metal-containing species, including byproducts from metathesis reactions, incomplete ion exchange, or contamination from clean-up columns.<sup>2–5</sup> Thus, improved techniques for IL synthesis and purification would drive the end product cost down and provide higher purity materials and consistency between batches, even between different suppliers.

Limited examples of imidazolium- or other cation-based halide-free synthesis of ILs are present in the literature; the most commonly known are replacements for haloalkyl alkylating agents like dialkyl sulfates<sup>6,7</sup> and dialkyl carbonates.<sup>8</sup> More recently, the use of alkane sulfonates<sup>9</sup> and alcohols in Mitsunobu alkylation reactions<sup>10</sup> for the synthesis of halide-free alkylated IL materials were reported. These salts, though halide-free, were then typically used as precursors for further ion exchange

reactions. Ideally, in order to obtain pure IL salts, the synthesis would have to be carried out directly with routes that are byproduct-free or that allow facile removal of byproducts by their evaporation, rather than by extraction.

The preparation of ILs *via* simple methods that result in formation of the desired salts and easily separated byproducts has been investigated for quite some time. Ohno and coworkers<sup>11</sup> have suggested using an ion exchange column in order to prepare hydroxide derivatives of ILs that later could be reacted with acid, forming the desired product with little but  $\text{H}_2\text{O}$  as a byproduct. In our work we have suggested,<sup>12</sup> along with Tommasi and Sorrentino,<sup>13</sup> the use of dialkylimidazolium-2-carboxylates and decarboxylation reactions in the presence of acids as robust IL precursors for the formation of pure, byproduct-free ILs. Utilizing this methodology, our laboratory successfully prepared the first proof of a stable dialkylimidazolium  $[\text{HCO}_3]^-$  salt that was then shown to easily react with acids.<sup>14</sup> Parallel to this work, recent patent literature has also proposed the usefulness of a  $[\text{HCO}_3]^-$ -based IL for the halide-free synthesis of many ILs through titration with a Brønsted acid,<sup>15</sup> and these salts have also recently appeared in the Sigma-Aldrich catalog.<sup>16</sup> Moreover, Zheng *et al.* report the formation of carbonate-based tetraalkylammonium salts *via* the reaction of ammonium carbonate with two equivalents of dimethyl carbonate, but with greatly depressed yields in the area of 2–45%.<sup>17</sup>

Although the utilization of zwitterionic carboxylate precursors and their use in halide-free synthesis of ILs as presented in our previous report appears attractive,<sup>18</sup> certain drawbacks of the system suggested that further research was needed toward other “green” IL precursors. While working on the imidazolium carboxylate zwitterionic systems, a few limitations

Center for Green Manufacturing and Department of Chemistry, The University of Alabama, Tuscaloosa, AL, 35487, USA

† Electronic supplementary information (ESI) available: Tables S1 and S2. CCDC reference numbers 752754–752756. For ESI and crystallographic data in CIF or other electronic format see DOI: 10.1039/b920003g

‡ Current address: Nuclear Radiation Center, Washington State University, Pullman, WA 99164, USA.

were recognized, including: (i) the necessity to use heterocyclic cation cores for formation of zwitterionic carboxylates, (ii) synthesis of the zwitterionic imidazolium carbonate precursor is a two-step reaction, where the second step (carboxylation) is rate-limiting, and often low-yielding, (iii) possible formation of regioisomeric products during the zwitterion synthesis having different reactivities in subsequent reactions, and (iv) need for use of low-volatile polar aprotic solvents such as DMSO for decarboxylation, which is very hygroscopic and hard to remove from the reaction mixture.

In our recent publication,<sup>14</sup> we focused on the synthesis of a hydrogen carbonate IL precursor by using the previously described conditions for the decarboxylation of the 1,3-dimethylimidazolium-2-carboxylate ([1,3-diMeIM-2-COO]) zwitterion. We have utilized the ability of [1,3-diMeIM-2-COO] to react with acids in polar solvents, followed by the zwitterionic decarboxylation, resulting in the formation of a new salt with a counterion from the acid used in the process. Carbonic acid ( $\text{H}_2\text{CO}_3$ ) was used to promote the protonation of the 2-carboxylate moiety, initially forming 2-carboxy-1,3-dimethylimidazolium hydrogen carbonate ([2-(COOH)-1,3-diMeIM][ $\text{HCO}_3^-$ ]), followed by the Krapcho decarboxylation reaction, with the [ $\text{HCO}_3^-$ ] anion serving as the weak nucleophile. This reaction yielded formation of 1,3-dimethylimidazolium hydrogen carbonate ([1,3-diMeIM][ $\text{HCO}_3^-$ ]).

We have also noted that that when [1,3-diMeIM][ $\text{HCO}_3^-$ ] is dissolved in pure MeOH, it slowly converts into [1,3-diMeIM][ $\text{MeCO}_3^-$ ] (Fig. 1a). As expected, this methyl carbonate anion in the presence of a strong protic acid could still undergo the decomposition reaction, forming MeOH,  $\text{H}_2\text{O}$ ,  $\text{CO}_2$ , and a new salt. Similarly, Tommasi and Sorrentino<sup>19</sup> described the utilization of 1,3-dialkylimidazolium-2-carboxylates as  $\text{CO}_2$  carriers for transcarboxylation reactions; for instance, the zwitterionic carboxylate was reacted with dry methanol and  $\text{NaBF}_4$  or  $\text{NaPF}_6$  to form dialkylimidazolium [ $\text{BF}_4^-$ ] or [ $\text{PF}_6^-$ ] salts and sodium methyl carbonate (Fig. 1b).

Both reactions presented in Fig. 1 suggest the possibility of forming the [ $\text{MeCO}_3^-$ ] anion directly from both the zwitterionic carboxylate precursor, as well as from the [ $\text{HCO}_3^-$ ] salt in the presence of dry MeOH. On the other hand, even though limited to only two literature examples, studies by Pocker *et al.*<sup>20</sup> and Mori *et al.*<sup>21</sup> helped to clarify the mechanism of the reaction as outlined in Fig. 1c, and showed that the reverse reaction is also possible. In the reverse pathway, the [ $\text{MeCO}_3^-$ ] anion reacts with  $\text{H}_2\text{O}$  and acids, with the consecutive formation of either

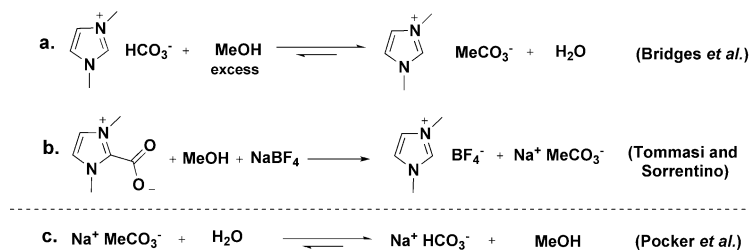
the [ $\text{HCO}_3^-$ ] anion, or alcohol and  $\text{CO}_2$ , depending on reaction conditions.

Pocker *et al.*<sup>20</sup> investigated the water- and acid-catalyzed decarboxylation of monosubstituted derivatives of carbonic acid (Fig. 1c), and concluded that the alkyl carbonate anions behave similarly to the [ $\text{HCO}_3^-$ ] anion in the presence of an acid and decompose to  $\text{CO}_2$  gas and alcohol, as opposed to  $\text{CO}_2$  and  $\text{H}_2\text{O}$  as in case of the [ $\text{HCO}_3^-$ ] anion. Another interesting result of this investigation was that the reaction of alkyl carbonate anions with water results in the decomposition of the alkyl carbonate anion with formation of an alcohol and [ $\text{HCO}_3^-$ ] anion. Similar findings have been reported by Mori *et al.*,<sup>21</sup> where the authors describe the conversion of tetraalkylammonium methyl carbonate to the corresponding hydrogen carbonate salt by addition of water. Unfortunately, no experimental data was presented to support this hypothesis in the patent.

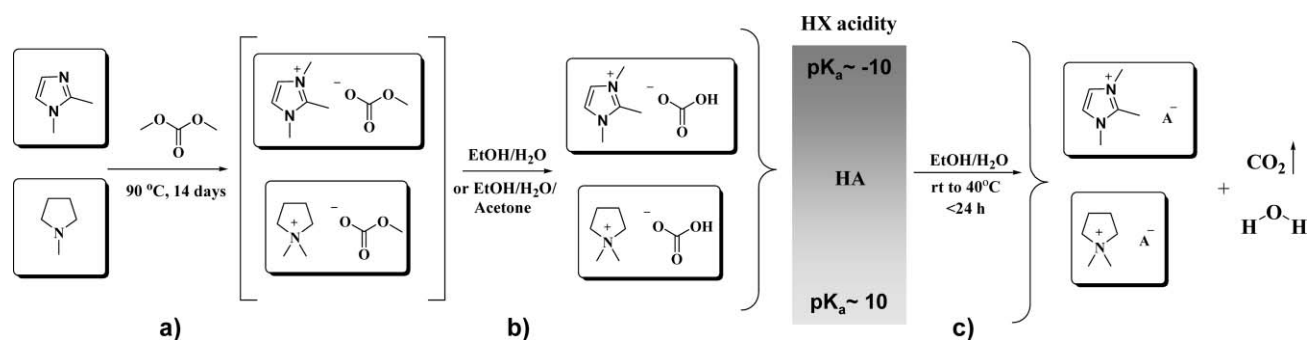
The results from the literature on the behavior of alkyl carbonates in water or in acids point to the conclusion that the reactions presented earlier by our group (Fig. 1a) might be reversible, depending on the solvent used. Thus it is anticipated that based on the solvent used for the dissolution of [ $\text{MeCO}_3^-$ ] or [ $\text{HCO}_3^-$ ]-containing salts, interconversion reactions may be seen between both anions, with both potentially present at the same time in equilibrium.

In this work, we have extended our research on the utility of dialkyl carbonates as alkylating agents to form new [ $\text{HCO}_3^-$ ] salt precursors for further halide-free syntheses of other ILs. In order to obtain [ $\text{MeCO}_3^-$ ]-based salts, we targeted two amines as prototypes: (i) 1,2-dimethylimidazole, since the carboxylation reaction at the C2 carbon during the imidazole alkylation process is prevented due to methyl group substitution (the carboxylation at C4/C5 position requires higher temperatures and should not occur with appropriate reaction conditions), and (ii) *N*-methylpyrrolidine, which due to lack of aromaticity or other conjugation, is less likely to undergo any carboxylation reaction to form a zwitterionic compound.

We report (Fig. 2) the formation of two new examples of [ $\text{HCO}_3^-$ ] IL precursors, 1,2,3-trimethylimidazolium hydrogen carbonate ([1,2,3-triMeIM][ $\text{HCO}_3^-$ ]) and *N,N*-dimethylpyrrolidinium hydrogen carbonate ([*N,N*-diMePyr][ $\text{HCO}_3^-$ ]) where the [ $\text{HCO}_3^-$ ] anion is generated by conversion of the [ $\text{MeCO}_3^-$ ] anion in the presence of excess water, and [1,2,3-triMeIM][ $\text{MeCO}_3^-$ ]. The crystallographic characterization of highly deliquescent crystals of [1,2,3-triMeIM][ $\text{HCO}_3^-$ ] $\cdot\text{H}_2\text{O}$  and [*N,N*-diMePyr][ $\text{HCO}_3^-$ ] was performed in order to further



**Fig. 1** Literature examples of possible conversions between [ $\text{HCO}_3^-$ ] and [ $\text{MeCO}_3^-$ ] anions depending on the reaction conditions and starting materials: a) conversion of [ $\text{HCO}_3^-$ ] anion to [ $\text{MeCO}_3^-$ ] in the presence of excess MeOH; b) conversion of dialkylimidazolium-2-carboxylate to dialkylimidazolium [ $\text{BF}_4^-$ ] salt in the presence of MeOH and inorganic salt; c) conversion of [ $\text{MeCO}_3^-$ ] anion to [ $\text{HCO}_3^-$ ] anion in the presence of an excess amount of  $\text{H}_2\text{O}$ .



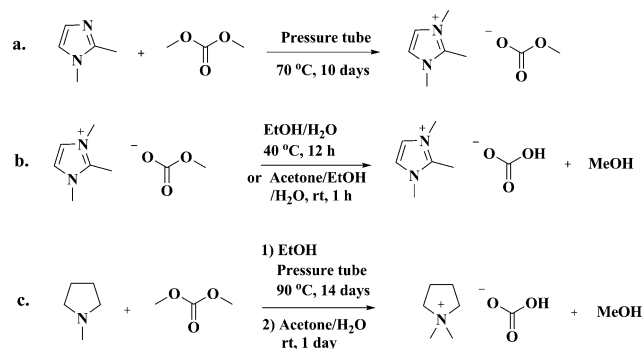
**Fig. 2** Efficient, three-step synthesis of halide-free imidazolium- and pyrrolidinium-based organic salts; a) alkylation reaction with formation of  $[\text{MeCO}_3]^-$  salts; b) conversion of  $[\text{MeCO}_3]^-$  into  $[\text{HCO}_3]^-$ ; c) reaction of  $[\text{HCO}_3]^-$  salt precursor with acid and formation of final product.

validate product formation of the three new IL precursors. The resulting salts were later used in reactions with several acids to prove their utility as IL precursors for the fast and efficient synthesis of imidazolium- and pyrrolidinium-based organic salts.

## Results and discussion

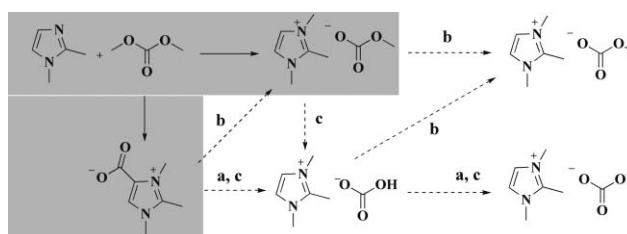
### Reactivity of 1,2,3-trimethylimidazolium methyl carbonate ( $[1,2,3\text{-triMeIM}][\text{MeCO}_3]$ )

The salt 1,2,3-trimethylimidazolium methyl carbonate ( $[1,2,3\text{-triMeIM}][\text{MeCO}_3]$ ) was synthesized by alkylation of 1,2-dimethylimidazole with dimethyl carbonate, at 70 °C for 10 days in a sealed pressure tube (Fig. 3a).<sup>18</sup> Because of the possible reaction outcomes (*i.e.*, formation of the desired  $[1,2,3\text{-triMeIM}][\text{MeCO}_3]$  or the 1,2,3-trimethylimidazolium-4-carboxylate ( $[1,2,3\text{-triMeIM-4-COO}]$ ) byproduct (Fig. 4)), the correct NMR solvent had to be used in order to provide reliable proof for the structure of the final product.



**Fig. 3** General protocol for the synthesis of a) 1,2,3-trimethylimidazolium methyl carbonate, b) 1,2,3-trimethylimidazolium hydrogen carbonate, and c) *N,N*-dimethylpyrrolidinium hydrogen carbonate.

From our experience, we knew that in the case where the product formed was the  $[1,2,3\text{-triMeIM-4-COO}]$  zwitterionic salt, the addition of a strongly polar aprotic solvent in the presence of trace amounts of water and atmospheric  $\text{CO}_2$  could cause the partial decarboxylation reaction and formation of  $[1,2,3\text{-triMeIM}][\text{HCO}_3]$  (Fig. 4, conditions a).<sup>14</sup> On the other hand, the use of pure deuterated MeOD as the NMR solvent could cause a reaction similar to the one reported by Tommasi and Sorrentino,<sup>19</sup> where transcarboxylation from the zwitterion



**Fig. 4** Possible products from the reaction of 1,2-diMeIM with DMC (highlighted area) and their expected reactivities in the presence of different deuterated solvents: a) polar aprotic solvent, trace  $\text{H}_2\text{O}$ , atmospheric  $\text{CO}_2$ ; b) MeOD; c)  $\text{D}_2\text{O}$ .

and formation of  $[1,2,3\text{-triMeIM}][\text{MeCO}_3]$  could occur (Fig. 4, conditions b). Such reactions would interfere with the NMR results if the real product of the reaction was actually the anticipated  $[1,2,3\text{-triMeIM}][\text{MeCO}_3]$ . Thus, the use of MeOD as the NMR solvent would prove the formation of  $[1,2,3\text{-triMeIM}][\text{MeCO}_3]$ , but could not rule out the possibility of its formation from the reaction of  $[1,2,3\text{-triMeIM-4-COO}]$  with the solvent. Also, the use of deuterated  $\text{H}_2\text{O}$  as the NMR solvent could greatly influence the experiment by possible conversion of  $[1,2,3\text{-triMeIM}][\text{MeCO}_3]$  into  $[1,2,3\text{-triMeIM}][\text{HCO}_3]$ , similar to work by Pocker *et al.*<sup>20</sup> In that case, the existence of the  $[\text{HCO}_3]^-$  salt could be proven, but the starting material from which it came could not (Fig. 4, conditions c). We therefore analyzed our product using  $^1\text{H}$  and  $^{13}\text{C}$  NMR in deuterated  $\text{CHCl}_3$  (chosen for its lower polarity than DMSO), relative immiscibility with water, low hygroscopicity, and inert character toward the product.

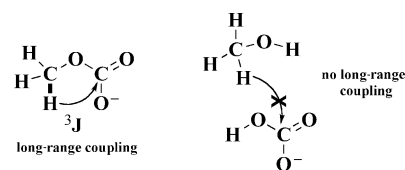
The results of the NMR analyses in  $\text{CDCl}_3$  confirmed the anticipated reaction outcome, the symmetric  $[1,2,3\text{-triMeIM}]^+$  cation core, by characteristic signals at 2.74 (C2- $\text{CH}_3$ ), 3.94 (N- $\text{CH}_3$ ), and 7.74 ppm (C4/C5-H) (Table S1a†). Moreover, the signal at 3.45 ppm has been identified as the  $\text{CH}_3\text{O}$ - group of the  $[\text{MeCO}_3]^-$  anion, which is highly suggestive of the formation of the desired  $[1,2,3\text{-triMeIM}][\text{MeCO}_3]$ . The  $^{13}\text{C}$  NMR also confirmed formation of pure  $[1,2,3\text{-triMeIM}][\text{MeCO}_3]$ , with  $[\text{MeCO}_3]^-$  anion signals appearing at 52.0 and 158.0 ppm (Table S1b). The other possibility for the assignment of these signals would be formation of  $[1,2,3\text{-triMeIM}][\text{HCO}_3]$  and the presence of MeOH formed during the decomposition of the  $[\text{MeCO}_3]^-$  anion. However, the signal at 52.0 ppm, due to its position slightly downfield from the expected position for MeOH (49.8 ppm), was assigned to the  $[\text{MeCO}_3]^-$  anion. A

shift in the position of the  $\text{CH}_3\text{O}^-$  signal was expected due to the electron-withdrawing effect of the carbonate group in the  $[\text{MeCO}_3]^-$  anion. Additionally, in the  $^1\text{H}$  NMR of  $[\text{1,2,3-triMeIM}][\text{MeCO}_3]$  (Table S1a), a small signal at 3.34 ppm was present. This was assigned to trace amounts of MeOH, possibly formed during the slow conversion process of the  $[\text{MeCO}_3]^-$  anion into MeOH and  $[\text{HCO}_3]^-$ .

Additional analysis of the same  $[\text{1,2,3-triMeIM}][\text{MeCO}_3]$  sample dissolved in  $\text{CDCl}_3$ , 24 h after the initial NMR experiment confirmed the earlier supposition of slow conversion of the  $[\text{MeCO}_3]^-$  anion into MeOH and  $[\text{HCO}_3]^-$ . In addition to the peaks observed during initial analysis, the signal suspected to be indicative of MeOH at 3.34 ppm appeared to be much more distinct (Table S1c). Additionally,  $^{13}\text{C}$  NMR of the same sample (after 24 h) (Table S1d) revealed the appearance of an additional peak at 49.63 ppm, slightly upfield from the signal of the methoxy group on the anion, thus again confirming slow conversion of the  $[\text{MeCO}_3]^-$  anion into MeOH and  $[\text{HCO}_3]^-$ . 24 h after NMR sample preparation, the ratio of the peak for MeOH (3.35 ppm) to the peak for  $[\text{MeCO}_3]^-$  (3.45 ppm) was 1:4.

A heteronuclear multiple bond correlation (HMBC) NMR experiment was performed to confirm the assumptions about the presence of the  $[\text{HCO}_3]^-$  anion in the product. The goal of this experiment was to correlate one of the  $\text{CH}_3\text{O}^-$  signals (at 3.45 or 3.35 ppm in the  $^1\text{H}$  NMR experiment) with the carbon atom of the carbonate group in  $[\text{MeCO}_3]^-$ , since only the  $[\text{MeCO}_3]^-$  could result in the appearance of the  $^3J$  cross-peak. In contrast, the hydrogen signal of MeOH was anticipated to show no  $^3J$ -coupling correlation with the carbonate signals (Fig. 5).

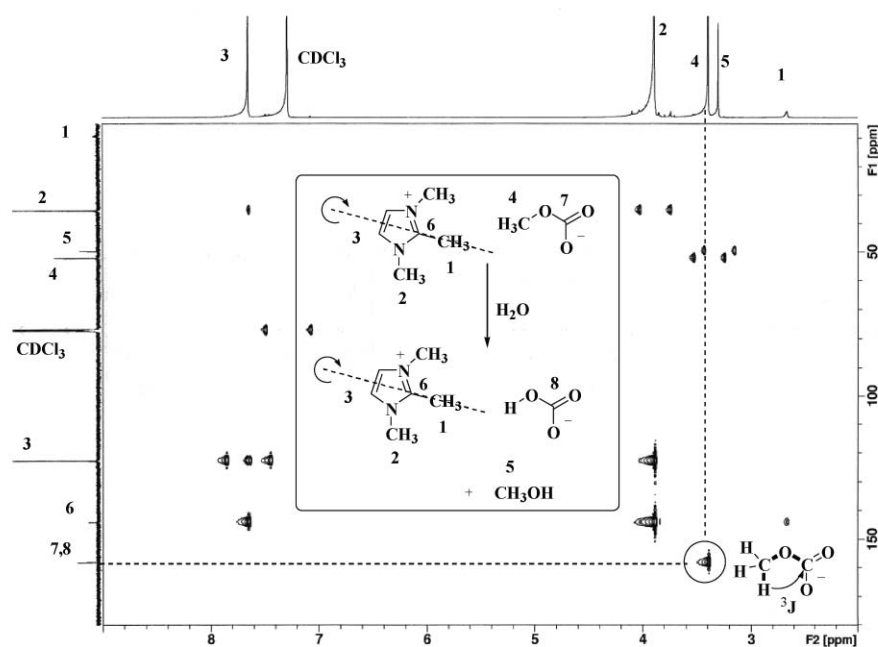
Of the two analyzed peaks at 3.45 and 3.35 ppm (NMR peaks 4 and 5, Fig. 6) only the peak at 3.45 ppm showed a cross-peak with the carbonate peak on the  $^{13}\text{C}$  NMR scale at 158.03 ppm. This directly indicated the presence of the  $[\text{MeCO}_3]^-$



**Fig. 5** Expected cross-peak correlation for the  $[\text{MeCO}_3]^-$  anion utilizing an HMBC NMR experiment.

species in the NMR solution. It was concluded from this NMR experiment that the starting material, before dissolution in  $\text{CDCl}_3$ , was pure  $[\text{1,2,3-triMeIM}][\text{MeCO}_3]$ , which after 24 h converted approximately 25% of the  $[\text{MeCO}_3]^-$  anion to  $[\text{HCO}_3]^-$  and MeOH. This finding is consistent with experimental results from the NMR experiment carried out in deuterated  $\text{H}_2\text{O}$  as solvent, and as discussed below.

To further investigate  $[\text{1,2,3-triMeIM}][\text{MeCO}_3]$  and its possible conversion to  $[\text{1,2,3-triMeIM}][\text{HCO}_3]$  in the presence of water, as reported by Mori *et al.*,<sup>21</sup> the NMR spectra of the raw sample, dissolved in deuterated  $\text{H}_2\text{O}$ , was analyzed (Table S1e–g). The first  $^1\text{H}$  NMR spectrum was taken ~10 min after dissolution in the NMR solvent and revealed two sets of signals at 3.37 and 3.54 ppm in a 3:1 ratio. As previously rationalized, the signal at 3.37 ppm was preliminarily assigned to the MeOH formed from decomposition of the  $[\text{MeCO}_3]^-$  anion, and a signal at 3.54 ppm was assigned to the remaining  $[\text{MeCO}_3]^-$  anion. The same sample was analyzed again after 1 h using the same NMR protocol and revealed the disappearance of the signal at 3.54 ppm and only the presence of a signal at 3.37 ppm, corresponding to MeOH being formed during the decomposition of  $[\text{MeCO}_3]^-$  in the presence of  $\text{D}_2\text{O}$ . A  $^{13}\text{C}$  NMR of the sample taken after 1 h (Table S1g) clearly shows (i) all signals present for the imidazolium cation, (ii) a signal at 160.9 ppm assigned to the carbonate group from the anion, and (iii) a signal at 49.6 ppm assigned to the formed MeOD.



**Fig. 6** HMBC NMR (ppm) of  $[\text{1,2,3-triMeIM}][\text{MeCO}_3]$  in  $\text{CDCl}_3$ , 24 h after initial sample preparation.

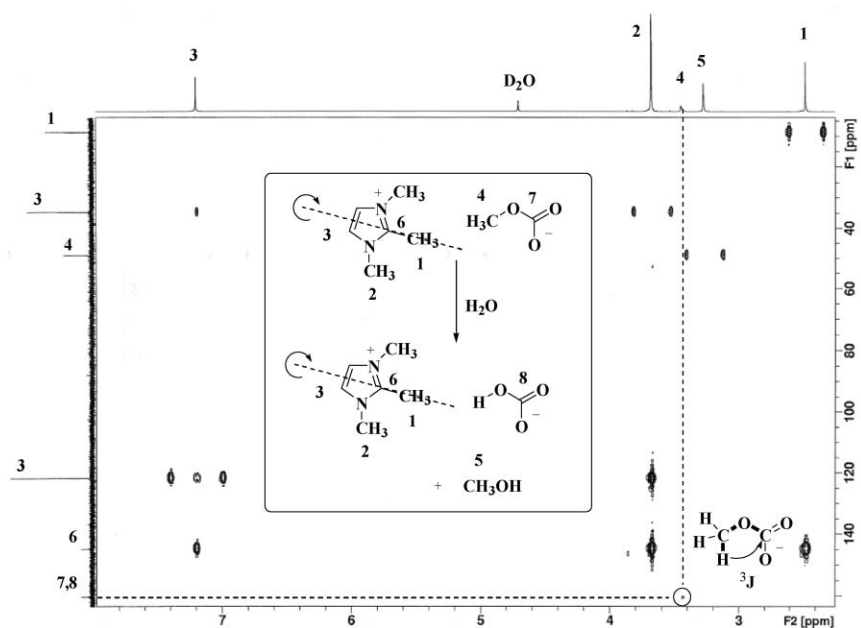


Fig. 7 HMBC NMR (ppm) of [1,2,3-triMeIM][MeCO<sub>3</sub>] in D<sub>2</sub>O 10 min after initial sample preparation.

Lastly, one more HMBC NMR experiment (Fig. 7) was performed to confirm the conversion reaction from [MeCO<sub>3</sub>]<sup>-</sup> to [HCO<sub>3</sub>]<sup>-</sup> in the presence of water, and to allow definite assignment of the observed NMR signals in D<sub>2</sub>O to the hypothesized products. Even though the HMBC experiment does not require a long time for data collection, it was noticed that over the time of the experiment, the signal at 3.54 ppm almost completely disappeared due to conversion of [MeCO<sub>3</sub>]<sup>-</sup> to MeOH and [HCO<sub>3</sub>]<sup>-</sup>. Fortunately, enough evidence of the cross-peak was found for this signal, and allowed for its successful correlation with the carbonate peak at 160.9 ppm.

To complete the NMR structural identification of crude [1,2,3-triMeIM][MeCO<sub>3</sub>], one further experiment was performed using deuterated MeOH to confirm its identity. In the <sup>1</sup>H NMR spectrum, the characteristic peak at 3.24 ppm was assigned to the CH<sub>3</sub>O- group of the [MeCO<sub>3</sub>]<sup>-</sup> anion. Also the <sup>13</sup>C NMR showed the peak for CH<sub>3</sub>O- at 49.9 ppm adjacent to the septet for MeOD. All chemical shifts for the sample run in MeOD are included in Table S1h-i.

Confirmation of the synthesis of [1,2,3-triMeIM][MeCO<sub>3</sub>] also came from single-crystal X-ray diffraction analysis (Fig. 8). An examination of the closest contacts suggests six anions surrounding each cation (and *vice versa*) in addition to one cation–cation stacking contact. The closest anion–cation contacts are the asymmetric and bifurcated contacts between the acidic ring hydrogen atoms at C4 and C5 with the carboxylate oxygen atoms of the anions (2.30(2) to 2.40(2) Å). The cation stacking interactions consist of parallel head-to-tail alignment over the N1–C2–N3 bond with a separation of 3.60(4) Å, calculated using centroid-to-centroid distances, where the centroid represents the center of the three atoms. Interestingly, the opposite face of each stacked cation pair is oriented toward the methyl-substituted oxygen in the anions with an O3-to-C2 separation of 2.960(1) Å.

#### Conversion of [1,2,3-triMeIM][MeCO<sub>3</sub>] to [1,2,3-triMeIM][HCO<sub>3</sub>]

As suggested by the results above, the conversion reaction of [MeCO<sub>3</sub>]<sup>-</sup> to [HCO<sub>3</sub>]<sup>-</sup> was attempted using EtOH as a solvent

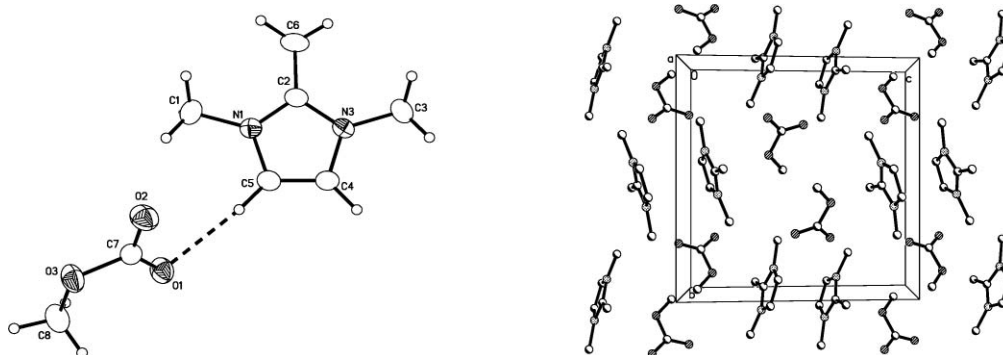


Fig. 8 Asymmetric unit (left, 50% probability thermal ellipsoids; closest anion–cation contact noted) and packing diagram (right, hydrogen atoms omitted for clarity) of [1,2,3-triMeIM][MeCO<sub>3</sub>].

and H<sub>2</sub>O as a reagent (in large excess over any other reactant). The reaction was stirred overnight at 40 °C, after which time the solvent was evaporated using a rotary evaporator and the product isolated (Fig. 3b). The NMR spectra of the product confirmed quantitative conversion to [1,2,3-triMeIM][HCO<sub>3</sub>], and the NMR signals were comparable with those for [1,2,3-triMeIM][MeCO<sub>3</sub>] analyzed in D<sub>2</sub>O 1 h after initial dissolution, as described above (Table S1f–g).

In an attempt to reduce the reaction steps and streamline the process, the same overall reaction was carried out by addition of wet acetone to [1,2,3-triMeIM][MeCO<sub>3</sub>] in EtOH resulting in the formation of [1,2,3-triMeIM][HCO<sub>3</sub>] directly as a solid precipitating out of solution. The solid was separated by centrifugation, the extract concentrated, and another portion of acetone added to the liquid phase, allowing more of the product to precipitate. (An additional advantage of this route is that colored impurities formed in the raw sample of [1,2,3-triMeIM][MeCO<sub>3</sub>] are retained in the mother liquor during the precipitation of pure [1,2,3-triMeIM][HCO<sub>3</sub>].) The total yield of the process (after drying the product under high vacuum) was calculated to be ~91%.

The NMR of [1,2,3-triMeIM][HCO<sub>3</sub>] was performed in D<sub>2</sub>O and MeOD separately (Table S1j–m). The NMR analyses in D<sub>2</sub>O confirmed the formation of pure [1,2,3-triMeIM][HCO<sub>3</sub>], evidenced by the lack of the distinctive peak for the CH<sub>3</sub>O-signal of [MeCO<sub>3</sub>]<sup>-</sup> at 59.9 ppm (<sup>13</sup>C NMR) and 3.2 ppm (<sup>1</sup>H NMR). A trace signal for the [MeCO<sub>3</sub>]<sup>-</sup> anion at 3.24 ppm was present in the <sup>1</sup>H NMR in MeOD after 1 h, indicating that back-conversion of [HCO<sub>3</sub>]<sup>-</sup> to [MeCO<sub>3</sub>]<sup>-</sup> was occurring,<sup>14</sup> but very slowly.

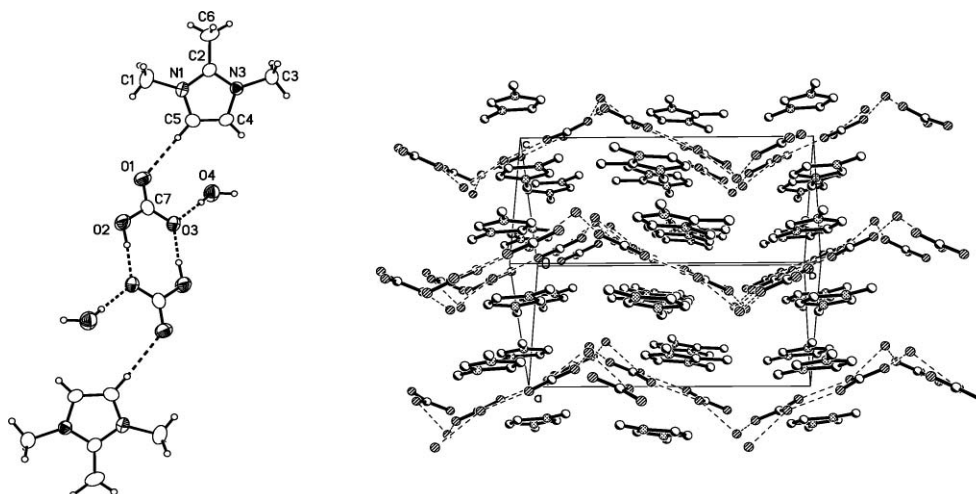
Slow precipitation of the product from solution produced single-crystals of [1,2,3-triMeIM][HCO<sub>3</sub>].H<sub>2</sub>O suitable for X-ray diffraction analysis. In the crystal structure (Fig. 9), one cation, one anion, and one water molecule complete the asymmetric unit. The [HCO<sub>3</sub>]<sup>-</sup> anions form classic head-to-head hydrogen bonded dimers around crystallographic centers of inversion, with each anion in the dimers accepting additional hydrogen bonds from the cation (the acidic proton on C5)

and the water molecule. The strong hydrogen bonds between the water and anions results in a corrugated 2D network with the cations residing between the sheets, similar to the crystal structure of [1,3-diMIM][HCO<sub>3</sub>].H<sub>2</sub>O.<sup>14</sup>

#### Formation of *N,N*-dimethylpyrrolidinium hydrogen carbonate ([*N,N*-diMePyr][HCO<sub>3</sub>])

The pyrrolidinium core was chosen for study to represent non-aromatic amines that would not undergo bonding of the carbonate group to the pyrrolidinium core, and thus not form a zwitterionic species. Another benefit of working with this cation core is its wide electrochemical window, thus having potential for use in electrochemical applications.<sup>22</sup> It was anticipated that in the reaction of *N,N*-dialkylpyrrolidine and dialkyl carbonate, only the *N,N*-dialkylpyrrolidinium alkyl carbonate would be formed. This could then undergo an anion conversion process, as described above, with clean formation of the [HCO<sub>3</sub>]<sup>-</sup>-based salt and alcohol as the byproduct.

Methylpyrrolidine and 200% excess of DMC were reacted at 90 °C for 14 days in a pressure tube. After this time, excess DMC and any possible unreacted *N*-methylpyrrolidine were removed using rotary evaporation; no solid precipitate was observed. Different solvent systems were tried to separate the product, [*N,N*-diMePyr][MeCO<sub>3</sub>], from the colored impurities without success. As in the previous experiments, solvents like DMSO, DMF, trialkylamine, acetone, water, and similar polar solvents had to be generally avoided due to the possible direct conversion of [MeCO<sub>3</sub>]<sup>-</sup> into [HCO<sub>3</sub>]<sup>-</sup> prior the isolation of [*N,N*-diMePyr][MeCO<sub>3</sub>]. Unfortunately, all the tested solvent systems failed to result in successful isolation of product from the reaction mixture. The only solvent system that successfully separated the product from the decomposition products was found to be acetone. It was also found that the use of acetone in product purification, as previously presented, facilitated the conversion of [MeCO<sub>3</sub>]<sup>-</sup> to [HCO<sub>3</sub>]<sup>-</sup> and MeOH, thus isolation of a pure [*N,N*-diMePyr][MeCO<sub>3</sub>] salt was not possible, and only a [HCO<sub>3</sub>]<sup>-</sup>-based salt could be isolated.



**Fig. 9** Crystal structure of [1,2,3-triMeIM][HCO<sub>3</sub>].H<sub>2</sub>O (left, 50% probability thermal ellipsoids; depicting the hydrogen bonded anion dimer and closest cation contact) and packing diagram (right, hydrogen atoms removed for clarity) showing the 2D corrugated sheets interpenetrated with stacked [1,2,3-triMeIM]<sup>+</sup> cations.



To the oily-red reaction mixture isolated from the rotary evaporation step above, wet acetone was added, resulting in the complete dissolution of the reaction mixture, from which, after 1 h, crystalline product slowly started to appear (Fig. 3c). This white, solid, crystalline, and very hygroscopic material was separated from the liquor by centrifugation, and washed twice with fresh acetone. After drying under high vacuum, NMR and X-ray diffraction analyses were performed.

The NMR spectra in D<sub>2</sub>O and DMSO (Table S2) clearly confirmed that the only isolated product was the [*N,N*-diMePyr][HCO<sub>3</sub>]<sup>-</sup> due to the lack of the CH<sub>3</sub>O- singlet signal of the [MeCO<sub>3</sub>]<sup>-</sup> anion expected at ~3.4–3.6 ppm. Additionally, in the NMR spectra in D<sub>2</sub>O, no MeOD signal was observed, which proved lack of conversion of [MeCO<sub>3</sub>]<sup>-</sup> to [HCO<sub>3</sub>]<sup>-</sup> and MeOH during the NMR experiment. Finally, an HMBC NMR experiment in D<sub>2</sub>O ruled out any possibility of the presence of [MeCO<sub>3</sub>]<sup>-</sup>, showing no cross-peaks between <sup>1</sup>H NMR signals and <sup>13</sup>C NMR peaks corresponding to the carbonate peak at ~160 ppm; thus it was concluded that the isolated product is pure [*N,N*-diMePyr][HCO<sub>3</sub>]<sup>-</sup>, as confirmed by X-ray diffraction.

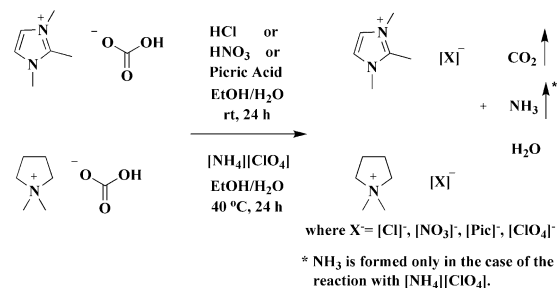
The crystal structure of the anhydrous [*N,N*-diMePyr][HCO<sub>3</sub>]<sup>-</sup> (Fig. 10) consists of hydrogen-bonded hydrogen carbonate dimers and discrete cations. Each anionic dimer is surrounded by eight nearest-neighbor cations, and each cation has four anion and two cation nearest neighbors.

#### Utilization of new hydrogen carbonate-based IL precursors in the synthesis of ILs and other organic salts

In order to show the possible synthetic applications of [HCO<sub>3</sub>]<sup>-</sup>-based salts as IL precursors, the newly formed [1,2,3-triMeIM][HCO<sub>3</sub>]<sup>-</sup> and [*N,N*-diMePyr][HCO<sub>3</sub>]<sup>-</sup> salts were reacted with a group of organic and inorganic acids (HCl, HNO<sub>3</sub>, picric acid), and ammonium perchlorate ([NH<sub>4</sub>][ClO<sub>4</sub>]; considered here as a very weak acid (p*K*<sub>a</sub> = 9.2)).<sup>23</sup> In all cases but one, [NH<sub>4</sub>][ClO<sub>4</sub>], the p*K*<sub>a</sub> values of the acids were lower than that of H<sub>2</sub>CO<sub>3</sub> (p*K*<sub>a1</sub> = 6.35),<sup>24</sup> thus complete conversion was expected with the formation of H<sub>2</sub>CO<sub>3</sub> as byproduct. H<sub>2</sub>CO<sub>3</sub>, due to its low stability, was expected to readily decompose to H<sub>2</sub>O and gaseous CO<sub>2</sub>, thus shifting the reaction equilibrium towards product formation, and after solvent evaporation, to result in byproduct-free salts.

In the case of the reaction of [HCO<sub>3</sub>]<sup>-</sup>-based IL precursors with [NH<sub>4</sub>][ClO<sub>4</sub>], a different reaction pathway was expected.

Instead of relying on a lower p*K*<sub>a</sub> of the acidic reagent in comparison to H<sub>2</sub>CO<sub>3</sub>, the kinetic equilibrium between [NH<sub>4</sub>]<sup>+</sup> + [HCO<sub>3</sub>]<sup>-</sup> and NH<sub>3</sub> + H<sub>2</sub>CO<sub>3</sub> was expected to produce volatile products which could be removed from the system, shifting the reaction toward products (Fig. 11, where [X]<sup>-</sup> = [ClO<sub>4</sub>]<sup>-</sup>).



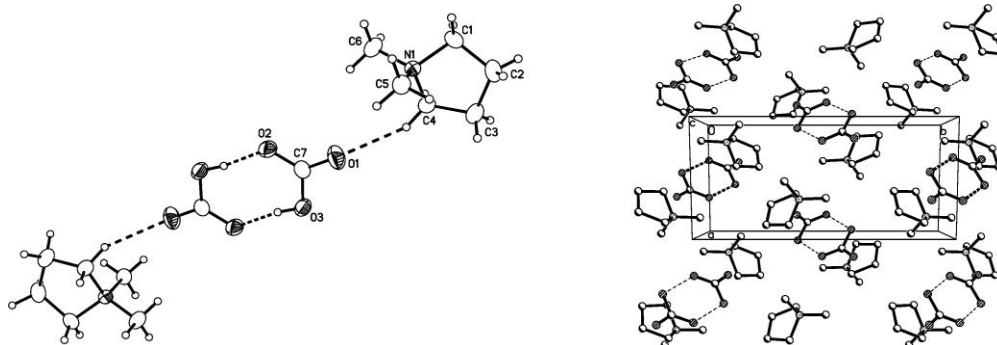
**Fig. 11** Reactions of [1,2,3-triMeIM][HCO<sub>3</sub>]<sup>-</sup> and [*N,N*-diMePyr][HCO<sub>3</sub>]<sup>-</sup> with hydrochloric, nitric, and picric acids, as well as ammonium perchlorate.

All eight product salts were confirmed using <sup>1</sup>H and <sup>13</sup>C NMR. In all cases, no remaining signal for [HCO<sub>3</sub>]<sup>-</sup> was recorded in the <sup>13</sup>C NMR, confirming the anticipated quantitative conversion of [HCO<sub>3</sub>]<sup>-</sup> IL precursors into new salt products.

#### Thermal analysis of synthesized salts

All synthesized compounds, along with their [HCO<sub>3</sub>]<sup>-</sup> IL precursors, were thermally characterized. Melting points and decomposition temperatures were analyzed (Table 1) using differential scanning calorimetry (DSC) and thermogravimetric analysis (TGA). The results indicated the thermal stabilities of [MeCO<sub>3</sub>]<sup>-</sup> and [HCO<sub>3</sub>]<sup>-</sup> salts to be very low, with the lowest thermal stability recorded for [1,2,3-triMeIM][MeCO<sub>3</sub>]<sup>-</sup> (onset temperature for 5% decomposition, *T*<sub>5%dec</sub> = 104 °C). The [HCO<sub>3</sub>]<sup>-</sup> salt of this cation exhibited a similar *T*<sub>5%dec</sub> of 112 °C. In comparison, the thermal stability of [*N,N*-diMePyr][HCO<sub>3</sub>]<sup>-</sup> was substantially higher (*T*<sub>5%dec</sub> = 158 °C) than observed for the imidazolium salts.

All of the analyzed salts formed by the reaction of the IL precursors with acids exhibited thermal stabilities >200 °C. This increase in stability was expected, since the new products are composed of stable anions that do not undergo any simple thermal decomposition, as normally found for [HCO<sub>3</sub>]<sup>-</sup> and [MeCO<sub>3</sub>]<sup>-</sup>. The thermal stabilities of the [1,2,3-triMeIM]<sup>+</sup>-based



**Fig. 10** Crystal structure of [*N,N*-diMePyr][HCO<sub>3</sub>]<sup>-</sup> (left, 50% probability thermal ellipsoids; depicting the hydrogen-bonded anion dimer and closest cation contact) and packing diagram (right, hydrogen atoms removed for clarity).

**Table 1** Melting point transitions and decomposition temperatures of the [1,2,3-triMeIM]<sup>+</sup> and [N,N-diMePyr]<sup>+</sup>-based salts<sup>a</sup>

Anion	[1,2,3-triMeIM] <sup>+</sup>		[N,N-diMePyr] <sup>+</sup>	
	m.p./°C	T <sup>5%dec</sup> /°C	m.p./°C	T <sup>5%dec</sup> /°C
[MeCO <sub>3</sub> ] <sup>-</sup>	<b>79</b>	104	n/a	n/a
[HCO <sub>3</sub> ] <sup>-</sup>	— <sup>c</sup>	112 <sup>d</sup>	— <sup>c</sup>	158
[Cl] <sup>-</sup>	<b>71</b>	205	~260 <sup>a</sup> (lit. >350) <sup>25</sup>	231
[NO <sub>3</sub> ] <sup>-</sup>	<b>63</b>	259	~220 <sup>b</sup>	276
[Pic] <sup>-</sup>	104	224	~280 <sup>b</sup> (lit. >310) <sup>26</sup>	269
[ClO <sub>4</sub> ] <sup>-</sup>	~220 <sup>b</sup> (lit >250) <sup>27</sup>	220	~280 <sup>b</sup> (lit. >330) <sup>28</sup>	254

<sup>a</sup> Salts melting below 100 °C are shown in **bold**. <sup>b</sup> Using a standard DSC protocol, the m.p. was not observed; visual m.p. analysis confirmed that the salt remains solid until its decomposition temperature, at which point it melts and decomposes simultaneously, changing to dark brown in color. <sup>c</sup> Due to the extreme hygroscopic nature of the sample, the determination of the m.p. was not possible. <sup>d</sup> Hydrated salt decomposition.

salts ranged from 205 °C for [1,2,3-triMeIM][Cl], to 258 °C for [1,2,3-triMeIM][NO<sub>3</sub>]. In the case of the [N,N-diMePyr]<sup>+</sup>-based salts, the thermal stabilities ranged between 231 °C for [N,N-diMePyr][Cl] to 276 °C [N,N-diMePyr][NO<sub>3</sub>].

The melting points of the obtained salts were also analyzed; however, due to the extreme hygroscopic nature of both [HCO<sub>3</sub>]<sup>-</sup>-based salts, the determination of the melting point using DSC did not provide reliable results, and visual melting point determination was attempted. In each of the [HCO<sub>3</sub>]<sup>-</sup>-based samples, placing them directly on a glass slide resulted in fast moisture absorption and deliquescence of the compounds due to the water absorbed from the atmosphere. When the glass slide was placed on the hot-stage apparatus and heated to ~100 °C, the absorbed water appeared to evaporate, leaving a white powder on the slide. Continuous heating of the sample was carried out to the decomposition temperature, at which point the compounds simultaneously melted, evolved gasses, and turned brown in color.

DSC analyses of the [1,2,3-triMeIM]<sup>+</sup> salts, except for the [HCO<sub>3</sub>]<sup>-</sup> and [ClO<sub>4</sub>]<sup>-</sup> analogs, exhibited a sharp melting transition (on heating) and a sharp crystallization transition (on cooling). The melting points of the [1,2,3-triMeIM]<sup>+</sup> salts were surprisingly low, considering the high symmetry of the cation, and were between 64 °C for [1,2,3-triMeIM][NO<sub>3</sub>] and 104 °C for [1,2,3-triMeIM][Pic]. The melting transition for [1,2,3-triMeIM][ClO<sub>4</sub>] was not detected on the DSC instrument due to the safety limitations set for the DSC experimental protocol. Visual melting point analysis revealed that the sample remained solid until ~220 °C, at which point it melted and decomposed simultaneously. This finding was supported by a literature report where the melting point for [1,2,3-triMeIM][ClO<sub>4</sub>] was reported to be >250 °C.<sup>27</sup>

DSC analysis of the melting points for the [N,N-diMePyr]<sup>+</sup>-based salts did not result in determination of any melting point transitions within the allowed DSC temperature ranges (up to T<sub>DSCmax</sub> = T<sup>5%dec</sup> - 50 °C to avoid decomposition of the analyzed

compound in the DCS cell and its contamination). Thus, visual melting point analyses were performed, and revealed that the analyzed salts remain solid until, or very close to, their decomposition temperatures. In all cases the melting points were recorded to be >220 °C, and the melting transition translated directly to the beginning of the decomposition process. Literature reports, although limited, confirm these findings.<sup>25,26,28</sup>

## Conclusions

In continuing the search toward novel halide- and metal-free synthetic protocols for the synthesis of ILs, two new [HCO<sub>3</sub>]<sup>-</sup> IL precursors ([1,2,3-triMeIM][HCO<sub>3</sub>] and [N,N-diMePyr][HCO<sub>3</sub>]) were developed and their structures were confirmed by NMR experiments and single-crystal X-ray diffraction. These salts were also evaluated for future possible applications in the syntheses of ILs by reacting them with a variety of acids and [NH<sub>4</sub>][ClO<sub>4</sub>], which resulted in the clean and quantitative formation of a family of [1,2,3-triMeIM]<sup>+</sup>- and [N,N-diMePyr]<sup>+</sup>-based salts. In the course of development of the synthetic protocols for the formation of [HCO<sub>3</sub>]<sup>-</sup> salts, the resulting alkylation reactions of the chosen neutral amines (in this case 1,2-dimethylimidazole and N-methylpyrrolidine) with DMC, and later conversion of the formed [MeCO<sub>3</sub>]<sup>-</sup> salts to [HCO<sub>3</sub>]<sup>-</sup> salts proceeded in one step at temperatures close to room temperature, using only water as reagent.

Previously reported routes to [1,3-diMeIM][HCO<sub>3</sub>]<sup>14</sup> were limited to the use of zwitterionic [1,3-diMeIM-2-COO], which upon reaction with carbonic acid, or water and CO<sub>2</sub>, led to the formation of the desired [HCO<sub>3</sub>]<sup>-</sup> salt. Here, we have presented a more generalized route to [HCO<sub>3</sub>]<sup>-</sup> salts which allows for more efficient and faster syntheses of ILs in comparison with the routes through zwitterionic feedstocks.

These new routes are advantageous for at least three reasons. First, the formation of the [HCO<sub>3</sub>]<sup>-</sup> precursor using the new synthetic protocol does not require prior formation of a zwitterionic salt, thus eliminating the need for a two-step reaction, with the carboxylation step requiring elevated temperatures and extended times. Second, the required formation of the [MeCO<sub>3</sub>]<sup>-</sup> intermediate *en route* to the [HCO<sub>3</sub>]<sup>-</sup> salts does not limit the range of cations to heterocycles that can undergo a carboxylation reaction; the only limitation is the ability of the starting amine to undergo alkylation with dialkyl carbonate. Finally, conversion of [MeCO<sub>3</sub>]<sup>-</sup> to [HCO<sub>3</sub>]<sup>-</sup>, and then consecutive reaction with the acid of choice, is simple in comparison with the requirements of the Krapcho decarboxylation reactions of the zwitterions, which often has to be performed in polar aprotic solvents, like DMSO, and proceeds in two steps.

The new [HCO<sub>3</sub>]<sup>-</sup>-based IL precursors were also used in reactions with several acids and [NH<sub>4</sub>][ClO<sub>4</sub>] to prove the potential of this family of salts for future applications in halide- and metal-free syntheses of ILs. As shown, it is possible to form virtually any salt from the [HCO<sub>3</sub>]<sup>-</sup> precursor when the pK<sub>a</sub> of the acidic reagent is lower than that of H<sub>2</sub>CO<sub>3</sub>. Also, the use of ammonium salts results in formation of ammonia gas, which can be evacuated from the system, shifting the equilibrium towards product formation. This reaction can be manipulated to accommodate a wide variety of anions by proper design of the reaction conditions.

## Experimental

### Chemicals

All reagents were purchased from Sigma-Aldrich (St. Louis, MO) and were used as received.

### Synthesis of 1,2,3-trimethylimidazolium methyl carbonate ((1,2,3-triMeIM][MeCO<sub>3</sub>])

The synthesis of [1,2,3-triMeIM][MeCO<sub>3</sub>] followed a previously published method for the synthesis of [1,3-diMeIM-2-COO] via an alkylation reaction of 1-methylimidazole with DMC.<sup>18</sup> 4.8 g (50 mmol) of 1,2-dimethylimidazole and 9 g (100 mmol) of DMC were placed in a 20 mL thick-walled glass pressure tube. The tube was sealed, placed in an oven, and heated to 70 °C for 10 days (Fig. 3a). The resulting yellow liquor was cooled to room temperature and unreacted substrates removed under high vacuum, at which time the product (7.44 g) crystallized in the form of slightly colored crystals.

**1,2,3-Trimethylimidazolium methyl carbonate ((1,2,3-triMeIM][MeCO<sub>3</sub>]).** White solid, very hygroscopic, 80% yield, m.p. 79 °C,  $T_{5\%dec} = 104$  °C; <sup>1</sup>H NMR (500 MHz, CDCl<sub>3</sub>)  $\delta = 2.74$  (s, 3H, C2-CH<sub>3</sub>), 3.45 (s, 3H, CH<sub>3</sub>CO<sub>3</sub>), 3.94 (s, 6H, N-CH<sub>3</sub>), 7.74 (s, 2H, C4/C5-H); <sup>13</sup>C NMR (125 MHz, CDCl<sub>3</sub>)  $\delta = 9.52$  (C2-CH<sub>3</sub>), 35.16 (N-CH<sub>3</sub>), 52.02 (CH<sub>3</sub>CO<sub>3</sub>), 122.69 (C4/C5), 143.99 (C2), 157.98 (CH<sub>3</sub>CO<sub>3</sub>); <sup>1</sup>H NMR (500 MHz, [D<sub>4</sub>]MeOH)  $\delta = 2.50$  (s, 3H; C2-CH<sub>3</sub>), 3.23 (s, 3H; CH<sub>3</sub>CO<sub>3</sub>), 3.71 (s, 6H, N-CH<sub>3</sub>), 7.35 (s, 2H, C4/C5-H); <sup>13</sup>C NMR (125 MHz, [D<sub>4</sub>]MeOH)  $\delta = 9.34$  (C2-CH<sub>3</sub>), 35.42 (N-CH<sub>3</sub>), 49.90 (CH<sub>3</sub>CO<sub>3</sub>), 123.35 (C4/C5), 146.52 (C2), 161.37 (CH<sub>3</sub>CO<sub>3</sub>). Single-crystal X-ray diffraction analysis: colorless plates; C<sub>8</sub>H<sub>14</sub>N<sub>2</sub>O<sub>3</sub>; MW 186.21;  $T = 173$  K; Monoclinic;  $P2_1/n$ ;  $a = 6.8805(6)$  Å;  $b = 11.6254(10)$  Å;  $c = 11.9614(11)$  Å;  $\beta = 96.229(2)^\circ$ ;  $V = 951.13(15)$  Å<sup>3</sup>;  $Z = 4$ ;  $D_c = 1.300$  g cm<sup>-3</sup>;  $R_1, wR_2$  [ $I > 2\sigma(I)$ ] = 0.0428, 0.1044;  $R_1, wR_2$  (all data) = 0.0510, 0.1087.

### Synthesis of 1,2,3-trimethylimidazolium hydrogen carbonate ((1,2,3-triMeIM][HCO<sub>3</sub>])

**By reaction in EtOH–H<sub>2</sub>O.** 0.5 g (2.7 mmol) of [1,2,3-triMeIM][MeCO<sub>3</sub>] was dissolved in 3 mL of EtOH and 1.5 mL (83 mmol) DI H<sub>2</sub>O was added (Fig. 3b). The reaction was stirred overnight at 40 °C, after which time the solvent was evaporated on the rotary evaporator, and the sample was analyzed by NMR. The NMR spectra confirmed the quantitative conversion to [1,2,3-triMeIM][HCO<sub>3</sub>]. The slightly colored solid product (0.46 g) was obtained in 99% yield.

**By reaction in EtOH–acetone.** 1.5 g (8.1 mmol) of [1,2,3-triMeIM][MeCO<sub>3</sub>] was dissolved in a minimum amount of EtOH (2 mL) and heated to 40 °C to allow complete dissolution of the starting material. 10 mL of acetone, spiked with 0.3 mL (16.7 mmol) DI H<sub>2</sub>O, was then added dropwise to the EtOH solution, producing a precipitate which was separated by centrifugation. The remaining solution was concentrated by partial evaporation of the solvent on a rotary evaporator at 40 °C, and another portion of acetone (10 mL) was added allowing for more precipitation. The process was repeated 2 more times

until no precipitate was noticed. The combined solid was dried under high vacuum at 40 °C for 12 h. A white, hygroscopic solid (1.39 g), with a melting point at the decomposition temperature was obtained with a total yield of 91%.

**1,2,3-Trimethylimidazolium hydrogen carbonate monohydrate ((1,2,3-triMeIM][HCO<sub>3</sub>]-H<sub>2</sub>O).** White solid, very hygroscopic, 91% yield, m.p. at  $T_{5\%dec}, T_{5\%dec} = 112$  °C; <sup>1</sup>H NMR (500 MHz, D<sub>2</sub>O)  $\delta = 2.57$  (s, 3H; C2-CH<sub>3</sub>), 3.78 (s, 6H, N-CH<sub>3</sub>), 7.30 (s, 2H, C4/C5-H); <sup>13</sup>C NMR (125 MHz, D<sub>2</sub>O)  $\delta = 9.41$  (C2-CH<sub>3</sub>), 35.32 (N-CH<sub>3</sub>), 122.55 (C4/C5), 145.50 (C2), 161.03 (HCO<sub>3</sub>); <sup>1</sup>H NMR (500 MHz, [D<sub>4</sub>]MeOH)  $\delta = 2.51$  (s, 3H; C2-CH<sub>3</sub>), 3.72 (s, 6H, N-CH<sub>3</sub>), 7.36 (s, 2H, C4/C5-H); <sup>13</sup>C NMR (125 MHz, [D<sub>4</sub>]MeOH)  $\delta = 9.37$  (C2-CH<sub>3</sub>), 35.44 (N-CH<sub>3</sub>), 123.35 (C4/C5), 146.48 (C2), 161.32 (CH<sub>3</sub>CO<sub>3</sub>). Single-crystal X-ray diffraction analysis of [1,2,3-triMeIM][HCO<sub>3</sub>]-H<sub>2</sub>O: colorless needles; C<sub>7</sub>H<sub>14</sub>N<sub>2</sub>O<sub>4</sub>; MW 190.20;  $T = 173$  K; monoclinic;  $P2_1/n$ ;  $a = 7.479(2)$  Å;  $b = 13.289(4)$  Å;  $c = 9.636(3)$  Å;  $\beta = 90.011(5)^\circ$ ;  $V = 954.0(5)$  Å<sup>3</sup>;  $Z = 4$ ;  $D_c = 1.324$  g cm<sup>-3</sup>;  $R_1, wR_2$  [ $I > 2\sigma(I)$ ] = 0.0719, 0.1097;  $R_1, wR_2$  (all data) = 0.1822, 0.1407.

### Synthesis of *N,N*-dimethylpyrrolidinium hydrogen carbonate ((*N,N*-diMePyr][HCO<sub>3</sub>])

4.0 g (50 mmol) of *N*-methypyrrolidine was initially dissolved in 5 mL of EtOH and transferred into a 20 mL thick-walled pressure tube. Next, 9 g (100 mmol) of DMC was added to the solution at room temperature. The tube was sealed, stirred vigorously, placed in the oven, and heated to 90 °C. The reaction mixture was kept under those conditions for 14 days, and then cooled to room temperature (Fig. 3c), giving a dark red liquor. Excess unreacted substrates were removed using a rotary evaporator at 90 °C, and later high vacuum at 70 °C. No product crystallized from the mother liquor.

Due to problems with isolating the product from the red liquor, the intermediate was converted *in situ* into *N,N*-dimethylpyrrolidinium hydrogen carbonate. To the oily-red concentrated reaction mixture 10 mL of wet acetone was added, resulting in the complete dissolution of reaction mixture. After 1 h a crystalline product slowly started to appear. After 24 h at room temperature, the vessel was placed in the refrigerator and kept at this temperature for an additional 72 h. A white, solid, very hygroscopic product was separated from the red liquor by centrifugation, and washed twice with cold acetone. The remaining extract was concentrated, more solid product precipitated, and later was separated by centrifugation. After combining the two precipitation batches, the product was dried under high vacuum for 12 h at room temperature, resulting in a white, hygroscopic solid (5.80 g; 72% total yield and 98% purity), with a melting point at the decomposition temperature.

***N,N*-Dimethylpyrrolidinium hydrogen carbonate ((*N,N*-diMePyr][HCO<sub>3</sub>]).** White solid, very hygroscopic, 72% yield, m.p. at  $T_{5\%dec}, T_{5\%dec} = 158$  °C; <sup>1</sup>H NMR (500 MHz, D<sub>2</sub>O)  $\delta = 2.23$  (t, 4H; CH<sub>2</sub>), 3.14 (s, 6H, N-CH<sub>3</sub>), 3.51 (t, 4H, N-CH<sub>2</sub>); <sup>13</sup>C NMR (125 MHz, D<sub>2</sub>O)  $\delta = 21.65$  (CH<sub>2</sub>), 51.67 (N-CH<sub>3</sub>), 65.82 (N-CH<sub>2</sub>), 160.17 (HCO<sub>3</sub>); <sup>1</sup>H NMR (500 MHz, [D<sub>6</sub>]DMSO)  $\delta = 2.08$  (t, 4H; CH<sub>2</sub>), 3.05 (s, 6H, N-CH<sub>3</sub>), 3.42 (t, 4H, N-CH<sub>2</sub>); <sup>13</sup>C NMR (125 MHz, [D<sub>6</sub>]DMSO)  $\delta = 21.76$  (CH<sub>2</sub>), 51.50 (N-CH<sub>3</sub>), 65.33 (N-CH<sub>2</sub>), 158.93 (HCO<sub>3</sub>). Single-crystal X-ray diffraction

analysis: colorless plates;  $C_7H_{15}NO_3$ ; MW 161.20; monoclinic;  $P2_1/n$ ;  $a = 6.6199(6) \text{ \AA}$ ;  $b = 13.9451(12) \text{ \AA}$ ;  $c = 9.2587(8) \text{ \AA}$ ;  $\beta = 101.760(2)^\circ$ ;  $V = 836.8(1) \text{ \AA}^3$ ;  $Z = 4$ ;  $D_c = 1.280 \text{ g cm}^{-3}$ ;  $R_1, wR_2 [I > 2\sigma(I)] = 0.0356, 0.0890$ ;  $R_1, wR_2$  (all data) = 0.0445, 0.0937.

**General procedure for the preparation of 1,2,3-trimethylimidazolium and *N,N*-dimethylpyrrolidinium chloride [Cl]<sup>-</sup>, nitrate [NO<sub>3</sub>]<sup>-</sup>, picrate [Pic]<sup>-</sup>, and perchlorate [ClO<sub>4</sub>]<sup>-</sup> salts**

All reactions were performed using the same procedure: 0.01 mol of the appropriate acid (HPF<sub>6</sub>, HCl, H<sub>2</sub>SO<sub>4</sub>, picric acid) or salt ([NH<sub>4</sub>][ClO<sub>4</sub>]) was dissolved in 10 mL of H<sub>2</sub>O (ethanol in the case of picric acid) and added dropwise, at room temperature (40 °C in case of [NH<sub>4</sub>][ClO<sub>4</sub>]), to a stirred solution of 0.01 mol of [1,2,3-triMeIM][HCO<sub>3</sub>] or [*N,N*-diMePyr][HCO<sub>3</sub>] in 50% aqueous ethanol (v/v, 20 mL). The mixture was stirred for an additional 24 h in a closed flask (to avoid inorganic acid evaporation) and the solvent and gaseous byproducts were evaporated on a rotary evaporator under vacuum. All samples were then dried under high vacuum at room temperature. All salts obtained were checked for the presence of starting material using <sup>1</sup>H and <sup>13</sup>C NMR, and none of the spectra revealed any residual peaks for the [HCO<sub>3</sub>]<sup>-</sup> anion.

**1,2,3-Trimethylimidazolium chloride ([1,2,3-triMeIM][Cl]).**

White solid, very hygroscopic, 99% yield, m.p. 71 °C,  $T_{5\%dec} = 205 \text{ }^\circ\text{C}$ ; <sup>1</sup>H NMR (500 MHz, [D<sub>4</sub>]MeOH)  $\delta = 2.62$  (s, 3H, C2-CH<sub>3</sub>), 3.83 (s, 6H, N-CH<sub>3</sub>), 7.46 (s, 2H, C4/C5-H); <sup>13</sup>C NMR (125 MHz [D<sub>4</sub>]MeOH)  $\delta = 10.38$  (C2-CH<sub>3</sub>), 35.57 (N-CH<sub>3</sub>), 123.26 (C4/C5), 146.45 (C2).

**1,2,3-Trimethylimidazolium nitrate ([1,2,3-triMeIM][NO<sub>3</sub>]).**

White crystalline solid, 98% yield, m.p. 63 °C,  $T_{5\%dec} = 259 \text{ }^\circ\text{C}$ ; <sup>1</sup>H NMR (500 MHz, [D<sub>4</sub>]MeOH)  $\delta = 2.60$  (s, 3H, C2-CH<sub>3</sub>), 3.84 (s, 6H, N-CH<sub>3</sub>), 7.43 (s, 2H, C4/C5-H); <sup>13</sup>C NMR (125 MHz [D<sub>4</sub>]MeOH)  $\delta = 10.01$  (C2-CH<sub>3</sub>), 35.34 (N-CH<sub>3</sub>), 123.26 (C4/C5), 146.40 (C2).

**1,2,3-Trimethylimidazolium picrate ([1,2,3-triMeIM][Pic]).**

Yellow crystalline solid, 98% yield, m.p. 104 °C,  $T_{5\%dec} = 224 \text{ }^\circ\text{C}$ ; <sup>1</sup>H NMR (500 MHz, [D<sub>4</sub>]MeOH)  $\delta = 2.56$  (s, 3H, C2-CH<sub>3</sub>), 3.76 (s, 6H, N-CH<sub>3</sub>), 7.58 (s, 2H, C4/C5-H), 8.59 (s, 2H, picrate); <sup>13</sup>C NMR (125 MHz [D<sub>4</sub>]MeOH)  $\delta = 9.48$  (C2-CH<sub>3</sub>), 34.54 (N-CH<sub>3</sub>), 121.82 (C4/C5), 124.03 (picrate), 125.07 (picrate), 141.73 (picrate), 144.59 (C2), 160.68 (picrate).

**1,2,3-Trimethylimidazolium perchlorate ([1,2,3-triMeIM][ClO<sub>4</sub>]).**

White crystalline solid, 98% yield, m.p. at  $T_{5\%dec}$  (hot-stage apparatus)  $\sim 220 \text{ }^\circ\text{C}$ ,  $T_{5\%dec} = 220 \text{ }^\circ\text{C}$ ; <sup>1</sup>H NMR (500 MHz, [D<sub>4</sub>]MeOH)  $\delta = 2.57$  (s, 3H, C2-CH<sub>3</sub>), 3.77 (s, 6H, N-CH<sub>3</sub>), 7.50 (s, 2H, C4/C5-H); <sup>13</sup>C NMR (125 MHz [D<sub>4</sub>]MeOH)  $\delta = 10.00$  (C2-CH<sub>3</sub>), 35.81 (N-CH<sub>3</sub>), 123.36 (C4/C5), 146.35 (C2).

***N,N*-Dimethylpyrrolidinium chloride ([*N,N*-diMePyr][Cl]).**

White solid, very hygroscopic, 99% yield, m.p. at  $T_{5\%dec}$  (hot-stage apparatus)  $\sim 260 \text{ }^\circ\text{C}$ ,  $T_{5\%dec} = 231 \text{ }^\circ\text{C}$ ; <sup>1</sup>H NMR (500 MHz, [D<sub>4</sub>]MeOH)  $\delta = 2.26$  (t, 4H, -CH<sub>2</sub>-), 3.20 (s, 6H, N-CH<sub>3</sub>), 3.58 (t, 4H, N-CH<sub>2</sub>); <sup>13</sup>C NMR (125 MHz [D<sub>4</sub>]MeOH)  $\delta = 22.99$  (-CH<sub>2</sub>-), 52.55 (t, N-CH<sub>3</sub>), 66.95 (t, N-CH<sub>2</sub>).

***N,N*-Dimethylpyrrolidinium nitrate ([*N,N*-diMePyr][NO<sub>3</sub>]).**

White solid, 98% yield, m.p. at  $T_{5\%dec}$  (hot-stage apparatus)  $\sim 220 \text{ }^\circ\text{C}$ ,  $T_{5\%dec} = 276 \text{ }^\circ\text{C}$ ; <sup>1</sup>H NMR (500 MHz, [D<sub>4</sub>]MeOH)  $\delta = 2.26$  (t, 4H, -CH<sub>2</sub>-), 3.18 (s, 6H, N-CH<sub>3</sub>), 3.55 (t, 4H, N-CH<sub>2</sub>); <sup>13</sup>C NMR (125 MHz [D<sub>4</sub>]MeOH)  $\delta = 22.97$  (-CH<sub>2</sub>-), 52.45 (t, N-CH<sub>3</sub>), 66.93 (t, N-CH<sub>2</sub>).

***N,N*-Dimethylpyrrolidinium picrate ([*N,N*-diMePyr][Pic]).**

Yellow crystalline solid, 98% yield, m.p. at  $T_{5\%dec}$  (hot-stage apparatus)  $\sim 280 \text{ }^\circ\text{C}$ ,  $T_{5\%dec} = 269 \text{ }^\circ\text{C}$ ; <sup>1</sup>H NMR (500 MHz, [D<sub>4</sub>]MeOH)  $\delta = 2.28$  (t, 4H, -CH<sub>2</sub>-), 3.19 (s, 6H, N-CH<sub>3</sub>), 3.56 (t, 4H, N-CH<sub>2</sub>), 8.87 (s, 2H, picrate); <sup>13</sup>C NMR (125 MHz [D<sub>4</sub>]MeOH)  $\delta = 22.79$  (-CH<sub>2</sub>-), 52.69 (N-CH<sub>3</sub>), 66.96 (N-CH<sub>2</sub>), 127.54 (picrate), 128.52 (picrate), 142.76 (picrate), 163.52 (picrate).

***N,N*-Dimethylpyrrolidinium perchlorate ([*N,N*-diMePyr][ClO<sub>4</sub>]).**

White solid, 97% yield, m.p. at  $T_{5\%dec}$  (hot-stage apparatus)  $\sim 280 \text{ }^\circ\text{C}$ ,  $T_{5\%dec} = 254 \text{ }^\circ\text{C}$ ; <sup>1</sup>H NMR (500 MHz, [D<sub>4</sub>]MeOH)  $\delta = 2.26$  (t, 4H, -CH<sub>2</sub>-), 3.17 (s, 6H, N-CH<sub>3</sub>), 3.55 (t, 4H, N-CH<sub>2</sub>); <sup>13</sup>C NMR (125 MHz [D<sub>4</sub>]MeOH)  $\delta = 22.97$  (-CH<sub>2</sub>-), 52.50 (N-CH<sub>3</sub>), 66.97 (N-CH<sub>2</sub>).

**X-Ray crystallographic studies**

Solid [1,2,3-triMeIM][MeCO<sub>3</sub>] was crystallized out of the reaction mixture after the excess of DMC was evaporated. The crystals of [1,2,3-triMeIM][HCO<sub>3</sub>] $\cdot$ H<sub>2</sub>O and [*N,N*-diMePyr][HCO<sub>3</sub>] were recrystallized from acetone, by dissolution of small amount of the sample in warm acetone, and slow cooling of the solution to room temperature.

Single crystals suitable for analysis were isolated in air, mounted on fibers, and transferred to the goniometer. The crystals were cooled to  $-100 \text{ }^\circ\text{C}$  with a stream of nitrogen gas and data were collected on a Siemens SMART diffractometer equipped with a CCD area detector, using graphite-monochromated MoK $\alpha$  radiation. The SHELXTL software package was used for each solution and refinement.<sup>29</sup> Absorption corrections were made with SADABS.<sup>30</sup> Each structure was refined by using full-matrix least-squares methods on  $F^2$ . All non-hydrogen atoms were readily located and their positions refined anisotropically, while all hydrogen atoms were located from difference Fourier maps and isotropically refined without restraint.

**Thermal analysis**

Thermal decomposition temperatures were measured in the dynamic heating regime using a TGA 2950 TA Instrument under dried air atmosphere. Samples between 5–15 mg were heated from 40–500 °C with an isocratic heating rate of 5 °C min<sup>-1</sup> under air atmosphere. Decomposition temperatures ( $T_{5\%dec}$ ) were determined from the onset to 5 wt% mass loss in an isocratic TGA experiment, which provides a more realistic representation of thermal stability at elevated temperatures.

Melting points were determined by differential scanning calorimetry (DSC) TA Instruments model 2920 Modulated DSC (New Castle, DE) cooled with a liquid nitrogen cryostat. The calorimeter was calibrated for temperature and cell constants using indium (mp 156.61 °C,  $\Delta H$  28.71 J g<sup>-1</sup>). Data were collected at constant atmospheric pressure, using samples between

10–40 mg in aluminium sample pans. Experiments were performed with heating at a rate of 5 °C min<sup>-1</sup> to the temperature 50 °C below the decomposition temperature ( $T_{5\%dec}$ ) and then cooled down to -100 °C. This heating and cooling cycle was repeated twice for each sample. The DSC instrument was adjusted so that zero heat flow was between 0 and -0.5 mW, and the baseline drift was less than 0.1 mW over the temperature range 0–180 °C. An empty sample pan was used as reference.

## Acknowledgements

This research was supported by the Air Force Office of Scientific Research (Grant F49620-03-1-0357).

## References

- 1 P. Wasserscheid and W. Keim, *Angew. Chem., Int. Ed.*, 2000, **39**, 3772.
- 2 Y. Yasaka, C. Wakai, N. Matubayasi and M. Nakahara, *Anal. Chem.*, 2009, **81**, 400.
- 3 M. Urbanek, A. Varenne, P. Gebauer, L. Krivankova and P. Gareil, *Electrophoresis*, 2006, **27**, 4859.
- 4 Z. Li, Z. Du, Y. Gu, L. Zhu, X. Zhang and Y. Deng, *Electrochem. Commun.*, 2006, **8**, 1270.
- 5 D. Berthier, A. Varenne, P. Gareil, M. Digne, C-P Lienemann, L. Magna and H. Olivier-Bourbigou, *Analyst*, 2004, **129**, 1257.
- 6 J. D. Holbrey, W. M. Reichert, R. P. Swatloski, G. A. Broker, W. R. Pitner, K. R. Seddon and R. D. Rogers, *Green Chem.*, 2002, **4**, 407.
- 7 P. Wasserscheid, R. van Hal, A. Boesmann, J. Esser and A. Jess, in *Ionic Liquids as Green Solvents: Progress and Prospects*, ed. R. D. Rogers and K. R. Seddon, ACS Symposium Series 856; American Chemical Society, Washington DC, 2003, pp. 57–69.
- 8 J. D. Holbrey, W. M. Reichert, I. Tkatchenko, E. Bouajila, O. Walter, I. Tommasi and R. D. Rogers, *Chem. Commun.*, 2003, 28.
- 9 C. C. Cassol, G. Ebeling, B. Ferrera and J. Duponta, *Adv. Synth. Catal.*, 2006, **348**, 243.
- 10 S. Petit, R. Azzouz, C. Fruit, L. Bischoff and F. Marsais, *Tetrahedron Lett.*, 2008, **49**, 3663.
- 11 W. Ogihara, M. Yoshizawa and H. Ohno, *Chem. Lett.*, 2004, **33**, 1022.
- 12 M. Smiglak, J. D. Holbrey, S. T. Griffin, W. M. Reichert, R. P. Swatloski, A. R. Katritzky, H. Yang, D. Zhang, K. Kirichenko and R. D. Rogers, *Green Chem.*, 2007, **9**, 90.
- 13 I. Tommasi and F. Sorrentino, *Tetrahedron Lett.*, 2006, **47**, 6453.
- 14 N. J. Bridges, C. C. Hines, M. Smiglak and R. D. Rogers, *Chem. Eur. J.*, 2007, **13**, 5207.
- 15 R. Kalb, W. Wesner, R. Hermann, M. Kotschan, M. Schelch and W. Staber, *PCT Int. Appl.*, WO 2005/021484, 2005.
- 16 [http://www.sigmaaldrich.com/etc/medialib/docs/Aldrich/Brochure/al\\_chemfile\\_v6\\_n9.Par.0001.File.tmp/al\\_chemfile\\_v6\\_n9.pdf](http://www.sigmaaldrich.com/etc/medialib/docs/Aldrich/Brochure/al_chemfile_v6_n9.Par.0001.File.tmp/al_chemfile_v6_n9.pdf), last accessed September 11, 2009.
- 17 Z. Zheng, T. Wu and X. Zhou, *Chem. Commun.*, 2006, 1864.
- 18 M. Smiglak, J. D. Holbrey, S. T. Griffin, W. M. Reichert, R. P. Swatloski, A. R. Katritzky, H. Yang, D. Zhang, K. Kirichenko and R. D. Rogers, *Green Chem.*, 2007, **9**, 90.
- 19 I. Tommasi and F. Sorrentino, *Tetrahedron Lett.*, 2005, **46**, 2141.
- 20 Y. Pocker, B. L. Davison and T. L. Deits, *J. Am. Chem. Soc.*, 1978, **100**, 3564.
- 21 S. Mori, K. Ida and M. Ue, Mitsubishi Petrochemical Co., Ltd, *US Pat.* 4892944, 1990.
- 22 Q. Zhu, Y. Song, X. Zhu and X. Wang, *J. Electroanal. Chem.*, 2007, **601**, 229.
- 23 [http://research.chem.psu.edu/brpgrp/pKa\\_compilation.pdf](http://research.chem.psu.edu/brpgrp/pKa_compilation.pdf), last accessed July 20, 2009.
- 24 G. Kortüm, W. Vogel and K. Andrussov, *Pure Appl. Chem.*, 1961, **1**, 364.
- 25 H. Kobler, R. Munz, G. Al Gasser and G. Simchen, *Justus Liebigs Ann. Chem.*, 1978, **12**, 1937.
- 26 W. Reppe, *Annalen*, 1956, **601**, 128.
- 27 J. A. Zoltewicz and J. K. O'Halloran, *J. Org. Chem.*, 1978, **43**, 1713.
- 28 N. J. Leonard and K. Jann, *J. Am. Chem. Soc.*, 1962, **84**, 4806.
- 29 G. M. Sheldrick, *SHELXTL, version 5.05*, Seimens Analytical X-ray Instruments Inc, 1996.
- 30 G. M. Sheldrick, *Program for Semiempirical Absorption Correction of Area Detector Data*, University of Göttingen, Germany, 1996.

# Microwave-assisted conversion of D-glucose into lactic acid under solvent-free conditions

Géraldine Epane,<sup>a</sup> Jean Claude Laguerre,<sup>a</sup> Anne Wadouachi<sup>\*b</sup> and Delphine Marek<sup>\*a</sup>

Received 28th October 2009, Accepted 26th November 2009

First published as an Advance Article on the web 29th January 2010

DOI: 10.1039/b922286c

The microwave-assisted alkaline degradation of D-glucose with alumina supported potassium hydroxide towards its conversion into lactic acid is reported. An experimental design approach was used to optimize the variables involved in this transformation. The reaction succeeded in yielding 75% of lactic acid starting from D-glucose using 1.5 equiv of KOH at 180 °C. The optimal conditions were applied to D-fructose, D-mannose and D-sucrose.

## Introduction

Lactic acid (2-hydroxypropanoic acid) is a feedstock with a growing market. It is used in food and pharmaceutical industries and has the potential to be used for the production of biodegradable polymers, such as poly(lactic acid).<sup>1</sup>

Currently, lactic acid is produced by a fermentative route starting from different sources of sugar, such as starch, sucrose, lactose, sugarcane bagass or apple pomace.<sup>2</sup> However, the biotechnology process presents some disadvantages, such as limited space–time yield and requires control and regulation of the microorganism pool.

Alternative chemical processes exist starting from monosaccharides treated in aqueous alkaline solution.<sup>3</sup> These processes are less constraining than the fermentative route. However, their limits are the release of a broad excess of by-products and the high concentration of alkaline used.

Recently, Onda *et al.* studied the conversion of D-glucose into lactic acid using noble metal supported catalyst with an alkaline in aqueous solution. This method allowed the reduction of the amount of complex by-products and lactic acid was obtained with 57% yield. Nevertheless, the reaction requires a broad alkali excess compared to the starting sugar (20 equiv compared to sugar).<sup>4</sup> In the last decades, microwave power has taken an undeniable place in chemical laboratory practice as a very effective and environmentally friendly process, particularly when it is carried out in solvent-less conditions. Microwave heating makes it convenient to perform reactions very efficiently in dry media conditions, and thus within the frame of the green chemistry concept. The advantages of using dry media conditions provide reaction rate enhancements with different selectivity compared to conventional conditions.<sup>5</sup>

In this study, we present the microwave-assisted conversion of D-glucose into lactic acid in dry media conditions using alumina supported potassium hydroxide. The effect of experimental

conditions such as power, time and concentration of alkali on the reaction of monosaccharide were investigated. An experimental design was used to obtain optimal conditions for conversion of D-glucose into lactic acid.

## Results and discussion

The CEM Discover MW allows for irradiation either by assigning the power with continuous measurement of the resulting temperature by an optic fiber captor or by assigning the temperature with continuous adjustment of irradiation power. In this study, we decided to employ the first mode of irradiation, in solventless media with assigned power in order to obtain a temperature profile. First, we investigated a microwave-assisted protocol in solvent-free conditions with an experiment field starting from the identification of the boundary values (*i.e.*, minima and maxima) for three variables, specific power applied SP (W g<sup>-1</sup> of product), alkali concentration (equiv) and time (min). We used the Box–Benkhen design to determine the reaction conditions with the three factors which could have a significant effect on the outcome of the reaction. The D-glucose mixed with previously crushed alumina supported potassium hydroxide was loaded in a glass tube and irradiated.

### Optimization of reaction conditions

The execution of the experimental design yielded approximately 50% of lactic acid. The experimental matrix of the executed Box–Benkhen design with the coded values (−1, 0, +1) is given in Table 1. The corresponding real values are given in the Table 2.

We employed a full three-level quadratic design giving 15 experiments, which lead to the formation of up to 50% of lactic acid according to reaction conditions. Experiment 5 represents the alkaline degradation of glucose supported on alumina at level-0 of potassium hydroxide level-0 of specific power and level-0 for the contact time. This reaction provided approximately 50% of lactic acid.

The identified quadratic model giving the lactic acid yield according to the experimental conditions is given in eqn (1)

$$Y = 31.25 + 8.875x_1 - 1.375x_2 + 6.5x_3 - 3.5x_1x_2 - 7.25x_1x_3 - 4.75x_2x_3 - 13.624x_1^2 - 6.125x_2^2 + 8.625x_3^2 \quad (1)$$

<sup>a</sup>Institut Polytechnique Lasalle Beauvais, 19 rue Pierre Wagnet, BP 30313, 60026, Beauvais cedex. E-mail: delphine.marek@lasalle-beauvais.fr

<sup>b</sup>Laboratoire des Glucides UMR CNRS 6219, 33 rue Saint-Leu, 80039, Amiens cedex. E-mail: anne.wadouachi@u-picardie.fr; Fax: +33 3 22 82 75 27

**Table 1** Full Experimental values of the Box-Benken design

Exp.	$x_1$	$x_2$	$x_3$	Lactic acid C-% yield	Total mass/g	Power/W	Final $T/^\circ\text{C}$
1	-1	-1	0	0	8	16	52
2	+1	-1	0	24	8	32	199
3	-1	+1	0	6	12	24	68
4	+1	+1	0	16	12	49	280
5	0	0	0	49	10	31	230
6	-1	0	-1	0	10	20	62
7	+1	0	-1	33	10	41	220
8	-1	0	+1	34	10	20	174
9	+1	0	+1	38	10	41	244
10	0	0	0	39	10	30	214
11	0	-1	-1	28	8	24	117
12	0	+1	-1	33	12	37	280
13	0	-1	+1	44	8	24	165
14	0	+1	+1	30	12	37	280
15	0	0	0	37	10	31	218

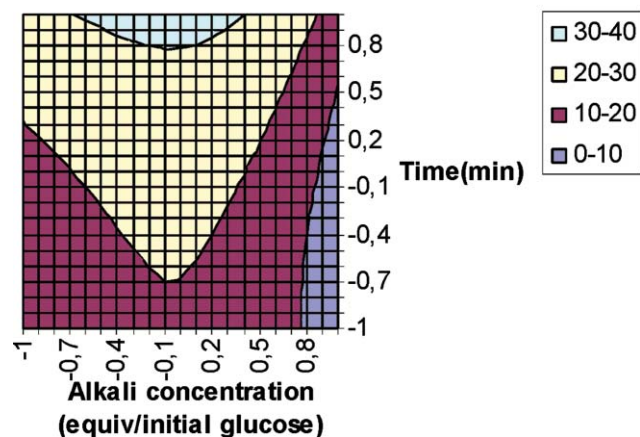
$x_1$ : microwave specific power SP ( $\text{W g}^{-1}$ ),  $x_2$ : potassium hydroxide (equiv/initial glucose),  $x_3$ : contact time (min).

**Table 2** Lactic acid yields starting from glucose at  $3.1 \text{ W g}^{-1}$  with 1.5 equiv of alkali at different reaction times in comparison to predicted experiment

Coded values	Real values of time/min	Predicted C-% yield in lactic acid	Observed C-% yield in Lactic acid	% Conversion of glucose
+1	30	48	49	99
+1.5	35	63	59	99
+2	40	82	75	99

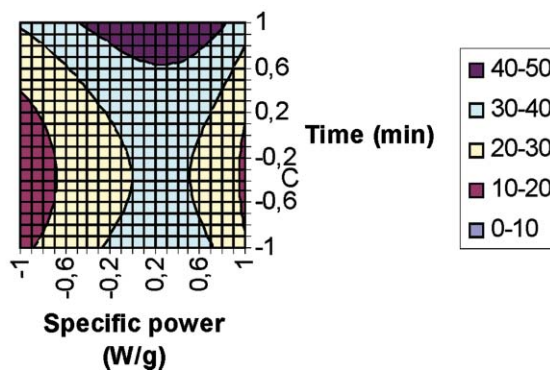
Different response surfaces were calculated from eqn (1) by setting alternatively one factor at a time at different levels (0, -1, +1). Only level-0 of both the specific power (*i.e.*  $3 \text{ W g}^{-1}$ ) and the concentration of KOH (*i.e.* 2 equiv/initial glucose) are shown in Fig. 1 and 2, respectively.

### Specific Power at level 0

**Fig. 1** Contour plot of lactic acid yield from regression analysis of experimental data at level-0 of the specific power.

As indicated by these plots, when the specific power was fixed at level-0 (*i.e.*  $3 \text{ W g}^{-1}$ ), it was possible to produce 30% of lactic acid at level-0 of KOH (*i.e.* 2 equiv/initial glucose) and level-1 for the time (*i.e.* 30 min). When the alkali concentration was

### Alkali concentration at level 0

**Fig. 2** Contour plot of lactic acid yield from regression analysis of experimental data at level-0 of alkali (equiv/initial glucose).

fixed at level-0 (*i.e.* 2 equiv/initial glucose) it is necessary to work around level-0.5 of the specific power (*i.e.*  $2.5 \text{ W g}^{-1}$ ) and level-1 for the time (*i.e.* 30 min) to produce 50% of lactic acid. Plots at other levels of alkali and power are qualitatively similar but the yields are lower. Analysis of variance indicates that the response models are suitable for lactic acid yields. Indeed the correlation coefficient ( $R^2 = 0.85$ ) indicated that the yield of lactic acid depended on the factors studied.

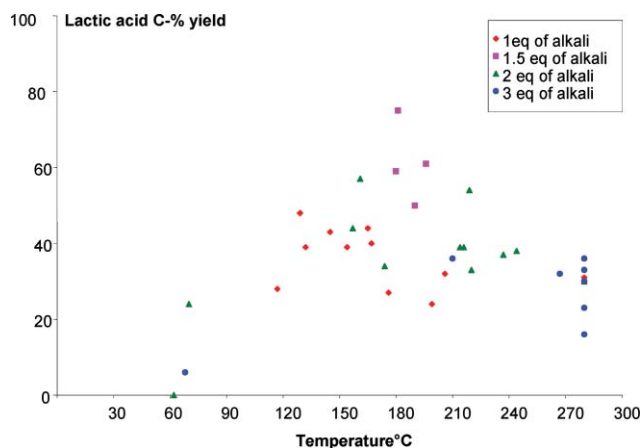
In the experimental design, the maximum product yield was obtained for a specific power of  $3 \text{ W g}^{-1}$ , 2 equiv of potassium hydroxide and 30 min reaction time conditions. Using these conditions, lactic acid yielded 49%. However, this result was obtained or accomplished along the boundary of the time parameter (*i.e.* after 30 min of reaction) in the design.

Experimental predictions were investigated using the quadratic model at different levels of specific power, concentration of potassium hydroxide and time. It appears that by working under  $3.1 \text{ W g}^{-1}$  and 1.5 equiv of alkali for 40 min, it can be possible to produce 82% of lactic acid. For this reason, additional experiments were carried out at different times while specific power and alkali concentration were set at  $3.1 \text{ W g}^{-1}$  and 1.5 equiv, respectively, to determine if mathematical simulations matched authentic experiments. The predicted values of the response under these experimental conditions and the values obtained experimentally are given in Table 2.

We observed that optimal conditions for the production of lactic acid based on these additional experiments occurred when glucose was irradiated at  $3.1 \text{ W g}^{-1}$  in the presence of 1.5 equiv of alkali for 40 min. Moreover, between 30 min and 40 min, the predictions fit the experiments. But working beyond 40 min proved to be harmful for the production of lactic acid.

### Impact of alkali concentration and the temperature on reaction conditions

Investigation of the experiments enabled us to study the effects of the temperature and the quantity of alkali on the output of the formed products. Fig. 3 demonstrated that lactic acid formation was enhanced by temperatures ranging between 180 and  $190^\circ\text{C}$  for 1.5 equiv of alkali compared to glucose. Under these conditions, it was then possible to achieve more than 50% of lactic acid.



**Fig. 3** Effect of alkali concentration and the temperature on the lactic acid yield.

Using the optimal conditions, we realized a reaction without solid support. In comparison with the reaction including solid support, the yield of lactic acid was four times less, as shown in Table 3. Solid support is thus an important component in the reaction.

In order to elucidate the importance of microwaves on these reactions, similar experiments were realized using conventional heating (Table 4).

As shown in Table 4, the use of microwave irradiation at fixed power is the best method for the production of lactic acid under dry media conditions, the yield reached 75 C-%. Indeed, when the reaction was accomplished in an oil bath, only 36% of lactic acid was obtained. Proceeding with fixed temperature with microwaves induced a lower yield in lactic acid, probably caused by a reduction of the power during the reaction. In contrast, executing the reaction at fixed power managed to stabilize the temperature during the reaction (Fig. 4).

**Table 3** Effect of solid support on the degradation of glucose using optimal conditions<sup>a</sup>

	Time/min	Final <i>T</i> /°C	C-% Lactic acid yield	% Conversion of glucose
Without solid support	40	180	19	99
With solid support	40	180	75	99

<sup>a</sup> Reactions were carried out with 11.1 mmol of D-glucose, 16.65 mmol of KOH and 200% w/w of alumina at 3.1 W g<sup>-1</sup> as specific power.

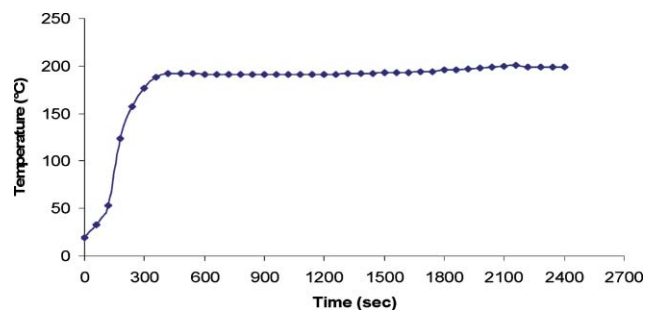
**Table 4** Comparison between microwave and conventional heating<sup>a</sup>

	Time/min	Final <i>T</i> /°C	C-% Lactic acid yield	% Conversion of glucose
Oil bath	40	180	36	99
MW <sup>b</sup>	40	180	75	99
MW <sup>c</sup>	40	180	21	99

<sup>a</sup> Reactions were carried out with 11.1 mmol of D-glucose, 16.65 mmol of KOH and 200% w/w of alumina at 3.1 W g<sup>-1</sup> as specific power. <sup>b</sup> With assigned power (specific power: 3 W g<sup>-1</sup>). <sup>c</sup> With assigned temperature: 180 °C.

**Table 5** Lactic acid yields obtained from different carbohydrates with optimized reaction conditions determined with D-glucose

Carbohydrates	% Conversion of glucose	%-C Lactic acid yield
D-Glucose	99	75
D-Mannose	99	41
D-Fructose	99	36
D-ribose	99	43
D-arabinose	99	35
D-Sucrose	99	23



**Fig. 4** Temperature profile of glucose irradiation at continuous power (28 W) during 40 min.

Similar studies have been conducted in the presence of hydroxalite-type catalysts to initiate the formation of lactic acid from glucose. These catalysts have Brønsted-base sites and are able to catalyze aldolization reaction.<sup>6</sup> The reaction mechanism of alkaline degradation of glucose into lactate has been described as a reverse aldol condensation and studied using <sup>13</sup>C-labeled glucose.<sup>7</sup>

The optimized conditions were applied to other sugars such D-mannose, D-fructose, D-ribose, D-arabinose and D-sucrose to compare the production of lactic acid (Table 5).

The yields obtained are lower for other sugars under the optimal conditions found for producing lactic acid from D-glucose. This means that it is necessary to perform another experimental designs for each type of sugar in order to maximize the lactic acid yield.

## Conclusion

Solvent-free organic syntheses combined with supported reagent and microwave irradiation is an effective process to obtain lactic acid starting from sugar source. Ideal temperature for the production of lactic acid is between 180 and 190 °C with a specific power of 3.1 W g<sup>-1</sup>. Compared to classical heating, MW accelerates the conversion rate of glucose and consequently enhance the yield of lactic acid, when the optimal temperature for this conversion is assigned, a lower yield in lactic acid is obtained.

These results suggest that beneficial rate enhancements are probably due to microwave effects, by comparing conventional and microwave heating. Pilot scales for industrial applications are being studied.



## Experimental

### Material

D-Glucose anhydrous and KOH (90%) were purchased from Verfilco and used without further purification.

Neutral alumina (150 mesh, 58 Å) was purchased from Sigma–Aldrich. Microwave irradiation was performed in a CEM Discover® System. This system operates at a frequency of 2.45 GHz with continuous MW irradiation power up to 300 W.

The reactions are carried out in round bottom pyrex tubes with a diameter of 38 mm and a height of 200 mm. Mechanical agitation is used.

### Reaction procedure

Glucose (11.1 mmol) and potassium hydroxide (16.65 mmol) were introduced into the reactor with alumina (200% w/w compared to initial glucose and alkali). The mixture (total mass of 9 g) was stirred for a minute then was irradiated by MW at the desired power and time. A mechanical system of agitation was used to homogenize the powder. After reaction, a solution of H<sub>2</sub>SO<sub>4</sub> 0.2 M was added so as to obtain a pH of approximately 2–3. The aqueous solution was separated from alumina by filtration for analysis.

### Product analysis

The filtrate was analyzed by HPLC (Surveyor photodiode array detector from ThermoFinnigan) with a UV detector (wavelength 220 nm). A Prevail Organic Acid column from Alltech (250 × 4.6 mm, 5 µm) was used with an aqueous solution of formic acid 0.15% as eluant at 0.5 mL min<sup>-1</sup> flow rate for 40 min.<sup>8</sup> The remaining sugar was quantified by HPLC analysis (Surveyor LC pump from ThermoFinnigan) coupled with an evaporative light scattering detector. A Prevail carbohydrates ES column, also from Alltech (250 × 4.6 mm, 5 µm), was used with a solution of 75% acetonitrile in water as eluant at 1 mL min<sup>-1</sup> flow rate for 30 min. In addition, a guard column of the same packing material was also used for both sugar and acid analysis.

Output in lactic acid and conversion of glucose were estimated on a carbon percentage basis (C-%) from eqn (2) and (3) in the following way:

$$\text{C-\% yield of lactic acid} = \frac{(\text{molar concentration of lactate formed} \times 3) \times 100}{(\text{molar concentration of introduced sugar} \times 6)} \quad (2)$$

$$\% \text{ glucose conversion} = \frac{\{1 - (\text{molar concentration of remained sugar})\} \times 100}{(\text{molar concentration of introduced sugar})} \quad (3)$$

### Optimization method

A response surface methodology (RSM) was used to find optimum operating conditions for the formation of lactic acid. Thus, a Box–Benkhen design, with three factors was chosen. The execution of such a design is a rapid and effective technique for finding the optimal operating conditions in order to improve the results.<sup>9,10</sup> The implementation of the design includes the setting

**Table 6** Box–Benkhen design reaction conditions

Parameter	Boundary values		
	-1	0	1
$x_1$ : Microwave specific power SP (W g <sup>-1</sup> )	2	3	4
$x_2$ : Alkali concentration (equiv/initial glucose)	1	2	3
$x_3$ : Time (min)	10	20	30

of the minima and maxima levels for all the retained factors of the experimental design (Table 5). That makes it possible to carry out the experiments under the conditions stipulated and to correlate the answers of the design (here the yield in lactic acid) to the experimental conditions (the factors of the experimental design) thanks to the quadratic model presented below (eqn (4)). The linear regression function on Excel® software was used in order to identify the coefficients  $a_i$ ,  $a_{ij}$  and  $a_{ii}$  of this quadratic model.

$$Y = a_0 + a_1x_1 + a_2x_2 + a_3x_3 + a_{12}x_1x_2 + a_{13}x_1x_3 + a_{23}x_2x_3 + a_{11}x_1^2 + a_{22}x_2^2 + a_{33}x_3^2 \quad (4)$$

Where:

$Y$  is the response (lactic acid C-%),

$a_0$  is the value of the response at the center point response of the design,

$a_i$ ,  $a_{ii}$  and  $a_{ij}$  are the coefficients of linear, quadratic and interactive effects respectively.

In our study, three reaction conditions designated by  $x_1$ ,  $x_2$ , and  $x_3$  for specific power applied (W g<sup>-1</sup> of product), alkali concentration (equiv/initial sugar) and time (min), respectively, were selected as being the experimental factors. For economic reasons, we have chosen to work between a specific power range of 2 W g<sup>-1</sup> to 4 W g<sup>-1</sup>. The coefficients ( $a_i$ ,  $a_{ij}$ ) in the model equation were determined using the linear regression function on Excel® software. The determination of optimum conditions and investigation of lactic acid output behaviour are illustrated by contour plots produced from eqn (1).

Table 6 presents the boundary values of reaction conditions in the experimental field.

## Acknowledgements

The authors thank the “Industries and Agrosources” competitiveness cluster and the “Conseil Régional de Picardie” for financial support.

## Notes and references

- (a) T. B. Vickroy, Lactic acid in: *Comprehensive Biotechnology*, Moo-Young Ed., Pergamon press, 1985, pp761-776; (b) Y. B. Wee, J. N. Kim and H. W. Ryu, *Food Technol. Biotechnol.*, 2006, **44**, 163; (c) R. P. John, K. M. Nampoothiri and A. Pandey, *Appl. Microbiol. Biotechnol.*, 2007, **74**, 524.
- (a) B. Gullon, R. Yanez, J. L. Alonso and J-C Parajo, *Bioresour. Technol.*, 2008, **99**, 308; (b) Y. J. Wee and H. W. Ryu, *Bioresour. Technol.*, 2009, **100**, 4262; (c) R. P. John, G. S. Anisha, K. M. Nampoothiri and A. Pandey, *Biotechnol. Adv.*, 2009, **27**, 145; (d) M. G. Adsul, A. J. Varma and D. V. Gokhale, *Green Chem.*, 2007, **9**, 58.

- 3 (a) B. Y. Yang and R. Montgomery, *Carbohydr. Res.*, 1996, **280**, 27; (b) B. Y. Yang and R. Montgomery, *Carbohydr. Res.*, 1996, **280**, 47.
- 4 A. Onda, T. Ochi, K. Kajiyoshi and K. Yanagisawa, *Appl. Catal., A*, 2008, **343**, 49.
- 5 (a) A. Loupy, *C. R. Chim.*, 2004, **7**, 103; (b) A. Loupy, A. Petit, D. Bogdal, *Microwaves in Organic Synthesis*, 2nd Edition, Wiley-VCH, Weinheim, Germany, 2006, pp278-326; (c) C. R. Strauss and R. S. Varma, *Top. Curr. Chem.*, 2006, **266**, 199; (d) R. S. Varma, *Green Chem.*, 1999, **1**, 43; (e) R. S. Varma, *Pure Appl. Chem.*, 2001, **73**, 193; (f) R. S. Varma, *Green Chem. Lett. Rev.*, 2007, **1**, 37.
- 6 (a) K. K. Rao, M. Gravelle, J. S. Valente and F. Figueras, *J. Catal.*, 1998, **173**, 115; (b) A. Onda, T. Ochi, K. Kajiyoshi and K. Yanagisawa, *Catal. Commun.*, 2008, **9**, 1050.
- 7 A. E. Ellis and M. A. Wilson, *J. Org. Chem.*, 2002, **67**, 8469.
- 8 J. Käkölä, R. Alen, H. Pakkanen, R. Matilainen and K. Lahti, *J. Chromatogr., A*, 2007, **1139**, 263.
- 9 J. Goupy and L. Creighton, in *Introduction aux plans d'expériences*, Dunod, 3rd edn, 2006, pp. 194-199.
- 10 D. C. Wadley, M. S. Tam, P. B. Kokitkar, J. E. Jackson and D. J. Miller, *J. Catal.*, 1997, **165**, 162.

# Cyto-toxicity and biocompatibility of a family of choline phosphate ionic liquids designed for pharmaceutical applications†

Katherine D. Weaver,<sup>a</sup> Hye Jin Kim,<sup>a</sup> Jiazeng Sun,<sup>b</sup> Douglas R. MacFarlane<sup>b</sup> and Gloria D. Elliott<sup>\*a</sup>

Received 10th September 2009, Accepted 21st December 2009

First published as an Advance Article on the web 29th January 2010

DOI: 10.1039/b918726j

Recently, the ionic liquid (IL) choline dihydrogen phosphate was demonstrated to improve the thermostability and shelf life of several model proteins, thus exhibiting potential as a stabilizing excipient or solvent for protein therapeutics. Before novel ILs can be used for biomedical applications, comprehensive data is required to establish biocompatibility, including cytotoxicity effects and solution behavior. In this study five phosphate-based anion moieties were analyzed:  $\text{H}_2\text{PO}_4^-$  (DHP), dibutyl phosphate (DBP), bis(2-ethylhexyl) phosphate (BEH), bis(2,4,4-trimethylpentyl) phosphinate (TMP), and *O,O'*-diethyl dithiophosphate (DEP), all paired with the cation choline (C). Toxicity levels for these ILs, and a common sugar and salts, were established using a J774 murine macrophage cell line. The sugar trehalose, and the simple salts sodium chloride and choline chloride yielded  $\text{EC}_{50}$  values of >100, 63 and 34 mM, respectively. The  $\text{EC}_{50}$  values (mM) of CDHP (20), CDBP (9.1), and CDEP (8.2) were lower than, but within the range of simple salts NaCl (62.8) and choline Cl (33.7). The  $\text{EC}_{50}$  values of CTMP and CBEH were considerably lower, 0.25 and 0.30 mM, respectively. CDHP and CBEH displayed a hormetic response. Osmolality measurements indicated that CDHP, CDBP, and CDEP exhibit nearly complete dissociation in aqueous solution, with osmotic coefficients of 1.0, 0.9, and 0.8, whereas CTMP and CBEH have coefficients of 0.5 and 0.3, and are more molecular in character. A high correlation between the  $\text{EC}_{50}$  value and the anion mass fraction indicated that anion size and the presence of moderately long and/or branched alkyl chains may affect viability.

## Introduction

Recently a number of ionic liquids (ILs) have been demonstrated to improve the thermal stability and shelf life of proteins in liquid formulations, and thus show great promise as stabilizing excipients or solvents for protein therapeutics.<sup>1–4</sup> Ionic liquids (ILs) consist of an anion and cation, but unlike typical salts, they are liquid at/near room temperature and can thus replace water and other solvents in a range of applications, potentially including protein-based pharmaceutical formulations intended for parenteral injection. The anion and cation choice can be tailored to provide desired solvent characteristics, such as polarity, viscosity, hydrogen bonding capacity, and conductivity. One of the elements considered mandatory for IL product development is the inclusion of a systematic evaluation of the toxicological properties.<sup>5</sup> An additional level of analysis requires the examination of side chains present on the ions, since ion effects on cytotoxicity have also been reported for ILs.<sup>6,7</sup>

When rationally designing new compounds for use within the body, it can be beneficial to use starting materials that are

already FDA-approved for drug formulation or alternatively are naturally found within the body. Because of the prevalence of choline and phosphates in the human body, a family of choline phosphate salts have been prepared and investigated for use in protein-based therapeutics.<sup>3</sup> The IL CDHP has been shown to dramatically improve the shelf life of cytochrome c when used as the major co-solvent with water, and in solution the protein was shown to retain both structure and activity.<sup>3,8</sup> The ability of proteins to retain a properly folded structure is paramount to their function *in vivo* and efficacy in therapeutic application. The potential benefit of affording storage and delivery in a liquid vehicle makes formulation in ILs like CDHP an alternative to costlier lyophilized products. The aim of this study was to evaluate the cytotoxicity of a panel of choline-based ILs in order to identify the least toxic for continued development as potential components in pharmaceutical formulations. Ionic liquids studied involve choline as a cation and a series of phosphate and phosphinate anions to investigate the possible roles of structural modifications, compared to choline dihydrogen phosphate itself, in the cytotoxicity of this family of compounds. The choline salts of: dihydrogen phosphate (CDHP), dibutyl phosphate (CDBP), bis(2-ethylhexyl) phosphate (CBEH), bis(2,4,4-trimethylpentyl) phosphinate (CTMP), and *O,O'*-diethyl dithiophosphate (CDEP) were investigated. Simple salts and sugars were included for comparison.

Another important consideration in the development of ILs for biological formulation is that the osmotic strength of IL

<sup>a</sup>Department of Mechanical Engineering and Engineering Science, University of North Carolina at Charlotte, Charlotte, North Carolina, 28223, USA. E-mail: gdelliot@uncc.edu

<sup>b</sup>School of Chemistry, Monash University, Clayton, VIC, 3800, Australia

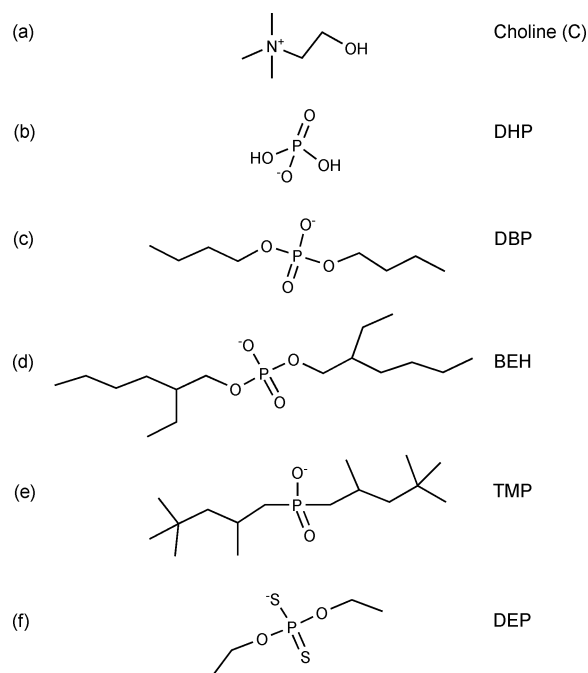
† Electronic supplementary information (ESI) available: Thermogravimetric analysis of choline ionic liquids. See DOI: 10.1039/b918726j

containing solutions must be well-defined. Recent work has shown that many of the ionic liquids that are of interest in bio-applications are not fully ionic; instead they exist as ion pairs in the neat liquid.<sup>9</sup> This observation indicates that an intermediate level of dissociation is occurring for these ILs where the solution behavior is between that of a fully ionic liquid and a molecular solvent such as water. Since the osmolality of the IL could potentially be much lower than one would expect for a simple salt, we have acquired osmolality measurements using a vapor pressure osmometer for the currently investigated family of choline salts.

## Results and discussion

The structures of the phosphate-based ILs included in this study are shown in Fig. 1. To establish the relative toxicity of these compounds, mouse macrophage cells (J774) were used as a model cell type. The J774 macrophage cell line was chosen due to proven applicability in particulate toxicity and intracellular drug effectiveness studies.<sup>10,11</sup> Cell viability following exposure to ILs was measured using a resazurin-based fluorometric assay to estimate the number of metabolically active cells in 96-well plates. Viable cells reduce resazurin to fluorescent resorufin whereas nonviable cells do not generate a significant fluorescent signal. Stock solutions of ionic liquids were prepared in culture medium composed of Dulbecco's modification of Eagle's medium (DMEM) with L-glutamine, 4.5 g L<sup>-1</sup> glucose and sodium pyruvate complemented with 10% fetal bovine serum and 1% penicillin/streptomycin. Cells were exposed to 1:1 serial dilutions of each IL compound in 96-well plates for 48 h. Each plate contained a negative control (media, no cells), and a vehicle control (untreated cells). Concentrations ranged from 0.2 to 113 mM, and were optimized for complete concentration–response curves including hormetic effects.

The simple sugar trehalose showed incomplete inhibition in the concentration range tested, and has an EC<sub>50</sub> >100 mM, while the simple salts (sodium chloride, and choline chloride) had EC<sub>50</sub> values of 63 and 34 mM respectively (Table 1). The EC<sub>50</sub> values (mM) of CDHP (20), CDBP (9.1), and CDEP (8.2) listed in Table 1 were lower than simple salts, suggesting that they were slightly more toxic, but still within the range of typical



**Fig. 1** Structures and names of compounds examined: (a) choline (C), (b) dihydrogen phosphate (DHP), (c) dibutyl phosphate (DBP), (d) bis(2-ethylhexyl) phosphate (BEH), (e) bis(2,4,4-trimethylpentyl) phosphinate (TMP), (f) *O,O'*-diethyl dithiophosphate (DEP).

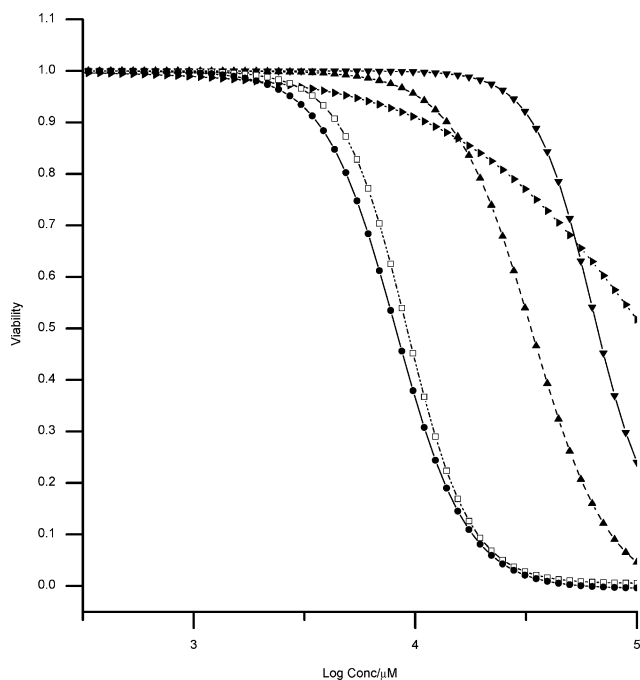
physiologic salts as shown in Fig. 2. The EC<sub>50</sub> value for CDHP is consistent with toxicity trends observed previously (Table 1).<sup>12</sup> The short sulfanyl and sulfanylidene groups on CDEP appear to yield similar toxicity effects to the four-carbon side chains on CDBP (Fig. 1 and 2); however, these two compounds were approximately two-fold more toxic than CDHP (Table 1).

The compounds CTMP and CBEH gave EC<sub>50</sub> values of <0.25 and 0.30 mM, respectively, lower than all the other compounds tested (Table 1). Media-based solutions prepared with CTMP appeared to form emulsions or micellar solutions that may have trapped, or even precipitated media nutrients. Due to these low solubility and solution characteristics, the EC<sub>50</sub> value for CTMP can only be estimated, and is assumed to be lower than 0.25 mM (Fig. 3). Since choline chloride did not display

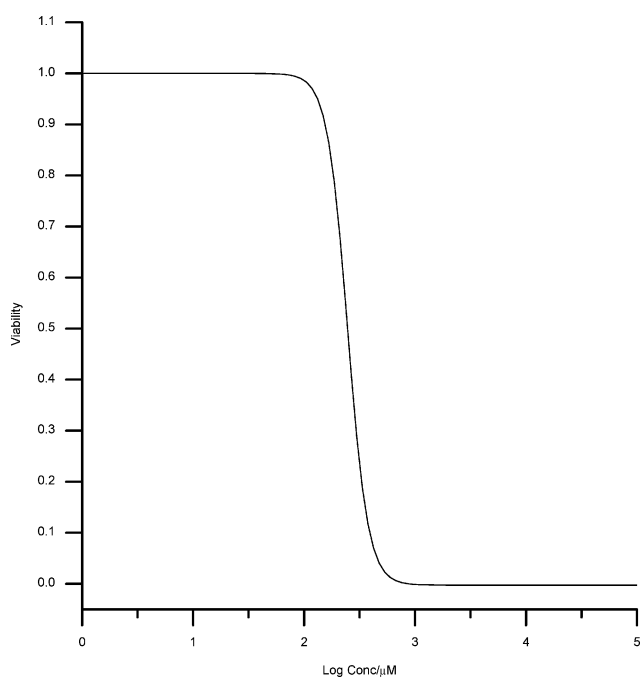
**Table 1** List of compounds, MWs, mass fractions, log EC<sub>50</sub> values, and osmotic coefficients

Compound (abbreviation)	MW/g mol <sup>-1</sup>	Anion mass fraction, $\chi^a$	log EC <sub>50</sub> /μM (dose–response model) <sup>b</sup>	log EC <sub>50</sub> /μM (logistic model) <sup>c</sup>	Osmotic coeff, $\phi$ in H <sub>2</sub> O <sup>d</sup>
Choline chloride (ChCl)	139.625	0.3	4.53(4)	n/a	0.86
Sodium chloride (NaCl)	58.443	0.6	4.8(1)	n/a	0.91
Trehalose (Tre)	378.33	n/a	5.1(5)	n/a	1.01
Choline dihydrogen phosphate (CDHP)	201.158	0.5	4.31(4)	4.28(6)	0.98
Choline dibutyl phosphate (CDBP)	313.366	0.7	3.96(3)	n/a	0.90
Choline bis(2-ethylhexyl) phosphate (CBEH)	425.574	0.8	2.47(3)	2.43(3)	0.31
Choline bis(2,4,4-trimethylpentyl) phosphinate (CTMP)	393.574	0.7	2.39(2)	n/a	0.48
Choline <i>O,O'</i> -diethyl dithiophosphate (CDEP)	289.382	0.6	3.91(2)	n/a	0.76

<sup>a</sup> Anion mass fraction,  $\chi = m_i/m$ , where  $m_i$  = mass of anion,  $m$  = total mass of substance in system. <sup>b</sup> Dose response model as defined in eqn (1). Error of last digit denoted in parentheses. <sup>c</sup> Modified dose–response model as defined in eqn (2). Error of last digit denoted in parentheses. <sup>d</sup> Osmotic coefficient,  $\phi = (\text{osmol/L})/nC$ , where  $n$  = number of particles,  $C$  = molar concentration of solute, osmol/L = osmolality. Measured for 100 mM solutions prepared in deionized water.



**Fig. 2** Dose response curves for J774 indicating toxicity effect of ionic liquids. Fitted concentration curves (dose–response model, eqn (1)) for trehalose  $\blacktriangle$ , NaCl  $\blacktriangledown$ , choline chloride  $\blacktriangle$ , CDBP  $\square$ , and CDEP  $\bullet$ .



**Fig. 3** Dose response curves for J774 indicating toxicity effect of ionic liquid CTMP. Fitted concentration curve (dose–response model, eqn (1)).

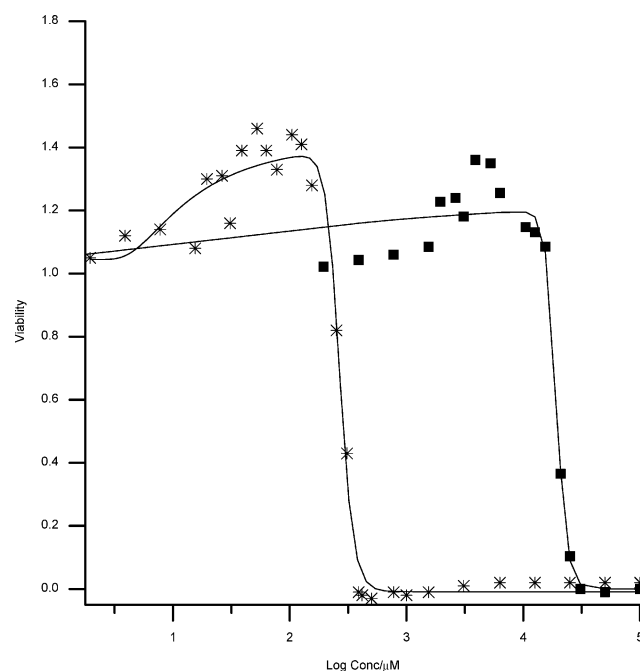
toxicity at the lower concentration level where the CTMP and CBEH  $EC_{50}$  values occur, it can be concluded that there is not an intrinsic cation effect on cytotoxicity. Thus, the toxicity of CTMP and CBEH can be attributed to the anion and in the case of CTMP and CBEH, perhaps the longer and branched

alkyl chain substituents. The alkyl substituents on both anions (TMP and BEH) would cause a larger degree of hydrophobic and perhaps amphiphilic character, making these anions potentially less miscible with water compared to the less toxic anions. These substituents may also be affecting the nature of cell membrane interactions, which could enhance toxicity. Although the R-group on BEH has a substituent that is one carbon longer than that of TMP, this anion exhibits a slightly lower toxicity. CTMP is a phosphinate ( $OP(OR)_2$ ) whereas the others (CDHP, CDBP, and CBEH) have the formula  $OP(OR)_3$ , that is, CTMP has two fewer oxygen atoms which could contribute to the observed difference in toxicity and possibly solubility. Additionally, CTMP may serve as a competing ligand for the metal components present in the media, limiting cellular availability or may even be inhibiting a membrane-associated enzyme. The causes for the differences in toxicity remain to be further investigated.

In the case of both CDHP and CBEH, cell viability *increased* with increasing concentration before passing through a maximum and eventually falling away with additional increasing ionic liquid concentration, *i.e.*, both compounds induced a subtoxic stimulus or hormetic response (Fig. 4). The inverted U-shaped dose response curves for both data sets were fit with a dose-response model (Experimental, eqn (1)) and a modified logistic model that includes a parameter that describes hormesis (Experimental, eqn (2)).

$$y = A1 + \frac{(A2 - A1)}{1 + 10^{(\log x_0 - x)^p}}, \quad (1)$$

$$y = A1 + \frac{A2 - A1 + f \exp(-1/x^\alpha)}{1 + \exp\{p[\ln(x) - \ln(x_0)]\}}, \quad (2)$$



**Fig. 4** Dose response curves for J774 indicating hormetic effects. Raw data and fitted concentration curves (modified logistic model, eqn (2)) for CBEH  $*$ , and CDHP  $\blacksquare$ .

See the experimental section, statistical analyses for a detailed description of the equation parameters. The  $EC_{50}$  values obtained from the two models were within error of one another, and the hormetic model appears to describe the toxicity behavior of CBEH reasonably well. However, the hormetic effect of CDHP showed considerable variability. The significant changes in the character of the hormetic trend for CDHP, especially the range of hormesis, were not accommodated well by the current model, indicating the need for improved hormesis model development, which will be addressed further elsewhere.

In addition, CDHP was observed to exceed the buffer capacity of the complemented media at high concentrations ( $\geq 50$  mM), as indicated by a color change in the pH indicator. At 100 and 50 mM CDHP, the pH was 6.48 and 6.77 ( $\pm 0.01$ ) respectively. After dilution with media to 25 mM, the solution had a pH of 7.52, close to that of the media alone. This concentration is higher than the  $EC_{50}$  value for CDHP. Although during the cell-based assay subtle changes in pH near the  $EC_{50}$  value cannot be ruled out, it is not clearly apparent whether toxicity can be attributed to pH effects where viability decreases as the buffer capacity is approached.

Choline is an essential nutrient, and serves many physiological roles due to its incorporation in membrane components, signaling molecules, and neurotransmitters.<sup>13</sup> It is reported that choline does not permeate cell membranes, but must be transported by a carrier-mediated system.<sup>13</sup> Inverted U-shaped dose-response curves have been reported for choline in cholinergic drug studies, and for high-affinity choline transporters.<sup>13,14</sup> Brock suggests that the biphasic effect of the dose-response curves indicates that more than one intracellular process is involved.<sup>13</sup> Biphasic dose-response curves indicate complex physiological action, and gave rise to the concept of hormesis described as low-dose stimulation followed by high-dose inhibition.<sup>13,15,16</sup> The fact that these effects were not observed with choline chloride or with the other choline-based ionic liquids included in this study seem to indicate that the effect in this test system is due to the anion (DHP or BEH). It does not appear that the hormetic effects can be attributed to pH changes, as pH was controlled by the media at the lower test compound concentrations where growth stimulus effects were observed. This raises an interesting question with respect to what exactly is occurring that manifests as the hormetic effect.

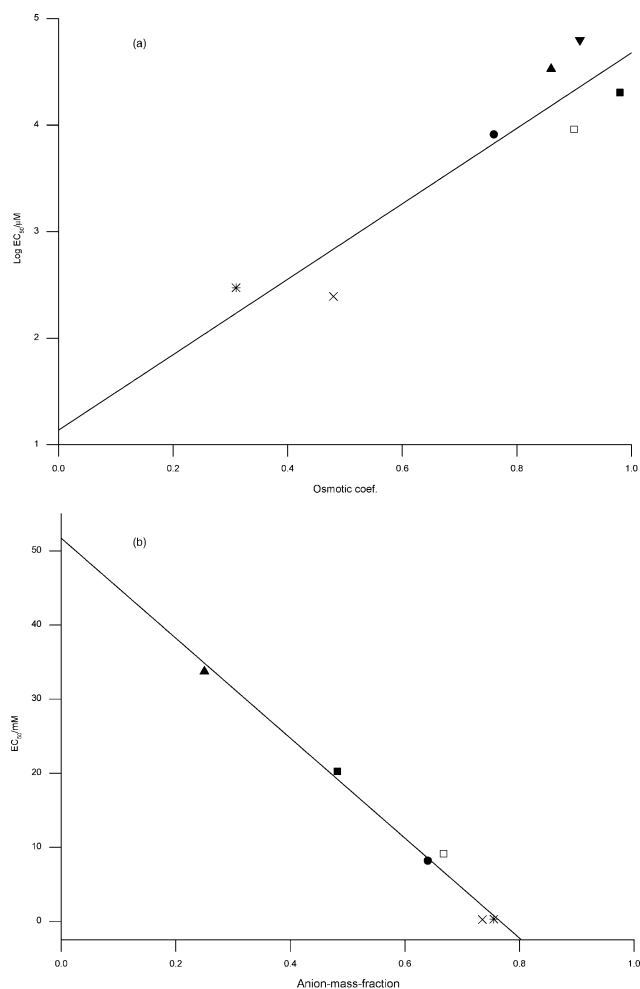
To improve the biocompatibility of injected therapeutics, the osmolality of such solutions are ideally formulated to be near that of extra- and intracellular fluids. Otherwise the imbalance in the chemical potential of water inside and outside the cells near the injection site will result in a rapid transport of water to/from the cells. This can cause cell injury, resulting in pain at the injection site. Because ionic liquids can exhibit solution behavior ranging from molecular in nature to that of a fully dissociated ionic solution, it is important to understand this behavior in order to predict final solution osmolalities in formulations.<sup>9,17</sup> Osmolality measurements of ILs formulated at 100 mM in water were determined using a vapor pressure osmometer. From these measurements, osmotic coefficients ( $\phi$ ) in water, which account for the degree of non-ideality of a solution, were calculated so that the degree of dissociation of each ionic liquid could be assessed. CDHP, CDBP, and CDEP have osmotic coefficients of  $\phi = 1.0$ , 0.9, and 0.8 respectively

at 100 mM (Table 1), where a value of 1 indicates 100% dissociation. CTMP ( $\phi = 0.5$ ) and CBEH ( $\phi = 0.3$ ) have very low coefficients (Table 1), and although these ionic liquids are composed of ionic salts, it appears that they may have not dissociated completely. While electrostatic effects can also cause depression in osmotic coefficients, osmotic coefficients at or below 0.5 for CTMP and CBEH seem to indicate more molecular *versus* ionic solution character. The observed limited dissociation for CTMP and CBEH indicates the possibility for ion pair formation in aqueous solution, suggesting that toxicity could be a result of membrane interactions as observed for other neutral and potentially lipophilic ILs.<sup>6</sup>

Although the other compounds were completely miscible with water and complemented media at all concentrations investigated, CTMP formulated at 10 and 100 mM appeared to precipitate at 4 °C, and form an emulsion or dispersion at 25 °C and 37 °C. The 1 mM CTMP used as the stock solution for the cell-based assays did not exhibit the same insolubility profile, *i.e.* CTMP appears to be miscible with water at 1 mM concentrations. Still, the characteristics of the CTMP emulsions remain to be elucidated, since potential particle formation in the solutions containing higher levels of CTMP might involve nutrient sequestration which would adversely affect cell viability in addition to lowering the osmolality.

It has been shown for a series of acetate-based ILs that higher anion molar concentrations enhanced the dissolution of substrates in the pure IL, but lowered enzyme activity, indicating that an optimum ion size is required to satisfy both sufficient substrate solution and enzyme activity conditions.<sup>18,19</sup> To determine if a similar anion size effect for toxicity could be occurring, the  $EC_{50}$  value was compared to both the osmotic coefficient and an approximate measure of anion size for this series of choline-based ILs (Fig. 5). The anion size is inferred from the calculated mass fraction of anion in the ionic liquid. Since the cation is common to all the salts studied and assuming that their densities are approximately the same, the mass fraction anion is a reflection of anion size. Looking at the log  $EC_{50}$  values *versus* the osmotic coefficients for the choline salts, it appears that there is clustering of the more toxic and molecular-like salts (Fig. 5A). Comparison of  $EC_{50}$  to the anion-mass-fraction shows that apparent anion size and toxicity are closely correlated (Fig. 5B), with a correlation coefficient of (adj.  $R^2 = 0.98$ ; note: the adjusted "adj."  $R^2$  statistic accounts for the degrees of freedom in the model, OriginPro 8). The trend observed for  $EC_{50}/mM$  *versus* anion mass fraction suggests that higher anion mass fractions correlate with higher J774 toxicity (Fig. 5B). This indicates that changes in anion size due to the incorporation of moderately long and or branched alkyl chains, or substitution with sulfur groups, may affect viability such as that seen for ILs CTMP, CBEH, and CDEP. The reason for this correlation is not clear, but could be related to interactions with lipid membranes, or possible electronic effects due to the differences in charge distribution of potential ion pairs within the solvent.

The anion effect was also examined through comparison of the ratio of the  $EC_{50}$  values of the chloride-containing choline reference salt and the  $EC_{50}$  for each of the choline-based IL compounds tested. The anion effect ratio (AR) (eqn (3)) was first used by Stolte to classify the toxicity of anions in ionic liquids, where AR values  $< 5$  were considered non-cytotoxic



**Fig. 5** Effect of osmotic coefficient and anion mass fraction on viability. (a) The osmotic coefficient of each anion is plotted against the log EC<sub>50</sub>/μM. Choline chloride ▲, CDHP ■, CDBP □, CBEH \*, CTMP ×, CDEP ●, and sodium chloride ▼. Adj. R<sup>2</sup> = 0.83. (b) The anion mass fraction versus EC<sub>50</sub>/mM. The mass fraction ( $\chi$ ) of each anion is expressed as in the equation  $\chi = m_i/m$ , where the mass of each component  $i$  is defined as its amount  $m_i$  divided by the total amount of substance in the system,  $m$ . Choline chloride ▲, CDHP ■, CDBP □, CBEH \*, CTMP ×, and CDEP ●. Adj. R<sup>2</sup> = 0.98. Data analyzed with OriginPro 8; the error of the last digit is in parenthesis.

or marginally cytotoxic, and values >5 were described as significantly influencing cytotoxicity,

$$AR = \frac{EC_{50}(CCI)}{EC_{50}(CY)}, \quad (3)$$

where CCI stands for choline chloride and CY stands for choline paired with anion Y.<sup>6</sup> CDHP has the lowest cytotoxicity with AR = 1.7, followed by CDBP = 3.7. The CDEP AR = 4.1 is approaching a borderline value of 5 and could be considered marginally cytotoxic. The AR values for CTMP (137) and CBEH (113) are over an order of magnitude greater than 5, and so these two anions (TMP and BEH) are considered to significantly influence the toxicity of these two ionic liquids, and therefore are not ideal for further exploration as excipients for pharmaceutical application. While the actual mode of CTMP and CBEH anion toxicity has yet to be determined,

it appears to be consistent with toxic effects observed for cations with longer alkyl chains.<sup>20,21</sup> Longer alkyl chains impart the anion with a hydrophobic tail that is lipophilic, and in an effort to escape contact with the aqueous environment it will associate and possibly intercalate with cell membranes. Still, the molecular nature of the ion pairs suggested by their osmotic coefficients may impart a mixed cytotoxicity in that an uncharged species introduced to the membrane may enable membrane interactions and increase cytotoxicity.<sup>22</sup> Future work in membrane perturbation and adjustments in lipophilicity will address the possibility of membrane interactions with this family of ILs.

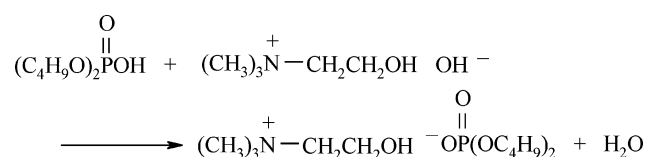
## Experimental

### Materials

Sodium chloride was purchased from VWR International,  $\alpha,\alpha$ -Trehalose dehydrate was purchased from Ferro Pfanstiehl Laboratories. Choline chloride, choline hydroxide, methanol, dihydrogen phosphate, dibutyl phosphate, bis(2-ethylhexyl) phosphate, and *O,O'*-diethyl dithiophosphate were obtained from Sigma-Aldrich. Bis(2,4,4-trimethylpentyl) phosphinate was obtained from Cytec. All chemicals were used as received, except as otherwise specified. ELGA Purelab Ultra water (18.2 M $\Omega$  cm) was used in the preparation of all water-based solutions.

### Ionic liquids

Choline dihydrogen phosphate (CDHP) was synthesized at Monash University according to previous methods.<sup>3,23</sup> Choline salts of dibutyl phosphate (CDBP), bis(2-ethylhexyl) phosphate (CBEH), bis(2,4,4-trimethylpentyl) phosphinate (CTMP), and *O,O'*-diethyl dithiophosphate (CDEP) were synthesized at Monash University as described below. Choline dibutyl phosphate (CDBP) was synthesized *via* a neutralization reaction as shown in Scheme 1.



**Scheme 1**

A typical procedure for the synthesis of CDBP is as follows: 3.342 g (0.0159 mol) dibutyl phosphate was dissolved in 4 g of ethanol, a choline hydroxide–methanol solution containing 0.0159 mol of choline hydroxide was added dropwise, and the mixture was stirred at room temperature for more than 4 h; the solvent was removed by distillation, and the product was dried under vacuum at 70 °C for at least 2 days. The other three choline ILs were synthesized *via* the same procedure as that of CDBP, using bis(2-ethylhexyl) phosphate instead of dibutyl phosphate for CBEH, using bis(2,4,4-trimethylpentyl) phosphinate for CTMP, and using *O,O'*-diethyl dithiophosphate for CDEP.

The resultant salts were characterized using electrospray mass spectrometry and thermogravimetric analysis. Electrospray mass spectrometry (cone  $\pm 35$  V),  $m/z$  (relative intensity, %)

for CDBP: ES<sup>+</sup>, 103.9 ([CH<sub>3</sub>]<sub>3</sub>[C<sub>2</sub>H<sub>4</sub>OH]N<sup>+</sup>, 100), 417.4 (M – [CH<sub>3</sub>]<sub>3</sub>[C<sub>2</sub>H<sub>4</sub>OH]N<sup>+</sup>, 10); ES<sup>-</sup>, 153.0 ([C<sub>4</sub>H<sub>9</sub>O]OPO<sup>-</sup>, 7); 209.2 ([C<sub>4</sub>H<sub>9</sub>O]<sub>2</sub>OPO<sup>-</sup>, 100). CBEH: ES<sup>+</sup>, 103.9 ([CH<sub>3</sub>]<sub>3</sub>[C<sub>2</sub>H<sub>4</sub>OH]N<sup>+</sup>, 100); ES<sup>-</sup>, 321.3 ([C<sub>8</sub>H<sub>17</sub>O]<sub>2</sub>OPO<sup>-</sup>, 100). CTMP: ES<sup>+</sup>, 103.9 ([CH<sub>3</sub>]<sub>3</sub>[C<sub>2</sub>H<sub>4</sub>OH]N<sup>+</sup>, 100), 497.5 (M – [CH<sub>3</sub>]<sub>3</sub>[C<sub>2</sub>H<sub>4</sub>OH]N<sup>+</sup>, 7); ES<sup>-</sup>, 289.4 ([C<sub>8</sub>H<sub>17</sub>O]<sub>2</sub>OPO<sup>-</sup>, 100), 579.4 ([C<sub>8</sub>H<sub>17</sub>]<sub>2</sub>OPOH – [C<sub>8</sub>H<sub>17</sub>]<sub>2</sub>OPO<sup>-</sup>, 10). CDEP: ES<sup>+</sup>, 103.8 ([CH<sub>3</sub>]<sub>3</sub>[C<sub>2</sub>H<sub>4</sub>OH]N<sup>+</sup>, 100); ES<sup>-</sup>, 156.8 ([C<sub>2</sub>H<sub>5</sub>O]SPS<sup>-</sup>, 18), 184.8 ([C<sub>2</sub>H<sub>5</sub>O]<sub>2</sub>SPS<sup>-</sup>, 100).

A PerkinElmer Thermogravimetric Analyzer (TGA) was used to test thermal stability of the choline ILs. Scan rate was 10.0 °C min<sup>-1</sup> from room temperature to 800 °C under a nitrogen atmosphere. See Fig. S1† for thermal traces.

Alkyl chain length and substituent composition were altered for the anions to test the influence of variation in the anion. The chemical structures of the compounds are given in Fig. 1.

### Cell line

Mouse macrophage cells (J774A.1) were obtained from American Type Culture Collection (ATCC® Number TIB-67™), Manassas, VA. Cultures of J774A.1 were grown at 37 °C in a humidified atmosphere in a total volume of 10 mL of Dulbecco's modification of Eagle's medium (DMEM, with phenol red) with L-glutamine, 4.5 g L<sup>-1</sup> glucose and sodium pyruvate (Mediatech, 10-013-CM) supplemented with 10% fetal bovine serum (FBS) (Atlanta Biologicals, S11150), 1% 5000 IU penicillin 5000 µg mL<sup>-1</sup> streptomycin (P/S) solution (Mediatech, 30-001-CI), pH 7.53 ± 0.01 under 5% CO<sub>2</sub> in 250 mL Cellstar® tissue culture flasks (Greiner bio-one). The cells were incubated for up to one week in order to obtain a population between 1 × 10<sup>5</sup> and 1 × 10<sup>6</sup> cells mL<sup>-1</sup>. The cells were scraped, centrifuged, and transferred to 20 mL spinner flasks where they were maintained at a density less than 1 × 10<sup>6</sup> cells mL<sup>-1</sup>. Under these culture conditions, the generation time of the cell line was about 24 h.

### Resazurin metabolism assay

All assays were conducted in 96-well Costar cell culture plates (Fisher) at 37 °C. The viability of J774 cells exposed to ionic liquids was measured using a fluorometric assay based on the reduction of resazurin (Sigma-Aldrich).<sup>24</sup> Resazurin was prepared as a stock solution of 0.437 mM in phosphate-buffered saline (PBS, 1X) without calcium and magnesium (Cellgro, Mediatech), and was stored in the dark at 4 °C. The stock resazurin solution was diluted to 0.0437 mM in DMEM containing 10% FBS and 1% P/S (full complement media). Stock solutions of ionic liquids (ILs) (1–100 mM) were prepared in full complement media. For comparison of toxicity, solutions of sodium chloride, choline chloride, and trehalose were included in the same concentration range. Each plate contained a negative (no-cell) control, a vehicle (untreated cell) control, and two IL dilution series with three replicates each. Cells in full complement media were plated at a density of 1 × 10<sup>4</sup> cells per well, and were incubated 2 h at 37 °C to allow attachment. After 2 h, the supernatant was removed, and IL supplemented media was added. The cell viability assays were carried out using a 1:1 dilution series in the range of 100 to 0.2 mM (CDHP, CDBP, and CDEP) or 1 to 0.002 mM (CTMP and CBEH). The cells were incubated for 48 h. After 44 h, the IL-

supplemented medium was removed, 0.0437 mM resazurin was added, and the cells were incubated for an additional 4 h. Assays were repeated in parallel on cells obtained from 3–5 different dates to allow for variability between cultures. Cell viability was measured at λ<sub>emis</sub> = 590 nm (λ<sub>excit</sub> = 560 nm) in a Synergy HT multi-detection microplate reader (Bio-Tek Instruments).

### Osmolality

In order to assess tonicity effects of the ILs, the osmolality of IL solutions (100 mM) prepared in water was measured using a Vapro™ vapor pressure osmometer (Wescor). The osmometer was calibrated against a set of 290, 1000, and 100 mmol kg<sup>-1</sup> osmometry standards prior to each sample.

### Statistical analyses

Background fluorescence was determined on wells containing resazurin but no cells (negative control), and this value was subtracted from all control and treated wells. Nonlinear regression was used to fit the relationship between cell viability (fluorescence) and the decadic logarithm of the tested concentrations. The general equation for a sigmoidal dose-response with variable slope (four-parameter logistic equation) was used to generate logEC<sub>50</sub> values for each compound (OriginPro 8.4) (eqn (1)) where  $x$  is the concentration of the substance to which the cells are exposed,  $y$  is the physiological response normalized for the interval from 1 to 0,  $A_2$  is the maximum  $y$  value at the top plateau ( $x = 0$ ),  $A_1$  is the minimum  $y$  value at the bottom plateau (0).  $\log x_0$  ( $\log EC_{50}$ ) is the  $x$  value when the response is halfway between the minimum and the maximum. The  $p$  value (Hill Slope) or slope factor describes the steepness of the curve and is negative, *i.e.*, the curve decrease as  $x$  increases (inhibitory response to growth).

In the case of compounds CDHP and CBEH, cell viability appeared to increase with increasing concentration until being reduced with increasing concentration, *i.e.*, these compounds induced a subtoxic stimulus or hormetic effect. The concentration–response curves were fit with both a dose–response (four-parameter logistic) model and a modification of the four-parameter logistic model (eqn (2)),<sup>25</sup> where  $f$  describes the hormetic effect and  $\alpha$  governs the rate of hormetic manifestation.  $A_1$  and  $A_2$  carry the same meaning as in eqn (1); however  $p$  no longer accurately describes the Hill Slope, and  $x_0$  provides a lower bound on the EC<sub>50</sub> level. The logEC<sub>50</sub> values derived from each model are within overlapping confidence intervals. The ability of the modified four-parameter logistic model to describe the hormetic responses and the level of hormesis for CDHP and CBEH are the subject of a separate body of work.

### Conclusion

Due to their low vapor pressure, ionic liquids have been used as green solvents, and are increasingly being examined for roles in non-aqueous enzymology and pharmaceutical protein stabilization.<sup>26</sup> Understanding the toxicity of this family of choline phosphate ionic liquids increases the knowledge of their utility for *in vivo* use as well as the potential ecological impacts due to their implementation in diverse applications. These choline-based ionic liquids exhibit a range of toxicities



from low (CDHP) and within the range of basic physiologic salts, to high (CTMP and CBEH) based on the anion effect ratio described by Stolte.<sup>6</sup> If a high IL concentration is required to achieve a biological stabilization effect, these ILs might be best implemented as co-formulation stabilizers within slow-release nano- and micro-particles to maximize the biocompatibility. We have observed that the choice of anion can greatly affect the osmotic coefficient of the solution. For example, CDHP dissociates completely at 100 mM, with an osmotic coefficient of 1.0, whereas CBEH has an osmotic coefficient of 0.3, and would be considered to have behavior more consistent with a molecular solvent. This would minimize the contribution to osmolality compared to traditional salts.

## Acknowledgements

This project was supported by a UNC Charlotte Junior Faculty Research Grant (to G.D.E.), a UNC Charlotte Bonnie Cone Award (NSF Institutional Award No. SBE0548401) (to G.D.E.), and Grant No. 1R21EB00740401A2 from the NIH (to G.D.E. and D.R.M.). D.R.M. is grateful to the Australian Research Council for a Federation Fellowship. K.D.W. is grateful for support provided by a Center for Biomedical Engineering Systems Duke Energy fellowship. We would like to thank Prof. Jiancheng Jiang, Department of Mathematics and Statistics, UNC-Charlotte, for his thoughtful assistance in the analysis of hormetic trends found in the cyto-toxicity data sets. We would also like to acknowledge Cytec Canada Inc. for provision of the chemicals used in this work.

## References

- J. P. Mann, A. McCluskey and R. Atkin, *Green Chem.*, 2009, **11**, 785–792.
- N. Byrne and C. A. Angell, *J. Mol. Biol.*, 2008, **378**, 707–714.
- K. Fujita, D. R. MacFarlane, M. Forsyth, M. Yoshizawa-Fujita, K. Murata, N. Nakamura and H. Ohno, *Biomacromolecules*, 2007, **8**, 2080–2086.
- S. N. Baker, T. M. McCleskey, S. Pandey and G. A. Baker, *Chem. Commun.*, 2004, 940–941.
- B. Jastorff, R. Störmann, J. Ranke, K. Mölter, F. Stock, B. Oberheitmann, W. Hoffmann, J. Hoffmann, M. Nüchter, B. Ondruschka and J. Filser, *Green Chem.*, 2003, **5**, 136–142.
- S. Stolte, J. Arning, U. Bottin-Weber, M. Matzke, F. Stock, K. Thiele, M. Uerdingen, U. Welz-Biermann, B. Jastorff and J. Ranke, *Green Chem.*, 2006, **8**, 621–629.
- M. Matzke, S. Stolte, K. Thiele, T. Juffernholz, J. Arning, J. Ranke, U. Welz-Biermann and B. Jastorff, *Green Chem.*, 2007, **9**, 1198–1207.
- K. Fujita, M. Forsyth, D. R. MacFarlane, R. W. Reid and G. D. Elliott, *Biotechnol. Bioeng.*, 2006, **94**, 1209–1213.
- K. J. Fraser, E. I. Izgorodina, M. Forsyth, J. L. Scott and D. R. MacFarlane, *Chem. Commun.*, 2007, 3817–3819.
- D. M. Brown, K. Donaldson and V. Stone, *Respir. Res.*, 2004, **5**: 29.
- E. L. Wright, D. C. Quenelle, W. J. Suling and W. W. Barrow, *Antimicrob. Agents Chemother.*, 1996, **40**, 2206–2208.
- R. M. Vrikkis, K. J. Fraser, K. Fujita, D. R. MacFarlane and G. D. Elliott, *J. Biomech. Eng.*, 2009, **131**, 074514.
- M. Brock, A. C. Nickel, B. Madziar, J. K. Blusztajn and B. Berse, *Brain Res.*, 2007, **1145**, 1–10.
- J. F. Flood, D. W. Landry and M. E. Jarvik, *Brain Res.*, 1981, **215**, 177–185.
- E. J. Calabrese and L. A. Baldwin, *Trends Pharmacol. Sci.*, 2002, **23**, 331–337.
- E. J. Calabrese and L. A. Baldwin, *Crit. Rev. Toxicol.*, 2001, **31**, 353–424.
- G. D. Elliott, R. Kemp and D. R. MacFarlane, in *Ionic Liquids: From Knowledge to Application*, eds. N. V. Plechkova, R. D. Rogers and K. R. Seddon, ACS, Washington, DC, 2009, vol. 1030, ch. 6, pp. 95–105.
- H. Zhao, G. A. Baker, Z. Song, O. Olubajo, T. Crittle and D. Peters, *Green Chem.*, 2008, **10**, 696–705.
- H. Zhao, C. L. Jones, G. A. Baker and J. V. Cowins, *Green Chem.*, 2009, **11**, 1128–1138.
- S. Stolte, M. Matzke, J. Arning, A. Bösch, W.-R. Pitner, U. Welz-Biermann, B. Jastorff and J. Ranke, *Green Chem.*, 2007, **9**, 1170–1179.
- R. A. Kumar, N. Papaiconomou, J.-M. Lee, J. Salminen, D. S. Clark and J. M. Prausnitz, *Environ. Toxicol.*, 2009, **24**, 388–395.
- E. Fulladosa, J.-C. Murat, J.-C. Bollinger and I. Villaescusa, *Sci. Total Environ.*, 2007, **377**, 207–213.
- K. Fujita, D. R. MacFarlane and M. Forsyth, *Chem. Commun.*, 2005, 4804–4806.
- B. Pagé, M. Pagé and C. Noël, *Int. J. Oncol.*, 1993, **3**, 473–476.
- N. Cedergreen, C. Ritz and J. C. Streibig, *Environ. Toxicol. Chem.*, 2005, **24**, 3166–3172.
- Z. Yang and W. Pan, *Enzyme Microb. Technol.*, 2005, **37**, 19–28.

# A simple, efficient and green procedure for Knoevenagel condensation catalyzed by [C<sub>4</sub>dabco][BF<sub>4</sub>] ionic liquid in water†

Da-Zhen Xu, Yingjun Liu, Sen Shi and Yongmei Wang\*

Received 9th September 2009, Accepted 21st November 2009

First published as an Advance Article on the web 29th January 2010

DOI: 10.1039/b918595j

A convenient and rapid method for Knoevenagel condensation has been developed by using DABCO-base ionic liquid catalysts. This method is applicable to a wide range of aromatic/aliphatic/heterocyclic/ $\alpha,\beta$ -unsaturated aldehydes and ketones with active methylene compounds, and affords the corresponding substituted electrophilic alkenes in excellent yields (up to 100%) in water at room temperature within short times. The method is operationally simple and the products do not need to be purified. The use of water as the reaction medium makes the process environmentally benign. The catalysts can be recycled seven times without activity loss.

## Introduction

In recent years, ionic liquids (ILs) have attracted significant attention as green solvents for many chemical and biochemical transformations.<sup>1</sup> Many functional ILs have also been synthesized and utilized as catalysts for different reactions, such as the Henry reaction,<sup>2</sup> direct Aldol reaction,<sup>3</sup> Mannich reaction,<sup>4</sup> Michael addition<sup>5</sup> and Knoevenagel condensation.<sup>6</sup>

The Knoevenagel condensation is one of the most important reactions in organic synthesis for carbon–carbon bond formation. It is usually performed in organic solvents in the presence of common bases such as ammonia, primary or secondary amines and their salts.<sup>7</sup> In recent years, a wide array of catalysts, including Lewis acids,<sup>8</sup> zeolites,<sup>9</sup> solid bases,<sup>10</sup> heterogeneous catalysts<sup>11</sup> and amines immobilized on polymers,<sup>12</sup> have been employed to catalyze this reaction, each affording variable yields of Knoevenagel condensation compounds in solution or under solvent-free conditions.

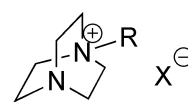
However there are still a lot of disadvantages of these new catalysts. For example, when the Lewis acidic catalysts, such as ZnCl<sub>2</sub>,<sup>13</sup> were used in the reaction, the conditions should be absent from water. In addition, these catalysts could not be reused because of the water made from the Knoevenagel reaction itself. Sometimes, the reaction time was too long,<sup>14</sup> and the reaction must be heated or it needed other special conditions,<sup>15</sup> such as microwave irradiation. In most cases, the range of carbonyl compounds was limited to aromatic aldehydes, and a few examples used aliphatic aldehydes and ketones at room temperature with excellent yields.<sup>6,16</sup>

One of the fundamental challenges and ultimate goals for organic reactions is to perform the reaction in water,<sup>17</sup> because in comparison with organic solvents, water is cheap, safe and

leads to the development of environmentally friendly chemical processes.<sup>18</sup>

As a result, a simple, efficient and green procedure for Knoevenagel condensation with excellent results with all kinds of aldehydes and ketones remains a major challenge in synthetic organic chemistry.

In this paper we report a class of catalysts which are compatible with various aldehydes (aromatic/aliphatic/heterocyclic/ $\alpha,\beta$ -unsaturated) and aliphatic ketones, providing excellent yields and with 100% selectivity. The DABCO-base ionic liquids (Fig. 1) as highly efficient and environmental friendly catalysts are used for Knoevenagel condensations. Moreover, the catalysis can be performed in water, and the catalysts can be recycled many times without loss of activity, offering a greener route to Knoevenagel condensation products.



[C<sub>2</sub>dabco]Br, X = Br, R = ethyl

[C<sub>2</sub>dabco][BF<sub>4</sub>], X = BF<sub>4</sub>, R = ethyl

[C<sub>4</sub>dabco]Br, X = Br, R = butyl

[C<sub>4</sub>dabco][BF<sub>4</sub>], X = BF<sub>4</sub>, R = butyl

[C<sub>8</sub>dabco]Br, X = Br, R = octyl

[Bndabco]Br, X = Br, R = benzyl

Fig. 1 Structures of the DABCO-base ionic liquids.

## Results and discussion

Compounds [C<sub>2</sub>dabco]Br, [C<sub>4</sub>dabco]Br, [C<sub>8</sub>dabco]Br and [Bndabco]Br were synthesized according to the literature.<sup>19</sup> The

Department of Chemistry, State Key Laboratory and Institute of Elemento-Organic Chemistry, Nankai University, Tianjin, 300071, China. E-mail: ymw@nankai.edu.cn; Fax: +86 22 2350 2654; Tel: +86 22 2350 3281

† Electronic supplementary information (ESI) available: Experimental details, analytical data and NMR spectra for catalysts. See DOI: 10.1039/b918595j

**Table 1** Knoevenagel condensation of benzaldehyde with malononitrile catalyzed by DABCO-base ionic liquids in solvent<sup>a</sup>

Entry	Cat. (15 mol%)	Solvent (0.5 mL)	Time/min	Yield (%) <sup>b</sup>
1	[C <sub>2</sub> dabco]Br	neat	5 s	83
2	[C <sub>2</sub> dabco]Br	[Bmim][BF <sub>4</sub> ]	4	98
3	[C <sub>4</sub> dabco]Br	[Bmim][BF <sub>4</sub> ]	7	99
4	[C <sub>8</sub> dabco]Br	[Bmim][BF <sub>4</sub> ]	13	99
5	[Bndabco]Br	[Bmim][BF <sub>4</sub> ]	10	98
6	[C <sub>2</sub> dabco][BF <sub>4</sub> ] <sup>d</sup>	[Bmim][BF <sub>4</sub> ]	< 1	100
7	[C <sub>4</sub> dabco][BF <sub>4</sub> ] <sup>e</sup>	[Bmim][BF <sub>4</sub> ]	< 1	100
8	[C <sub>4</sub> dabco][BF <sub>4</sub> ] <sup>f</sup>	H <sub>2</sub> O	< 1	100
9	[C <sub>4</sub> dabco][BF <sub>4</sub> ] <sup>g</sup>	H <sub>2</sub> O	8	95
10	[C <sub>4</sub> dabco][BF <sub>4</sub> ] <sup>h</sup>	H <sub>2</sub> O	20	94
11	[C <sub>4</sub> dabco][BF <sub>4</sub> ] <sup>i</sup>	neat	20	84
12	[C <sub>4</sub> dabco][BF <sub>4</sub> ] <sup>j</sup>	neat	120	85
13	[C <sub>4</sub> dabco][BF <sub>4</sub> ] <sup>k</sup>	neat	15 h	73
14	Catalyst free	neat	20 h	15

<sup>a</sup> Reaction conditions: benzaldehyde (0.5 mmol), malononitrile (0.5 mmol), catalyst (15 mol%), water (0.5 mL), room temperature.

<sup>b</sup> Isolated yield of product. <sup>c</sup> Catalyst 10 mol%. <sup>d</sup> Catalyst 5 mol%.

<sup>e</sup> Catalyst 1 mol%. <sup>f</sup> Catalyst 0.2 mol%.

method of synthesis of [C<sub>2</sub>dabco][BF<sub>4</sub>] and [C<sub>4</sub>dabco][BF<sub>4</sub>] is described in the Experimental.

The Knoevenagel reaction of benzaldehyde with malononitrile was initially carried out under solvent-free conditions, in which the compound [C<sub>2</sub>dabco]Br served as the catalyst. But the reaction was very fast, and the mixture solidified as soon as the catalyst was added. The yield was not so high, because the reaction mixture could not stir well enough (Entry 1, Table 1). In order to improve the yield, we chose IL [Bmim][BF<sub>4</sub>] as solvent. The results are summarized in Table 1, Entries 2–5. The condensation of benzaldehyde with malononitrile in the solvent of [Bmim][BF<sub>4</sub>] catalyzed by any one of [C<sub>2</sub>dabco]Br, [C<sub>4</sub>dabco]Br or [Bndabco]Br proceeded efficiently, resulting in near a quantitative yield of the product. Then, we changed to BF<sub>4</sub><sup>-</sup> instead of Br<sup>-</sup> as the anion in the catalysts of [C<sub>2</sub>dabco]Br and [C<sub>4</sub>dabco]Br. Under the same conditions, the reactions finished in less than one minute (Entries 6 and 7, Table 1). But the product, which was generated by [C<sub>4</sub>dabco][BF<sub>4</sub>], was solidified from the solvent which made the reaction easy to handle. Catalyst [C<sub>4</sub>dabco][BF<sub>4</sub>] was used as the catalyst of choice. We found that, when the reaction was performed in water, the reaction proceeded as well as in IL [Bmim][BF<sub>4</sub>] (Entry 8, Table 1). The reactions, using water as solvent, allowed Knoevenagel condensation compounds to be performed in a very simple, cheap and green manner. The product, which solidified from the system in a few minutes, was filtered and did not need to be purified. When we reduced the amount of the catalyst [C<sub>4</sub>dabco][BF<sub>4</sub>], the reactions needed more time to finish, but the yields were also very high (Entries 9 and 10, Table 1).

We also used the catalyst [C<sub>4</sub>dabco][BF<sub>4</sub>] to promote the condensation under solvent free conditions. We found that the product **3a** was formed in high yields when 5 mol% and 1% catalyst were used (Entries 11 and 12, Table 1). When we reduced

the amount of the catalyst [C<sub>4</sub>dabco][BF<sub>4</sub>] to 0.2 mol%, the reaction mixture solidified in 15 h with 73% yield (Entry 13, Table 1). The product was obtained with very low yield when no catalyst was added (Entry 14, Table 1).

This shows that, (1) all the DABCO-base ILs can very efficiently catalyze the Knoevenagel condensation, even when 0.2 mol% of the catalyst was used; (2) when the catalysts with aliphatic substituents had less hindrance, or the anions in the ILs had weaker ionicity, the reaction would proceed more efficiently.

Next, the Knoevenagel condensation reactions of various aldehydes, including aromatic/aliphatic/heterocyclic/ $\alpha$ ,  $\beta$ -unsaturated aldehydes, and cyclic and acyclic ketones, were also examined in the presence of [C<sub>4</sub>dabco][BF<sub>4</sub>] (15 mol%) in water with active methylene compounds, and the products were isolated all in excellent yields (>90% yield)(Table 2). The reaction is highly stereoselective with only an *E*-geometry.

**Table 2** Knoevenagel condensations catalyzed by [C<sub>4</sub>dabco][BF<sub>4</sub>]<sup>a</sup>

Entry	1	E	Product	Time/min	Yield [%] <sup>b</sup>
1		CN	<b>3a</b>	< 1	100
2		CN	<b>3b</b>	2	95
3		CN	<b>3c</b>	< 1	100
4		CN	<b>3d</b>	2	100
5		CN	<b>3e</b>	10	97
6		CN	<b>3f</b>	< 1	100
7		CN	<b>3g</b>	1	98
8		CN	<b>3h</b>	2	100
9		CN	<b>3i</b>	1	97
10		CN	<b>3j</b>	15	91

Table 2 (Contd.)

Entry	1	E	Product	Time/min	Yield [%] <sup>b</sup>
11		CN	<b>3k</b>	2	100
12		CN	<b>3l</b>	9	93
13		CN	<b>3m</b>	2	95
14		CO <sub>2</sub> Et	<b>3n</b>	2d	94
15		CO <sub>2</sub> Et	<b>3n</b>	40 <sup>c</sup>	96
16		CO <sub>2</sub> Et	<b>3o</b>	4	96
17		CO <sub>2</sub> Et	<b>3p</b>	5	90

<sup>a</sup> Reaction conditions: carbonyl compound (0.5 mmol), active methylene compound (0.5 mmol), catalyst [C<sub>4</sub>dabco][BF<sub>4</sub>] (19 mg, 15 mol%), water (0.5 mL), room temperature. <sup>b</sup> Isolated yield of product. <sup>c</sup> The Knoevenagel condensation reaction was made at 100 °C.

Compared to the Knoevenagel reactions of malononitrile with aromatic aldehydes, the reactions of ethyl cyanoacetate with the same aromatic aldehydes needed more time. Because the electron-withdrawing ability of the CN group is stronger than that of the carbonyl or carboxylic group, the methylene group of malononitrile is more activated than ethyl cyanoacetate, and readily reacts with aromatic aldehydes. If the reactions of aldehydes with ethyl cyanoacetate were carried out at 100 °C, the Knoevenagel condensations were also very fast (Entry 15, Table 2).

We examined the recyclability of the catalyst. Once product **3a** had been filtered from the mixture, more water was evaporated from the IL [C<sub>4</sub>dabco][BF<sub>4</sub>] under vacuum, and the catalyst was reused for the same reaction. The catalyst showed no substantial reduction in activity even after the seventh run. All reactions were completed in 1–2 min and afforded yields of 92–100%, with no apparent tendency to decline (Table 3).

We have developed an improved process which offered several advantages over this procedure. In this process, after stirring for a few minutes, the product solidified from the mixture, which was filtered and did not need to be purified. The catalyst was an ionic liquid, which was easily recovered and could be reused more than six times. Water as solvent in the reaction made the process very cheap and green. This is a simpler and very mild reaction,

Table 3 Recycling of the catalyst [C<sub>4</sub>dabco][BF<sub>4</sub>] in the Knoevenagel condensation reaction between benzaldehyde and malononitrile<sup>a</sup>

Run	Time/min	Yield (%) <sup>b</sup>
1	< 1	100
2	1	95
3	2	95
4	2	96
5	1	92
6	2	95
7	2	94

<sup>a</sup> Reaction conditions: benzaldehyde (0.5 mmol), malononitrile (0.5 mmol), catalyst ([C<sub>4</sub>dabco][BF<sub>4</sub>], 15 mol%), water (0.5 mL), room temperature. <sup>b</sup> Isolated yield of product.

which is readily amenable to large-scale synthesis. Using this procedure, we tried this reaction out on a one-mol scale, and 145 g of **3a** were prepared in 94% yield. This is therefore an easy access to these substituted electrophilic alkenes on a large scale, using DABCO-base ILs as catalysts.

## Conclusions

In summary, it was demonstrated that the readily available, economic DABCO-base ILs could behave as recyclable catalysts for the Knoevenagel condensation reaction of a broad range of aldehydes (aromatic/aliphatic/heterocyclic/ $\alpha,\beta$ -unsaturated) and ketones with active methylene compounds, offering excellent yields in short times. The reactions, using water as solvent, allowed Knoevenagel condensation reactions to be performed in a very simple, clean and green manner. The products, which solidified from the system in a few minutes, did not need to be purified. What is more, only the *E*-isomers were detected. The catalysts can be recycled many times without activity loss. It is a simple route to large scale synthesis of substituted electrophilic alkenes. We believe that this new synthetic method reported here would greatly contribute to environmentally greener and safer processes.

## Experimental

### Preparation of the catalyst 1-ethyl-4-aza-1-azoniabicyclo[2.2.2]octane tetrafluoroborate ([C<sub>4</sub>dabco][BF<sub>4</sub>])

To a solution of 1-ethyl-4-aza-1-azoniabicyclo[2.2.2]octane bromide (1.78 g, 8.1 mmol) in ethanol (50 mL) was added freshly prepared silver tetrafluoroborate (1.57 g, 8.1 mmol). The mixture was stirred at room temperature for 30 min, then the precipitate was removed by filtration, and the resulting colourless solution was evaporated at reduced pressure (50 °C) to give [C<sub>4</sub>dabco][BF<sub>4</sub>] (1.72 g, 93%). <sup>1</sup>H NMR (300 MHz, D<sub>2</sub>O):  $\delta$  1.19–1.26 (m, 3H), 3.1 (t, 6H,  $J = 7.6$  Hz), 3.19–3.29 (m, 8H); <sup>13</sup>C NMR (75 MHz, D<sub>2</sub>O):  $\delta$  6.75 (CH<sub>3</sub>), 44.20 (CH<sub>2</sub>), 51.56 (NCH<sub>2</sub>), 60.03 (N<sup>+</sup>CH<sub>2</sub>); Anal. Calcd. for C<sub>8</sub>H<sub>17</sub>BF<sub>4</sub>N<sub>2</sub>: C, 42.14; H, 7.51; N, 12.28. Found C, 42.23; H, 7.48; N, 12.34.

### Preparation of the catalyst 1-butyl-4-aza-1-azoniabicyclo[2.2.2]-octane tetrafluoroborate ([C<sub>4</sub>dabco][BF<sub>4</sub>])

[C<sub>4</sub>dabco][BF<sub>4</sub>] was prepared as per our general procedure. <sup>1</sup>H NMR (300 MHz, D<sub>2</sub>O): δ 0.82 (t, 3H, *J* = 7.5 Hz), 1.21–1.38 (m, 2H), 1.55–1.66 (m, 2H), 3.05–3.15 (m, 8H), 3.27 (t, 6H, *J* = 7.6 Hz); <sup>13</sup>C NMR (75 MHz, D<sub>2</sub>O): δ 12.76 (CH<sub>3</sub>), 19.14 (CH<sub>2</sub>), 23.12 (CH<sub>2</sub>), 44.18 (CH<sub>2</sub>), 52.03 (NCH<sub>2</sub>), 64.48 (N<sup>+</sup>CH<sub>2</sub>); Anal. Calcd. for C<sub>10</sub>H<sub>21</sub>BF<sub>4</sub>N<sub>2</sub>: C, 46.90; H, 8.27; N, 10.94. Found C, 47.17; H, 8.12; N, 10.98.

### General procedure for Knoevenagel condensation

A 5-mL round bottomed flask was charged with the carbonyl compound (0.5 mmol), active methylene compound (0.5 mmol), ionic liquid catalyst [C<sub>4</sub>dabco][BF<sub>4</sub>] (19 mg, 15 mol% of the substrates) and water (0.5 mL). The reaction mixture was stirred at the room temperature. The formation of the products was monitored by TLC. After completion of the reaction, the reaction mixture often solidified in the round bottomed flask. The solid mixture was filtered and washed with cold water (5 mL) to remove the catalyst, and then dried to obtain the products. In general, no further purification method was required. All the products were previously reported and were characterized by melting point determination and <sup>1</sup>H NMR spectroscopy. The ionic liquid catalysts were recovered by removing the water of the filtrate and reused in the reaction for seven times. In the case of liquid products, GC was used for yield determination. Selected data for typical compounds are given below.

**2-(Phenylmethylene)malononitrile (3a).** White solid, (78 mg, 100%). M.p. 83–84 °C. <sup>1</sup>H NMR (400 MHz, CDCl<sub>3</sub>): δ 7.54 (2H, t, *J* = 8.0 Hz, ArH), 7.63 (1H, t, *J* = 7.6 Hz, ArH), 7.79 (1H, s, ArH), 7.91 (2H, d, *J* = 7.6 Hz, ArH).

**2-(4-Methylphenylmethylene)malononitrile (3b).** White solid, (84 mg, 95%). M.p. 133–134 °C. <sup>1</sup>H NMR (400 MHz, CDCl<sub>3</sub>): δ 2.46 (2H, s, CH<sub>3</sub>), 7.34 (2H, d, *J* = 8.0 Hz, ArH), 7.22 (1H, s, ArH), 7.81 (2H, d, *J* = 8.0 Hz, ArH).

**2-(2-Furylmethylene)malononitrile (3f).** Red solid, (72 mg, 100%). M.p. 68–69 °C. <sup>1</sup>H NMR (400 MHz, CDCl<sub>3</sub>): δ 6.72 (1H, dd, *J*<sub>1</sub> = 1.6 Hz, *J*<sub>2</sub> = 3.6 Hz), 7.36 (1H, d, *J* = 3.6 Hz), 7.53 (1H, s, CH=), 7.81 (1H, d, *J* = 1.2 Hz).

**2-(Cyclohexylidene)malononitrile (3k).** Colourless liquid, (73 mg, 100%). <sup>1</sup>H NMR (400 MHz, CDCl<sub>3</sub>): δ 1.66–1.73 (2H, m), 1.78–1.84 (4H, m), 2.66 (4H, t, *J* = 6.0 Hz).

**2-(Butan-2-ylidene)malononitrile (3l).** colourless liquid (56 mg, 93%). <sup>1</sup>H NMR (400 MHz, CDCl<sub>3</sub>): δ 1.21 (3H, t, *J* = 7.6 Hz, CH<sub>2</sub>CH<sub>3</sub>), 2.29 (3H, s, CCH<sub>3</sub>), 2.62 (2H, q, *J* = 7.6 Hz, CH<sub>2</sub>CH<sub>3</sub>).

**(E)-ethyl-3-phenyl-2-cyanoacrylate (3n).** white solid, (95 mg, 94%). M.p. 48–49 °C. <sup>1</sup>H NMR (400 MHz, CDCl<sub>3</sub>): δ 1.39 (3H, t, *J* = 7.2 Hz, CH<sub>3</sub>), 4.38 (2H, q, *J* = 6.8 Hz, CH<sub>2</sub>), 7.40–7.55 (3H, m, ArH), 7.88–7.95 (2H, m, ArH), 8.21 (1H, s, ArH).

**(E)-ethyl-3-(3-nitrophenyl)-2-cyanoacrylate (3p).** Orange solid, (111 mg, 90%). M.p. 166–168 °C. <sup>1</sup>H NMR (400 MHz,

CDCl<sub>3</sub>): δ 1.42 (3H, t, *J* = 7.2 Hz, CH<sub>3</sub>), 4.42 (2H, q, *J* = 7.2 Hz, CH<sub>2</sub>), 7.75 (1H, t, *J* = 8.0 Hz, ArH), 8.31 (1H, s, CH=), 8.39–8.43 (2H, m, ArH), 8.70 (1H, s, ArH).

### Acknowledgements

This work was financially supported by the National Natural Science Foundation of China (grant no. 20672061, China) and 863 Project (no. 2007AA05Z102, China). We also thank the Nankai University State Key Laboratory of Elemento-Organic Chemistry for support.

### Notes and references

- (a) N. Jain, A. Kumar, S. Chauhan and S. M. S. Chauhan, *Tetrahedron*, 2005, **61**, 1015; (b) S. Park and J. Kazlauskas, *Curr. Opin. Biotechnol.*, 2003, **14**, 432.
- T. Jiang, H. Gao, B. X. Han, G. Zhao, Y. Chang, W. Wu, L. Gao and G. Yang, *Tetrahedron Lett.*, 2004, **45**, 2699.
- (a) A. L. Zhu, T. Jiang, D. Wang, B. X. Han, L. Liu, J. Huang, J. C. Zhang and D. H. Sun, *Green Chem.*, 2005, **7**, 514; (b) A. L. Zhu, T. Jiang, B. X. Han, J. Huang, J. C. Zhang and X. M. Ma, *New J. Chem.*, 2006, **30**, 736.
- G. Y. Zhao, T. Jiang, B. X. Han, Y. H. Chang, H. X. Gao, J. Huang and D. H. Sun, *Green Chem.*, 2004, **6**, 75.
- (a) B. C. Ranu, S. Banerjee and R. Jana, *Tetrahedron*, 2007, **63**, 776; (b) J.-M. Xu, Q. Wu, Q.-Y. Zhang, F. Zhang and X.-F. Lin, *Eur. J. Org. Chem.*, 2007, 1798.
- (a) B. C. Ranu and R. Jana, *Eur. J. Org. Chem.*, 2006, 3767; (b) Y. O. Sharma and M. S. Degani, *Green Chem.*, 2009, **11**, 526.
- (a) G. Jones, *Org. React.*, 1967, **15**, 204; (b) L. F. Tietze, *Chem. Rev.*, 1996, **96**, 115.
- P. Leelavathi and S. R. Kumar, *J. Mol. Catal. A: Chem.*, 2004, **240**, 99.
- T. I. Reddy and R. S. Varma, *Tetrahedron Lett.*, 1997, **38**, 1721.
- Y. Goa, P. Wu and T. Tatsumi, *J. Catal.*, 2004, **224**, 107.
- S. Nakamura, H. Hirao and T. J. Ohwada, *J. Org. Chem.*, 2004, **69**, 4309.
- B. Tamami and A. Fadavi, *Catal. Commun.*, 2005, **6**, 747.
- F. Delgado, J. Tamariz, G. Zepeda, M. Landa, R. Miranda and J. Garcia, *Synth. Commun.*, 1995, **25**, 753.
- (a) Y. Hu, J. Chen, Z.-G. Le and Q.-G. Zheng, *Synth. Commun.*, 2005, **35**, 739; (b) K. Yamashita, T. Tanaka and M. Hayashi, *Tetrahedron*, 2005, **61**, 7981; (c) G. Lai, J. Peng, J. Li, H. Qiu, J. Jiang, K. Jiang and Y. Shen, *Tetrahedron Lett.*, 2006, **47**, 6951; (d) R. Troztki, M. M. Hoffmann and B. Ondruschka, *Green Chem.*, 2008, **10**, 873.
- (a) S. A.-E. Ayoubi, F. Texier-Boulet and J. Hamelin, *Synthesis*, 1994, 258; (b) J. S. Yadav, B. V. Subba Reddy, A. K. Basak, B. Visali, A. V. Narsaiah and K. Nagaiah, *Eur. J. Org. Chem.*, 2004, 546; (c) F. Bigi, M. L. Conforti, R. Maggi, A. Piccinno and G. Sartori, *Green Chem.*, 2000, **2**, 101; (d) Y. Liu, J. Peng, S. Zhai, J. Li, J. Mao, M. Li, H. Qiu and G. Lai, *Eur. J. Inorg. Chem.*, 2006, 2947; (e) K. Komura, T. Kawamura and Y. Sugi, *Catal. Commun.*, 2007, **8**, 644; (f) R. Troztki, M. M. Hoffmann and B. Ondruschka, *Green Chem.*, 2008, **10**, 767.
- (a) C. Paun, J. Barklie, P. Goodrich, H. Q. N. Gunaratne, A. McKeown, V. I. Pärulescu and C. Hardacre, *J. Mol. Catal. A: Chem.*, 2007, **269**, 64; (b) M. Feroci, M. Orsini, L. Palombi and A. Inesi, *Green Chem.*, 2007, **9**, 323.
- C.-J. Li and L. Chen, *Chem. Soc. Rev.*, 2006, **35**, 68.
- (a) P. Anastas and J. C. Warner, *Green Chemistry: Theory and practice*, Oxford University Press, Oxford, 1998; (b) D. Dallinger and C. O. Kappe, *Chem. Rev.*, 2007, **107**, 2563; (c) V. Polshettiwar and R. S. Varma, *J. Org. Chem.*, 2007, **72**, 7420.
- (a) A. Marra, A. Vecchi, C. Chiappe, B. Melai and A. Dondoni, *J. Org. Chem.*, 2008, **73**, 2458; (b) A. R. Hajipour, H. R. Bagheri and A. E. Ruohob, *Phosphorus, Sulfur Silicon Relat. Elem.*, 2003, **178**, 2441; (c) S. Lall, V. Behaj, D. Mancheno, R. Casiano, M. Thomas, A. Rikin, J. Gaillard, R. Raju, A. Scumpia, S. Castro, R. Engel and J. I. Cohen, *Synthesis*, 2002, 1530.

# A new journal from RSC Publishing Launching mid 2010

Rapid communication of research  
in medicinal chemistry

## MedChemComm



Official journal of:



A new, peer-reviewed journal publishing medicinal chemistry research, including new studies related to biologically-active chemical or biochemical entities that can act as pharmacological agents with therapeutic potential or relevance.

The journal will publish monthly issues from mid 2010 and will contain a mix of vibrant and concise research and review articles. *MedChemComm* will complement the existing RSC Publishing portfolio of bioscience journals, providing authors in the field with a dedicated subject-specific publication.

From launch, the current issue of *MedChemComm* will be freely available to all readers via the website. Free institutional online access to all 2010/2011 content will be available following a simple registration process at [www.rsc.org/medchemcomm\\_registration](http://www.rsc.org/medchemcomm_registration)

Co-Editor-in-Chief: **Dr Anthony Wood**, Pfizer, UK

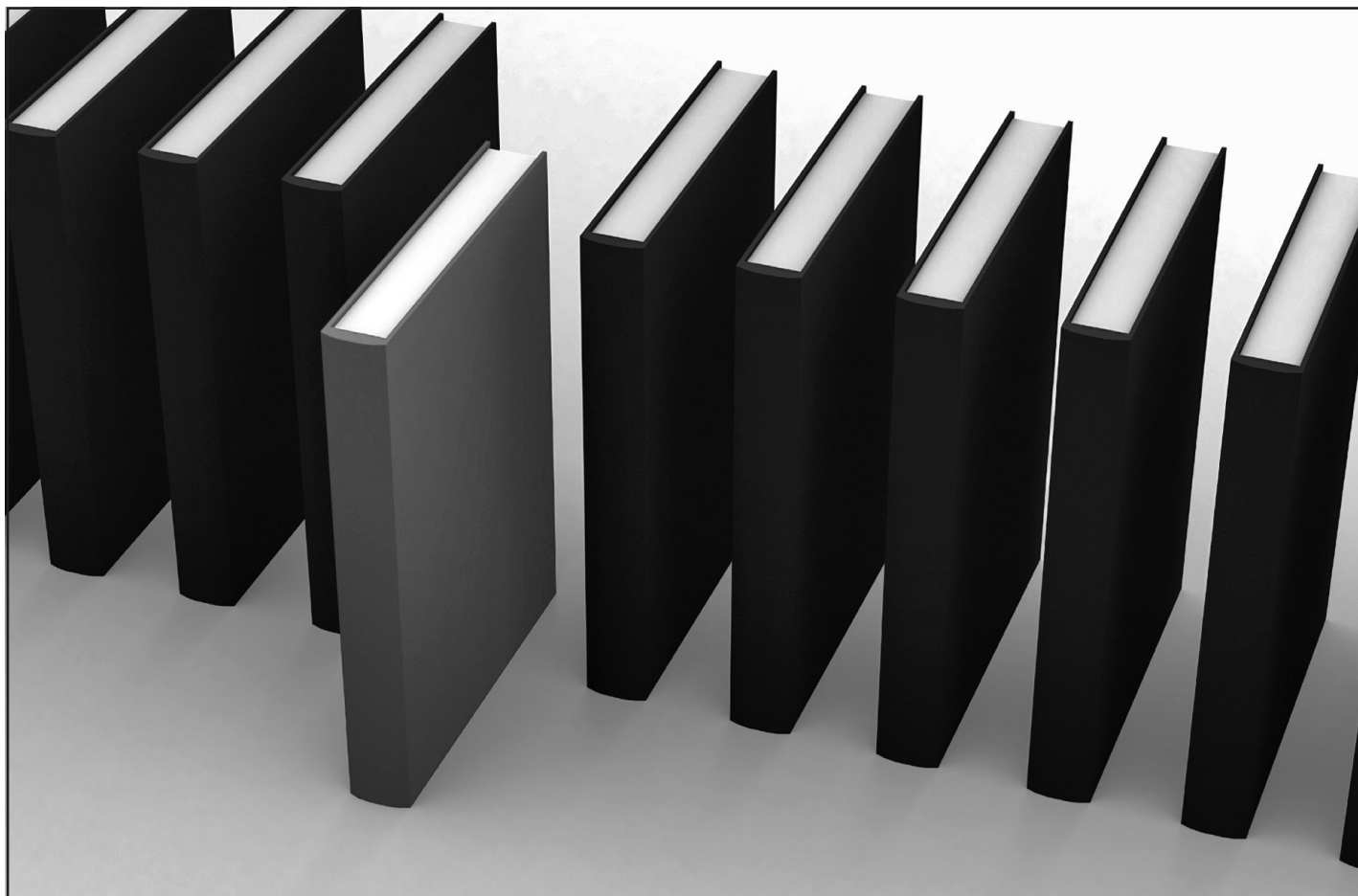
Co-Editor-in-Chief: **Professor Gregory Verdine**, Harvard University, USA

**Sign up for free access today!**

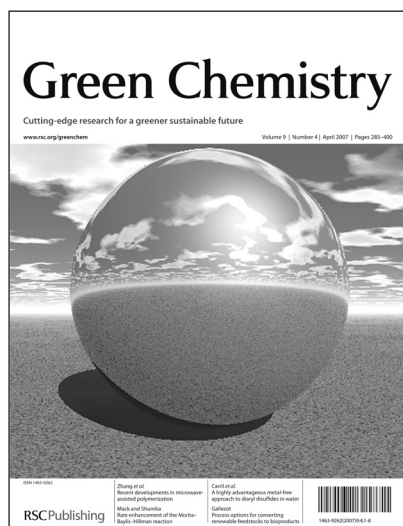
RSC Publishing

[www.rsc.org/medchemcomm](http://www.rsc.org/medchemcomm)

Registered Charity Number 207890



## 'Green Chemistry book of choice'



Why not take advantage of free book chapters from the RSC? Through our 'Green Chemistry book of choice' scheme *Green Chemistry* will regularly highlight a book from the RSC eBook Collection relevant to your research interests. Read the latest chapter today by visiting the *Green Chemistry* website.

The RSC eBook Collection offers:

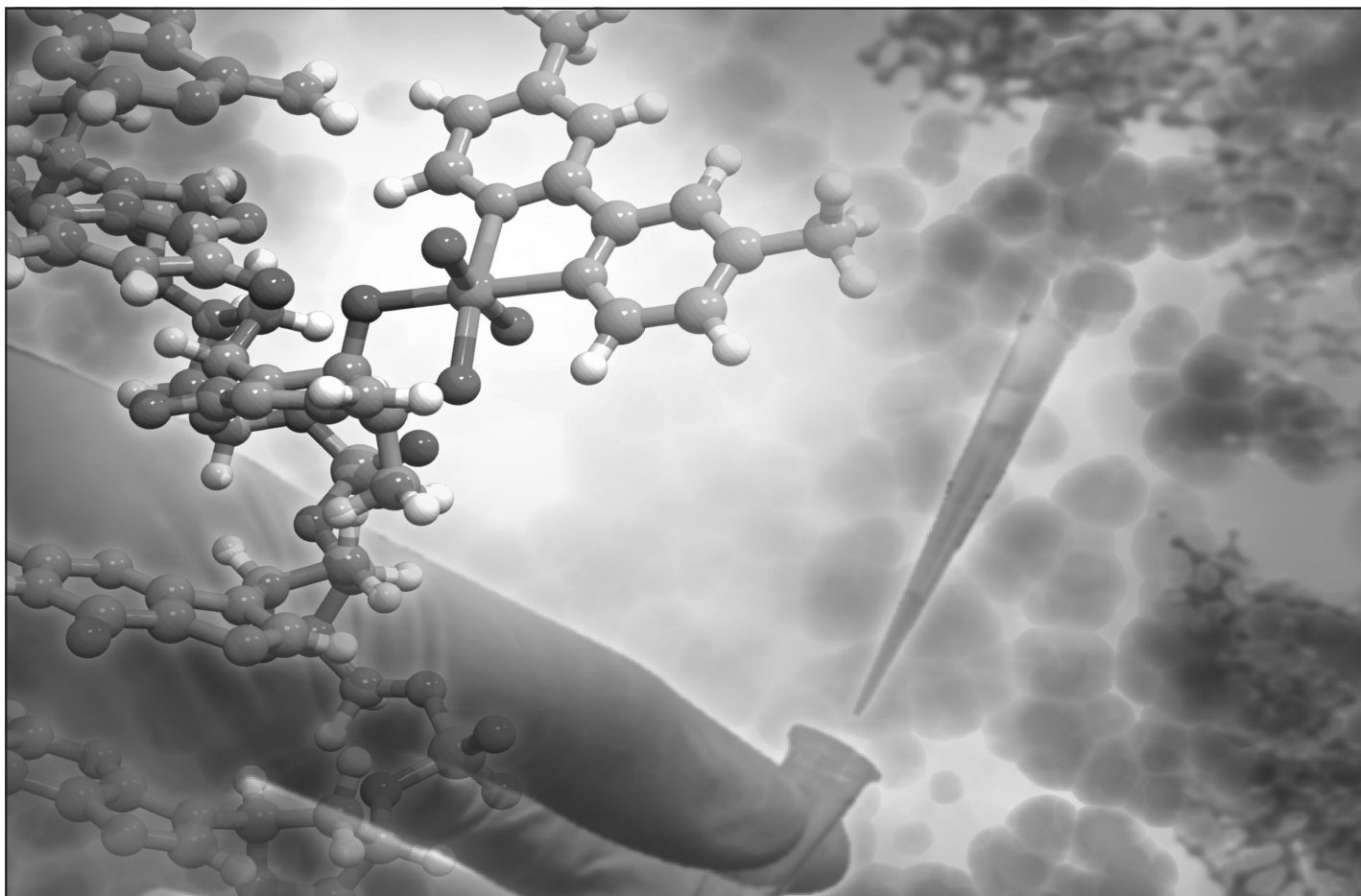
- Over 900 new and existing books
- Fully searchable
- Unlimited access

Why not take a look today? Go online to find out more!

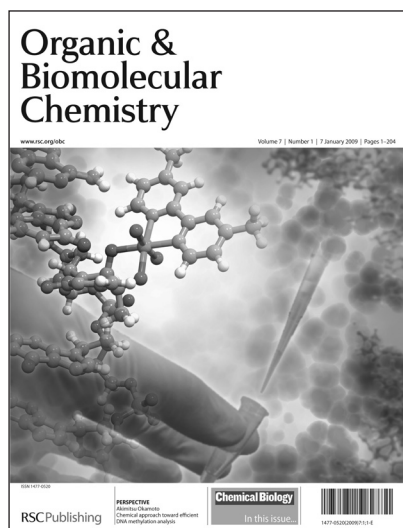
RSC Publishing

[www.rsc.org/greenchem](http://www.rsc.org/greenchem)

Registered Charity Number 207890



# Organic & Biomolecular Chemistry



OBC has achieved tremendous success since the first issue was published in January 2003. Can any other 'young' journal boast such highly cited papers, published quickly after independent peer review to such exacting standards?

- A leading journal in the field
- High impact factor 3.550\*
- Short publication times
- World renowned editorial board

\* 2008 Thomson Scientific (ISI) Journal Citation Reports®

**... high quality - high impact!**

RSC Publishing

[www.rsc.org/obc](http://www.rsc.org/obc)

Registered Charity Number 207890



# Stimulating reviews on natural products and related areas

*Natural Product Reports* publishes highlights (topical areas of interest) and reviews in key areas including: bioorganic chemistry, chemical biology, chemical ecology and carbohydrates

- Impact factor 7.450\*
- High visibility – cited in MEDLINE
- Hot off the Press literature highlights published in each issue for the benefit of the community



\*2008 Thomson Scientific (ISI) Journal Citation Reports®

RSC Publishing

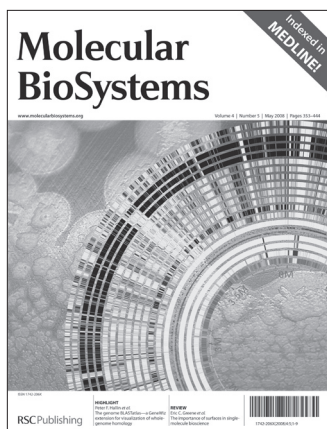
[www.rsc.org/npr](http://www.rsc.org/npr)

Registered Charity Number 207890

# Research at the interface between chemistry, the –omic sciences and systems biology

IMPACT FACTOR  
4.236\*

0886077a



- High impact, high visibility
- Fast publication times (average 80 days from receipt)
- Enhanced HTML articles, including:
  - Hyperlinked compound information, including downloadable structures in text
  - Gene, Sequence and Cell Ontology terms linked to definitions and related articles
  - IUPAC Gold Book terms linked

\*2008 Thomson Scientific (ISI) Journal Citation Reports<sup>®</sup>

RSC Publishing

[www.molecularbiosystems.org](http://www.molecularbiosystems.org)

Registered Charity Number 207890



# Top science ...free institutional access



## New for 2010

**Chemical Science** - a new journal presenting findings of exceptional significance from across the chemical sciences. [www.rsc.org/chemicalscience](http://www.rsc.org/chemicalscience)

**MedChemComm** - focusing on medicinal chemistry research, including new studies related to biologically-active chemical or biochemical entities that can act as pharmacological agents with therapeutic potential or relevance. [www.rsc.org/medchemcomm](http://www.rsc.org/medchemcomm)

**Polymer Chemistry** - publishing advances in polymer chemistry covering all aspects of synthetic and biological macromolecules, and related emerging areas. [www.rsc.org/polymers](http://www.rsc.org/polymers)

## New for 2009

**Analytical Methods** - highlights new and improved methods for the practical application of analytical science. This monthly journal will communicate research in the advancement of analytical techniques for use by the wider scientific community. [www.rsc.org/methods](http://www.rsc.org/methods)

**Integrative Biology** - focusing on quantitative multi-scale biology using enabling technologies and tools to exploit the convergence of biology with physics, chemistry, engineering, imaging and informatics. [www.rsc.org/ibiology](http://www.rsc.org/ibiology)

**Metallomics** - covering the research fields related to metals in biological, environmental and clinical systems. [www.rsc.org/metallomics](http://www.rsc.org/metallomics)

**Nanoscale** - publishing experimental and theoretical work across the breadth of nanoscience and nanotechnology. [www.rsc.org/nanoscale](http://www.rsc.org/nanoscale)

Free institutional access, managed by IP address, is available on all these titles. For more details, and to register, visit [www.rsc.org/free\\_access\\_registration](http://www.rsc.org/free_access_registration)